TESTING AND ANALYSIS OF THE PEELING OF MEDICAL ADHESIVES FROM HUMAN SKIN

Alicia Corrine Karwoski

Thesis submitted to the Faculty of the
Virginia Polytechnic Institute and State University
In partial fulfillment of the requirements for the degree of

MASTER OF SCIENCE
IN
CIVIL ENGINEERING

Approved by:

_____
Raymond H. Plaut, Chairman

_____ _____
Carin L. Roberts-Wollmann David A. Dillard

April 29, 2003
Blacksburg, Virginia

Key Words: Adhesion, Peel, Pressure Sensitive Adhesives, Skin

TESTING AND ANALYSIS OF THE PEELING OF MEDICAL ADHESIVES FROM HUMAN SKIN

Alicia Corrine Karwoski

Raymond H. Plaut, Chairman
Civil and Environmental Engineering

(ABSTRACT)

The analysis of peeling tape or a bandage from skin is a challenging problem. Skin is a very complex material made of many layers with anisotropic material properties. Adhesives that bond tapes or patches to skin must attach to skin through moisture and skin movement, but then be removed with little skin trauma. A computer model of peeling from skin apparently has not been developed previously. With experiments and the application of mechanics, research was conducted to analyze adhesion to skin.

Numerous peeling experiments were performed on human subject arms using 2.54-cm-wide pressure sensitive tape Durapore™ by 3M. Various rates, angles, and dwell times were tested. Testing machines recorded peel force and the displacement of the end of the tape. A range of maximum and average peeling force values were noted for human subjects, along with the influence of angle, rate, order of testing, dwell time, and subject. Also, rigid substrates were tested for comparison with human skin.

Computer models were also developed to simulate peeling and skin behavior. Initial models dealt with peeling from a rigid surface, and intermediate models concerned plucking skin. The final model involved peeling a piece of tape from skin, the overall goal of this research. The skin and tape were modeled as they behave during peeling. With the final model, the peel angle, debonding moment, normal force on the skin, and net shear force tangential to the skin were analyzed.

Results from the experiments and computer models of this research will increase knowledge of skin behavior and could contribute to improvements in the design of adhesives that contact the skin.

Acknowledgements

I would like to thank Dr. R. H. Plaut for his time, patience, and this intriguing research opportunity. I would also like to thank Dr. D. A. Dillard and Dr. C. L. Roberts-Wollmann for their advice and for serving as committee members.

Special thanks to Rachel Roop, Daniel Kozink, Bob Simonds, and the technicians in the ESM Machine Shop for helping with the testing phase.

I would also like to thank the Carilion Biomedical Institute through the Optical Sciences and Engineering Research Center (OSER) at Virginia Tech for providing the funding for this research.

Finally, thanks to my mom, dad, and sister for all their love and support.

Table of Contents

Table of Contents, Continued

Table of Contents, Continued

List of Figures

Figures, Continued

Figures, Continued

Figures, Continued

List of Tables

Chapter 1. Introduction and Literature Review

1.0 Introduction

Skin is important to the human body because it provides support and protection to internal organs. Scientists have long studied skin to understand its properties, behavior, and structure. Skin properties change depending on age, sex, weight, environmental exposure, pregnancy, disease, exposure to drugs and chemicals, and place on the body, making it a complex material to study. Several models, tests, and testing devices exist to study skin properties and behavior. The use of bandages and medical dressings on skin also factor into skin research. As a result, scientists study the behavior and performance of pressure sensitive adhesive tapes on skin and other surfaces along with the basic principles of adhesion. The study of skin behavior benefits disease research, cosmetic product development, knowledge of skin in the aging process, plastic surgery research, and skin adhesives development (Lanir, 1987; Diridollou et al., 1998).

1.1. Overview of Skin

1.1.1. Skin Composition

Skin makes up approximately 16% of human adult body weight and has many heterogeneous and anisotropic tissue layers. The four main categories of layers are the outer layer or stratum corneum, the epidermis, the dermis, and the hypodermis or subcutaneous fat layer. The dermis is further divided into the papillary dermis and reticular dermis, which contain collagen, elastin, reticulin, fibrocytes, blood and lymph vessels, nerve endings, hair, hair follicles, and glands and ducts in a “ground substance”. The “ground substance” is made up of water, mucopolysaccharides, proteins, enzymes, and electrolytes, and occupies the majority of the dermis layer along with collagen fibers (Lanir, 1987; Diridollou et al., 1998). Table 1.1 shows the main skin components with corresponding materials exhibiting similar behavior.

Table 1.1: Major Components of the Skin and Materials Showing Similar Behavior

Skin Component	Similar Material
Collagen	Crystalline
Elastin	Rubber-like materials
"Ground substance"	Gels made of hyaluronic acid and water

1.1.2. Mechanical Properties

The major mechanical properties of skin include hardness, tensile strength, stiffness, and elasticity (Gniadecka and Serup, 1995). Hardness is defined by Graves and Edwards (2002) as "resistance to wear, indentation, and scratching." Tensile strength is the amount of force applied to stretch the skin when it breaks. Stiffness is the skin's ability to resist deformation, or change in shape. Elasticity is the skin's ability to recover its original shape after deformation. Collagen and elastin mainly influence tensile strength, stiffness, and elasticity (Oikarinen and Knuutinen, 2002).

1.1.3. Collagen and Elastin

Collagen fibers are the major mechanical element of skin. Collagen fibers are viscoelastic, provide structure and tensile strength, and vary in thickness and density throughout the dermis layer (Lanir, 1987; Oikarinen and Knuutinen, 2002). When skin is stretched, the collagen fibers dominate over the other elements of skin and can be stretched reversibly up to two to four percent. Collagen fibers have a high tensile strength of about 150 to 350 MPa and a high stiffness of around 1 GPa (Lanir, 1987).

Like collagen, elastin is also important to mechanical skin properties. The elasticity and resilience in skin can be attributed to elastin fibers. Elastin fibers are fine and wind through and around thick collagen fibers in the interior of the dermis (Elsner et al., 2002). The stiffness of an elastin fiber is less than that of a collagen fiber, but can be reversibly stretched more than a collagen fiber. Furthermore, elastin fibers stretch first when skin tissue is strained (Lanir, 1987).

Skin tissues containing both collagen and elastin fibers in the "ground substance" are known as fibrous connective tissues. Fibrous connective tissues consist of many individual components called phases, which are organized in a "typical structure," and react and interact with each other when skin is deformed. Upon deformation, fibers rotate, stretch, and push out fluids in the "ground substance" with the pressure of their movements. The resulting fluid flow in skin is slow because of the dense network of fibers and highly viscous fluid (Lanir, 1983).

1.1.4. Langer's Lines

Skin attached to the body is normally under tension. Once removed from the body, skin retracts about 5 to 30%. Both tension and retraction depend on place on the body, direction, and body posture (Lanir, 1987).

In 1861, Langer investigated the tension and retraction of skin by making circular punctures into dead human skin. The skin revealed elliptical shapes where the circular punctures were made, showing tension in the direction of the ellipse's major axis. By repeating punctures over the surface of cadavers, Langer established lines connecting the major axes of the ellipses. These lines indicated the direction of maximum tension, stress, and strain over the body and are known as Langer's lines (Thacker et al., 1977). In addition, skin's mechanical anisotropy follows the same direction as Langer's lines such that skin extensibility is lowest in the direction of Langer's lines *in vivo* and *in vitro*. Also, skin stiffness tends to be highest in the direction of Langer's lines at low strain levels, but similar in all directions at high strain levels (Lanir, 1987).

Collagen and elastin fibers are preferentially positioned in the direction of Langer's lines. The collagen and elastin fibers that run along Langer's lines are stretched more than the collagen and elastin fibers that run across Langer's lines. As a result, *in vivo*, the collagen and elastin along Langer's lines have a higher tension and stretch, but a lower extensibility and higher initial stiffness in the direction of Langer's lines (Lanir, 1987).

1.2. Skin Tests and Testing Devices

1.2.1. *In Vitro* and *In Vivo*

Skin tests are divided into two categories, *in vitro* (*ex vivo*) and *in vivo*. *In vitro* testing involves testing the skin after it has been removed from the living being, while *in vivo* tests examine the skin while it is still attached. The disadvantage of performing *in vitro* tests is that the skin is away from its influential surroundings: blood, blood pressure, lymphatic drainage, *in vivo* metabolism, and nervous and hormonal controls. On the other hand, establishing a uniform strain field in the sample and controlling boundary conditions are very difficult when performing *in vivo* tests. According to Lanir (1987), skin tests should always include measurements of the skin's resting tension, deformation, and thickness. Table 1.2 shows various skin testing techniques, their corresponding uniform strain parameter, and their advantages.

Table 1.2: Testing Techniques Table

Test Type		Comments
Uniaxial	*In Vivo*	No uniform strain in tissue, but show directional effects
Uniaxial	*In Vitro*	Improved uniform strain in tissue
Strip Biaxial	*In Vivo*	
Strip Biaxial	*In Vitro*	
Suction Tests with Racetrack-shaped Cups	*In Vivo*	Uniform strain in tissue and show anisotropic constitutive behavior
Biaxial	*In Vitro*	
Torsional	*In Vitro*	No uniform strain in tissue, easy to perform
Suction Tests with Circular Cups	*In Vivo*	
Suction Tests with Circular Cups	*In Vitro*	
Skin-fold Compressibility	*In Vivo*	No uniform strain in tissue, but easy to perform and useful in parametric studies of compressive response of skin
Indentation	*In Vivo*	

In vitro tests typically involve removing animal or dead human skin and testing the skin in tension. The excised skin is modified into a dumbbell shape so the ends may be gripped by an Instron testing machine, enabling experimenters to test for strength, time-dependent values, and non-time-dependent values. *In vitro* test samples cannot be kept for an extended amount of time, usually shrink once removed, and cannot be further modified *in vivo* (Edwards and Marks, 1995).

Suction, tonometric, traction, indentation, and torsion tests are examples of *in vivo* tests. Suction tests exert negative pressure on the skin, and tonometric tests place vertical forces of extension on the skin. Traction tests exert linear displacement in the horizontal plane of the skin, and indentation tests push inward on discs or points glued to the skin. Lastly, torsion tests apply torques on the skin (Diridollou et al., 1998).

1.2.2. Skin Testing Devices

Researchers have developed certain devices to perform the above-mentioned tests and determine skin's mechanical properties. The devices are even commercially available. Some of the basic devices used to study skin properties include the Cutometer®, the Dermaflex A®, the "echorheometer," Gas-Bearing Electrodynamometer and Linear Skin Rheometer, the extensometers, the Durometer®, the Microindentometer, and the Dermal Torque Meter®, and the Ballistometer. Scientists have learned about various skin properties through the use of these devices.

1.2.2.1. The Cutometer®

The Cutometer® performs suction *in vivo* tests on human skin and measures the upward displacement of the skin. The device indicates elastic and viscoelastic properties of skin by measuring vertical displacement, but does not record skin thickness or changes to thickness in deeper skin layers (Diridollou et al., 1998). The Cutometer® is on the market and known for being easy to use. Through use of a variable vacuum, the device pulls skin into the opening of a probe and generates resulting stress versus strain and strain versus time curves. Cutometer® users can evaluate the effects of aging, anatomical skin sites, gender, and topical dermatocosmetic treatments (Barel et al., 1998).

Through use of the Cutometer®, Barel et al. (1998) found many trends in skin behavior due to applied suction pressure and physiological parameters. First they found that skin deformation parameters increased nonlinearly with increasing suction and that the coefficient of elasticity was pressure dependent. They also noticed that pretensioning the skin increased elasticity parameters and helped the skin revert to its initial position after deformation. In addition, Barel et al. (1998) found that elastic parameters differed among anatomical sites and that the coefficient of elasticity increased with sun exposure. Furthermore, the elasticity ratio dropped in older subjects, whereas the viscoelasticity ratio and coefficient of elasticity increased. The removal of upper layers of skin (approximately 40 strippings) revealed a small decrease in elasticity and a large increase in viscoelastic parameters.

1.2.2.2. The Dermaflex A®

Like the Cutometer®, the Dermaflex A® is commercially sold and performs suction on skin *in vivo*. The Dermaflex A also measures the vertical displacement of the skin without concern for skin thickness or change in thickness of the deeper layers of skin (Diridollou et al., 1998). Mechanical parameters of skin such as distensibility, elasticity, and hysteresis can be read with use of the Dermaflex A®. The device consists of a vacuum generator connected to a suction probe to place on the skin. The probe diameter for the Dermaflex A® is larger than that of the Cutometer®, making it more suitable for measuring mechanical properties of the dermis or deeper skin layers (Gniadecka and Serup, 1995).

Through use of the Dermaflex A®, several authors have found that skin properties vary with anatomical site, age, and time of the day. Specifically, anatomical sites that are closer to the body, like on the thighs, are less stiff than anatomical sites that are further from the body, such as forearms. Also, skin elasticity is less for subjects of greater age. Furthermore, skin's stiffness and elasticity vary throughout the day (Gniadecka and Serup, 1995).

1.2.2.3. The "Echorheometer"

The "echorheometer" is a third *in vivo* suction device worth mentioning. Incorporating a suction system, combined probe, and ultrasound scanner, the "echorheometer" examines the effects of mechanical stresses applied to deeper layers of skin and quantifies deformation of skin structures. In contrast to the Cutometer® and the Dermaflex A®, the "echorheometer" records dermal and hypodermal thicknesses before, during, and after the skin undergoes suction (Diridollou et al., 1998).

The creators of the "echorheometer" performed numerous tests to observe skin's mechanical properties. They found that the effects of suction stress on skin cannot be distinguished from the effects on the subcutaneous fat layer because of thickness changes in the subcutaneous fat layer with suction. In addition, the dermis layer of the skin provides the primary resistance to applied suction. Moreover, when suction is applied to skin, fluid infiltrates into the tissues experiencing the suction pressure and lingers for a period of time after suction ceases (Diridollou et al., 1998).

1.2.2.4. The Gas-Bearing Electrodynamometer and Linear Skin Rheometer

The Gas-Bearing Electrodynamometer and Linear Skin Rheometer test skin tension *in vivo*. The Linear Skin Rheometer was built to improve the Gas-Bearing Electrodynamometer. Tabs are attached to the outer edge of skin with adhesives and apply stress to the skin. The tests indicate changes in the mechanical properties of the human stratum corneum. Specifically, the effect of moisturizers can be evaluated (Matts, 2002).

1.2.2.5. The Extensometers

Extensometers are not widely used skin-testing devices, but are novel in their indication of the anisotropy of skin. Extensometers typically involve two pads attached to skin *in vivo* by means of a double-sided adhesive tape. The pads can either be moved

so the experimenter can read the force on the pads, or can be loaded so the experimenter can measure displacement between the pads (Vescovo et al., 2002).

One study by Thacker et al. (1977) utilized a uniaxial extensometer to provide information for making excisions and incisions based on static and dynamic skin tensions. Static tensions are natural tensions present in normal skin, and dynamic tensions result from joint movement, gravity, and mimetic and other voluntary muscle activity. Thacker et al. found that static and dynamic tensions influence the load-extension properties of human skin *in vivo*. For instance, some body areas have a defined orientation of static tensions. Furthermore, when a joint moves, the dynamic tensions change in terms of magnitude and direction.

According to Vescovo et al. (2002), extensometers are very valuable tools, but need improvement. Their size should be minimized and they should perform force or displacement servo-controlled tests. Also, they should be sized to fit in an optical device for finding the strain field, and to an ultrasonic device. Lastly, they should be simple to use and provide precise information on skin's mechanical behavior.

1.2.2.6. The Durometer®

The Durometer® is a portable and commercially sold indentation device used to measure skin hardness (Rodrigues, 2001). The Durometer® consists of a gauge for measurement at the top, a spring-loaded interior, and a small, dull indentor at the bottom. The Durometer®'s gauge displays hardness as the Durometer® rests by gravity on the skin surface, which primarily pertains to the stratum corneum. The device provides reproducible results and can be used on patients with skin disorders such as scleroderma to assess treatment (Romanelli and Falanga, 2002).

1.2.2.7. The Microindentometer

Also employing indentation methods is the microindentometer. The microindentometer targets the stratum corneum layer of the skin for indentation. The device uses a needle to indent the skin and records the reaction force. The reaction force provides indication of stiffness, tensile strength, and hardness properties for the stratum corneum. The stratum corneum serves as a protective layer for the body, making the stiffness, tensile strength, and hardness properties significant. Scientists have tested different subjects in callus and thenar eminence regions to compare resulting reaction

forces and verify the performance of the device (Graves and Edwards, 2002). The callus region is the top portion of the palm where the fingers attach to the palm and the thenar eminence region is the fleshy portion of the palm that lies at the base of the thumb (Van De Graaff, 2002).

1.2.2.8. The Dermal Torque Meter®

The Dermal Torque Meter® is a device used to apply torsion to skin. Known as the Twistometer in its early stages, the Dermal Torque Meter® applies stress in rotation in the plane of skin provided the body area is flat and about 5 cm in width. The device involves a probe containing a torque motor connected to a disk that twists and is surrounded by a "guard ring," which holds the outside edge of skin in place. The "guard ring" and disk adhere to the skin by means of a double-sided adhesive tape. The results from the tests are in terms of elasticity, viscosity, and plasticity variables. The Dermal Torque Meter® can be used for exploring age, sun, cosmetic, and dermatology effects (Rigal, 2002).

1.2.2.9. The Ballistometer

The Ballistometer performs impact testing on skin, which means "a vibrational movement is imposed to the skin through a ballistomer hammer being dropped on the surface of the skin" (Rodrigues, 2001). The resulting response and displacement of the hammer are recorded with time to determine parameters of amplitude, stiffness, cutaneous absorption coefficient, and coefficient of restitution. The Ballistometer is mainly used to evaluate viscoelastic properties of the skin (Pugliese and Potts, 2002).

Pugliese and Potts (2002) performed a study using the Ballistometer on female subjects. They found a decrease in amplitude and coefficient of restitution with age. However, they found an increase in cutaneous absorption coefficient with age. Furthermore, stiffness decreased until the age of 50 years, and then began to increase.

1.2.3. Peel Tests on Skin

In addition, to testing skin with devices *in vivo*, researchers have performed peel tests on the skin *in vivo*. Bothwell (1970) examined effects of skin trauma due to peeling by peel testing subjects' backs with 2.54 cm x 5.08 cm surgical tape. The dwell time was varied and 40 repeated peelings were conducted on one spot of skin. In the dwell time tests, Bothwell found that peel force increased for up to 4 hours of dwell time and then

decreased. In the repeated peelings, Bothwell found peel force to increase up to the 20th peel and then decrease.

Other authors have presented additional varying dwell time results. Lucast (1990) and Taylor tested back skin with a 180-degree peel and used dwell times up to 48 hours. Spencer et al. (1990) used an Instron Tensile Tester to peel patches of tape at 180 degrees after one to seven days. They present a plot of adhesion versus time that starts at zero, ascends to a plateau and then descends back to zero. In addition, Horstmann et al. (1999) shows unpublished work of Lücker et al. on peel force after 1 and 24 hours. They also point out the difference of force values among subjects.

Certain studies also examine different peeling rates and evaluate pain. Andrews et al. (1987) peel tested skin by using a weight attached to the free end of tape for removal. The weight was varied and the resulting peeling speeds were recorded. Schiraldi (1990) ran peel tests at speeds of 300 to 5,000 mm/min and observed cohesive failure at lower rates and adhesive failure at higher rates. Cohesive failure is when part of the adhesive remains on the surface after removal and adhesive failure means that the adhesive is removed cleanly from the surface. Maillard-Salin et al. (2000) performed 90-degree peel tests with transdermal patches at 100 mm/min and found an average peel force of 1.2 N. Mayrovitz and Carta (1996) peeled acrylic adhesive strips from subject arms after 24 hours and then measured skin blood perfusion as a measure of trauma. Also relating peeling to trauma, Ko (1996) experimented with transdermal patches and had participants describe the level of pain felt as the peel force was recorded.

Some peel tests have been performed on animal skin. Mouse skin was used by Dong et al. (1993) for peeling at a 180-degree angle. Also, Bundy et al. (2000) peeled tissues from mouse skin clamped in a peel tester at a 90-degree angle.

In addition to animal skin testing, some studies place a focus on the skin and its mechanical behavior. The work of Aubert et al. (1985) and Agache (1995) applied a torsional device to skin to evaluate biomechanical skin properties and cosmetic effects;. Aubert et al. studied forearm skin and Agache presented work performed on forehead, forearm, cheeks, and abdomen. Lastly, Kenney et al. (1992) tested the "wear performance" of adhesives on skin.

1.3. Skin Models

According to Lanir (1987), there are three major classes of numerical models for skin: continuum models, phenomenological models, and structural models. The continuum models use general material theories to demonstrate the skin's multiaxial behavior. The phenomenological models apply mathematical formulas to imitate skin's response to various types of deformation. The structural models analyze skin by combining and analyzing the behavior of its individual components. Models have been made to consider viscoelastic behavior or a simplified pseudoelastic behavior, skin as a membrane, time-dependent behavior, and compressive response.

1.3.1. Lanir's Model

Lanir's skin model is a structural model that considers the viscoelastic, nonlinear, and anisotropic behavior of skin *in vivo*. The skin is divided into three layers: the epidermis, the dermis, and the hypodermis. The epidermis contacts the dermis in a "wavy and fingerlike-folded way ensuring that the epidermis can not glide over the dermis" (Douven et al., 2000). The hypodermis and dermis are loosely connected and the dermis is thicker than the epidermis so as to prevail in the skin's in-plane mechanical response. Collagen and elastin fibers in a "ground substance" make up the dermis layer (Douven et al., 2000).

The assumptions made in Lanir's model according to Douven et al. (2000) are as follows:

- Each fiber is thin and perfectly flexible with no compressive strength. If contracted, the fiber will buckle under zero load and wavy fibers do not bear load until they are completely straight.
- When a fiber stretches, it experiences a uniaxial strain that is the tensorial transformation of the overall strain in the fiber's direction.
- Fibers are linearly elastic under stretch.
- The fraction of fibers that are straight and stretched increases when the skin is stretched, causing increased resistance against the stretch.
- Skin is incompressible.

- During deformation, the fibers unfold and rotate, placing pressure on the "ground substance." The "ground substance" responds with hydrostatic pressure only.

The research and experimentation of Douven et al. (2000) demonstrates some inconsistencies of Lanir's skin model. The probable errors in Lanir's skin model include:

- The characterization of skin by the dermis only, neglecting the epidermis and hypodermis.
- The interaction of the fibers and the "ground substance" is not considered.
- The epidermis is assumed to behave the same as the dermis during deformation.
- Only elastic behavior is taken into consideration when the skin is not fully relaxed at the end of the final relaxation period.
- Deformations are assumed to be homogeneous throughout the skin's thickness.

1.3.2. Manschot and Brakkee's Model

Manschot and Brakkee (1985) also developed a structural model for *in vivo* human skin behavior. Their model concentrates on the time-independent stress-strain relationship of human skin and thus, the purely elastic properties of skin. The Manschot and Brakkee model is based on the following:

- An increasing stress is required to unwind each originally wavy collagen fiber.
- Collagen fibers dominate over the elastin fibers in determining the skin's purely elastic behavior.
- Tendon fibrils behave as elastic springs with a periodic corrugation given by a planar sinusoidal waveform.
- After preconditioning the skin with a high uniaxial load, collagen fibers in the skin are parallel and aligned.

Manschot and Brakkee (1985) compared their model with experimental results and found the following:

- Elastin fibers contribute substantially less to the skin's purely elastic behavior than collagen fibers.

- Ultimate skin stiffness correlates to the initial skin stiffness.
- Elastin fibers may influence the viscoelastic process after loading.

1.4. Adhesion and Skin

1.4.1. Adhesion Definition and History

Adhesion is defined by Pocius (1997) as "the phenomenon which allows the adhesive to transfer a load from the adherend to the adhesive joint." Pocius describes the adhesive joint as "the assembly made by the use of an adhesive" and the adherend as "solid materials in the adhesive joint other than the adhesive." In general, an adhesive has high adhesive and cohesive forces that transfer the force of the adhesive bond between the adherend and substrate (Horstmann et al., 1999). Figure 1.1 shows an adhesive joint. Adhesives have been around for many years. Adhesives are referenced in the Bible and were used in ancient Egypt and Rome for furniture and wooden musical instruments. Also, in modern times, adhesives are widely used in industry. Airplanes, automobiles, houses, and medical bandages are just a few of the everyday items that use adhesives (Pocius, 1997).

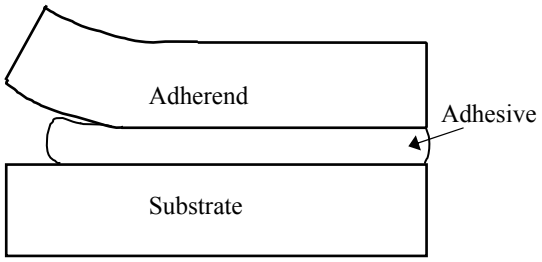

Figure 1.1: Adhesive Joint

1.4.2. Beam Theory

When adhesive joints experience a force or an adherend is separated from the adhesive, a flexible adherend sometimes may be modeled as a bending beam or a beam on an elastic foundation. Using principles from statics and Newton's Laws of Motion, scientists can develop equations and relations among the forces, moments, and shears for the beam (Pocius, 1997). This thesis utilizes beam theory in developing the mathematical models presented in the following chapters.

1.4.3. Pressure Sensitive Adhesives

Pressure sensitive adhesives are one specific type of adhesive. The medical industry typically uses pressure sensitive adhesives for medical bandages, tape, and transdermal therapeutic systems (TTS or transdermal patches). Transdermal patches are "pharmaceutical sustained-release devices that operate in a state firmly attached to human skin" (Horstmann et al., 1999). When pressed to the skin, a pressure sensitive adhesive "will instantly interact with surface lipids, provide mechanical flow into the "valleys" of the rough surface, and finally adhere directly to the keratin backbone" (Horstmann et al., 1999). The Pressure-Sensitive Tape Council describes pressure sensitive adhesives with the following characteristics (Pocius, 1997):

- Aggressive and permanent tack.
- Adheres with no more than finger pressure.
- Requires no activation by any energy source.
- Has sufficient ability to hold onto the adherend.
- Has enough cohesive strength to be able to be removed cleanly from the adherend.

Medical dressings and transdermal patches have special adhesive requirements due to the fact that they contact human skin. They must securely attach to the skin around a wound, but also allow easy and painless removal after some time without damaging the skin or wound (Chivers, 2001).

1.4.3.1. Failure Modes

Important to the study of adhesives are the different mechanisms of failure. Pressure sensitive adhesives exhibit the following progression of failure (Andrews et al., 1985):

- Cohesive failure at low peel rates where the adhesive failure energy increases with peel rate.
- Transition region between cohesive and adhesive failure where the adhesive failure energy may fall sharply with peel rate.
- Adhesive failure where adhesive failure energy increases with peel rate.
- Adhesive failure where adhesive failure energy falls with peel rate.

According to Horstmann et al. (1999), the typical failures of adhesive behavior for transdermal patches include:

- Adhesion to pouch during storage.
- Formation of adhesive residue on skin.
- Adhesion failure of backing layer.
- Protective foil difficult to detach.
- Poor adhesion to skin.

1.4.4. Adhesive Tests

As there are numerous skin tests, there are also several adhesion tests. The major test methods for adhesion include (Horstmann et al., 1999):

- Rolling ball tack.
- Surface tension.
- Probe tack.
- Peel adhesion test.
- Viscoelastic properties.

1.4.4.1. Peel Adhesion Test

The main adhesion test of relevance to this thesis is the peel adhesion test. In a peel adhesion test, adhesive tape is placed on a test surface (like skin) and then peeled from the surface at a fixed rate. The maximum detachment force is noted and considered a measure of adhesive force (Horstmann et al., 1999).

1.4.4.1.1. Hard Versus Soft Machine Tests

Andrews et al. (1985) performed peel tests with uncrosslinked elastomeric polymers with hard- and soft-machines. The difference between hard- and soft-machine tests is that the soft-machine test incorporates a spring between the cross-head of the testing machine and the peel strip; in the hard-machine test, the spring is omitted. Soft-machine tests let the peel strip peel at a rate according to the adhesive properties and instantaneous load. The authors ran peel tests at 90 degrees only and utilized a free-running trolley to maintain the peel angle. They found the following:

- One soft-machine test produces data for a range of peeling velocities, thus saving time.

- Soft-machine tests produce new information about peel tests including the lower bound behavior of adhesive failure energy per unit area and the transition peel velocity.
- Soft-machine tests can enhance quality control testing for pressure sensitive adhesives since the transition peel velocity and the difference of lower and upper bound adhesive failure energies per unit area are sensitive to thickness and rheology.

1.4.4.1.2. Reducing Peel Force

Many studies have shown a correlation of greater skin trauma with higher peel force, leading scientists to believe peel force should be minimized in order to ease medical dressing removal (Chivers, 2001). There are various physical means of reducing peel force. Most relevant to this thesis is the peel angle. According to Chivers, peel force decreases with an increasing peel angle up to 135 degrees, and then levels off. Other ways to decrease peel force is to alter the elasticity of the backing, restrain substrate deformation, modify adhesive structure, alter rate effects, and/or use a thin barrier film under the adhesive or solvent to pour over the adhesive. One chemical means for reducing peel force involves using additives to enable turning the adhesive from on to off with water contact or the heat of a hair dryer. Another chemical way of reducing peel force requires linking molecules in the pressure sensitive adhesive. Removal for different types of chemically cross-linked pressure sensitive adhesives is possible with a cold compress in one type and the exposure of the adhesive to visible light for another type (Chivers, 2001). Boyne et al. and Webster also presented switching an adhesive to a lower level with light (2001, 1999).

1.5. Models of Peeling from a Non-Rigid Surface

Most standard peel tests involve peeling from a flat, rigid substrate or surface. Peeling tape from skin is unique as skin is not a rigid surface nor is it always flat. Various researchers have examined peeling from a non-rigid surface. Roop et al. (2002) modeled and experimented with peeling from an initially-slack thin solid film. In addition, Steven-Fountain et al. (2002) analyzed and tested peeling from flexible substrates.

1.5.1. Roop et al.

Roop et al. (2002) developed a mathematical model for finding the adhesive fracture energy when peeling from an initially-slack thin solid film. The model considers geometry, fracture mechanics, slackness of the film, distance between supports, angle of the force, and the tape's extensibility. Roop et al. peeled pressure sensitive adhesive tape at 90 and 180 degrees from a strip of transparency film loosely attached to a standard machinist vise in their experiments. They recorded peel force and displacement at the end of the tape, and their results corresponded with the model in that the force slowly increases as the end of the tape is pulled upward.

1.5.2. Steven-Fountain et al.

Steven-Fountain et al. (2002) developed a mathematical model to determine the adhesive fracture energy when peeling from a flexible substrate. The model uses geometry, fracture mechanics, nonlinear elasticity, and equilibrium. They modify the fracture toughness or adhesive fracture energy equation for a rigid substrate by including a strain energy component. Steven-Fountain et al. also performed 90-degree peel tests, peeling pressure sensitive adhesive tape from both latex and neoprene substrates to verify their model. The substrates are initially straight and they stretch as the tape is peeled.

1.6. Artificial Skin

Researchers have developed materials to serve as artificial skin for testing purposes. One study by Young et al. (1998) produced artificial skin membranes from pHEMA-based composites with and without fiber reinforcement. Recently, in another study, Coulthard and Roop (2002) developed an artificial skin foundation in the shape of a half cylinder made of a gelatinous foundation material, silicone, on the bottom and an adhesive tape/fabric layer over top. Coulthard and Roop ran 90-degree peel tests on their artificial skin foundation and on their own arms with the medical tape Durapore™. They found that the magnitude of force required to pull the tape from the artificial skin was less than that of the human skin, which could indicate that the foundation represented very young skin. In addition, Coulthard and Roop found the deformation of the artificial skin to be constant as it was with the human skin. Overall, the authors recommend additional research on the artificial skin foundation.

1.7. Summary and Beginning of Research

Skin is a complex organ with great variability. There are many ways to test the skin to examine its mechanical properties and adhesive contact. There are also many mathematical models of the skin; however, as stated by Chivers (2001), "models of skin are numerous, but none has yet reproduced all the properties of skin relevant to dressing removal, and certainly not the variability." This thesis will investigate the peeling of adhesives from skin with experiments and will provide mathematical models of tape peeling from skin. Such research will hopefully increase peel testing knowledge to improve dressings and patches developed for contact with skin.

One preliminary exercise performed to provide information about skin behavior was photography of the skin up close during peeling. Two subjects, Subject A (age 22) and Subject D (age 60), were photographed for analyzing the displacement of the skin during peeling up close. The pictures were taken in front of a grid for reference when positioning the tape and the subject. Also, the subjects pulled the tape from their own arms for the photos. The subjects attempted to keep a constant peeling force. Figures 1.2-1.4 show sample photographs taken of Subject A's skin at various angles. From each photograph, two angles were obtained. The first angle, θ_o, is the angle the tape makes with the arm. The second angle, β, is the angle between the arm and the skin that lifts as a result of the tape. Figure 1.5 shows the angles on a sample picture. Both subjects were photographed the first day and only Subject A was photographed the second day. The values of all the angles were measured and tabulated. Figure 1.6 plots the angle β for both subjects versus the angle θ_o. These photographs and results will provide a base for experimenting and developing the models. The angle β mostly decreased as the angle θ_o increased. In addition, on the second day of photographs on Subject A, the β values were higher than on the first day. This could be due to a different peel force applied.

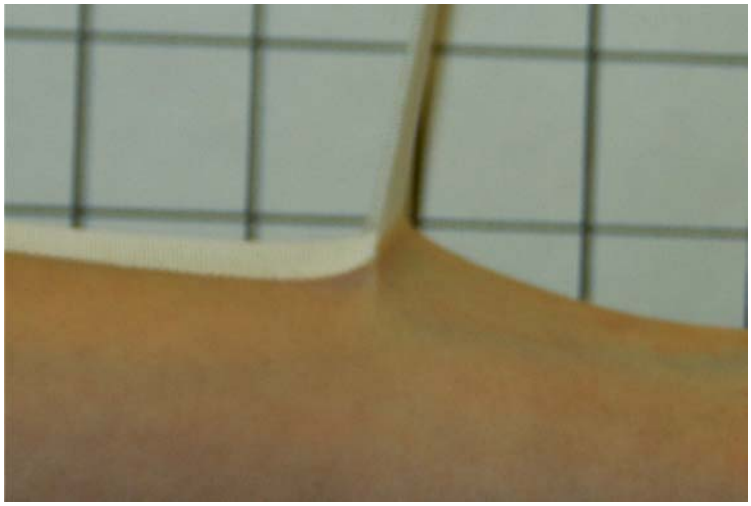

Figure 1.2: Photograph of Peeling at About 90 degrees

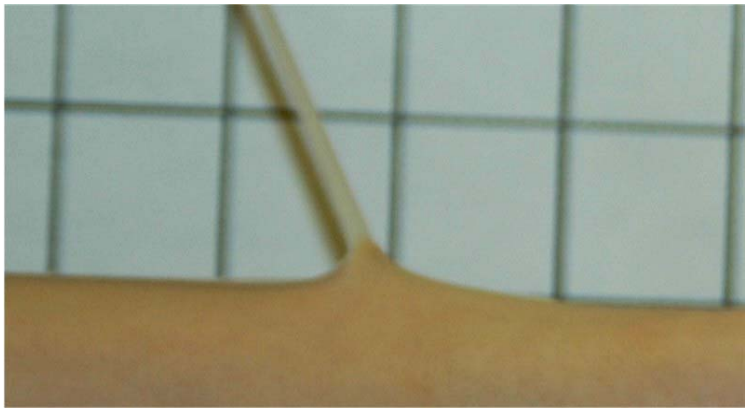

Figure 1.3: Photograph of Peeling at About 120 degrees

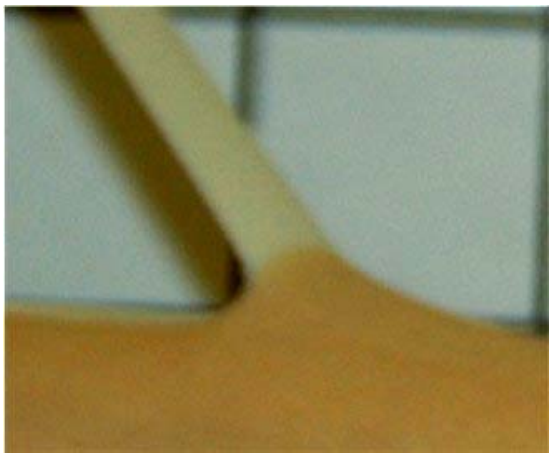

Figure 1.4: Photograph of Peeling at About 150 degrees

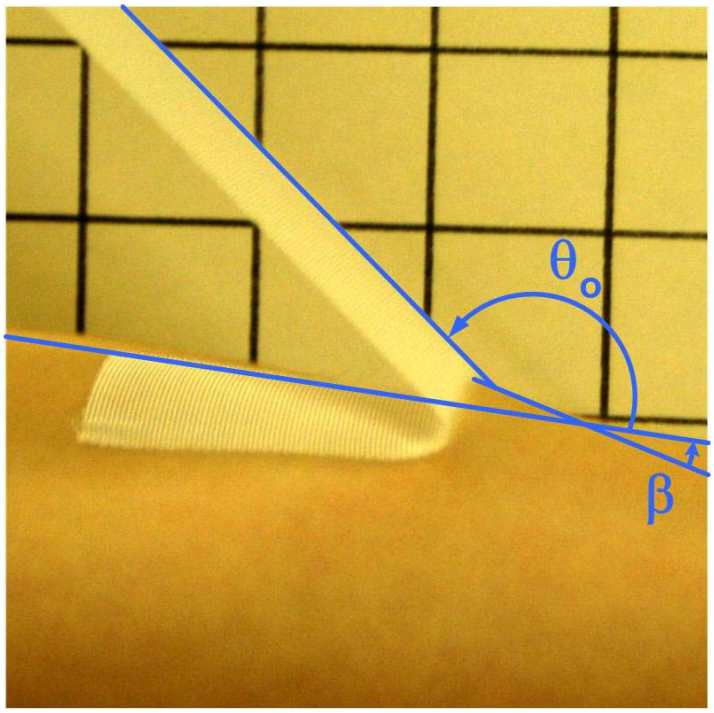

Figure 1.5: Schematic of Angles θ_o and β

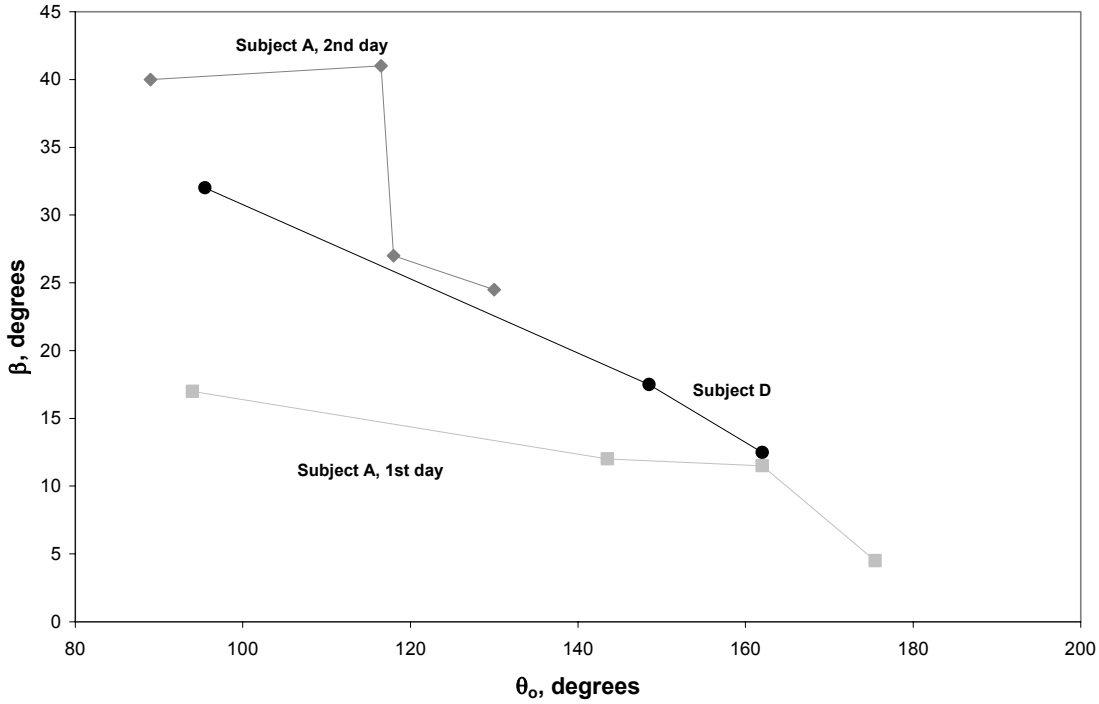

Figure 1.6: β Versus θ_o

Chapter 2. Experimentation Series One

2.0 Introduction

As mentioned in the literature, skin is an anisotropic and heterogeneous material that renews itself every two to three weeks (Edwards and Marks, 1995). In order to better understand and accurately model such a complex material, experimental peel tests were performed. The peel tests focused on the skin of the forearm region due to lack of hair and layout of the testing machines employed. The experiments are categorized into two series, Series One and Series Two. This chapter focuses on Series One experiments performed in the fall of 2002.

2.1. Materials and Equipment

Series One peel tests were performed in the Engineering Science and Mechanics Adhesion Mechanics Laboratory on the Virginia Tech campus. Equipment included an Instron 4505 tensile testing machine and LabVIEW™ software to record load versus displacement for each test. Experiments required attachments such as a sliding trolley for changing peel angle and maintaining a constant 90-degree angle (Figure 2.1), a clamp to secure the free end of tape (Figure 2.2), an L-shaped plate for securing the string in the trolley to the top of the Instron (Figure 2.2), and a turnbuckle to tighten the slack in the string (Figure 2.2). Figure 2.3 shows the testing machine and the various attachments. Attachments were selected according to the designated peel angle of each test. Table 2.1 lists the attachments for each angle setting. In addition to the Instron attachments, we used a ruler, level, timer, rubbing alcohol, cotton balls, scissors, cylindrical weight of about 10 N, and the medical tape Durapore™. Durapore™ is manufactured by 3M, and is 2.54 cm in width and 0.19 mm in thickness. Tension tests showed that the Durapore™ had a modulus of elasticity (E) of 0.81 GPa and are featured in Appendix A.

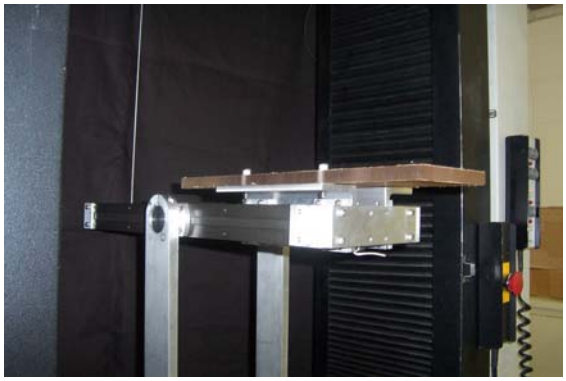

Figure 2.1: Sliding Trolley where Subject Rests Arm

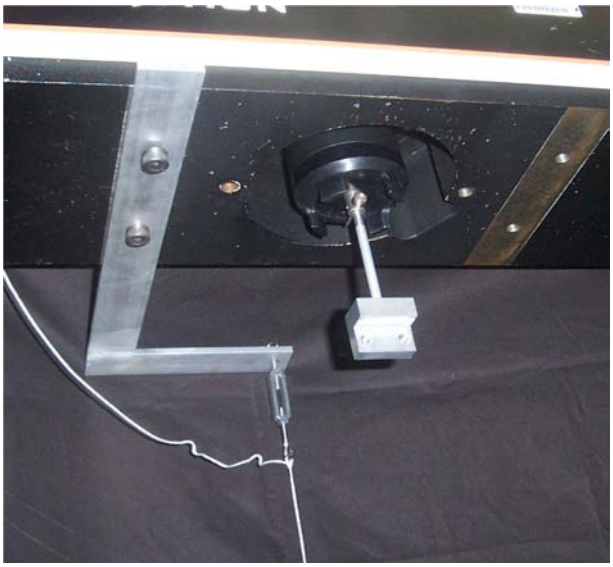

Figure 2.2: Instron Attachments in Place

Table 2.1: Equipment Attached to the Instron

Angle	Attachments Used
90^o	Clamp, sliding trolley, L-shaped plate, turnbuckle
120^o	Clamp, sliding trolley
150^o	Clamp, sliding trolley
180^o	Clamp

Figure 2.3: Experimental Setup with Instron 4505 Testing Machine

Four main subjects were tested. Table 2.2 lists subject, age, gender, angles tested, and speeds tested.

Table 2.2: Series One Peel Test Subjects

Subject	Age	Gender	Angles Tested	Speed Ranges Tested (mm/min)	Tape Dwell Time (min)
A	22	female	90^o, 120^o, 150^o, 180^o	100-500	1, 5, 10, 15
B	22	female	90^o, 180^o	100-500	1
C	24	male	90^o, 180^o	100-500	1
D	60	male	90^o, 120^o, 150^o, 180^o	100-500	1

2.2. Procedure

2.2.1. Subject Preparation

Each participant cleaned his/her forearm prior to the tests with rubbing alcohol and allowed the area to dry. The end of the tape was positioned approximately three inches from the elbow and the tape had a contact length of about 7.62 cm on the skin. Following tape application, the tape was further pressed to the skin by rolling the 10 N weight over the length of the tape four times. After the selected contact time for the peel test, the subject's arm was placed in the Instron testing machine with the appropriate attachments. The tape was then attached to the clamp approximately 41 cm above the peel front on the skin. Figure 2.4 shows the test setup including subject for a 90-degree test. The trolley is adjusted for tests at 120- and 150-degree angles and removed for tests at a 180-degree angle as in Figure 2.5.

Figure 2.4: Experimental Setup for 90-degree Tests Including Subject with Instron 4505 Testing Machine

Figure 2.5: Experimental Setup for 180-degree Tests Including Subject with Instron 4505 Testing Machine

2.2.2. Data Acquisition

When the tape and subject were in position, the load was set to read zero on the Instron. Then the peel test was executed by moving the ledge of the Instron downward with the machine controls. Three to five tests were run on each subject at different speeds, angles, and dwell times. The Instron 4505 and LabView™ Software recorded data for the peel force and the displacement of the end of the tape.

2.3. Results and Discussion

2.3.1. 90- and 180-degree Tests

The recorded peel force and displacement of the end of the tape were plotted separately for each individual peel test. Also, the data points recorded from each set of tests were averaged to make one average plot of load versus displacement for the subject, angle, speed, and contact time. Figure 2.6 shows a sample average peel test plot from Subject A at a 90-degree angle and speed of 400 mm/min (also available in Appendix B). Figure 2.7 displays a sample average peel test plot from Subject B at a 180-degree angle and speed of 100 mm/min (also available in Appendix B). Appendix B contains a complete record of individual peel test plots and averaged peel test plots acquired in Series One.

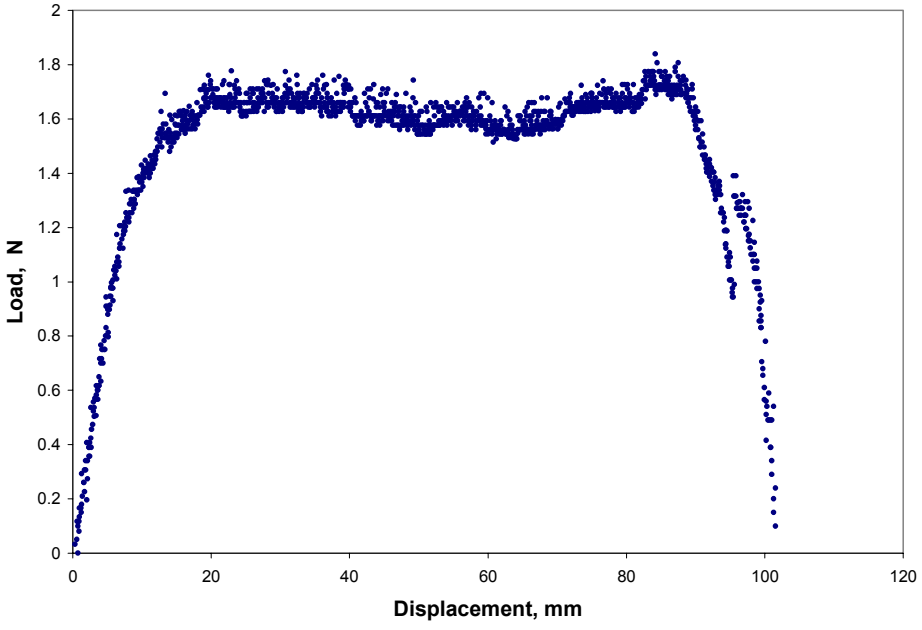

Figure 2.6: Averaged 90-degree Peel Test Run on Subject A at 400 mm/min

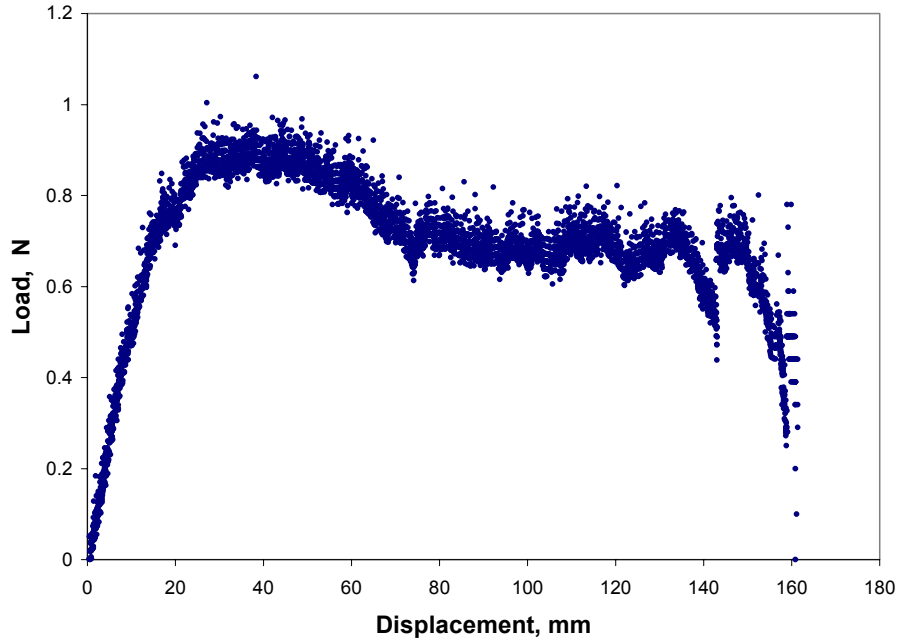

Figure 2.7: Averaged 180-degree Peel Test Run on Subject A at 400 mm/min

The individual peel test plots were used to find the average and maximum peel force for the subject, angle, and speed. Dwell time was held constant at one minute for all tests except those described in Section 2.3.2. The average peel force was measured by taking an average of the load values on the plateau region of the average plot and the maximum peel force was simply the greatest load recorded throughout the entire test. On each test a value for average and maximum peel force was obtained. Then, the average and maximum force values from the three to five tests were averaged and the coefficient of variation was computed.

Also computed from the peel tests were initial slope, and maximum displacement before peeling starts, which were obtained from the average test plots. The initial slope is taken from the beginning positive data points found in the rising portion of the graph. The maximum displacement before peeling starts is the displacement value of the tape end when the tape begins to lift off the skin. Thus, it is the displacement value at the point where the plateau region starts since we set the starting displacement to zero on the machine. Figure 2.8 shows average peel force, maximum peel force, initial slope, and maximum displacement before peeling starts labeled on a test plot. Table 2.3 lists

subjects' average peel force, maximum peel force, initial slope, and maximum displacement at different speeds for 90-degree peel tests. Also found in Table 2.3 is the coefficient of variation, denoted CV, for the average and maximum peel force results.

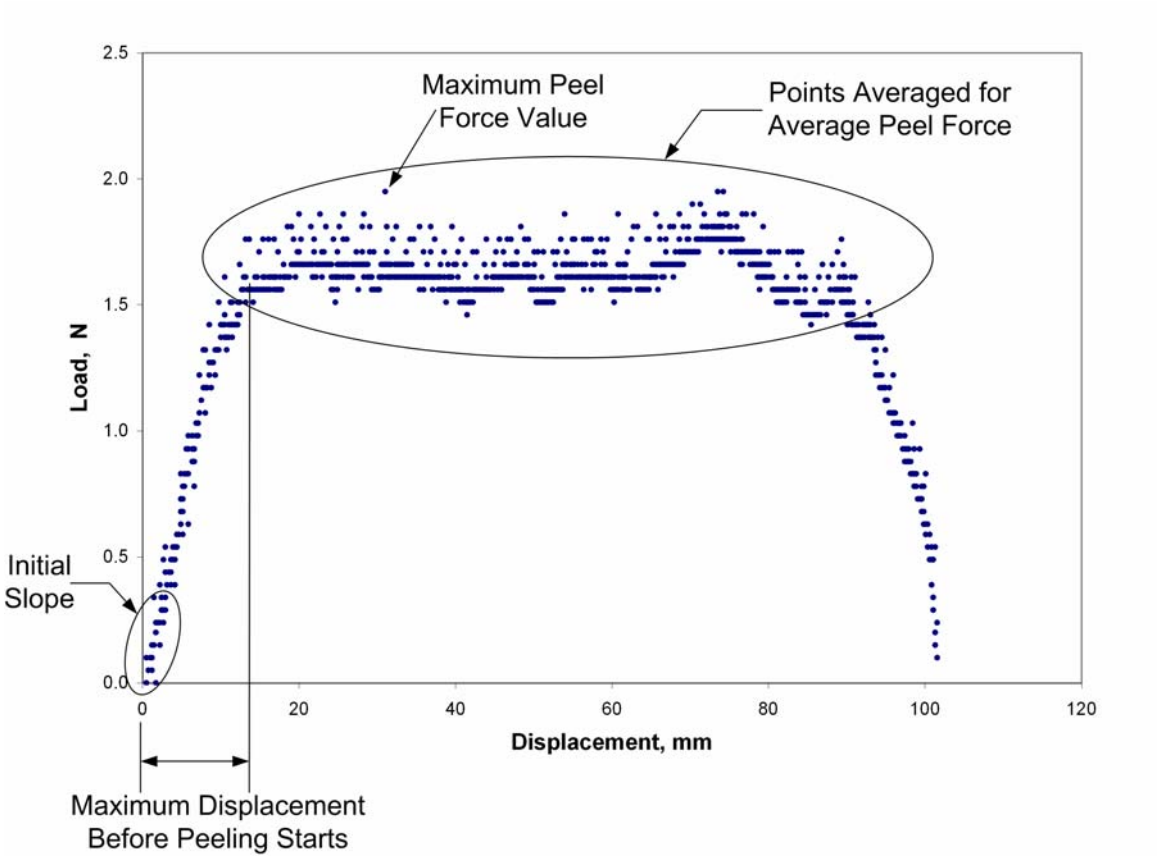

Figure 2.8: Showing Average Peel Force, Maximum Peel Force, Initial Slope, and Maximum Displacement Before Peeling Starts

Figure 2.9 shows a comparison for each subject of his/her average peel force with corresponding rate for the 90-degree peel tests with error bars. The error bars represent coefficient of variation for the three to five tests that were averaged to produce the point shown in Figure 2.9. The average peel force for all subjects ranged between about 0.69 N and 2.44 N. Figure 2.10 compares the maximum peel force for each subject for the 90-degree peel tests with error bars for coefficient of variation. The maximum peel force for all subjects ranged between about 1.08 N and 2.98 N. For the majority of the speeds, Subject B, the youngest subject, had the lowest average peel force and lowest maximum peel force for almost all the rates. Furthermore, the male subjects, C and D, consistently experienced forces that were larger than those for the female subjects, A and B. Force

did not consistently increase with an increase in rate for all subjects. Most subjects' forces increased and then decreased, creating a zigzag shape on the graph. However, adding a linear trend line to the plots of average force and maximum force versus displacement demonstrated a small positive slope, or increase in force with rate, ranging from about 0.001 to 0.002 N/mm.

Table 2.3: Average Peel Force, Maximum Peel Force, Initial Slope, and Maximum Displacement Results for 90-degree Tests

Subject	Age	Rate (mm/min)	Average Force (N)	CV	Maximum Force (N)	CV	Initial Slope (N/mm)	Maximum Displacement (mm)	Day Tested
A	22	100	0.6875	0.14	1.2380	0.09	0.1247	8.3	9/20/02
A	22	200	1.0637	0.09	1.4167	0.08	0.1296	12.0	10/12/02
A	22	300	1.0860	0.10	1.4560	0.07	0.116	11.1	9/13/02
A	22	400	1.6388	0.07	2.0500	0.07	0.1803	19.0	10/12/02
A	22	500	1.1798	0.10	1.4167	0.05	0.0922	10.3	9/13/02
B	22	100	0.7333	0.11	1.2200	0.06	0.1519	5.1	9/20/02
B	22	200	0.7407	0.13	1.0767	0.20	0.1740	7.0	10/12/02
B	22	300	1.2268	0.08	1.6200	0.21	0.1634	8.8	9/20/02
B	22	400	1.0353	0.12	1.3580	0.17	0.2201	6.7	9/13/02
B	22	500	1.2143	0.12	1.6325	0.17	0.1818	10.1	9/13/02
C	24	100	1.1824	0.17	2.3467	0.10	0.2344	8.5	11/15/02
C	24	200	1.4615	0.10	2.3467	0.15	0.2625	10.3	11/15/02
C	24	300	1.9515	0.12	2.9800	0.12	0.2811	7.4	11/15/02
C	24	400	1.7068	0.11	2.4900	0.22	0.3035	7.2	11/15/02
C	24	500	1.7245	0.11	2.5700	0.06	0.3337	4.8	11/15/02
D	60	100	1.3156	0.12	1.7960	0.17	0.1678	13.1	9/13/02
D	60	200	1.9566	0.08	2.5100	0.15	0.1975	12.1	10/11/02
D	60	300	1.9397	0.09	2.4220	0.06	0.2333	13.1	9/13/02
D	60	400	2.4368	0.06	2.8720	0.11	0.1455	15.8	10/11/02
D	60	500	1.7665	0.09	2.1760	0.16	0.1720	18.2	9/13/02

The 90-degree initial slopes for all subjects ranged between approximately 0.1 and 0.3 N/mm. Subject C had the largest initial slopes of all subjects and increasing initial slopes with rate. The other subjects, A, B, and D, simply maintained a range of initial slope values showing no major trends.

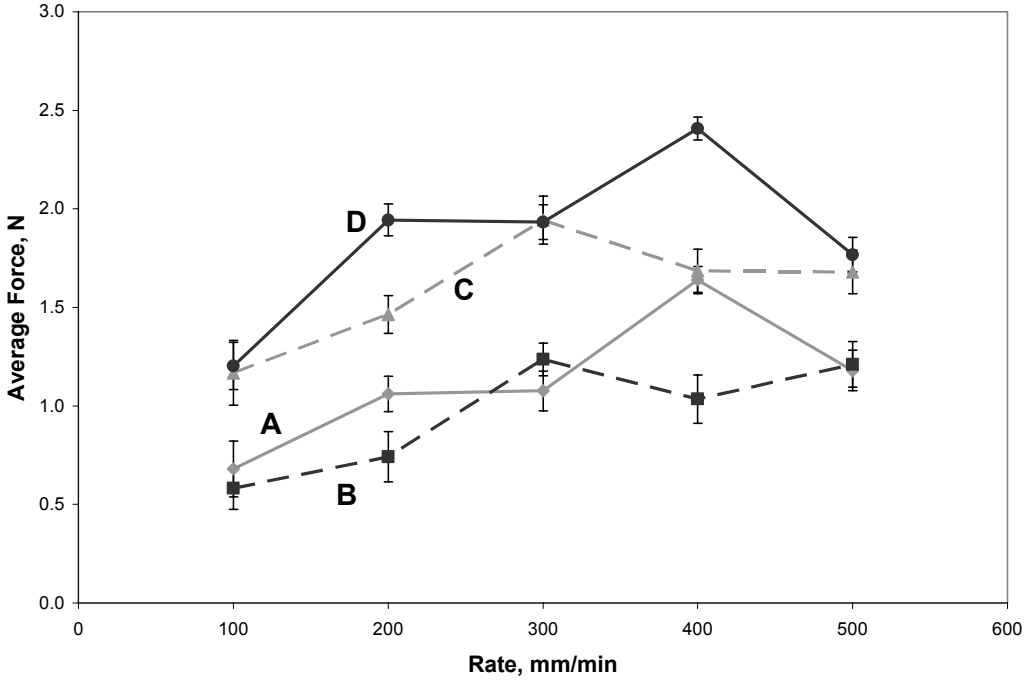

Figure 2.9: 90-degree Peel Test, Average Force Versus Rate from All Subjects and Speeds with Error Bars

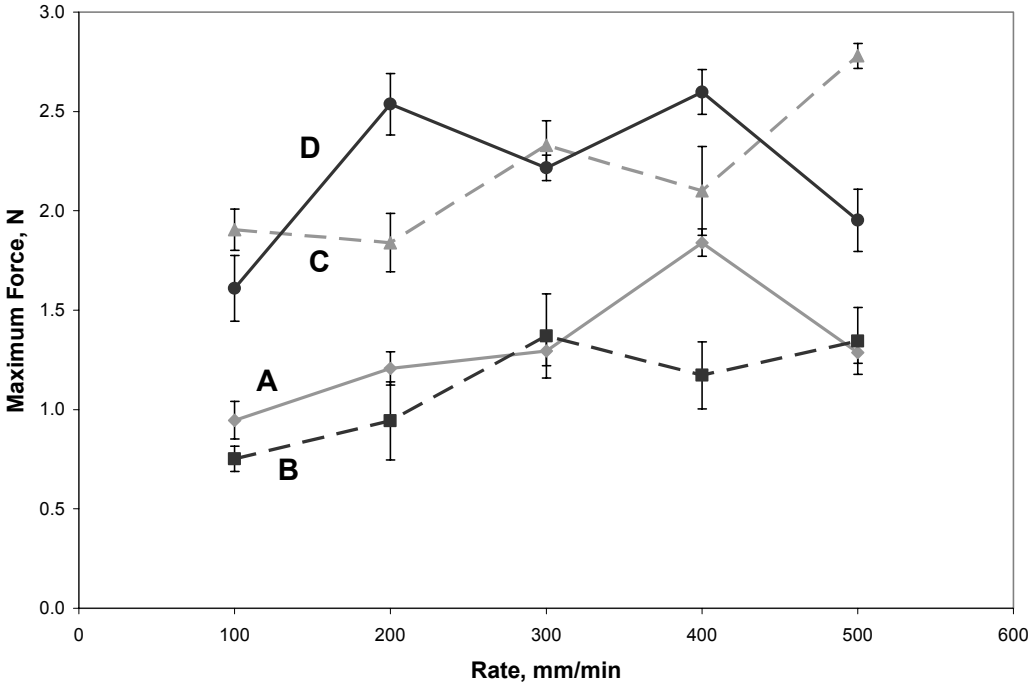

Figure 2.10: 90-degree Peel Test, Maximum Force Versus Rate from All Subjects and Speeds with Error Bars

The maximum displacement results are compared among subjects in Figures 2.11-2.13. Figure 2.11 presents the average peel force values versus the maximum displacement values for all rates and subjects. Figure 2.12 shows the maximum peel force values versus maximum displacement values for all rates and subjects. For the most part, Subject D had the highest maximum displacement values and Subject B had the lowest maximum displacement values. Figure 2.13 demonstrates maximum displacement versus rate for all subjects. Based on Figure 2.13, there is no clear correlation between rate and maximum displacement.

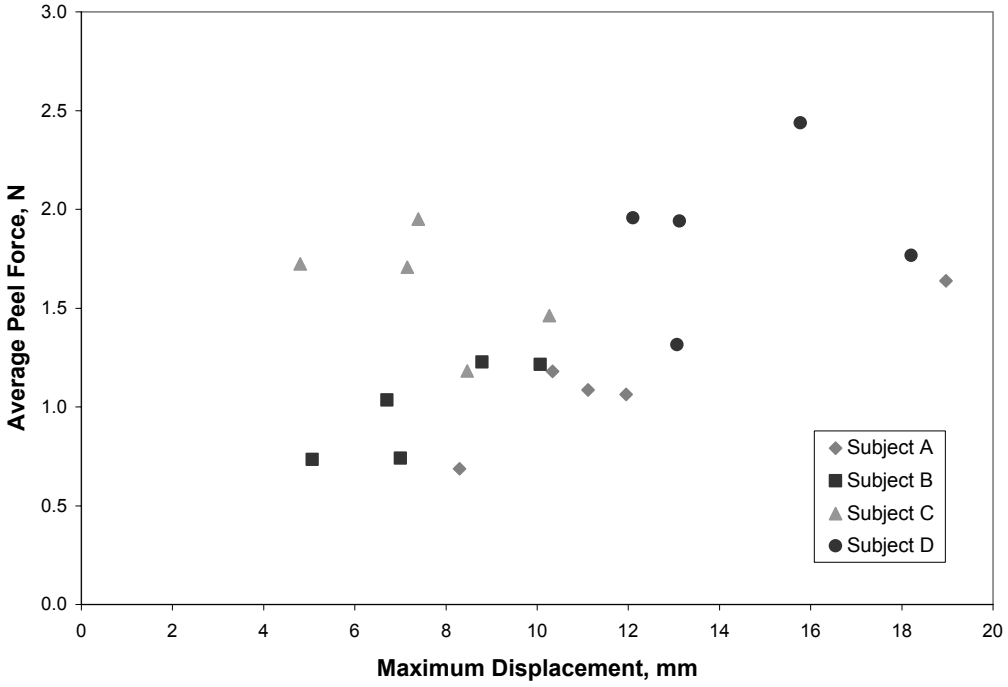

Figure 2.11: Average Peel Force Versus Maximum Displacement for All Subjects Tested at Various Rates for 90-degree Peel Tests

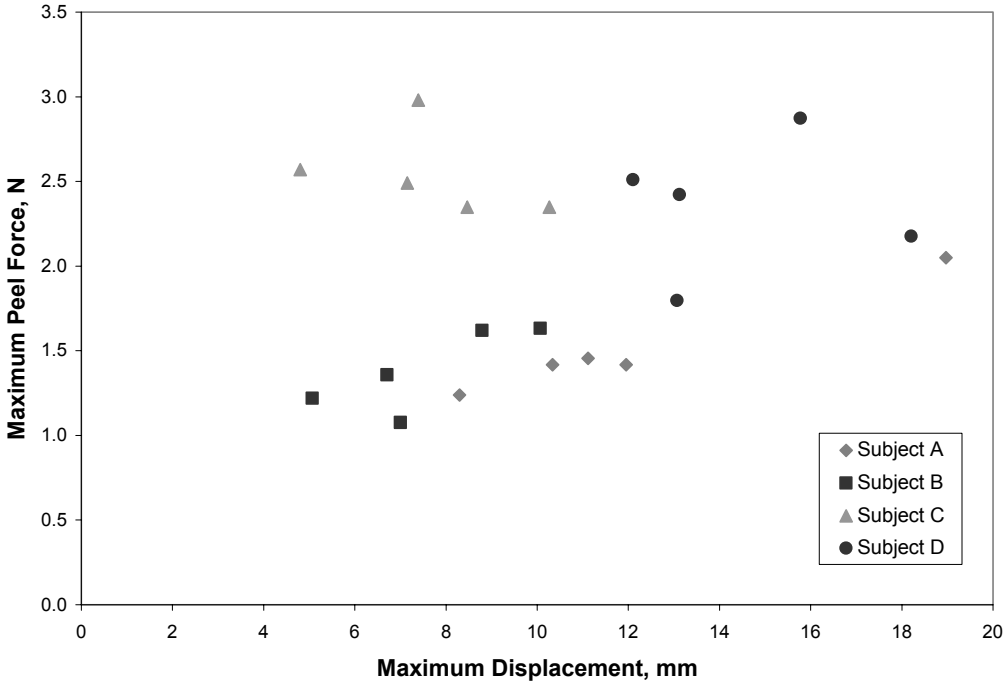

Figure 2.12: Maximum Peel Force Versus Maximum Displacement for All Subjects Tested at Various Rates for 90-degree Peel Tests

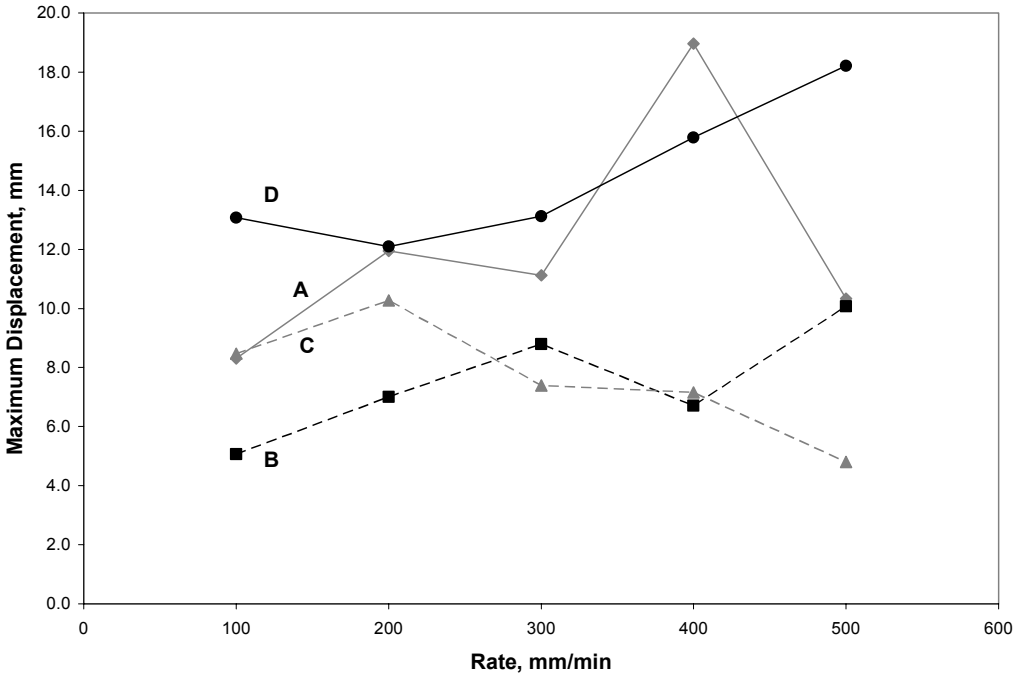

Figure 2.13: Maximum Displacement Versus Rate for All Subjects for 90-degree Peel Tests

The 180-degree tests tended to show distinct "waves" or "wrinkles" in the arm and on some of the plots of force versus displacement. The plots from Subject D especially demonstrate this trend as can be seen in Figure 2.14, a single test performed on Subject D. Figure 2.15 also shows the wrinkling of the skin underneath the tape on Subject D. Table 2.4 lists results for all subjects' average peel force, coefficient of variation (CV) for average peel force, maximum peel force, coefficient of variation (CV) for maximum peel force, and initial slope at different speeds for 180-degree peel tests.

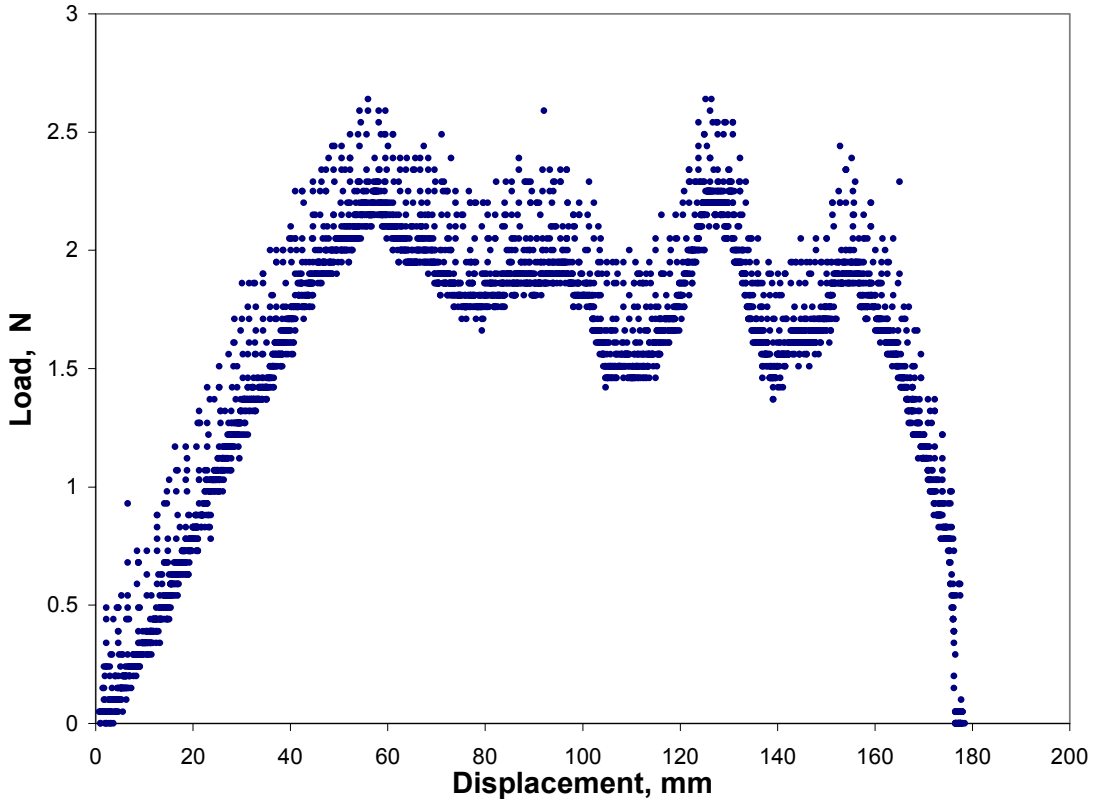

Figure 2.14: Single 180-degree Peel Test Run on Subject D at 200 mm/min

Figure 2.15: Subject D Skin Demonstrating "Waves" Underneath Tape

Table 2.4: Average Peel Force, Maximum Peel Force, Initial Slope, and Maximum Deflection Results for 180-degree Tests

Subject	Age	Rate (mm/min)	Average Force (N)	CV	Maximum Force (N)	CV	Initial Slope (N/mm)	Maximum Displacement (mm)	Day Tested
A	22	100	0.5656	0.16	1.0100	0.08	0.0485	17.0	9/20/02
A	22	200	0.6020	0.13	0.9600	0.15	0.0474	17.7	9/6/02
A	22	300	0.6249	0.10	0.8111	0.27	0.0685	14.3	9/6/02
A	22	400	0.6651	0.12	0.9767	0.08	0.1182	11.4	10/18/02
A	22	500	0.5661	0.10	0.9467	0.05	0.0709	9.9	9/27/02
B	22	100	0.7497	0.13	1.1693	0.22	0.0564	24.2	9/27/02
B	22	200	0.8051	0.16	1.2033	0.08	0.0630	23.9	10/18/02
B	22	300	0.6252	0.13	0.9633	0.06	0.0556	20.9	9/27/02
B	22	400	0.5739	0.08	0.7055	0.05	0.1026	8.7	9/6/02
B	22	500	0.7735	0.09	0.9027	0.09	0.0735	13.9	9/6/02
C	24	100	0.7648	0.14	1.5767	0.01	0.0685	13.2	11/1/02
C	24	200	0.7148	0.17	1.6850	0.16	0.1126	12.6	11/1/02
C	24	300	0.7660	0.08	1.5975	0.08	0.0991	11.3	11/1/02
C	24	400	0.9581	0.14	1.6725	0.03	0.1321	14.4	11/1/02
C	24	500	0.7364	0.23	1.4967	0.08	0.0960	17.7	11/15/02
D	60	100	1.6616	0.10	2.2180	0.11	0.0397	34.5	9/20/02
D	60	200	1.9421	0.12	2.7920	0.03	0.0543	41.2	10/4/02
D	60	300	1.7255	0.11	2.3040	0.10	0.0514	24.7	9/20/02
D	60	400	2.0047	0.10	2.7920	0.02	0.0480	34.8	10/4/02
D	60	500	1.7707	0.09	2.2060	0.08	0.0448	40.7	9/20/02

Figure 2.16 shows a comparison of average peel force with corresponding rate for the 180-degree peel tests with error bars. As with the 90-degree test results, the error bars represent coefficient of variation from the averaged three to five tests. The average peel force for all subjects ranged between about 0.57 N and 2.00 N. Figure 2.17 compares the maximum peel force and rate for each subject for the 180-degree peel tests. The maximum peel force for all subjects ranged between about 0.71 N and 2.79 N. For all speeds, Subject D maintained the largest average peel force and maximum peel force. Also, as with the 90-degree result, force sometimes increased and sometimes decreased with increasing rate, making a zigzag shape on the graph. Adding a linear trend line to the plots of average force and maximum force versus displacement showed very small and sometimes negative slopes ranging from about -0.0008 to 0.0003 N/mm.

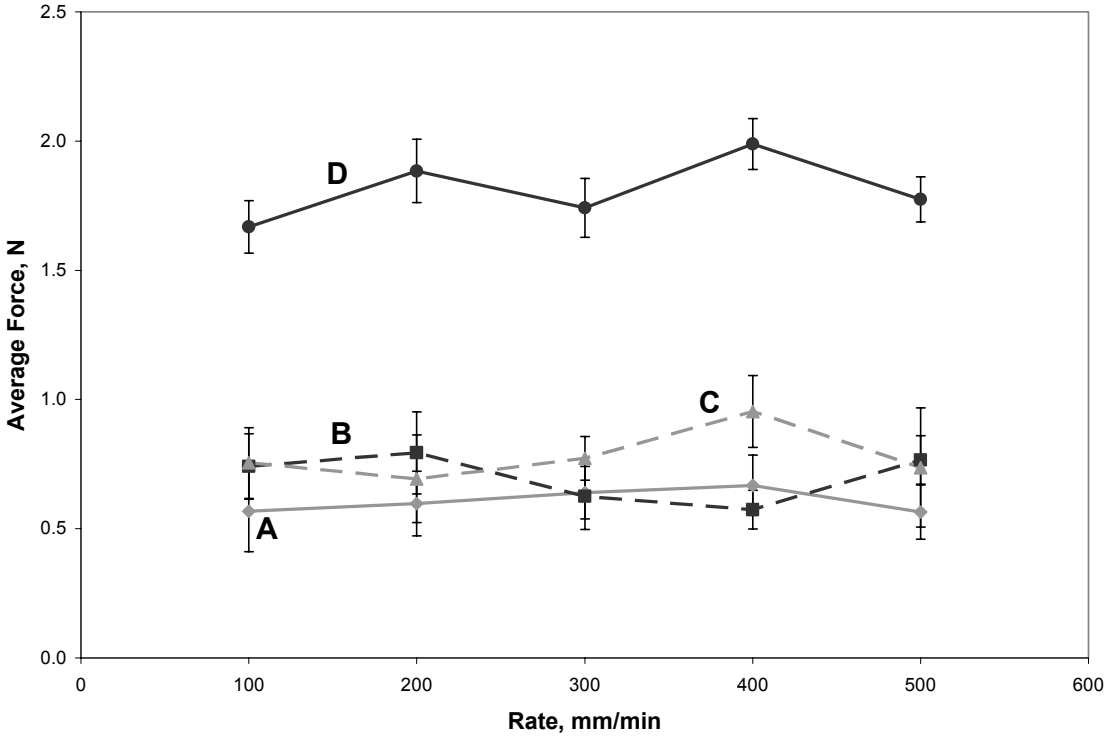

Figure 2.16: 180-degree Peel Test, Average Force Versus Rate from All Subjects and Speeds with Error Bars

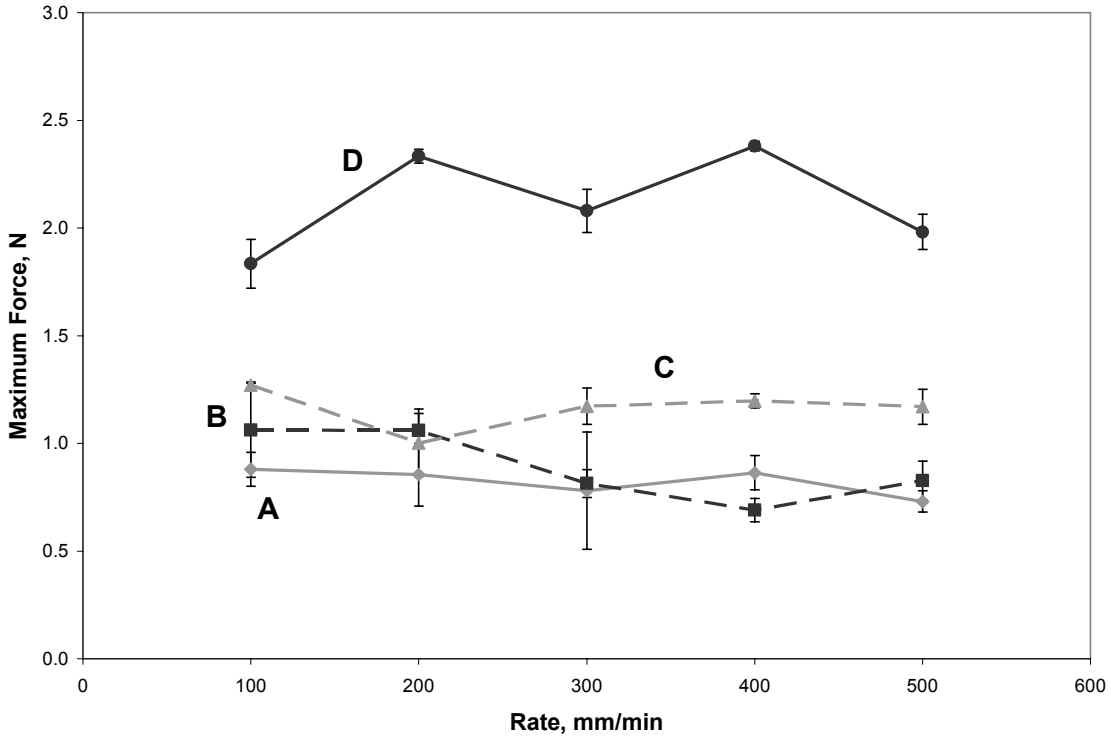

Figure 2.17: 180-degree Peel Test, Maximum Force Versus Rate from All Subjects and Speeds with Error Bars

The 180-degree initial slopes for all subjects ranged between approximately 0.04 and 0.1 N/mm. As with the 90-degree initial slopes, all subjects maintained a range of initial slope values and showed no major trends.

The maximum displacement results are compared in Figures 2.18-2.20. Figure 2.18 presents the average peel force values versus the maximum displacement values for all rates and subjects, and Figure 2.19 shows the maximum peel force values versus maximum displacement values for all rates and subjects. Like the 90-degree test results, Subject D had the highest maximum displacement values and Subject B had the lowest maximum displacement values. Figure 2.20 exhibits maximum displacement versus rate for all subjects. Again there is no clear correlation between rate and maximum displacement.

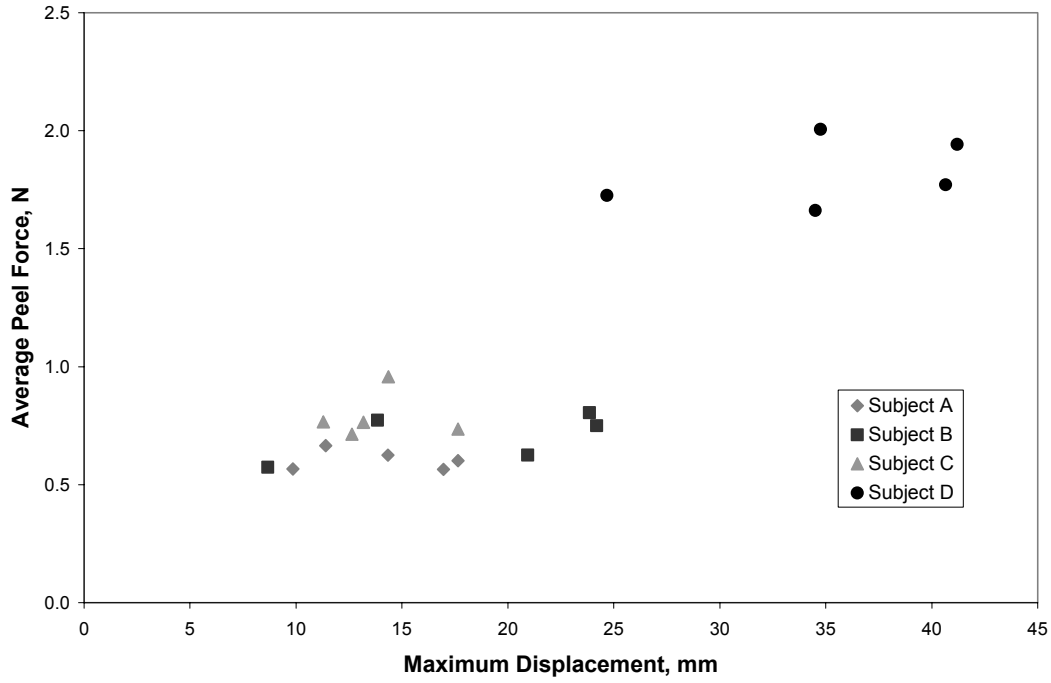

Figure 2.18: Average Peel Force Versus Maximum Displacement for all Subjects Tested at Various Rates for 180-degree Peel Tests

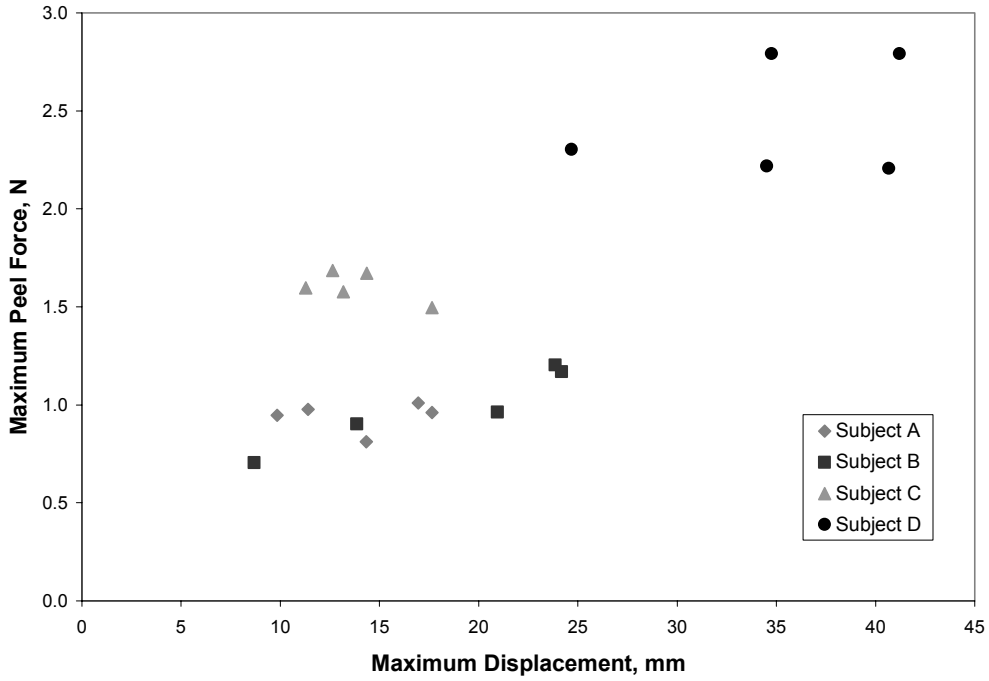

Figure 2.19: Maximum Peel Force Versus Maximum Displacement for all Subjects Tested at Various Rates for 180-degree Peel Tests

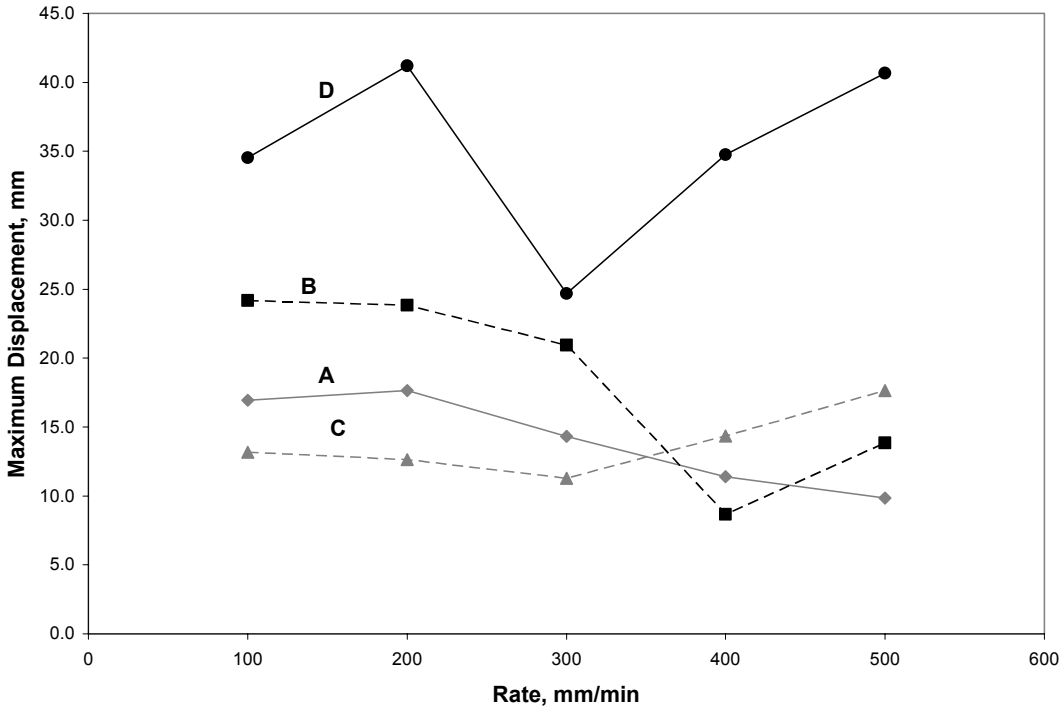

Figure 2.20: Maximum Displacement Versus Rate for All Subjects for 180-degree Peel Tests

2.3.2. Changing Dwell Time

Dwell time, or contact time, was varied on Subject A only. Three 180-degree peel tests were run at 500 mm/min at each dwell time. As with the 90- and 180-degree tests mentioned earlier, the results of the individual three tests evaluated separately for average and maximum peel force. Also, the results were averaged to make one average plot of load versus displacement for finding initial slope. Table 2.5 lists Subject A's average peel force, maximum peel force, average and maximum peel force coefficients of variation (CV), and initial slope at all dwell times tested.

Table 2.5: Average Peel Force, Maximum Peel Force, and Initial Slope Results for 180-degree Tests Run on Subject A at 500 mm/min and Several Dwell Times

Age	Dwell Time (min)	Average Force (N)	CV	Maximum Force (N)	CV	Initial Slope (N/mm)	Day Tested
22	1	0.5661	0.10	0.9467	0.05	0.0709	9/27/02
22	5	0.7936	0.12	1.1533	0.02	0.0743	9/27/02
22	10	1.0506	0.11	1.4300	0.06	0.0854	10/18/02
22	15	1.0812	0.10	1.4000	0.08	0.1002	10/18/02

Figure 2.21 shows a plot of the average peel force versus dwell time for the 180-degree peel tests run on Subject A. In addition, Figure 2.22 displays a plot of the maximum peel force versus dwell time for the same tests. Both figures show error bars representing coefficient of variation. The average peel force ranged between about 0.57 N and 1.08 N, and the maximum peel force ranged between approximately 0.95 N and 1.43 N. For the most part, both average and maximum forces increased with dwell time, indicating that the adhesive achieved a stronger attachment to the skin the longer it was exposed to the skin. The initial slopes of peel force versus displacement for the dwell time tests ranged from 0.07 and 0.10 N/mm and they increased with contact time.

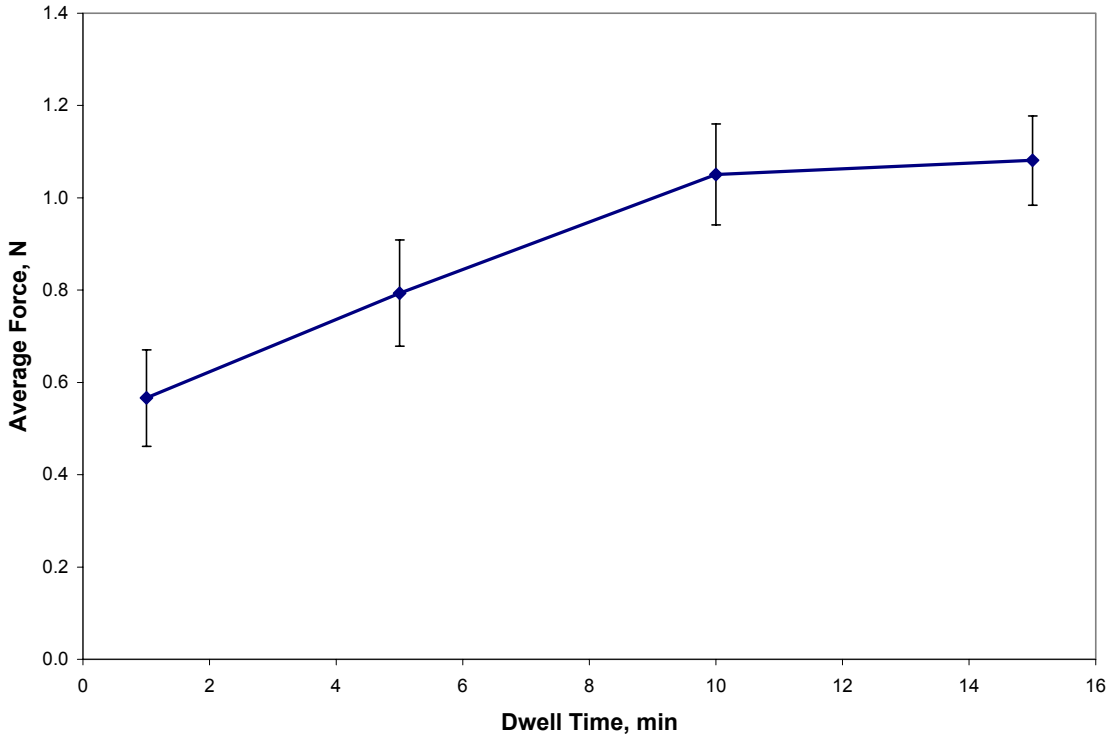

Figure 2.21: 180-degree Peel Test, Average Force Versus Dwell Time from Subject A with Error Bars

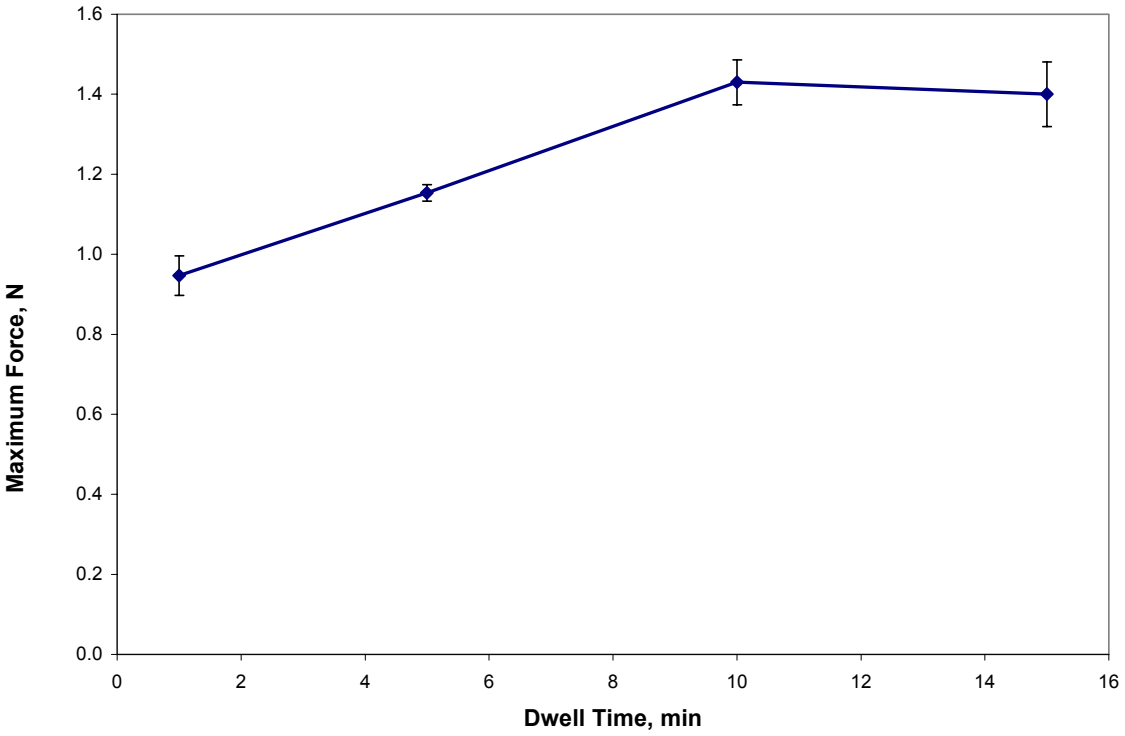

Figure 2.22: 180-degree Peel Test, Maximum Force Versus Dwell Time from Subject A with Error Bars

2.3.3. 120- and 150-degree Tests

Subjects A and D were used for the 120- and 150-degree tests. Speeds were 100, 300, and 500 mm/min. The individual test peel force results were again averaged to obtain one force value for the set of tests. The dwell time was 1 minute for all 120- and 150- degree tests. Figure 2.23 shows a sample average peel test plot from Subject A at a 120-degree angle and speed of 100 mm/min. Figure 2.24 displays a sample average peel test plot from Subject D at a 150-degree angle and speed of 100 mm/min.

The 120- and 150-degree plots were used to find the initial peel force for the subject, angle, and speed. Only initial peel force was recorded because the angle was not exactly constant throughout the tests. The initial peel force was measured by finding the point on the graph where the graph begins to exhibit a plateau. This corresponds to the point after the tape has been pulled taut by the machine. Figure 2.23 illustrates the initial peel force on the sample 120-degree test plot. Table 2.6 lists subjects' initial peel force and coefficient of variation (CV) at different speeds for the 120- and 150-degree peel tests.

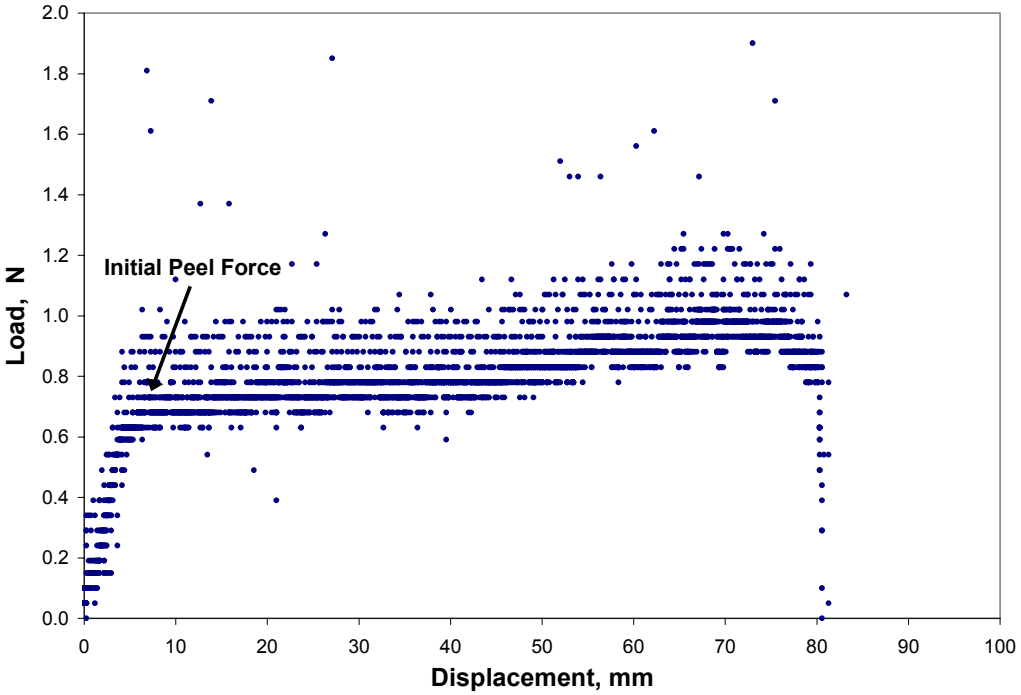

Figure 2.23: Sample 120-degree Peel Test Run on Subject A at 100 mm/min Showing Initial Peel Force

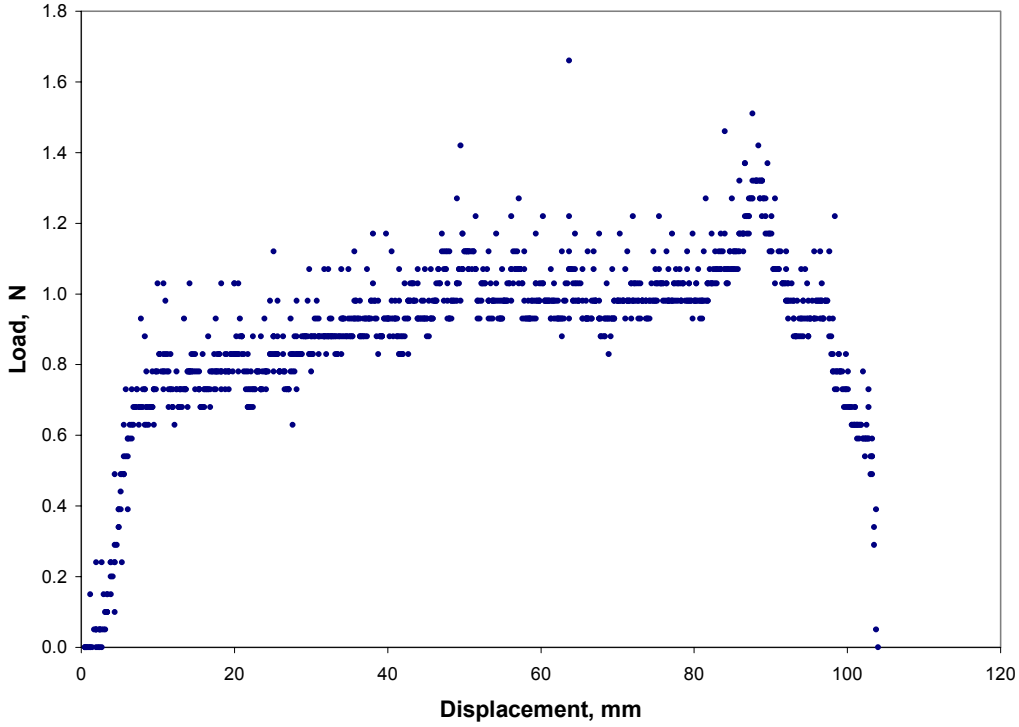

Figure 2.24: Sample 150-degree Peel Test Run on Subject D at 500 mm/min

Table 2.6: Initial Peel Force Results for 120- and 150-degree Tests Run on Subjects A and D

Subject	Age	Peel Angle (degrees)	Rate (mm/min)	Initial Peel Force (N)	CV	Day Tested
A	22	120	100	0.65	0.15	12/3/02
A	22	120	300	0.62	0.20	12/3/02
A	22	120	500	0.72	0.12	11/1/02
A	22	150	100	0.59	0.11	11/20/02
A	22	150	300	0.47	0.05	11/20/02
A	22	150	500	0.38	0.12	11/1/02
D	60	120	100	2.15	0.15	11/20/02
D	60	120	300	1.64	0.21	12/3/02
D	60	120	500	1.76	0.11	11/1/02
D	60	150	100	1.24	0.08	11/20/02
D	60	150	300	1.72	0.22	11/20/02
D	60	150	500	0.80	0.18	11/1/02

Figure 2.25 shows a comparison of initial peel force with corresponding rate for the 120-degree peel tests with error bars representing coefficient of variation. The initial peel force for all subjects tested ranged between about 0.62 N and 2.15 N. For all speeds, Subject D had the highest initial peel force. Linear trend lines through the data indicate that the initial peel force increased slightly with rate for Subject A, but decreased with rate for Subject D.

Figure 2.26 demonstrates initial peel force versus rate for the 150-degree peel tests. Again, error bars represent coefficient of variation. Initial peel force values ranged from approximately 0.38 N to 1.72 N. Again, at all rates, Subject D had the largest initial peel force values.

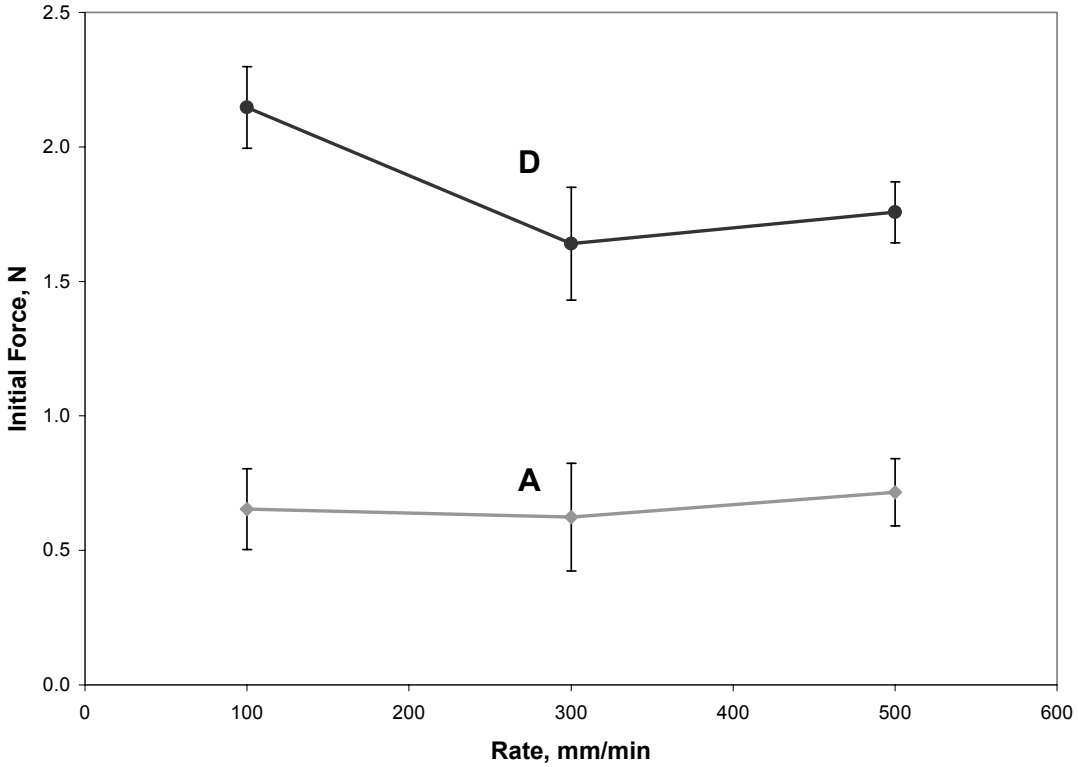

Figure 2.25: 120-degree Peel Test, Initial Force Versus Rate for Subjects A and D

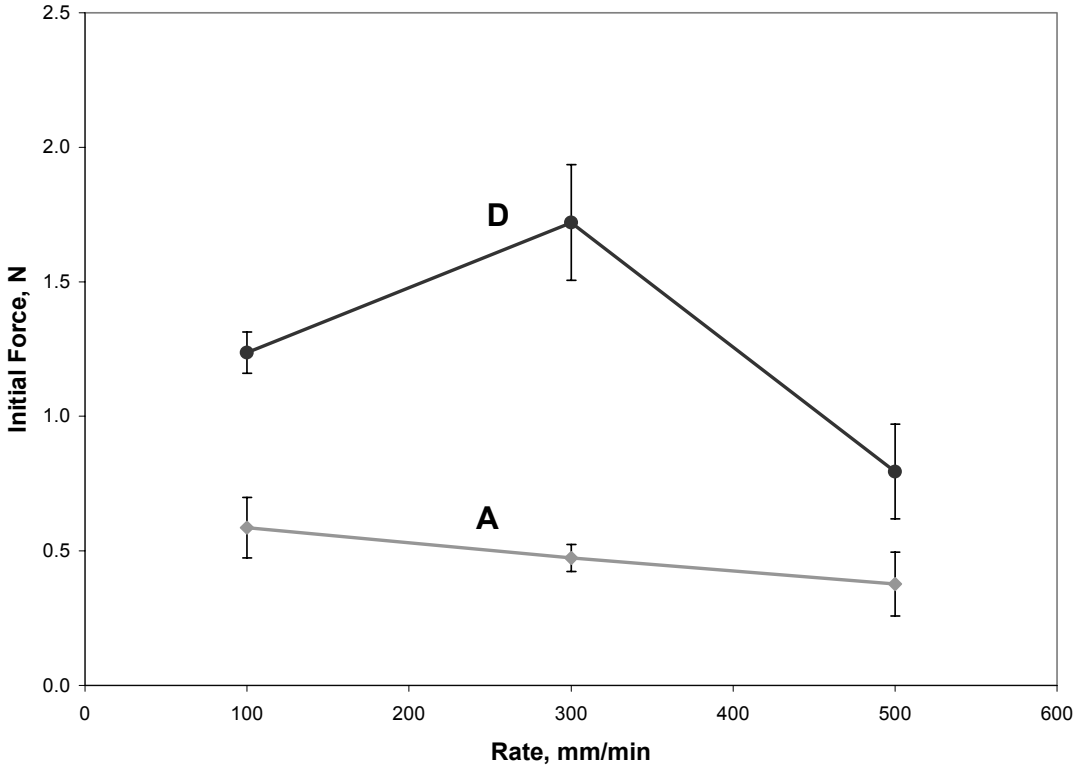

Figure 2.26: 150-degree Peel Test, Initial Force Versus Rate for Subjects A and D

2.3.4. Angle Comparison

Peel force data from Subjects A and D for 90-, 120-, 150-, and 180-degree peel tests were combined to evaluate the effect of peel angle on force. The forces compared were average peel force from 90- and 180-degree tests at 500 mm/min and initial peel forces from 120- and 150-degree tests at the same speed. Figure 2.27 shows the comparison for Subject A and Figure 2.28 shows the comparison for Subject D. Figures 2.27 and 2.28 also include error bars for coefficient of variation. Both subjects had a minimum force value at 150 degrees, which may be an optimum angle for peeling with minimal pain.

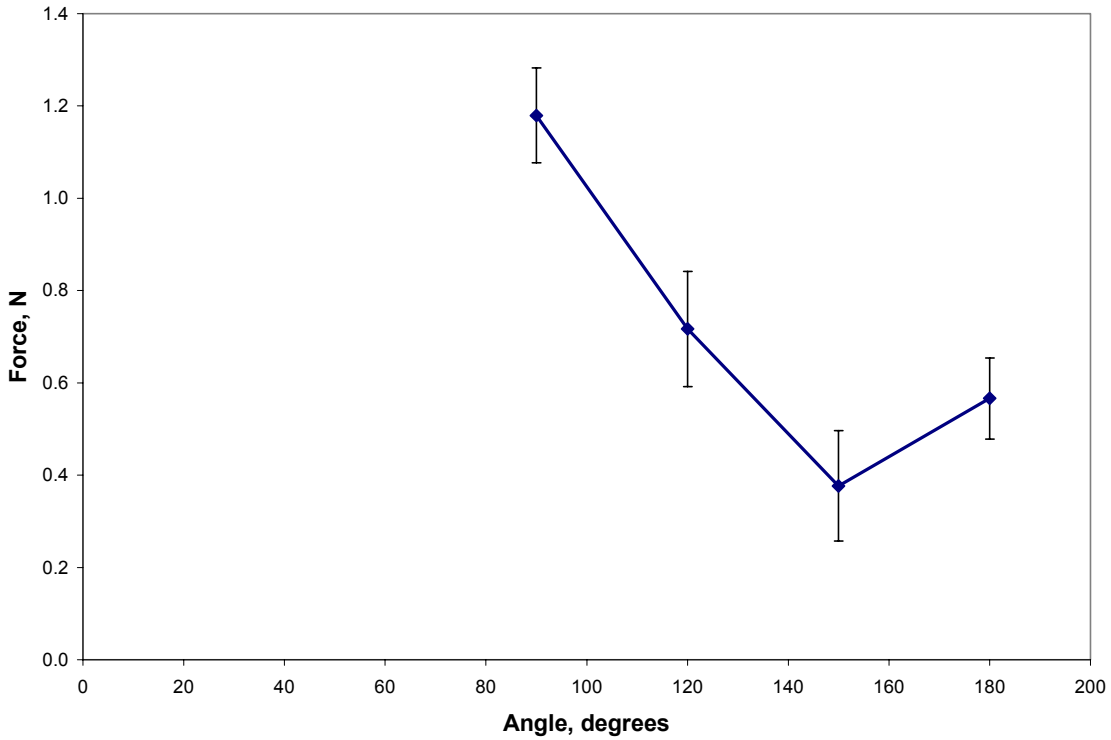

Figure 2.27: Peel Force Versus Peel Angle for Subject A at 500 mm/min with Error Bars

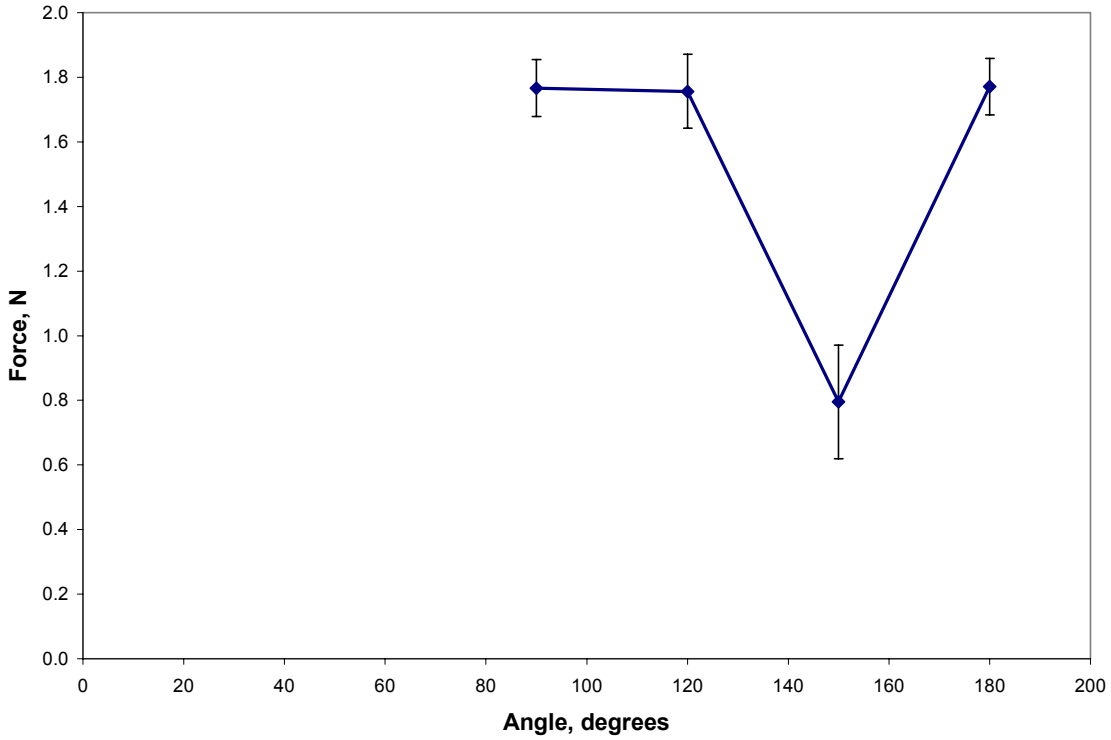

Figure 2.28: Peel Force Versus Peel Angle for Subject D at 500 mm/min with Error Bars

2.4. Conclusions

Numerous peel tests were run on four subjects at 90- and 180-degree angles. They showed no major correlation between force and speed of tape removal. Tests run at 120- and 150-degree angles also did not show a definite increase or decrease in force with speed. However, for all tests, the force required to remove the tape from the skin fell into a range of about 0.4 N and 3.0 N. Subject D typically required the highest forces for tape removal at all angles tested. Also, the 150-degree peel angle required the lowest force for tape removal of all the angles. Comparing different dwell times indicated that the longer tape contacts the skin before removal, the higher the force required to remove the tape, but after a certain dwell time the force does not increase appreciably.

The experiments in Series One were not performed in any particular order. Because the skin changes as tape is peeled from it and layers are removed, the order of the tests may be significant. In the next round of experiments, Series Two, the sequence of peel tests was altered to determine this effect on the average and maximum peel forces, and testing incorporated peel speeds greater than 500 mm/min.

Chapter 3. Experimentation Series Two

3.0 Introduction

The experiments in Series One varied peel angles, subjects, dwell time, and rate of peeling. The rates of peeling for Series One were within the range of 100 to 500 mm/min. To further explore the influence of peel rate and to continue analyzing skin behavior during peeling, Series Two of experiments was established with peeling rates up to 10,000 mm/min. Again, experiments involved peel tests on the skin of the forearm of human subjects. This chapter focuses on Series Two experiments performed in spring of 2003.

3.1. Materials and Equipment

Series Two peel tests were performed in the Biomechanics Laboratory of the Department of Engineering Science and Mechanics on the Virginia Tech campus. Equipment included an MTS Tytron 250 testing machine to record load versus displacement for each test. Experiments required attaching a clamp for the tape to the load cell and blocks to provide a level arm rest. In addition to the testing machine setup, we used a ruler, rubbing alcohol, scissors, cylindrical weight of about 10 N, and the 2.54-cm-wide Durapore™ tape as used in Series One. The entire test setup is shown in Figure 3.1. Figure 3.2 displays a close-up view of the clamp that held the tape.

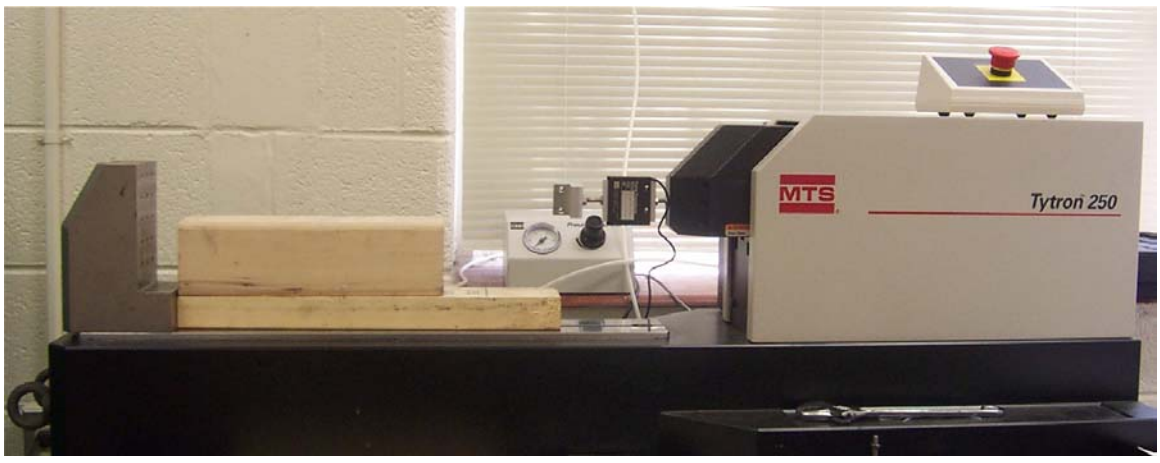

Figure 3.1: Experimental Setup with MTS Tytron 250 Testing Machine

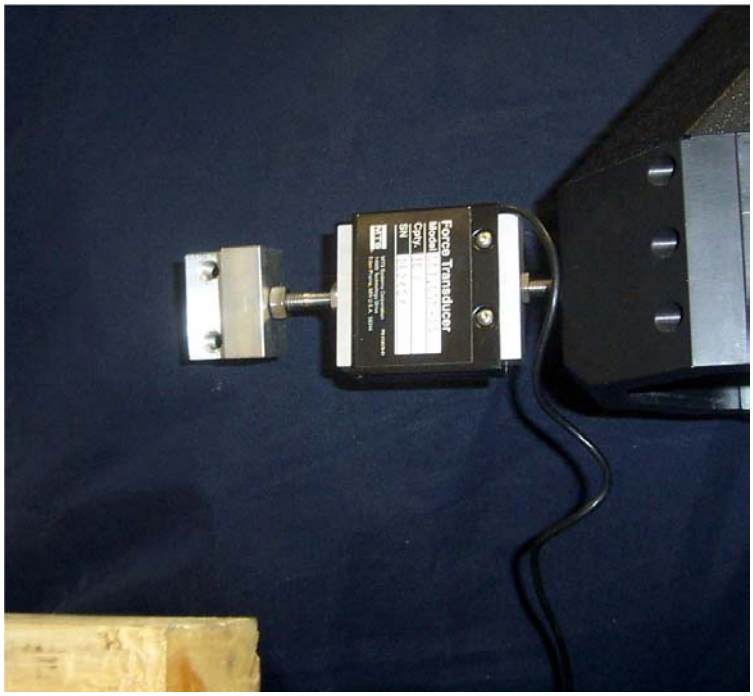

Figure 3.2: Clamp Used to Connect Load Cell to Tape End

Series Two experiments involved two subjects only. The subjects were assigned the same letters as those given in Series One experiments. Table 3.1 lists subject, age, gender, angle tested, and speeds tested. Only 180-degree tests were performed in Series Two because of the setup of the testing machine.

Table 3.1: Series Two Peel Test Subjects

Subject	Age	Gender	Angle Tested	Speed Ranges Tested (mm/min)	Tape Dwell Time (min)
A	22	female	180^{o}	200-10,000	1
D	60	male	180^{o}	200-10,000	1

3.2. Procedure

3.2.1. Subject Preparation

Subject preparation of Series Two experiments followed the same guidelines as those for Series One experiments (refer to Section 2.2.1). Once the tape was in position on the subject, the subject's (left) arm was placed in the Tytron testing machine and rested against the blocks and the end plate of the machine. The free end of tape was then

attached to the clamp approximately 38 cm from the peel front on the skin. Figure 3.3 displays the subject's positioning with the testing machine.

Figure 3.3: Experimental Setup Including Subject with MTS Tytron 250 Testing Machine

3.2.2. Data Acquisition

After situating subject and tape in the testing machine, the load was set to read zero on the Tytron. Then the peel test was executed by moving the load cell to the right with the computer controls for the machine. Dwell time was held constant at one minute for all tests. Three to five tests were run on each subject at different speeds. The MTS Tytron 250 recorded data for the peel force and the displacement of the end of the tape attached to the machine.

3.3. Results and Discussion

3.3.1. 180-degree Tests

The load versus displacement data from each individual test was analyzed in Series Two. Figure 3.4 shows a sample plot of load versus displacement from Subject A at a speed of 2400 mm/min (also available in Appendix C). Figure 3.5 shows a sample plot of load versus displacement from Subject D at the same speed (also available in Appendix C). The "waves" or "wrinkles" in the arm and plots mentioned in Section 2.3.1

were also present in Series Two experiments and are shown in Figure 3.5. Appendix C contains a complete record of individual peel test plots acquired in Series Two. In most tests in Series Two, the tape was not completely removed from the subjects' arms when the load cell stopped moving. Therefore, the sample plots show a rise and plateau, but do not return to zero at the conclusion of the test.

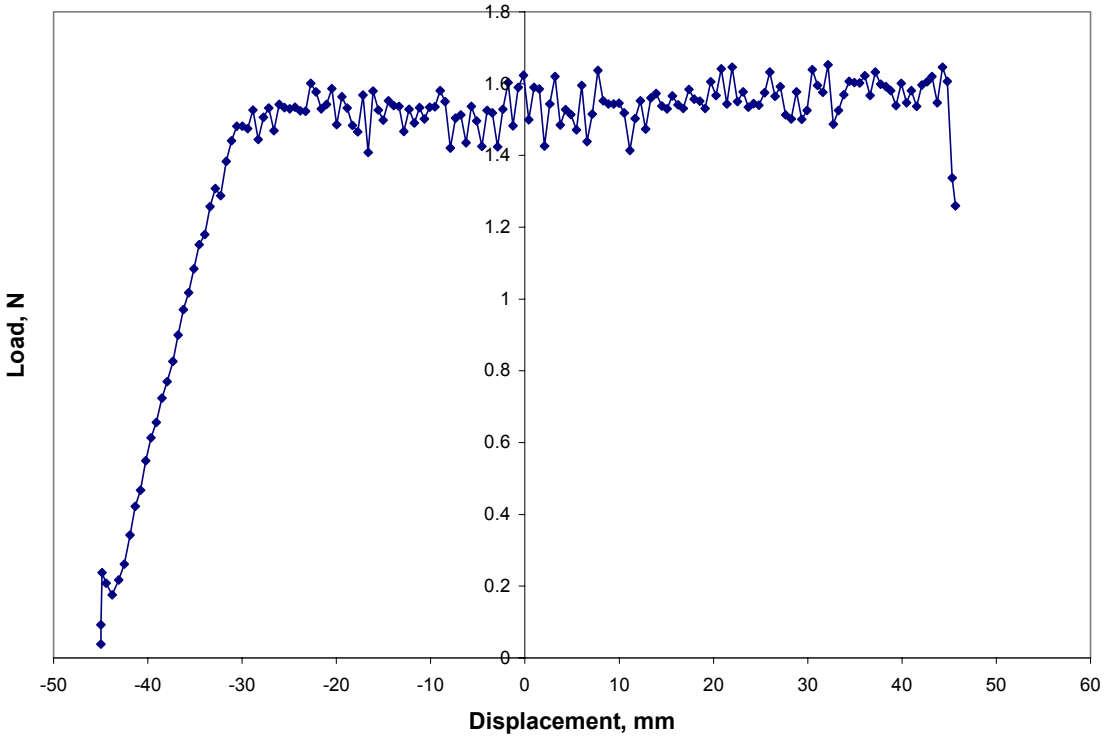

Figure 3.4: 180-degree Peel Test Run on Subject A at 2400 mm/min

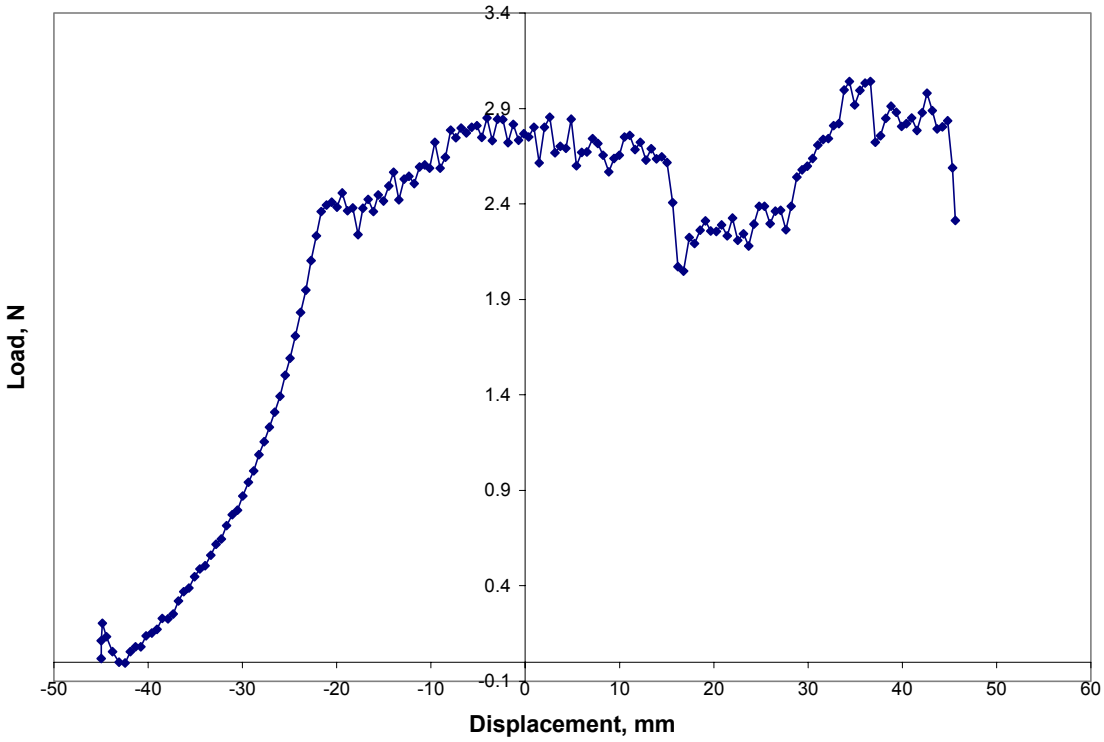

Figure 3.5: 180-degree Peel Test Run on Subject D at 2400 mm/min

For each speed and subject, the peel test data were analyzed to find values of average peel force, maximum peel force, linear slope, initial slope, and maximum displacement before peeling starts. The average peel force was found by taking an average of the load values on the plateau region of the single test plot. The plateau regions were different from those in Series One experiments because the tape was not completely peeled from the skin. The maximum peel force was recorded as the maximum load value reached per each individual test. Linear slope refers to the slope of the rise of the graph just before peel begins, which appears to be almost linear. Figure 3.4 exemplifies a distinct line that begins when the test starts and ends as the graph plateaus. Initial slope refers to the very beginning of the test when the tape is first pulled and corresponds to a slight curvature in the graph as in Figure 3.5. Not all tests demonstrated an initial slope different from the linear slope. Primarily, peel tests on Subject D demonstrated this behavior. Maximum displacement before peeling starts is the displacement value when the tape begins to lift off the skin and was taken as the point

where the plateau starts minus -45 mm (the set starting point on the machine). Figure 3.6 illustrates the average peel force, maximum peel force, linear slope, initial slope, and maximum displacement before peel as it was read from each test plot. Each peel test had its own value for average peel force, maximum peel force, linear slope, initial slope, and maximum displacement. To attain an overall value for each speed and subject, the values of each of these parameters for the three to five tests were averaged and the coefficient of variation was computed.

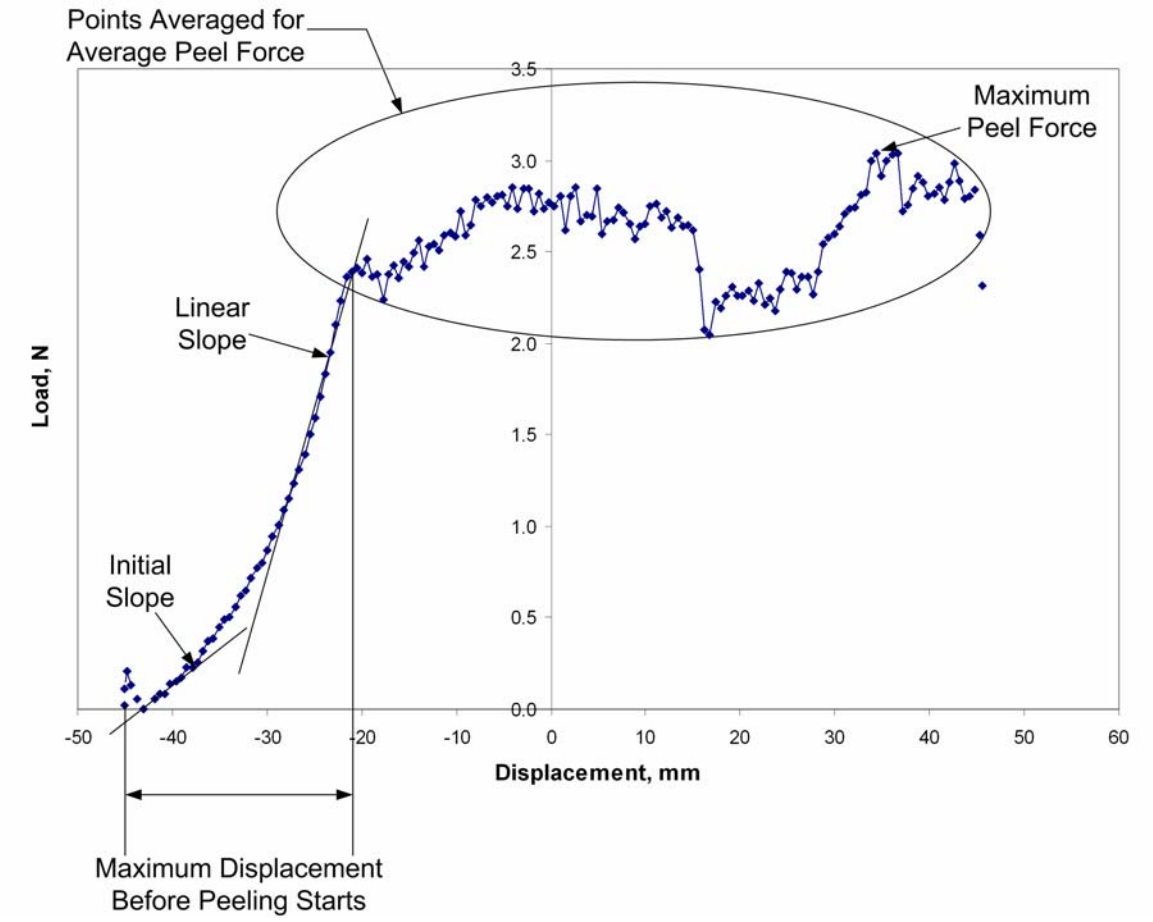

Figure 3.6: Showing Average Peel Force, Maximum Peel Force, Initial Slope, Linear Slope, and Maximum Displacement Before Peeling Starts

Tables 3.2 and 3.3 list average peel force, maximum peel force, linear slope, initial slope, and maximum displacement where applicable, for the different rates tested. Table 3.2 corresponds to Subject A and Table 3.3 corresponds to Subject D. Rates tested were 200 to 2800 mm/min in increments of 200 mm/min, and 5000, 7500, and 10,000

mm/min. The rates 5000, 7500, and 10,000 mm/min were tested to see if the force would drastically increase with a large increase in rate.

The results displayed in Tables 3.2 and 3.3 are plotted in Figures 3.7-3.10. Figures 3.7 and 3.8 show only the results for rates 200 to 2800 mm/min because the lower speeds are difficult to read when all the rates are plotted. Figure 3.7 displays the average peel force versus rate for both subjects tested and Figure 3.8 shows the maximum peel force versus rate for both subjects tested. Figures 3.9 and 3.10 show results from all rates tested. Figure 3.9 shows the average peel force versus rate for both subjects at all speeds tested and Figure 3.10 depicts the maximum peel force versus rate for both subjects at all speeds tested. In Figures 3.7-3.10, the lines connecting the points for each subject are broken when a new day of testing began. In addition, the numbers (1, 2, 3, 4) associated with the data points indicate the testing order of the rates. Error bars in Figures 3.7-3.10 represent the coefficient of variation for the three to five tests conducted at each rate per subject.

The average peel force for both subjects ranged between about 0.74 N and 2.92 N. The maximum peel force for both subjects ranged between about 0.83 N and 3.58N. For all speeds, Subject D, the 60-year-old male subject, experienced higher average peel force and maximum peel force values than Subject A, the 22-year-old female subject.

The range of slope values was similar for both subjects. Linear slopes ranged from 0.07 to 0.21 N/mm and initial slopes ranged from 0.02 to 0.06 N/mm. There was only one test that yielded a distinct initial slope for Subject A, which was a 600 mm/min test. This initial slope value, 0.029 N/mm, closely matches Subject D's initial slope value of 0.028 N/mm at 600 mm/min.

Table 3.2: Average Peel Force, Maximum Peel Force, Linear Slope, and Initial Slope Results for Subject A's Series Two 180-degree Tests

Subject	Age	Rate	Average Peel Force		Maximum Peel Force		Linear Slope		Initial Slope		Maximum	Day
			Mean	CV	Mean	CV	Mean	CV	Mean	CV	Displacement	Tested
		(mm/min)	(N)		(N)		(N/mm)		(N/mm)		(mm)	
A	22	200	0.738	0.063	0.834	0.095	0.077	0.235			14.9	2/14/03
A	22	400	1.176	0.052	1.299	0.154	0.094	0.141			16.9	2/14/03
A	22	600	1.034	0.032	1.110	0.165	0.075	0.134	0.029		27.4	1/23/03
A	22	800	1.390	0.058	1.472	0.120	0.091	0.043			35.7	1/23/03
A	22	1000	1.125	0.048	1.240	0.155	0.071	0.229			18.5	1/24/03
A	22	1200	1.539	0.045	1.696	0.109	0.093	0.112			20.0	1/24/03
A	22	1400	1.390	0.033	1.500	0.093	0.125	0.086			14.4	1/24/03
A	22	1600	1.647	0.058	1.842	0.052	0.115	0.019			18.1	1/24/03
A	22	1800	1.197	0.075	1.382	0.139	0.101	0.062			15.0	1/29/03
A	22	2000	1.382	0.056	1.534	0.130	0.110	0.052			14.5	1/29/03
A	22	2200	1.618	0.036	1.762	0.018	0.103	0.062			20.9	1/29/03
A	22	2400	1.620	0.063	1.818	0.068	0.108	0.044			17.3	2/14/03
A	22	2600	1.438	0.049	1.579	0.021	0.108	0.019			14.1	2/14/03
A	22	2800	1.539	0.059	1.767	0.086	0.125	0.130			16.7	2/14/03
A	22	5000	0.958	0.100	1.176	0.127	0.108	0.046			11.6	2/21/03
A	22	7500	1.593	0.124	2.076	0.015	0.156	0.070			16.0	2/21/03
A	22	10000	1.336	0.128	1.756	0.038	0.201	0.099			12.1	2/21/03

Table 3.3: Average Peel Force, Maximum Peel Force, Linear Slope, and Initial Slope Results for Subject D's Series Two 180-degree Tests

Subject	Age	Rate	Average Peel Force		Maximum Peel Force		Linear Slope		Initial Slope		Maximum	Day
			Mean	CV	Mean	CV	Mean	CV	Mean	CV	Displacement	Tested
		(mm/min)	(N)		(N)		(N/mm)		(N/mm)		(mm)	
D	60	200	1.598	0.046	1.777	0.064	0.097	0.312	0.021	0.475	27.7	2/14/03
D	60	400	1.834	0.075	2.121	0.154	0.108	0.189	0.060		34.0	2/14/03
D	60	600	1.945	0.058	2.163	0.151	0.098	0.357	0.028	0.659	40.9	1/23/03
D	60	800	2.294	0.048	2.523	0.109	0.085	0.528	0.062	0.521	38.2	1/23/03
D	60	1000	2.158	0.066	2.411	0.116	0.150	0.345	0.038	0.439	36.6	1/24/03
D	60	1200	2.297	0.072	2.616	0.071	0.142	0.420	0.045	0.617	28.7	1/24/03
D	60	1400	2.315	0.070	2.626	0.046	0.121	0.350	0.039	0.472	32.0	1/24/03
D	60	1600	2.574	0.058	2.831	0.038	0.136	0.341	0.044	0.323	36.5	1/24/03
D	60	1800	1.734	0.093	2.045	0.069	0.107	0.147	0.046		39.8	1/29/03
D	60	2000	2.090	0.095	2.503	0.064	0.098	0.111	0.029		35.7	1/29/03
D	60	2200	2.634	0.095	3.138	0.084	0.188	0.341	0.052		25.5	1/29/03
D	60	2400	2.482	0.088	2.914	0.084	0.189	0.110	0.053		21.2	2/14/03
D	60	2600	2.306	0.079	2.641	0.063	0.146	0.157			28.5	2/14/03
D	60	2800	2.108	0.096	2.459	0.088	0.147	0.158			16.6	2/14/03
D	60	5000	2.280	0.108	2.800	0.129	0.153	0.075			21.8	2/21/03
D	60	7500	2.918	0.107	3.576	0.066	0.211	0.197			21.0	2/21/03
D	60	10000	2.415	0.131	3.117	0.016	0.192	0.032			24.1	2/21/03

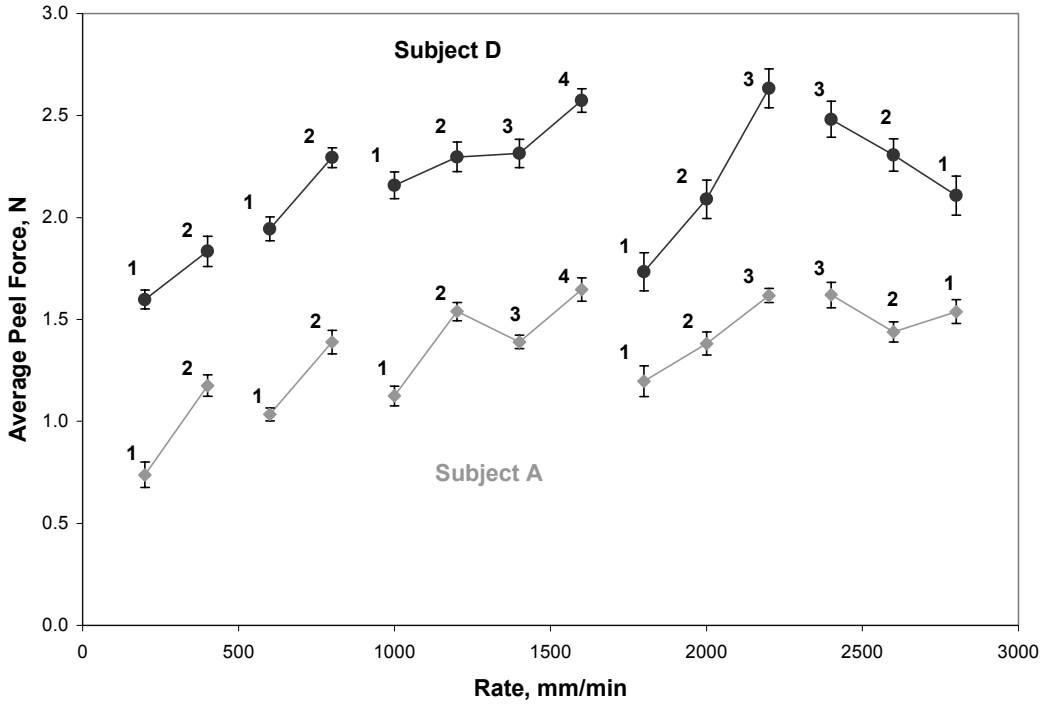

Figure 3.7: 180-degree Peel Tests, Average Peel Force Versus Rate for Both Subjects and Speeds 200 to 2800 mm/min with Error Bars

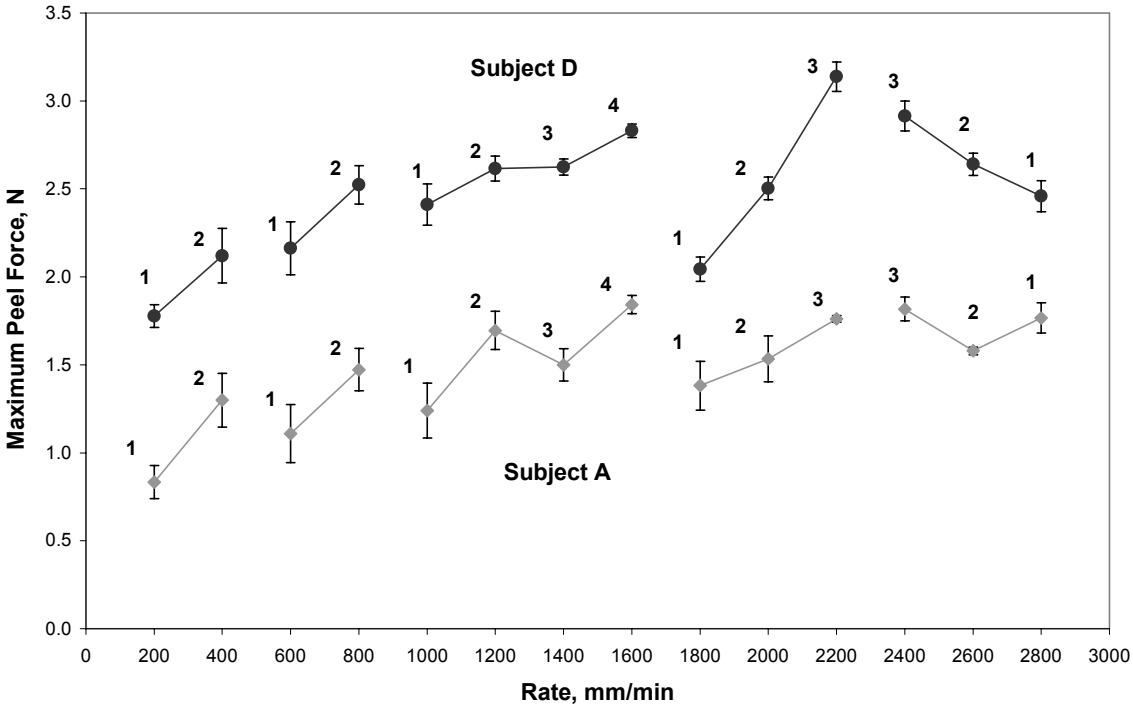

Figure 3.8: 180-degree Peel Tests, Maximum Peel Force Versus Rate for Both Subjects and Speeds 200 to 2800 mm/min with Error Bars

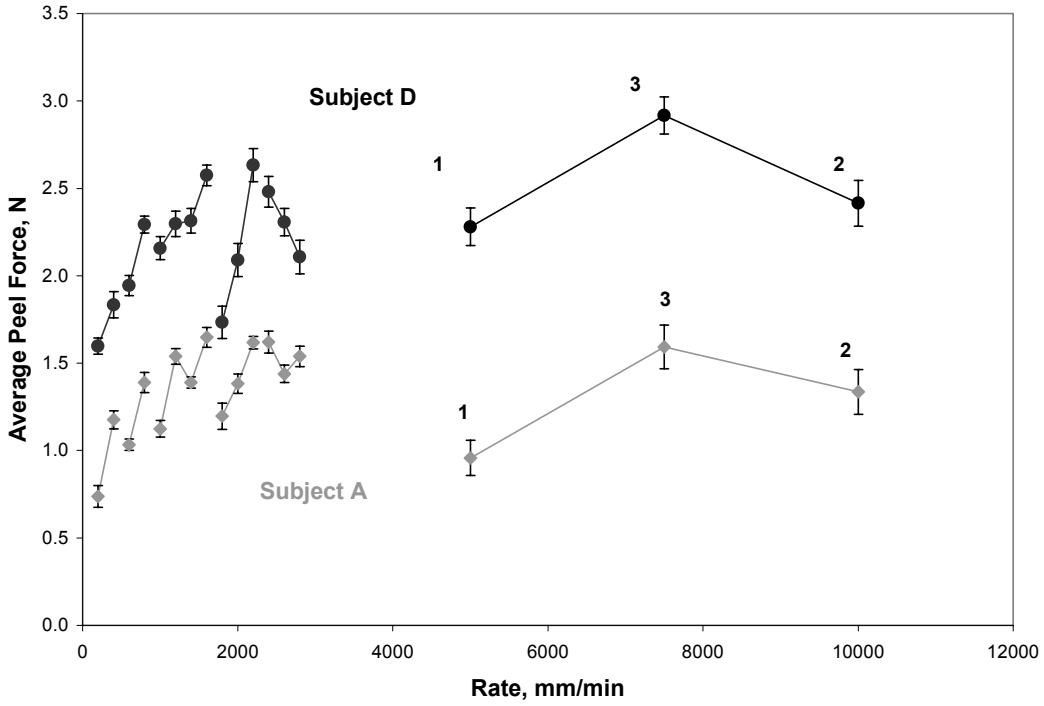

Figure 3.9: 180-degree Peel Tests, Average Peel Force Versus Rate for Both Subjects and All Speeds with Error Bars

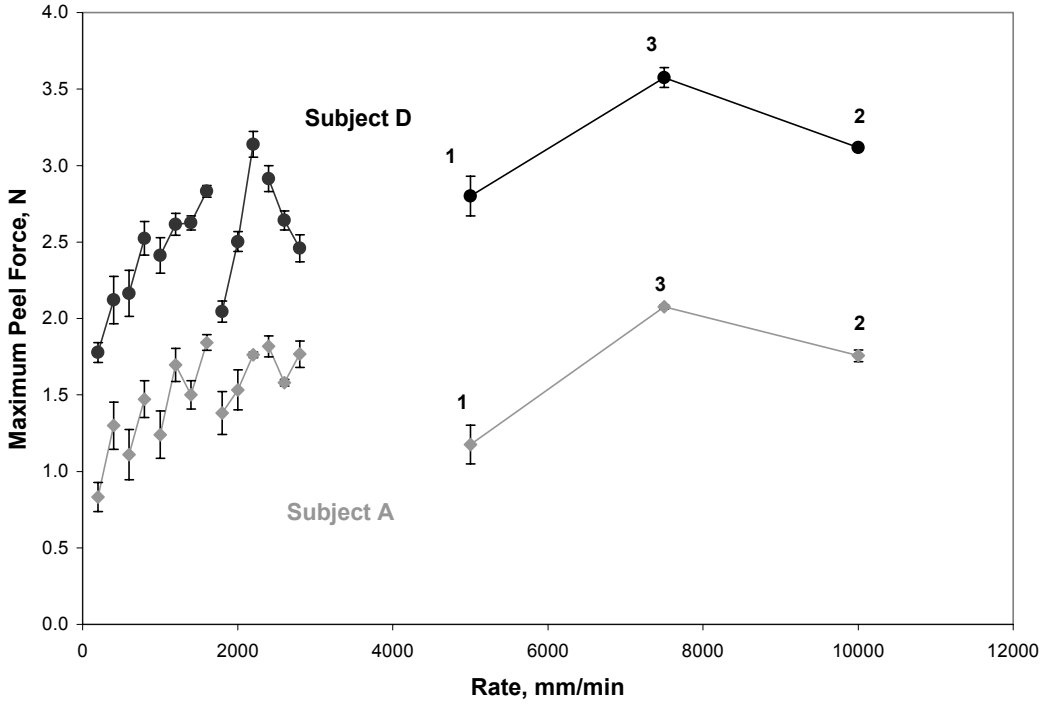

Figure 3.10: 180-degree Peel Tests, Maximum Peel Force Versus Rate for Both Subjects and All Speeds with Error Bars

The maximum displacement results are shown in Figures 3.11-3.14. Figure 3.11 shows the average peel force versus maximum displacement for all rates tested and both subjects. Figure 3.12 displays the maximum peel force versus maximum displacement for all rates tested and both subjects. Subject D consistently has a higher maximum displacement than Subject A. Figure 3.13 exhibits the maximum displacement versus rate for both subjects for rates up to 2800 mm/min. Figure 3.14 shows maximum displacement versus rate for both subjects at all rates tested. The lines are separated in Figures 3.13 and 3.14 for different days of testing. Both subjects show a rise and fall of maximum displacement with increase in rate.

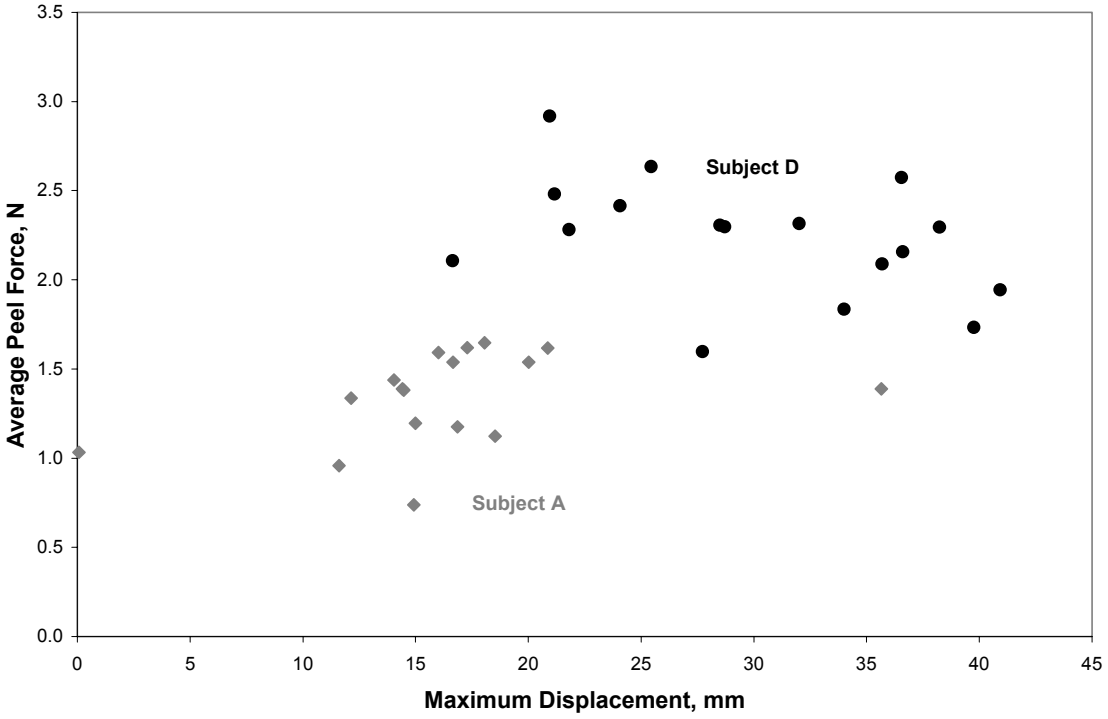

Figure 3.11: Average Peel Force Versus Maximum Displacement for Both Subjects Tested at Various Rates

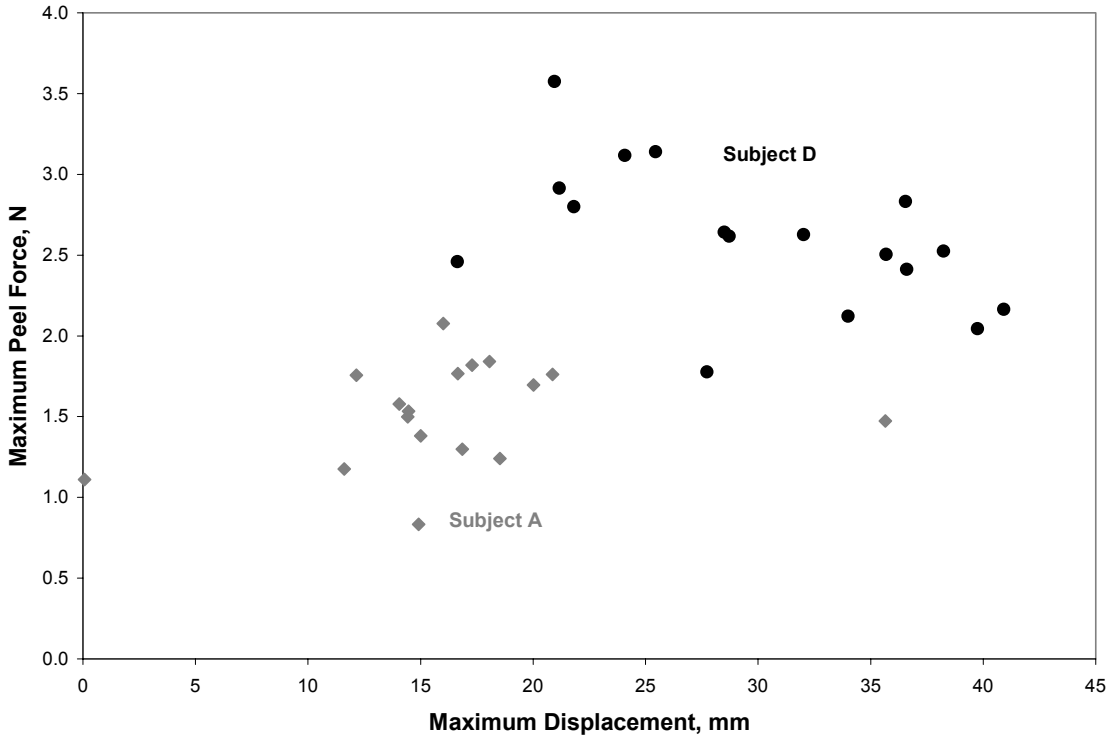

Figure 3.12: Maximum Peel Force Versus Maximum Displacement for Both Subjects Tested at Various Rates

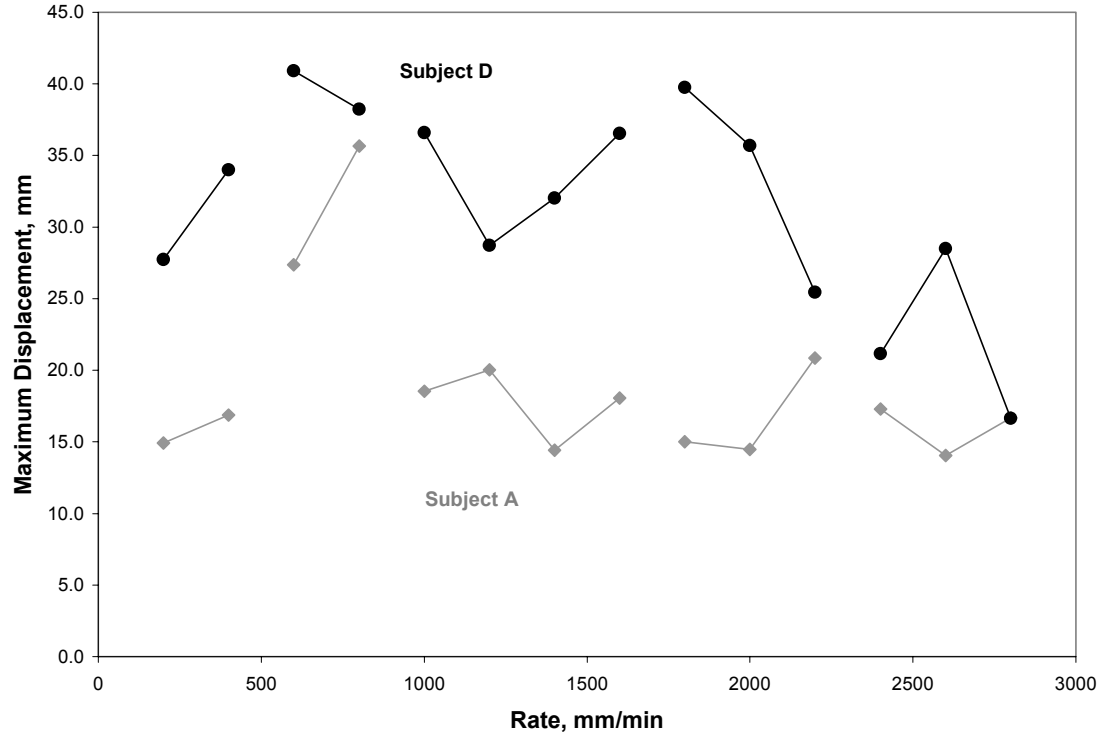

Figure 3.13: Maximum Displacement Versus Rate for All Subjects Showing Tests up to 2800 mm/min

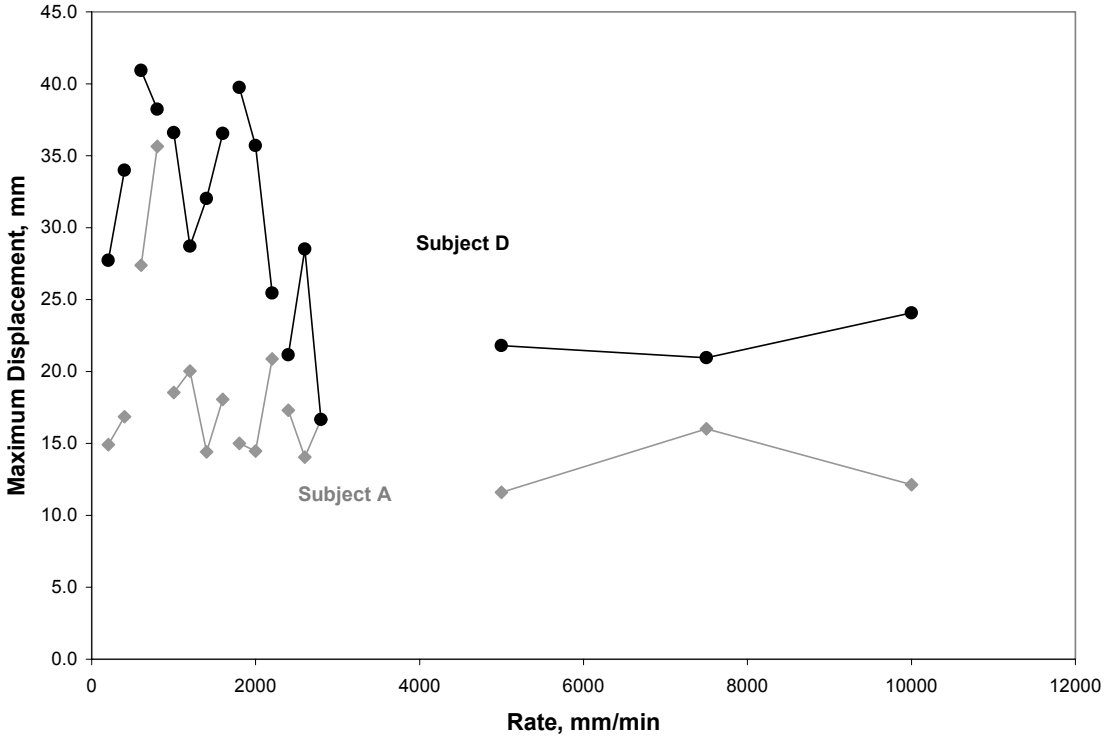

Figure 3.14: Maximum Displacement Versus Rate for All Subjects Showing All Tests in Series Two

3.3.2. Influence of Testing Order and Rate

The order of experiments in Series Two was recorded, as shown in Figures 3.7-3.10. Experiments at rates of 200 through 2200 mm/min were performed in order of increasing speed. This order mainly showed an increase in average and maximum peel force values as rate increased for both subjects. Alternatively, experiments at rates of 2400 through 2800 mm/min were performed in order of decreasing speed. The reversed order showed decreasing average and maximum peel force values with rate increase for Subject D. Subject A's average and maximum peel force values decreased at 2600 mm/min, but increased at 2400 mm/min. However, adding a best fit line to Subject A's force data shows a decreasing slope with increase in rate. The peel tests run at 5000, 7500, and 10,000 mm/min were performed in the following order: 5000, 10,000, 7500. Evident in Figures 3.9 and 3.10 for both subjects, these tests show that force usually increased with increase in test number (1, 2, 3).

The variation of average and maximum force values with testing order demonstrates that skin changes as tape is removed and layers of skin are removed with the tape. As layers are removed, the skin tends to get stiffer and a higher force is required to peel the tape from the skin. The change in the skin is not always visible. In Series Two testing, a change in the appearance of the skin on the forearm was only visible after several tests had been run on the same day and the arm was slightly pink in the region where the tape had been placed.

For peel tests on rigid surfaces, the peel force tends to increase as the peel rate increases according to research conducted by Aubrey (1977), Skeist (1990), and Yarusso (1999), but also exhibits some erratic behavior involving both increasing and decreasing peel force. Here the effect of peel rate can be examined essentially independently of testing order by considering the results marked "1" (i.e., the first set of tests on a day). These tests are referred to as "initial tests." Figures 3.15 and 3.16 show peel force versus peel rate for only the initial tests. Force values in Figure 3.15 are averaged values and force values in Figure 3.16 are the maximum values. Subject A's average peel force ranged between 0.738 N and 1.620 N, and maximum peel force ranged between 0.834 N and 1.818 N for the initial tests. Subject D's average peel force ranged between 1.598 N and 2.482 N, and maximum peel force ranged between 1.777 N and 2.914 N for the initial tests. On both subjects, the smallest force value correlates to the 200 mm/min speed and the largest force value correlates to the 2400 mm/min speed. Furthermore, the peel force tended to increase with an increasing rate up to 2400 mm/min and then decrease for a higher rate.

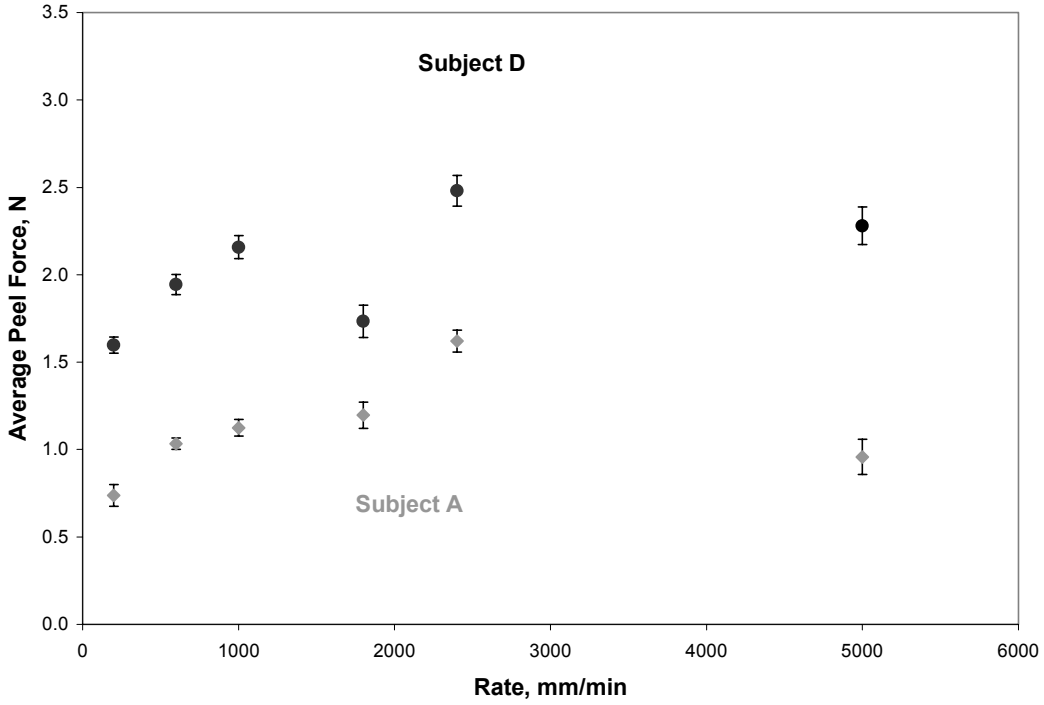

Figure 3.15: 180-degree Initial Peel Tests, Average Peel Force Versus Rate for Both Subjects with Error Bars

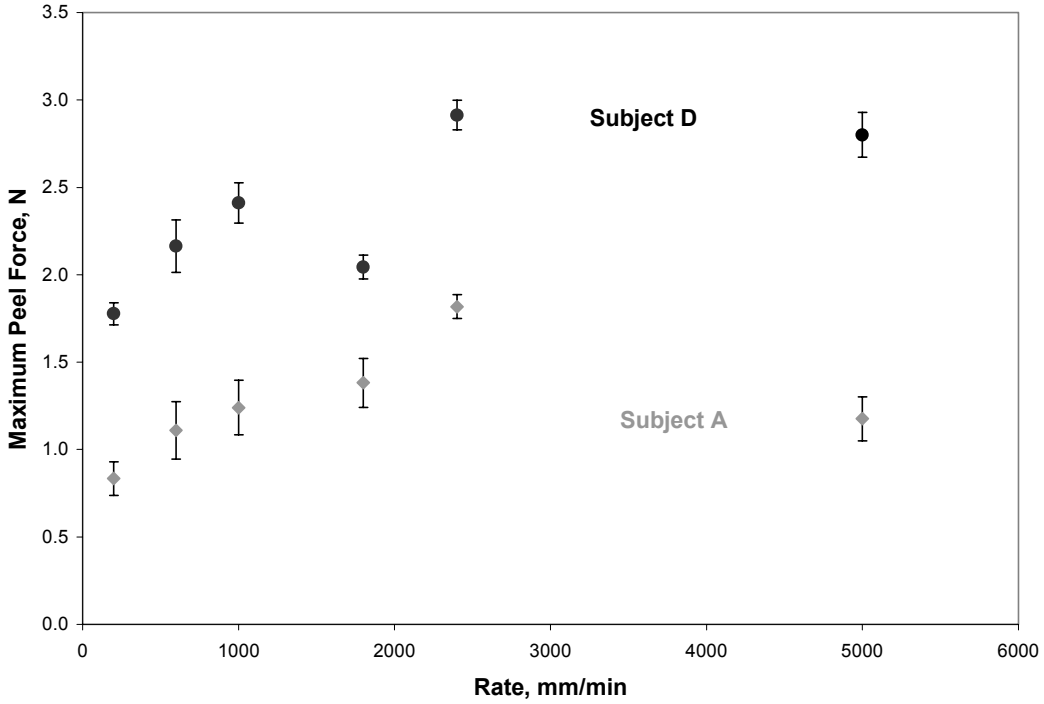

Figure 3.16: 180-degree Initial Peel Tests, Maximum Peel Force Versus Rate for Both Subjects with Error Bars

3.3.3. Influence of Tape's Position on Arm

All experiments presented thus far involved tape being peeled from the forearm region of the body. To compare the behavior of skin in different body regions where the skin may have a different foundation in terms of geometry, experiments were performed on the side of the arm as well (Figure 3.17). Subjects were prepared for the peel tests as in the previous experiments and described in Section 3.2.1. Separate peel tests on the side of the arm were run on both subjects at a speed of 1200 mm/min and dwell time of one minute. The results from the side arm tests were analyzed for average peel force and maximum peel force values as in the experiments on the forearm and as described in Section 3.3.1.

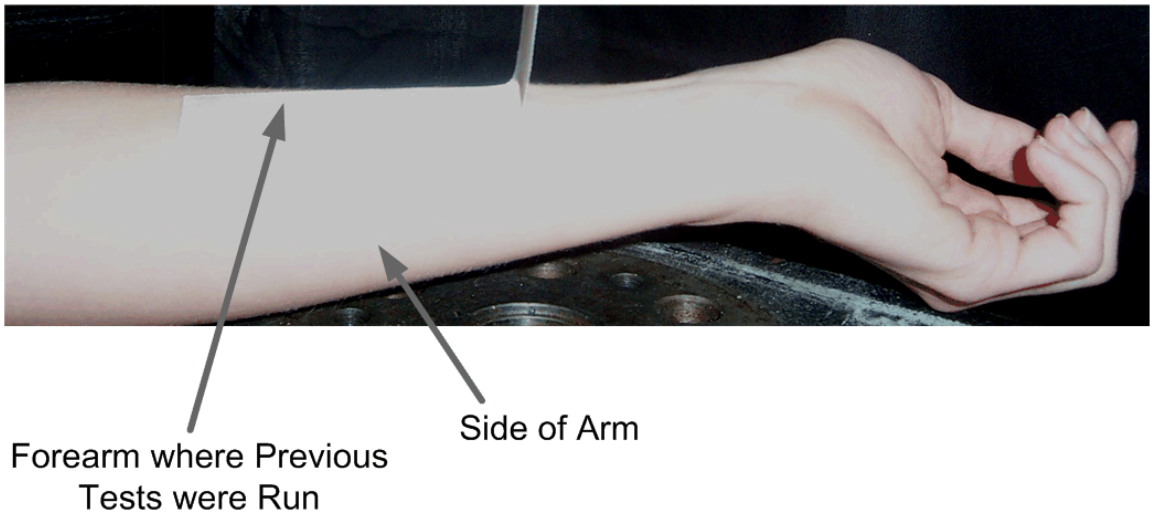

Figure 3.17: Regions of the Arm Tested

Tables 3.4 and 3.5 display the results from peel tests run on the side of the arm and the forearm. Table 3.4 lists results for Subject A and Table 3.5 lists results for Subject D. Both subjects experienced lower average peel force and maximum peel force values on the side of the arm than the forearm region. The difference between the two body locations was around 0.6 N for Subject A and approximately 1 N for Subject D.

Table 3.4: Subject A Force Comparison from 1200 mm/min Tests

Body Location	Average Peel Force (N)	Maximum Peel Force (N)
Forearm	1.539	1.696
Side of arm	0.948	1.050

Table 3.5: Subject D Force Comparison from 1200 mm/min Tests

Body Location	Average Peel Force (N)	Maximum Peel Force (N)
Forearm	2.297	2.616
Side of arm	1.277	1.436

3.3.4. Comparison of Series One Tests with Series Two Tests

Series Two tests primarily involved speeds greater than 500 mm/min, which were unattainable with the Instron 4505 testing machine used in Series One. However, tests run at 200 and 400 mm/min with the Tytron 250 testing machine allow comparison with the180-degree tests of the same speeds in Series One. Table 3.6 lists the Instron 4505 and Tytron 250 results for 200 mm/min and 400 mm/min. Series One in Table 3.6 refers to the Instron 4505 and Series Two corresponds to the Tytron 250.

Table 3.6: Series One and Two Results for 200 mm/min and 400 mm/min Peel Tests on Subjects A and D

Test Series	Subject	Gender	Age	Peel Angle (degrees)	Rate (mm/min)	Average Peel Force (N)	Maximum Peel Force (N)
One	A	female	22	180	200	0.602	0.960
Two	A	female	22	180	200	0.738	0.834
One	A	female	22	180	400	0.665	0.977
Two	A	female	22	180	400	1.176	1.299
One	D	male	60	180	200	1.942	2.792
Two	D	male	60	180	200	1.598	1.777
One	D	male	60	180	400	2.005	2.792
Two	D	male	60	180	400	1.834	2.121

The test results from Series One and Two are similar, but not exactly the same. The maximum difference between Series One and Two tests is approximately 1 N. Most Series One values are lower than Series Two values for Subject A. However, Series One values were higher than Series Two values for Subject D. The difference in the two testing methods could be due to the order of the tests, as mentioned in Section 3.3.2.

Series Two tests for the 200 and 400 mm/min speeds were performed on the same day in ascending speed for both subjects. Series One tests for the 200 and 400 mm/min speeds on Subject D were also performed on the same day in ascending speed. Conversely, Subject A was tested at the 200 and 400 mm/min speeds in Series One on separate days in separate months. Another theory on the cause of different values is the different orientation of pulling. Series One tests involved the arm positioned vertically and Series Two tests positioned the arm horizontally, which caused different gravitational effects on the skin.

3.3.5. Testing Rigid Substrates

Numerous peel tests have been performed on rigid substrates, or surfaces, and presented in the literature. In this section, additional peel tests are run on rigid surfaces for comparison with the skin results. The same 2.54-cm-wide Durapore™ tape is used. Peel tests were run with the Tytron 250 testing machine at 180 degrees on aluminum, polycarbonate, and steel surfaces. The 180-degree peel tests are compared with the skin results from Series Two.

3.3.5.1. Substrate Preparation

The aluminum, polycarbonate, and steel surfaces used were thin, flat plates. The aluminum and steel surfaces were wiped with a degreaser before each test. The 180-degree tests required positioning the plate to lie flat on the blocks used to rest the arm from the skin peel tests. The tape was attached to the plate and clamp (shown in Figure 3.2). Then, 7.62 cm of tape was bonded with the plate and a 10 N cylindrical weight was rolled over the tape to secure the tape's grip, as in the skin tests.

3.3.5.2. Substrate Peel Results and Comparison with Skin

Three peel tests were run on each substrate. The speed of the tests was held constant at 200 mm/min and dwell time was one minute for all tests. Figures 3.18-3.19 show sample 180-degree peel tests from the aluminum and polycarbonate surfaces, respectively. Figures 3.20-3.22 show all the peel tests performed on the steel surface. The plot of load versus displacement for two of the steel tests was very flat, indicating that the peel force for steel may be higher than what was recorded due to the load cell for the machine. Nevertheless, the steel surface achieved the largest forces, overall. Appendix D contains the complete record of 180-degree rigid surface tests.

As with the skin peel tests, average peel force and maximum peel force were computed. Table 3.7 lists the force results from rigid substrates and skin substrates for comparison. Figures 3.23 and 3.24 graphically display the results and compare the different substrates. Steel had the largest average peel force of about 4.7 N and largest maximum peel force of about 5.1 N. The substrate with the lowest force values was Subject A's skin. Subject A had an average peel force of about 0.7 N and a maximum peel force of about 0.8 N.

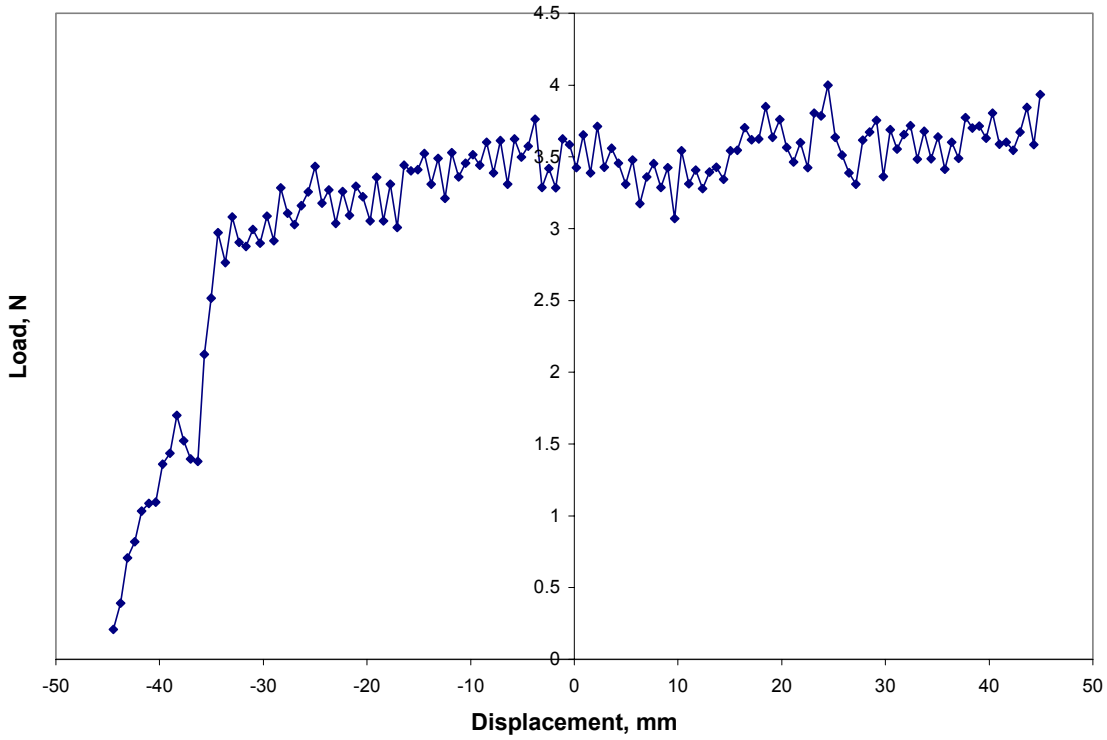

Figure 3.18: 180-degree Peel Test on Aluminum Substrate at 200 mm/min

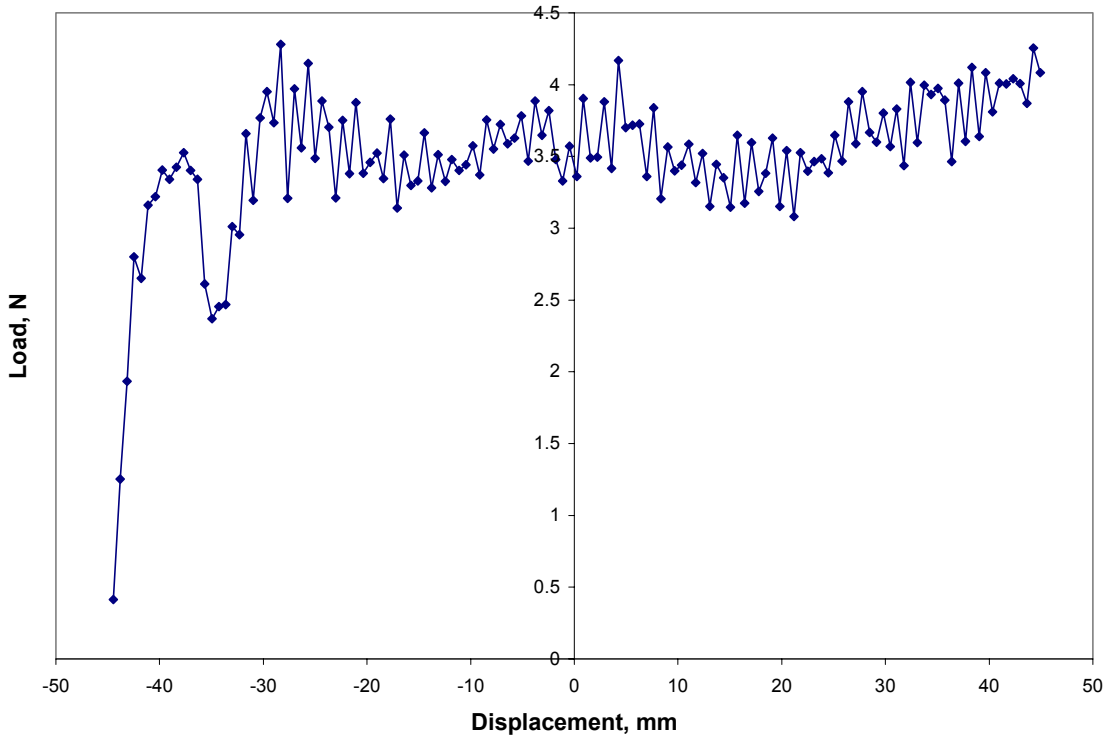

Figure 3.19: 180-degree Peel Test on Polycarbonate Substrate at 200 mm/min

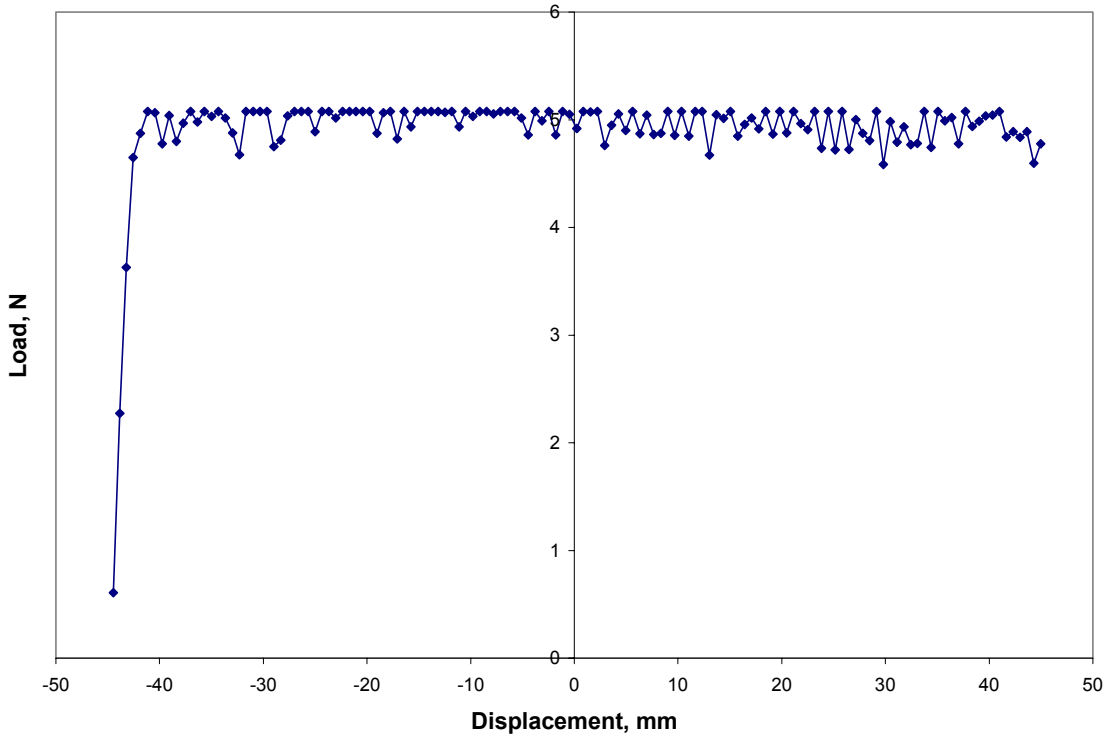

Figure 3.20: 180-degree Peel Test on Steel Substrate at 200 mm/min, Test 1

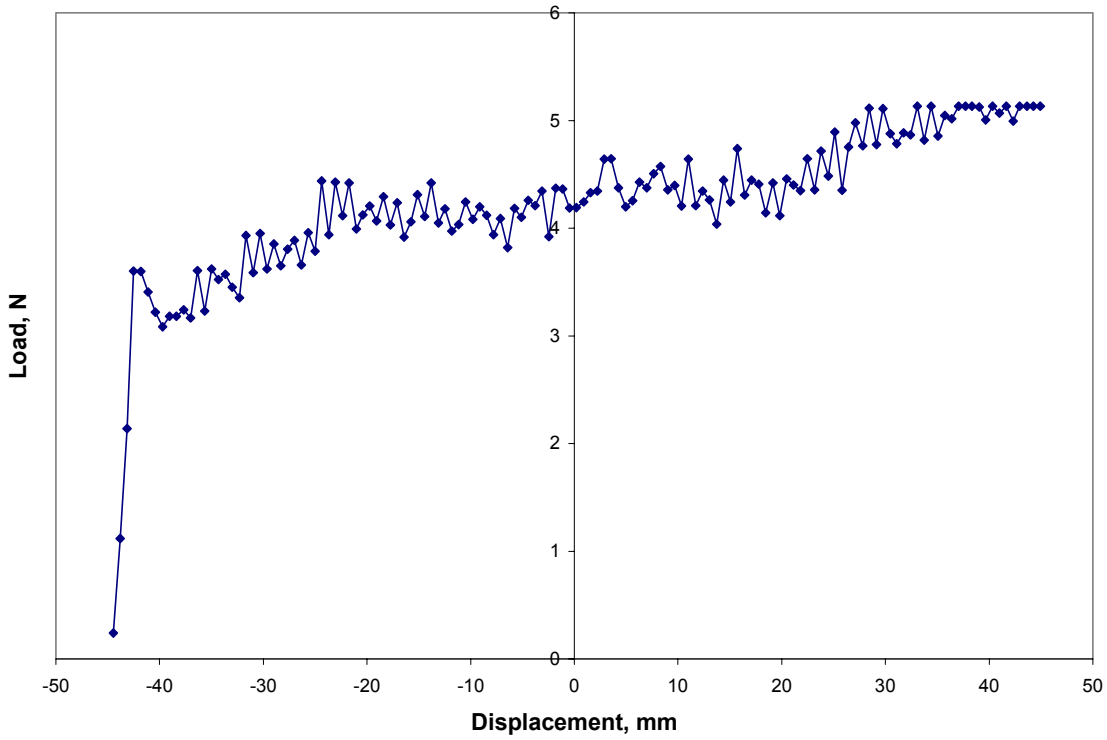

Figure 3.21: 180-degree Peel Test on Steel Substrate at 200 mm/min, Test 2

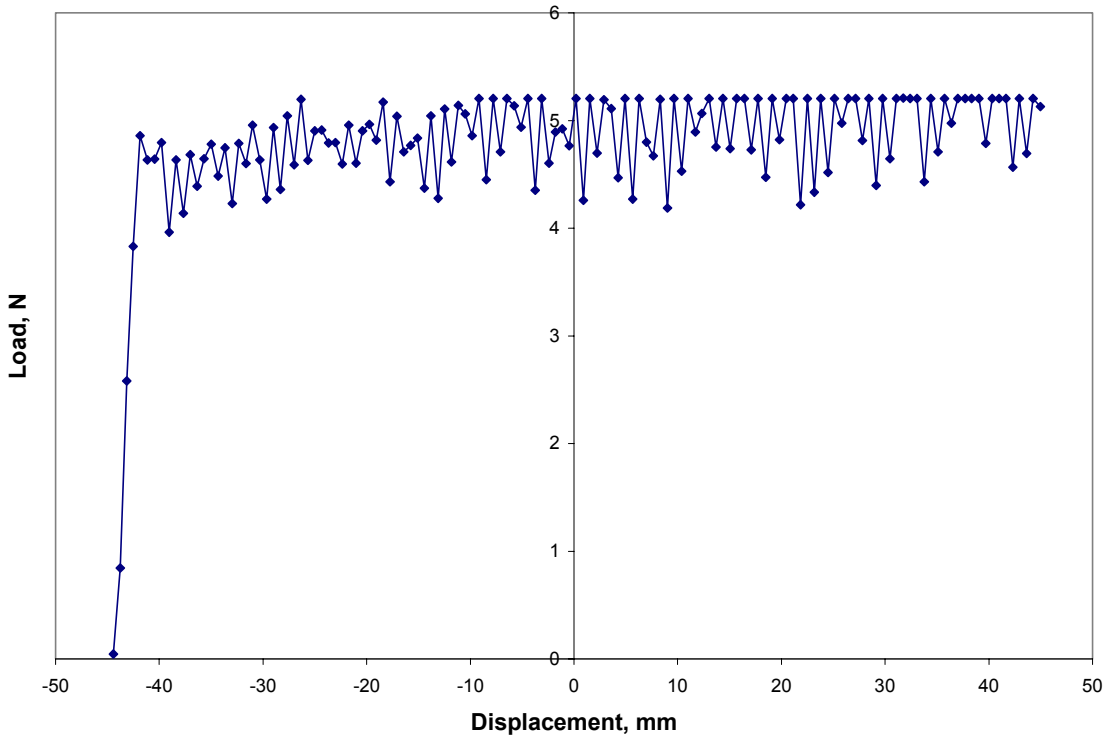

Figure 3.22: 180-degree Peel Test on Steel Substrate at 200 mm/min, Test 3

Table 3.7: Comparison of Different Substrates for Peel Tests at 200 mm/min

Substrate	Age	Peel Angle (degrees)	Average Peel Force		Maximum Peel Force		Day Tested
			Mean (N)	CV	Mean (N)	CV	
Subject A Skin	22	180	0.74	0.06	0.83	0.10	2/14/03
Subject D Skin	60	180	1.60	0.05	1.78	0.06	2/14/03
Aluminum	-	180	3.29	0.07	3.78	0.12	2/20/03
Polycarbonate	-	180	3.69	0.12	4.91	0.09	2/20/03
Steel	-	180	4.71	0.07	5.14	0.01	2/20/03

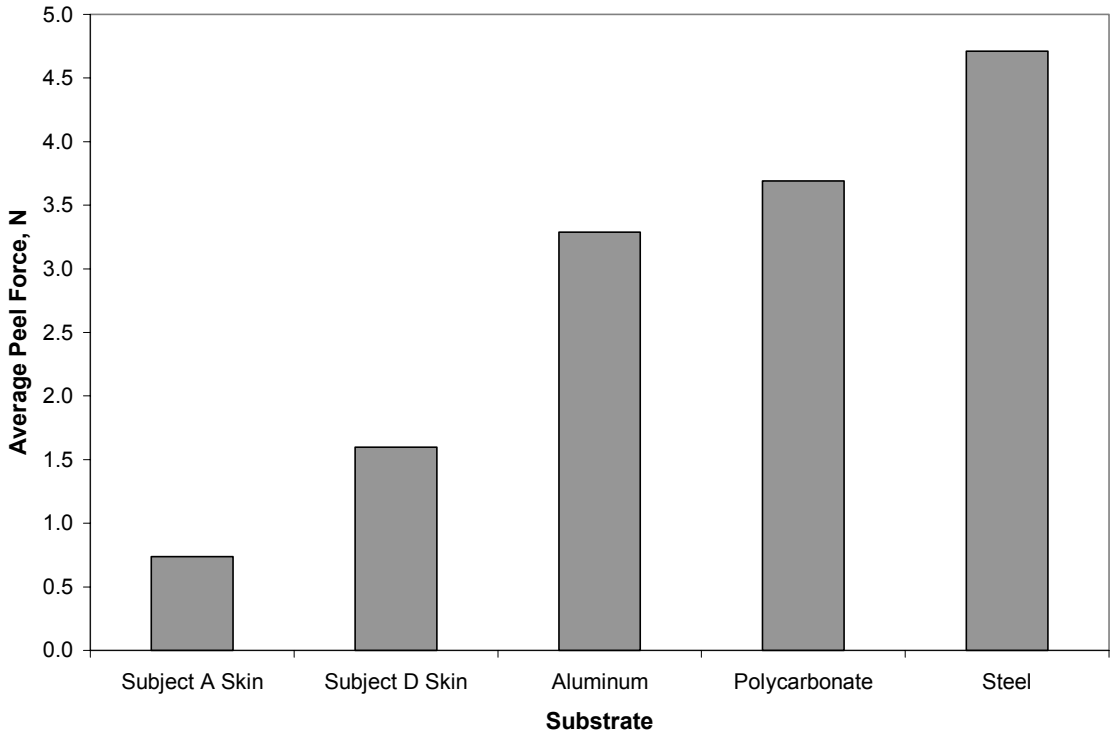

Figure 3.23: Average Peel Forces for 180-degree Peel Tests on Different Substrates at 200 mm/min

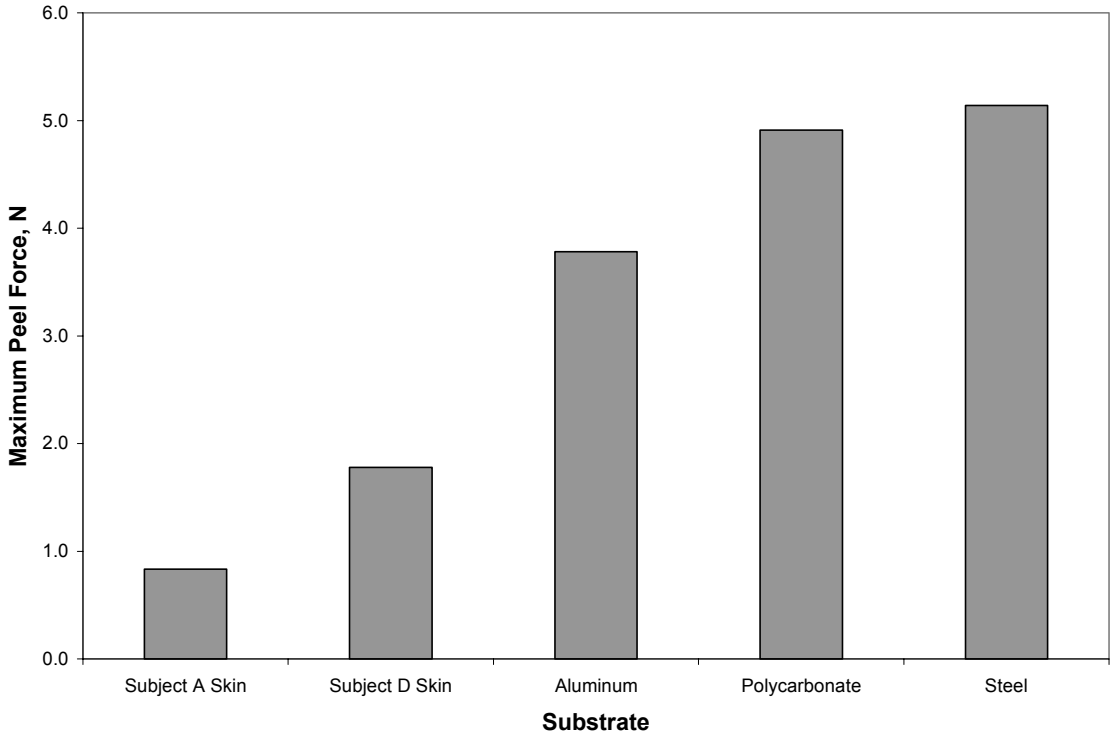

Figure 3.24: Maximum Peel Forces for 180-degree Peel Tests on Different Substrates at 200 mm/min

As shown in Figures 3.23 and 3.24, human skin requires less force for tape removal than rigid surfaces. This could be because of the curved skin surface and the moisture in the skin. The models involving skin in the following chapters will take this flexible behavior into account.

3.4. Conclusions

Peel tests at 180 degrees were run on two subjects at speeds between 200 and 10,000 mm/min. The peel force to remove the tape ranged from about 0.7 N to 3.6 N for the 2.54-cm-wide Durapore™ tape. Overall, Subject D had the larger average force and maximum peel force compared to Subject A. Both subjects had similar linear and initial slopes. Changing the testing order from increasing speed to decreasing speed showed that after each peel test, the skin changes and typically requires a higher force to remove the tape. Peel tests on the side of the arm showed that the arm region is not uniform in force required for peeling; the side of the arm required less force for peeling than the forearm region. Series Two tests produced different values for forces than Series One tests. The results that could be compared were within a range of 1 N. Comparing peeling

from skin with peeling from a rigid surface showed that Subject A required the least force for peeling and steel surfaces require the most force for peeling. In general, skin requires less force than an aluminum, polycarbonate, or steel surface.

The results from Series One and Two provide a foundation for developing mathematical models of peeling from skin and rigid surfaces. The next chapter will introduce mathematical modeling with a working model of peeling from a rigid substrate. Models following the rigid substrate models will involve tape peeling from a skin surface.

Chapter 4. Mathematical Model Research

4.0 Introduction

As mentioned in the literature review and shown in Chapters 2 and 3, peeling tape from various types of surfaces is often used to test adhesives for a variety of uses. Various models were created as research for this thesis with the overall goal being a model of peeling tape from skin. This chapter provides a brief description of all models attempted. Not all models were successful in yielding results or meaningful solutions. There were eleven models overall and the computer inputs and commands for the executable models are presented in Appendix E. The three most promising models will be featured with results in Chapters 5 and 6.

4.1. Foundation Principles for the Models

All mathematical models developed are two-dimensional; they analyze the tape and skin in a vertical plane. The skin and tape are modeled as flexible beams with axial force taken into account. The models or model components may treat the skin with tape attached as one unit or as two separate entities. In some cases, a free, unattached portion of the tape is included. The springs in the models represent skin's resistance and are positioned on the sides, ends, underneath, or a combination of these three positions. The tape backing and skin are modeled as an elastica with bending moment proportional to curvature. Also, the extensibility or inextensibility of skin and tape factors into all the models.

The displacements and rotations of the skin and tape are functions of the arc length of the component, and may be large. In some previous models, like that in Kaelble (1960), only small slopes and deflections, and linear equations, are used. To simulate peeling tape from skin, the models here focus on large rotations of the skin and peel angles between 90 and 180 degrees. Moreover, skin resists bending and has a continuous slope, making the inclusion of bending stiffness significant, though neglected in Stephen-Fountain et al. (2002) and Roop et al. (2002).

One objective for the models is to model the shapes of the skin and tape during peeling, and the forces and moments throughout the skin and tape, especially at the peel front. Another objective is to determine an appropriate debonding criterion, though this

is not the major focus of this basic study. The strain in the adhesive at the peel front has been used in prior research and a critical strain will be considered as the debonding criterion in one model.

4.2. The Shooting Method

The numerical analysis for all models was performed using the program Mathematica (Wolfram, 1996). Within Mathematica, the shooting method was employed to execute the analysis. The shooting method involves inputting initial guesses of unknown parameters and some boundary conditions to the model's differential equations. The program iterates and tries new values based on the results from the initial guesses until a solution is discovered for the differential equations. Not every solution obtained is a correct or logical solution to the specific problem, and care must be taken to verify the appropriateness of the solution.

4.3. Peeling Off a Rigid Surface

Models 1-4 simulate peeling tape from a rigid surface. The tape is broken down into two components, backing and adhesive. The backing of the tape is modeled as a beam with forces and moments, and the adhesive of the tape is modeled as a series of springs or fibrils. The tape backing is considered inextensible in Models 1 and 2, and the adhesive has a negligible effect on the tape's bending stiffness in all eleven models.

4.3.1. Model 1

Figure 4.1 shows the basis for Model 1. Only the tape is modeled as it is peeled upward from the rigid surface. The adhesive is modeled as a Winkler foundation, i.e., as a uniform continuous distribution of independent springs. In the first variation, the program computes adhesive strain based on the forces acting on the end of the tape. In the second variation of the program, the strain at the end of the tape is specified to allow the computer to compute the force applied there. Additionally, the program displays the shape of the tape backing as forces and/or moments pull it, and checks to assure that the fibrils from the adhesive do not wrap around the tape backing as the tape deflects. Results from Model 1 are presented in Chapter 5.

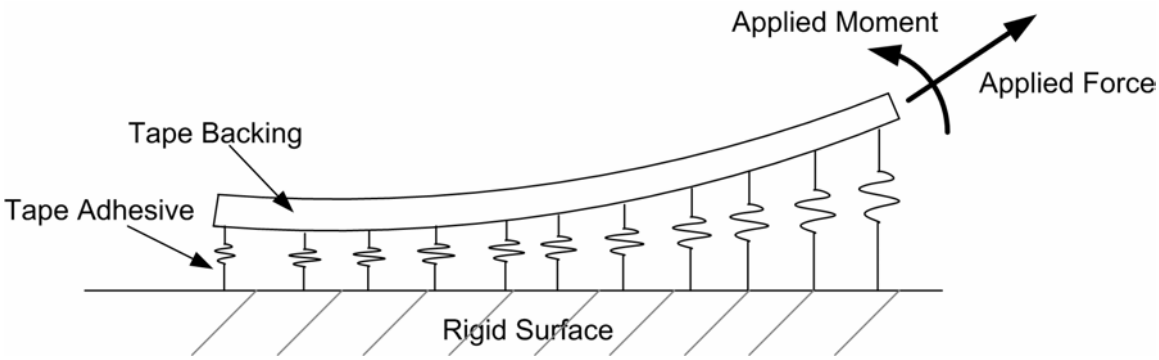

Figure 4.1: Illustration of Rigid Surface Peeling Model with Tape Divided into Backing and Adhesive (Model 1)

4.3.2. Model 2

Model 2 augments Model 1 by adding a free piece of tape that is unattached to the surface. The tape is then peeled up from the surface with the free end. Figure 4.2 shows a schematic illustrating Model 2. Model 2 requires the results from Model 1, and also considers the tape backing inextensible and the adhesive's effect on the tape's bending stiffness negligible. Model 2 works by first applying a moment to the end of the tape that is fully attached to the surface (Model 1) and pulling up at a specified angle. Using the outputs of Model 1, Model 2 computes the resulting rotation at the attached tape end and the resulting force which causes a specified strain value in the adhesive at that location (which is the debonding criterion being used). Next, the rotation, force, and moment are applied to Model 2 to allow it to solve for the length of the unattached portion of tape that is pulled. Like Model 1, Model 2 also plots the shape of the tape as it is pulled from the surface. Model 2 results are presented in Chapter 5.

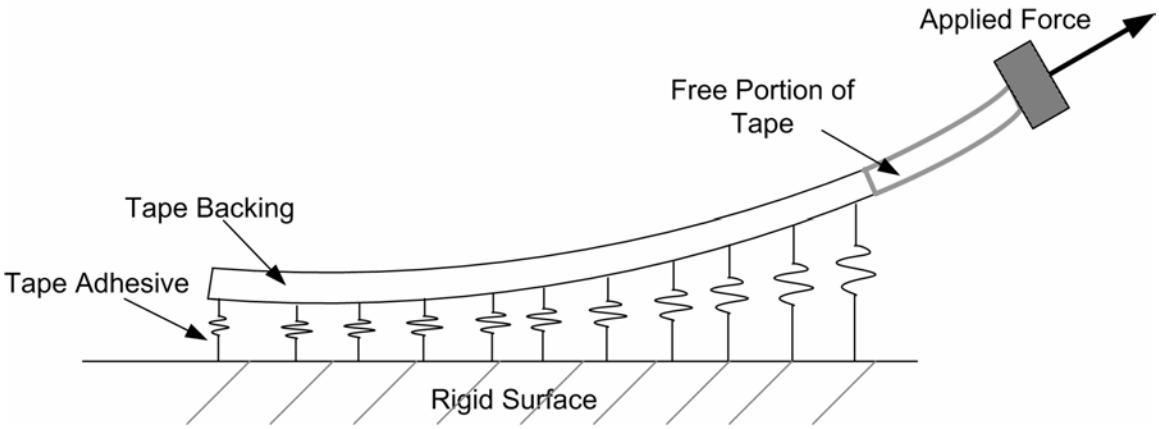

Figure 4.2: Illustration of Rigid Surface Peeling Model Including Free Portion of Tape (Model 2)

4.3.3. Models 3 and 4

Models 3 and 4 are based on Models 1 and 2. Models 3 and 4 modify the equations of Models 1 and 2 to account for extensibility in the tape by incorporating the deformed length of the tape backing. Model 3 adds the extensibility conditions into Model 1, and Model 4 adds it to Model 2. However, the shooting conditions for Models 3 and 4 are different from those of Models 1 and 2 in that they are based on the input forces and moments at the end of the tape. Models 3 and 4 were unsuccessful in yielding results. The models produced a result showing the tape compressing into the rigid surface, which is incorrect. Instead of modifying Models 3 and 4 to rectify this problem, it was decided to move on to models that included the deflection of the skin.

4.4. Plucking Skin

Models 5-8 consider the skin's response to an upward plucking motion. The skin is analyzed as a beam attached to a uniform distribution of springs (i.e., a Winkler foundation). The skin end conditions are represented as fixed or fixed with a horizontal spring.

4.4.1. Model 5

Model 5 is shown in Figure 4.3. In this model, the tape is positioned on the left side. In nondimensional terms, the length of tape (a), slackness of skin (c), spring constants for the skin (k and K_1), force applied (F), angle of force application (θ), spring exponent as in equation 4.1 (n), and skin bending stiffness (η) are inputs for the program.

$$\text{Spring Force} = K_1\left[x_1(0)\right]^n \tag{4.1}$$

The program displays a resulting shape of the skin based on the inputs. Figure 4.4 shows a sample output shape.

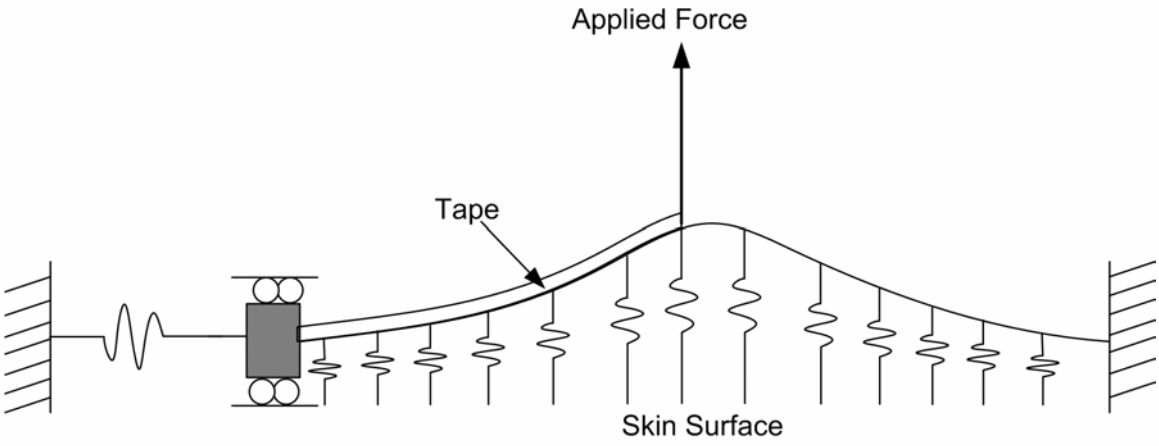

Figure 4.3: Illustration of Skin Model During Plucking with Tape (Model 5)

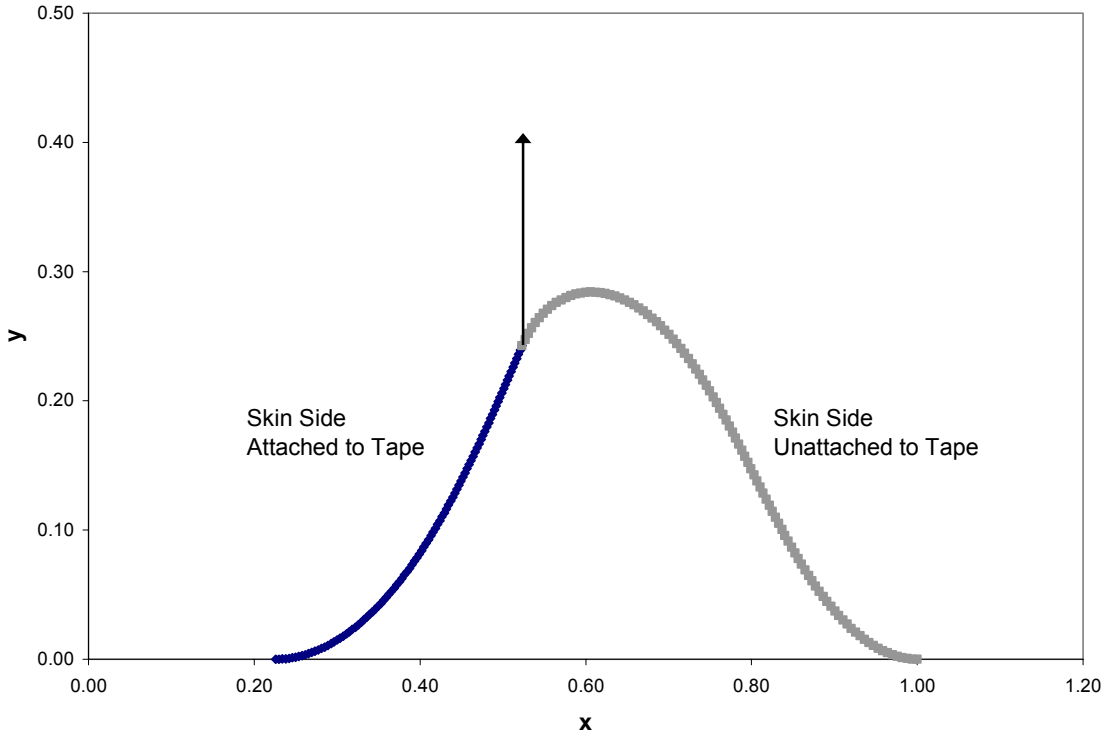

Figure 4.4: Model 5 Sample Output Shape Showing Skin's Behavior, Arrow Designates Force (Slightly Exaggerated Scale)

Studies were performed to increase the height of the skin and modify various inputs to see their effects on the skin's behavior. Not all studies converged; however, the

model performed well when the length of the tape was 40% of the total skin length. Adjusting the applied force, for this case to a large value, say 10,000, did not increase the height of the skin significantly. Moreover, the k values were varied for this case and showed very little influence on the model outputs. Also analyzed for this case was the displacement of the end of the tape. Figure 4.5 shows the resulting plot of applied force versus the displacement of the end of the tape.

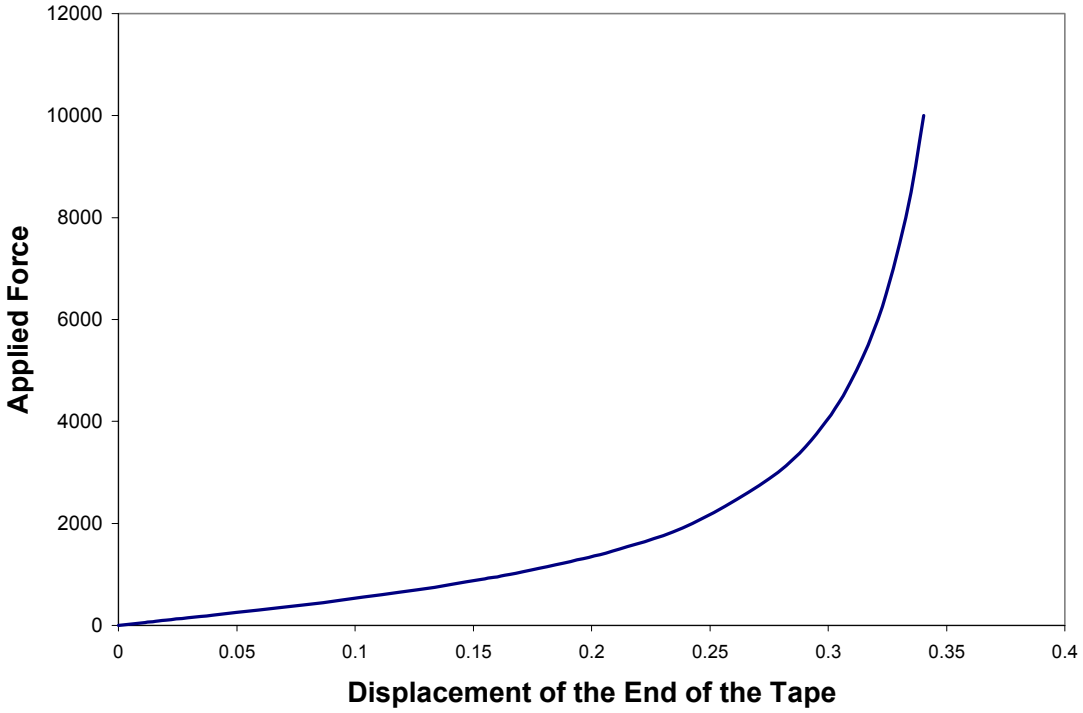

Figure 4.5: Applied Force Versus Displacement of the End of the Tape For 90^o Force in Model 5

4.4.2. Model 6

Model 6 enhances Model 5 by adding a free portion to the tape that is pulled upward. Figure 4.6 displays a schematic of Model 6. The tape is assumed to be inextensible and is modeled in terms of backing and adhesive. In nondimensional terms, the nondimensional inputs for Model 6 consisted of skin, tape adhesive and tape backing bending stiffnesses (ρ_a, ρ_s), adhesive height (h_a), backing height (h_b), skin height (h_s), spring constants (K_1, k), applied force (f_o), angle of applied force (θ_o), length of free portion of tape (d), slackness of skin (c), and length of skin unattached to tape (r).

Convergence problems were encountered with Model 6, which involved ten unknown parameters to be determined by the shooting method.

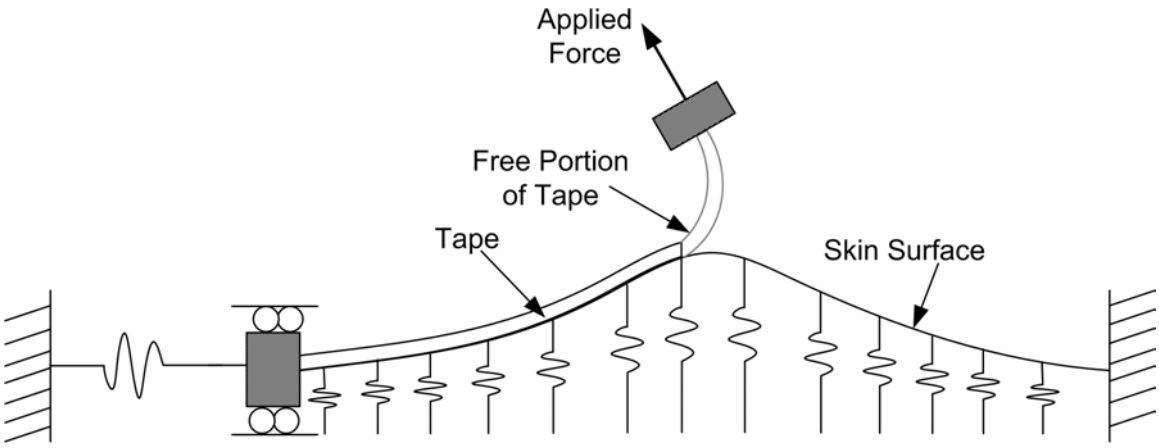

Figure 4.6: Illustration of Skin Model During Plucking with Tape Including Free Portion (Model 6)

4.4.3. Models 7 and 8

Models 7 and 8 alter Models 5 and 6 to include a horizontal spring on the right side of the system as well as the left side. Figures 4.7 and 4.8 show this change for each model. While no results were achieved with Model 8 due to convergence problems, Model 7 did yield results. As with Model 5, the force was varied in Model 7 to develop a plot of applied force versus the displacement of the end of the tape. Figure 4.9 shows force versus displacement of the end of the tape with the input parameters $a = 0.4$, $c = 1$, $\theta = 90^{o}$, $k = 1$, $K_1 = 100$, $\eta = 100$, and $n = 3$. The values K_1 and n were set to 1 for additional cases and showed little variation from the results with the aforementioned parameters. Furthermore, Model 5 was compared with Model 7 in terms of force versus displacement of the end of the tape. Figure 4.10 compares Model 5 and Model 7 results. The models are very similar in the skin's response to force.

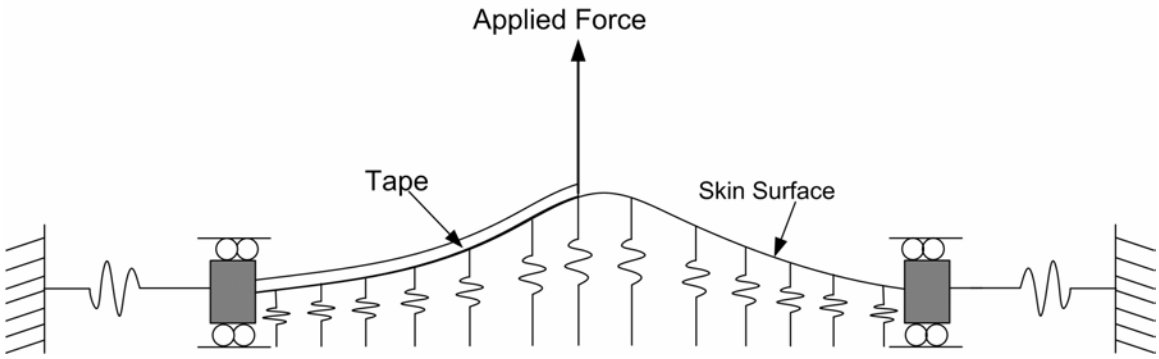

Figure 4.7: Illustration of Skin Model During Plucking with Two End Springs (Model 7)

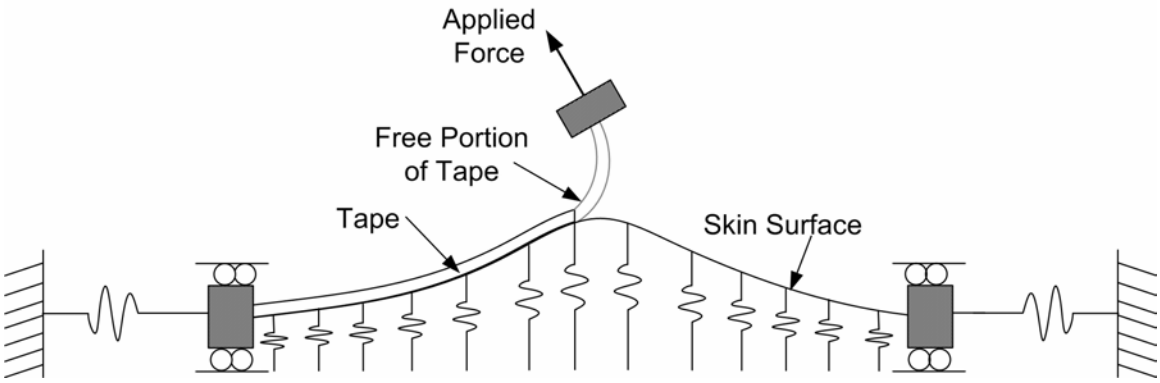

Figure 4.8: Illustration of Skin Model During Plucking with Tape Including Free Portion and Two End Springs (Model 8)

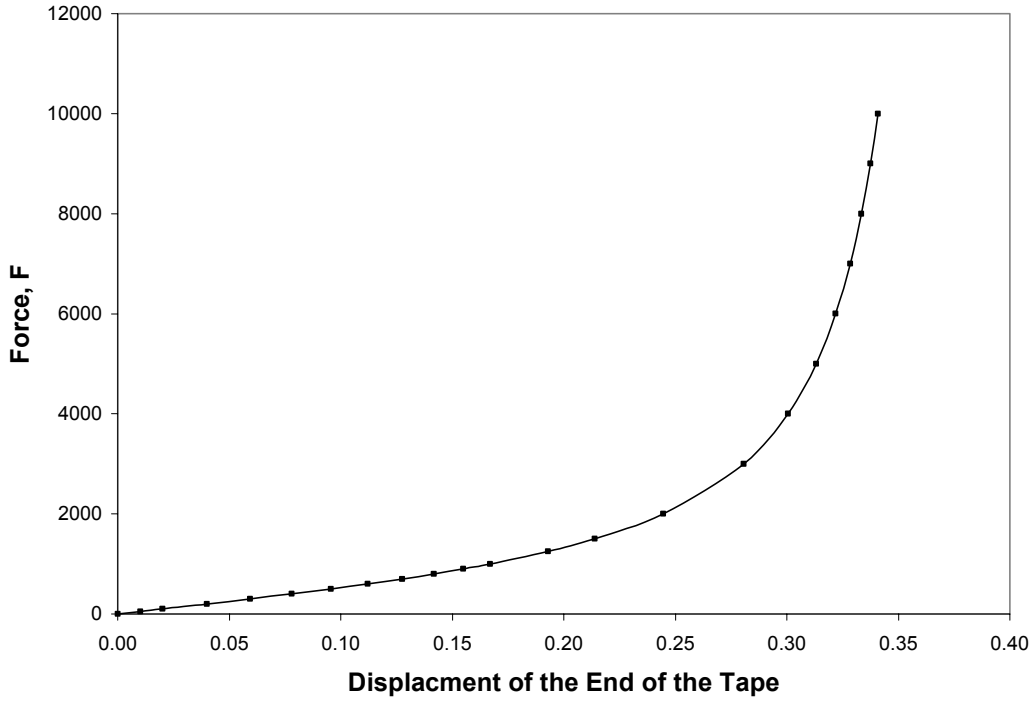

Figure 4.9: Applied Force Versus Displacement of the End of the Tape For 90^{o} Force in Model 7

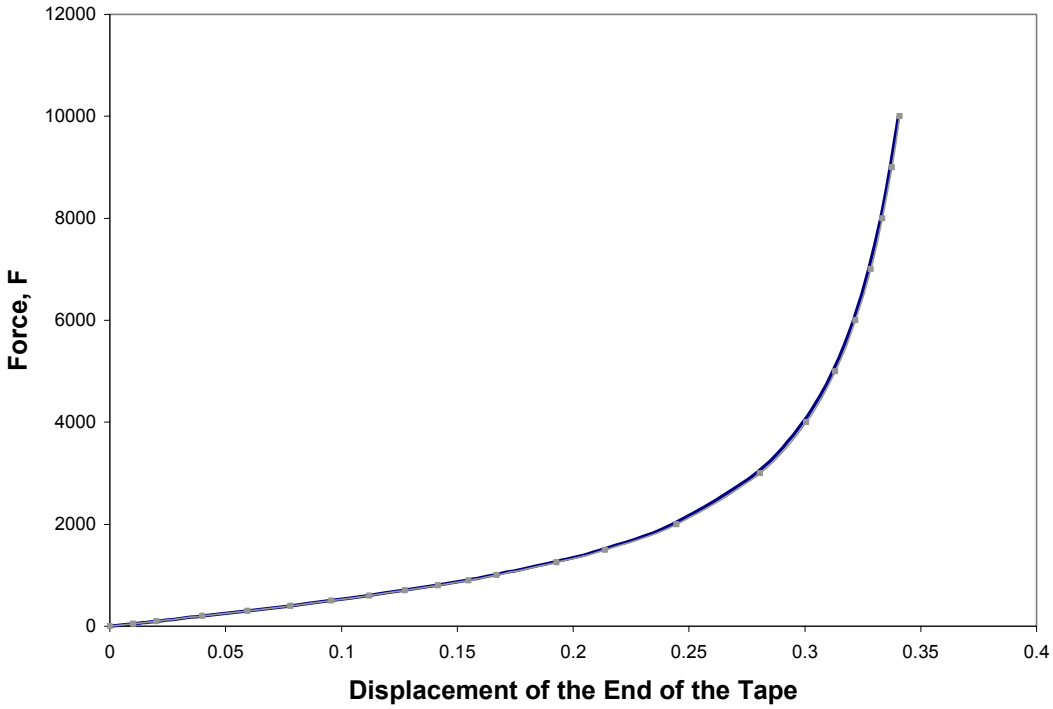

Figure 4.10: Applied Force Versus Displacement of the End of the Tape For 90^{o} Force in Models 5 and 7

Another variation was carried out with Model 7 using symmetry to quicken program operation. Essentially, the left side of the model was analyzed in the model and the right side was assumed to perform the same as the left. The value a = 0.5 to allow symmetry and signify that the tape covered exactly half the length of the skin. A sample output shape is shown in Figure 4.11, where only half of the skin is plotted. The relationship between force and displacement of the end of the tape was analyzed using the symmetrical Model 7, and Figure 4.12 displays the results. The parameter n was set to 1, 3, and 5 for these results and, as evident in Figure 4.12, these values of n produced very similar results.

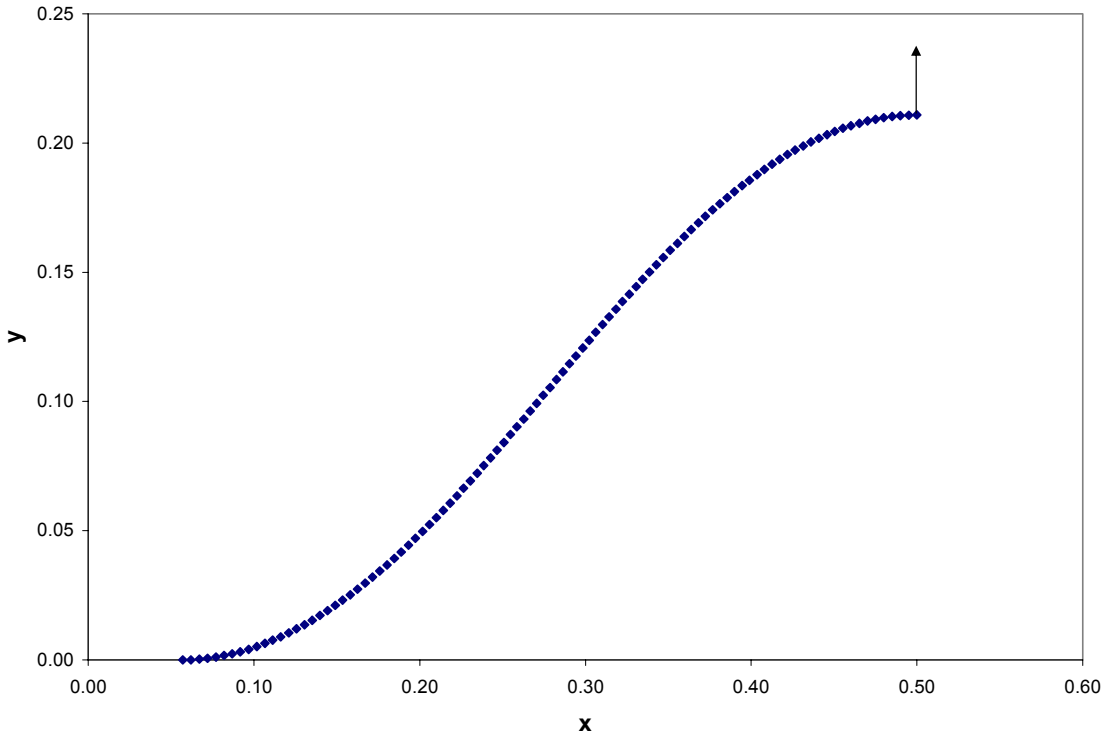

Figure 4.11: Model 7 Sample Output Shape When Symmetry is Used, Arrow Designates Force (Slightly Exaggerated Scale)

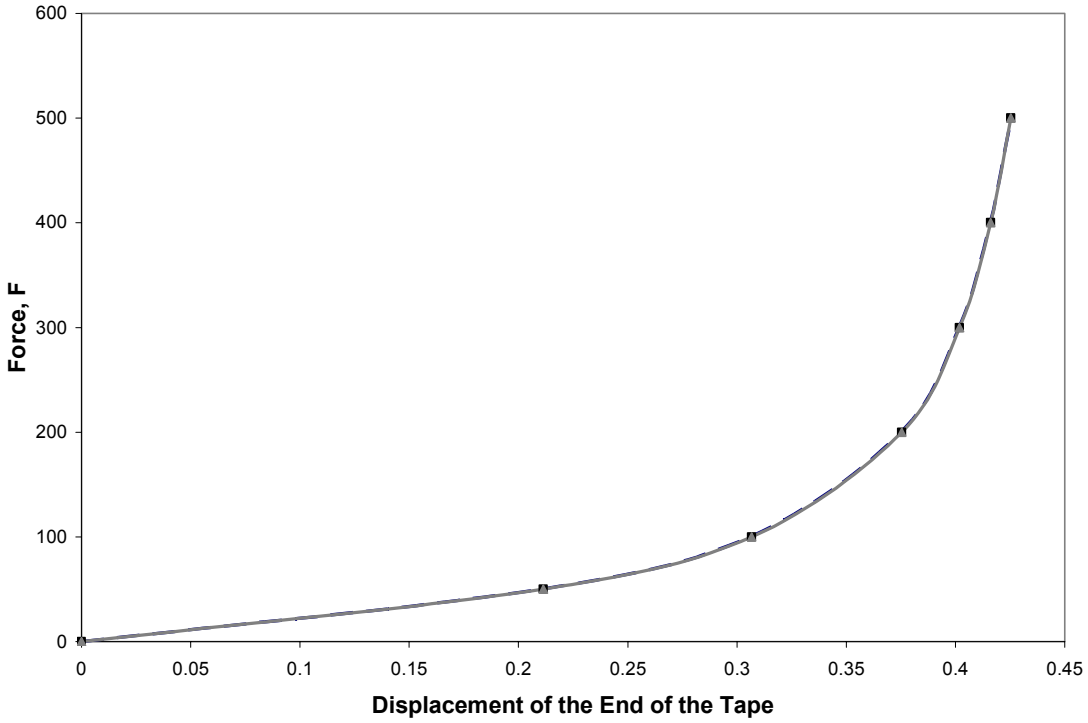

Figure 4.12: Applied Force Versus Displacement of the End of the Tape For 90^{o} Force in the Symmetrical Variation of Model 7

4.5. Skin During Peeling

The final three models, Models 9, 10, and 11, simulate peeling tape from a skin surface. Model 9 involves peeling by an applied force and moment, and the skin is made up of a beam attached to a uniform distribution of springs (i.e., a Winkler foundation) and horizontal springs at the left and right ends with roller supports. Model 10 augments Model 9 by peeling with a distributed force over the entire strip of tape instead of the single force and moment. Model 11 peels with a force and moment like Model 9; however, the skin is represented by one spring resisting the peel in the vertical direction and one end spring resisting the peel in the horizontal direction.

4.5.1. Model 9

Model 9 is displayed in Figure 4.13 with the skin colored gray for clarity. There are two separate diagrams, one before the peel and one after the peel. The tape is not separate from the skin in Model 9 and therefore the tape adhesive is not modeled. Symmetry implies that the springs on each side stretch the same amount. Nondimensional inputs for the program include curvature of the arm (a_o, b_o), the length of

skin untouched by tape (d), spring constants for the springs representing the skin (k_1, k_2, k_s), the applied force (f_o), the angle of the force (θ_o), the spring exponent (n), the stiffness of the skin (η), and the applied moment (m_o). Figure 4.14 further depicts the curvature of the arm with springs.

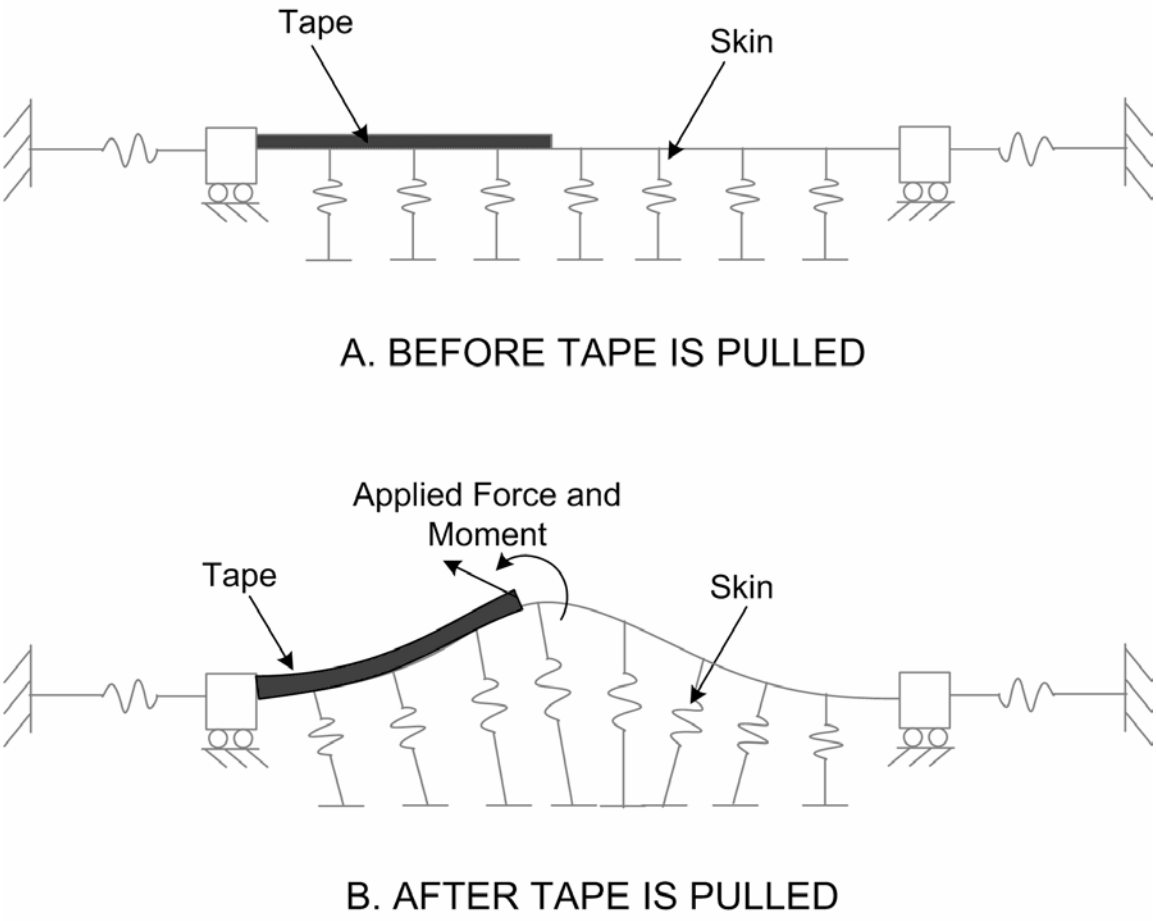

Figure 4.13: Illustration of Peeling Tape from a Skin Surface with Force and Moment (Model 9)

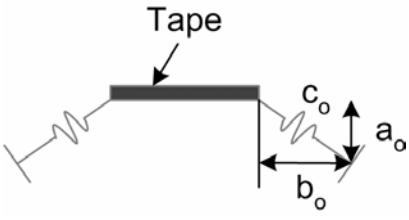

Figure 4.14: End View of Tape and Skin, Accounting for Curvature of the Arm with Springs

Two separate cases were evaluated for Model 9. First, the model was executed with n = 1. An initial case used an applied force of 100. Then the force was increased to bring the height of the skin up to around 1 or 2 relative to the skin length of 2. The program experienced convergence problems when the force went over 120. A sample shape of the skin when the force was 120 is shown in Figure 4.15. In addition to adjusting the force, the angle of the force was changed to evaluate the effect of this angle. Changing the angle also caused the program to experience difficulties and, therefore, correct solutions were not obtained.

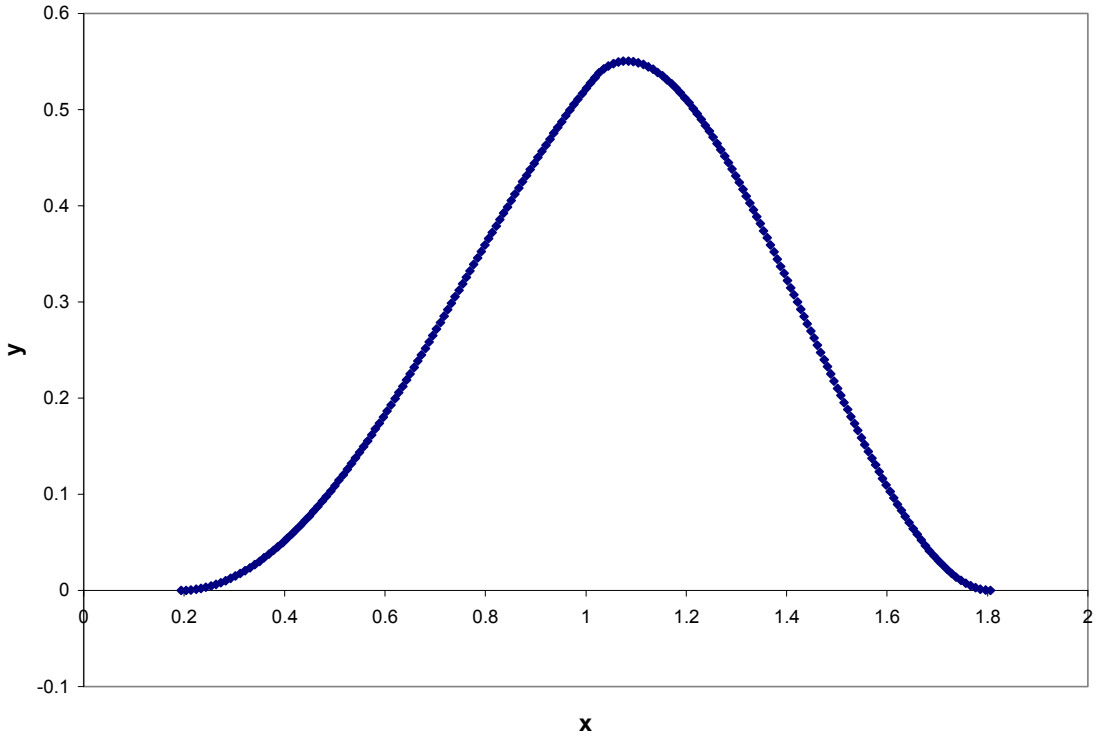

Figure 4.15: Skin Shape Produced with Model 9 when n = 1 (Slightly Exaggerated Scale)

Building on the n = 1 results, n was increased to 3 for further analysis. When n was set to 3, the program became very slow and solving for correct solutions was difficult. Numerous incorrect responses were achieved, such as the case displayed in Figure 4.16. This demonstrates the importance of verifying the solutions produced with the shooting method.

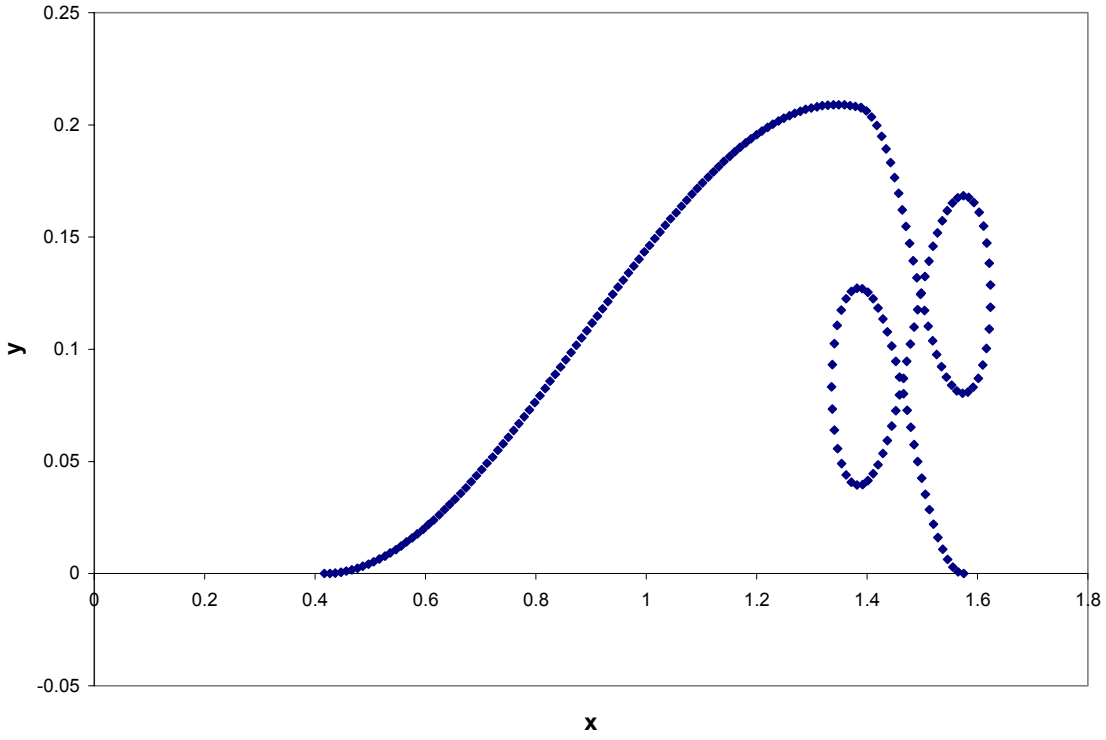

Figure 4.16: Skin Shape Produced with Model 9 Showing Non-Physical Solution at n = 3 (Slightly Exaggerated Scale)

4.5.2. Model 10

An illustration of Model 10 is displayed in Figure 4.17. Again, the skin is shown in gray for clarity. The distributed force in Model 10 is a normal or cleavage force per unit length from the solution in Kaelble (1960) and Kaelble and Ho (1974) of the cleavage stress function for peeling from a rigid surface. The tape is not separate from the skin, like Model 9. Nondimensional inputs for the program include curvature of the arm (a_o, b_o), the length of skin untouched by tape (d), spring constants for the springs representing the skin (k_1, k_2, k_s), the applied force (f_A), the spring exponent (n), the stiffness of the skin (η), and Kaelble's decay rate of the distributed force from the peel front (β). The properties of the skin and adhesive are not based on experimental data.

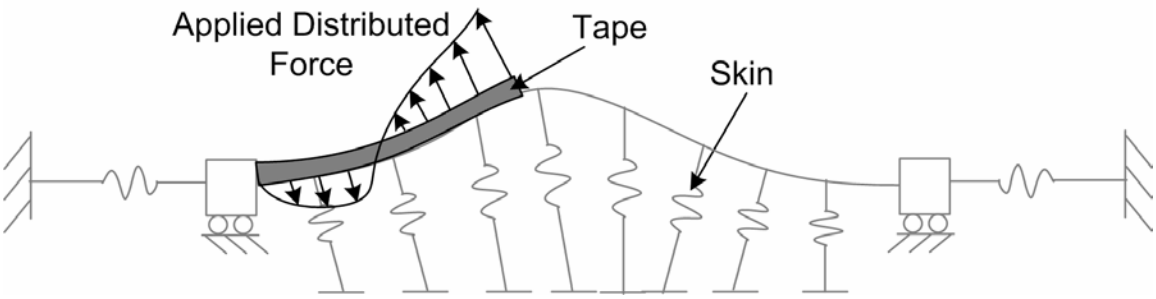

Figure 4.17: Illustration of Peeling Tape from a Skin Surface with Distributed Force (Model 10)

Analysis for Model 10 involved increasing the force to achieve a skin height of 1 or 2 and increasing β to 50 for more localized action near the peel front while n was set at 1. The resulting skin shape when β = 50 from the highest force obtained is displayed in Figure 4.18. The skin did not achieve a height of 1 or 2, but the skin does show a logical shape.

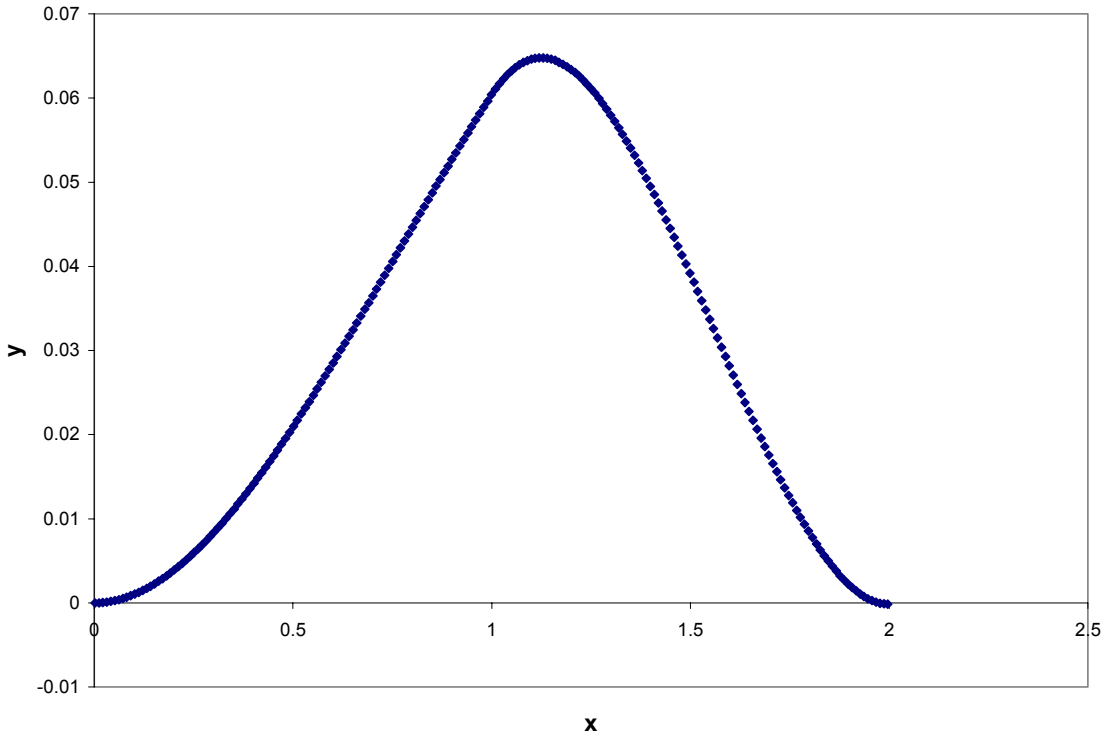

Figure 4.18: Skin Shape Produced with Model 10 when β = 50, f_A = 410, and n = 1 (Slightly Exaggerated Scale)

4.5.3. Model 11

A schematic of Model 11 is found in Figure 4.19. The tape is inextensible and the springs are linear. In addition, the skin has no slackness. Various results were found with Model 11 and are presented in Chapter 6.

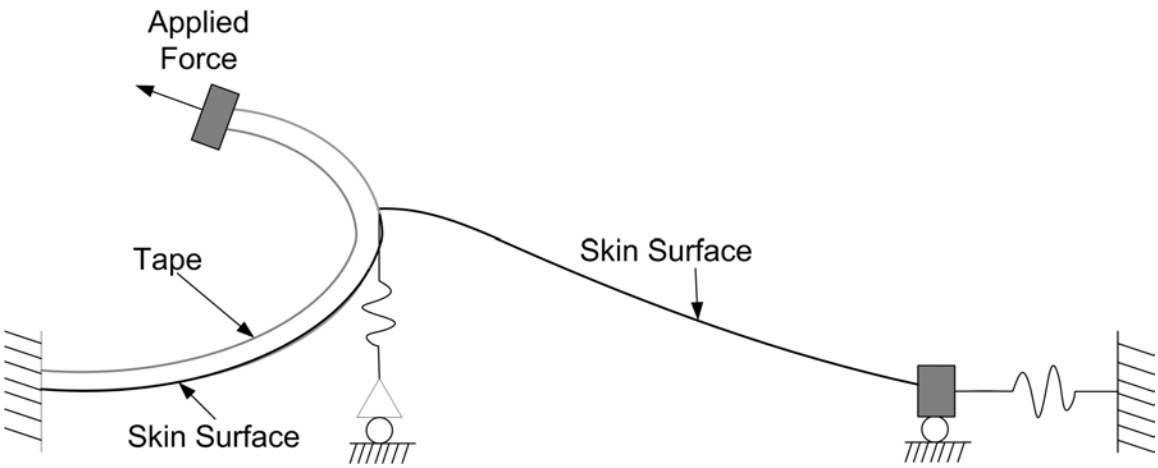

Figure 4.19: Illustration of Peeling Tape from a Skin Surface with Force and Moment (Model 11)

4.6. Conclusions

Various models were considered and analyzed by evaluating the governing differential equations to display tape and skin behavior. There were 11 models in all. The most successful models are presented in the following chapters with a full description of their formulation and the results achieved.

Chapter 5. Model of Peeling Tape from Rigid Surface

5.0 Introduction

The first two models that will be explained in detail in this thesis are Models 1 and 2. These models simulate peeling tape from a rigid surface, and developed a foundation for the various other models visualized and evaluated. This chapter presents the formulation of Models 1 and 2 along with results from program execution.

5.1. Assumptions and Formulation of Model 1

The major pieces of Model 1 consist of a rigid foundation, such as a tabletop, and a piece of tape broken into two components, backing and adhesive. The backing of the tape is modeled as an elastica, i.e., a flexible beam with forces and moments, and the adhesive of the tape is modeled as a series of elastic springs or fibrils. The tape backing is considered inextensible and the adhesive has a negligible effect on the tape's bending stiffness in this model. In addition, equilibrium during pulling is assumed, and there are no forces or bending moment at the left (free) end of the tape attached to the surface. The equations presented were derived by Professor Raymond H. Plaut, and the numerical analysis was performed as part of the research for this thesis.

Figures 5.1 and 5.2 show a schematic of the system with labeled coordinates, angles, forces, and moment. Figure 5.1 depicts the system before the application of the moment and forces, i.e., before the tape is peeled. Figure 5.2 illustrates the system after the application of the moment and forces. Starting at A and D, the left end of the system, S is the arc length and θ is the rotation along the arc length. Also,

b is the width of the backing;

H_b is the thickness of the backing;

E_b is the modulus of elasticity of the backing;

I_b is the moment of inertia of the backing;

H_a is the thickness of the adhesive;

E_a is the modulus of elasticity of the adhesive;

L is the length of the tape;

X_A is the horizontal distance point A moves due to moment and forces;

Y_A is the vertical distance point A moves due to moment and forces;

Γ is the length of the last spring (at the peel front) making up the adhesive after moment and forces are applied;

M_B is the applied moment at point B, the right end of the backing;

P_B is the applied horizontal force at point B;

Q_B is the applied vertical force at point B.

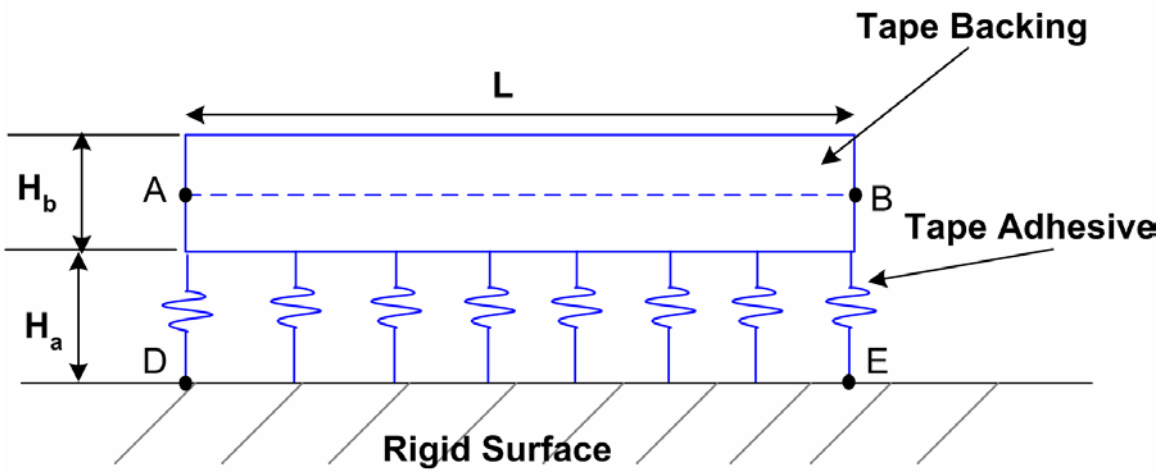

Figure 5.1: Tape (Backing and Adhesive) Adhered to a Rigid Surface Before Application of Moment and Forces

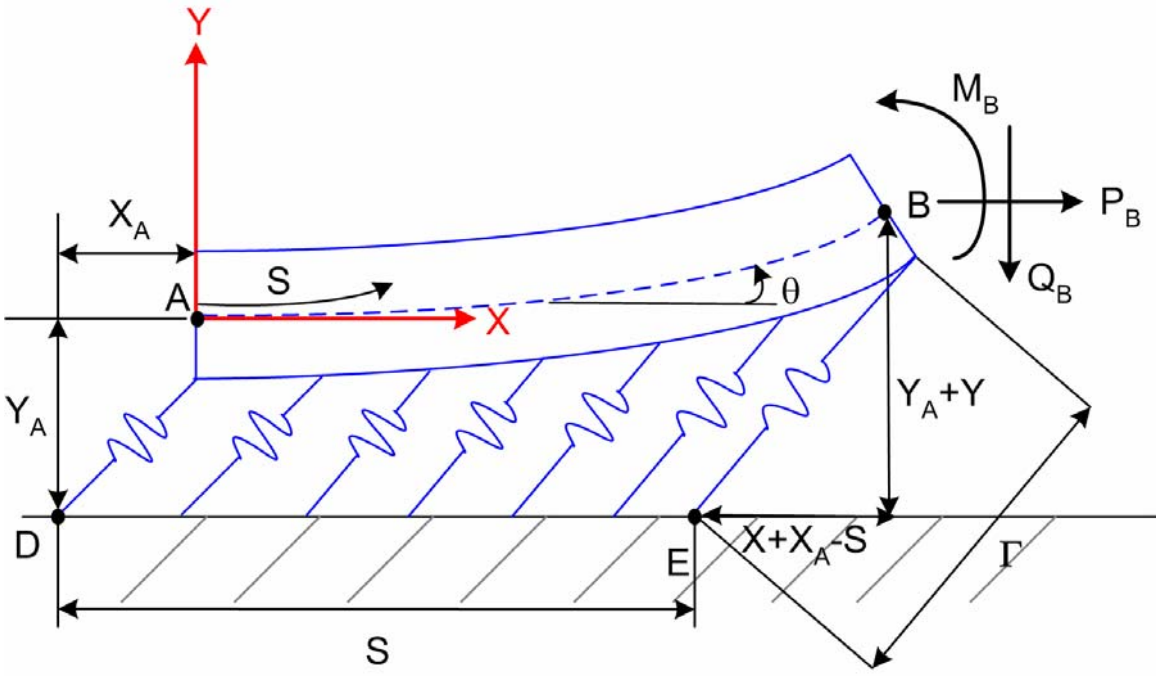

Figure 5.2: Tape (Backing and Adhesive) Adhered to a Rigid Surface After Application of Moment and Forces

First, consider the forces on the backing due to the adhesive. Figure 5.3 shows the geometry of a spring in the adhesive. Starting with the definition of strain, the change in length divided by original length, we have

$$\varepsilon_a = \frac{\Gamma - H_a}{H_a}, \tag{5.1}$$

$$\text{where } \Gamma(S) = \sqrt{\left(Y_A + Y - \frac{1}{2}H_b\cos\theta\right)^2 + \left(X + X_A - S + \frac{1}{2}H_b\sin\theta\right)^2} \tag{5.2}$$

Since the spring is linearly elastic, stress relates to strain with

$$\sigma_a = E_a\varepsilon_a \tag{5.3}$$

$$\text{or } \sigma_a = E_a\left(\frac{\Gamma - H_a}{H_a}\right) \tag{5.4}$$

Thus, the force per length along the backing is $b\sigma_a$ and can be divided into vertical and horizontal components as follows:

$$\text{Vertical Component: } F = b\sigma_a\left(\frac{Y_A + Y - \frac{1}{2}H_b\cos\theta}{\Gamma}\right) \tag{5.5}$$

$$\text{Horizontal Component: } G = b\sigma_a\left(\frac{X + X_A - S + \frac{1}{2}H_b\sin\theta}{\Gamma}\right) \tag{5.6}$$

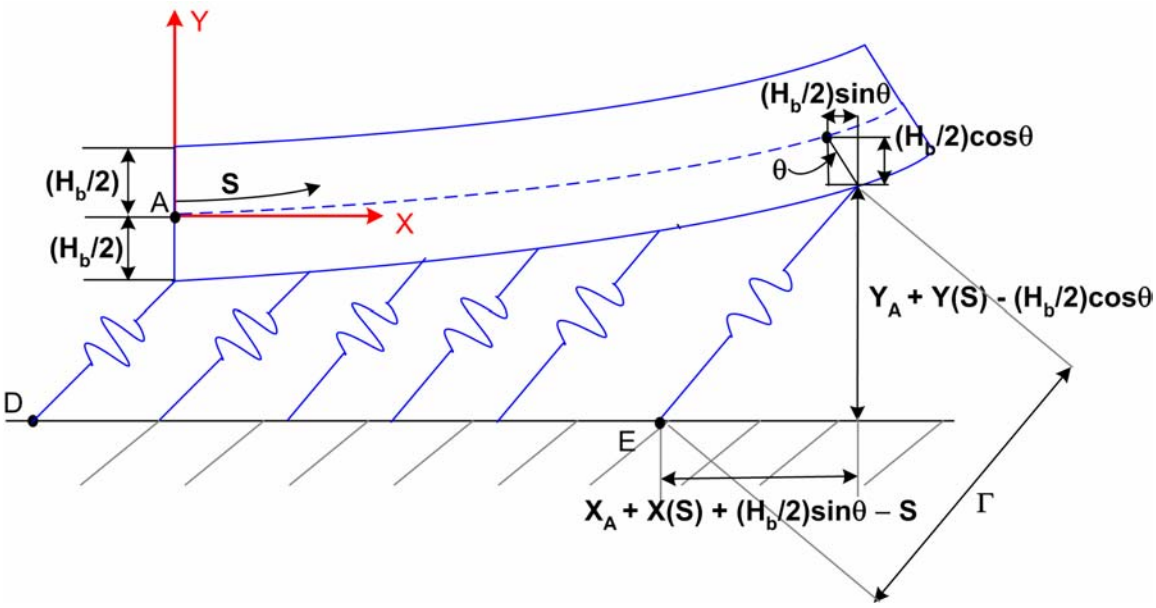

Figure 5.3: Tape (Backing and Adhesive) Showing Geometry to Measure Length of Spring (Adhesive)

Figure 5.4 shows the sign conventions of the forces and moments on an element of backing *dS*. Replacing σ_a in the vertical and horizontal components leaves:

Vertical Component: $$F = bE_a\left(\frac{\Gamma - H_a}{H_a}\right)\left(\frac{Y_A + Y - \frac{1}{2}H_b\cos\theta}{\Gamma}\right) \tag{5.7}$$

Horizontal Component: $$G = bE_a\left(\frac{\Gamma - H_a}{H_a}\right)\left(\frac{X + X_A - S + \frac{1}{2}H_b\sin\theta}{\Gamma}\right) \tag{5.8}$$

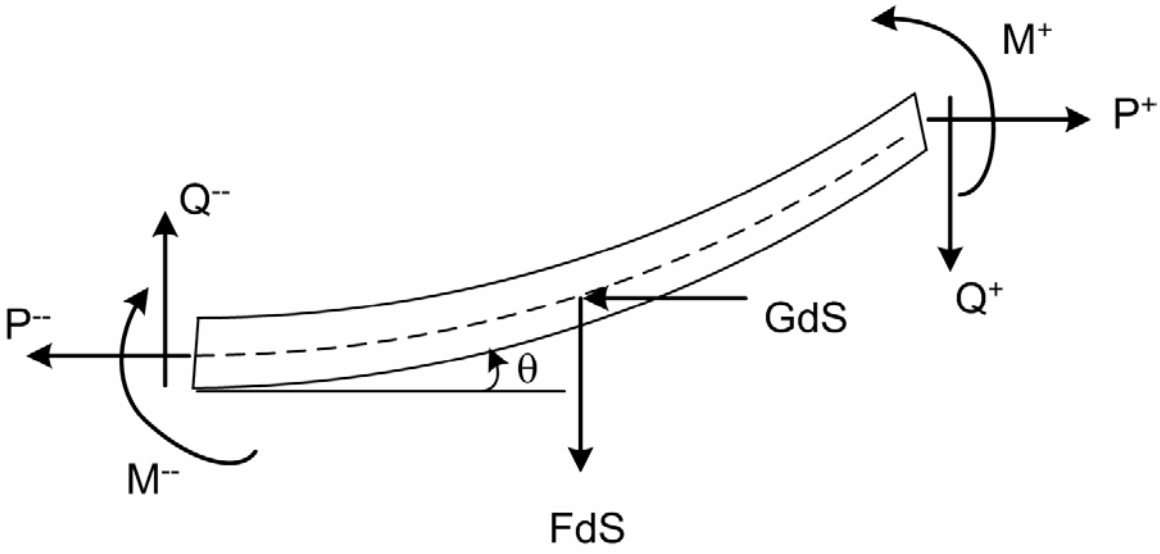

Figure 5.4: Free-body Diagram of Element of Tape Backing, *dS*, with Sign Convention for Adhesive Forces and Backing Forces and Moments

From geometry, the properties of the elastica, and equilibrium, we establish the following main relations for the model:

$$\frac{dX}{dS} = \cos\theta \tag{5.9}$$

$$\frac{dY}{dS} = \sin\theta \tag{5.10}$$

$$E_b I_b \frac{d\theta}{dS} = M \tag{5.11}$$

$$\frac{dQ}{dS} = -F \tag{5.12}$$

$$\frac{dP}{dS} = G \tag{5.13}$$

$$\frac{dM}{dS} = Q\cos\theta + P\sin\theta + \frac{1}{2}H_b G\cos\theta + \frac{1}{2}H_b F\sin\theta \tag{5.14}$$

To avoid using units on each quantity, the variables of the system are non-dimensionalized as follows:

$$x = \frac{X}{L}, y = \frac{Y}{L}, s = \frac{S}{L}, x_A = \frac{X_A}{L}, y_A = \frac{Y_A}{L}, \gamma = \frac{\Gamma}{L}, h_a = \frac{H_a}{L}, h_b = \frac{H_b}{L},$$
$$\eta = 12\left(\frac{E_a}{E_b}\right)\left(\frac{L}{H_b}\right)^3, p = \frac{PL^2}{E_b I_b}, q = \frac{QL^2}{E_b I_b}, m = \frac{ML}{E_b I_b} \tag{5.15-5.26}$$

After nondimensionalizing each variable, the main relations for the model become:

$$\frac{dx}{ds} = \cos\theta \tag{5.27}$$

$$\frac{dy}{ds} = \sin\theta \tag{5.28}$$

$$\frac{d\theta}{ds} = m \tag{5.29}$$

$$\frac{dq}{ds} = \eta\left(\frac{1}{\gamma} - \frac{1}{h_a}\right)\left(y + y_A - \frac{1}{2}h_b\cos\theta\right) \tag{5.30}$$

$$\frac{dp}{ds} = \eta\left(\frac{1}{\gamma} - \frac{1}{h_a}\right)\left(s - x - x_A - \frac{1}{2}h_b\sin\theta\right) \tag{5.31}$$

$$\frac{dm}{ds} = q\cos\theta + p\sin\theta$$
$$-\frac{1}{2}\eta h_b\left(\frac{1}{\gamma} - \frac{1}{h_a}\right)\left[\left(y + y_A - \frac{1}{2}h_b\cos\theta\right)\sin\theta + \left(x + x_A - s + \frac{1}{2}h_b\sin\theta\right)\cos\theta\right] \tag{5.32}$$

$$\text{where } \gamma = \sqrt{\left(y_A + y - \frac{1}{2}h_b\cos\theta\right)^2 + \left(x + x_A - s + \frac{1}{2}h_b\sin\theta\right)^2} \tag{5.33}$$

The strain for the adhesive with non-dimensional variables is:

$$\varepsilon_a = \frac{\gamma - h_a}{h_a} = \frac{\sqrt{\left(y_A + y - \frac{1}{2}h_b\cos\theta\right)^2 + \left(x + x_A - s + \frac{1}{2}h_b\sin\theta\right)^2} - h_a}{h_a} \tag{5.34}$$

The applied forces, q and p, are vectorally summed to produce a resultant, f_o, at an angle of θ_o from the X-axis as shown in Figure 5.5.

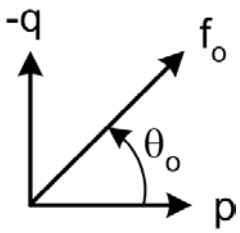

Figure 5.5: Applied Loads q and p Resolved Into the Resultant Force, f_o

The components of the resultant f_o become those of equations 5.35 and 5.36 because of the sign convention shown in Figure 5.4.

$$q = -f_o \sin\theta_o \tag{5.35}$$

$$p = f_o \cos\theta_o \tag{5.36}$$

5.2. Avoiding Penetration of Tape into Surface

In some numerical solutions the springs rotated by about 180 degrees along a portion of the tape, and the tape was below the rigid surface. An "if" statement was included in the computer program to ensure that the tape did not penetrate into the rigid surface and produce an illogical solution. The "if" statement condition affected equations (5.30) - (5.32). They were modified when $y + y_A - \frac{1}{2} h_b \cos\theta \le h_a$ (i.e., when the springs are compressed) to the following new equations involving vertical spring forces plus some horizontal resistance with an assumed coefficient of 0.35:

$$\frac{dq}{ds} = \frac{-\eta}{h_a}\left(y + y_A - \frac{1}{2} h_b \cos\theta - h_a \right) \tag{5.34}$$

$$\frac{dp}{ds} = 0.35\eta \frac{\left(x + x_A + \frac{1}{2} h_b \sin\theta - s \right)}{h_a} \tag{5.35}$$

$$\frac{dm}{ds} = q\cos\theta + \frac{1}{2}\eta \frac{h_b}{h_a}\left(y + y_A - \frac{1}{2} h_b \cos\theta - h_a \right)\sin\theta \tag{5.36}$$

5.3. Numerical Solution

The assumed boundary conditions for the tape's behavior during peeling from a rigid surface consist of the following:

At s = 0: x = 0, y = 0, $\theta = \theta_A$ (unknown), m = 0, q = 0, p = 0

At s = 1: $m = m_B$, $q/p = -\tan\theta_o$, $\varepsilon_a = 2$

These conditions govern the tape's position. At one end the tape is attached to the surface and the other end is assumed to debond when the strain in the adhesive equals 2.

Based on the input values and boundary conditions, the shooting method will iterate until the program converges. The values for x_A, y_A, θ_A, are returned and then set for the rest of the program. A sample output shape produced by the program is shown in

Figure 5.6. The shape represents the center of the tape backing. The inputs to the program required to achieve this result include the following:
$\eta = 1$, $h_a = 0.0005$, $h_b = 0.005$, $\theta_o = 135^o$, $m_B = 0$, $gx_A = -0.0002$, $gy_A = 0.003$, $g\theta_A = -0.0001$. The variables gx_A, gy_A, $g\theta_A$ are guesses that the program uses to begin the shooting method. The Mathematica program codes for Models 1 and 2 are located in Appendix E.

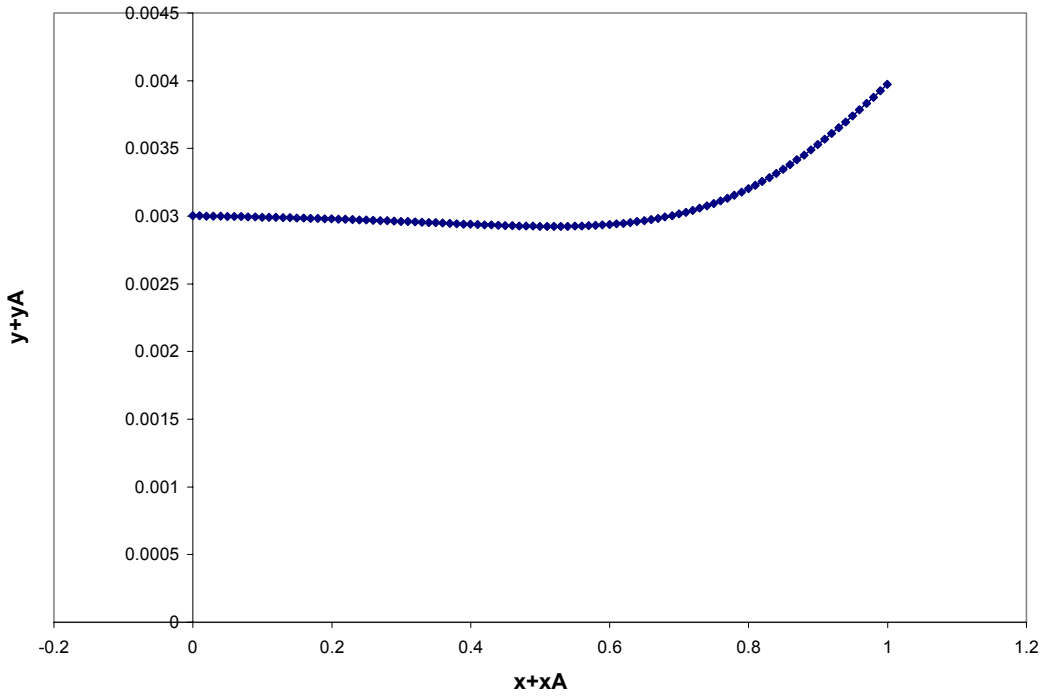

Figure 5.6: Sample Output Shape From Model 1 Representing Tape Backing Centerline Peeled at 135^o (Exaggerated Scale)

In analyzing this model, θ_o, the angle of peel, was increased to determine the effect of the angle of peel on the peel force. Figure 5.7 displays the peel force versus peel angle. The force decreased when the peel angle was between 45 and 95 degrees. Between 95 and 165 degrees, the force increased. This trend disagrees with those from the model of Kaelble (1999), which shows the angle decreasing until around 180 degrees. Kaelble also presents experiments that closely match his model, but have minimum force values at about 140 degrees. In addition, experimental results presented in Satas (1989) from peel tests show a decrease to around 120 to 140 degrees followed by an increase depending on rate of peel and tape. Furthermore, Aubrey et al. (1969) peeled tape from a

glass surface at various angles and found a peel force versus peel angle plot that resembled the shape of the model of Kaelble, but with minimum force at about 120 degrees. Lastly, Dahlquist (1969) presents rigid surface peel test results with low peel forces between 100 and120 degrees, and 120 and 140 degrees, depending on rate.

Working with a peel angle greater than 165 degrees caused problems in the program with convergence, and thus prevented us from comparing peel test data from Chapters 2 and 3.

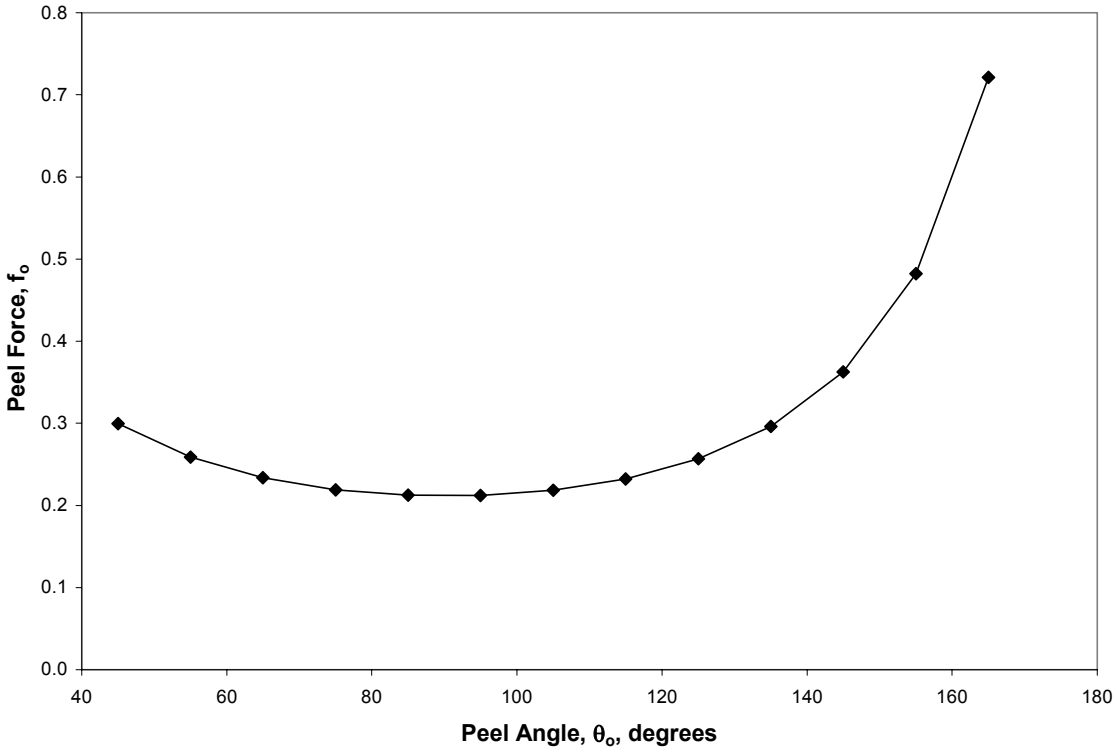

Figure 5.7: Peel Force Versus Peel Angle

The specified maximum strain in the adhesive governs the program in the boundary conditions. Set at 2 initially, the strain was increased to 3 and 4, and decreased to 1. The resulting plots of force versus angle for strain values of 1, 3, and 4 have the same shape as that for end strain equal to 2. Figure 5.8 displays peel force versus peel angle found with the program with each strain value. As evident in Figure 5.8, the higher the end strain in the adhesive, the higher the peel force at all angles.

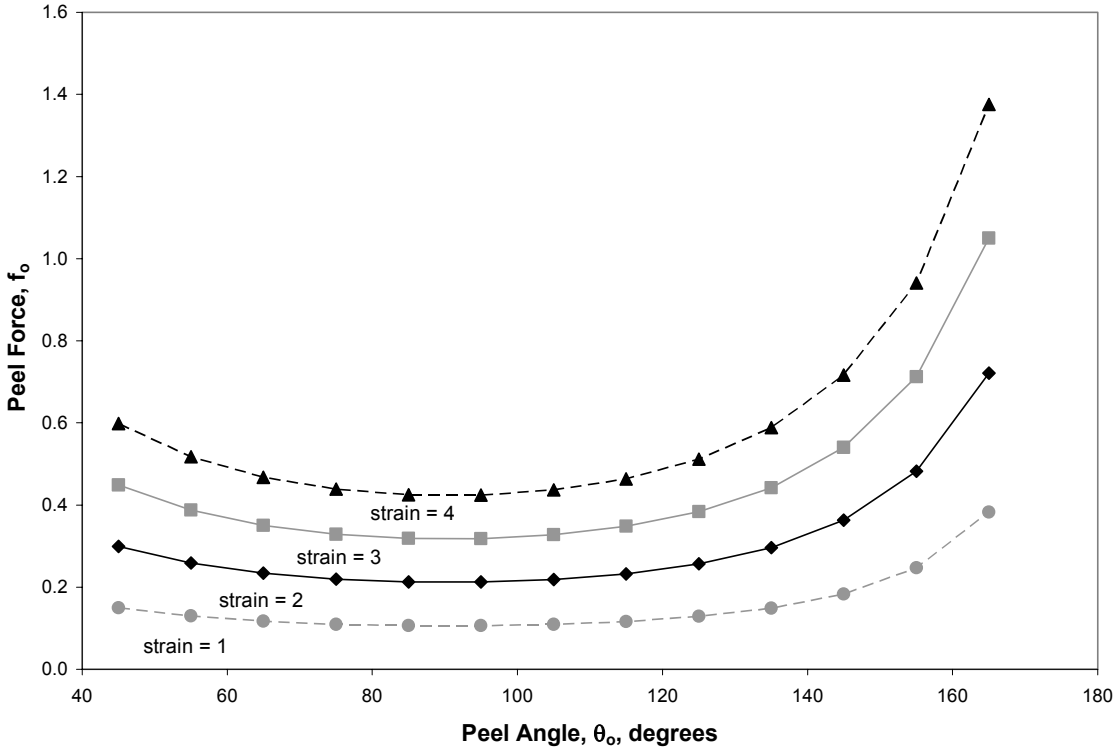

Figure 5.8: Peel Force Versus Peel Angle at End Strains of 1, 2, 3, and 4

5.4. Addition of Unattached Elastica (Model 2)

As explained in Chapter 4, Model 2 was constructed using Model 1 as a base model. Model 2 adds a free or unattached portion to the tape. The tape is again peeled from the rigid surface, however this time a portion of the tape is not connected.

Using the same slope, θ_B, and moment, m_B, at the endpoint of the tape in Model 1, Model 2 builds on Model 1 to define the free portion of tape as an addition to a previously solved Model 1 solution. The equations governing the Model 2 addition include:

$$\frac{dx}{ds} = \cos\theta \tag{5.37}$$

$$\frac{dy}{ds} = \sin\theta \tag{5.38}$$

$$\frac{d\theta}{ds} = m \tag{5.39}$$

$$\frac{dm}{ds} = f_o \sin(\theta - \theta_o) \tag{5.40}$$

The total length of the tape is *(1+d)L*. In the program, the nondimensional arc length *s* along the unattached portion is scaled by *d* so the coordinate runs from 0 to 1.

The boundary conditions for the free, unattached piece of tape's behavior during peeling consist of the following:

At s = 0: x = 0, y = 0, $\theta = \theta_B$ (from Model 1), $m = m_B$ (from Model 1)

At s = d: m = 0

These conditions carry over the conditions from Model 1 to the free portion of the tape and govern the free portion of tape's behavior.

The shooting method is employed again to solve the differential equations. The value for d is determined and then used to evaluate the shape of the tape. A sample output shape produced by the program showing the Model 1 component and the Model 2 component is shown in Figure 5.9. The shape corresponds to the center of the tape backing and has an exaggerated scale. The input to the program required to achieve this result is simply gd = 0.2, which is a guess to initiate the shooting method. However, Model 1 was run first with the following inputs:

$\eta = 1$, $h_a = 0.0005$, $h_b = 0.005$, $\theta_o = 135^o$, $m_B = 0.04$, $gx_A = -0.00011$, $gy_A = 0.003$, $g\theta_A = -0.00013$. These inputs produce a value of 0.00896 for θ_B and about 0.0313 for f_o, which are carried through Model 2.

In analyzing Model 2, attempts were made to decrease the value of d and the stiffness of the tape backing. Due to the sensitivity of the shooting method running on both models in tandem, this proved impossible. As apparent in Figure 5.9, the free portion of the tape does not pull back as it would in a real life situation because of the high stiffness of the tape backing.

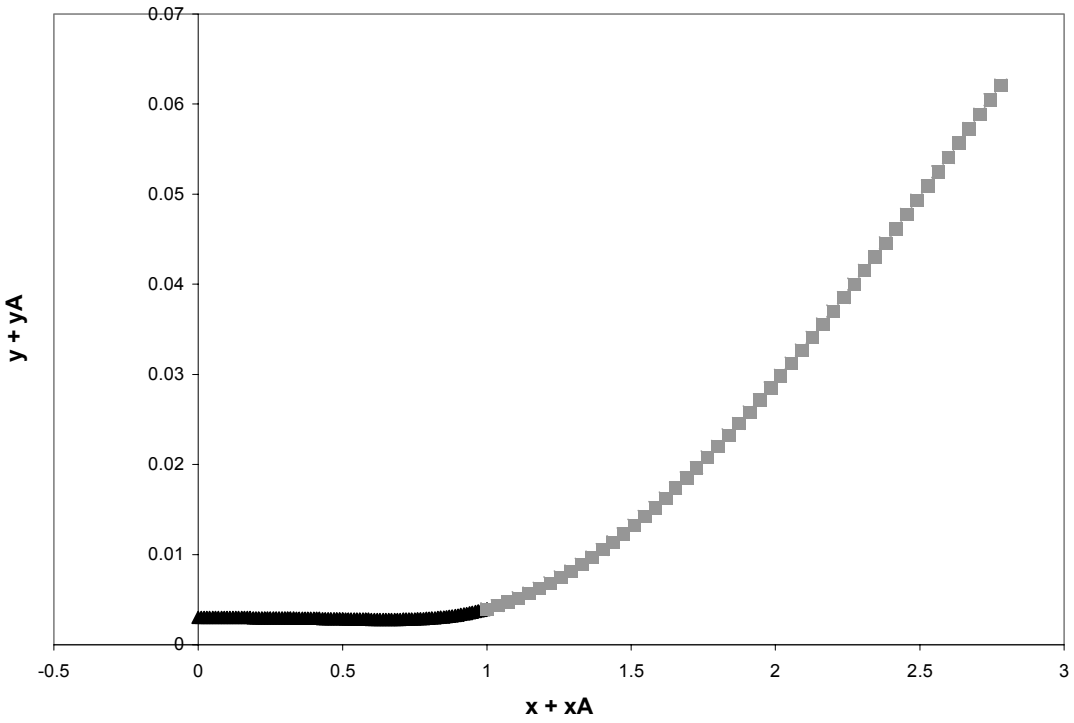

Figure 5.9: Sample Output Shape Showing Components From Model 1 (in black) and Model 2 (in gray) Tape Backing Centerline Peeled at 135^{o} (Exaggerated Scale)

5.5. Conclusions

Models 1 and 2 are preliminary models for evaluating tape as it peels from a rigid surface. They allow for large rotations of the tape and consider rotations of the springs, as done previously in Chang (1960) and Lin et al. (2002). Furthermore, Models 1 and 2 feature a finite length of the attached tape. The shooting method was applied to differential equations developed from geometry, the properties of the elastica, and equilibrium. Evaluation with the shooting method proved difficult because of the "if" statements to prevent the tape from penetrating into the rigid foundation. Nevertheless, the models successfully depict the shape of the tape during peeling and execute between the angles of 45 and 165 degrees. Between 45 and 165 degrees, the peel force decreases with increasing angle to 95 degrees, and then increases with angle increase, if a constant maximum adhesive strain is assumed. In addition, fixing a higher adhesive strain in the models causes an increase in peel force for all angles. Experiments often show the minimum peel force occurring at higher peel angles (e.g., 120 to 150 degrees).

In the next chapter, a final model will be presented. This model analyzes the skin surface during peeling and includes an unattached portion of tape as in Model 2.

Chapter 6. Model of Skin During Peeling

6.0 Introduction

The final model presented in detail simulates the skin response during peeling. The model formulation and results are explained in this chapter.

6.1. Assumptions and Formulation of Model 11

Model 11 involves the skin surface and a piece of tape attached to the skin. Not all of the tape is attached to the skin. The unattached end of the tape is clamped and pulled at some angle for peeling. As the tape is pulled, the skin lifts up. The skin and the tape are modeled together. The tape is assumed to be inextensible and the skin has no slackness. Springs are incorporated into the model to mimic skin behavior. There are two linear springs resisting the peel. The equations presented were derived by Professor Raymond H. Plaut, and the numerical analysis was performed as part of the research for this thesis.

Figures 6.1 and 6.2 display the system for Model 11. Figure 6.1 shows the skin and tape before the peeling begins. Figure 6.2 shows the new layout after peeling. Coordinates, angles, force, moment, and spring constants are labeled. There are three sets of coordinates, as each side is analyzed separately and then combined to form a final shape. The variables S_1, S_2, S_3 are the arc lengths for each coordinate system, θ_1, θ_2, θ_3 are the rotations along the arc lengths, and K_2, K_3 are the spring constants. Also,

L is the length of the skin attached to tape;

D is the length of the tape unattached to skin;

R is the length of the skin unattached to tape;

E_1 is the modulus of elasticity of the tape and skin as a composite;

I_1 is the moment of inertia of the tape and skin as a composite;

E_2 is the modulus of elasticity of the skin only;

I_2 is the moment of inertia of the skin only;

E_3 is the modulus of elasticity of the tape only;

I_3 is the moment of inertia of the tape only;

M_o is the moment exerted on the tape end by the clamp;

F_o is the force applied to peel the tape;

θ_o is the angle of the applied force with respect to the skin.

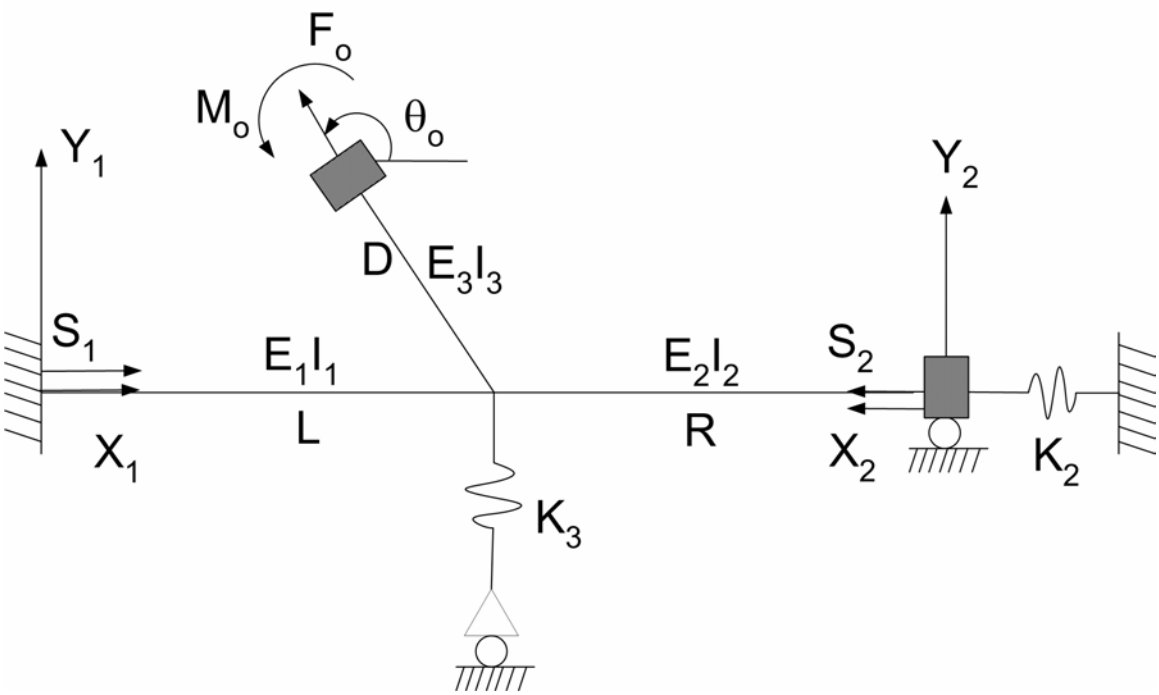

Figure 6.1: Skin and Tape Orientation Before Peeling Starts

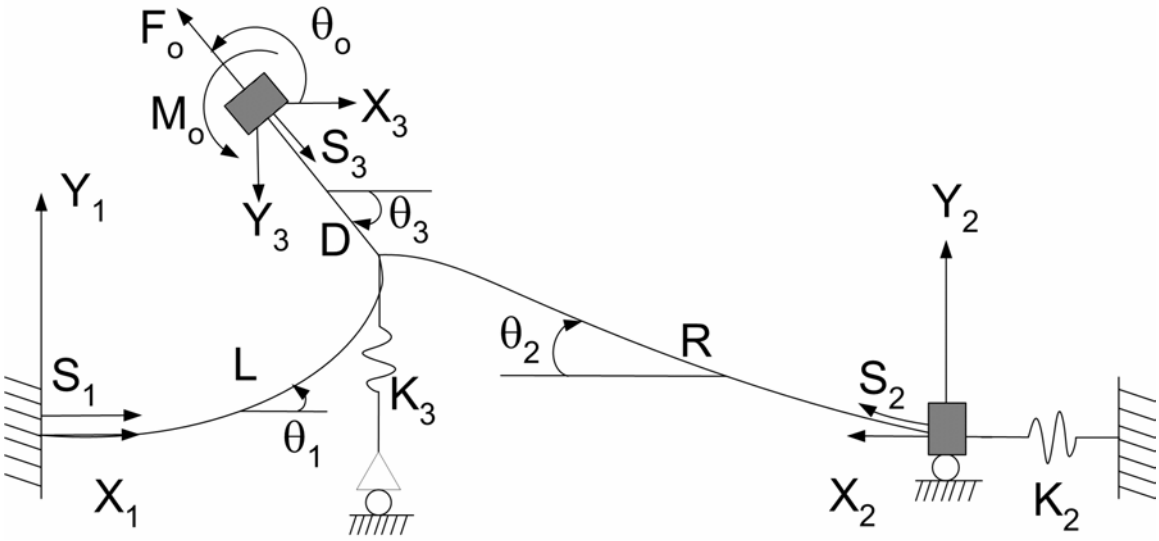

Figure 6.2: Skin and Tape Orientation After Peeling Starts

First, we separate each component in its coordinate system and apply principles of geometry, beam bending, and equilibrium. The variables P_1, P_2, P_3, are the horizontal force components and Q_1, Q_2, Q_3 are the vertical force components. These P and Q

variables do not depend on arc length. Figure 6.3 shows element 1, the skin and tape composite.

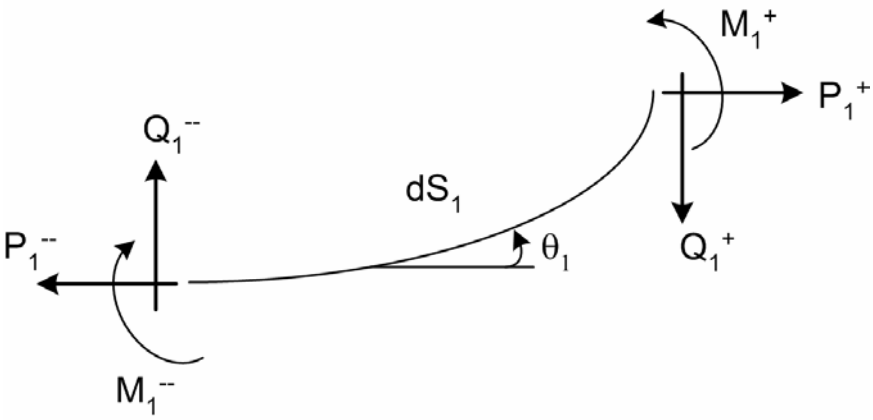

Figure 6.3: Free-body Diagram of Element 1 (Skin and Tape), dS_1, With Sign Convention for Forces and Moments

The equations from geometry, beam bending, and equilibrium are as follows:

$$\frac{dX_1}{dS_1} = \cos\theta_1 \tag{6.1}$$

$$\frac{dY_1}{dS_1} = \sin\theta_1 \tag{6.2}$$

$$E_1 I_1 \frac{d\theta_1}{dS_1} = M_1 \tag{6.3}$$

$$\frac{dM_1}{dS_1} = Q_1 \cos\theta_1 + P_1 \sin\theta_1 \tag{6.4}$$

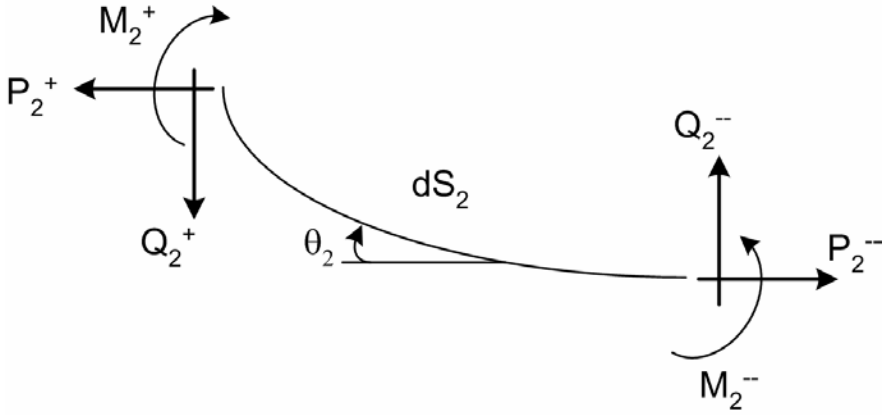

Figure 6.4: Free-body Diagram of Element 2 (Skin), dS_2, With Sign Convention for Forces and Moments

Figure 6.4 displays element 2, the skin only, and corresponding relations are:

$$\frac{dX_2}{dS_2} = \cos\theta_2 \tag{6.5}$$

$$\frac{dY_2}{dS_2} = \sin\theta_2 \tag{6.6}$$

$$E_2 I_2 \frac{d\theta_2}{dS_2} = M_2 \tag{6.7}$$

$$\frac{dM_2}{dS_2} = Q_2 \cos\theta_2 + P_2 \sin\theta_2 \tag{6.8}$$

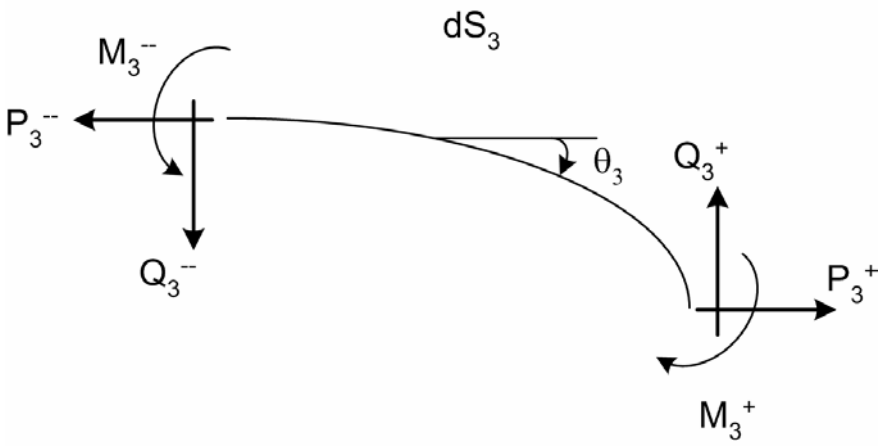

Figure 6.5: Free-body Diagram of Element 3 (Tape), dS_3, With Sign Convention for Forces and Moments

Figure 6.5 displays element 3, the tape only, and corresponding relations are:

$$\frac{dX_3}{dS_3} = \cos\theta_3 \tag{6.9}$$

$$\frac{dY_3}{dS_3} = \sin\theta_3 \tag{6.10}$$

$$E_3 I_3 \frac{d\theta_3}{dS_3} = M_3 \tag{6.11}$$

$$\frac{dM_3}{dS_3} = Q_3 \cos\theta_3 + P_3 \sin\theta_3 \tag{6.12}$$

Applying equilibrium at the peel front gives the following equations (see Figure 6.6):

$$M_1(L) = M_3(D) + M_2(R) \tag{6.13}$$

$$P_1 = P_2 - P_3 \tag{6.14}$$

$$Q_2 = Q_3 - Q_1 + K_3 Y_1(L) \tag{6.15}$$

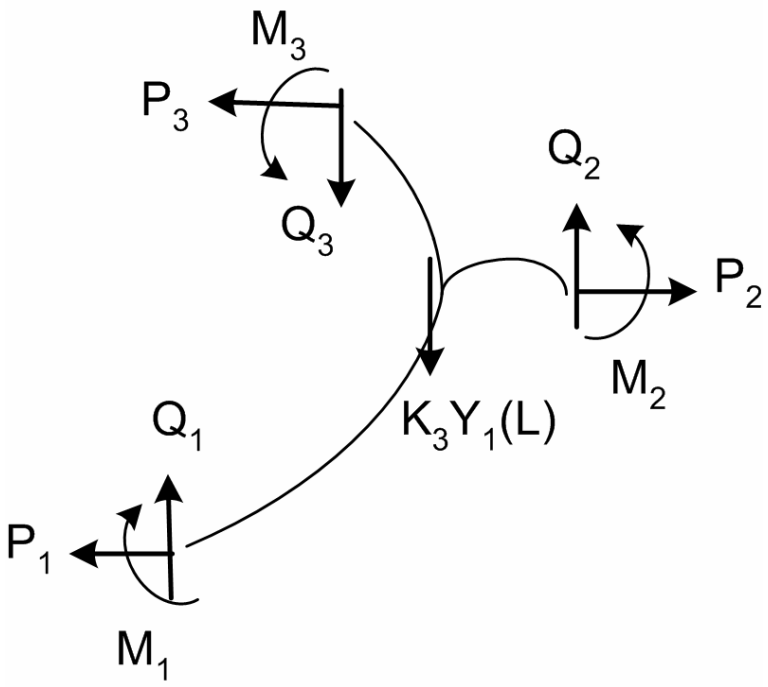

Figure 6.6: Free-body Diagram of All Elements Combined

Also from combining the elements and geometry we have:

$$\theta_2(R) = -\theta_1(L) \tag{6.16}$$

$$\theta_3(D) = \pi - \theta_1(L) \tag{6.17}$$

$$Y_2(R) = Y_1(L) \tag{6.18}$$

Applying equilibrium to the whole system is shown in Figure 6.7. The resulting equations used are:

$$P_1 = P_2 + F_o \cos\theta_o \tag{6.19}$$

$$Q_2 = -F_o \sin\theta_o - Q_1 + K_3 Y_1(L) \tag{6.20}$$

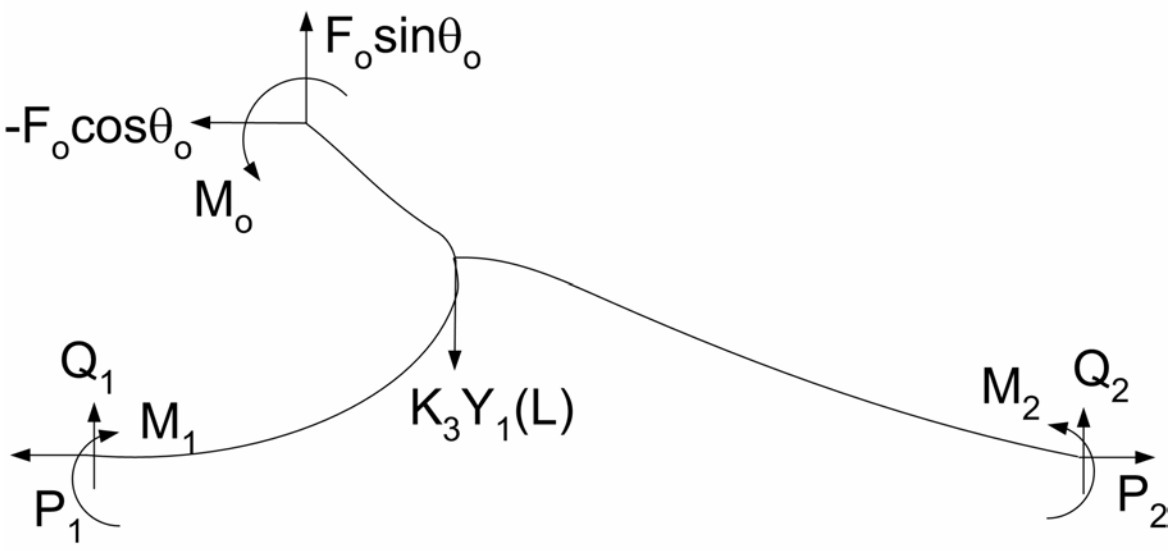

Figure 6.7: Free-body Diagram of Entire System

Comparing equations 6.14 and 6.15 with 6.19 and 6.20 produces:

$$P_3 = -F_o \cos\theta_o \tag{6.21}$$

$$Q_3 = -F_o \sin\theta_o \tag{6.22}$$

Also, equilibrium in the skin at the right spring yields:

$$P_2 = K_2\left[L + R - X_1(L) - X_2(R)\right] \tag{6.23}$$

To avoid using units on each quantity, the variables of the system are non-dimensionalized as follows (j = 1, 2, 3):

Lengths

$$x_j = \frac{X_j}{L},\ y_j = \frac{Y_j}{L},\ s_j = \frac{S_j}{L},\ r = \frac{R}{L},\ d = \frac{D}{L} \tag{6.24-6.28}$$

Forces

$$f_o = \frac{F_o L^2}{E_1 I_1},\ p_j = \frac{P_j L^2}{E_1 I_1},\ q_j = \frac{Q_j L^2}{E_1 I_1} \tag{6.29-6.31}$$

Moments

$$m_o = \frac{M_o L}{E_1 I_1},\ m_j = \frac{M_j L}{E_1 I_1} \tag{6.32-6.33}$$

Stiffness and Spring Constants

$$\eta_1 = \frac{E_1 I_1}{E_1 I_1} = 1, \;\; \eta_2 = \frac{E_2 I_2}{E_1 I_1}, \;\; \eta_3 = \frac{E_3 I_3}{E_1 I_1}, \;\; k_j = \frac{K_j L^3}{E_1 I_1} \tag{6.34-6.37}$$

After nondimensionalizing each variable, the differential equations for the model become:

$$\frac{dx_j}{ds_j} = \cos\theta_j \tag{6.38}$$

$$\frac{dy_j}{ds_j} = \sin\theta_j \tag{6.39}$$

$$\frac{d\theta_j}{ds_j} = \frac{m_j}{\eta_j} \tag{6.40}$$

$$\frac{dm_j}{ds_j} = q_j \cos\theta_j + p_j \sin\theta_j \tag{6.41}$$

Furthermore, equations 6.19, 6.21, and 6.22 allow replacing the following variables as follows:

$$p_3 = -f_o \cos\theta_o \tag{6.42}$$

$$q_3 = -f_o \sin\theta_o \tag{6.43}$$

$$p_1 = p_2 + f_o \cos\theta_o \tag{6.44}$$

The arc lengths s_2 and s_3 are scaled so that a single arc length s, $0 < s < 1$ is used in the numerical solution:

$$s_1 = s \tag{6.45}$$

$$s_2 = sr \tag{6.46}$$

$$s_3 = sd \tag{6.47}$$

The shooting conditions are taken from equations 6.13, 6.15, 6.16, 6.17, 6.18, and 6.20. After substitution and nondimensionalization, the shooting conditions are:

$$m_1 = m_3 + m_2 \tag{6.48}$$

$$k_3 y_1(1) = q_2 + q_1 + f_o \sin\theta_o \tag{6.49}$$

$$\theta_2(r) = -\theta_1(1) \tag{6.50}$$

$$\theta_1(1) + \theta_3(d) = \pi \tag{6.51}$$

$$y_1(1) = y_2(r) \tag{6.52}$$

$$k_2\left[1 + r - x_1(1) - x_2(r)\right] = p_2 \tag{6.53}$$

6.2. Numerical Solution

The boundary conditions for the skin and tape's behavior during peeling consist of the following:

At s = 0: $x_1 = 0,\ y_1 = 0,\ \theta_1 = 0,\ m_1 = m_1$ (unknown),

$x_2 = 0,\ y_2 = 0,\ \theta_2 = 0,\ m_2 = m_2$ (unknown),

$x_3 = 0,\ y_3 = 0,\ \theta_3 = \pi - \theta_o,\ m_3 = m_3$ (unknown)

At s = 1: see equations 6.48-6.53

These conditions govern the skin and tape position. The skin is fixed at both ends and the tape is clamped at its unattached end. Forces and moments within the system satisfy equilibrium.

The shooting method solves the differential equations using the boundary conditions and input values from the user. Values of q_1, p_2, q_2, m_1, m_2, and m_3 are returned and then set for the rest of the program. A sample output shape produced by the program is shown in Figure 6.8. The shape shows all three components of the system combined. The inputs to the program that were used to achieve this result include the following:

$f_o = 1$, $\theta_o = 90^o$, r = 1, d = 1, $\eta_2 = 0.1$, $\eta_3 = 0.9$, $k_2 = 1$, $k_3 = 1$, $gq_1 = 0.3$, $gp_2 = 0.12$, $gq_2 = -0.78$, $gm_1 = 0.47$, $gm_2 = 0.28$, $gm_3 = 0.75$. The variables gq_1, gp_2, gq_2, gm_1, gm_2, and gm_3 are guesses that the program uses to begin the shooting method. The Mathematica program code for Model 11 is located in Appendix E.

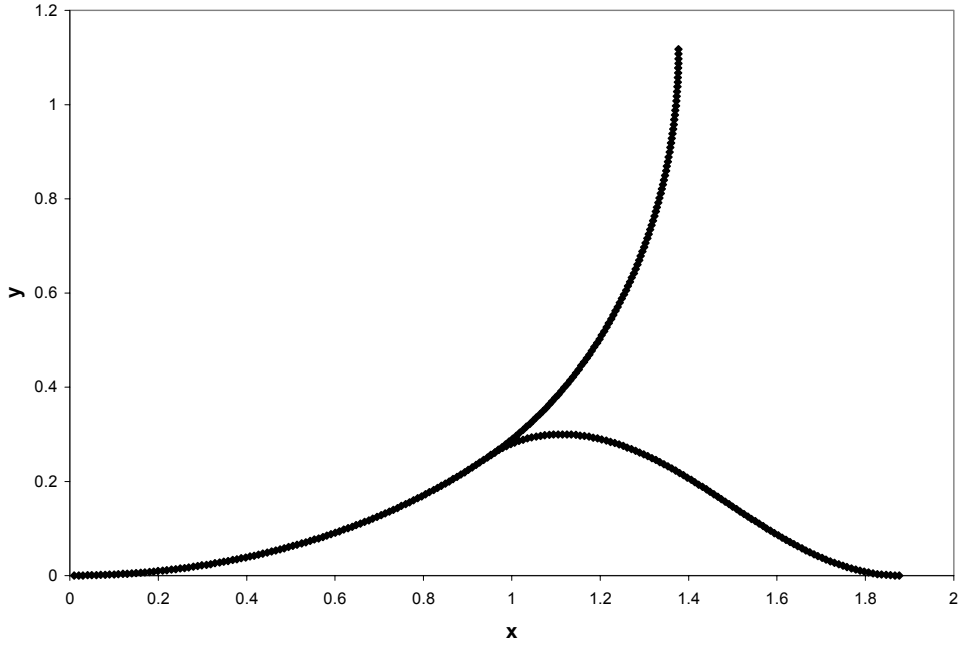

Figure 6.8: Sample Output Shape From Model 11 With 90-degree Peel (Slightly Exaggerated Scale)

6.3. Adjusting Input Parameters

The goal of this research is to closely simulate the tape and skin behavior. Pictures taken of a 90-degree peel on skin show the unattached Durapore™ tape as very straight. Also, the skin makes a "tent" shape with a pointy interface at the peel front. Figure 6.9 shows peeling from human skin at a 90-degree angle. In order to improve the model, various program inputs were adjusted. The values of η_2 and η_3, were varied to straighten the free end of tape. After varying the values of η_2 and η_3, it was apparent that η_3 has to be smaller than η_2. Also, k_2 and k_3 were decreased and f_o was increased in an attempt to produce a "tent" shape and possibly a higher y value. However, adjusting k_2 and k_3 did not make the model look more realistic, and higher values of f_o caused convergence difficulties in the program. Figure 6.10 shows the improved output shape with the straightened tape. For this example, the input values were: $f_o = 5$, $\theta_o = 90^o$, r = 1, d = 1, $\eta_2 = 0.05$, $\eta_3 = 0.005$, $k_2 = 0.01$, $k_3 = 0$, $gq_1 = -3.5$, $gp_2 = 0.002$, $gq_2 = -0.05$, $gm_1 = 1.6$, $gm_2 = 0.2$, $gm_3 = 6.3*10\text{^}-15$.

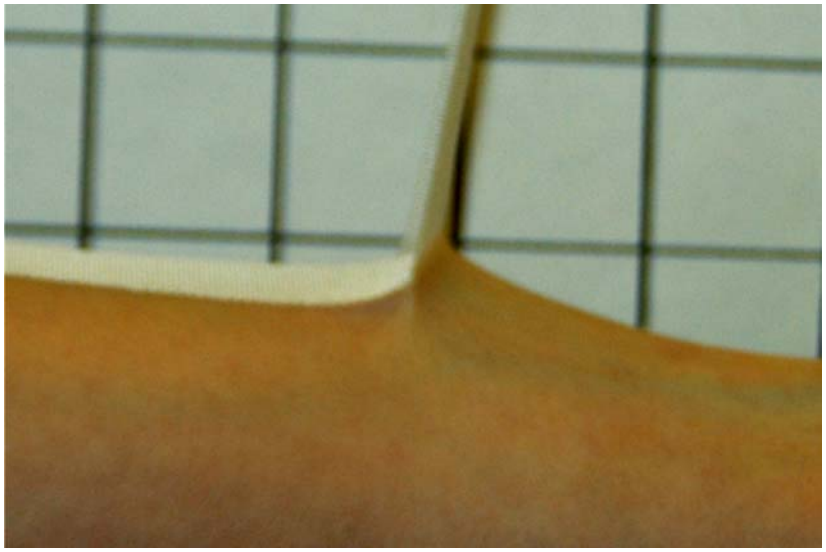

Figure 6.9: Peeling at Approximately 90 degrees

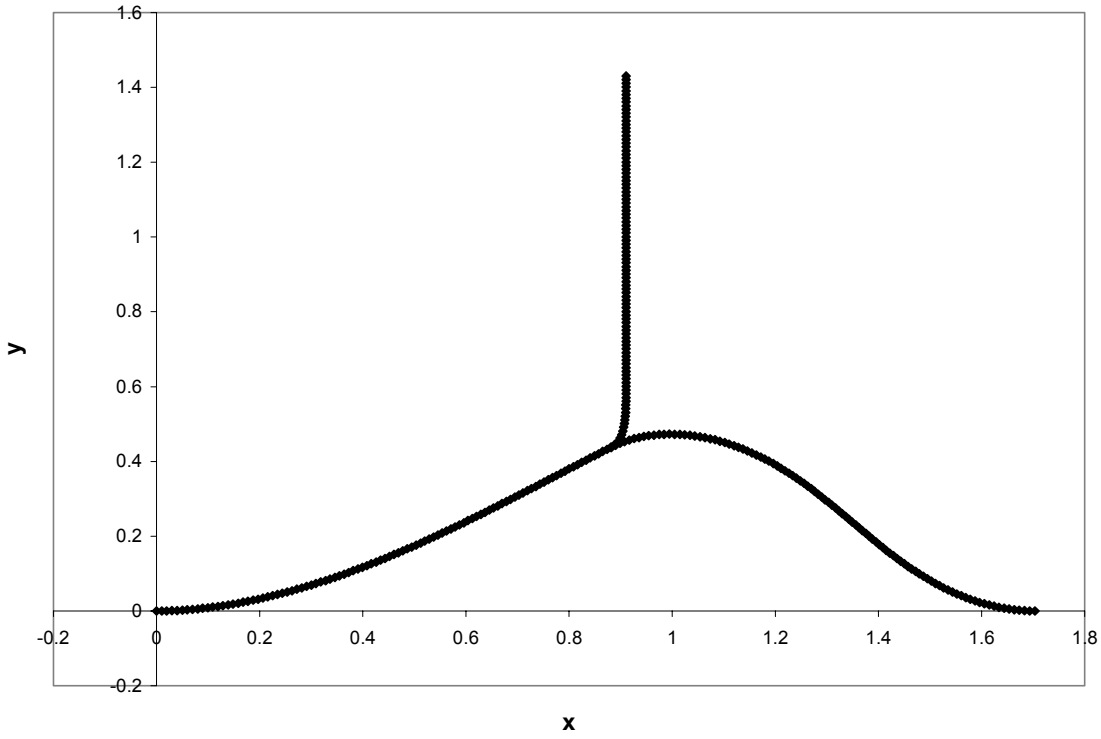

Figure 6.10: Improved Output Shape With Straight Free End of Tape During 90-degree Peel (Slightly Exaggerated Scale)

6.4. Examining Displacement of the Tape End

Once the tape was pulling straight in the model, the displacement of the tape was examined. The model was run at applied forces between zero and five and the

displacement of the free end of the tape was computed. Figure 6.11 shows results from changing the applied force. The inputs that were held constant were: $\theta_o = 90^o$, r = 1, d = 1, $\eta_2 = 0.05$, $\eta_3 = 0.005$, $k_2 = 0.01$, $k_3 = 0$, $gq_1 = -3.5$, $gp_2 = 0.002$, $gq_2 = -0.05$, $gm_1 = 1.6$, $gm_2 = 0.2$, $gm_3 = 6.3*10\text{^}-15$. Although the force was only increased to a value of five, it is evident that the displacement of the free end of the tape increases as force increases. Also, as the force increases continuously by one, the displacement of the free end of the tape increases by smaller and smaller amounts, giving the graph a parabolic appearance. The graph resembles a peel test plot that exhibits initial curvature in Figure 6.12.

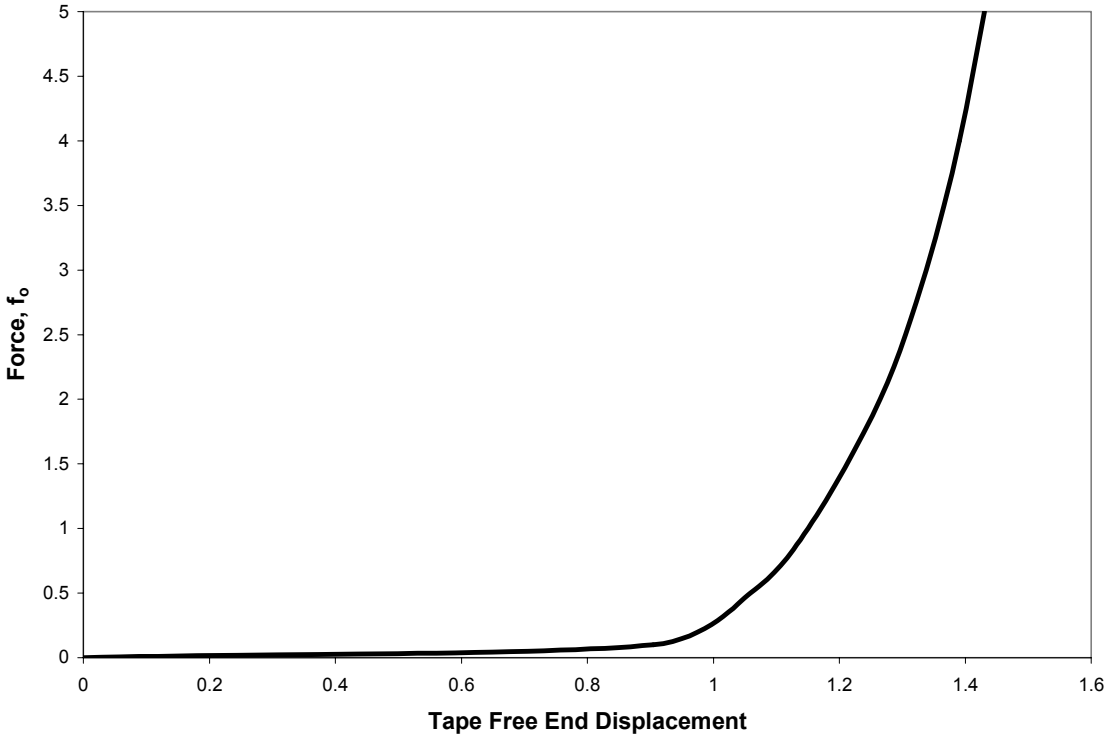

Figure 6.11: Force Versus Tape Free End Displacement for 90-degree Peel

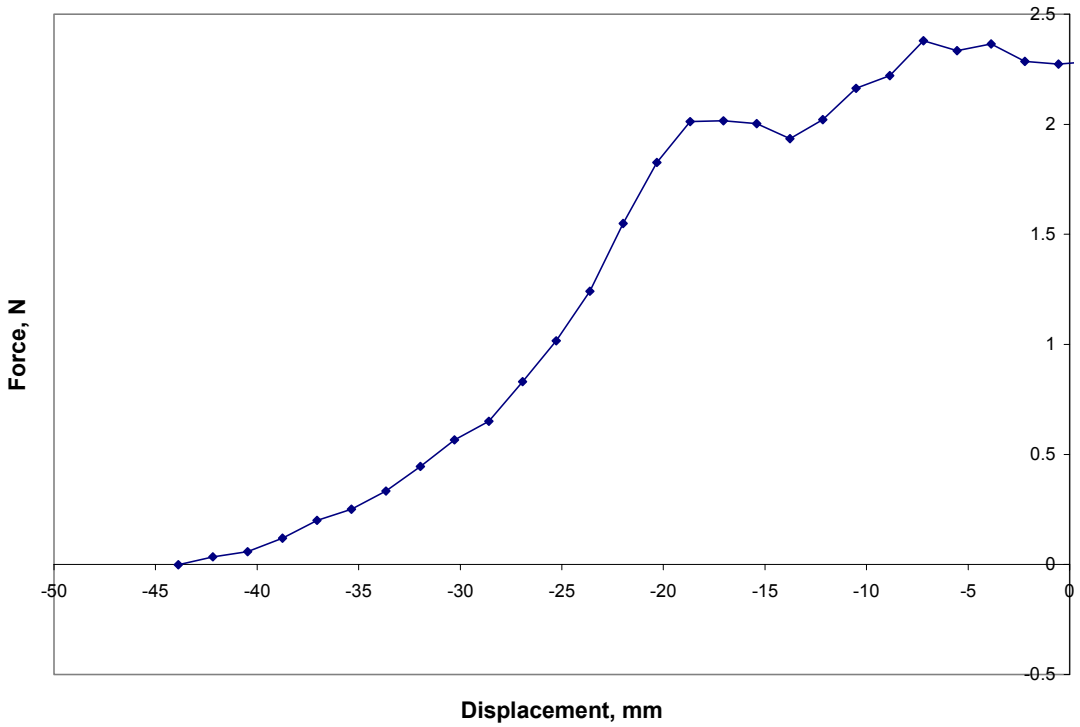

Figure 6.12: Force Versus Displacement Showing Initial Curvature for 180-degree Peel on Subject D at 1000 mm/min

In addition to 90 degrees, the tape end displacement was evaluated for peel angles of 120 and 150 degrees. The displacements increased by about 0.04 for the 120-degree case and approximately 0.16 for the 150-degree case.

6.5. Changing The Angle of Peel

The angle of the force applied to the tape (θ_o), or the peel angle, was changed to see if Model 11 would accurately depict the tape's behavior at angles other than 90 degrees. The peel angles tested during experimental peel tests for this thesis were 90, 120, 150, and 180 degrees. Therefore, Model 11 was next evaluated at 120, 150, and 180 degrees. Figure 6.12 shows the 90, 120, and 150 degree cases together. The inputs held constant at each angle were: $f_o = 5$, $r = 1$, $d = 1$, $\eta_2 = 0.05$, $\eta_3 = 0.005$, $k_2 = 0.01$, $k_3 = 0$, $gq_1 = -3.5$, $gp_2 = 0.002$, $gq_2 = -0.05$, $gm_1 = 1.6$, $gm_2 = 0.2$, $gm_3 = 6.3*10\text{^}-15$. These inputs are the same as those for Figure 6.10. The 180-degree peel case did not produce a logical result with Model 11. The tape showed curvature toward the left side of the graph instead of remaining straight as in the 90-, 120-, and 150-degree peel cases.

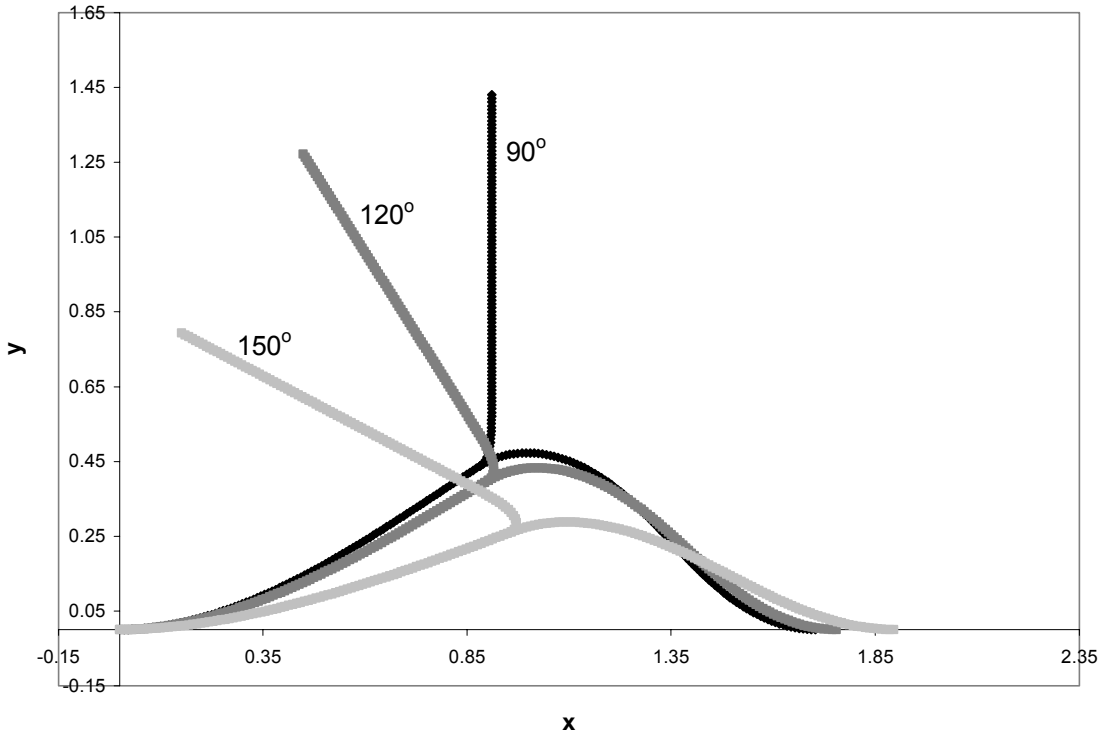

Figure 6.13: Model 11 Output Shapes for 90, 120, and 150-degree Peels

Figure 6.13 proves useful when comparing the model with the actual skin behavior. Figures 6.14 and 6.15 show photos of the skin peeled at 120 and 150 degrees for comparison with Figure 6.13. Model 11 does not accurately portray the skin, but does represent the tape behavior well. The tape pulls straight and matches the angles closely in Figures 6.14 and 6.15.

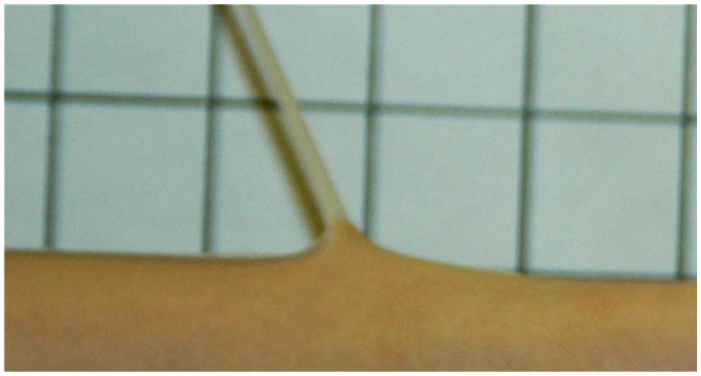

Figure 6.14: Peeling at Approximately 120 degrees

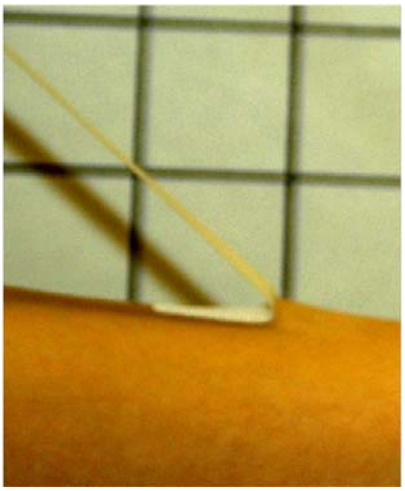

Figure 6.15: Peeling at Approximately 150 degrees

6.6. Evaluating Debonding Moment, Normal Force, and Net Tangential Shear Force

Debonding moment, normal force, and net tangential shear force are the main quantities that were analyzed with this model. The debonding moment is defined here as the resultant moment trying to separate the free portion of the tape from the skin at the peel front. Figure 6.16 provides a visual representation of the debonding moment. Also, the following equation presents the relationship:

$$m_d = m_3(1) - m_2(1) \tag{6.54}$$

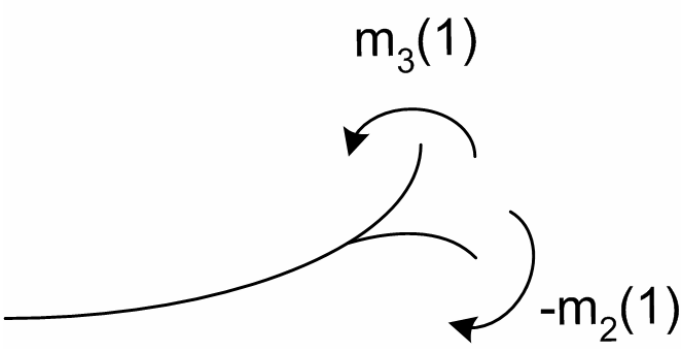

Figure 6.16: Debonding Moment, m_d

The normal force is defined here as the net force components in the tape and the unattached skin that acts normal to the tape and skin at the peel front. Equation 6.55 and Figure 6.17 depict this quantity:

$$f_n = f_{n1} + f_{n2} = f_o \sin[\theta_o - \theta_1(1)] + p_2 \sin[\theta_1(1)] - q_2 \cos[\theta_1(1)] \tag{6.55}$$

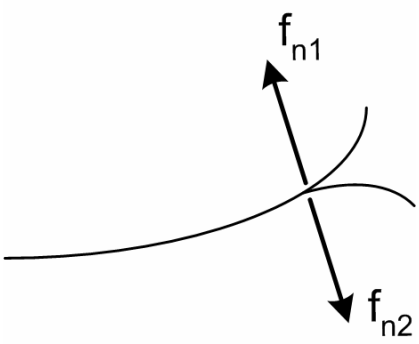

Figure 6.17: Normal Force, f_n

The net tangential shear force is defined here as the difference between the tangential force components in the tape and the skin at the peel front. Equation 6.56 and Figure 6.18 display the net tangential shear force:

$$f_t = -p_2 \cos[\theta_1(1)] - q_2 \sin[\theta_1(1)] + f_o \cos[\theta_o - \theta_1(1)] \tag{6.56}$$

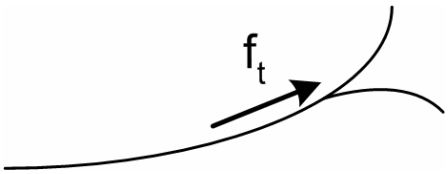

Figure 6.18: Net Tangential Shear Force, f_t

Model 11 was run at various values of applied force, f_o, and debonding moment, normal force, and net tangential shear force were recorded. The inputs held constant for the evaluation were: $\theta_o = 90^o$, r = 1, d = 1, $\eta_2 = 0.05$, $\eta_3 = 0.005$, $k_2 = 0.01$, $k_3 = 0$, gq_1 = -3.5, $gp_2 = 0.002$, $gq_2 = -0.05$, $gm_1 = 1.6$, $gm_2 = 0.2$, $gm_3 = 6.3*10\text{^}-15$. Figures 6.19-6.21 show the resulting trends of each value for the 90-, 120-, and 150-degree peel, respectively. The applied force, f_o, was only increased to five because the program would not converge when f_o exceeded five. The debonding moment, m_d, varied slightly and the normal force, f_n, varied the most. Also, Figures 6.19-6.21 show that the force normal to the skin is larger than the net tangential shear force during peeling. Overall, all three of these quantities increased with an increase in applied force for the 90- and 120-degree angles. On the other hand, the 150-degree case showed that only debonding moment and normal force increased with an increase in applied force and the net tangential shear force decreased with an increase in applied force. Therefore, debonding of the tape from the skin will depend on these quantities.

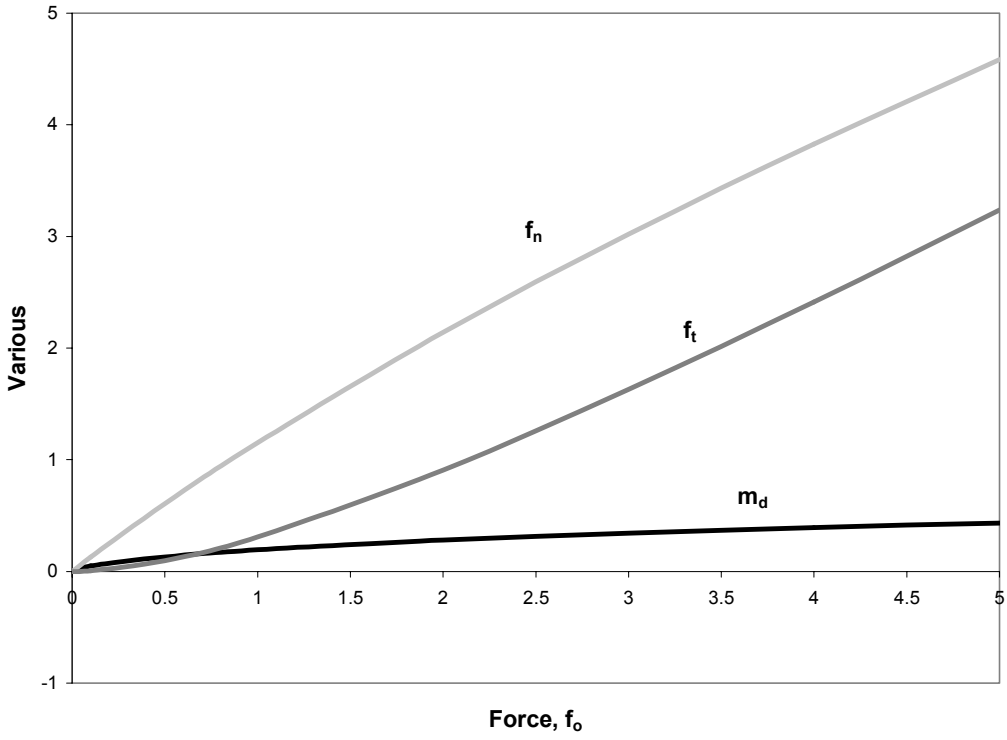

Figure 6.19: f_n, f_t, and m_d Versus Force for 90-degree Peel

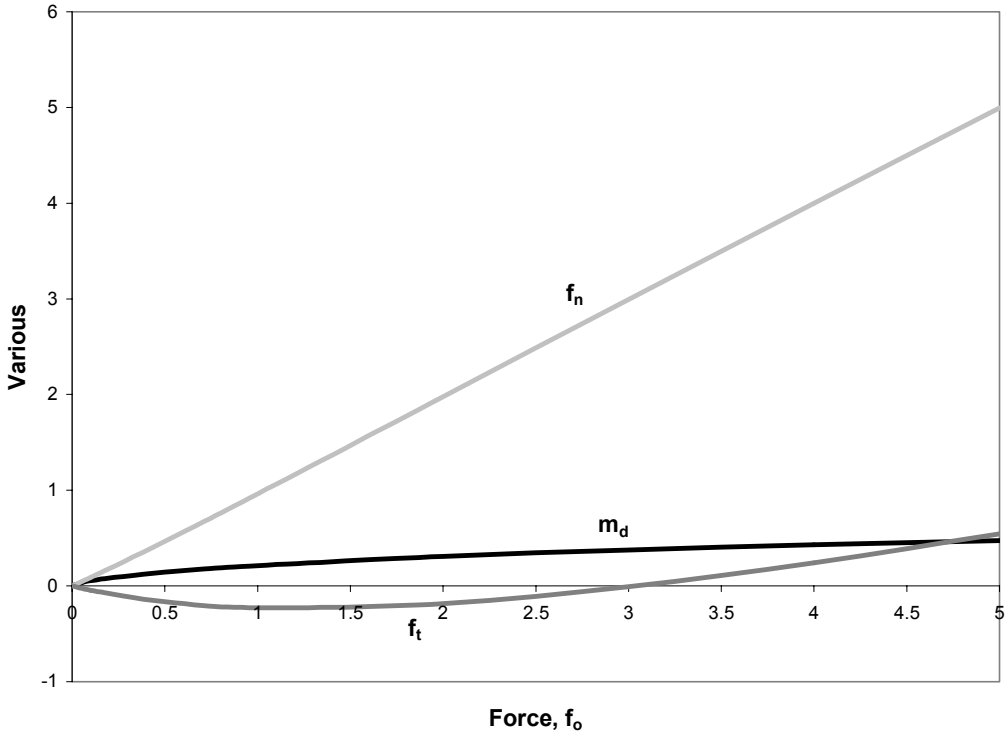

Figure 6.20: f_n, f_t, and m_d Versus Force for 120-degree Peel

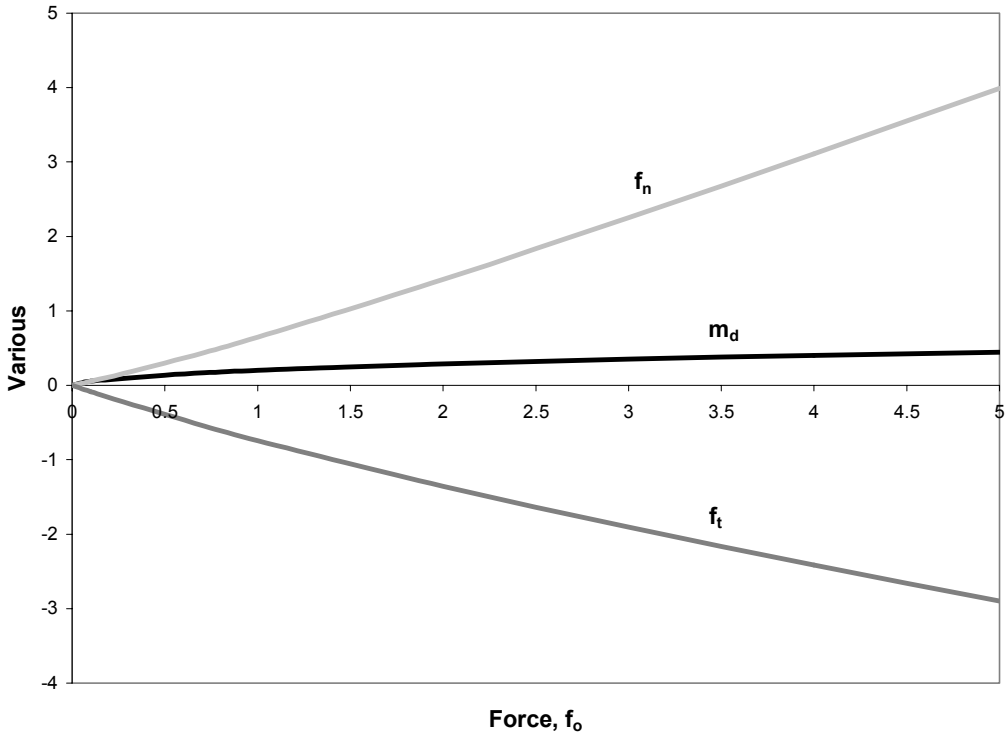

Figure 6.21: f_n, f_t, and m_d Versus Force for 150-degree Peel

6.7. Final Modification to Match Skin

One last attempt was made to make Model 11 match the skin's behavior. The two conditions on the continuity of slopes at the peel front were replaced by plastic hinges. The plastic hinges were placed at the end of the free portion of tape that meets the skin and the end of the right-hand skin portion that meets the tape. Two plastic moments were added as inputs into the program, one for the skin (ms) and one for the tape (mt). A sample output shape after the modification is shown in Figure 6.22. This shape more closely matches a "tent" shape and the skin's behavior as shown in Figure 6.14.

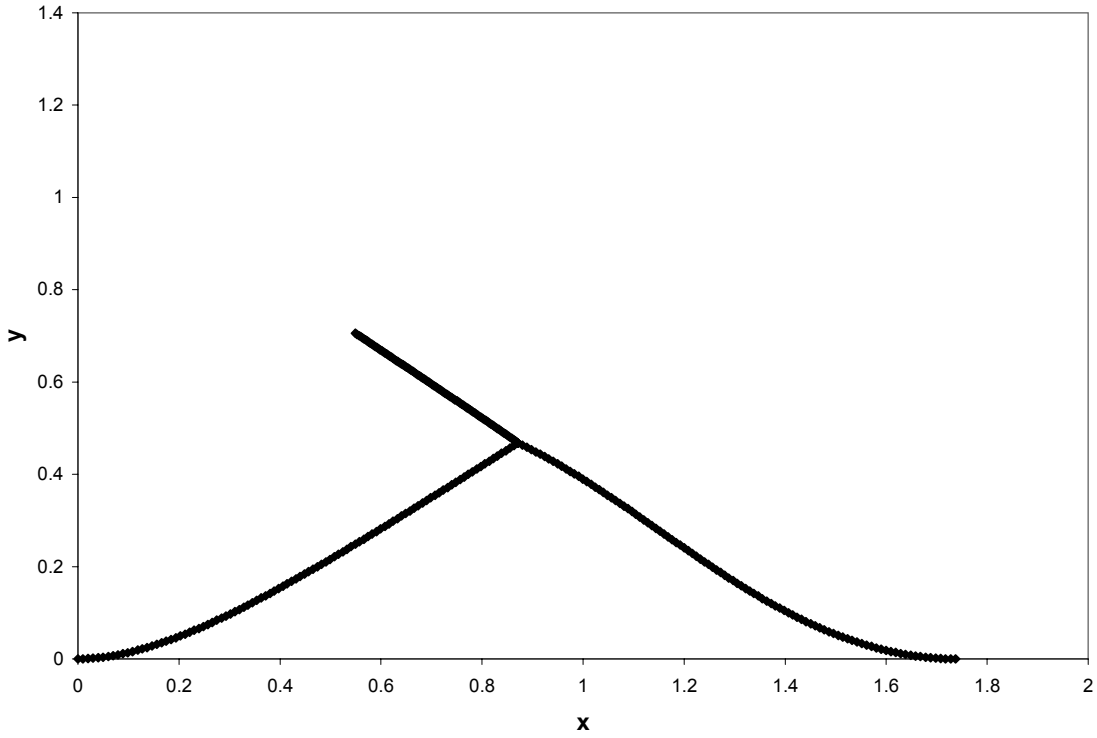

Figure 6.22: Improved Output Shape With "Tent" Shaped Skin

6.8. Conclusions

Model 11 analyzes peeling tape from a skin surface using differential equations based on geometry and equilibrium, and the shooting method. The model was found to depict the skin and tape correctly during peeling in part. The skin takes the shape of a round bump in Model 11 as opposed to a "tent-like" shape that is seen in experimental peel tests. Attempts at creating the "tent-like" shape were only successful when adding plastic hinges at the peel front. Moreover, the tape was pulled straight as in an experiment with modification of input parameters. When the tape was made straight, the model's tape matched experimental peel tests at peel angles of 90, 120, and 150 degrees. Furthermore, the displacement of the free end of the tape, debonding moment, normal force, and net tangential shear force at the peel front were also evaluated with Model 11. All quantities increased with applied for 90-, 120-, and 150-degree angles except for net tangential shear force for the 150-degree case.

Model 11 completes the research for this thesis. The final chapter will provide conclusions and recommendations for further research.

Chapter 7. Conclusions and Recommendations for Further Research

7.0 Summary

Peeling from skin requires careful study of skin and adhesives. To increase knowledge of skin and adhesive behavior, experimental peel tests were performed on the arms of human subjects. Also, a few rigid substrates were tested. Angles, rates, dwell times, testing machines, and subjects were varied in the study. In addition to the experimental work, mathematical models were developed using experimental results and principles of mechanics. The mathematical models represented peeling tape from rigid substrates, plucking skin, and peeling tape from skin. The goal of the study was to model peeling tape from skin, and the final model was the most promising in terms of simulating peeling tape from skin.

7.1. Conclusions

The first round of experiments offered a variety of results. First of all, 90-, 120-, 150-, and 180-degree peel tests showed no major correlation between peel force and rate at which the tape was peeled. In general, the force required to peel the tape from the skin ranged between about 0.4 N and 3.0 N for a 2.54-cm-wide Durapore™ tape. The oldest subject, Subject D, typically experienced the highest peel forces. Moreover, the longer the dwell time of tape on the skin, the higher the peel force. Furthermore, a 150-degree angle causes the lowest peel force compared with 90-, 120-, and 180- degree angles of peel.

The second round of experiments explored peeling at higher speeds. The required peel force for peeling at 180 degrees ranged between about 0.7 N and 3.6 N for a 2.54-cm-wide Durapore™ tape. Again, the oldest subject, Subject D, had the largest peel forces. Repeated peeling from the skin caused higher peel forces, and different body sites yielded different peel force values. In addition, the skin required a lower peel force than a rigid substrate, such as steel.

Results from both sets of experiments show that peel force will most likely be under 3.6 N for the tape used in this study. The peel force value is proportional to tape width based on comparison with previous unpublished research performed by Rachel Roop. Also, older subjects may experience larger peel forces than younger subjects.

Lastly, testing on a different testing machine and changing orientation of the arm with respect to gravity may cause variations in results.

The mathematical models showed that modeling the skin can be very difficult. The rigid substrate models (Models 1 and 2) and the final model (Model 11) provided the most meaningful results. Models 1 and 2 showed an increase in peel force for all angles with higher critical adhesive strain. Models 1 and 2 also showed a trend between force and peel angle that conflicted with previous experimental work. Model 11 successfully depicted tape and skin behavior after numerous modifications to the original program. In addition, the model simulated the tape's behavior at peel angles of 90, 120, and 150 degrees. Additionally, Model 11 showed how the displacement of the free end of the tape, the peel front debonding moment, the peel front normal force, and the peel front net tangential force increased with greater applied force for a 90-degree peel angle.

7.2. Recommendations for Further Research

Further study on skin and adhesives during peeling should involve more experiments. Peel tests could be run on a broader range of subjects in terms of gender and age. Also, experiments could test some additional brands, sizes, and types of tape. Since the experiments in this thesis tended to show an influence of testing order and frequency, it would be good to test the area of skin no more than three times once a week.

Researchers trying to model skin might try a new method or computer program. The shooting method tended to experience convergence problems with many of the models mentioned and its operation was slow at times. Also, researchers might develop new model formulations, improving the models presented in this thesis. Models 1, 2, and 11 provide a base and could be improved further.

In conclusion, testing and modeling skin could improve scientists' understanding of skin behavior. A computer program developed from skin models would be useful in predicting skin and/or tape behavior, and assist in producing commercially-sold skin adhesives that would cause less trauma when peeled off the skin.

References

Agache, P. G. (1995). "Twistometry Measurement of Skin Elasticity." *Handbook of Non-Invasive Methods and the Skin*, J. Serup and G. B. E. Jemec, eds., CRC Press, Boca Raton, Florida, pp. 319-328.

Alexander, H. and Cook, T. H. (1977). "Accounting for Natural Tension in the Mechanical Testing of Human Skin." *Journal of Investigative Dermatology*, Vol. 69, pp. 310-314.

Andrews, E. H., Khan, T. A., and Majid, H. A. (1985). "Adhesion to Skin, Part 1: Peel Tests with Hard and Soft Machines." *Journal of Materials Science*, Vol. 20, pp. 3621-3630.

Andrews, E. H., Khan, T. A., and Lockington, N. A. (1987). "Adhesion to Skin, Part 2: Measurement of Interfacial Energies for Pressure Sensitive Adhesives." *Journal of Materials Science*, Vol. 22, pp. 2833-2841.

Andrews, E. H., Khan, T. A., Drew, P., and Rance, R. (1990). "Design of Pressure-Sensitive Adhesives." *Journal of Applied Polymer Science*, Vol. 41, pp. 595-611.

Aubert, L., Anthoine, P., De Rigal, J., and Léveque, J.-L. (1985). "An *In Vivo* Assessment of the Biomechanical Properties of Cosmetic Products." *International Journal of Cosmetic Science*, Vol. 7, pp. 51-59.

Aubrey, D. W. (1977). "Pressure-Sensitive Adhesives—Principles of Formulation." *Developments in Adhesives*, W. C. Wake, ed., Vol. 1, pp. 133-143.

Aubrey, D. W., Welding, G. N., and Wong, T. (1969). "Failure Mechanisms in Peeling of Pressure-Sensitive Adhesive Tape." *Journal of Applied Polymer Science*, Vol. 13, pp. 2193-2207.

Barel, A. O., Courage, W., and Clarys, P. (1995). "Suction Method for Measurement of Skin Mechanical Properties: The Cutometer." *Handbook of Non-Invasive Methods and the Skin*, J. Serup and G. B. E. Jemec, eds., CRC Press, Boca Raton, Florida, pp. 335-340.

Barel, A. O., Lambrecht, R., and Clarys, P. (1998). "Mechanical Function of the Skin: State of the Art." *Skin Bioengineering Techniques and Applications in Dermatology and Cosmetology*, Vol. 26, pp. 69-83.

Berndt, U. and Elsner, P. (2002). "Hardware and Measuring Principle: The Cutometer®." *Bioengineering of the Skin: Skin Biomechanics*, P. Elsner, E. Berardesca, K.-P. Wilhelm, and H. I. Maibach, eds., CRC Press, Boca Raton, Florida, pp. 91-97.

Bothwell, J. W. (1970). "Effects of Surgical Tapes on Skin." *Adhesion in Biological Systems*, R. S. Manly, ed., Academic Press, New York, 215-221.

References, Continued

Boyne, J. M., Millan, E. J., and Webster, I. (2001). "Peeling Performance of a Novel Light Switchable Pressure-Sensitive Adhesive." *International Journal of Adhesion and Adhesives*, Vol. 21, pp. 49-53.

Bundy, K., Schlegel, U., Rahn, B., Geret, V., and Perren, S. (2000). "An Improved Peel Test Method for Measurement of Adhesion to Biomaterials." *Journal of Materials Science: Materials in Medicine*, Vol. 11, pp. 517-521.

Chang, F. S. C. (1960). "The Peeling Force of Adhesive Joints." *Transactions of the Society of Rheology*, Vol. 4, pp. 75-89.

Chivers, R. A. (2001). "Easy Removal of Pressure Sensitive Adhesive for Skin Applications." *International Journal of Adhesion and Adhesives*, Vol. 21, pp. 381-388.

Coulthard, S. and Roop, R. (2002). Artificial Skin Foundation System for Use in Biomedical Pressure-Sensitive Adhesive Peel Testing. Technical Report, Department of Engineering Science and Mechanics, Virginia Tech, Blacksburg, Virginia.

Dahlquist, C. A. (1969). "Pressure-Sensitive Adhesives." Treatise on Adhesion and Adhesives, R. L. Patrick, ed., Marcel Dekker, New York, pp. 219-260.

Diridollou, S. et al. (1998). "An *in Vivo* Method for Measuring the Mechanical Properties of the Skin Using Ultrasound." *Ultrasound in Medicine and Biology*, Vol. 24, pp. 215-224.

Diridollou, S., Patat, F., Gens, F., Vaillant, L., Black, D., Lagarde, J. M., Gall, Y., and Berson, M. (2000). "*In Vivo* Model of the Mechanical Properties of the Human Skin under Suction." *Skin Research and Technology*, Vol. 6, pp. 214-221.

Dong, C., et al. (1993). "Development of a Device for Measuring Adherence of Skin Grafts to the Wound Surface." *Annals of Biomedical Engineering*, Vol. 21, pp. 51-55.

Douven, L. F. A., Meijer, R., and Oomens, C. W. J. (2000). "Characterisation of Mechanical Behaviour of Human Skin *In Vivo*." *Laser-Tissue Interaction XI: Photochemical, Photothermal, and Photomechanical*, D. D. Duncan, J. O. Hollinger, and S. L. Jacques, eds., Proceedings of the International Society for Optical Engineering, Vol. 3914, pp. 618-626.

Edwards, C. and Marks, R. (1995). "Evaluation of Biomechanical Properties of Human Skin." *Clinics in Dermatology*, Vol. 13, pp. 375-380.

Gniadecka, M. and Serup, J. (1995). "Suction Chamber Method for Measurement of Skin Mechanical Properties: The Dermaflex." *Handbook of Non-Invasive Methods and the Skin*, J. Serup and G. B. E. Jemec, eds., CRC Press, Boca Raton, Florida, pp. 329-334.

References, Continued

Graves, C. J. and Edwards, C. (2002). "Hardware and Measuring Principles: The Microindentometer." *Bioengineering of the Skin: Skin Biomechanics*, P. Elsner, E. Berardesca, K.-P. Wilhelm, and H. I. Maibach, eds., CRC Press, Boca Raton, Florida, pp. 161-178.

Horstmann, M., Müller, W., and Asmussen, B. (1999). "Principles of Skin Adhesion and Methods for Measuring Adhesion of Transdermal Systems." *Bioadhesive Drug Delivery Systems: Fundamentals, Novel Approaches, and Development*, E. Mathiowitz, D. E. Chickering III, and C.-M. Lehr, eds., Marcel Dekker, New York, pp. 175-195.

Kaelble, D. H. (1960). "Theory and Analysis of Peel Adhesion: Bond Stresses and Distributions." *Transactions of the Society of Rheology*, Vol. 4, pp. 45-73.

Kaelble, D. H. (1999). "Theory and Analysis of Peel Adhesion." *Handbook of Pressure Sensitive Adhesive Technology*, D. Satas, ed., Satas and Associates, Warwick, Rhode Island, pp. 87-120.

Kaelble, D. H. and Ho, C. L. (1974). "Biaxial Bond Stress Analysis in Peeling." *Transactions of the Society of Rheology*, Vol. 18, pp. 219-235.

Kenney, J. F., Haddock, T. H., Sun, R. L., and Parreira, H. C. (1992). "Medical-Grade Acrylic Adhesives for Skin Contact." *Journal of Applied Polymer Science*, Vol. 45, pp. 355-361.

Ko, C. U. (1996). "Effect of Skin Penetration Enhancers in Transdermal Drug Delivery Adhesives on Skin Adhesion and Irritation." Proceedings of the 23rd International Symposium on Controlled Release of Bioactive Materials, pp. 281-282.

Lanir, Y. (1983). "Constitutive Equations for Fibrous Connective Tissues." *Journal of Biomechanics*, Vol. 16, pp. 1-12.

Lanir, Y. (1987). "Skin Mechanics." *Handbook of Bioengineering*, R. Skalak and S. Chien, eds., McGraw-Hill, New York, pp. 11.1-11.25.

Lin, Y. Y., Hui, C. Y., and Wang, Y. C. (2002). "Modeling the Failure of an Adhesive Layer in a Peel Test." *Journal of Polymer Science Part B*, Vol. 40, pp. 2277-2291.

Lucast, D. H., and Taylor, C. W. (1990). "Cross-Linked Acrylate Adhesives for Use on Skin." *TAPPI Journal*, Vol. 73, pp. 159-163.

Maillard-Salin, D. G., Bécourt, P., and Couarraze, G. (2000). "Physical Evaluation of a New Patch Made of a Progestomimetic in a Silicone Matrix." *International Journal of Pharmaceutics*, Vol. 199, pp. 29-38.

References, Continued

Manschot, J. F. M. and Brakkee, A. J. M. (1986). "The Measurement and Modelling of the Mechanical Properties of Human Skin *in Vivo*—II. The Model." *Journal of Biomechanics*, Vol. 19, pp. 517-521.

Matts, P. J. (2002). "Hardware and Measurement Principles: The Gas-Bearing Electrodynamometer and Linear Skin Rheometer." *Bioengineering of the Skin: Skin Biomechanics*, P. Elsner, E. Berardesca, K.-P. Wilhelm, and H. I. Maibach, eds., CRC Press, Boca Raton, Florida, pp. 99-109.

Mayrovitz, H. N., and Carta, S. G. (1996). "Laser-Doppler Imaging Assessment of Skin Hyperemia as an Indicator of Trauma After Adhesive Strip Removal." *Advances in Wound Care*, Vol. 9, pp. 38-42.

Oikarinen, A. and Knuutinen, A. (2002). "Mechanical Properties of Human Skin: Biochemical Aspects." *Bioengineering of the Skin: Skin Biomechanics*, P. Elsner, E. Berardesca, K.-P. Wilhelm, and H. I. Maibach, eds., CRC Press, Boca Raton, Florida, pp. 3-16.

Piérard, G. E., Nikkels-Tassoudji, N., and Piérard-Franchimont, C. (1995). "Influence of the Test Area on the Mechanical Properties of Skin." *Dermatology*, Vol. 191, pp. 9-15.

Pocius, A. V. (1997). *Adhesion and Adhesives Technology: an Introduction*. Hanser Publishers, New York.

Pugliese, P. T. and Potts, J. R. (2002). "Hardware and Measuring Principles: The Ballistometer." *Bioengineering of the Skin: Skin Biomechanics*, P. Elsner, E. Berardesca, K.-P. Wilhelm, and H. I. Maibach, eds., CRC Press, Boca Raton, Florida, pp. 147-159.

Rigal, J. (2002). "Hardware and Basic Principles of the Dermal Torque Meter." *Bioengineering of the Skin: Skin Biomechanics*, P. Elsner, E. Berardesca, K.-P. Wilhelm, and H. I. Maibach, eds., CRC Press, Boca Raton, Florida, pp. 63-76.

Rodrigues, L. (2001). "EEMCO Guidance to the *in Vivo* Assessment of Tensile Functional Properties of the Skin, Part 2: Instrumentation and Test Modes." *Skin Pharmacology and Applied Skin Physiology*, Vol. 14, pp. 52-67.

Romanelli, M. and Falanga, V. (2002). "Hardware and Measuring Principles: The Durometer." *Bioengineering of the Skin: Skin Biomechanics*, P. Elsner, E. Berardesca, K.-P. Wilhelm, and H. I. Maibach, eds., CRC Press, Boca Raton, Florida, pp. 139-145.

References, Continued

Roop, R. V., Plaut, R. H., Dillard, D. A., and Ohanehi, D. C. (2002). "Peeling Pressure-Sensitive Adhesive Tape From Initially-Slack Thin Solid Film." Proceedings of the 25th Annual Meeting of the Adhesion Society and the Second World Congress on Adhesion and Related Phenomena (WCARP-II). Orlando, Florida. February 10-14, Poster Presentations, pp. 129-131.

Satas, D. (1989). "Peel." *Handbook of Pressure-Sensitive Adhesive Technology*, Second Edition, D. Satas, ed., Van Nostrand Reinhold Co., New York.

Schiraldi, M. T. (1990). "Peel Adhesion of Tapes from Skin." The Proceedings of the Polymers, Laminations and Coatings Conference, Boston, Massachusetts, September 4-7, pp. 63-70.

Serup, J. (2002a). "Mechanical Properties of Human Skin: Elasticity Parameters and Their Relevance." *Bioengineering of the Skin: Skin Biomechanics*, P. Elsner, E. Berardesca, K.-P. Wilhelm, and H. I. Maibach, eds., CRC Press, Boca Raton, Florida, pp. 41-47.

Serup, J. (2002b). "Hardware and Measuring Principles: The Dermaflex A." *Bioengineering of the Skin: Skin Biomechanics*, P. Elsner, E. Berardesca, K.-P. Wilhelm, and H. I. Maibach, eds., CRC Press, Boca Raton, Florida, pp. 111-115.

Skeist, I., ed. (1990). "Pressure-Sensitive Adhesives for Tapes and Labels." *Handbook of Adhesives*, Third Edition, Van Nostrand Reinhold Co., New York.

Spencer, T. S., Smith, S. E., and Conjeevaram, S. (1990). "Adhesive Interactions Between Polymers and Skin in Transdermal Delivery Systems." *Polymeric Materials: Science and Engineering*, Vol. 63, American Chemical Society, Washington, DC, pp. 337-339.

Steven-Fountain, A. J., Atkins, A. G., Jeronimidis, G., Vincent, J. F. V., Farrar, D. F., and Chivers, R. A. (2002). "The Effect of Flexible Substrates on Pressure-Sensitive Adhesive Performance." *International Journal of Adhesion and Adhesives*, Vol. 22, pp. 423-430.

Thacker, J. G., Iachetta, F. A., Allaire, P. E., Edgerton, M. T., Rodeheaver, G. T., and Edlich, R. F. (1977). "*In Vivo* Extensometer for Measurement of the Biomechanical Properties of Human Skin." *Review of Scientific Instruments*, Vol. 48, pp. 181-185.

Van De Graaff, K. M. (2002). *Human Anatomy*, Sixth Edition, McGraw-Hill, New York.

Vescovo, P., Varchon, D., and Humbert, P. (2002). "*In Vivo* Tensile Tests on Human Skin: The Extensometers." *Bioengineering of the Skin: Skin Biomechanics*, P. Elsner, E. Berardesca, K.-P. Wilhelm, and H. I. Maibach, eds., CRC Press, Boca Raton, Florida, pp. 77-90.

References, Continued

Vogel, H. G. (2002). "Mechanical Properties of Human Skin: Animal Models." *Bioengineering of the Skin: Skin Biomechanics*, P. Elsner, E. Berardesca, K.-P. Wilhelm, and H. I. Maibach, eds., CRC Press, Boca Raton, Florida, pp. 17-39.

Webster, I. (1999). "The Development of a Pressure-Sensitive Adhesive for Trauma-Free Removal." *International Journal of Adhesion and Adhesives*, Vol. 19, pp. 29-34.

Williams, N. L. (2000). Elastic Analysis of the Loop Tack Test for Pressure Sensitive Adhesives. Master of Science Thesis, Department of Civil and Environmental Engineering, Virginia Tech, Blacksburg, Virginia.

Wolfram, S. (1996). *The Mathematica Book*, Third Edition. Wolfram Media, Champaign, Illinois.

Yarusso, D. J. (1999). "Quantifying the Relationship Between Peel and Rheology for Pressure Sensitive Adhesives." *Journal of Adhesion*, Vol. 70, pp. 299-320.

Young, C.-D., Wu, J.-R., and Tsou, T.-L. (1998). "High-Strength, Ultra-Thin and Fiber-Reinforced pHEMA Artificial Skin." Biomaterials, Vol. 19, pp. 1745-1752.

Appendix A

Tension Test Results

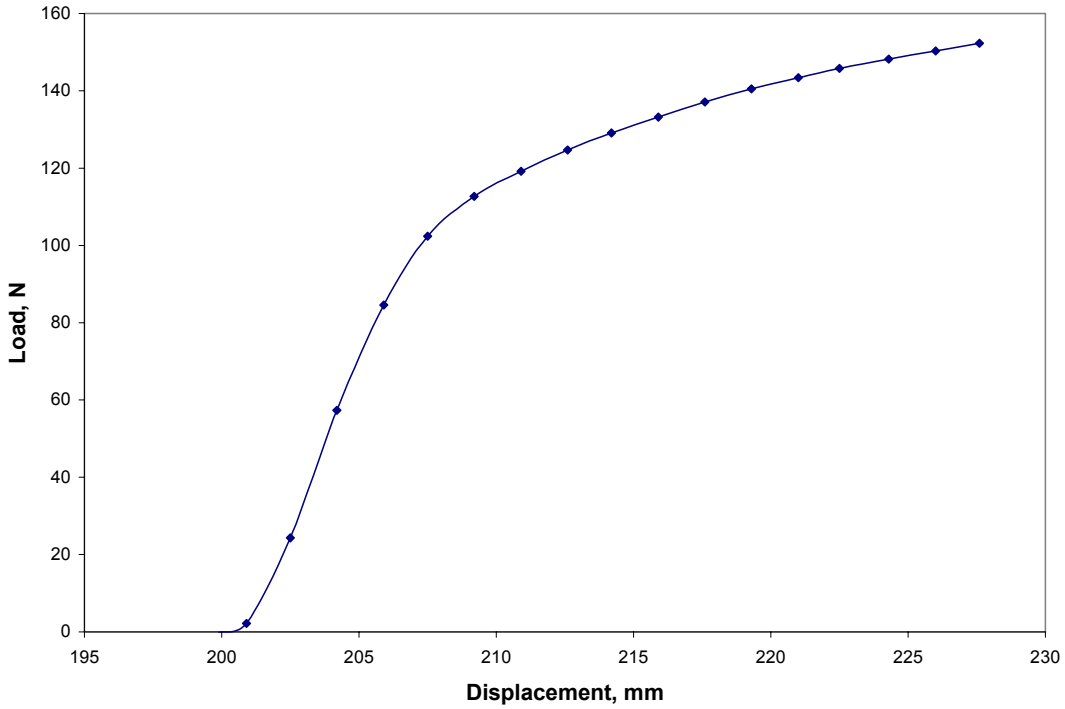

Figure A.1: Load Versus Displacement for Durapore™, Test 1, 10/11/2002

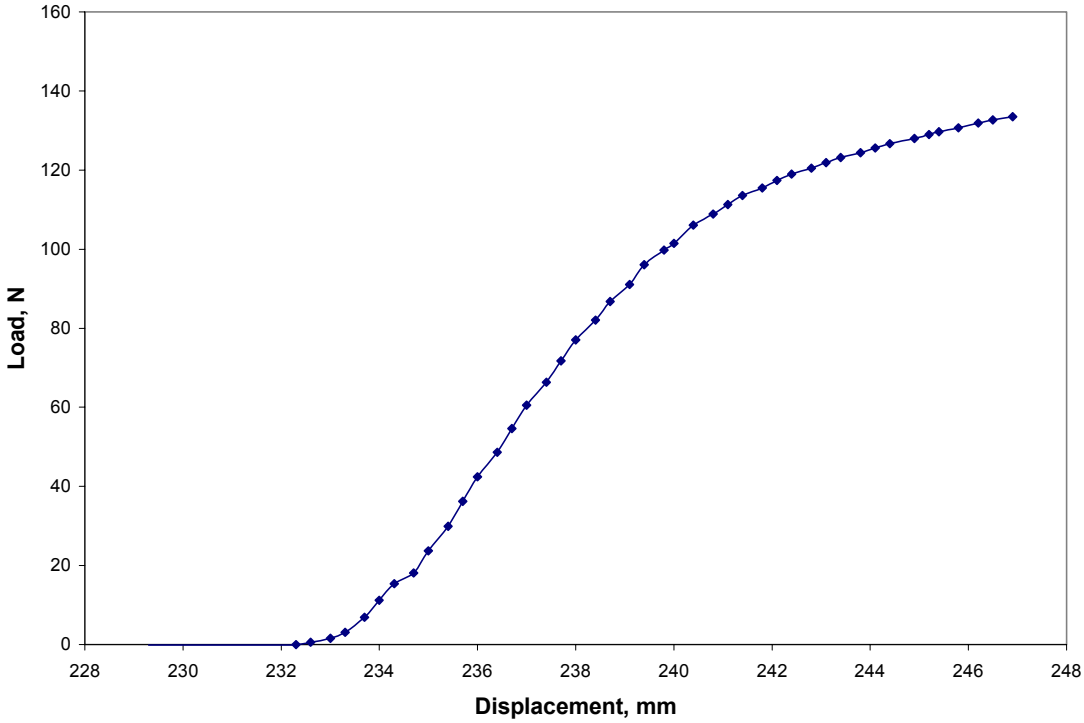

Figure A.2: Load Versus Displacement for Durapore™, Test 2, 10/11/2002

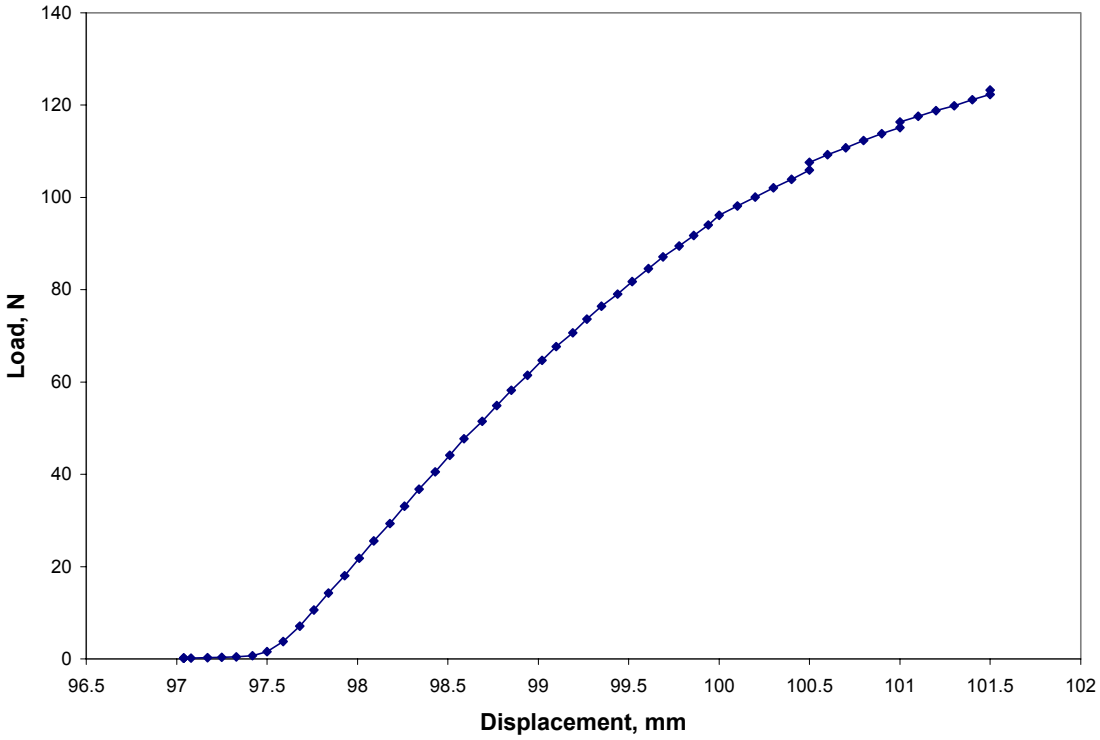

Figure A.3: Load Versus Displacement for Durapore™, Test 1, 4/24/2003

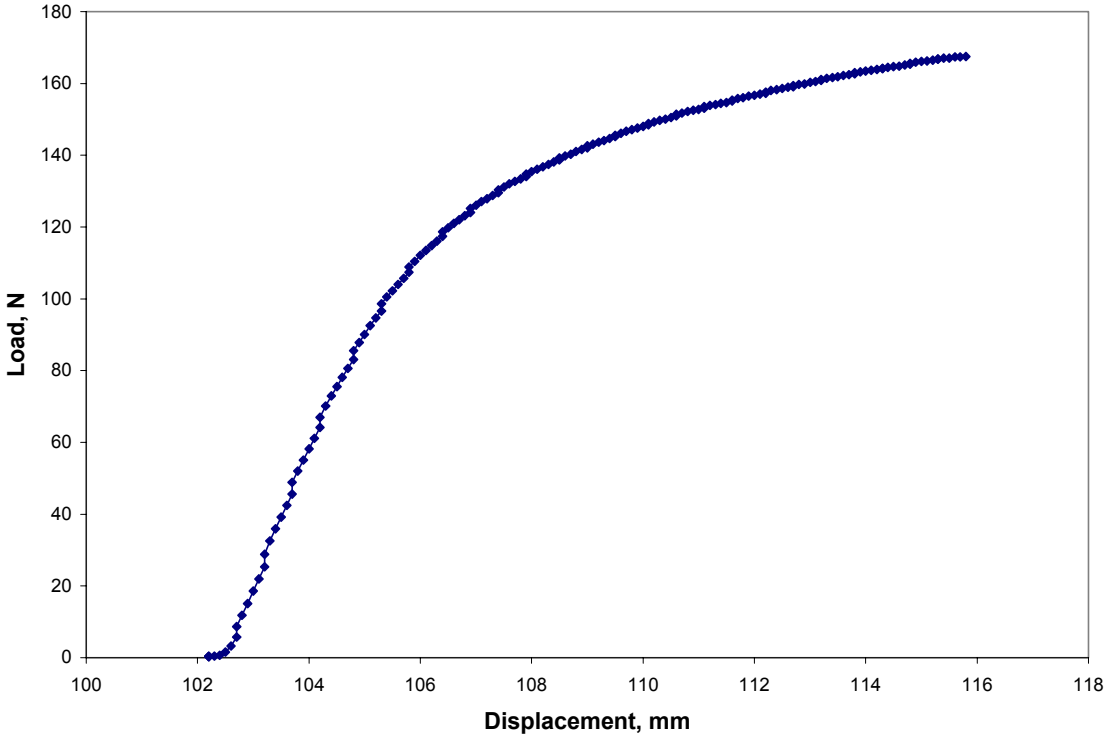

Figure A.4: Load Versus Displacement for Durapore™, Test 2, 4/24/2003

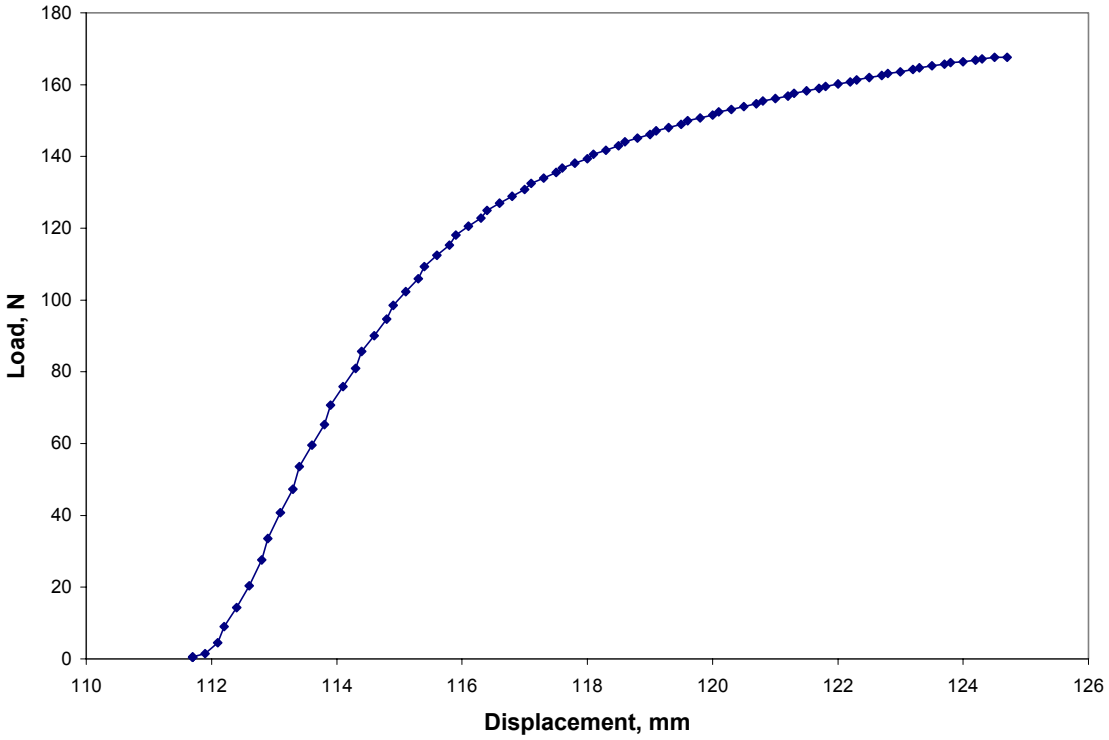

Figure A.5: Load Versus Displacement for Durapore™, Test 3, 4/24/2003

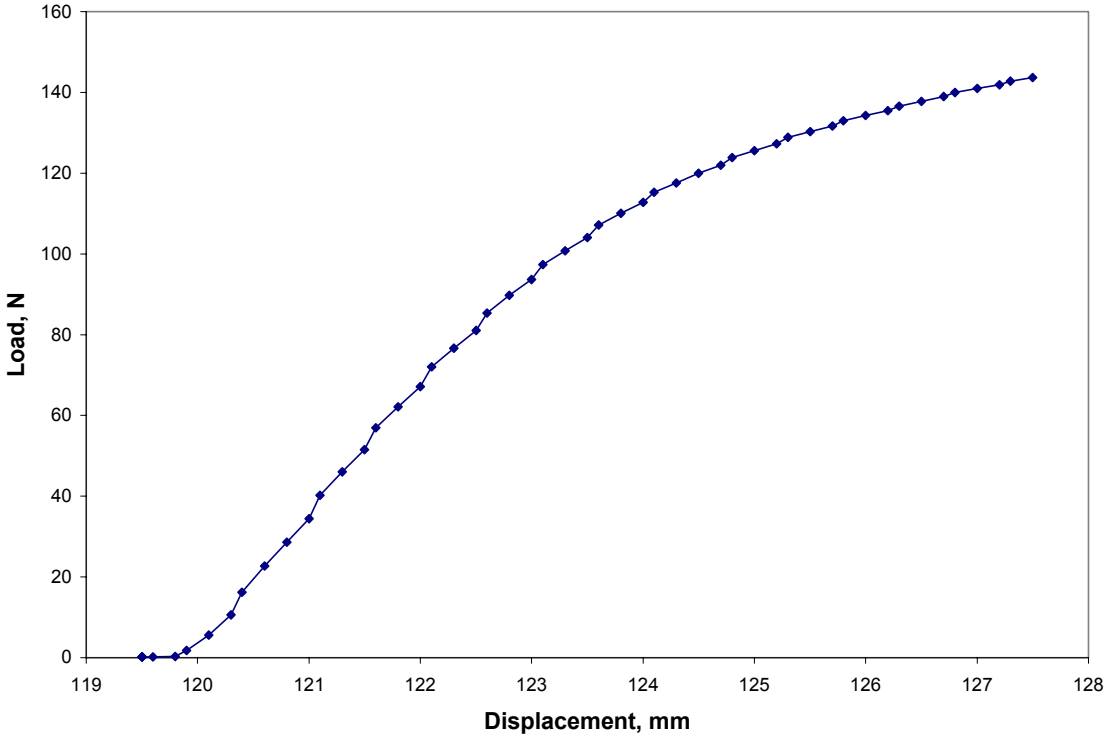

Figure A.6: Load Versus Displacement for Durapore™, Test 4, 4/24/2003

Appendix B

Experimentation Series One Results

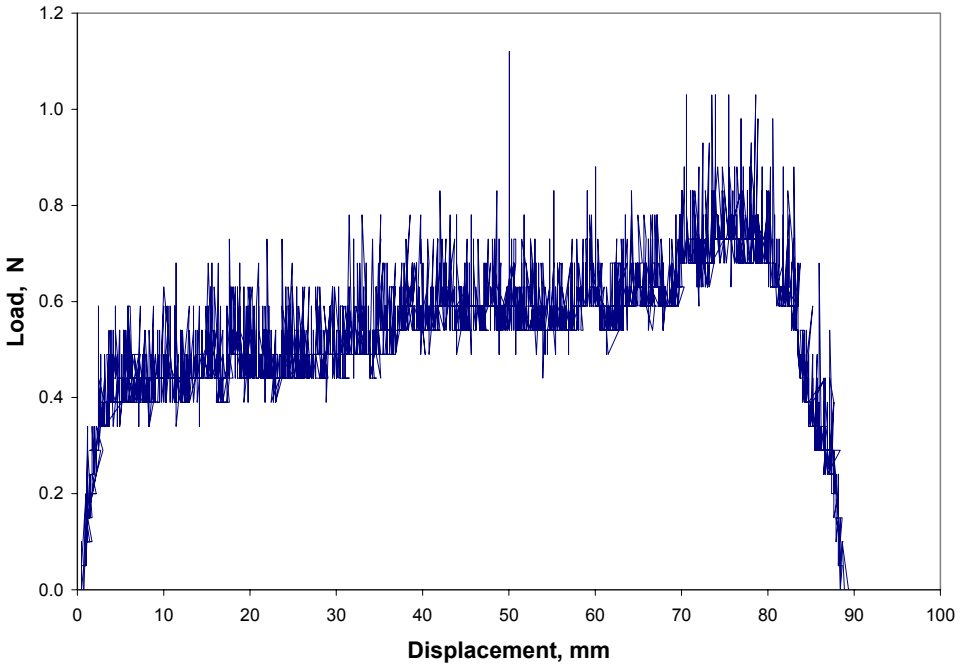

Figure B.1: Load Versus Displacement for Subject A, 90 degrees, 1 min, 100 mm/min, Test 1

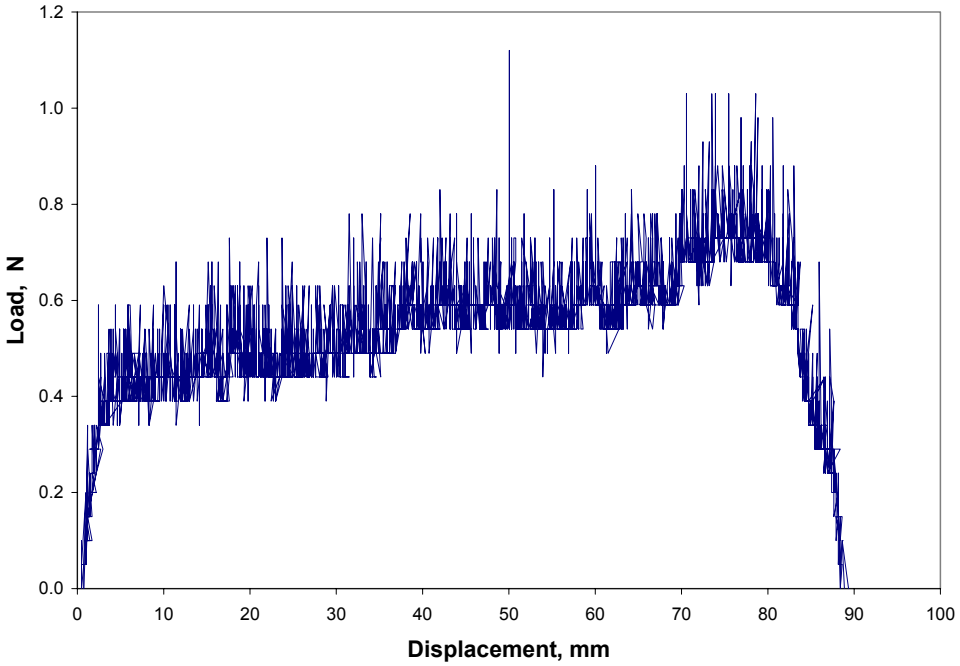

Figure B.2: Load Versus Displacement for Subject A, 90 degrees, 1 min, 100 mm/min, Test 2

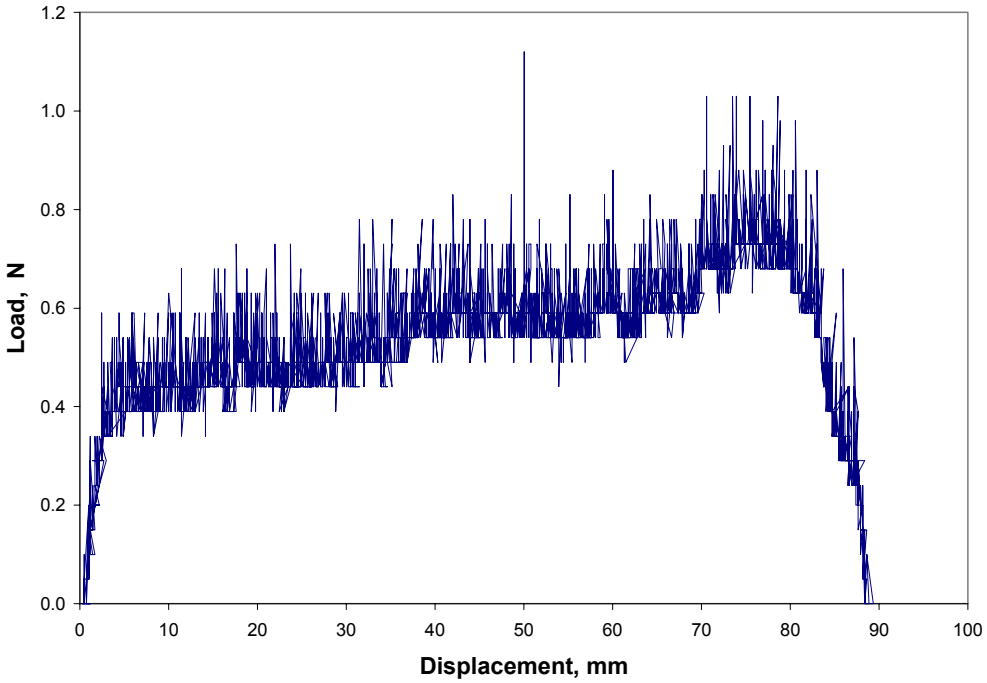

Figure B.3: Load Versus Displacement for Subject A, 90 degrees, 1 min, 100 mm/min, Test 3

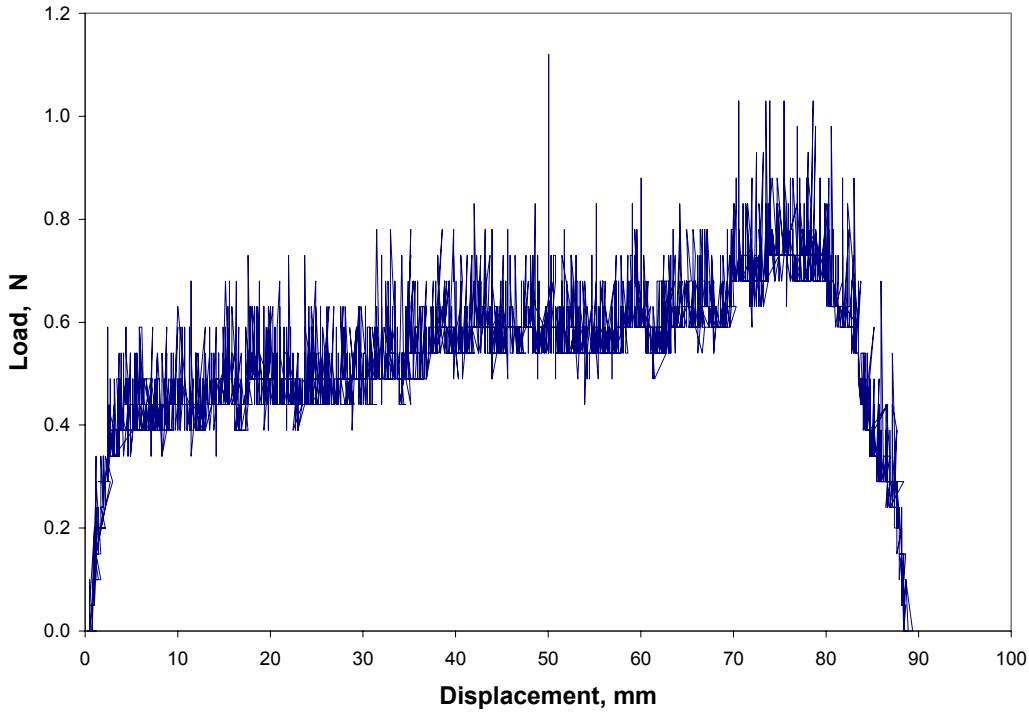

Figure B.4: Load Versus Displacement for Subject A, 90 degrees, 1 min, 100 mm/min, Test 4

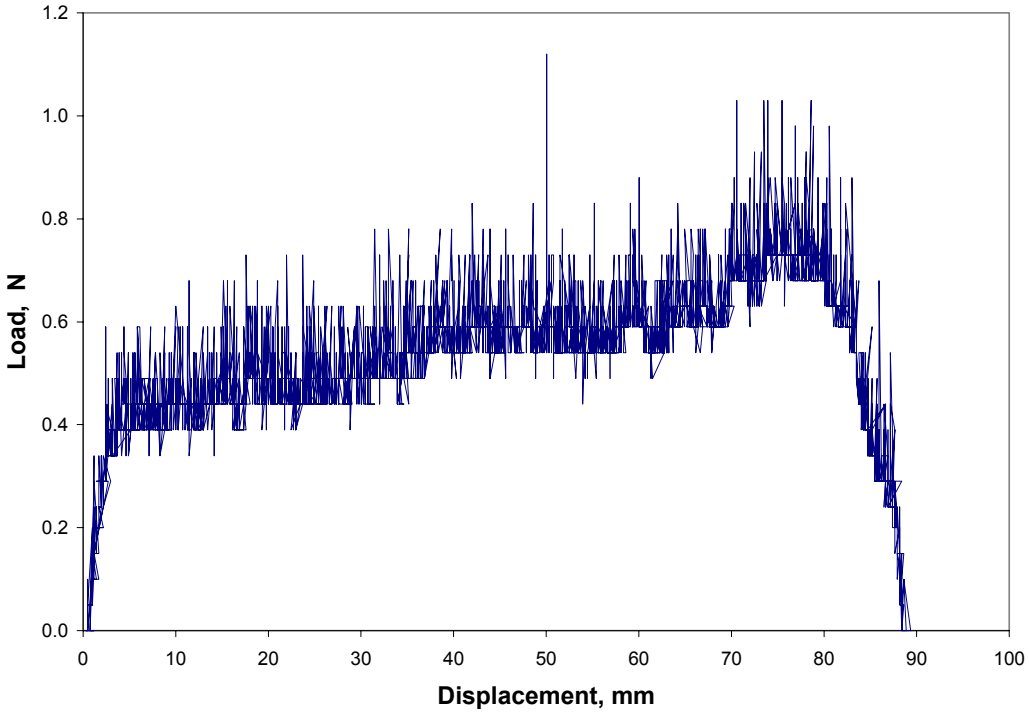

Figure B.5: Load Versus Displacement for Subject A, 90 degrees, 1 min, 100 mm/min, Test 5

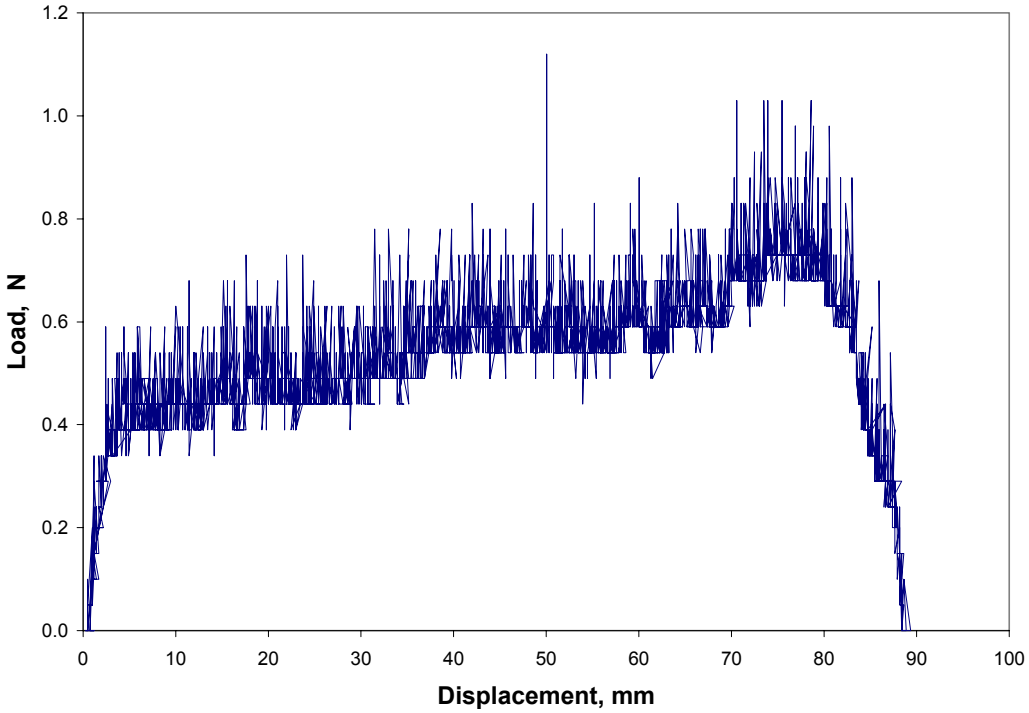

Figure B.6: Load Versus Displacement for Subject A, 90 degrees, 1 min, 100 mm/min, Average

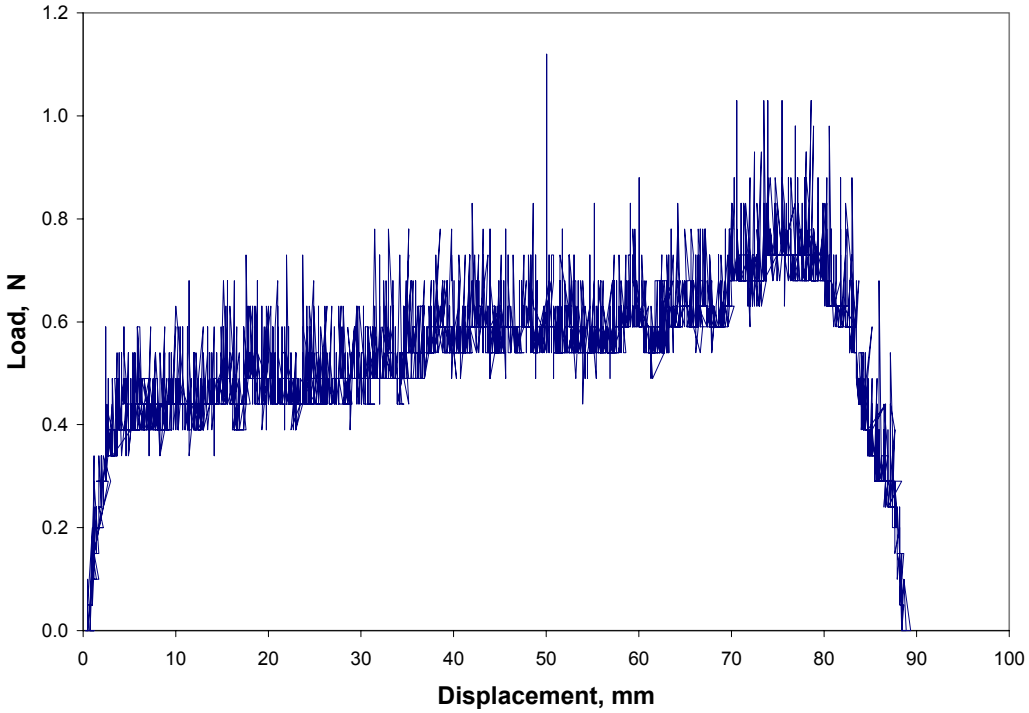

Figure B.7: Load Versus Displacement for Subject A, 90 degrees, 1 min, 200 mm/min, Test 1

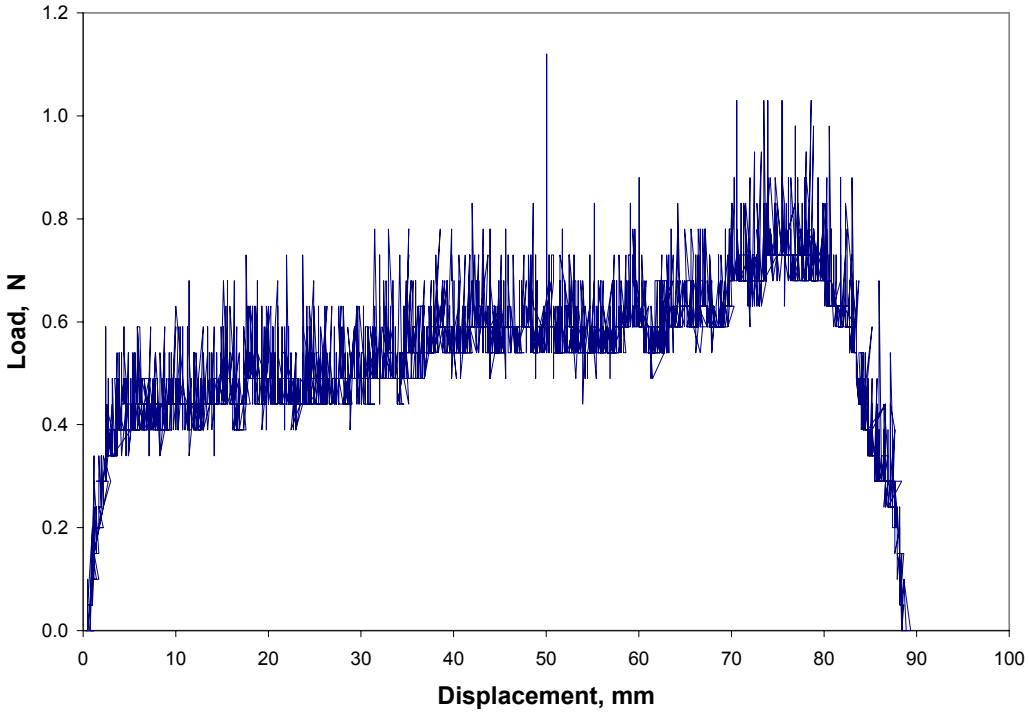

Figure B.8: Load Versus Displacement for Subject A, 90 degrees, 1 min, 200 mm/min, Test 2

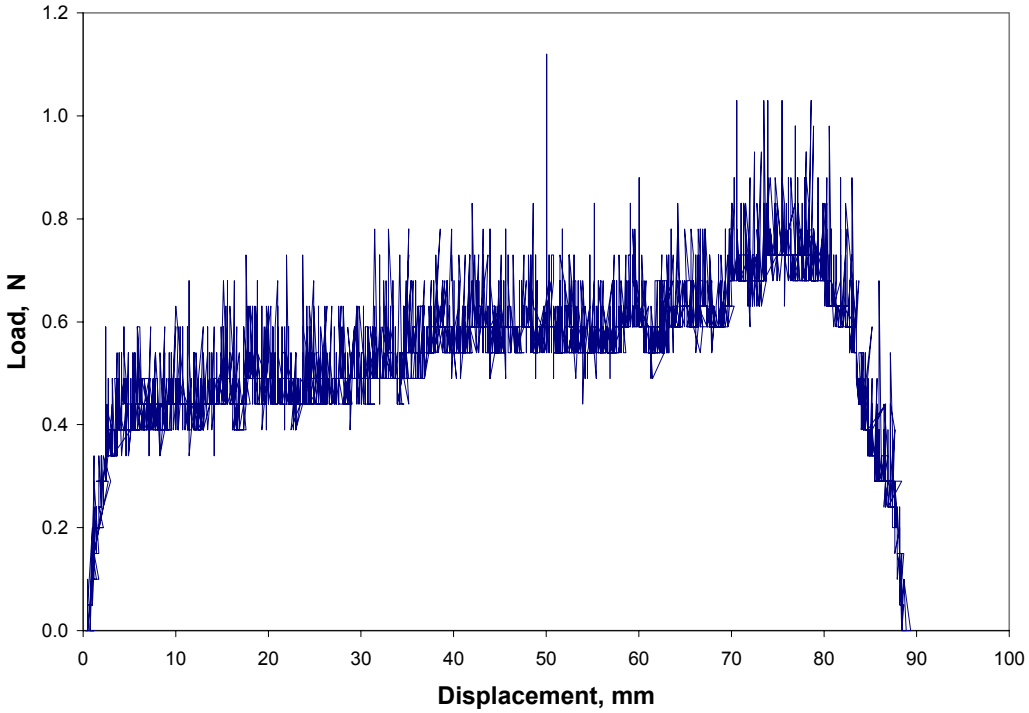

Figure B.9: Load Versus Displacement for Subject A, 90 degrees, 1 min, 200 mm/min, Test 3

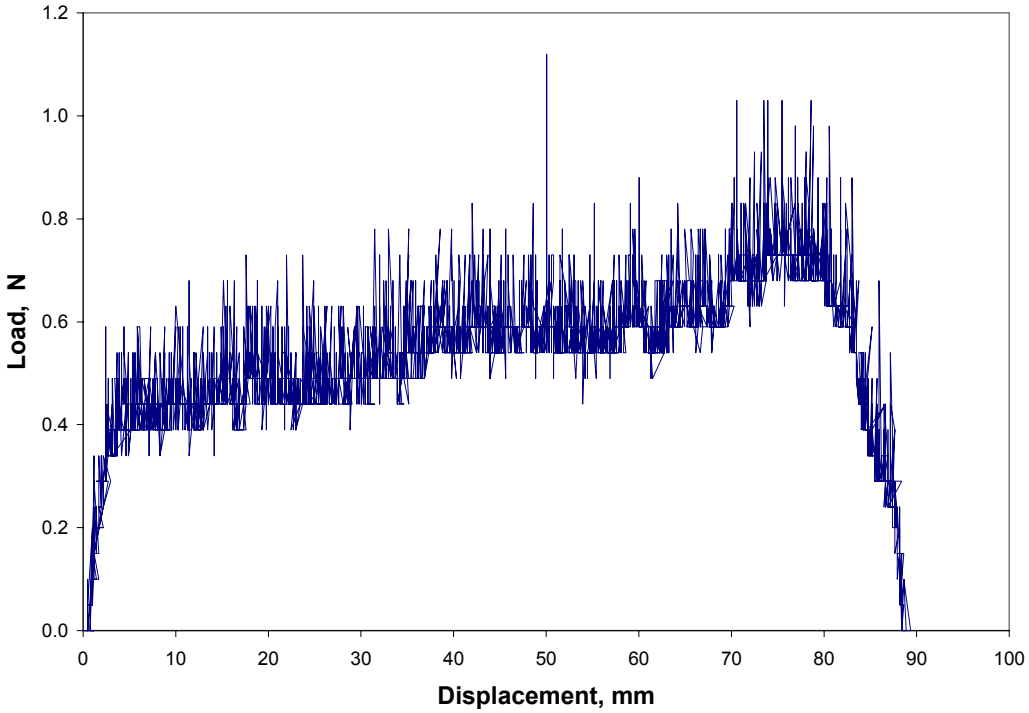

Figure B.10: Load Versus Displacement for Subject A, 90 degrees, 1 min, 200 mm/min, Average

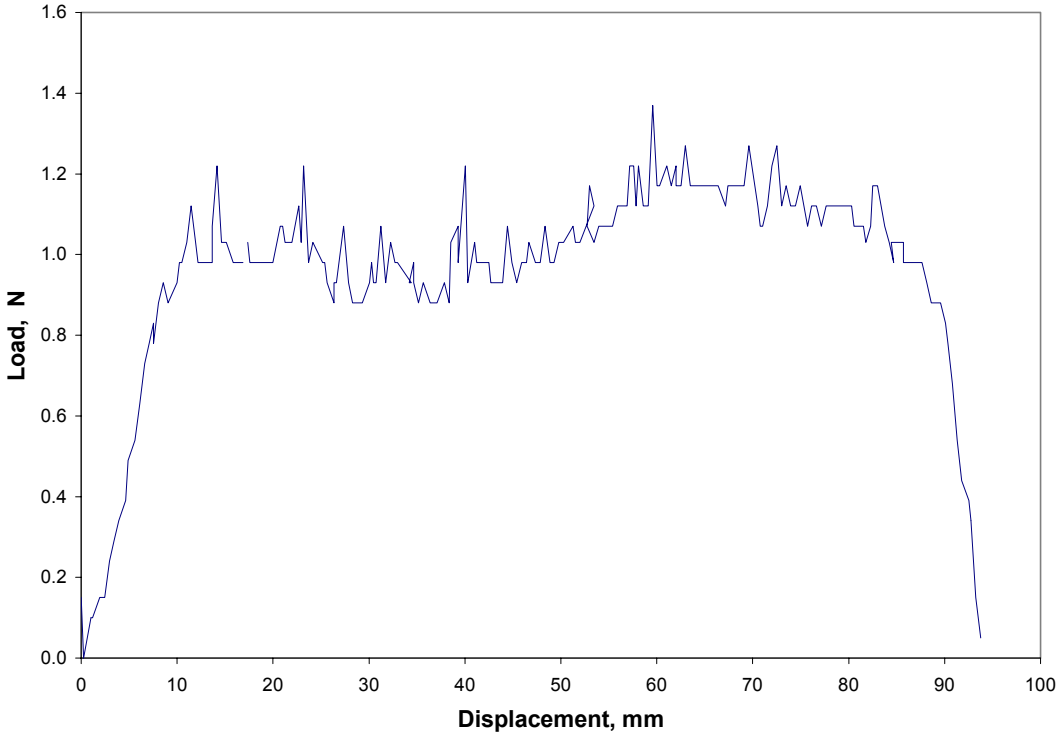

Figure B.11: Load Versus Displacement for Subject A, 90 degrees, 1 min, 300 mm/min, Test 1

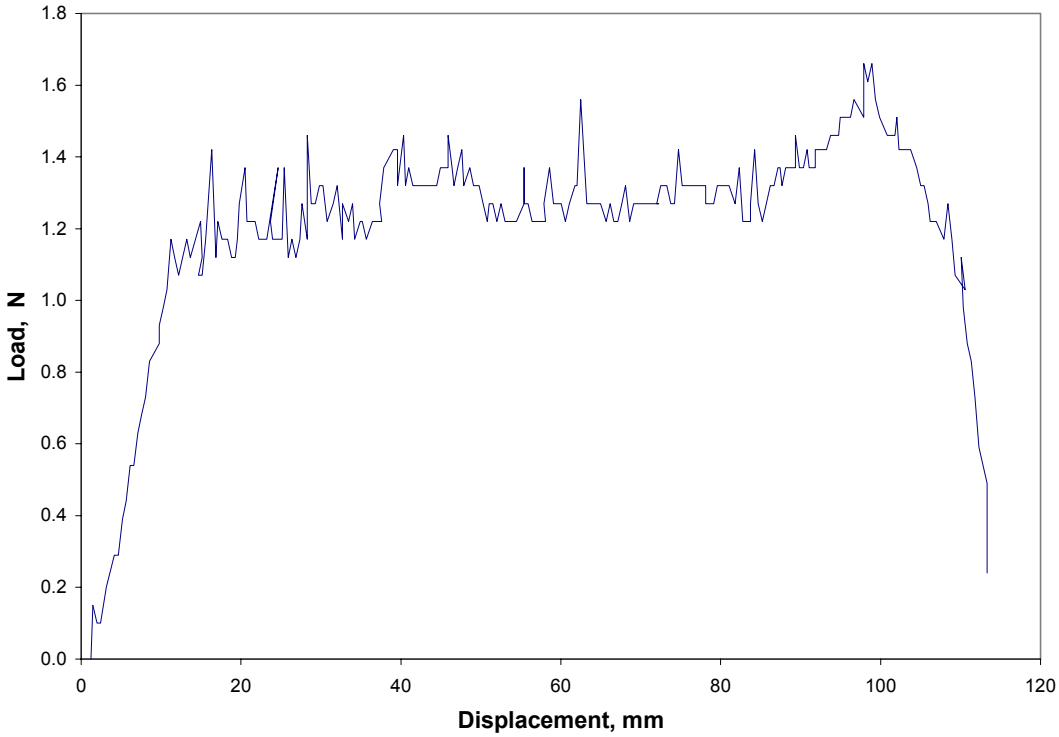

Figure B.12: Load Versus Displacement for Subject A, 90 degrees, 1 min, 300 mm/min, Test 2

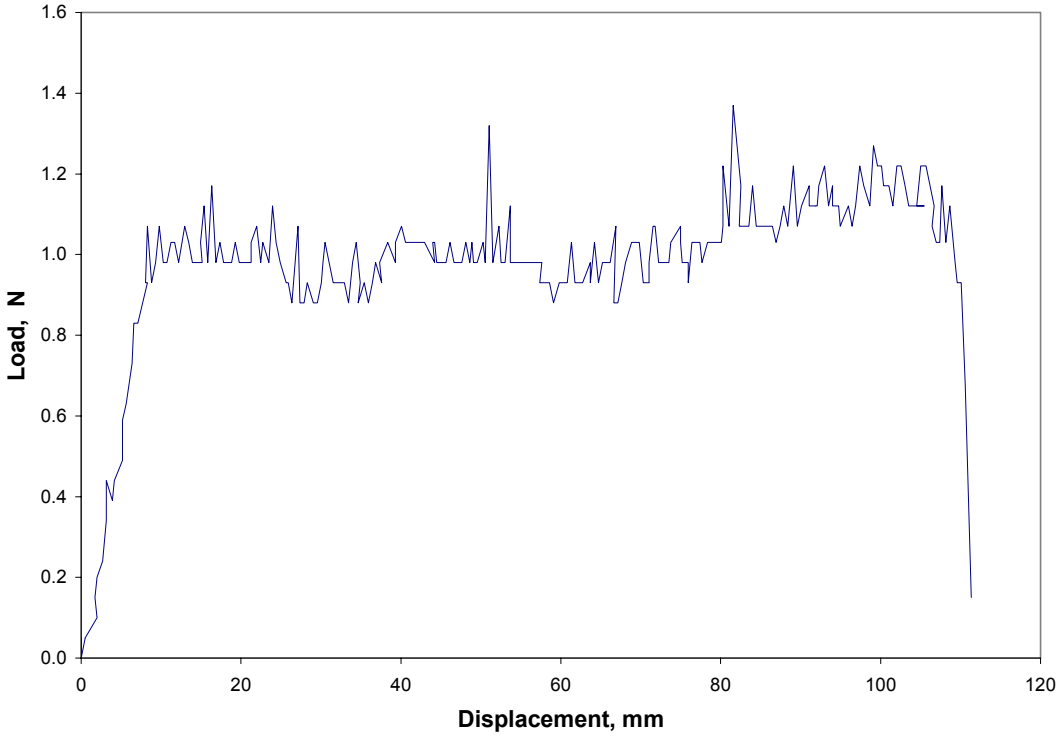

Figure B.13: Load Versus Displacement for Subject A, 90 degrees, 1 min, 300 mm/min, Test 3

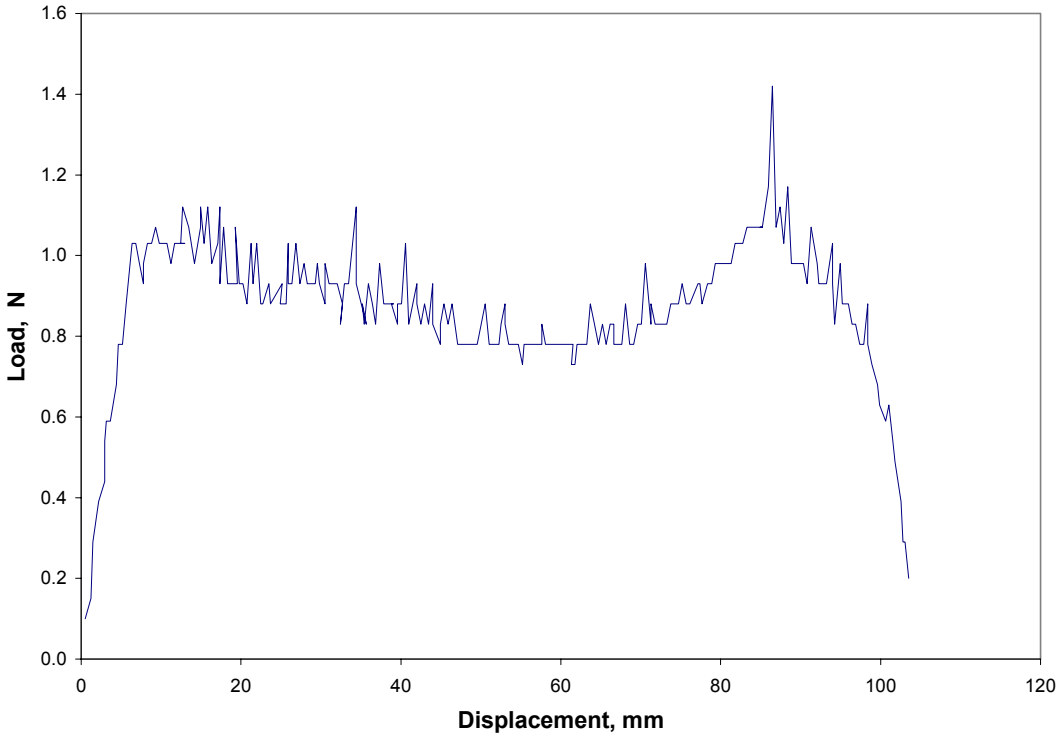

Figure B.14: Load Versus Displacement for Subject A, 90 degrees, 1 min, 300 mm/min, Test 4

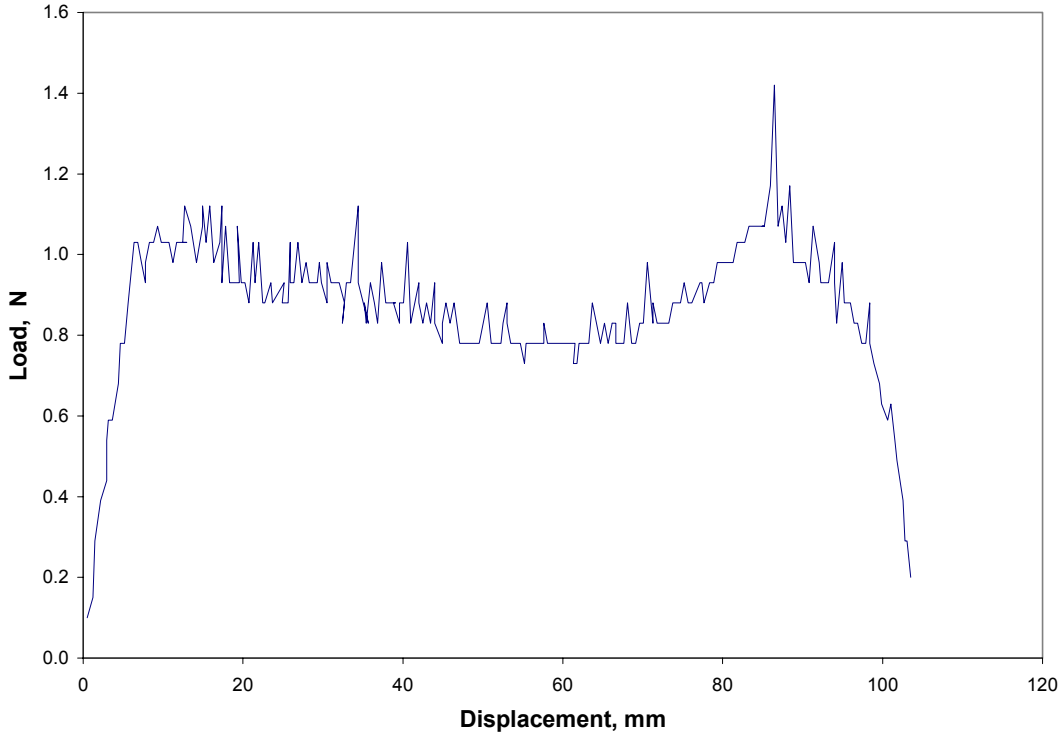

Figure B.15: Load Versus Displacement for Subject A, 90 degrees, 1min, 300 mm/min, Test 5

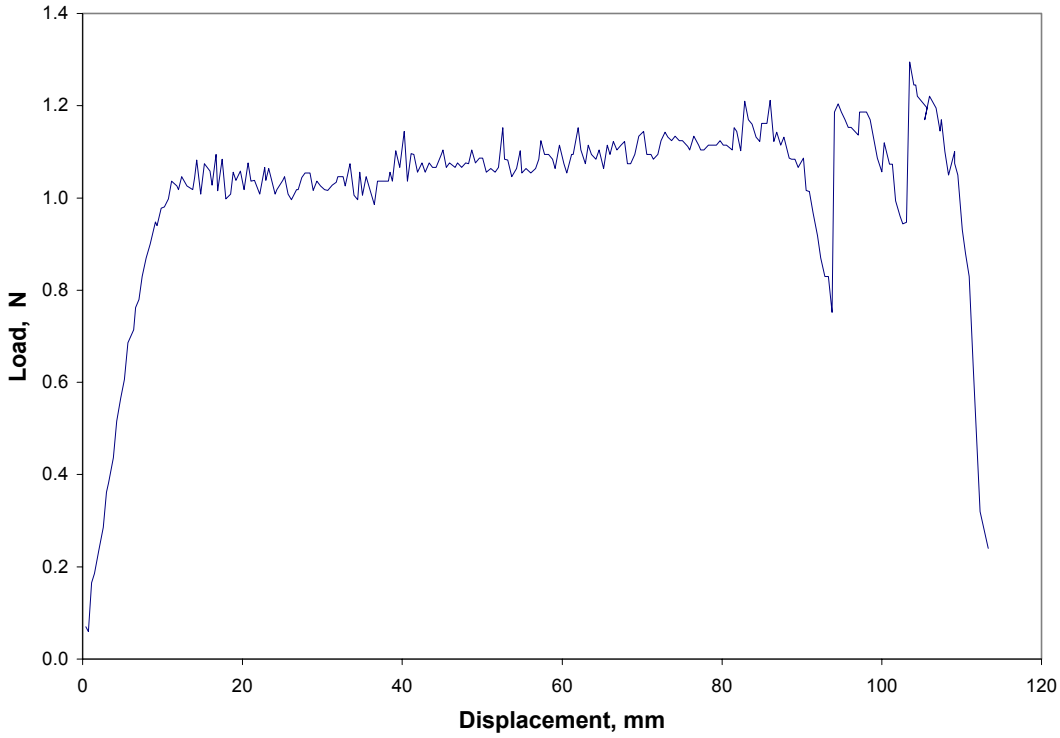

Figure B.16: Load Versus Displacement for Subject A, 90 degrees, 1 min, 300 mm/min, Average

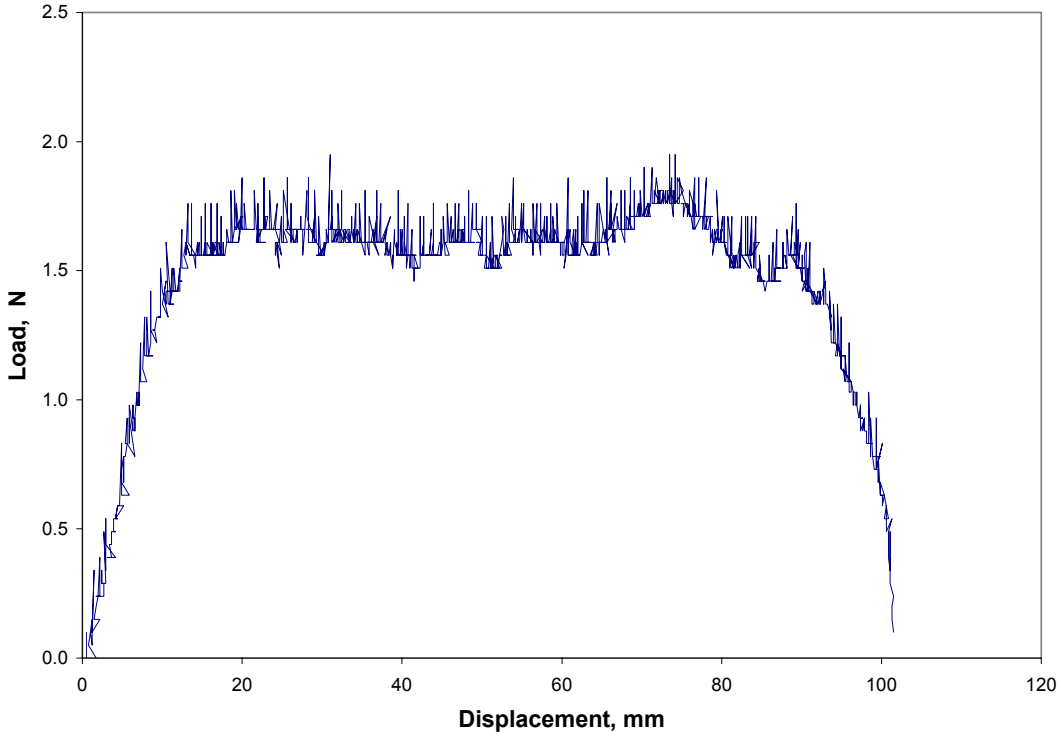

Figure B.17: Load Versus Displacement for Subject A, 90 degrees, 1 min, 400 mm/min, Test 1

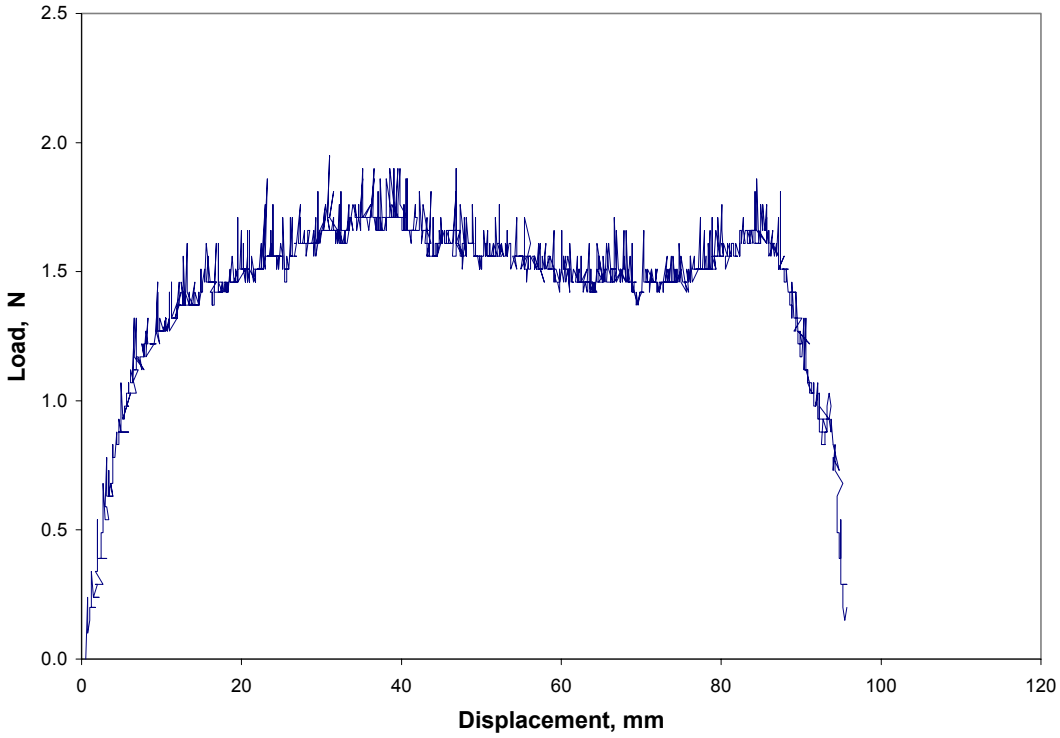

Figure B.18: Load Versus Displacement for Subject A, 90 degrees, 1 min, 400 mm/min, Test 2

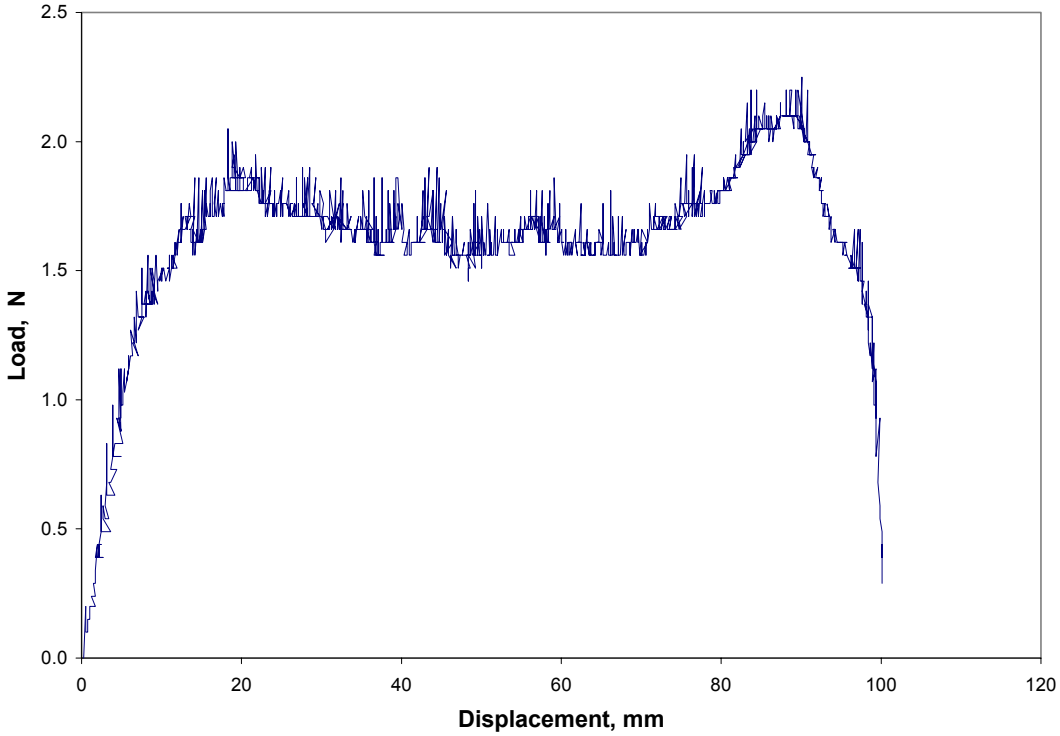

Figure B.19: Load Versus Displacement for Subject A, 90 degrees, 1 min, 400 mm/min, Test 3

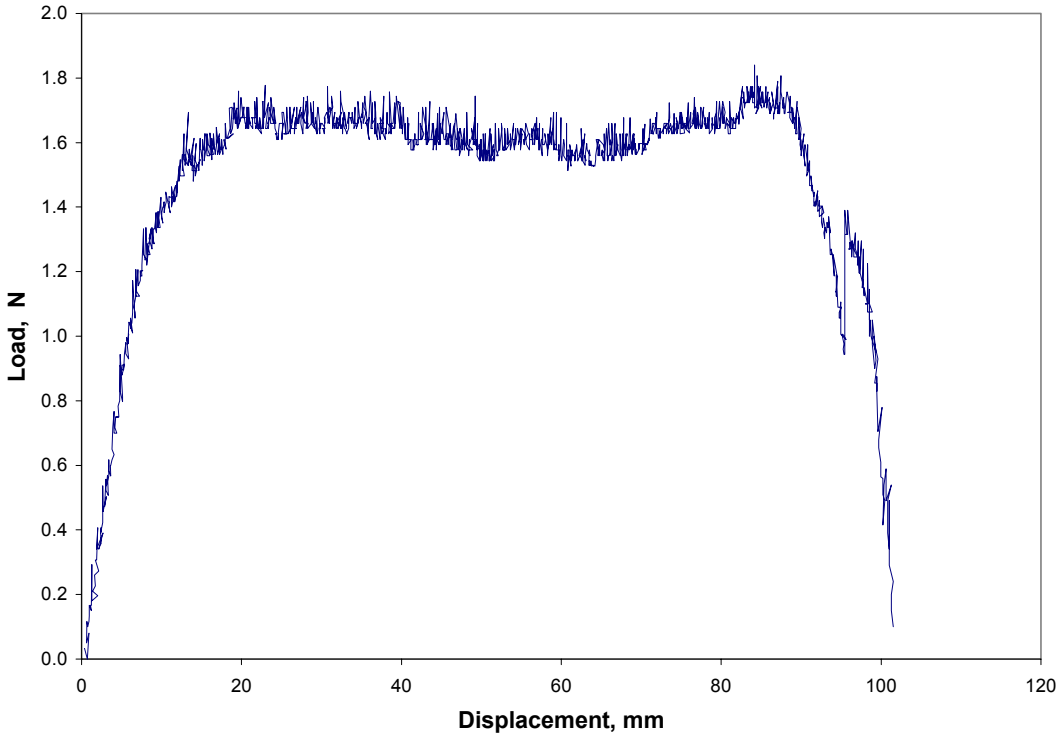

Figure B.20: Load Versus Displacement for Subject A, 90 degrees, 1 min, 400 mm/min, Average

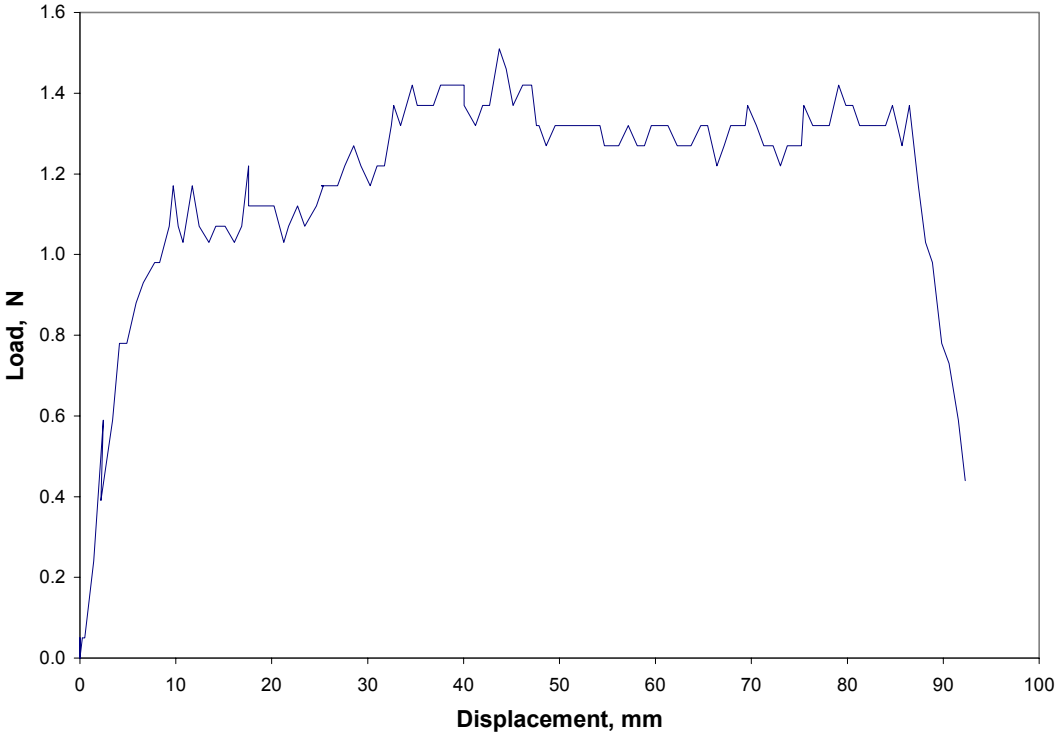

Figure B.21: Load Versus Displacement for Subject A, 90 degrees, 1 min, 500 mm/min, Test 1

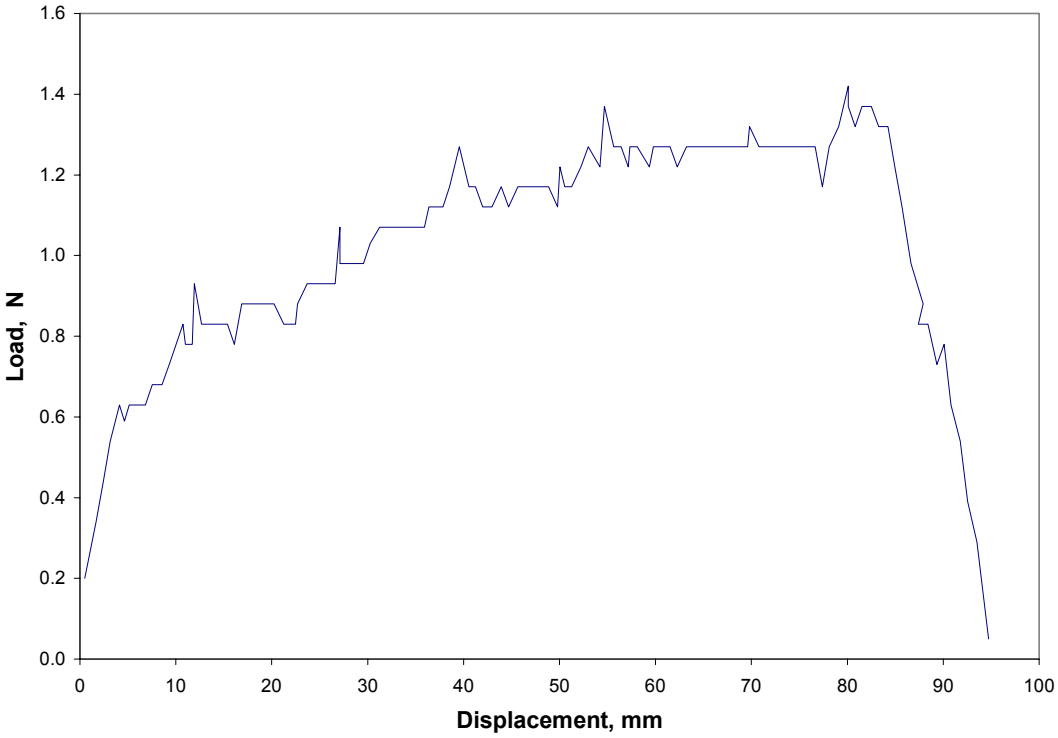

Figure B.22: Load Versus Displacement for Subject A, 90 degrees, 1 min, 500 mm/min, Test 2

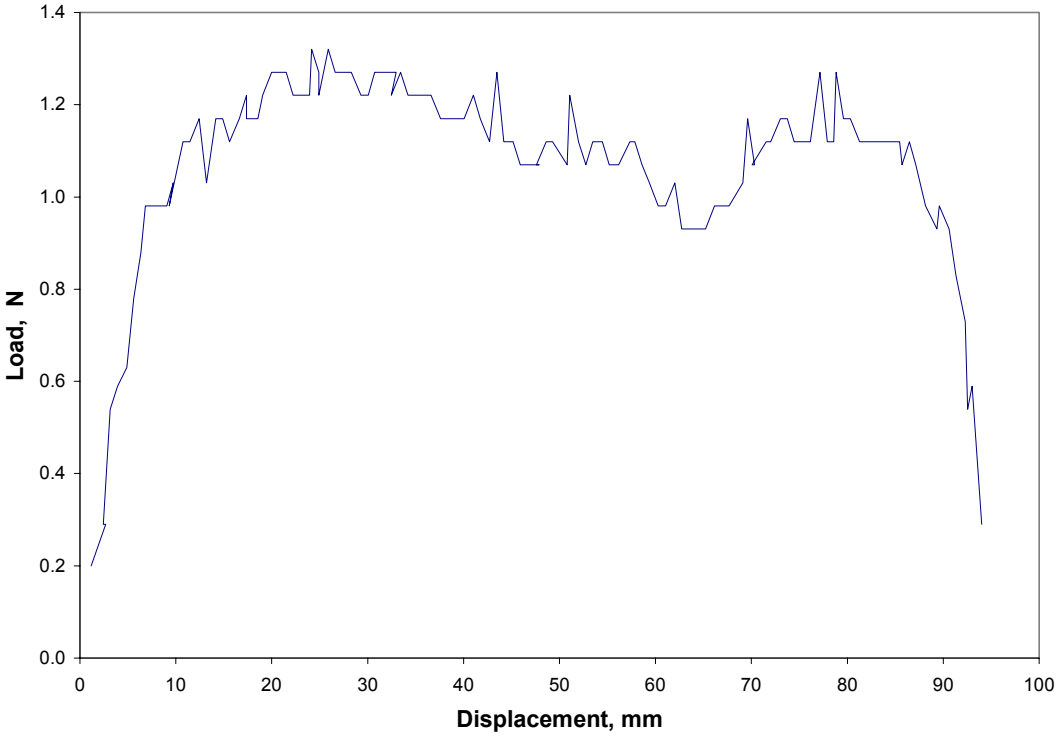

Figure B.23: Load Versus Displacement for Subject A, 90 degrees, 1 min, 500 mm/min, Test 3

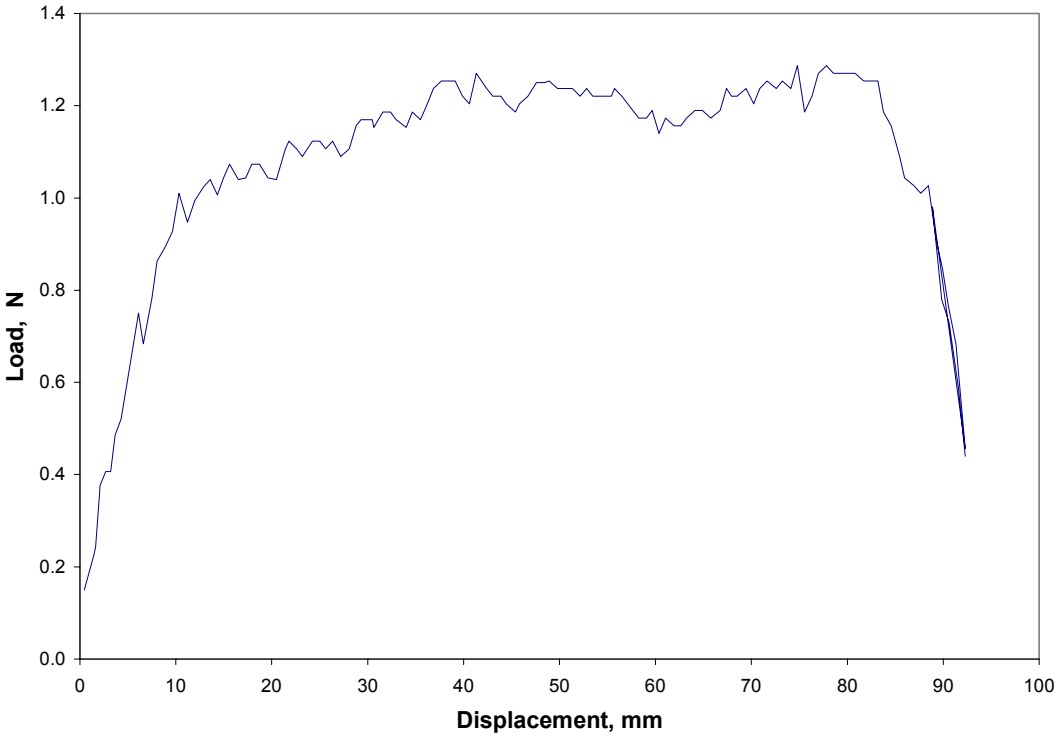

Figure B.24: Load Versus Displacement for Subject A, 90 degrees, 1 min, 500 mm/min, Average

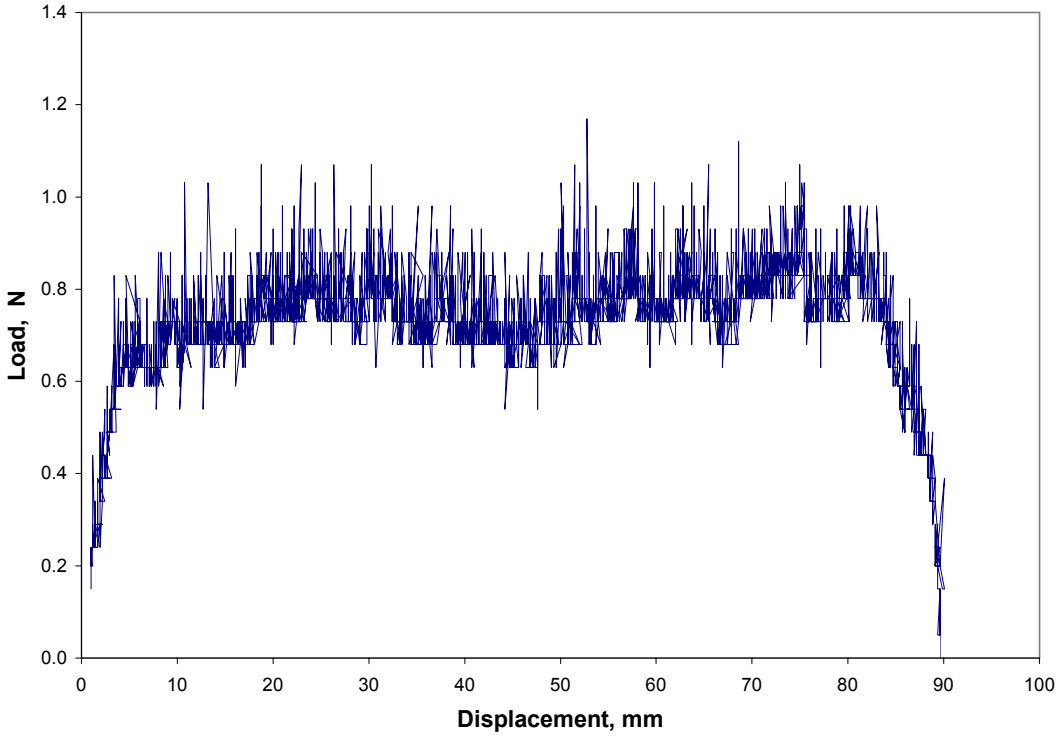

Figure B.25: Load Versus Displacement for Subject B, 90 degrees, 1 min, 100 mm/min, Test 1

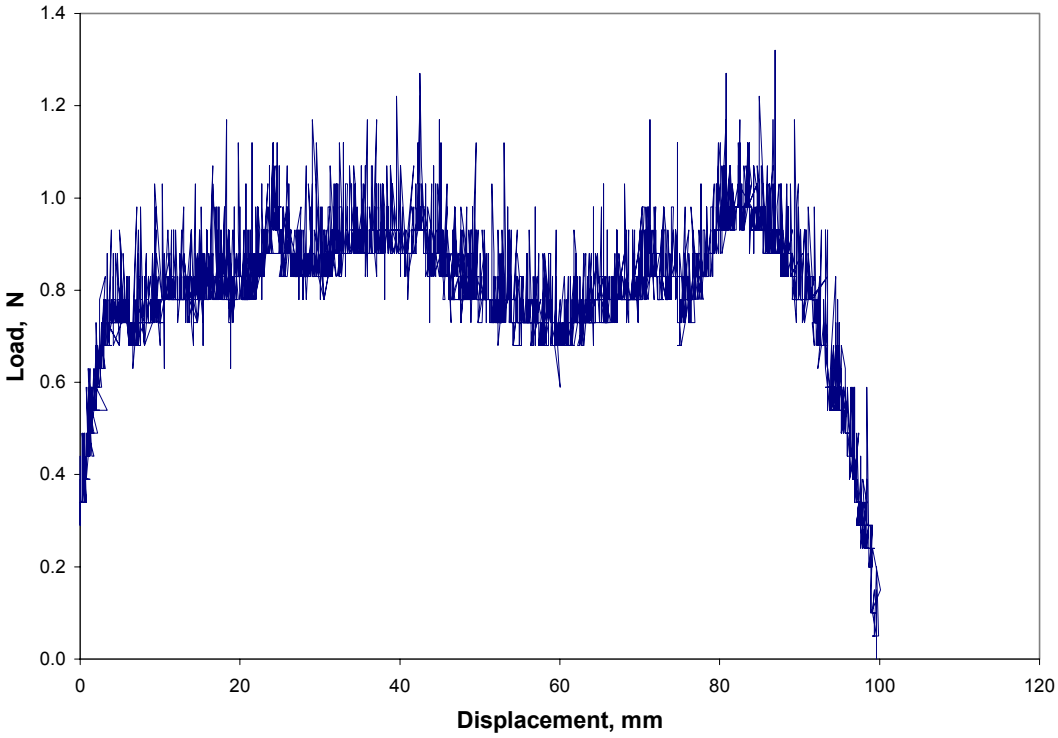

Figure B.26: Load Versus Displacement for Subject B, 90 degrees, 1 min, 100 mm/min, Test 2

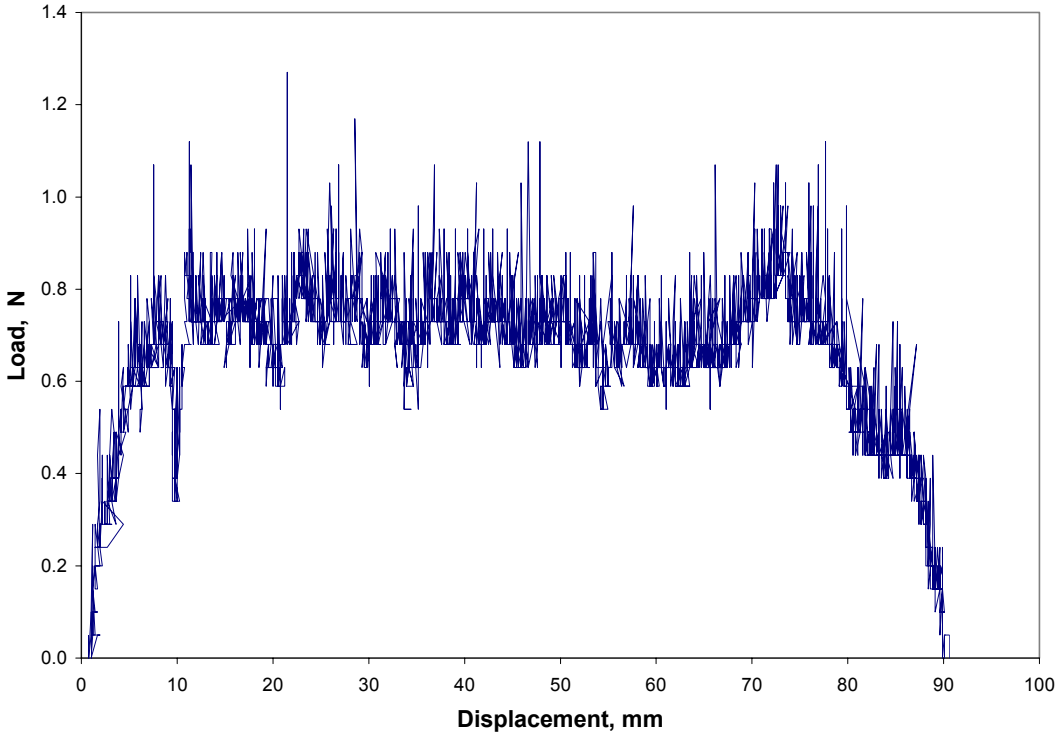

Figure B.27: Load Versus Displacement for Subject B, 90 degrees, 1 min, 100 mm/min, Test 3

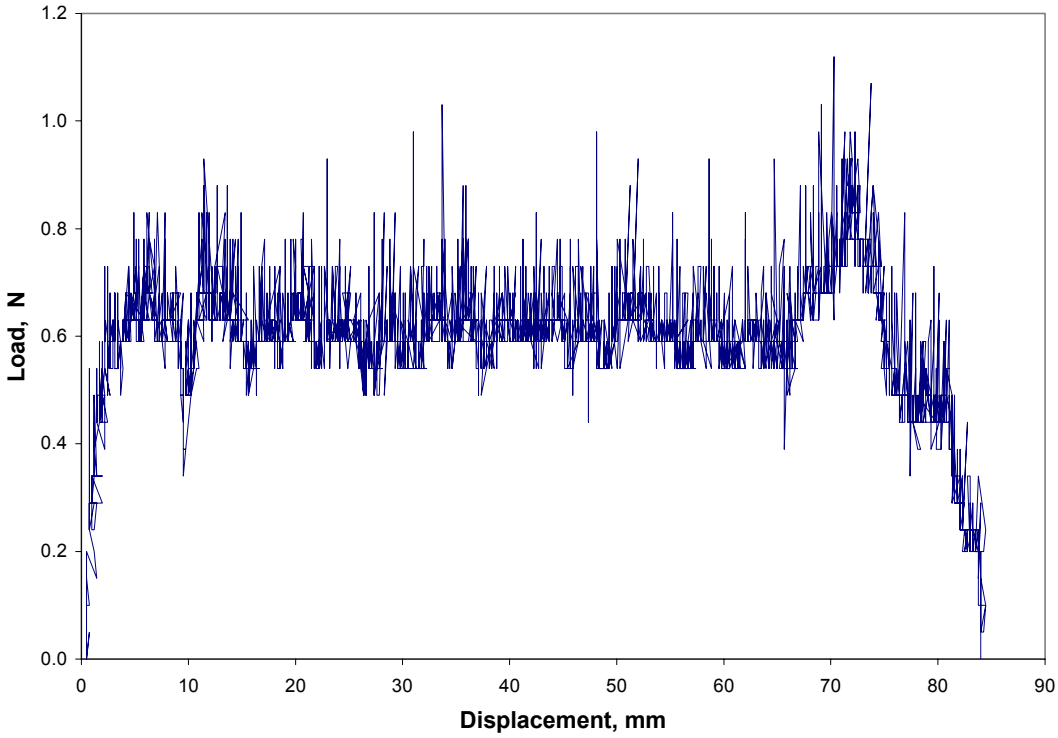

Figure B.28: Load Versus Displacement for Subject B, 90 degrees, 1 min, 100 mm/min, Test 4

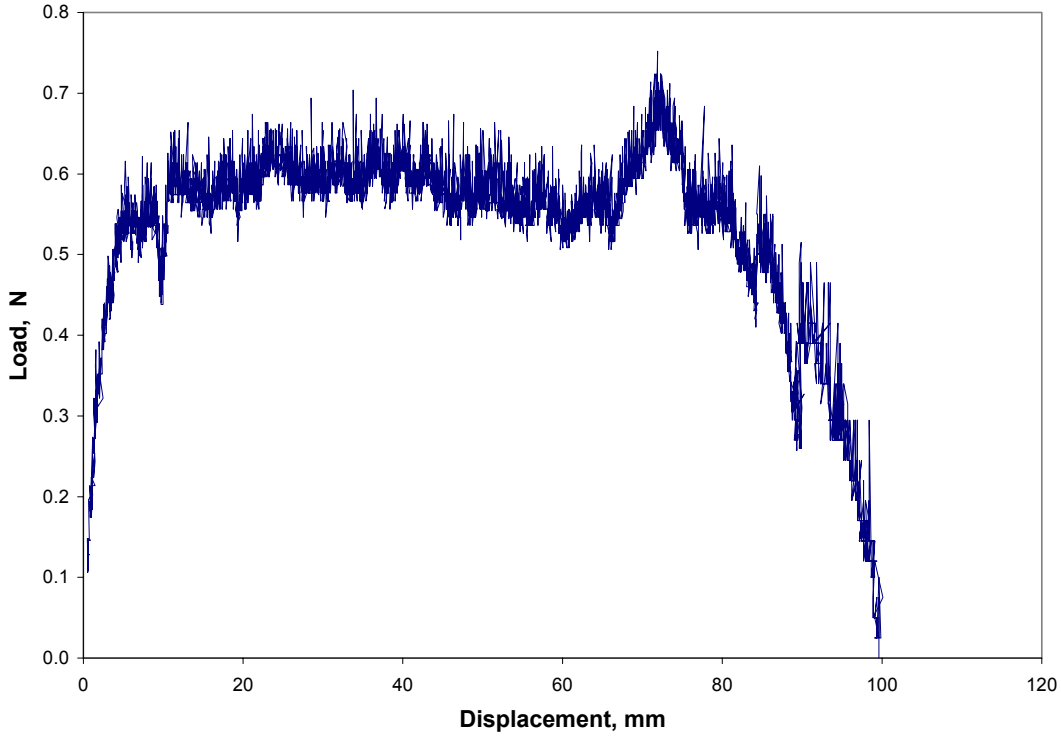

Figure B.29: Load Versus Displacement for Subject B, 90 degrees, 1 min, 100 mm/min, Average

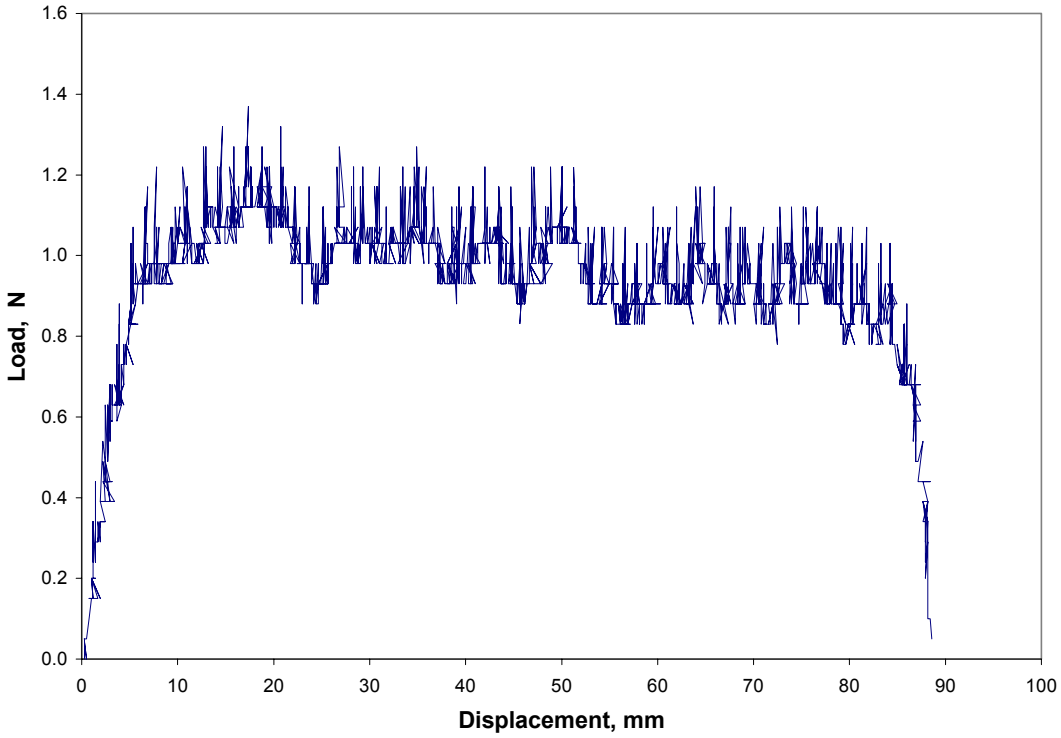

Figure B.30: Load Versus Displacement for Subject B, 90 degrees, 1 min, 200 mm/min, Test 1

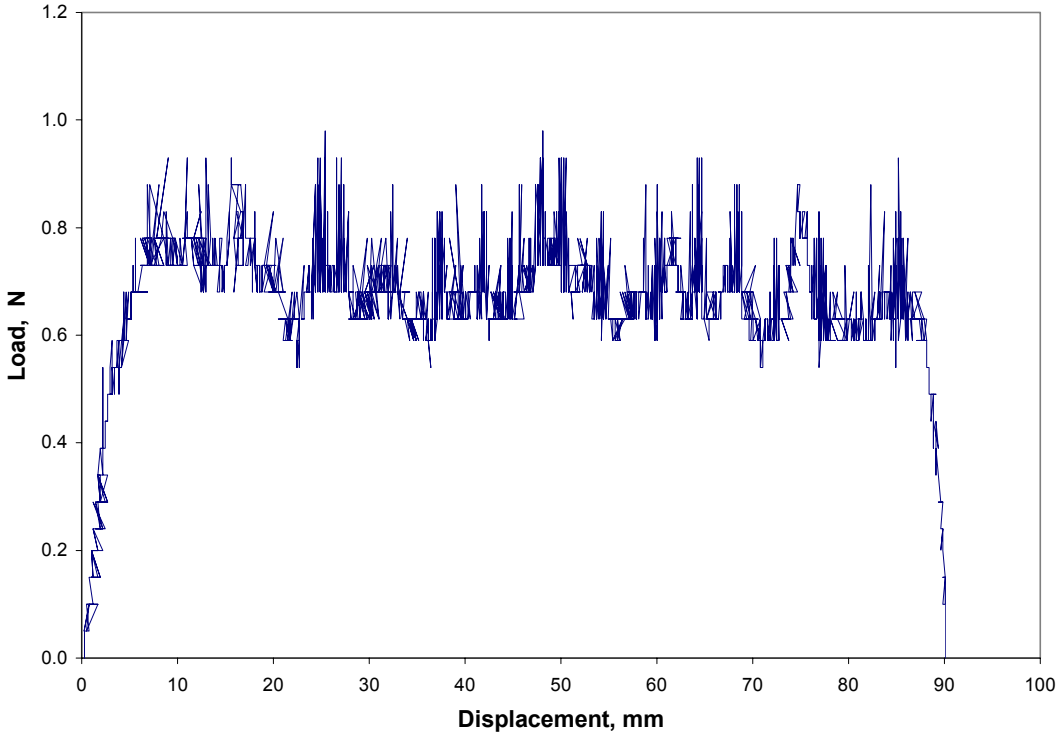

Figure B.31: Load Versus Displacement for Subject B, 90 degrees, 1 min, 200 mm/min, Test 2

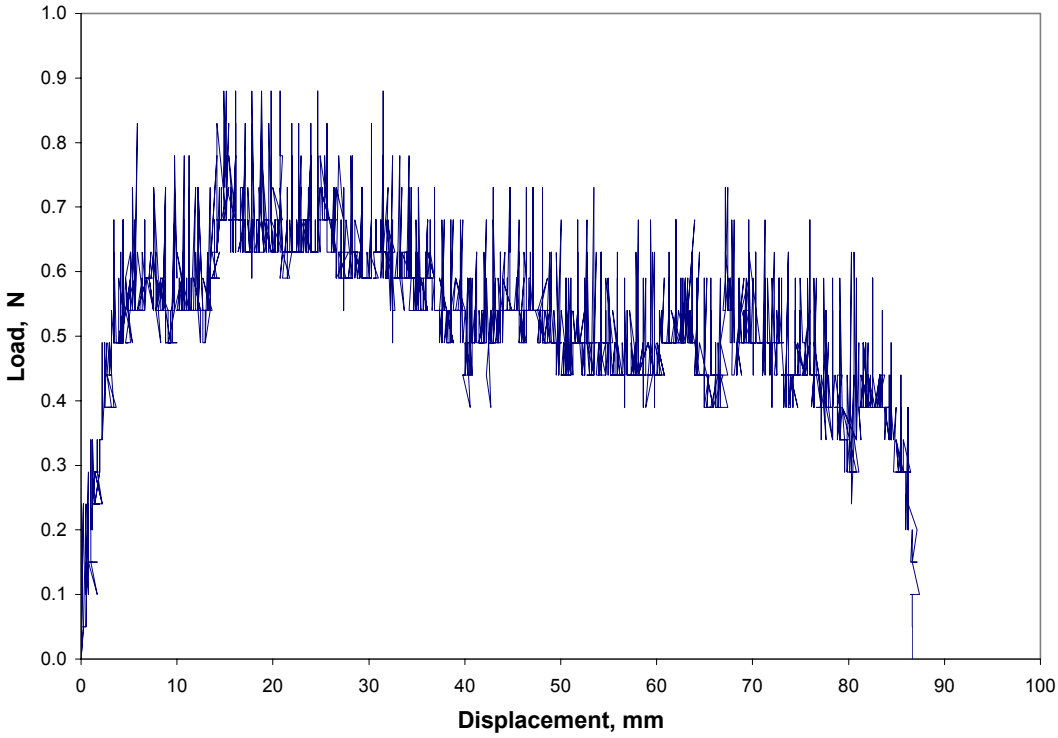

Figure B.32: Load Versus Displacement for Subject B, 90 degrees, 1 min, 200 mm/min, Test 3

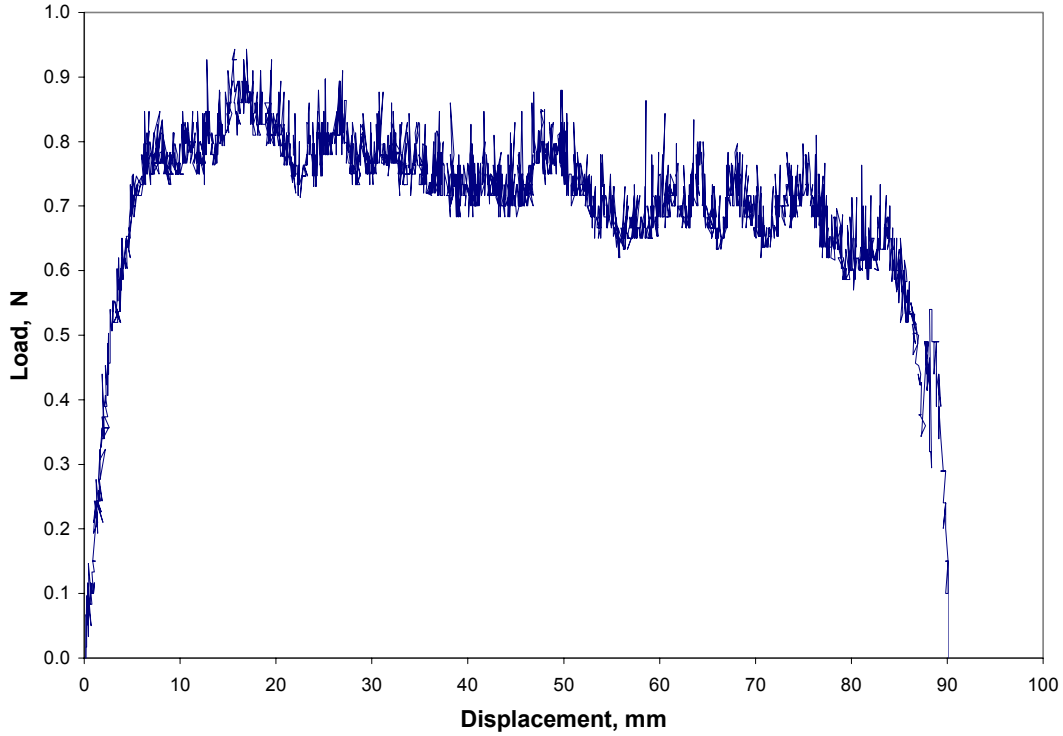

Figure B.33: Load Versus Displacement for Subject B, 90 degrees, 1 min, 200 mm/min, Average

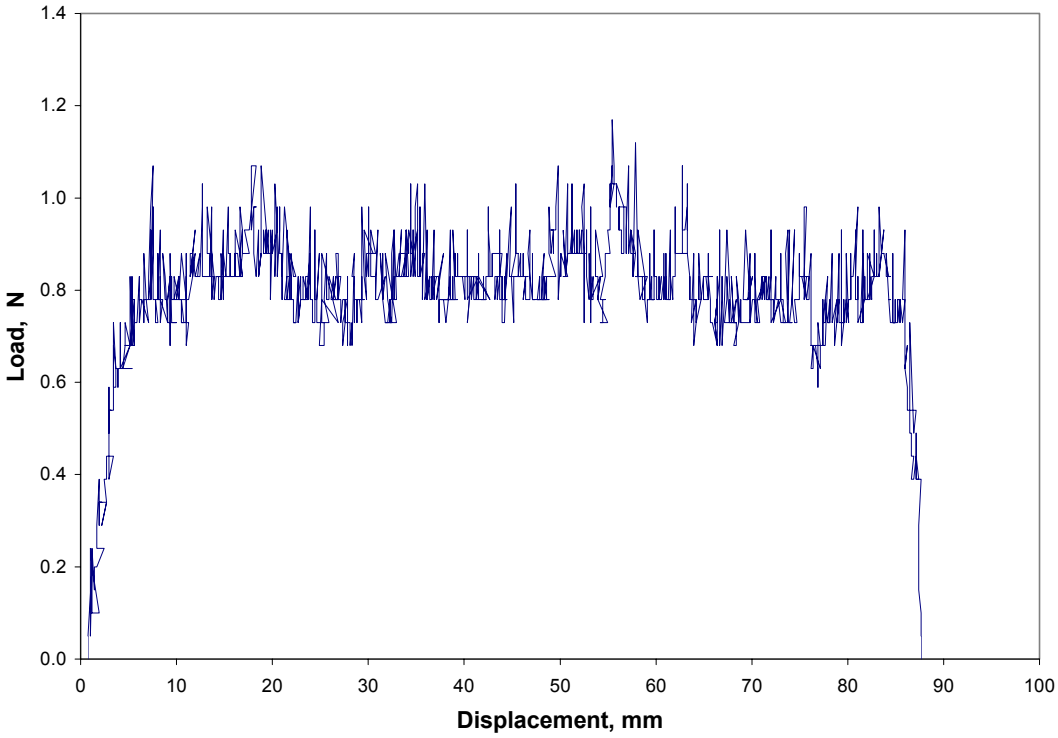

Figure B.34: Load Versus Displacement for Subject B, 90 degrees, 1 min, 300 mm/min, Test 1

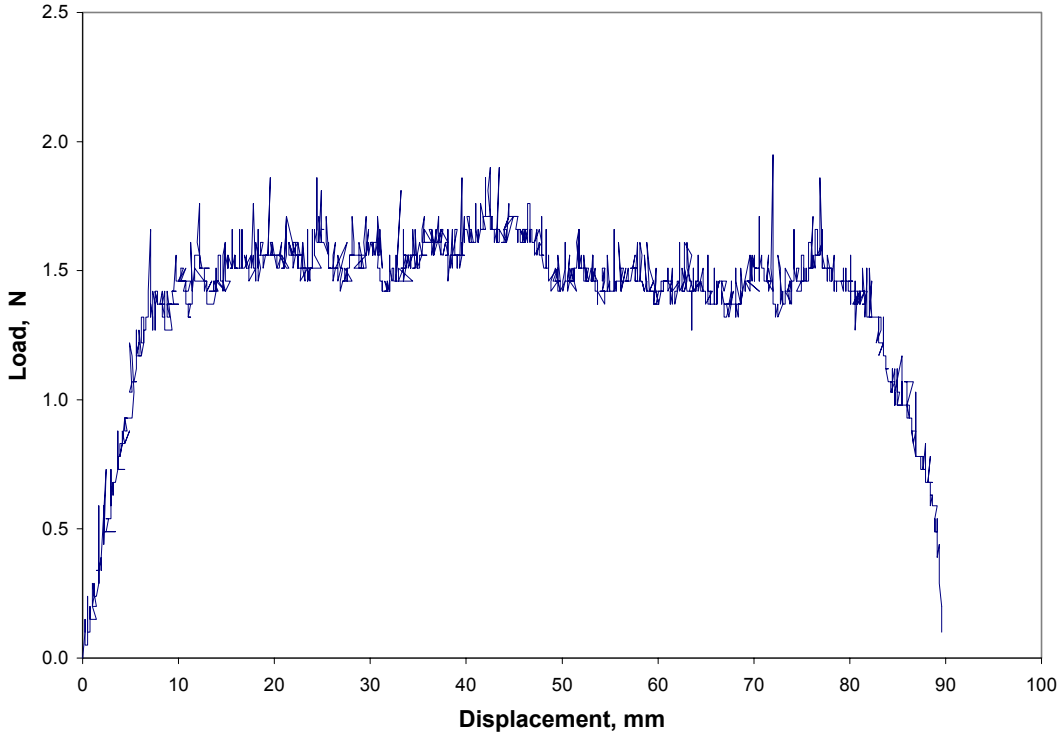

Figure B.35: Load Versus Displacement for Subject B, 90 degrees, 1 min, 300 mm/min, Test 2

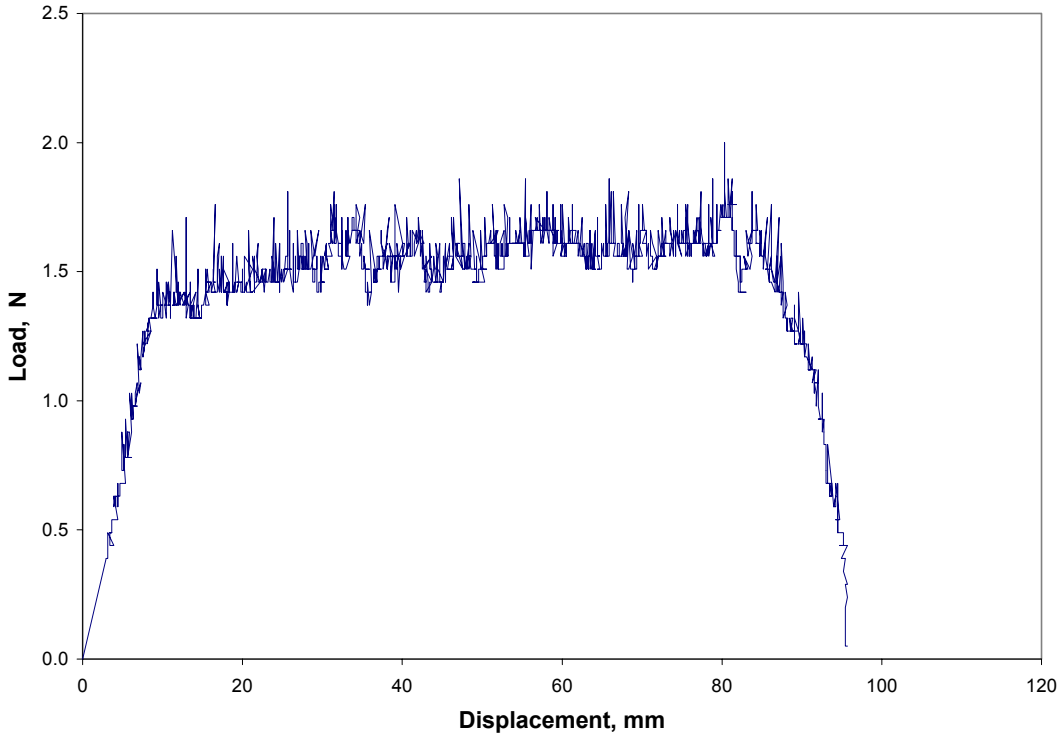

Figure B.36: Load Versus Displacement for Subject B, 90 degrees, 1 min, 300 mm/min, Test 3

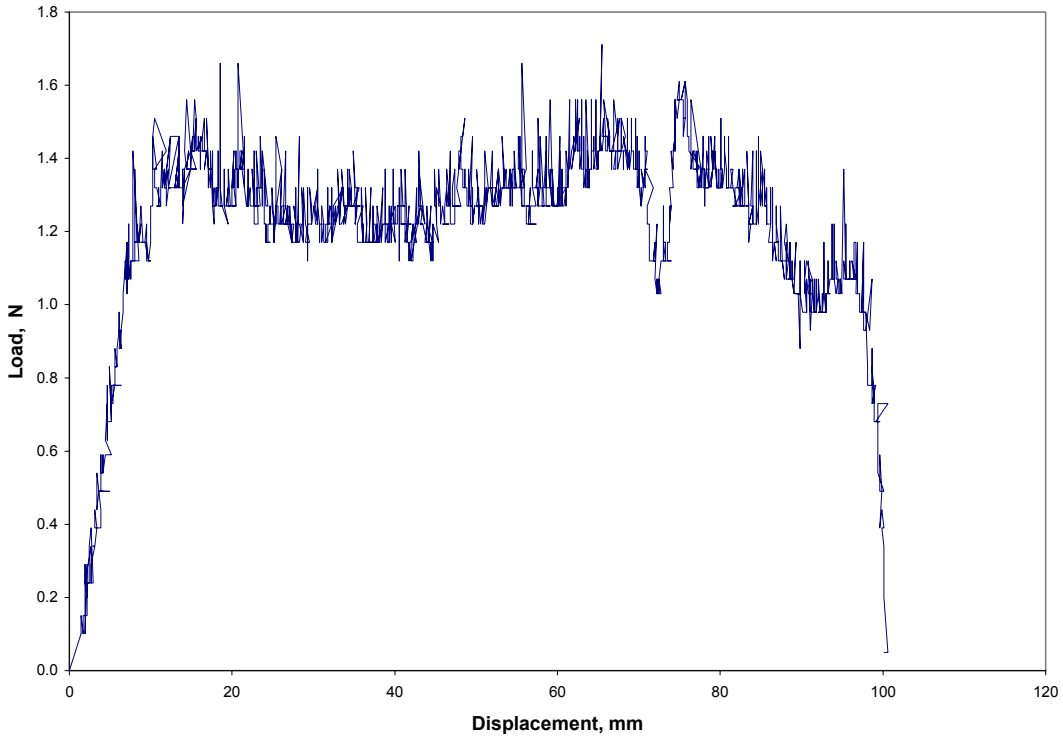

Figure B.37: Load Versus Displacement for Subject B, 90 degrees, 1 min, 300 mm/min, Test 4

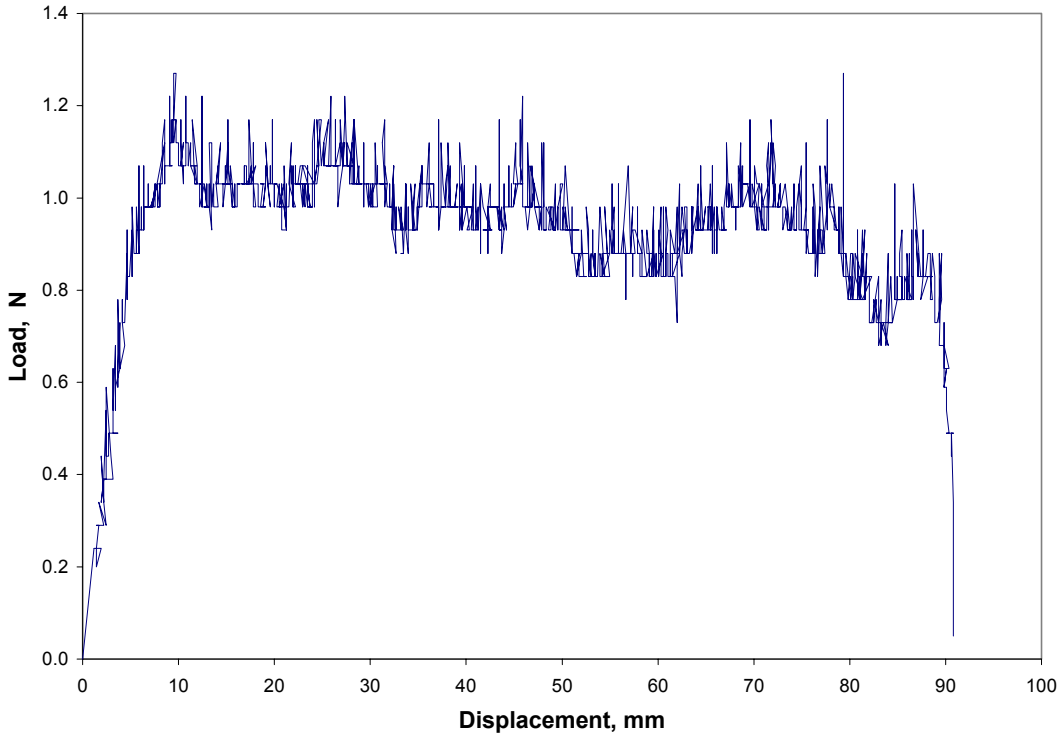

Figure B.38: Load Versus Displacement for Subject B, 90 degrees, 1 min, 300 mm/min, Test 5

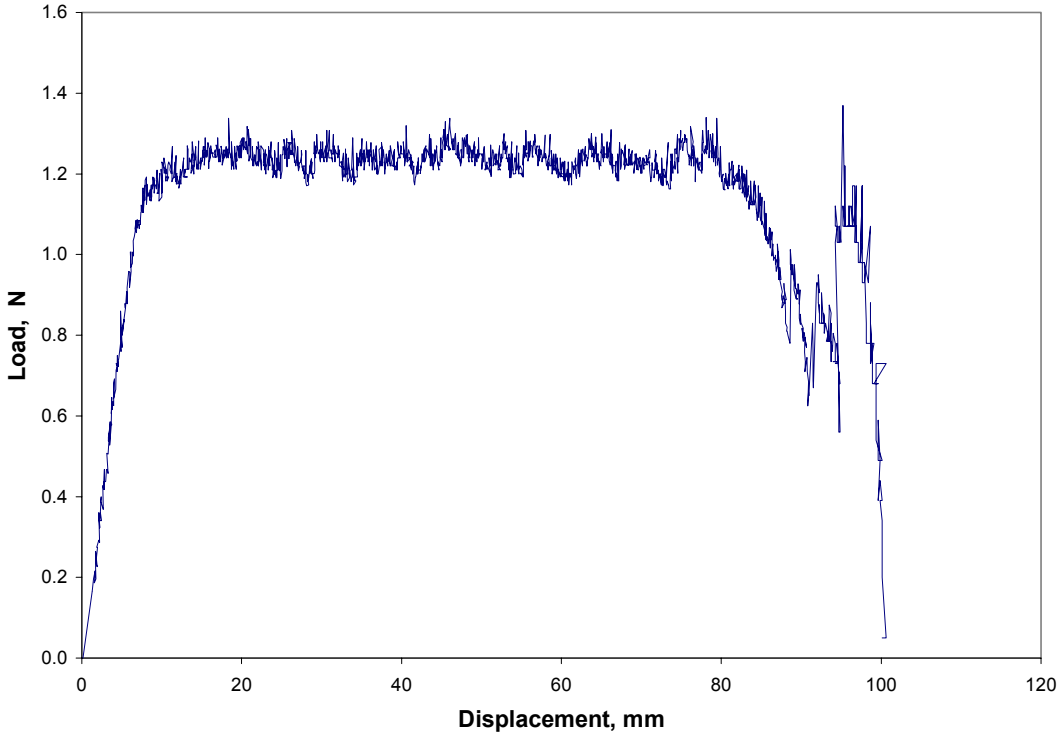

Figure B.39: Load Versus Displacement for Subject B, 90 degrees, 1 min, 300 mm/min, Average

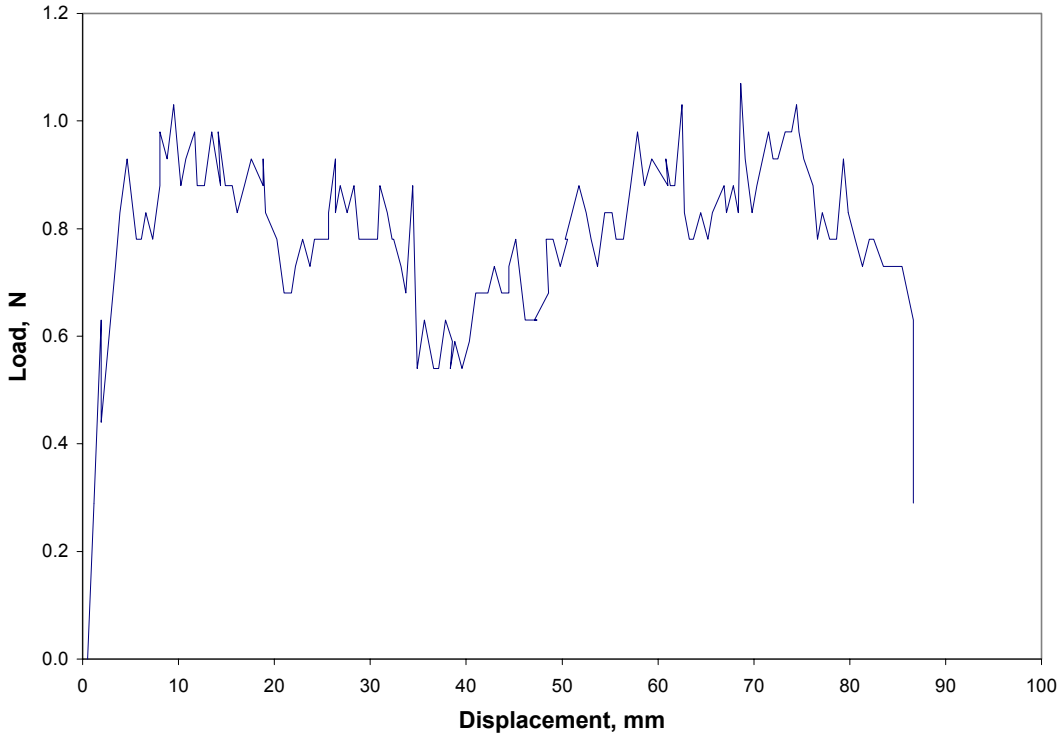

Figure B.40: Load Versus Displacement for Subject B, 90 degrees, 1 min, 400 mm/min, Test 1

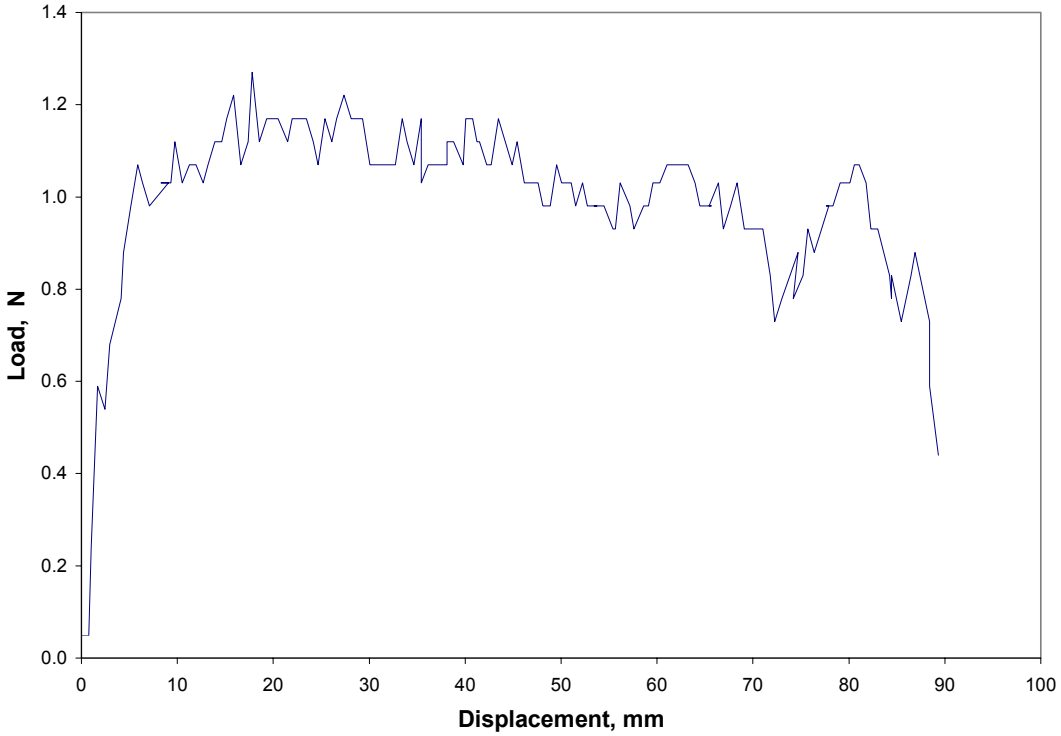

Figure B.41: Load Versus Displacement for Subject B, 90 degrees, 1 min, 400 mm/min, Test 2

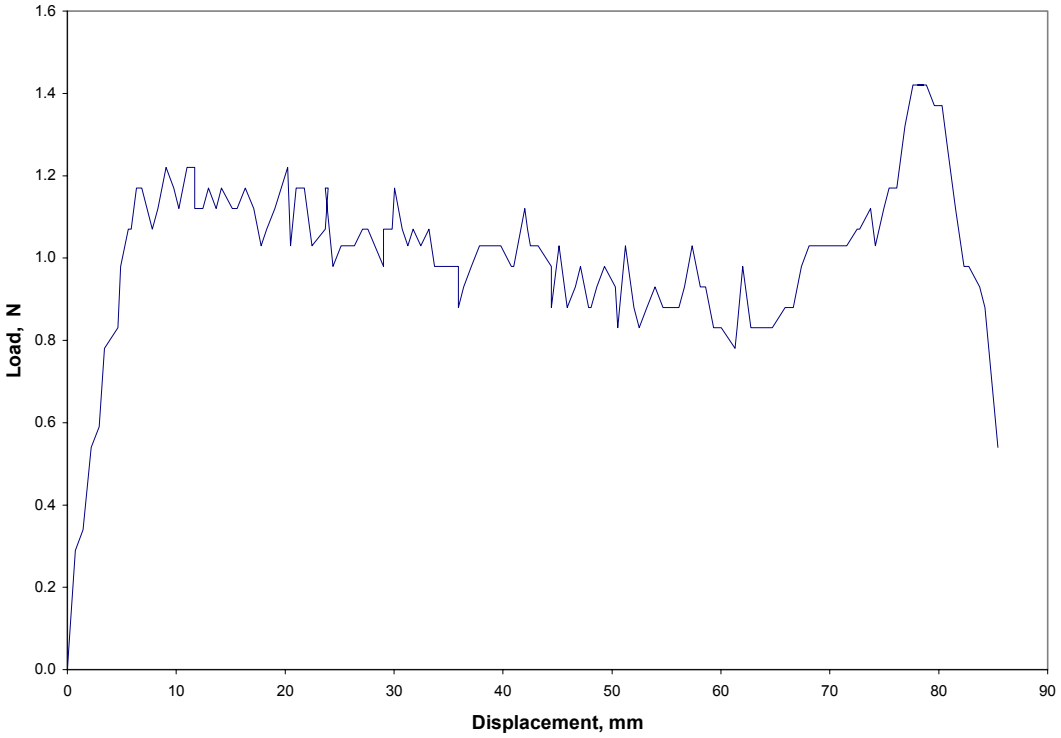

Figure B.42: Load Versus Displacement for Subject B, 90 degrees, 1 min, 400 mm/min, Test 3

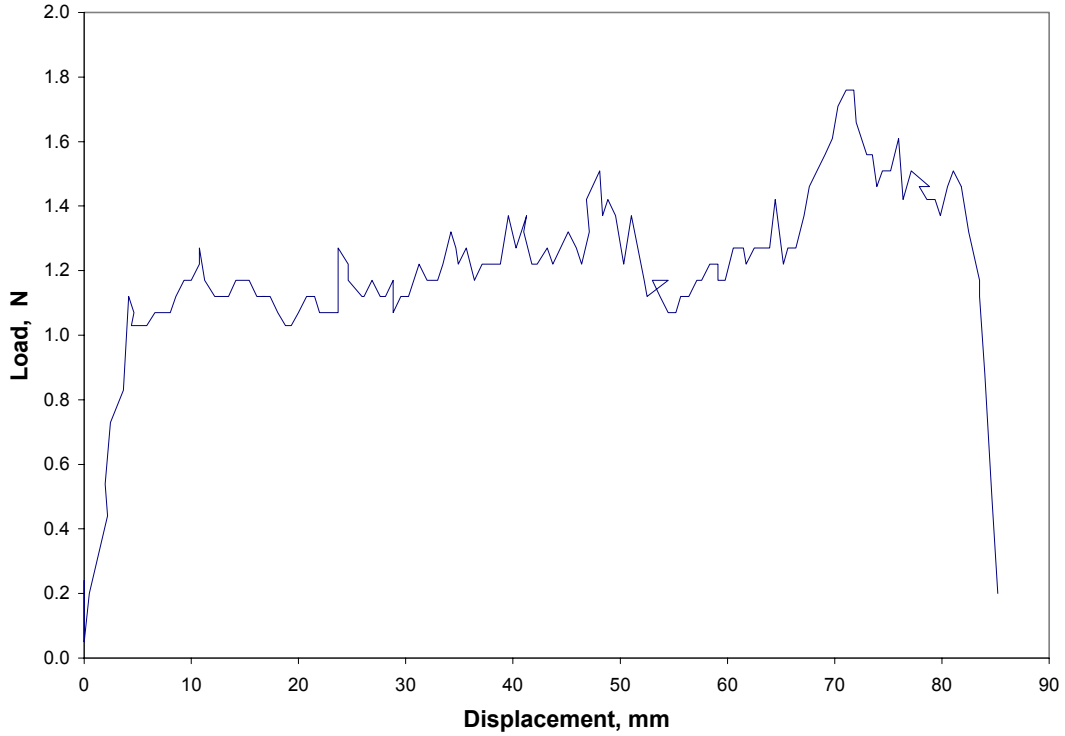

Figure B.43: Load Versus Displacement for Subject B, 90 degrees, 1 min, 400 mm/min, Test 4

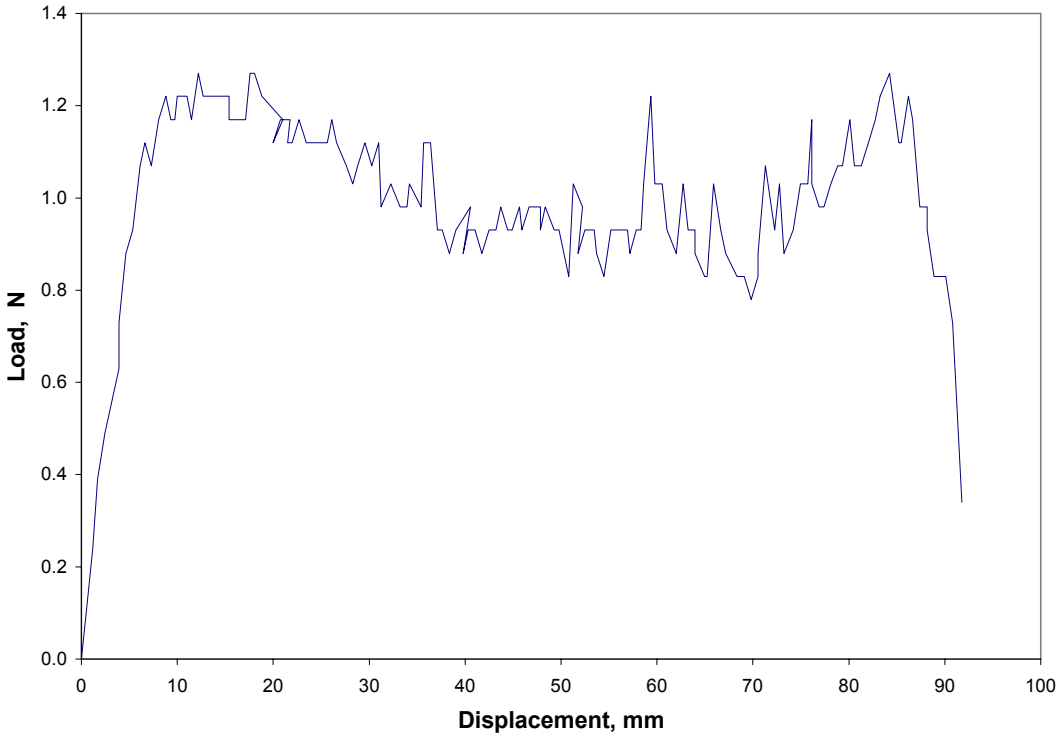

Figure B.44: Load Versus Displacement for Subject B, 90 degrees, 1 min, 400 mm/min, Test 5

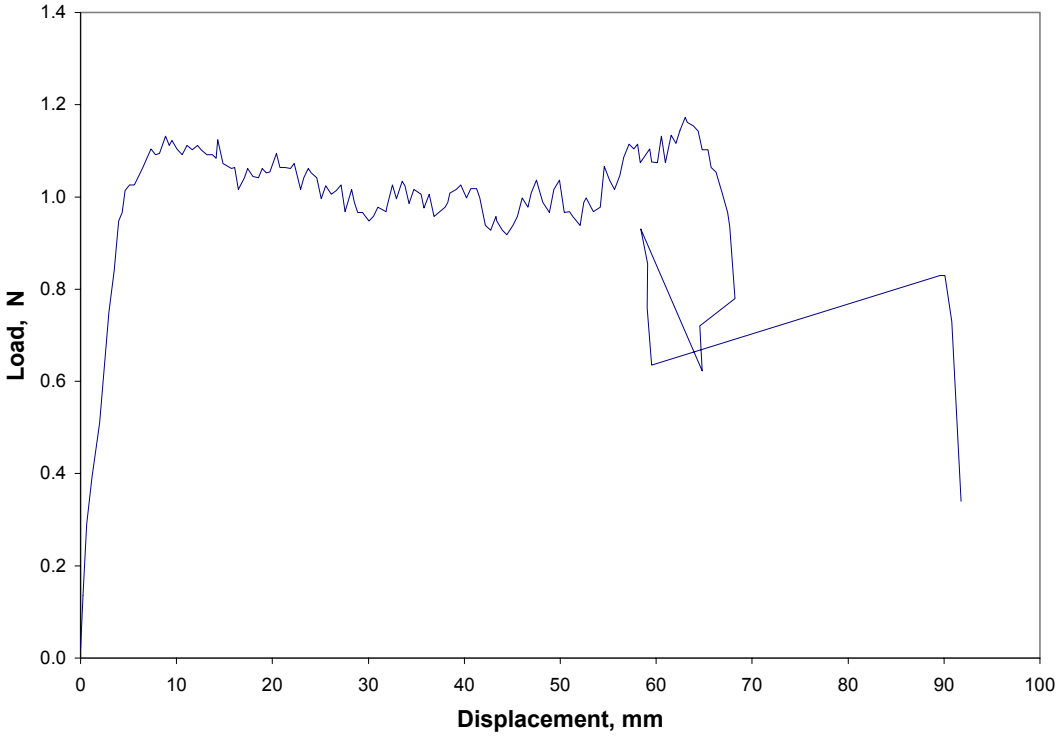

Figure B.45: Load Versus Displacement for Subject B, 90 degrees, 1 min, 400 mm/min, Average

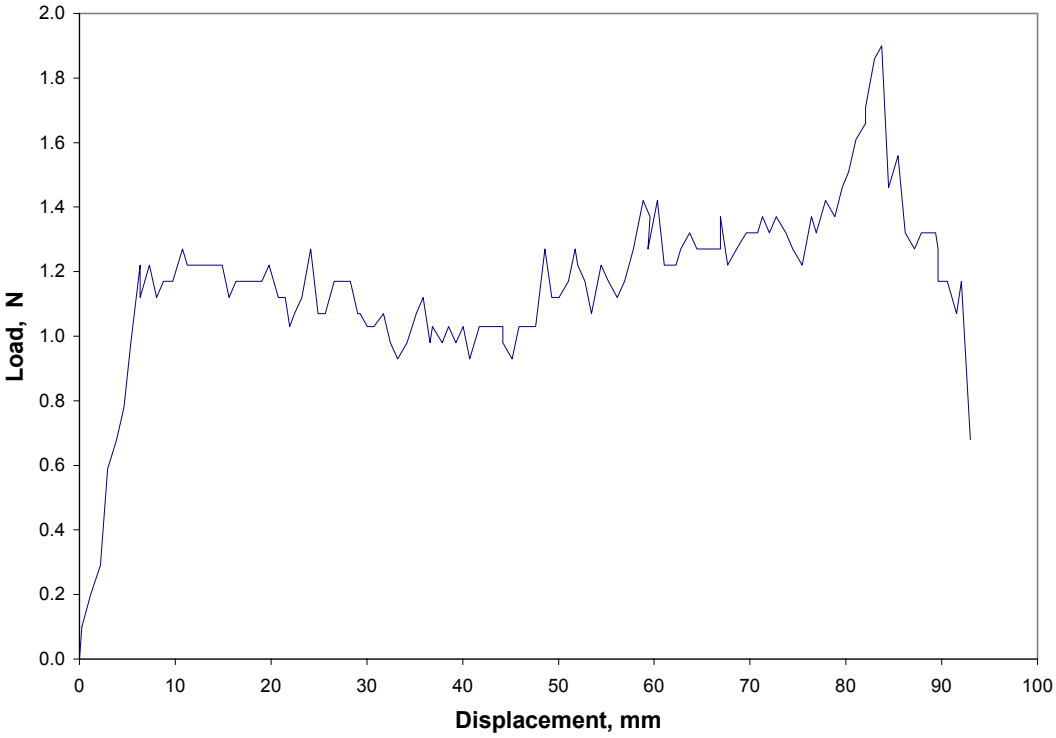

Figure B.46: Load Versus Displacement for Subject B, 90 degrees, 1 min, 500 mm/min, Test 1

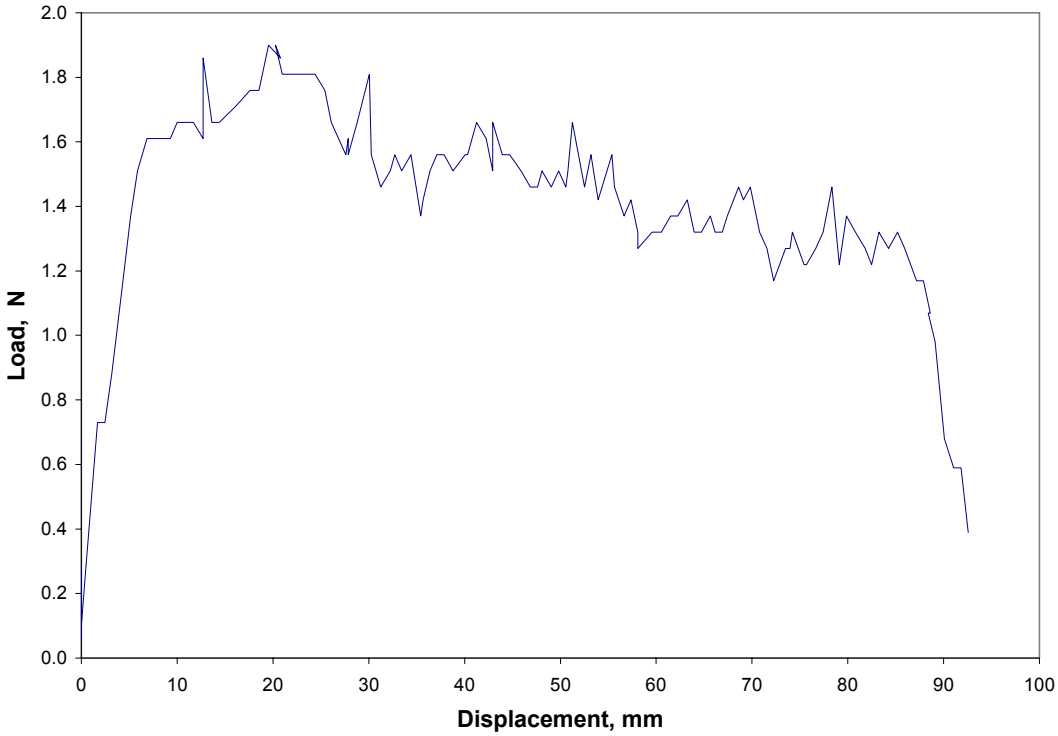

Figure B.47: Load Versus Displacement for Subject B, 90 degrees, 1 min, 500 mm/min, Test 2

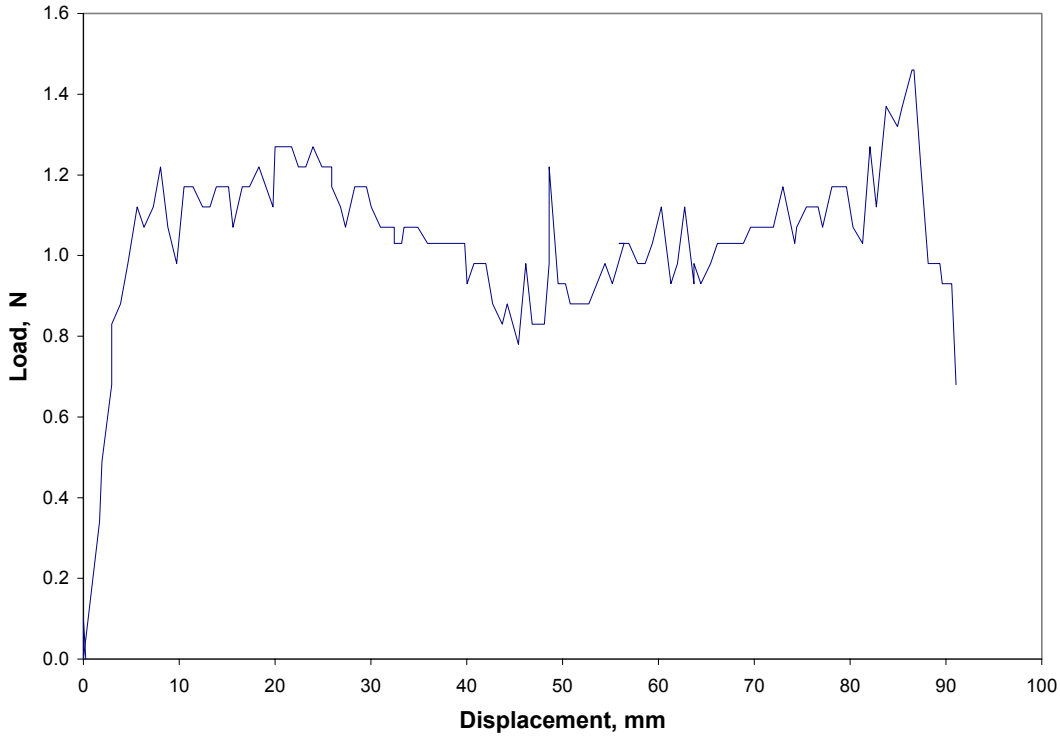

Figure B.48: Load Versus Displacement for Subject B, 90 degrees, 1 min, 500 mm/min, Test 3

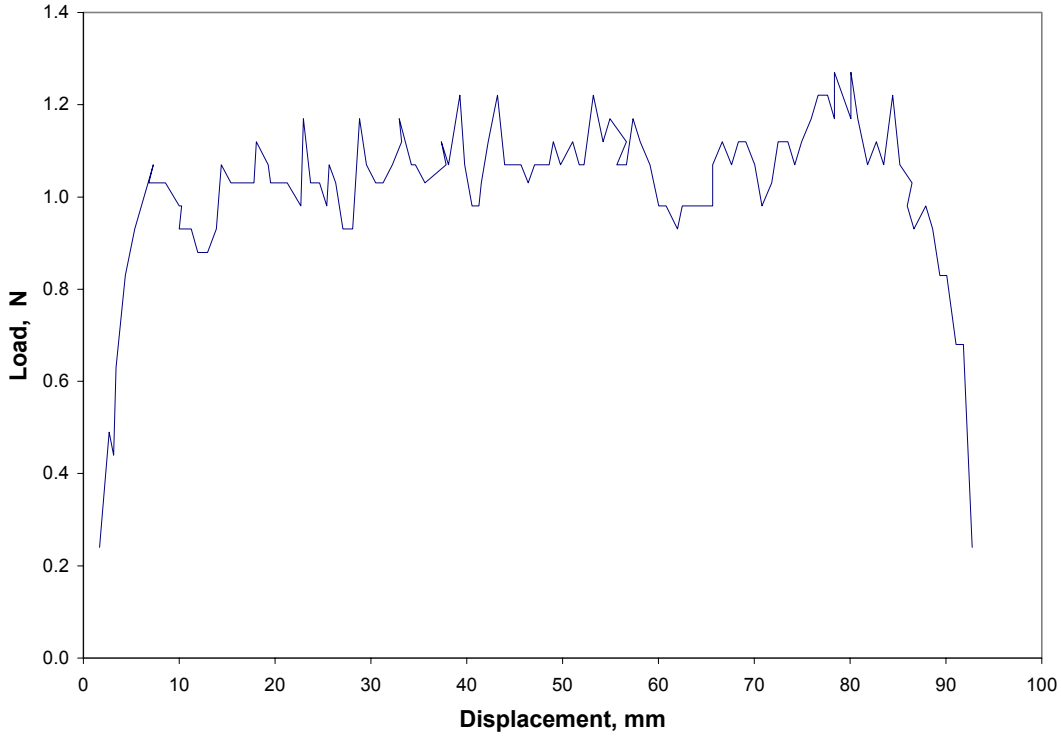

Figure B.49: Load Versus Displacement for Subject B, 90 degrees, 1 min, 500 mm/min, Test 4

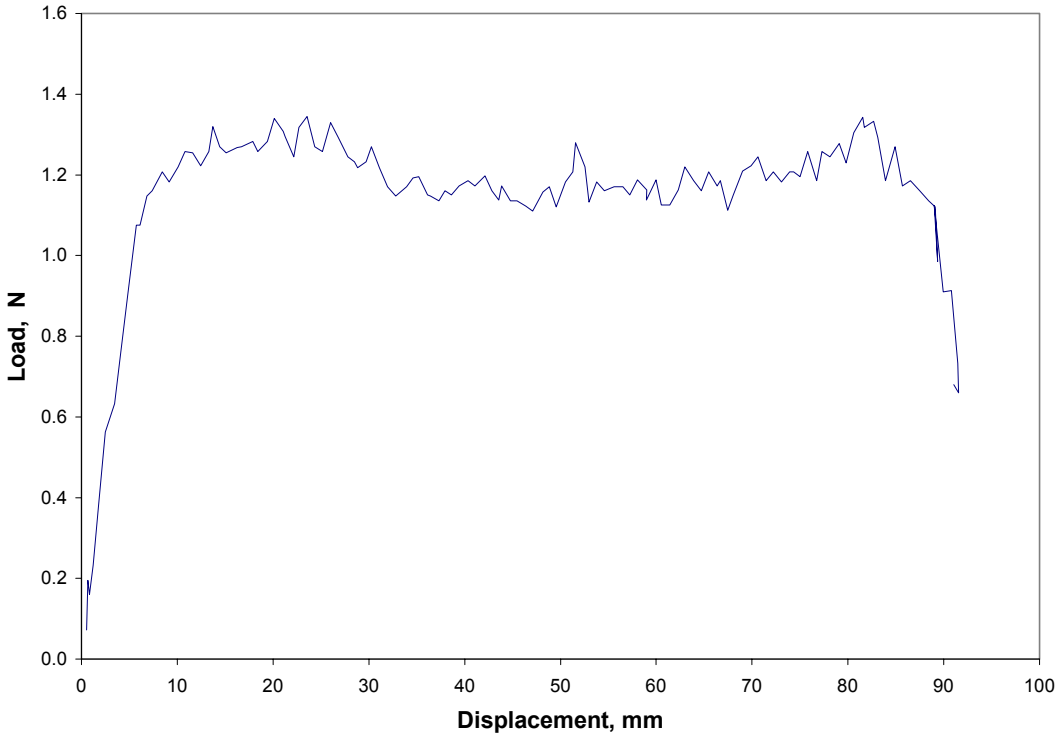

Figure B.50: Load Versus Displacement for Subject B, 90 degrees, 1 min, 500 mm/min, Average

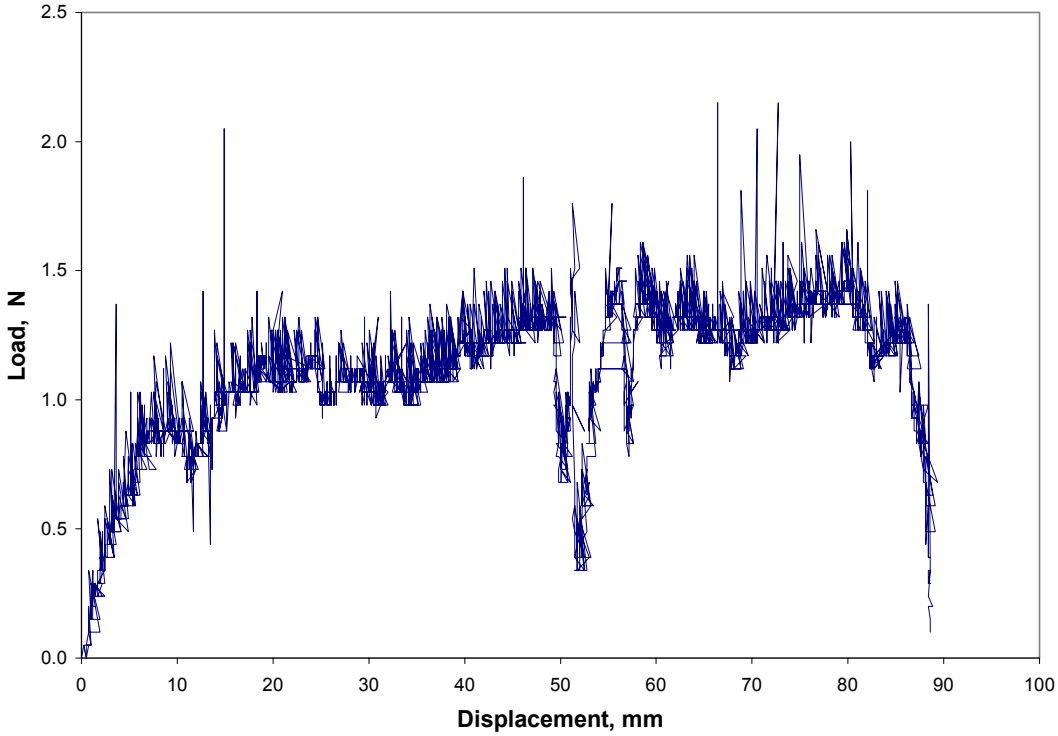

Figure B.51: Load Versus Displacement for Subject C, 90 degrees, 1 min, 100 mm/min, Test 1

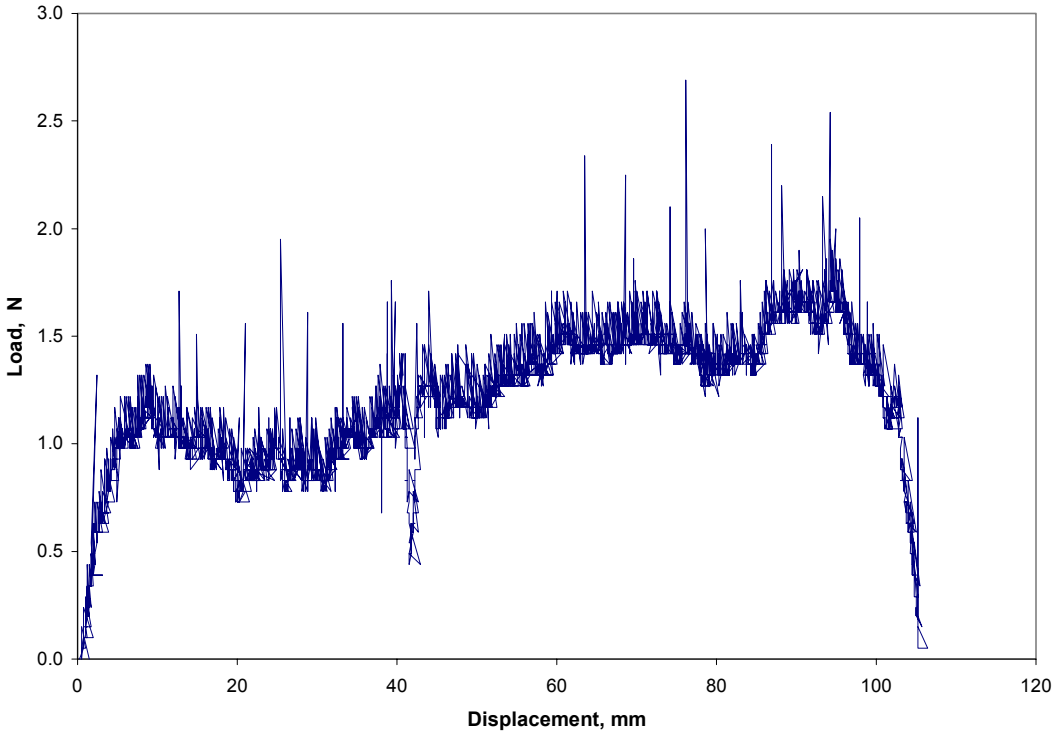

Figure B.52: Load Versus Displacement for Subject C, 90 degrees, 1 min, 100 mm/min, Test 2

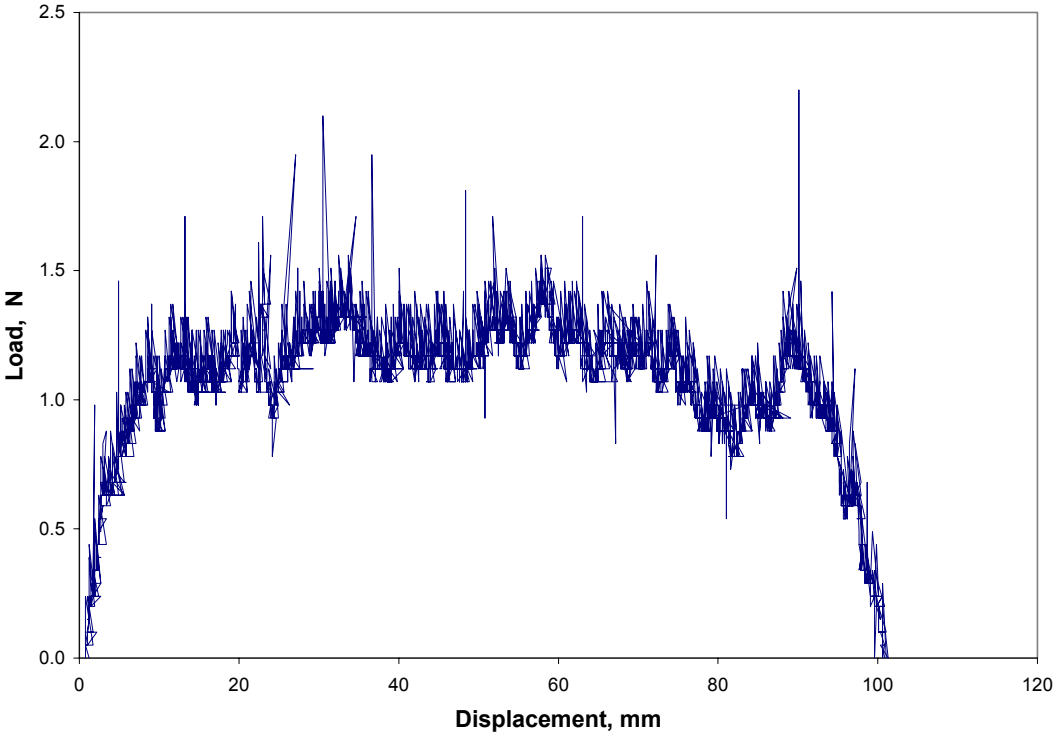

Figure B.53: Load Versus Displacement for Subject C, 90 degrees, 1 min, 100 mm/min, Test 3

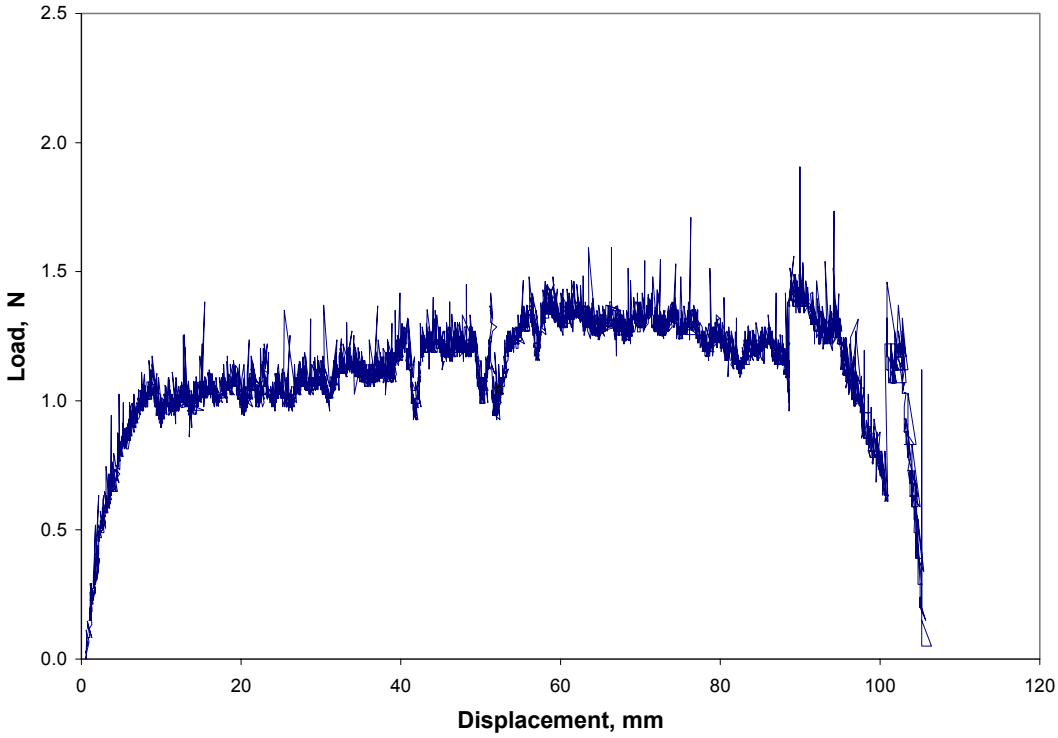

Figure B.54: Load Versus Displacement for Subject C, 90 degrees, 1 min, 100 mm/min, Average

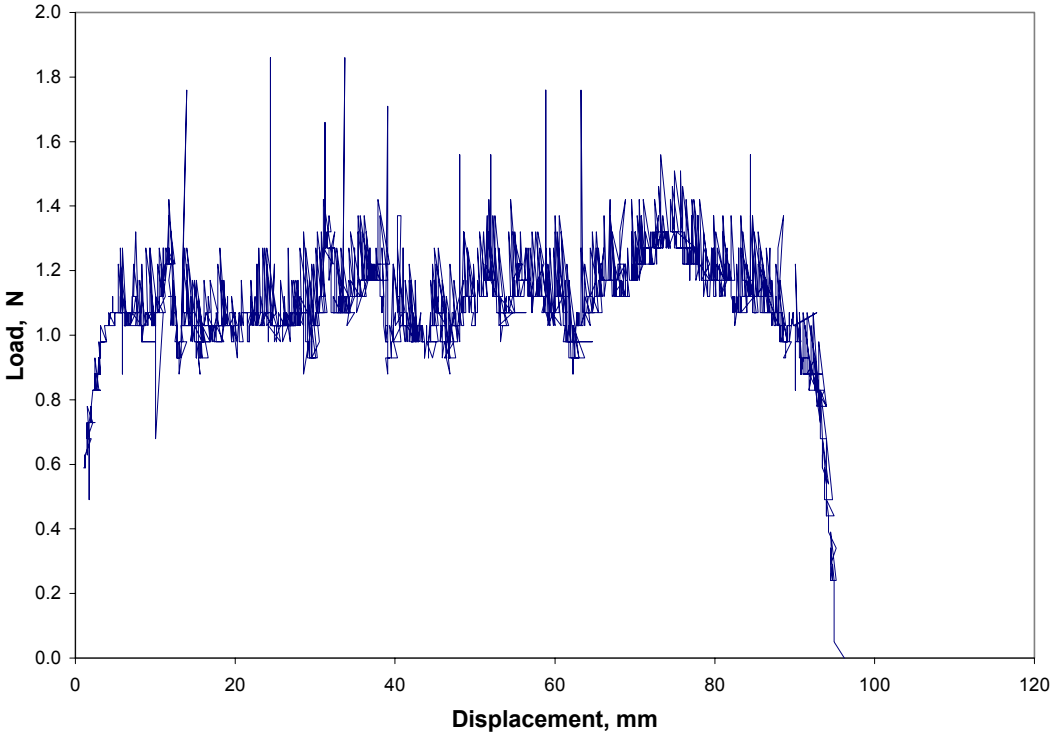

Figure B.55: Load Versus Displacement for Subject C, 90 degrees, 1 min, 200 mm/min, Test 1

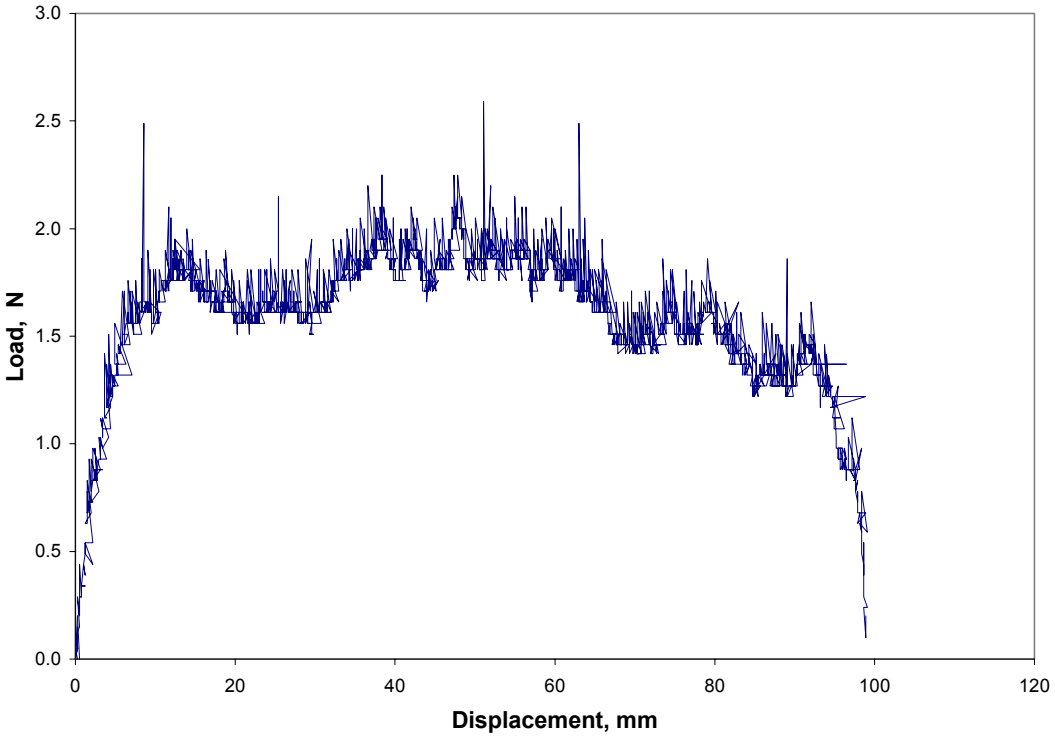

Figure B.56: Load Versus Displacement for Subject C, 90 degrees, 1 min, 200 mm/min, Test 2

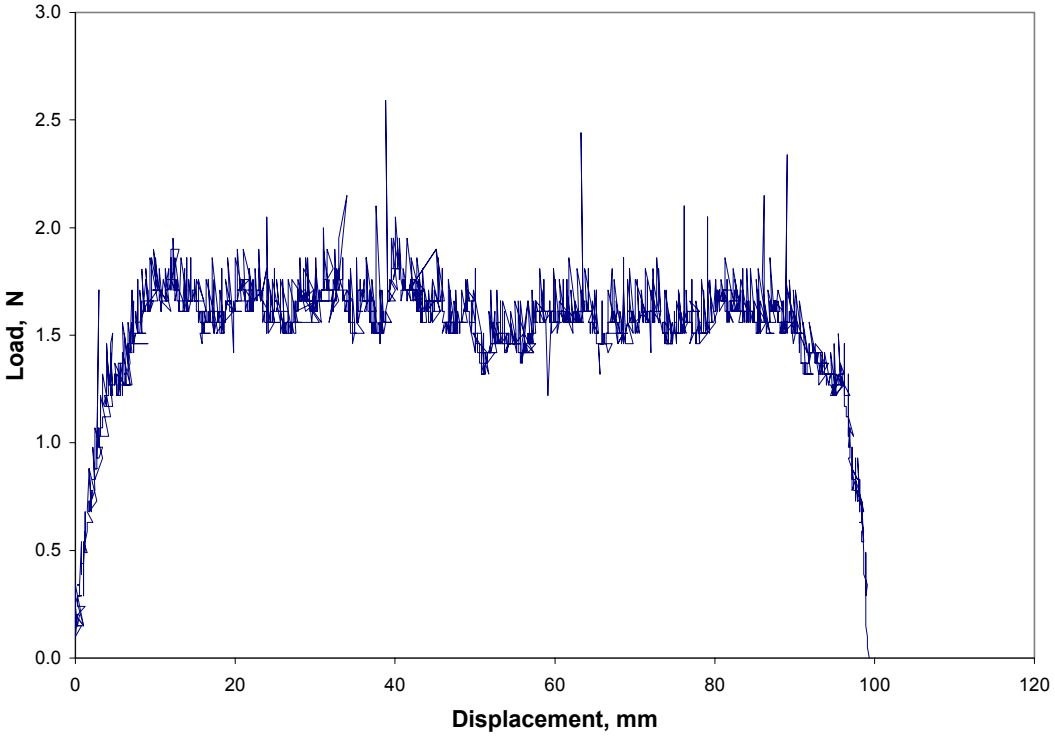

Figure B.57: Load Versus Displacement for Subject C, 90 degrees, 1 min, 200 mm/min, Test 3

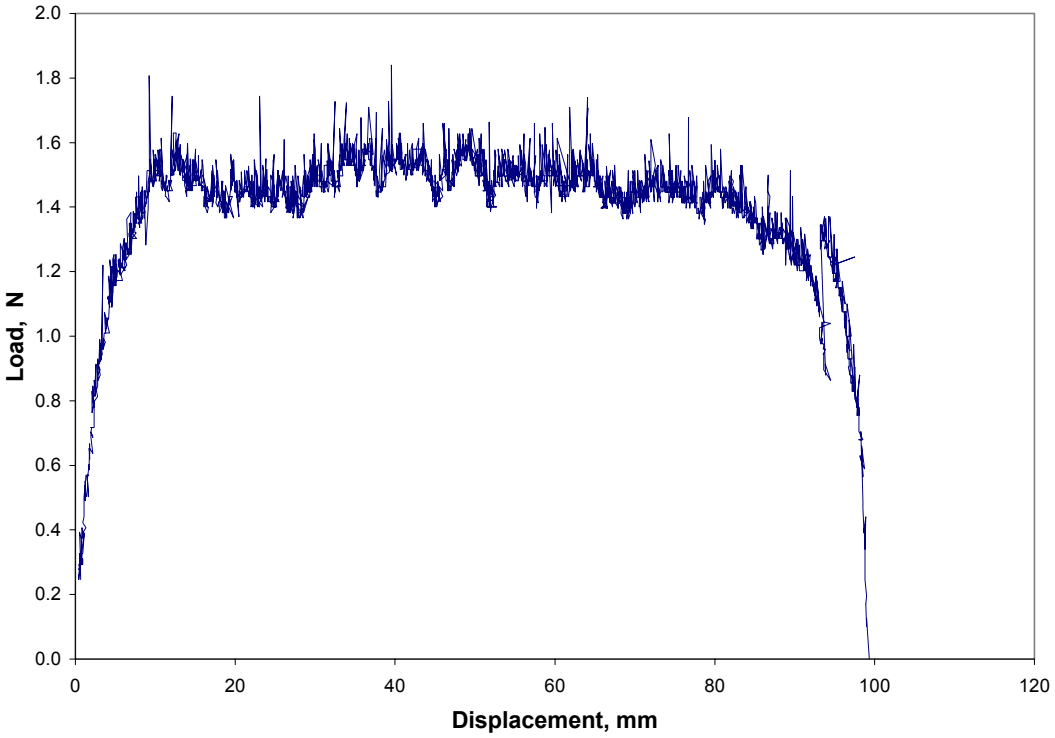

Figure B.58: Load Versus Displacement for Subject C, 90 degrees, 1 min, 200 mm/min, Average

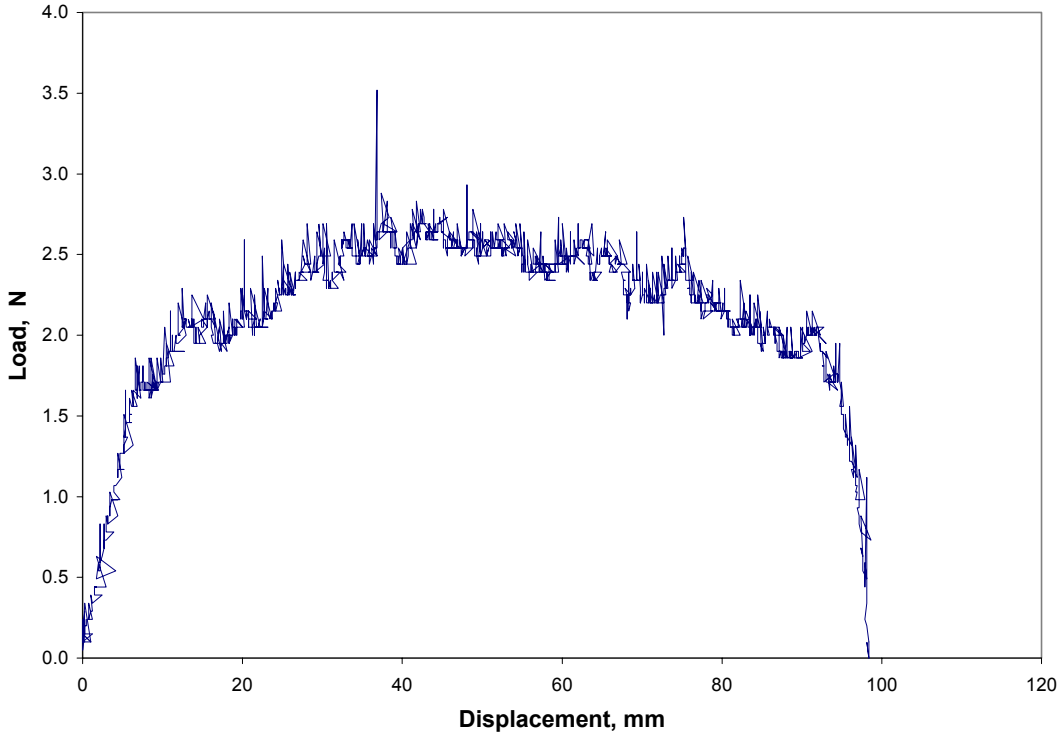

Figure B.59: Load Versus Displacement for Subject C, 90 degrees, 1 min, 300 mm/min, Test 1

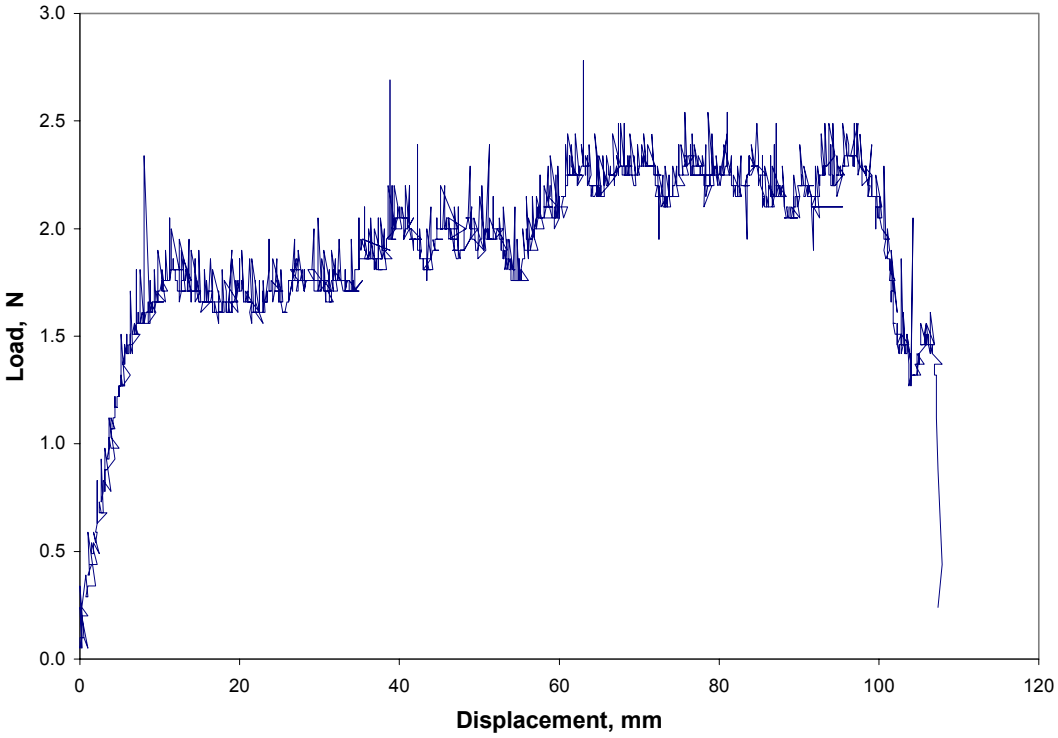

Figure B.60: Load Versus Displacement for Subject C, 90 degrees, 1 min, 300 mm/min, Test 2

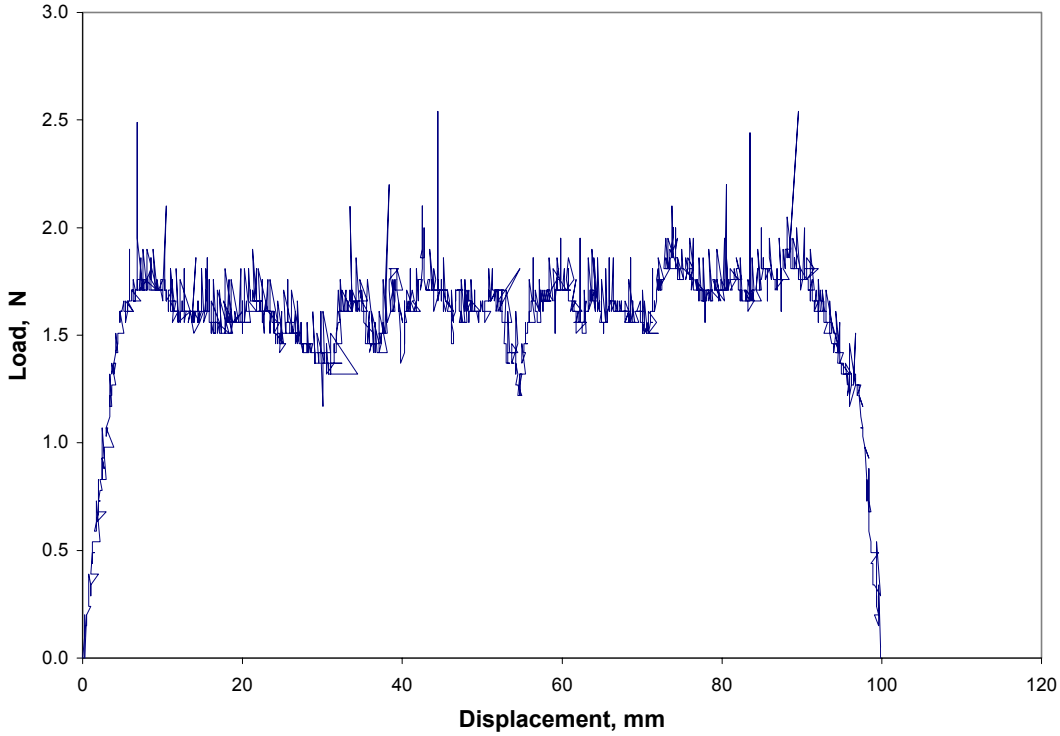

Figure B.61: Load Versus Displacement for Subject C, 90 degrees, 1 min, 300 mm/min, Test 3

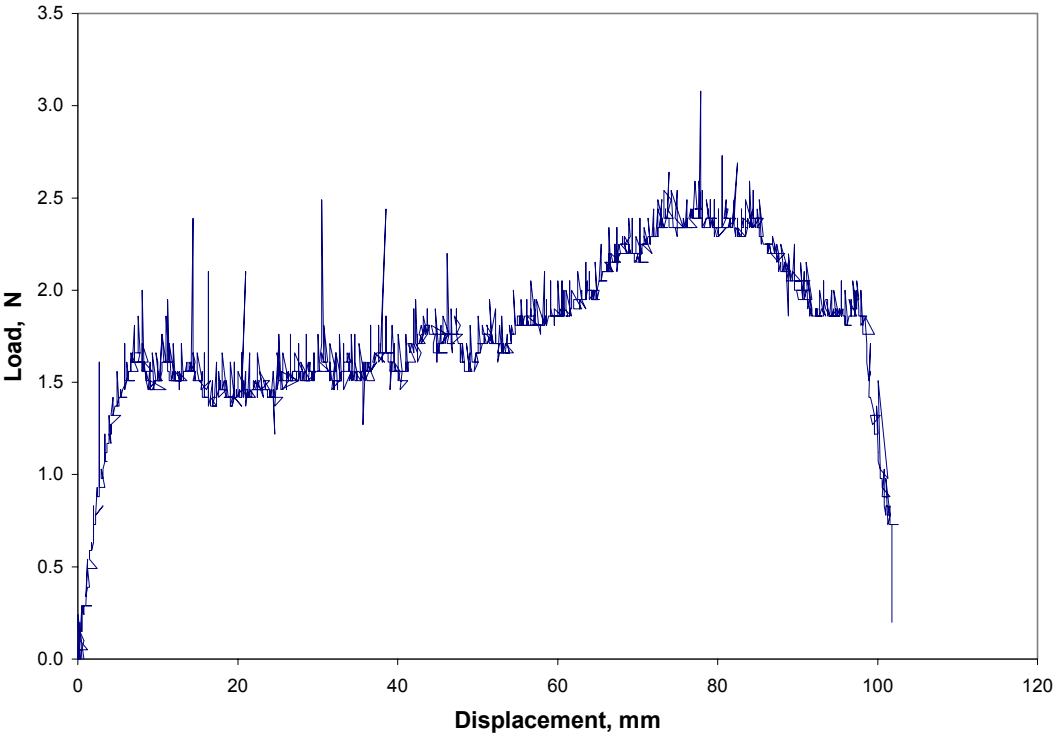

Figure B.62: Load Versus Displacement for Subject C, 90 degrees, 1 min, 300 mm/min, Test 4

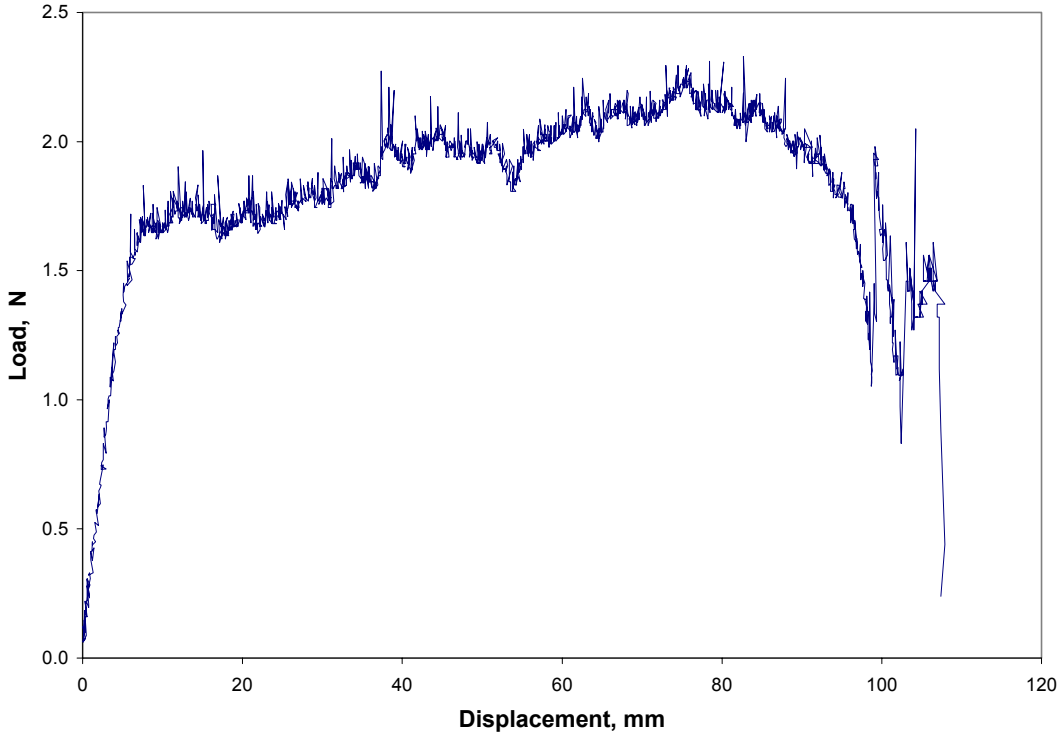

Figure B.63: Load Versus Displacement for Subject C, 90 degrees, 1 min, 300 mm/min, Average

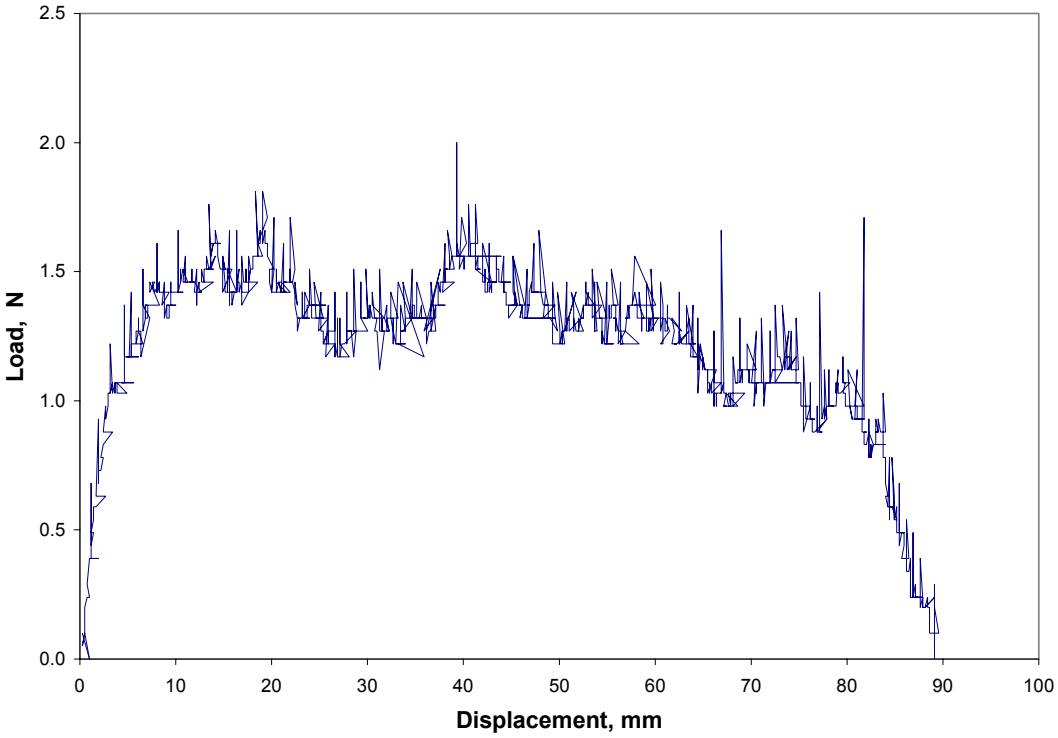

Figure B.64: Load Versus Displacement for Subject C, 90 degrees, 1 min, 400 mm/min, Test 1

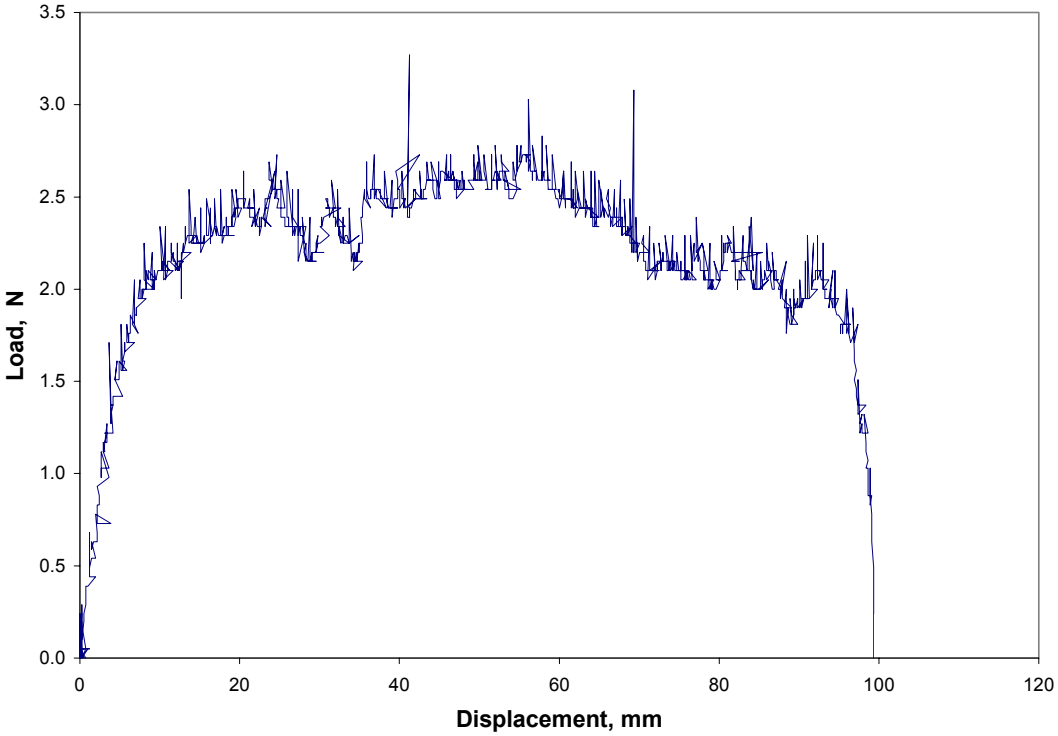

Figure B.65: Load Versus Displacement for Subject C, 90 degrees, 1 min, 400 mm/min, Test 2

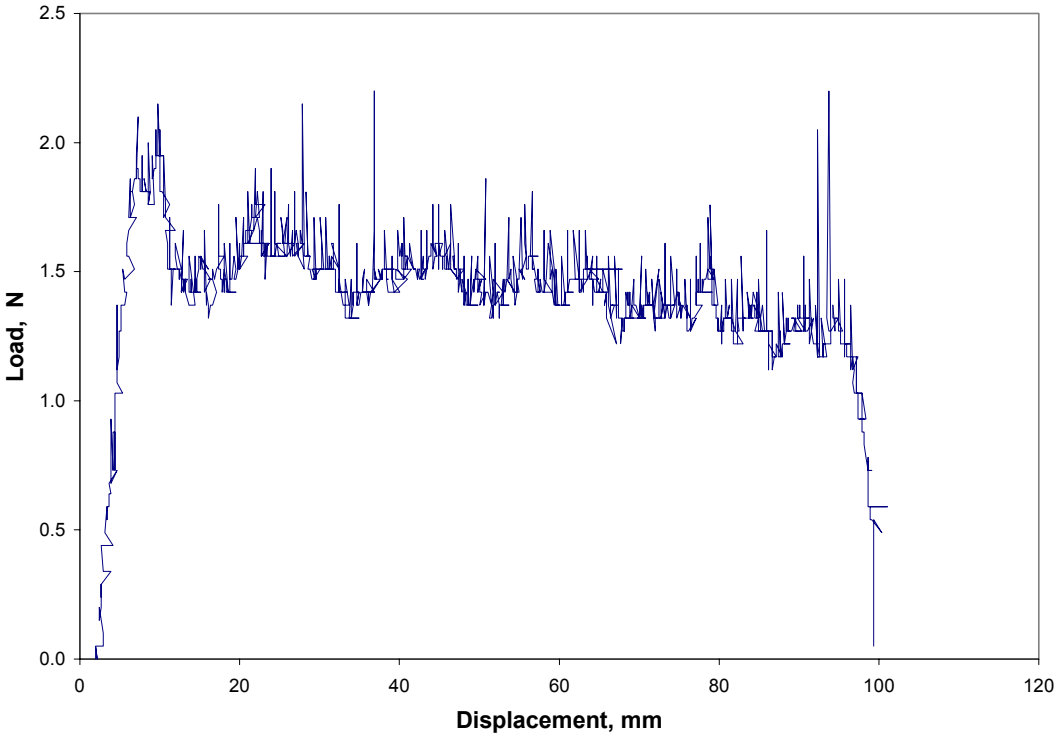

Figure B.66: Load Versus Displacement for Subject C, 90 degrees, 1 min, 400 mm/min, Test 3

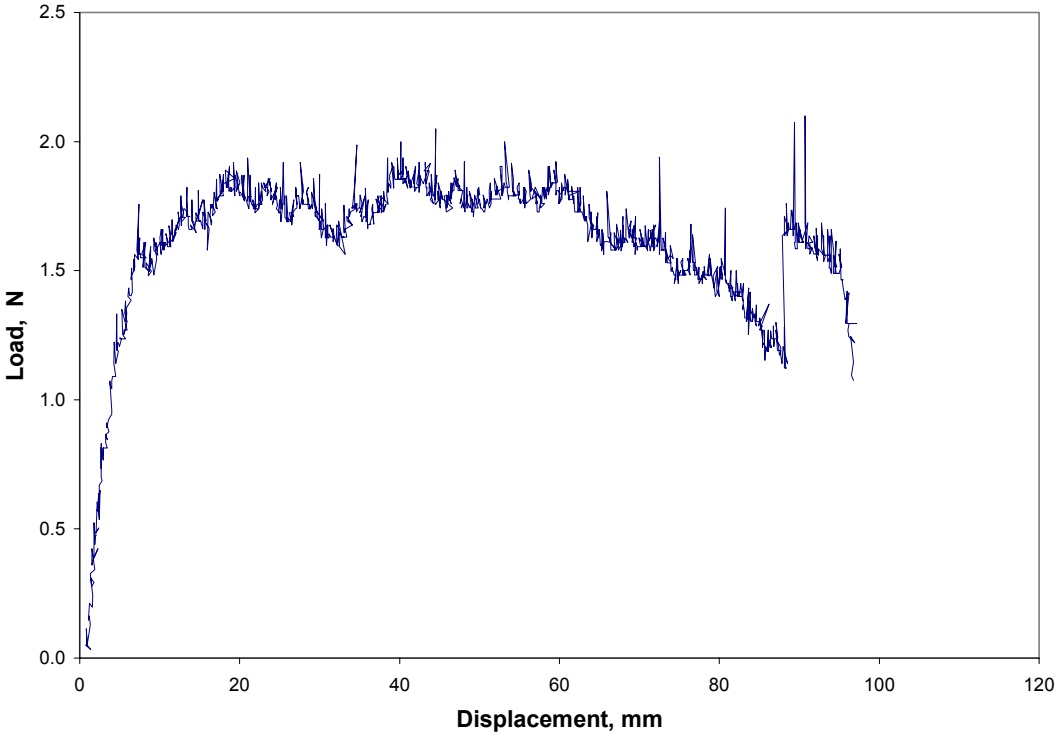

Figure B.67: Load Versus Displacement for Subject C, 90 degrees, 1 min, 400 mm/min, Average

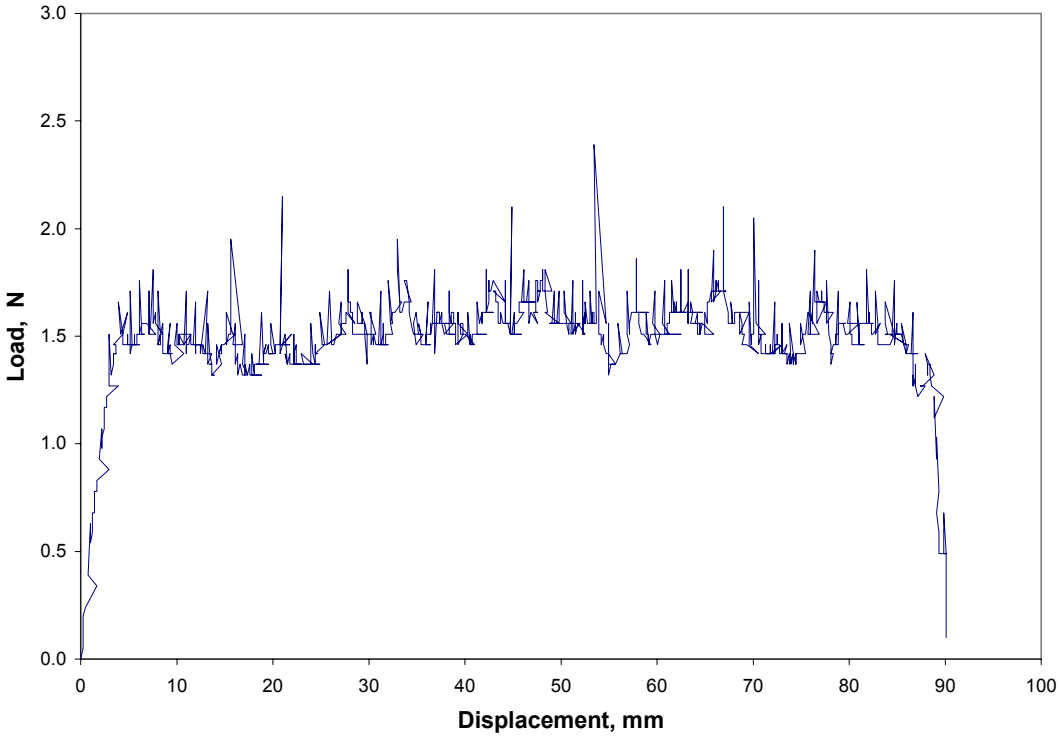

Figure B.68: Load Versus Displacement for Subject C, 90 degrees, 1 min, 500 mm/min, Test 1

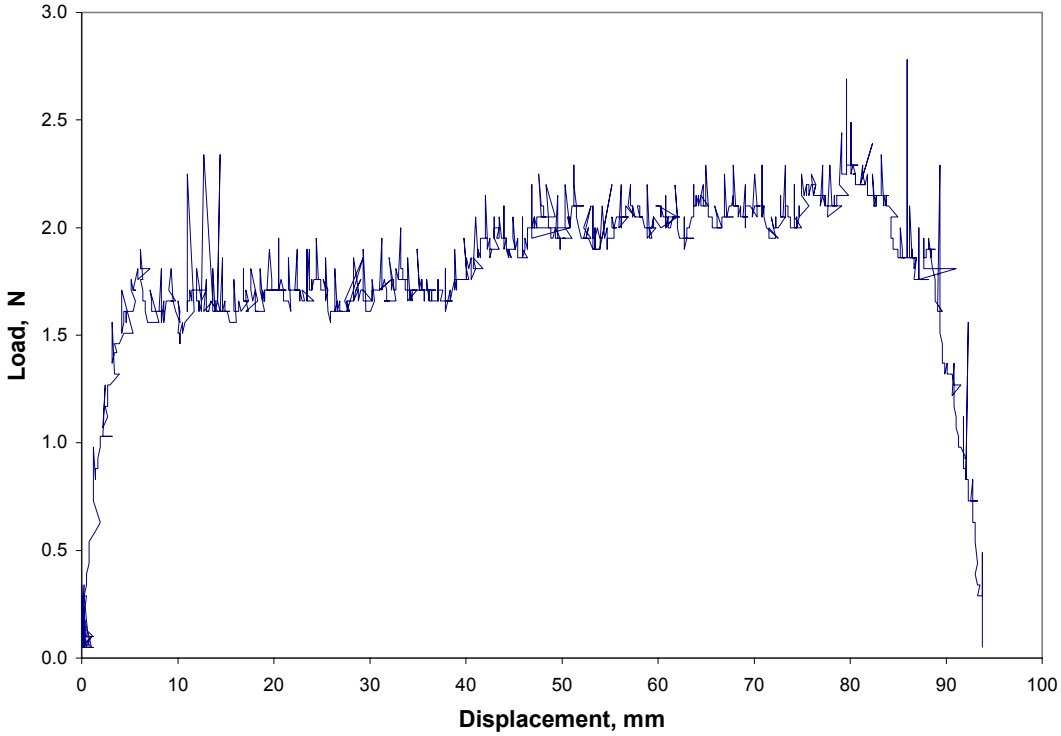

Figure B.69: Load Versus Displacement for Subject C, 90 degrees, 1 min, 500 mm/min, Test 2

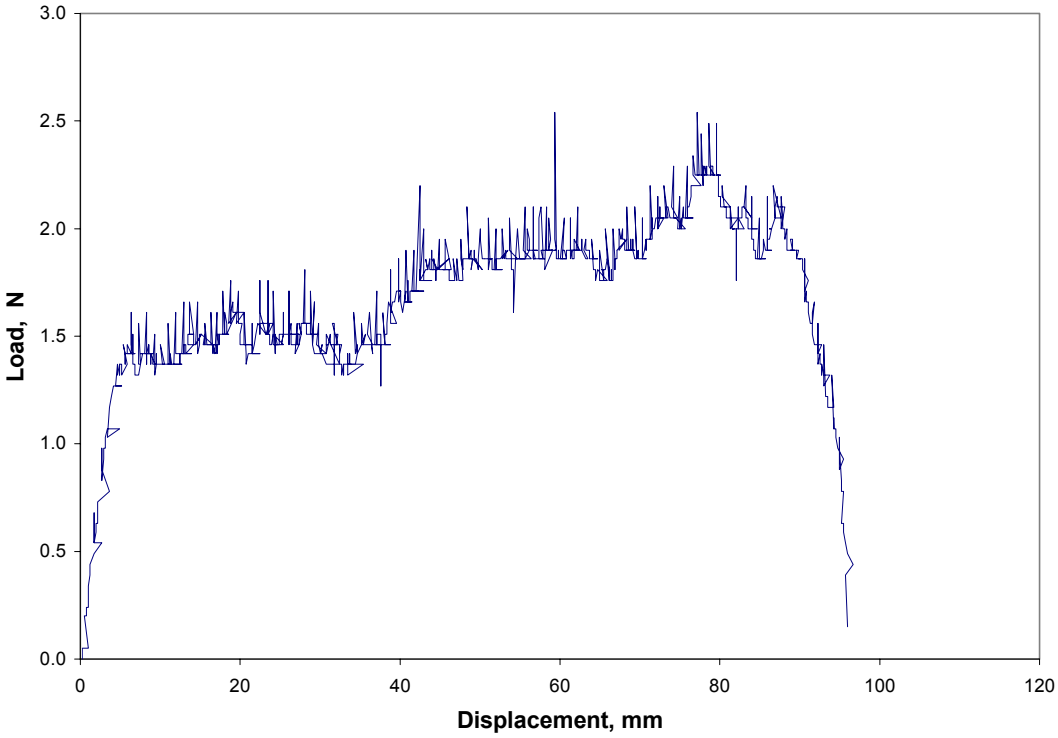

Figure B.70: Load Versus Displacement for Subject C, 90 degrees, 1 min, 500 mm/min, Test 3

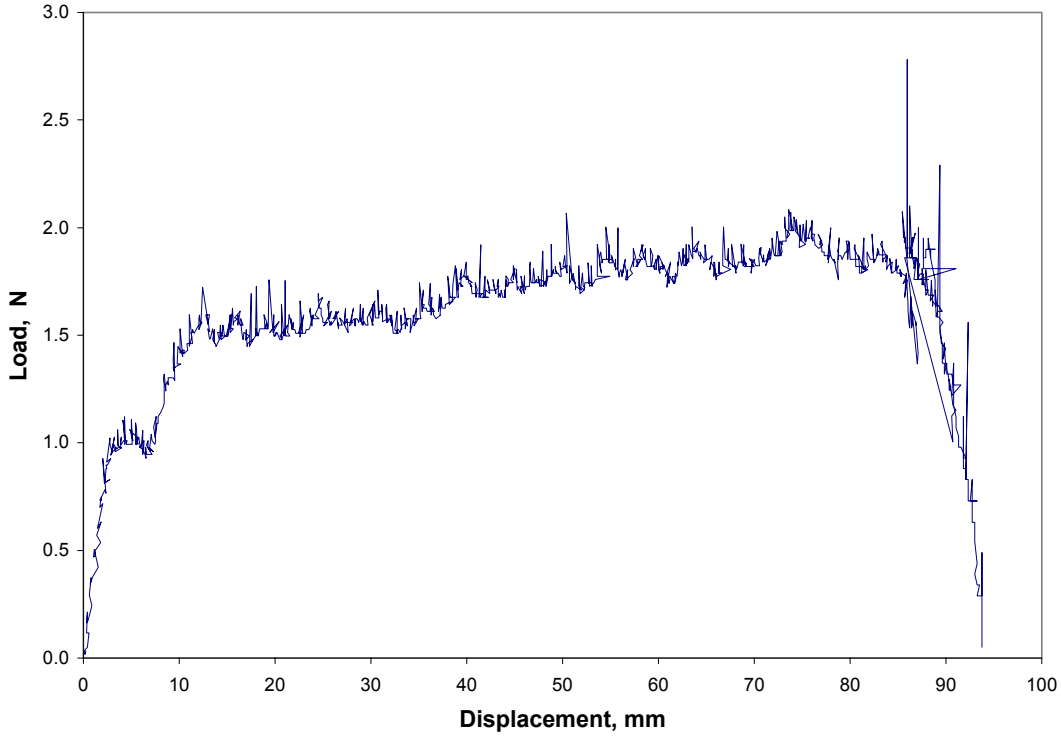

Figure B.71: Load Versus Displacement for Subject C, 90 degrees, 1 min, 500 mm/min, Average

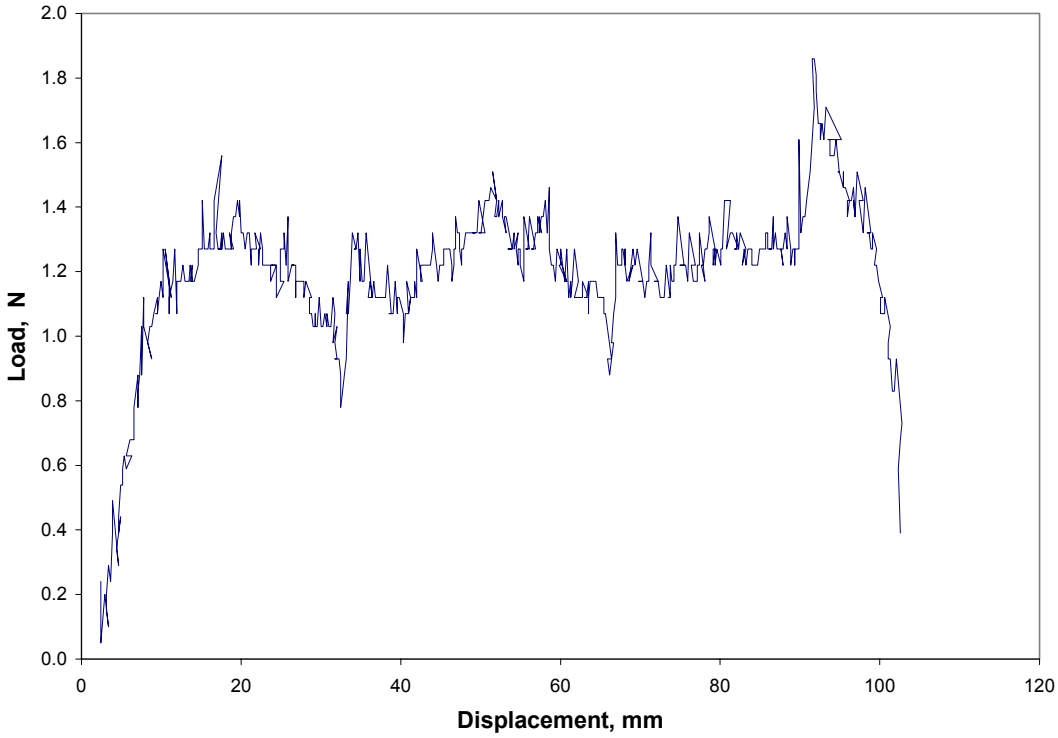

Figure B.72: Load Versus Displacement for Subject D, 90 degrees, 1 min, 100 mm/min, Test 1

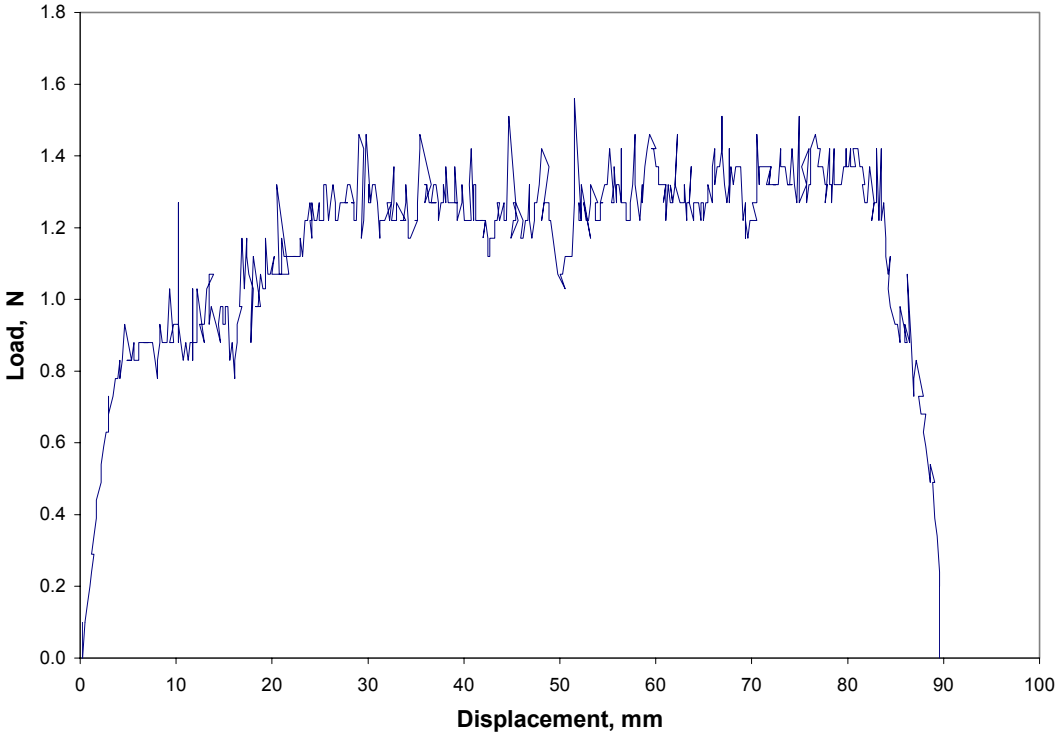

Figure B.73: Load Versus Displacement for Subject D, 90 degrees, 1 min, 100 mm/min, Test 2

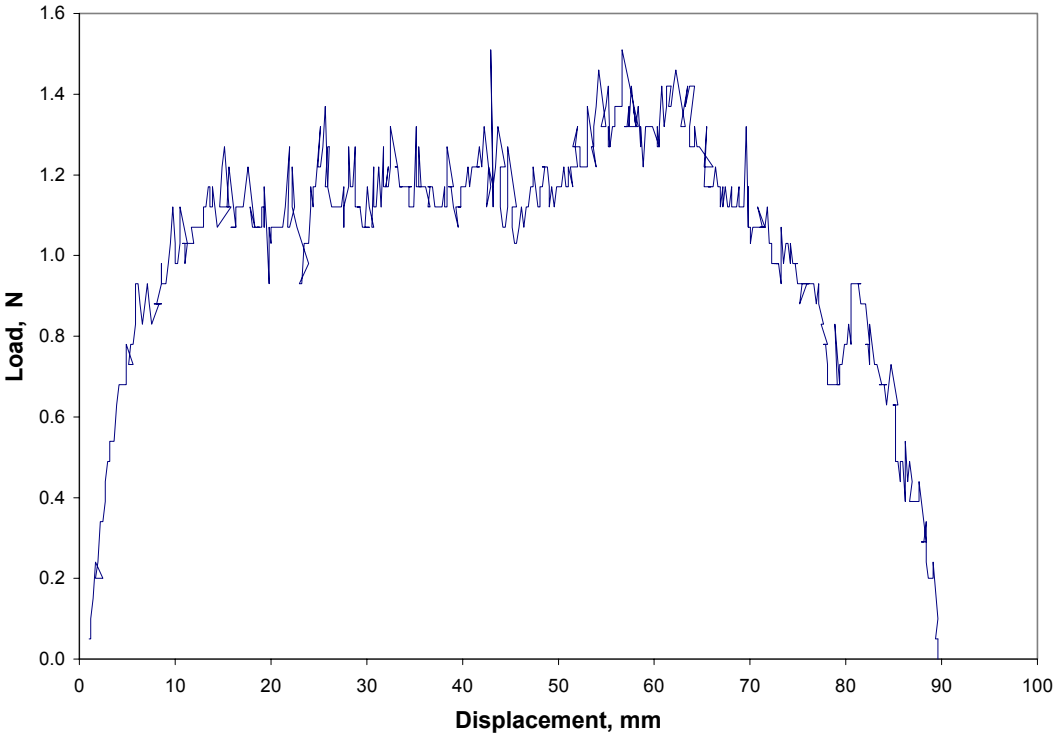

Figure B.74: Load Versus Displacement for Subject D, 90 degrees, 1 min, 100 mm/min, Test 3

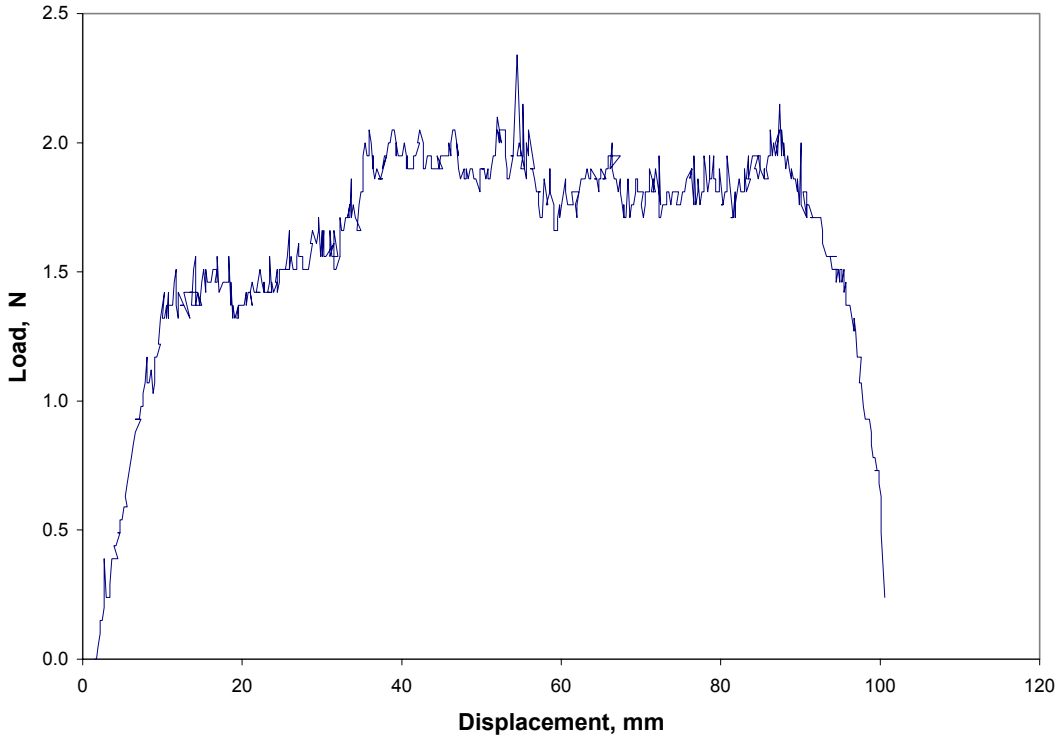

Figure B.75: Load Versus Displacement for Subject D, 90 degrees, 1 min, 100 mm/min, Test 4

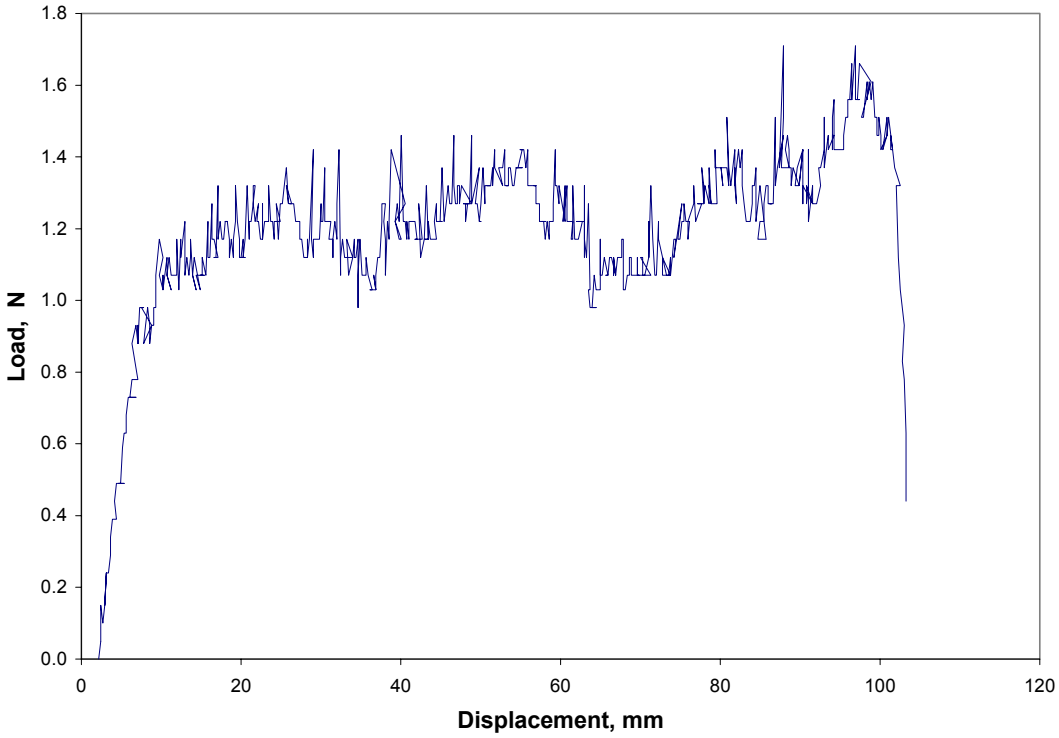

Figure B.76: Load Versus Displacement for Subject D, 90 degrees, 1 min, 100 mm/min, Test 5

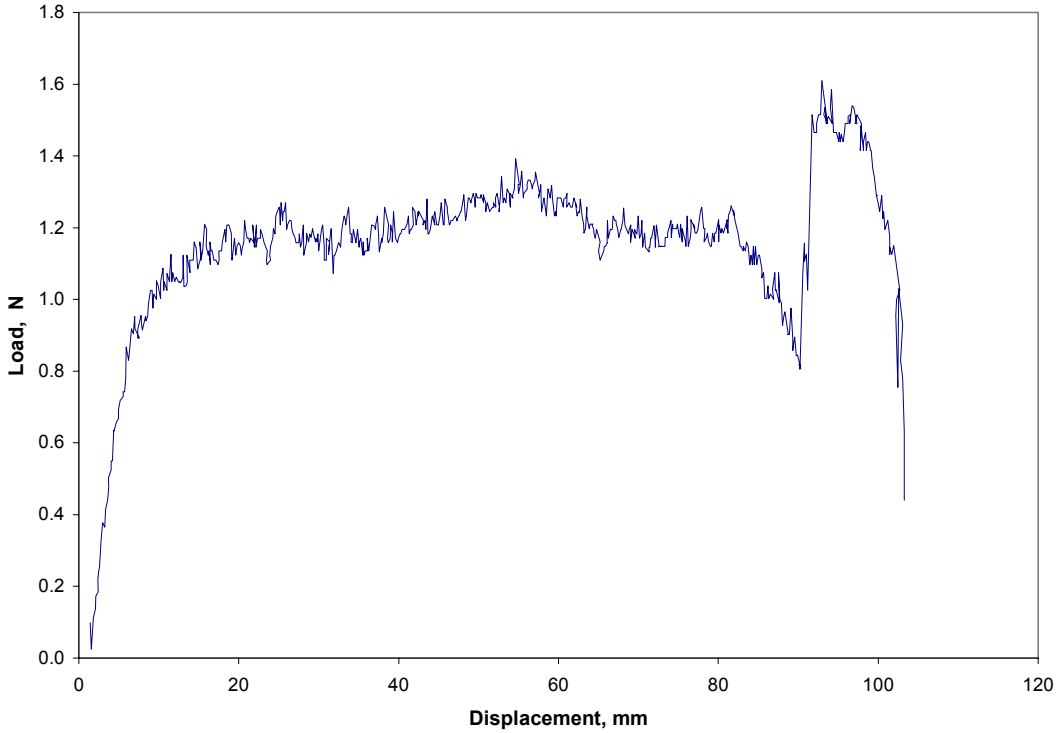

Figure B.77: Load Versus Displacement for Subject D, 90 degrees, 1 min, 100 mm/min, Average

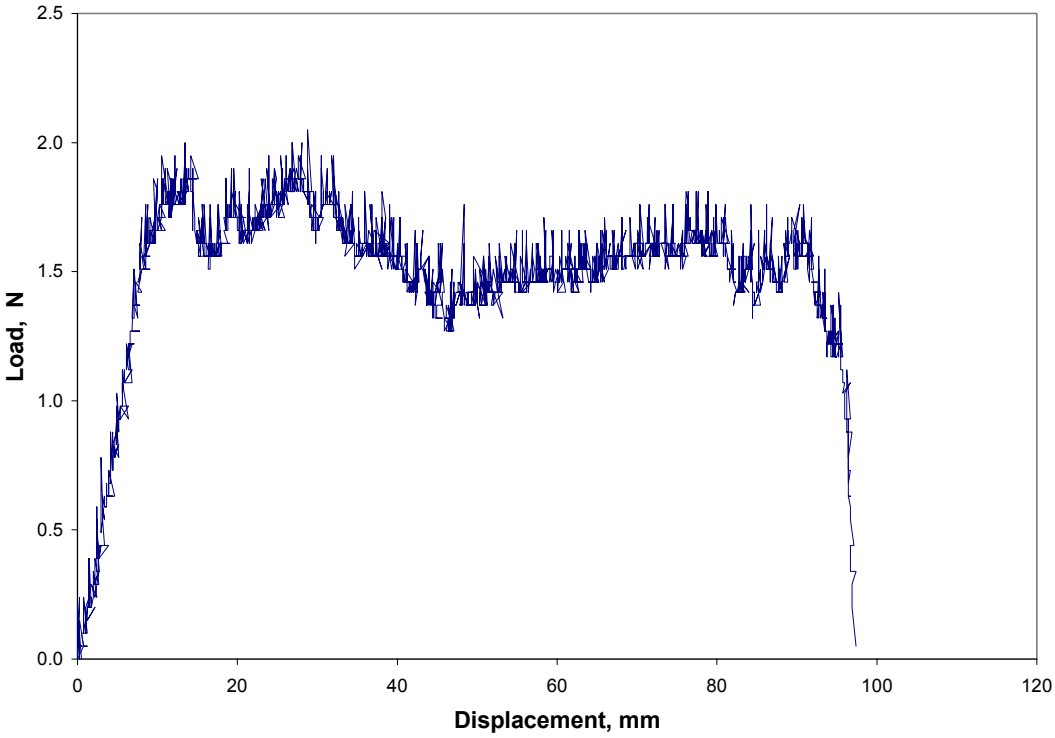

Figure B.78: Load Versus Displacement for Subject D, 90 degrees, 1 min, 200 mm/min, Test 1

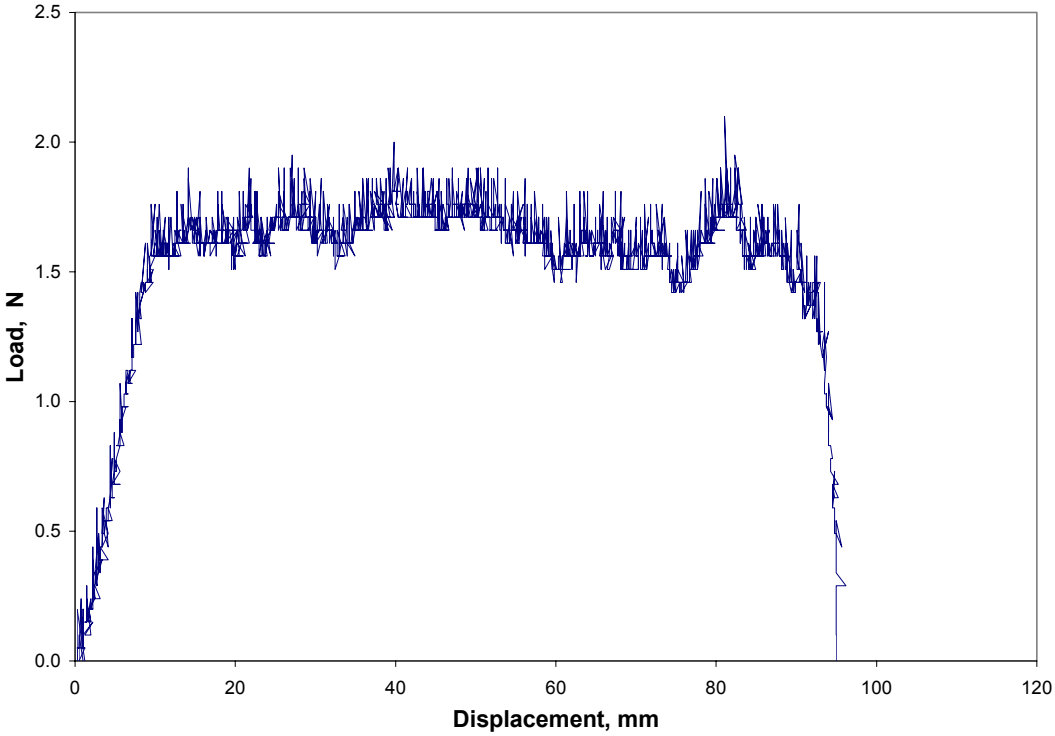

Figure B.79: Load Versus Displacement for Subject D, 90 degrees, 1 min, 200 mm/min, Test 2

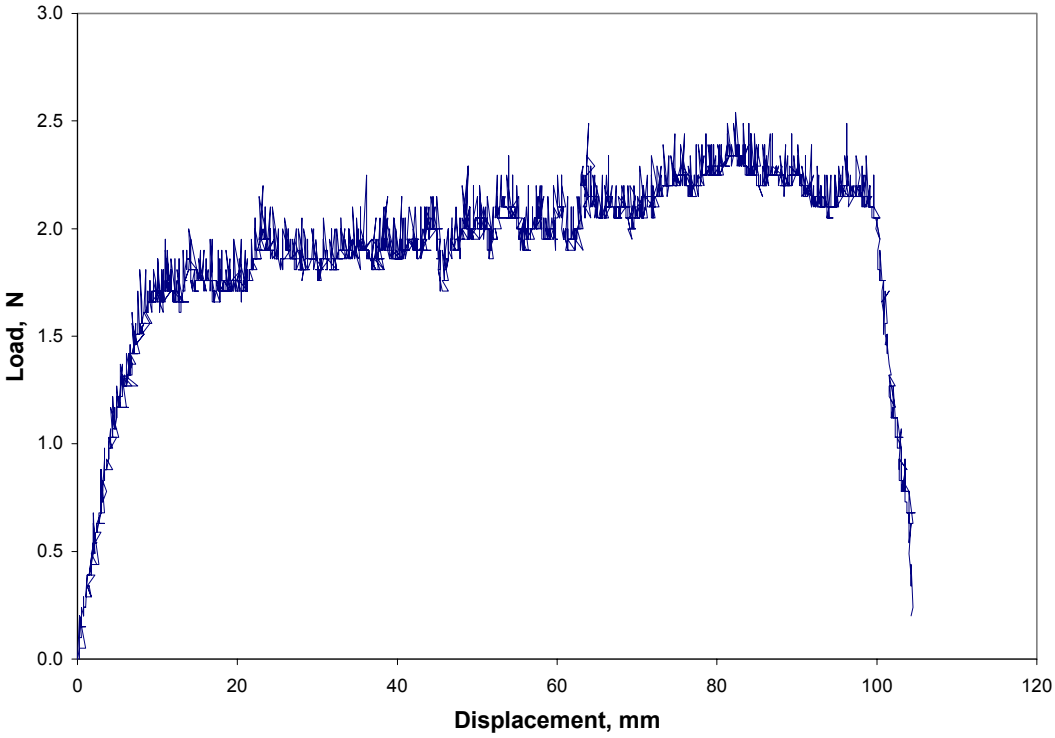

Figure B.80: Load Versus Displacement for Subject D, 90 degrees, 1 min, 200 mm/min, Test 3

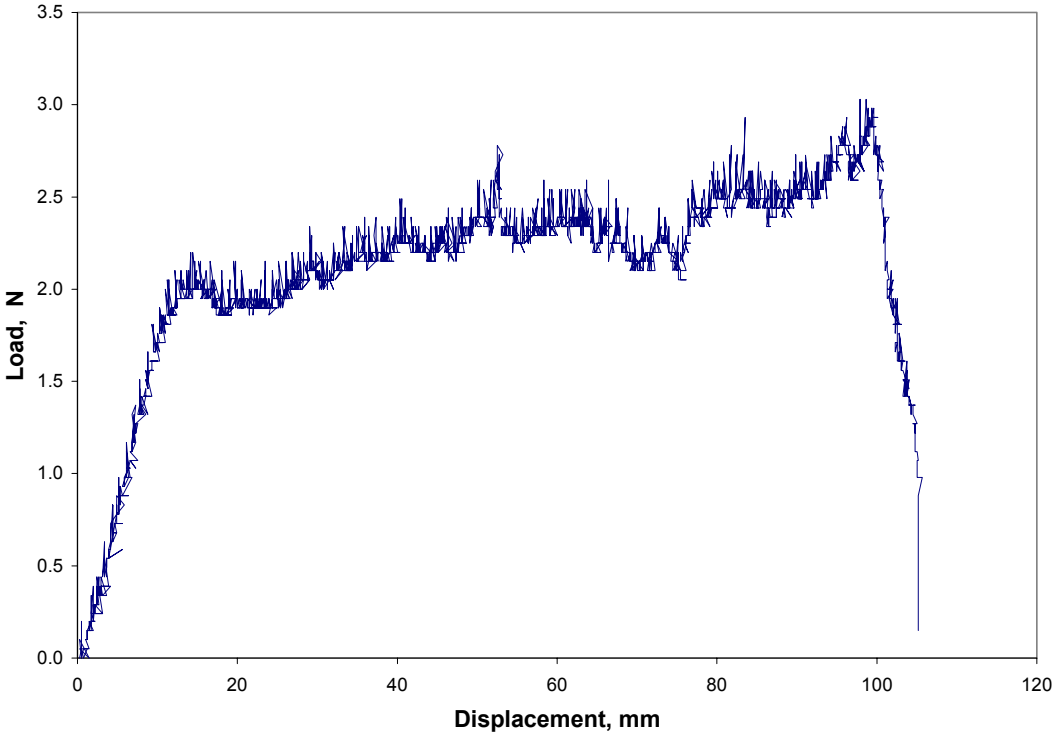

Figure B.81: Load Versus Displacement for Subject D, 90 degrees, 1 min, 200 mm/min, Test 4

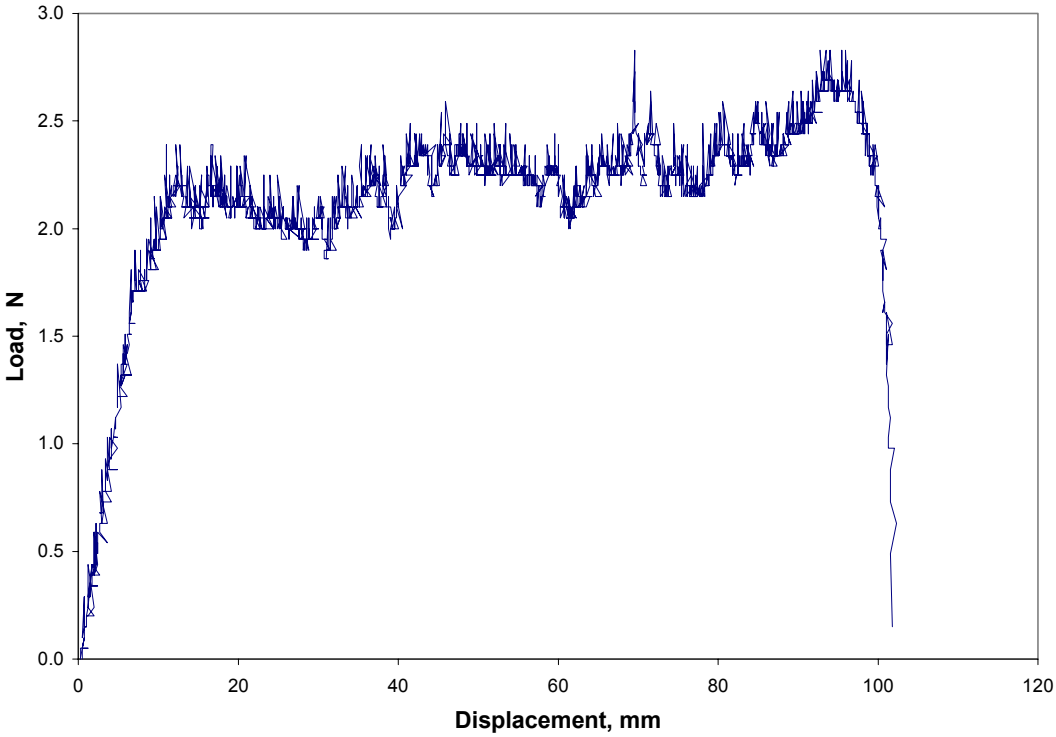

Figure B.82: Load Versus Displacement for Subject D, 90 degrees, 1 min, 200 mm/min, Test 5

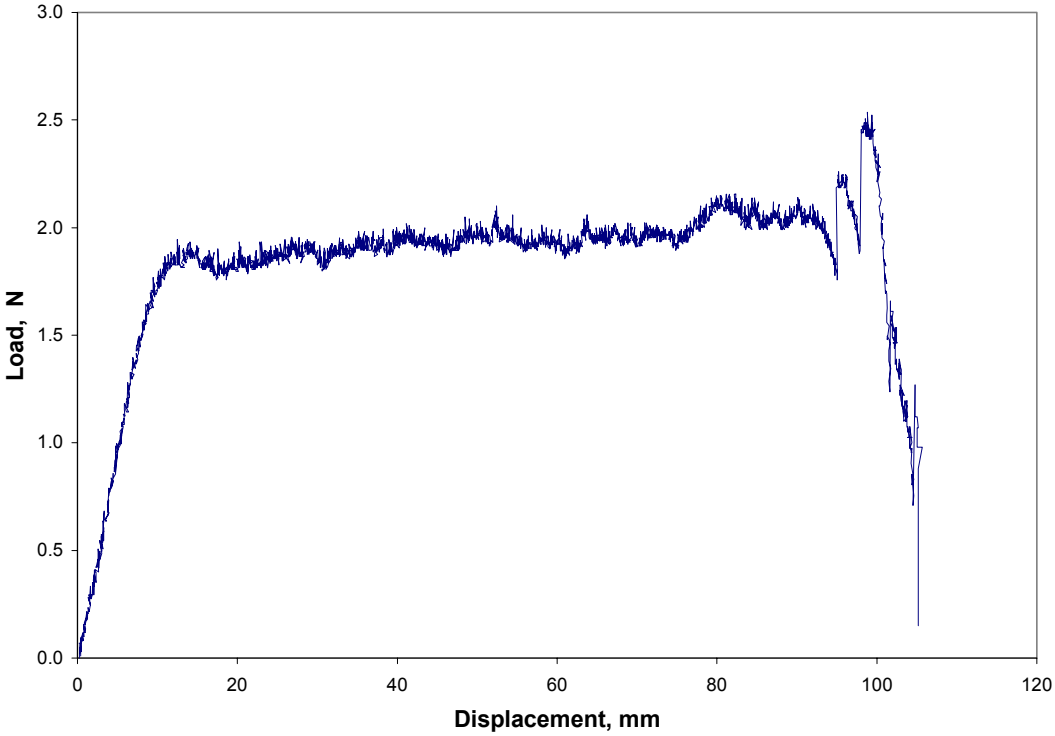

Figure B.83: Load Versus Displacement for Subject D, 90 degrees, 1 min, 200 mm/min, Average

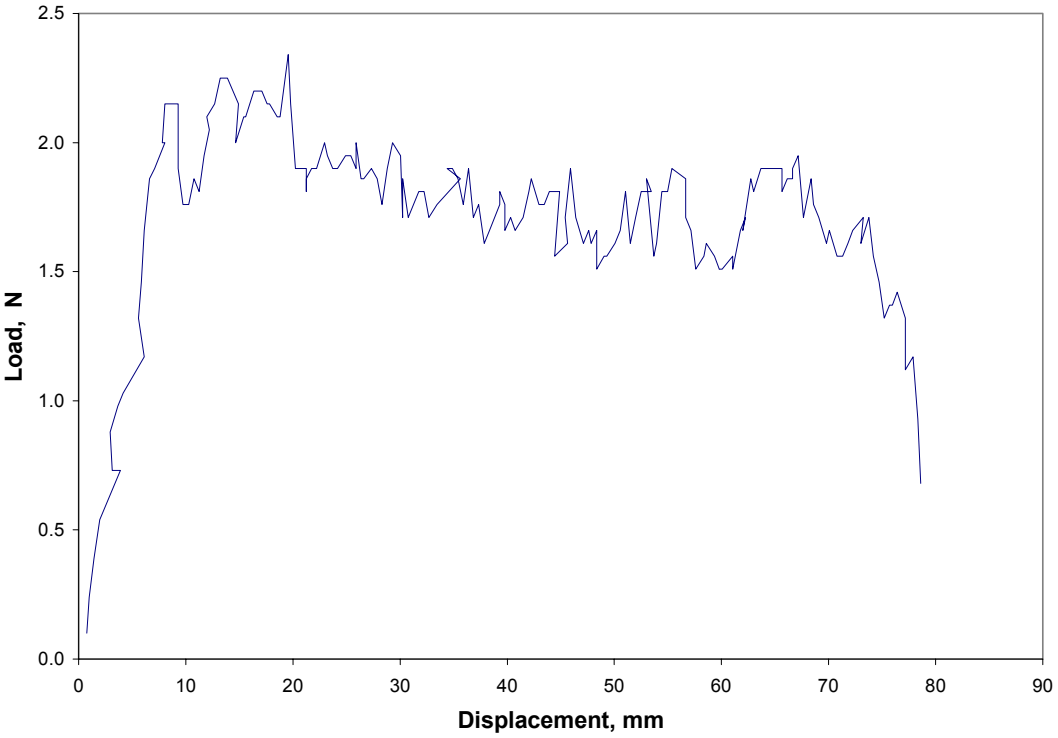

Figure B.84: Load Versus Displacement for Subject D, 90 degrees, 1 min, 300 mm/min, Test 1

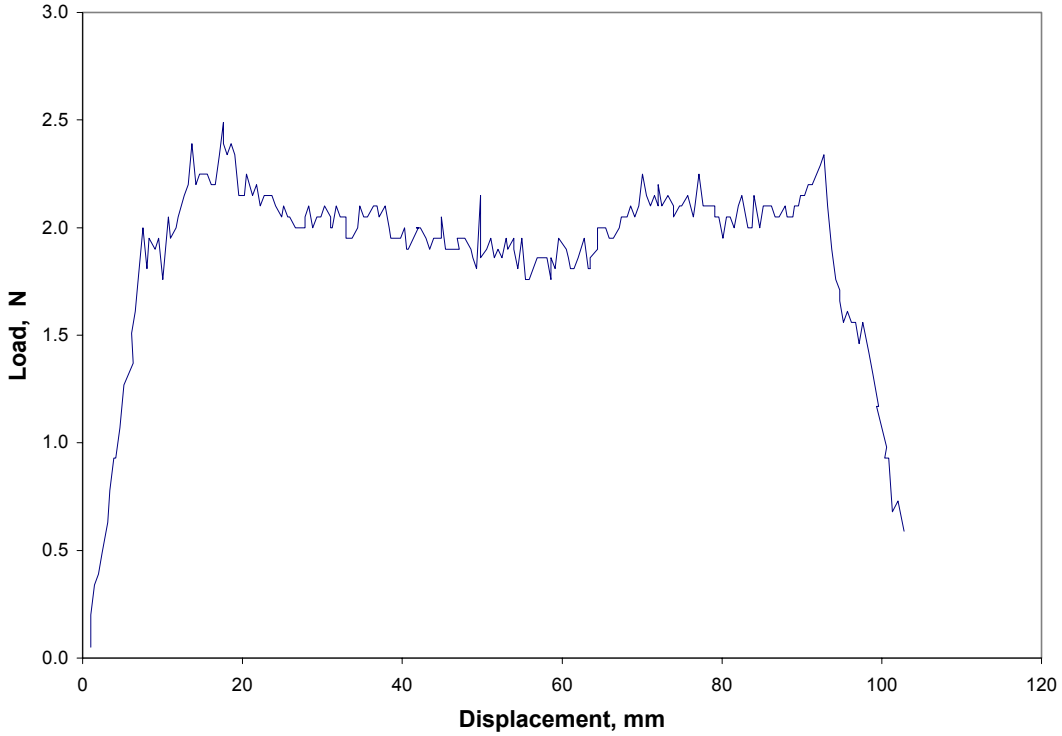

Figure B.85: Load Versus Displacement for Subject D, 90 degrees, 1 min, 300 mm/min, Test 2

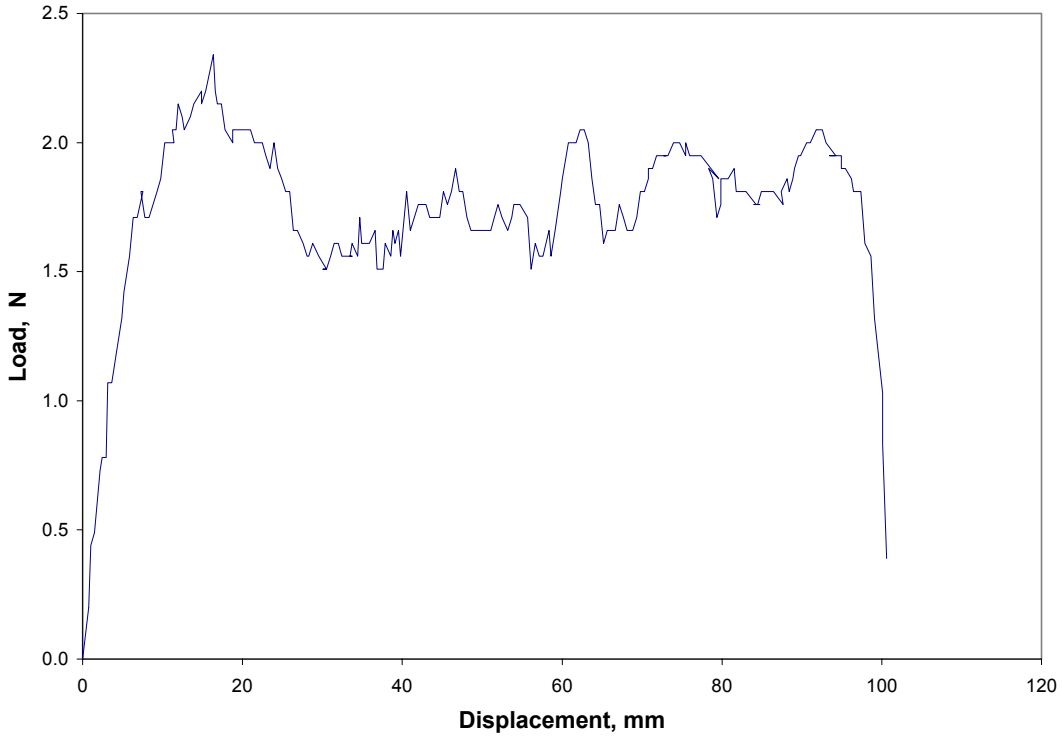

Figure B.86: Load Versus Displacement for Subject D, 90 degrees, 1 min, 300 mm/min, Test 3

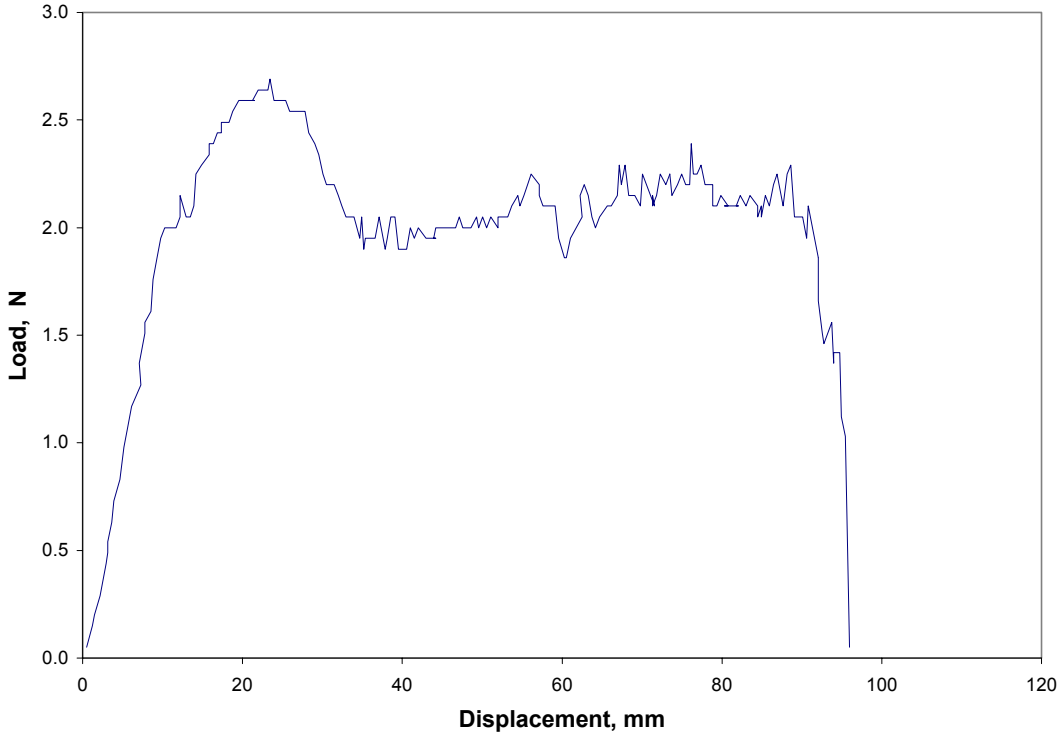

Figure B.87: Load Versus Displacement for Subject D, 90 degrees, 1 min, 300 mm/min, Test 4

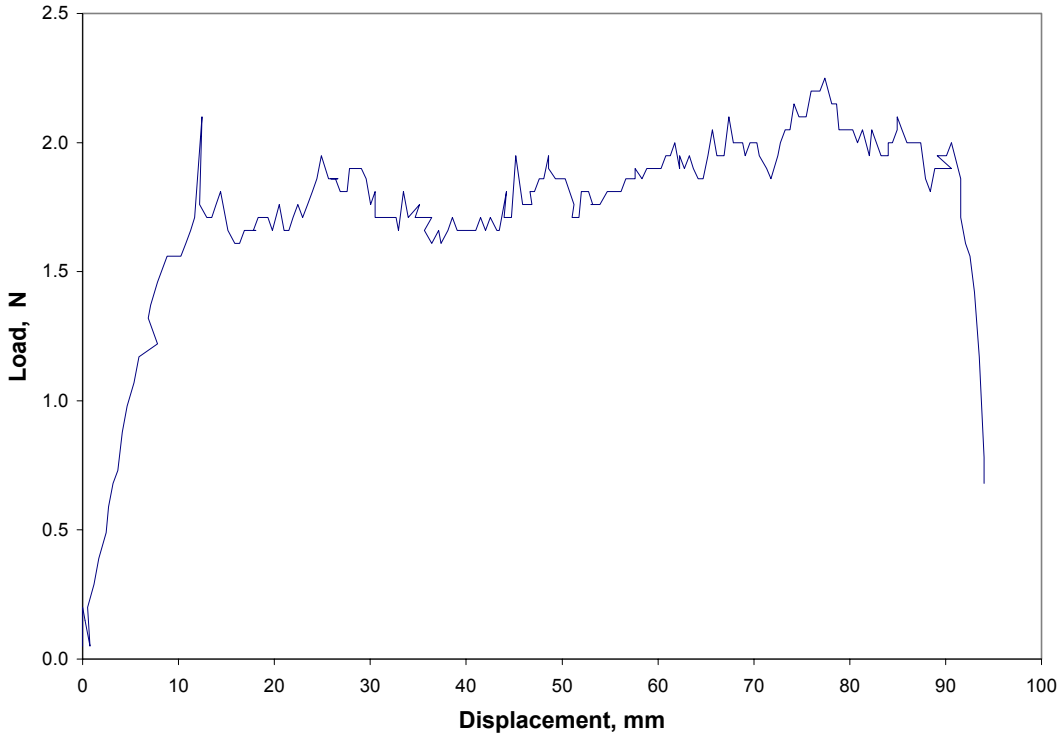

Figure B.88: Load Versus Displacement for Subject D, 90 degrees, 1 min, 300 mm/min, Test 5

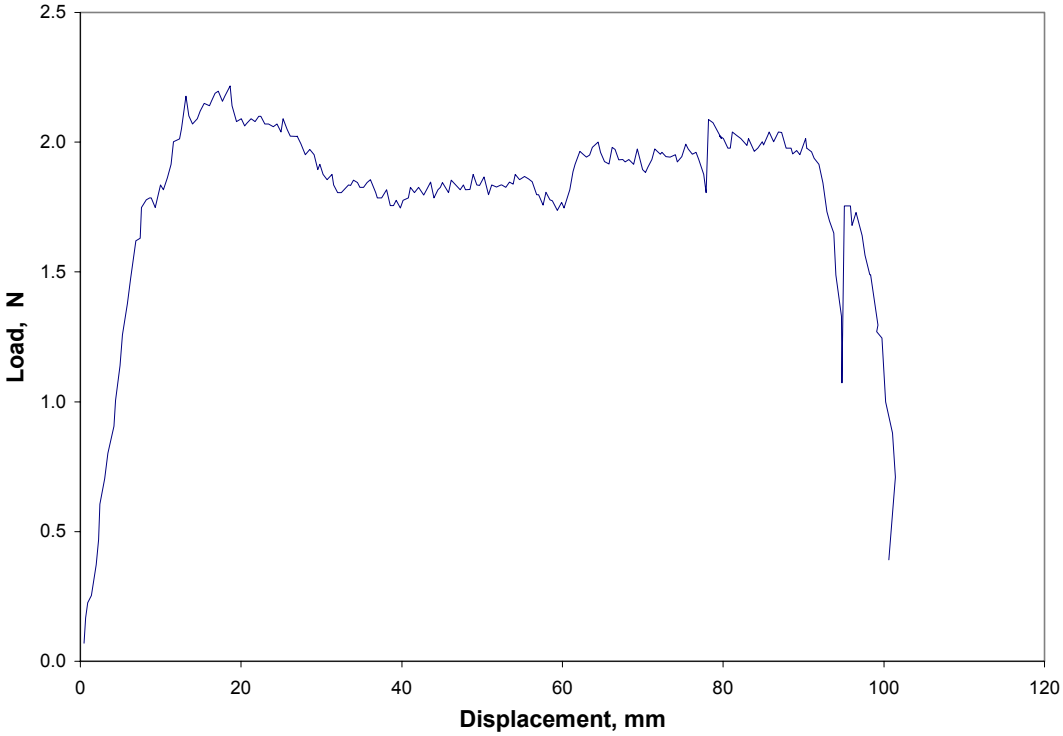

Figure B.89: Load Versus Displacement for Subject D, 90 degrees, 1 min, 300 mm/min, Average

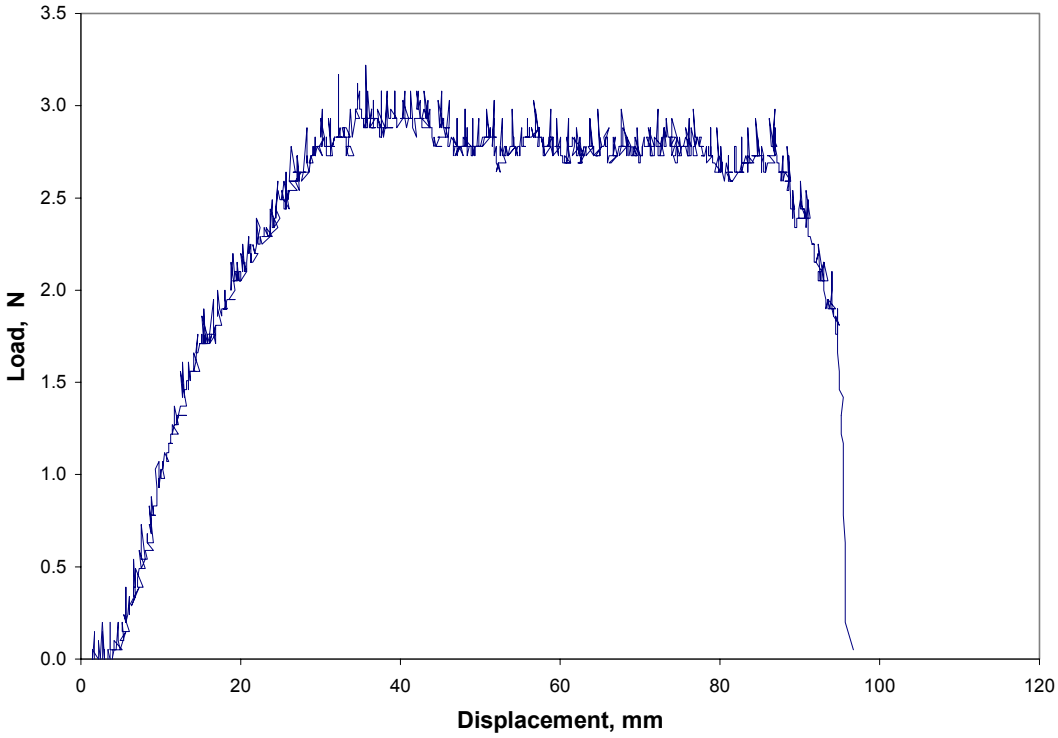

Figure B.90: Load Versus Displacement for Subject D, 90 degrees, 1 min, 400 mm/min, Test 1

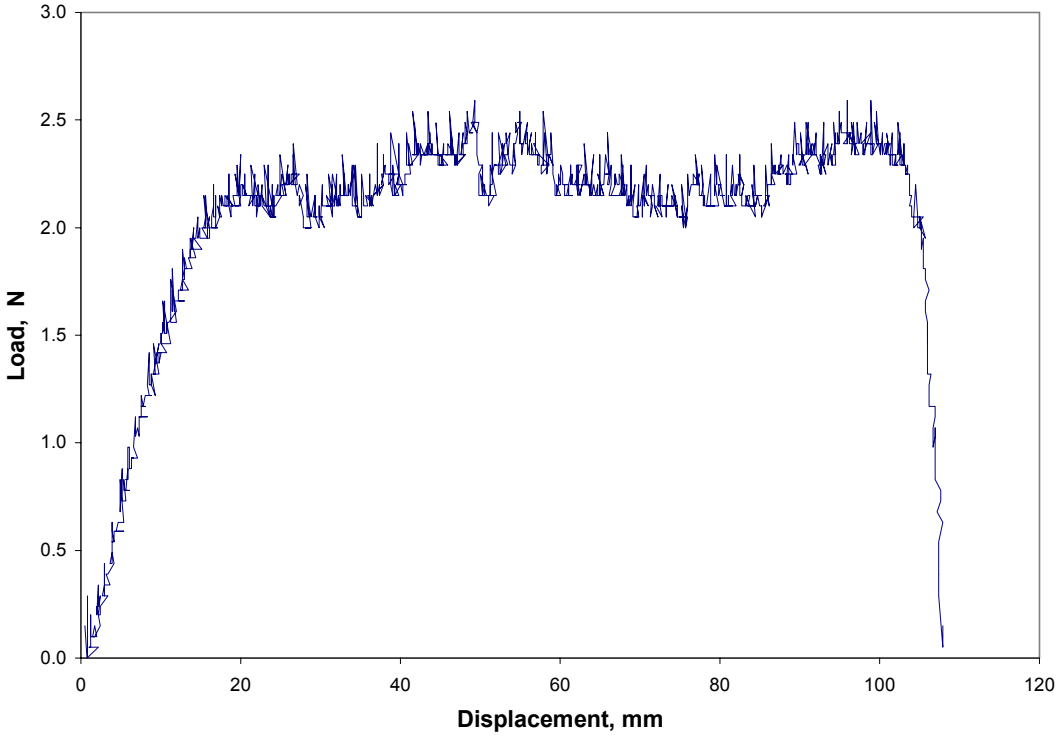

Figure B.91: Load Versus Displacement for Subject D, 90 degrees, 1 min, 400 mm/min, Test 2

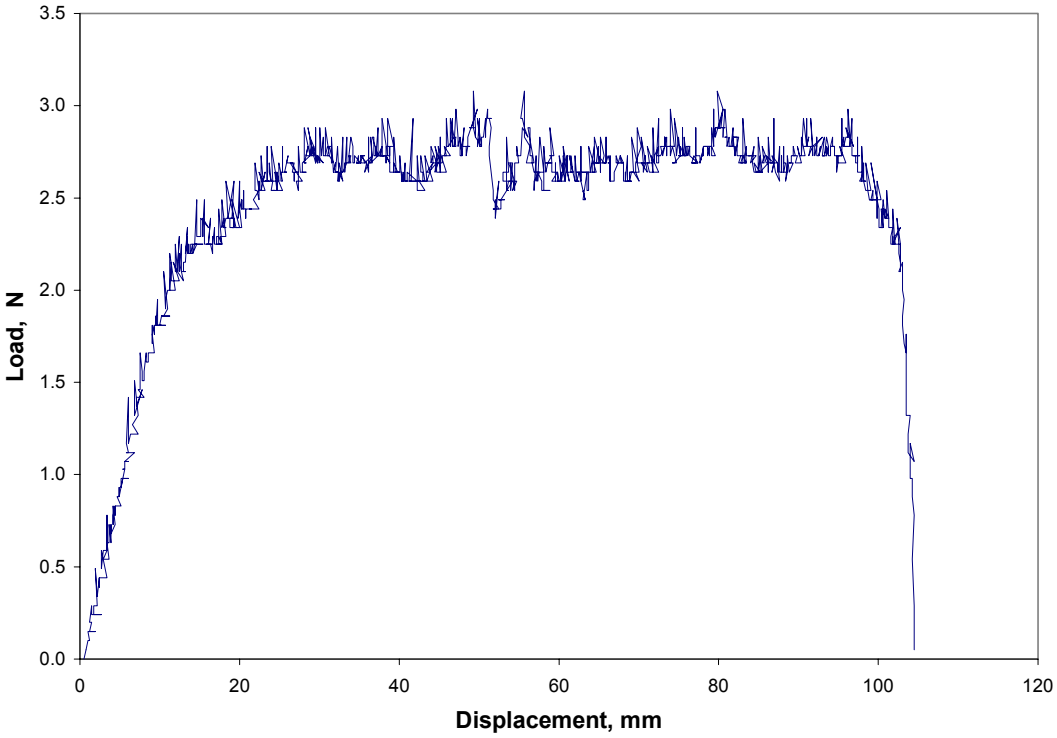

Figure B.92: Load Versus Displacement for Subject D, 90 degrees, 1 min, 400 mm/min, Test 3

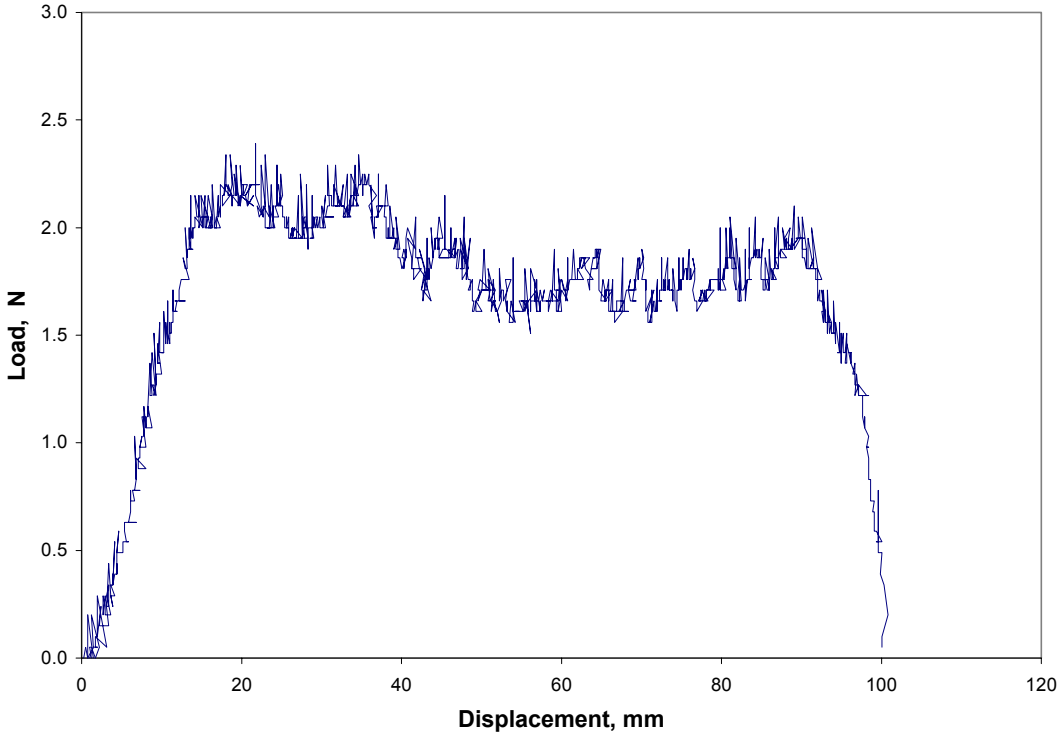

Figure B.93: Load Versus Displacement for Subject D, 90 degrees, 1 min, 400 mm/min, Test 4

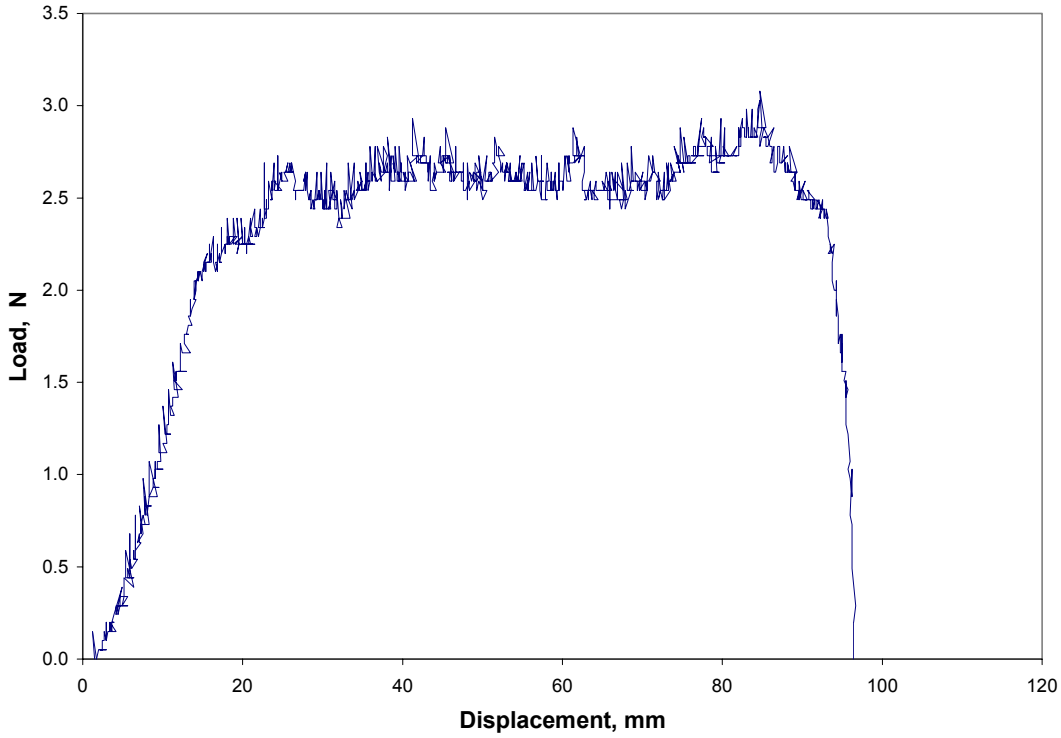

Figure B.94: Load Versus Displacement for Subject D, 90 degrees, 1 min, 400 mm/min, Test 5

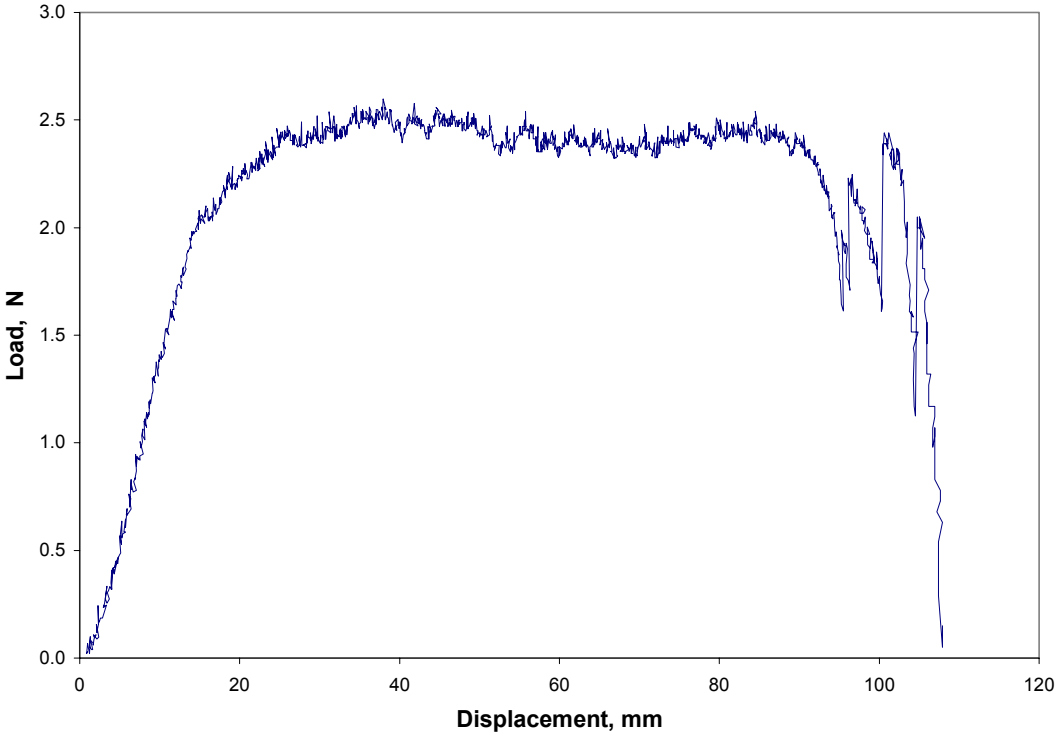

Figure B.95: Load Versus Displacement for Subject D, 90 degrees, 1 min, 400 mm/min, Average

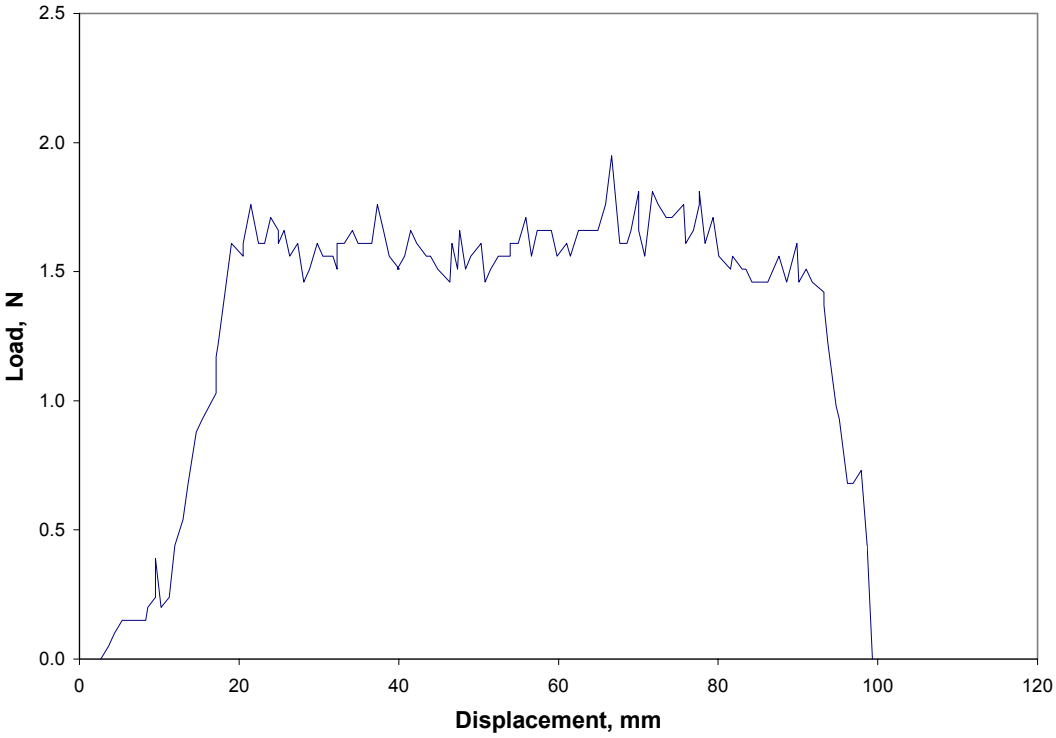

Figure B.96: Load Versus Displacement for Subject D, 90 degrees, 1 min, 500 mm/min, Test 1

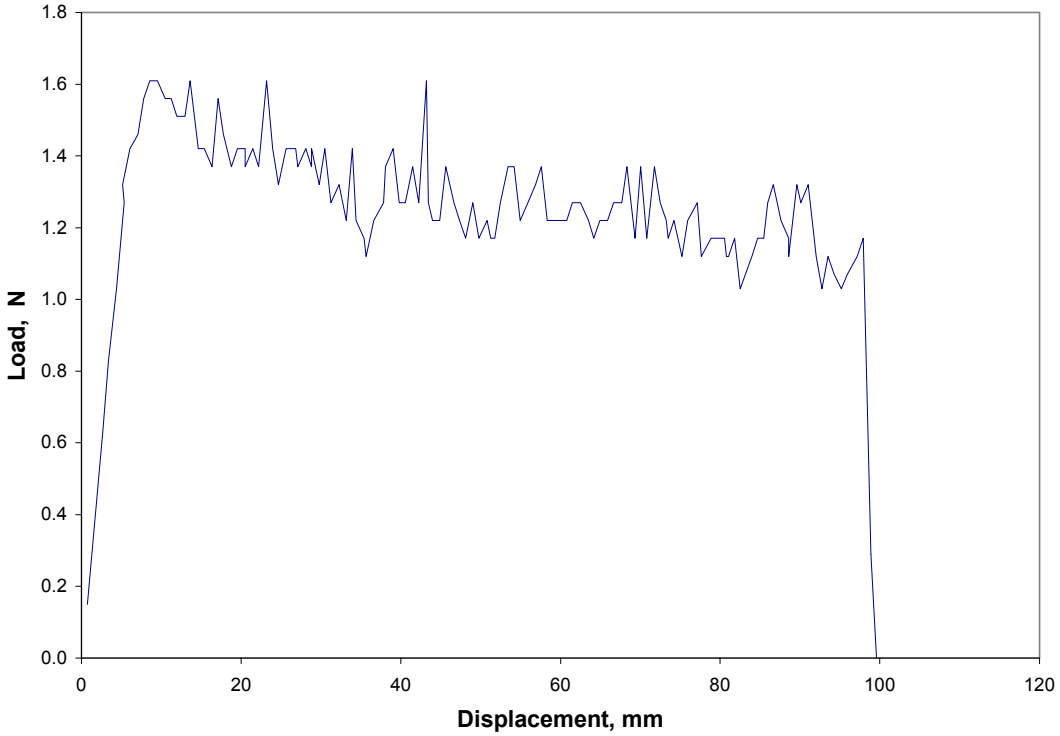

Figure B.97: Load Versus Displacement for Subject D, 90 degrees, 1 min, 500 mm/min, Test 2

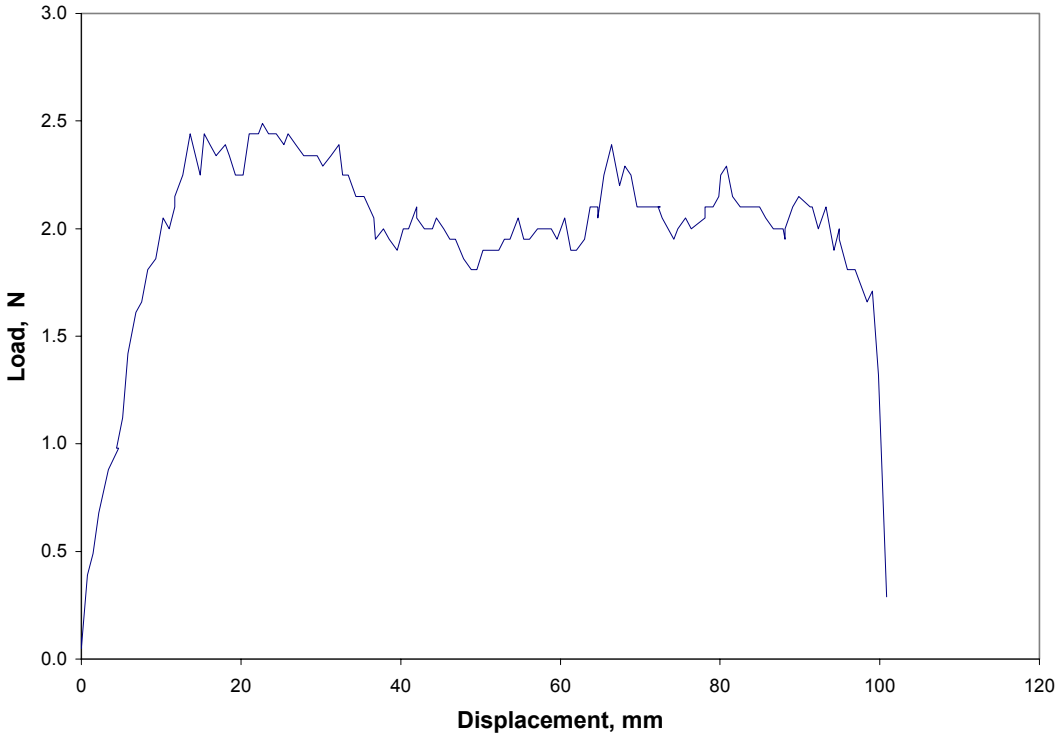

Figure B.98: Load Versus Displacement for Subject D, 90 degrees, 1 min, 500 mm/min, Test 3

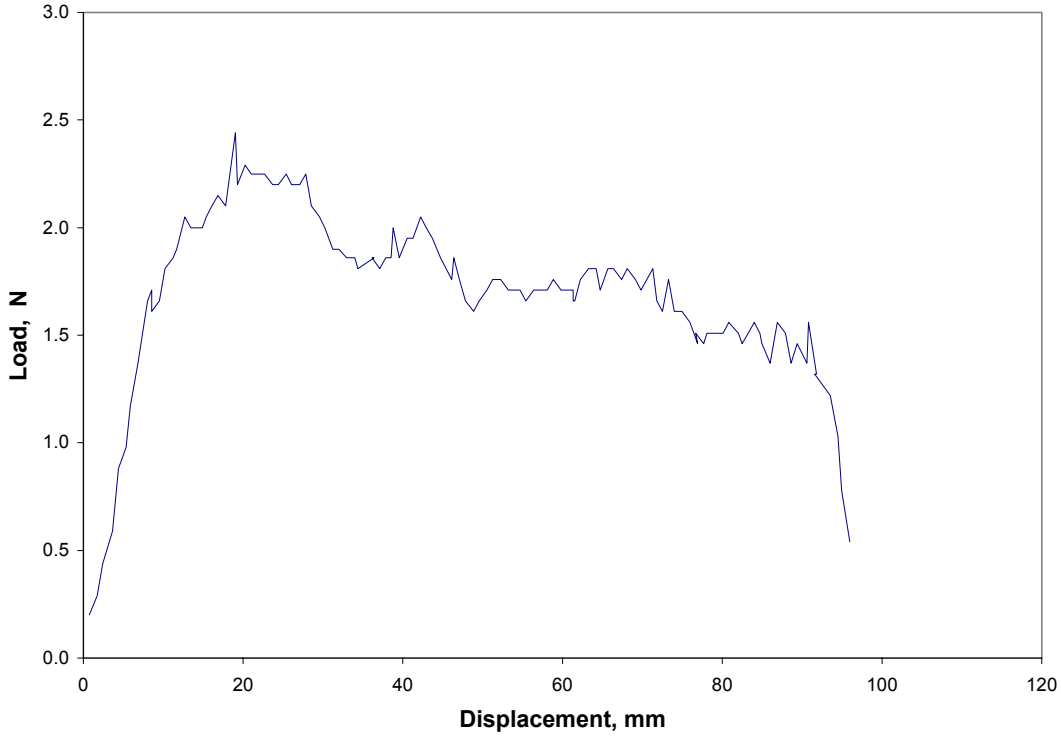

Figure B.99: Load Versus Displacement for Subject D, 90 degrees, 1 min, 500 mm/min, Test 4

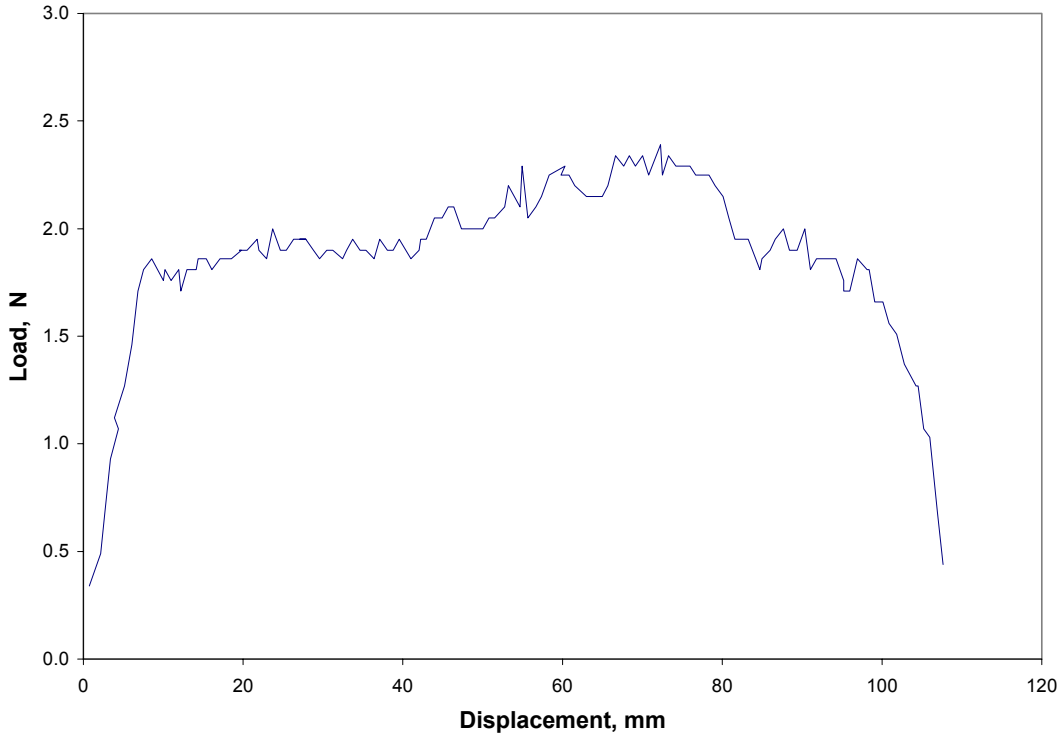

Figure B.100: Load Versus Displacement for Subject D, 90 degrees, 1 min, 500 mm/min, Test 5

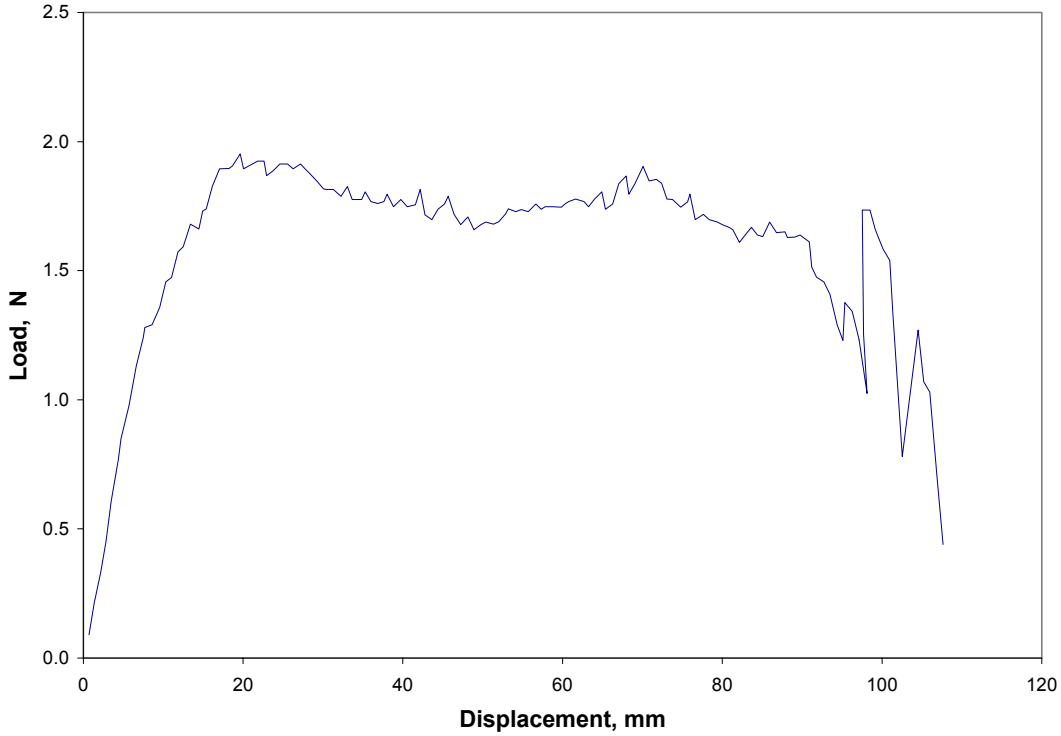

Figure B.101: Load Versus Displacement for Subject D, 90 degrees, 1 min, 500 mm/min, Average

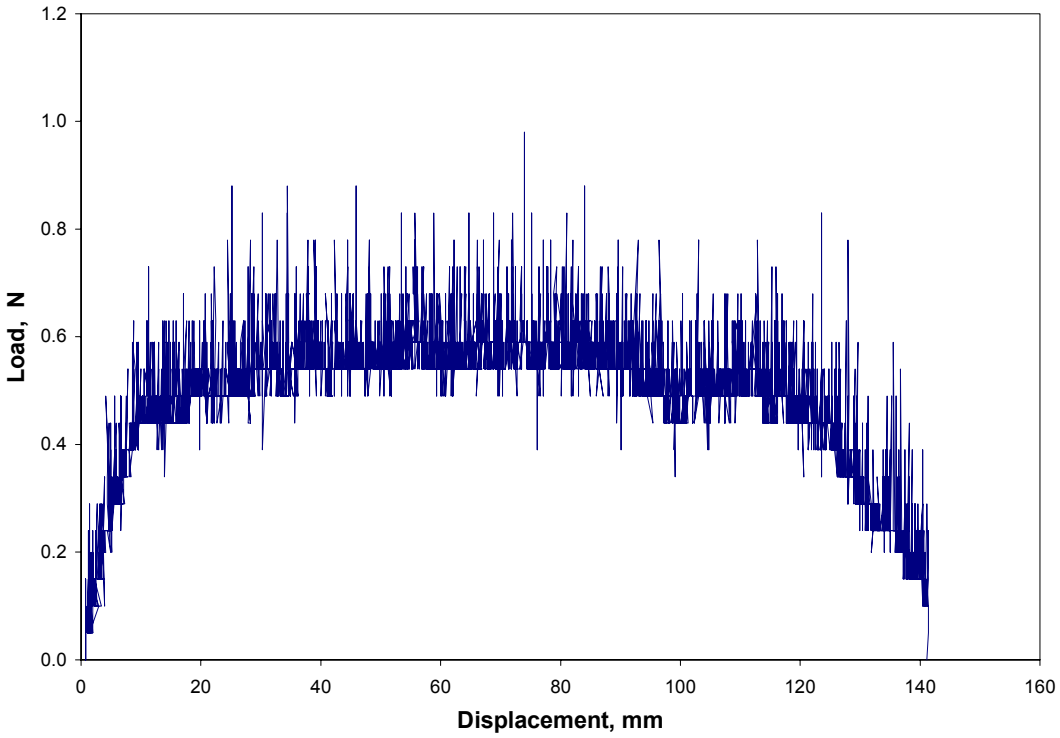

Figure B.102: Load Versus Displacement for Subject A, 180 degrees, 1 min, 100 mm/min, Test 1

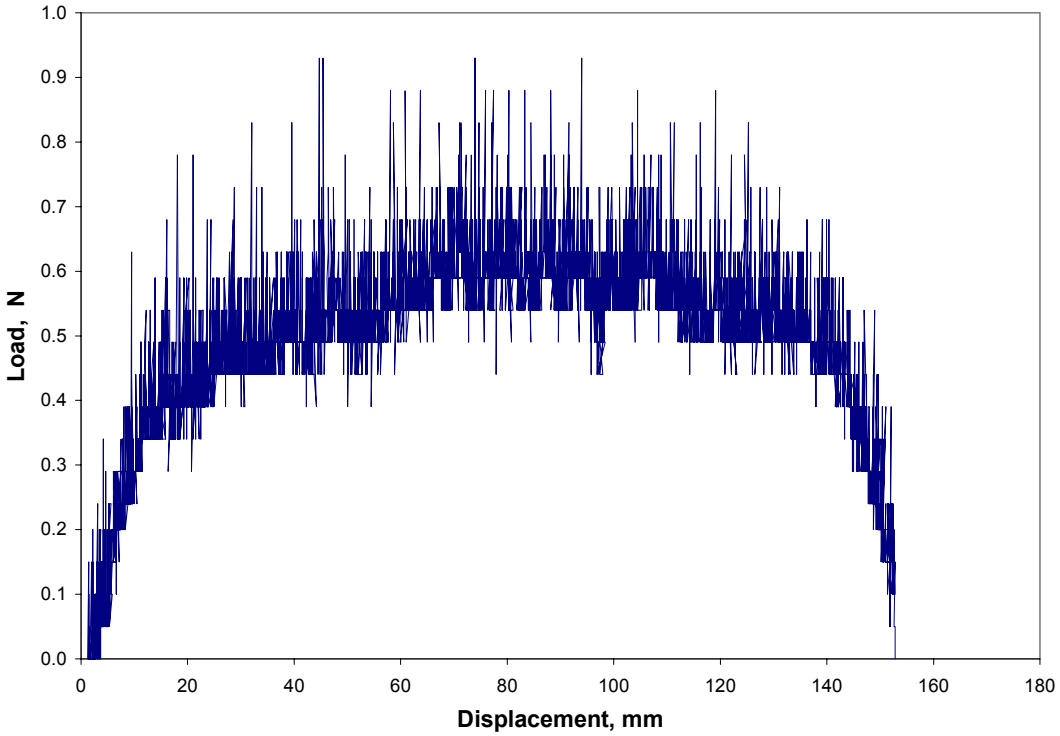

Figure B.103: Load Versus Displacement for Subject A, 180 degrees, 1 min, 100 mm/min, Test 2

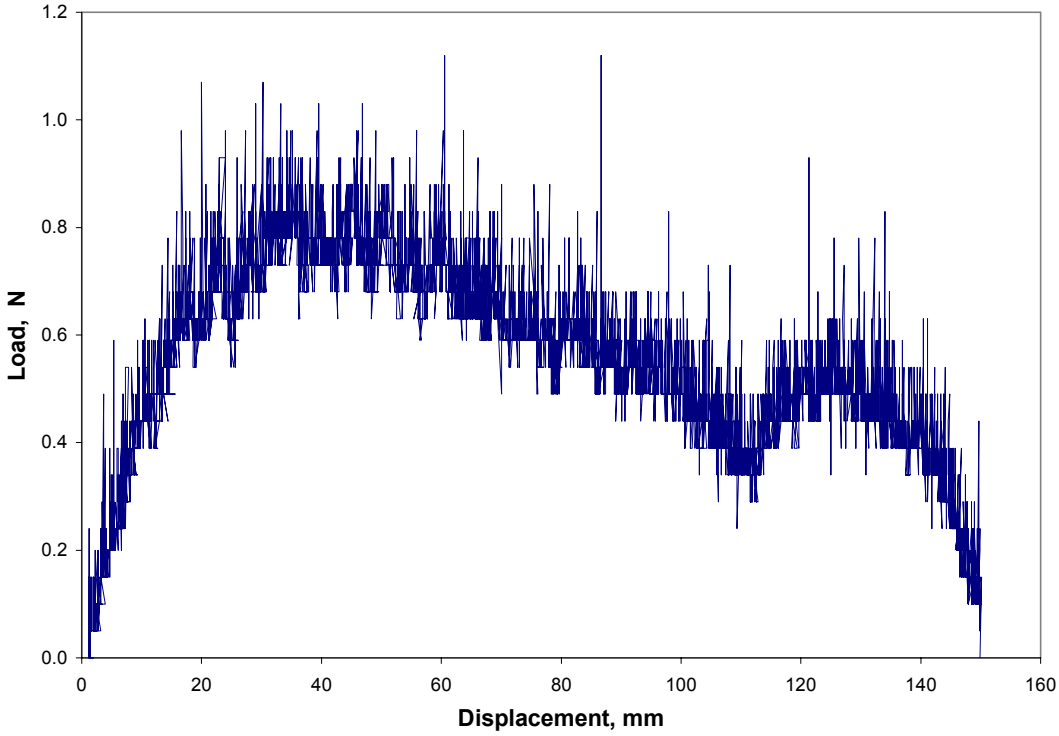

Figure B.104: Load Versus Displacement for Subject A, 180 degrees, 1 min, 100 mm/min, Test 3

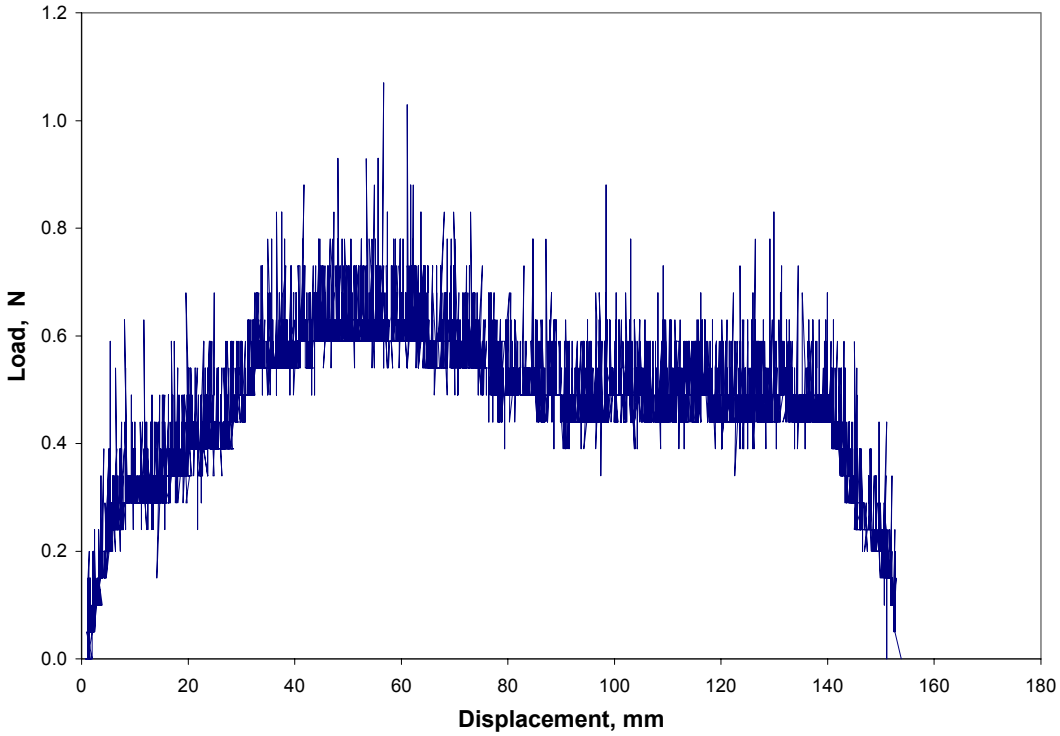

Figure B.105: Load Versus Displacement for Subject A, 180 degrees, 1 min, 100 mm/min, Test 4

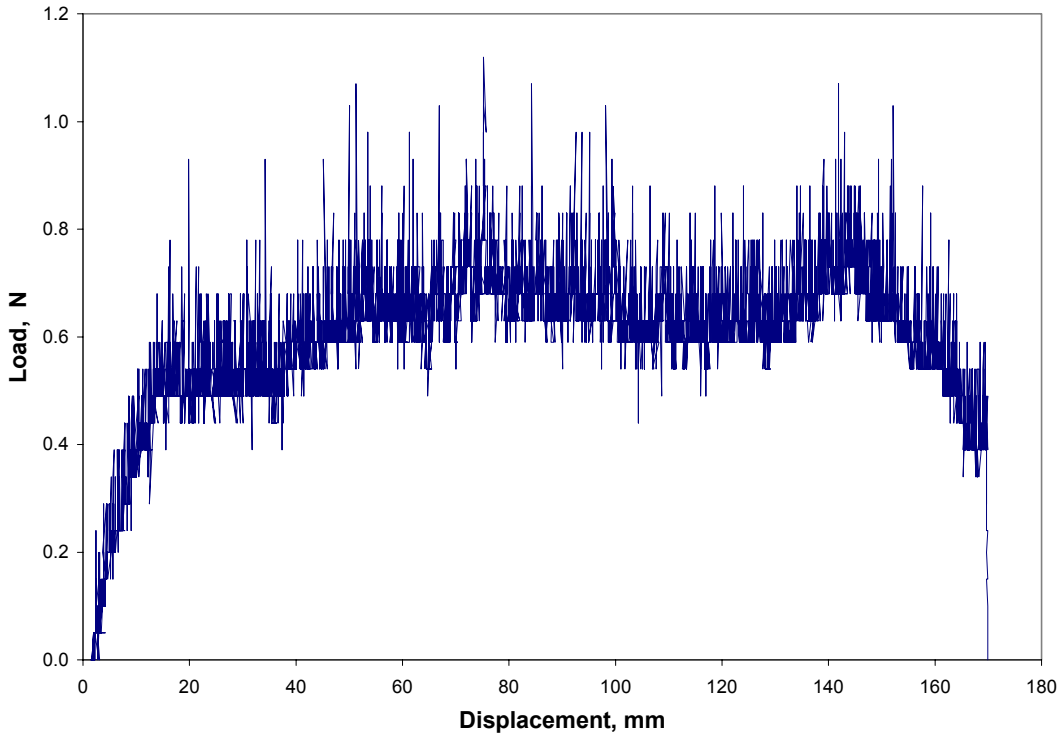

Figure B.106: Load Versus Displacement for Subject A, 180 degrees, 1 min, 100 mm/min, Test 5

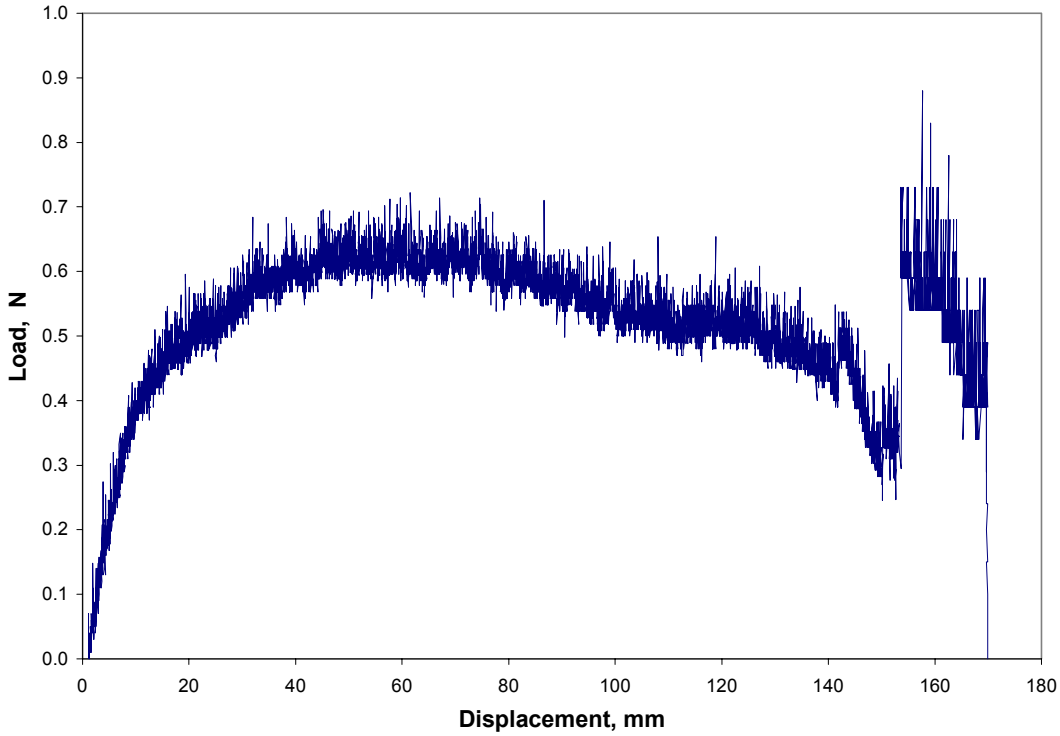

Figure B.107: Load Versus Displacement for Subject A, 180 degrees, 1 min, 100 mm/min, Average

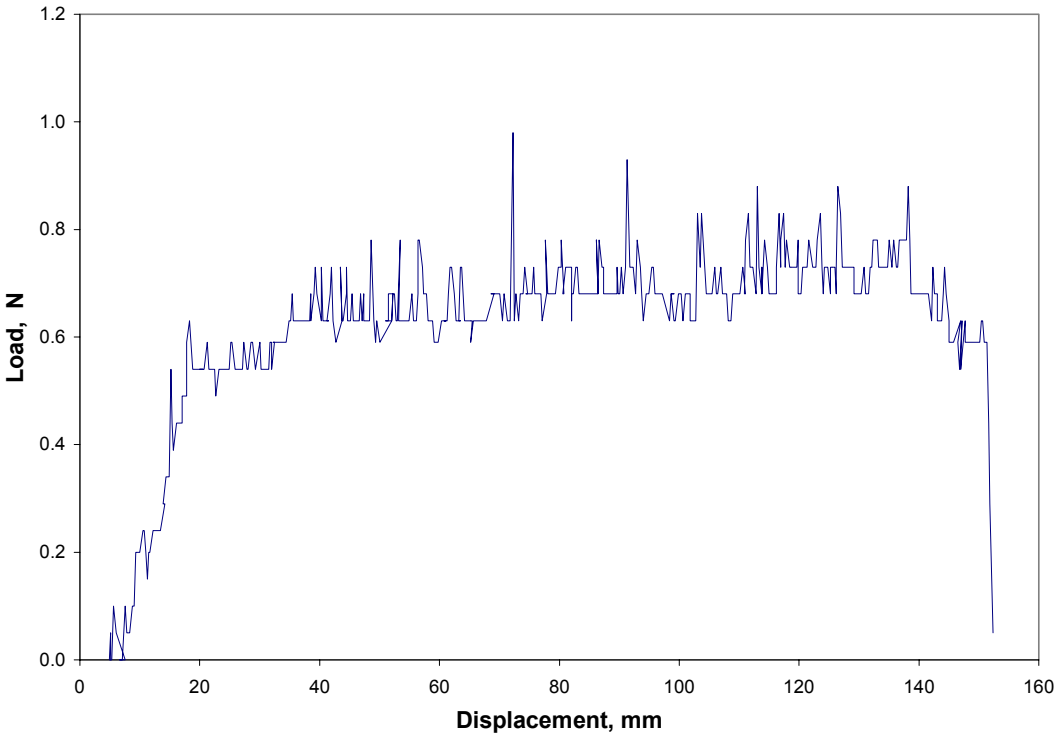

Figure B.108: Load Versus Displacement for Subject A, 180 degrees, 1 min, 200 mm/min, Test 1

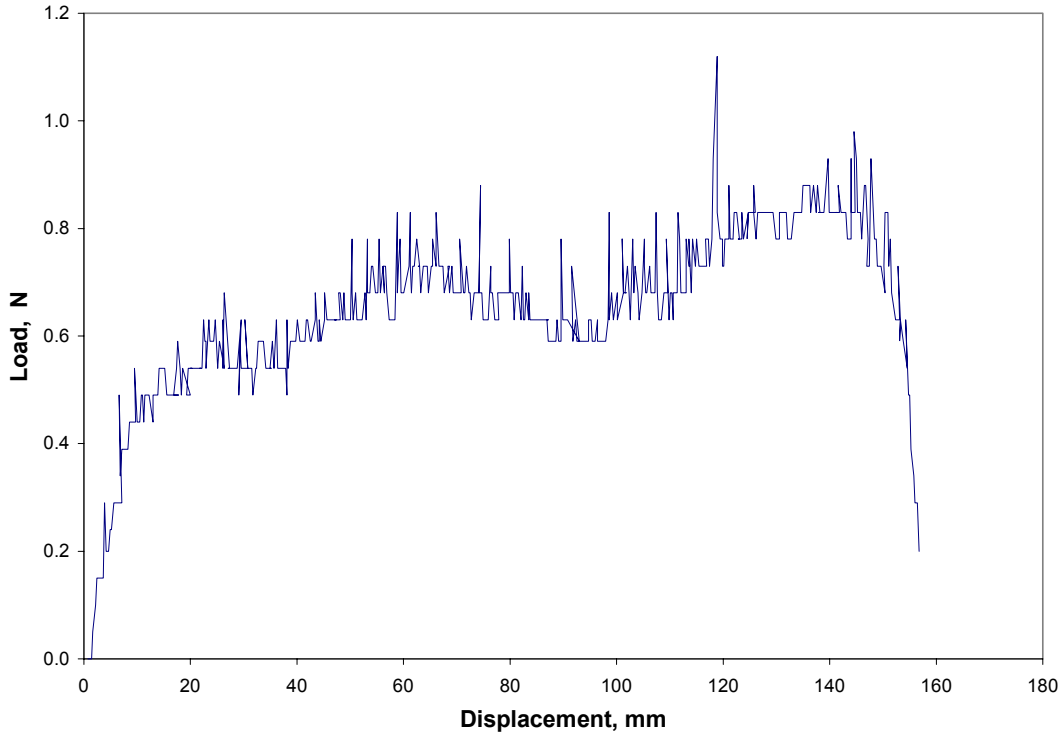

Figure B.109: Load Versus Displacement for Subject A, 180 degrees, 1 min, 200 mm/min, Test 2

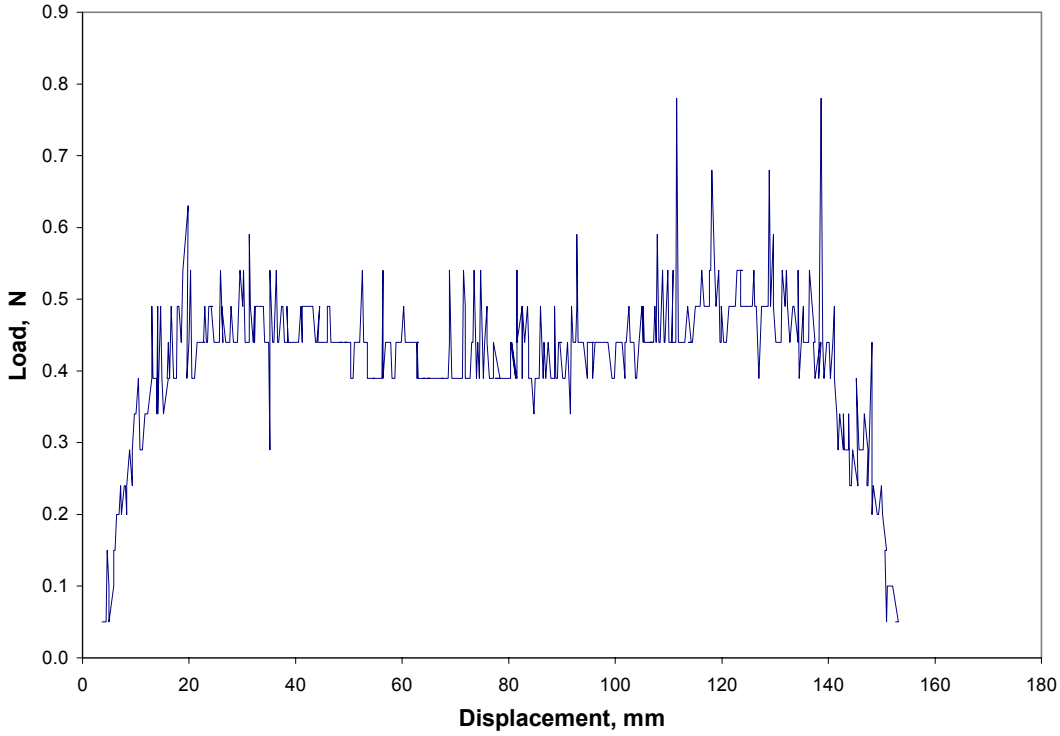

Figure B.110: Load Versus Displacement for Subject A, 180 degrees, 1 min, 200 mm/min, Test 3

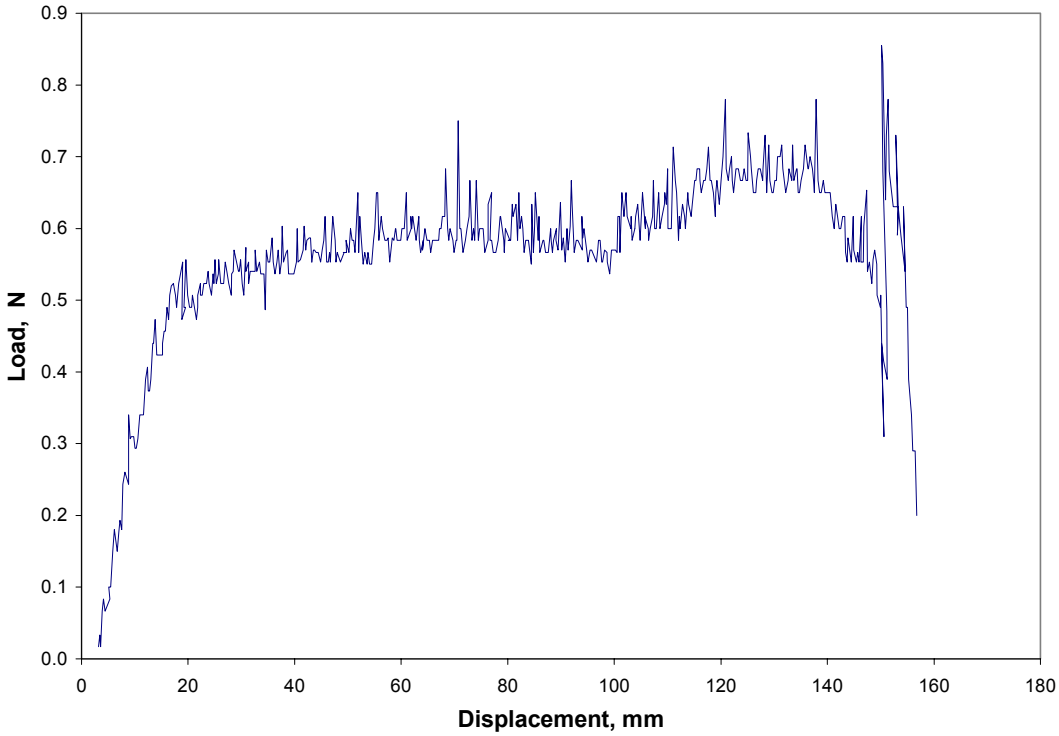

Figure B.111: Load Versus Displacement for Subject A, 180 degrees, 1 min, 200 mm/min, Average

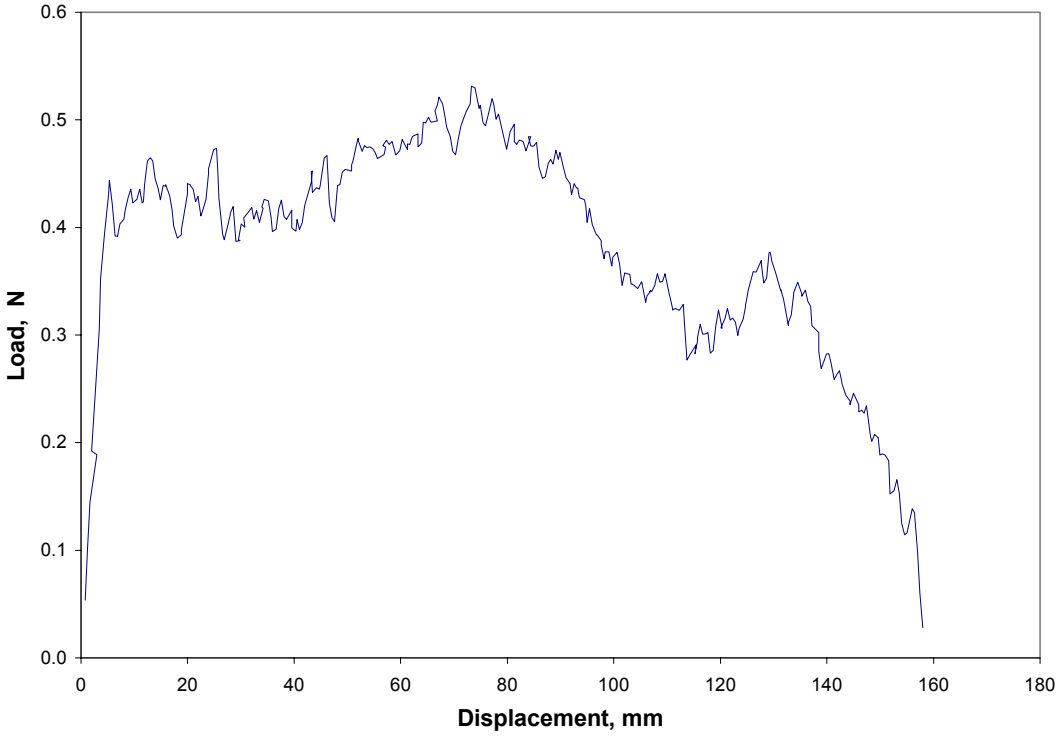

Figure B.112: Load Versus Displacement for Subject A, 180 degrees, 1 min, 300 mm/min, Test 1

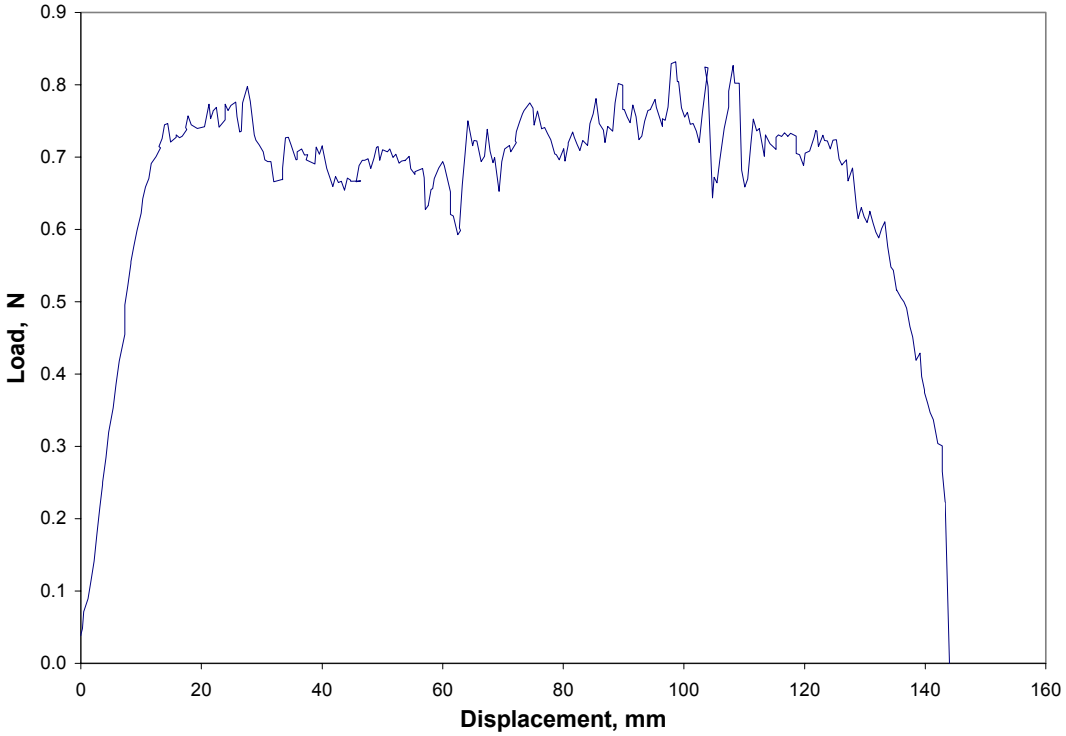

Figure B.113: Load Versus Displacement for Subject A, 180 degrees, 1 min, 300 mm/min, Test 2

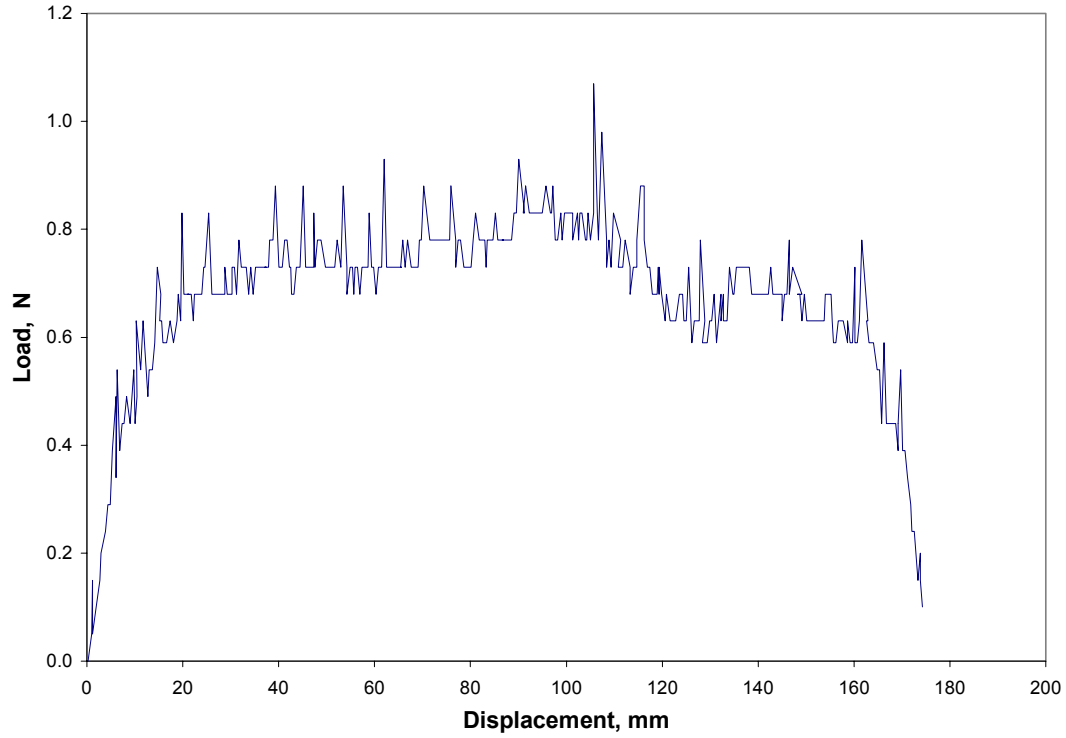

Figure B.114: Load Versus Displacement for Subject A, 180 degrees, 1 min, 300 mm/min, Test 3

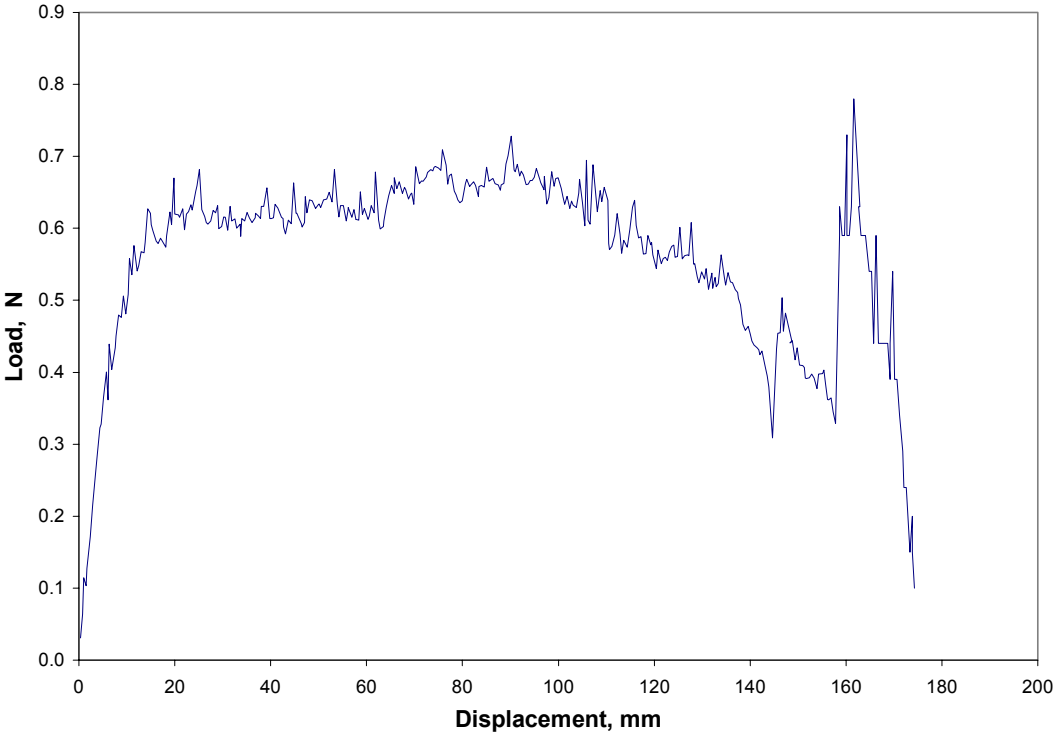

Figure B.115: Load Versus Displacement for Subject A, 180 degrees, 1 min, 300 mm/min, Average

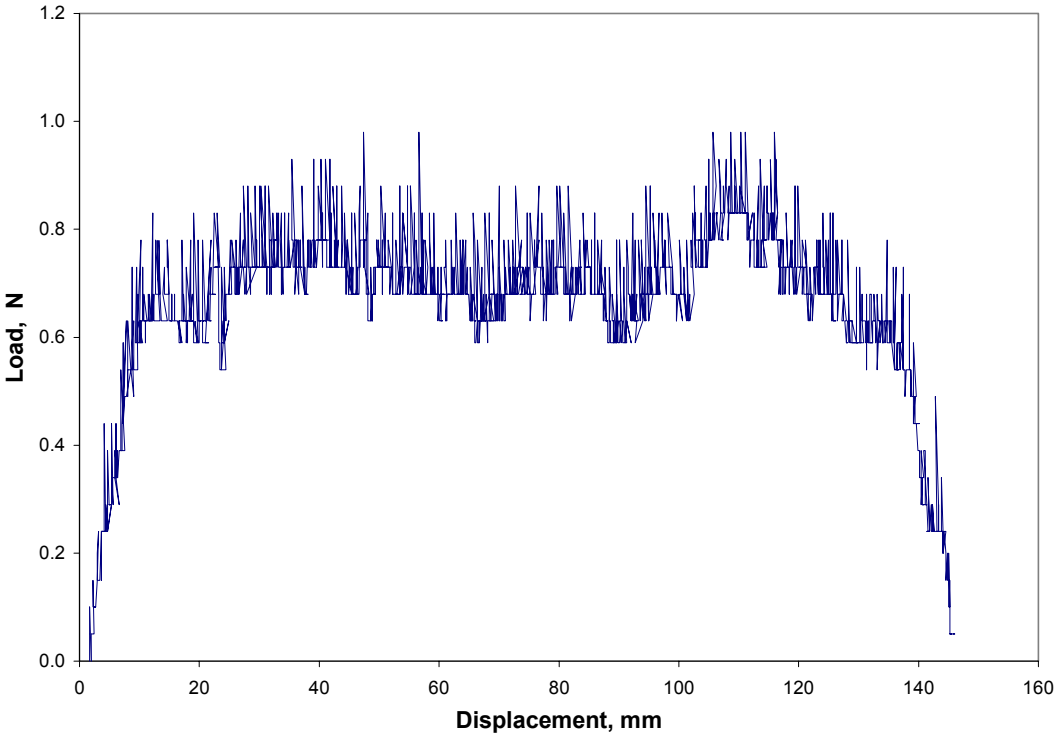

Figure B.116: Load Versus Displacement for Subject A, 180 degrees, 1 min, 400 mm/min, Test 1

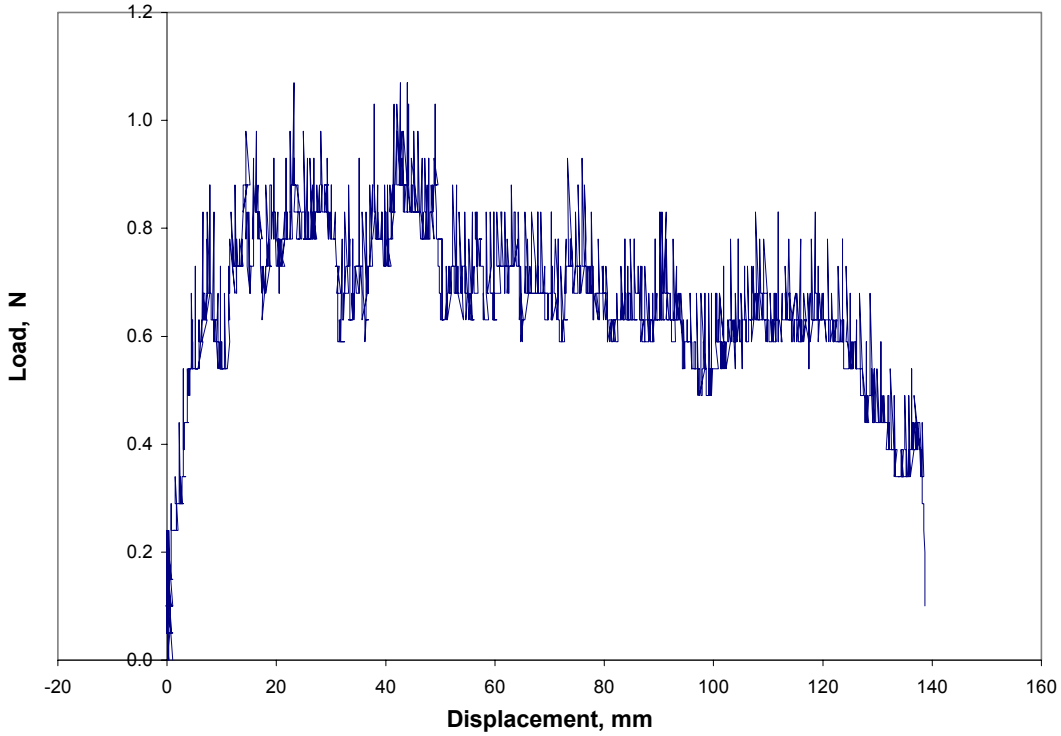

Figure B.117: Load Versus Displacement for Subject A, 180 degrees, 1 min, 400 mm/min, Test 2

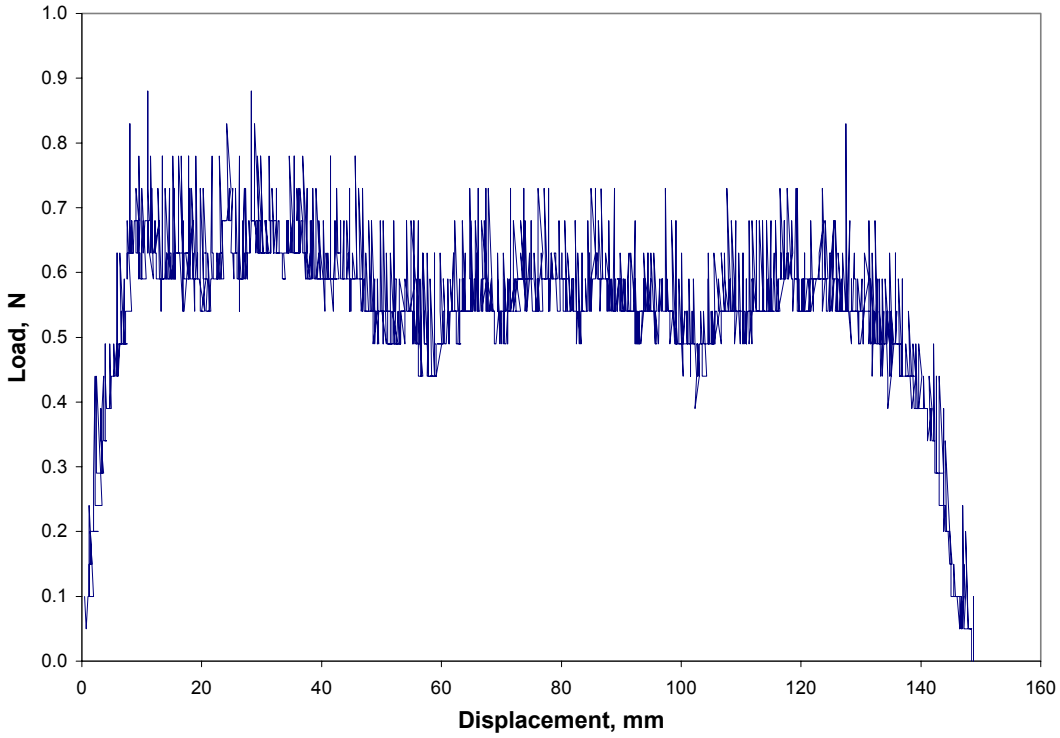

Figure B.118: Load Versus Displacement for Subject A, 180 degrees, 1 min, 400 mm/min, Test 3

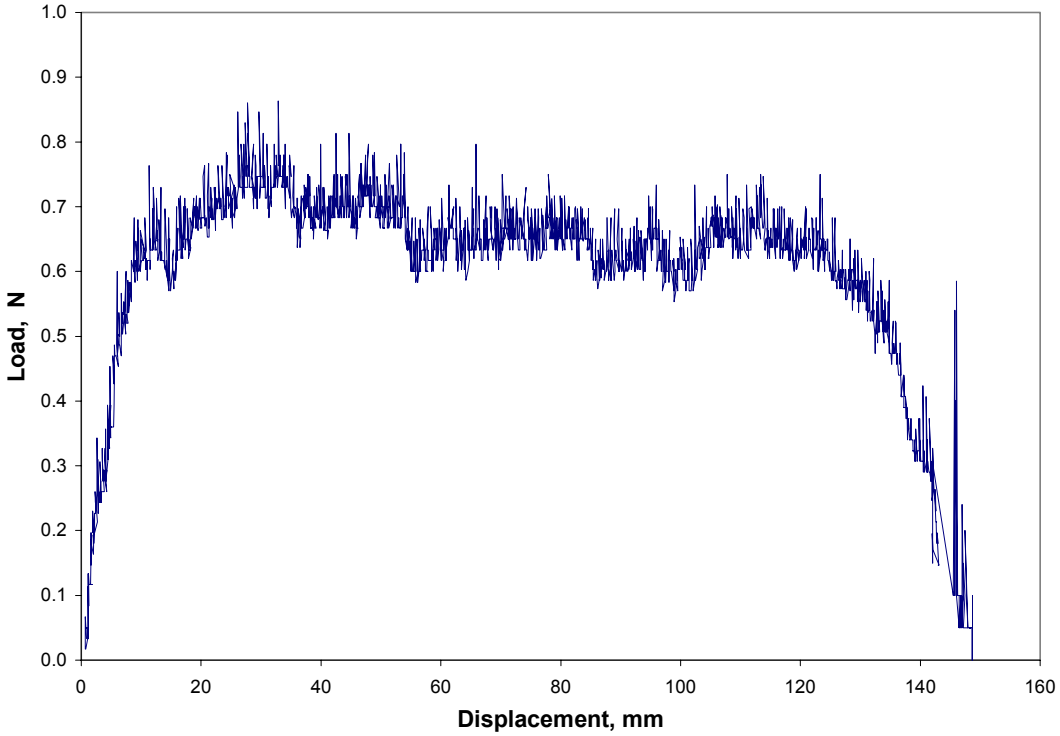

Figure B.119: Load Versus Displacement for Subject A, 180 degrees, 1 min, 400 mm/min, Average

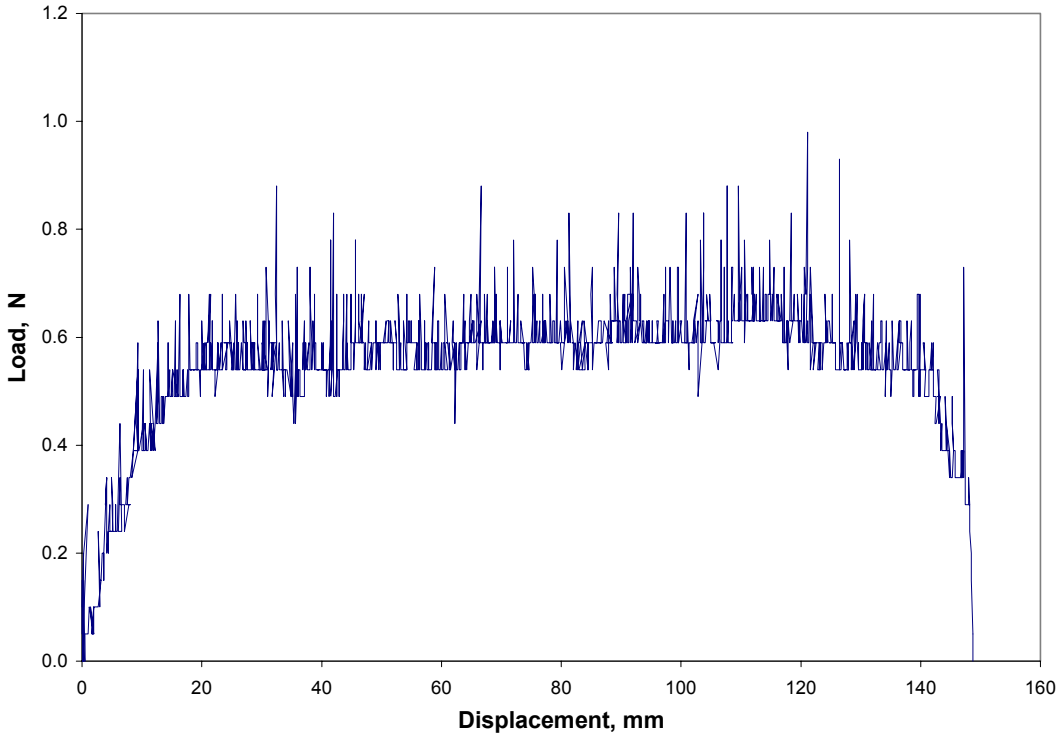

Figure B.120: Load Versus Displacement for Subject A, 180 degrees, 1 min, 500 mm/min, Test 1

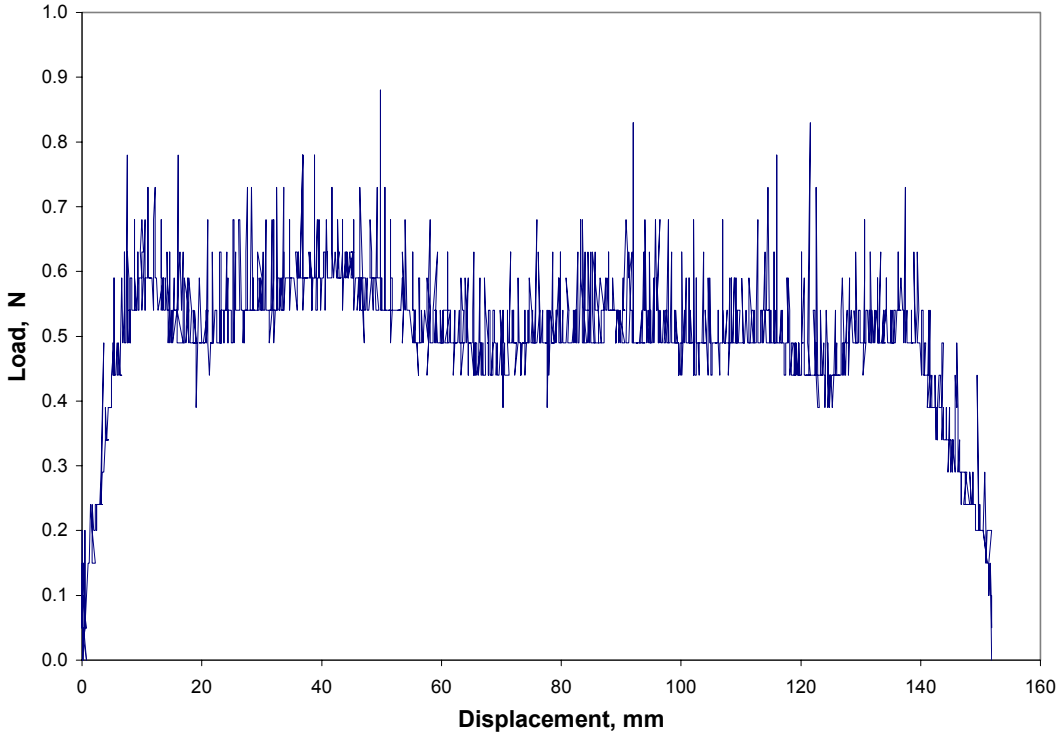

Figure B.121: Load Versus Displacement for Subject A, 180 degrees, 1 min, 500 mm/min, Test 2

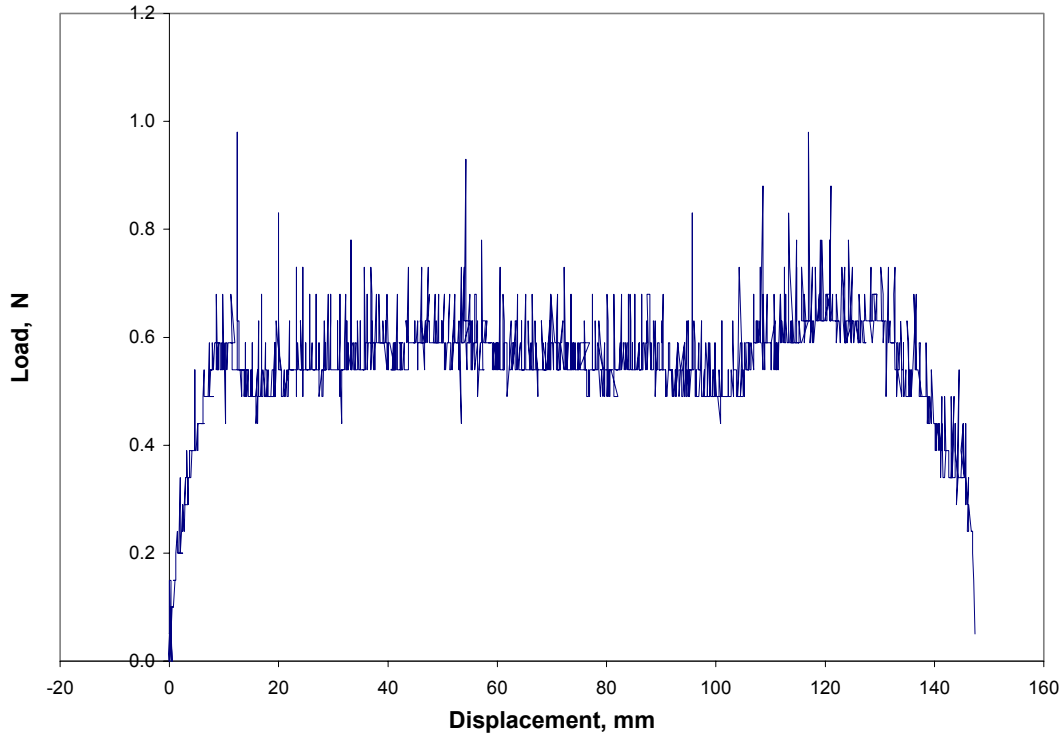

Figure B.122: Load Versus Displacement for Subject A, 180 degrees, 1 min, 500 mm/min, Test 3

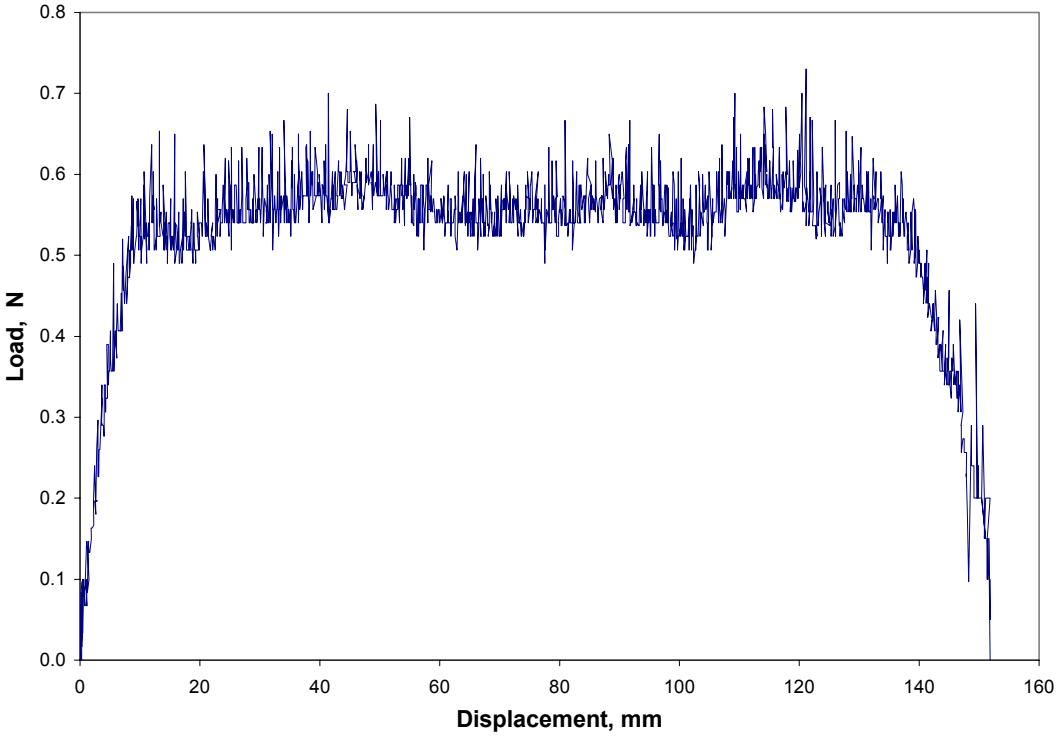

Figure B.123: Load Versus Displacement for Subject A, 180 degrees, 1 min, 500 mm/min, Average

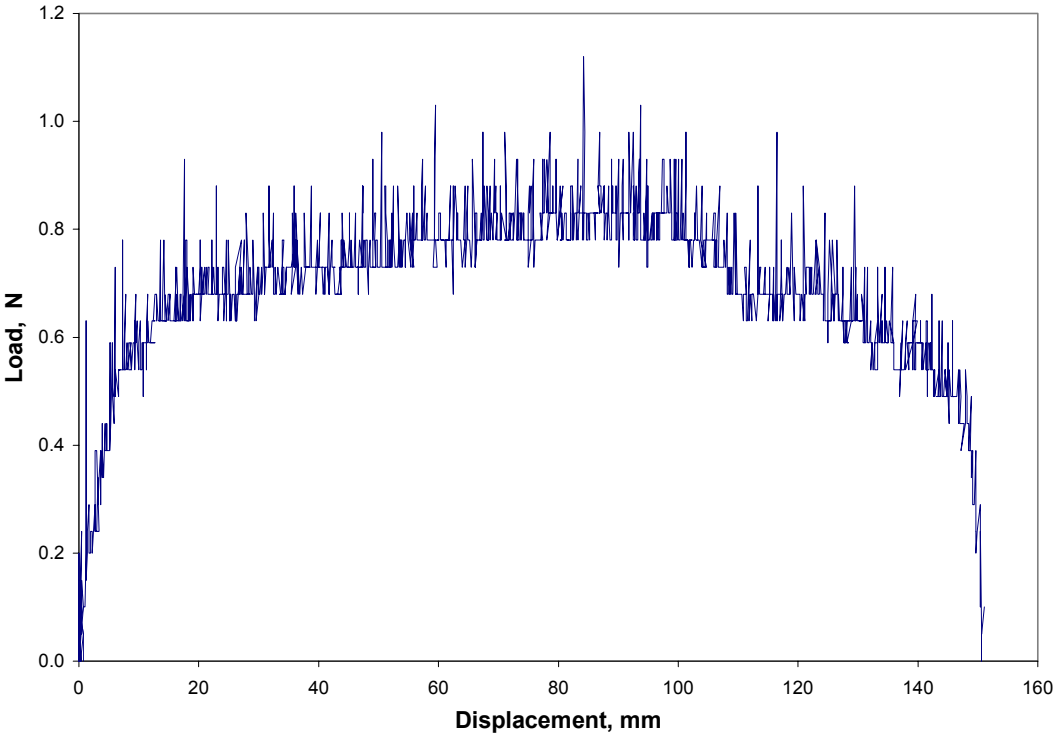

Figure B.124: Load Versus Displacement for Subject A, 180 degrees, 5 min, 500 mm/min, Test 1

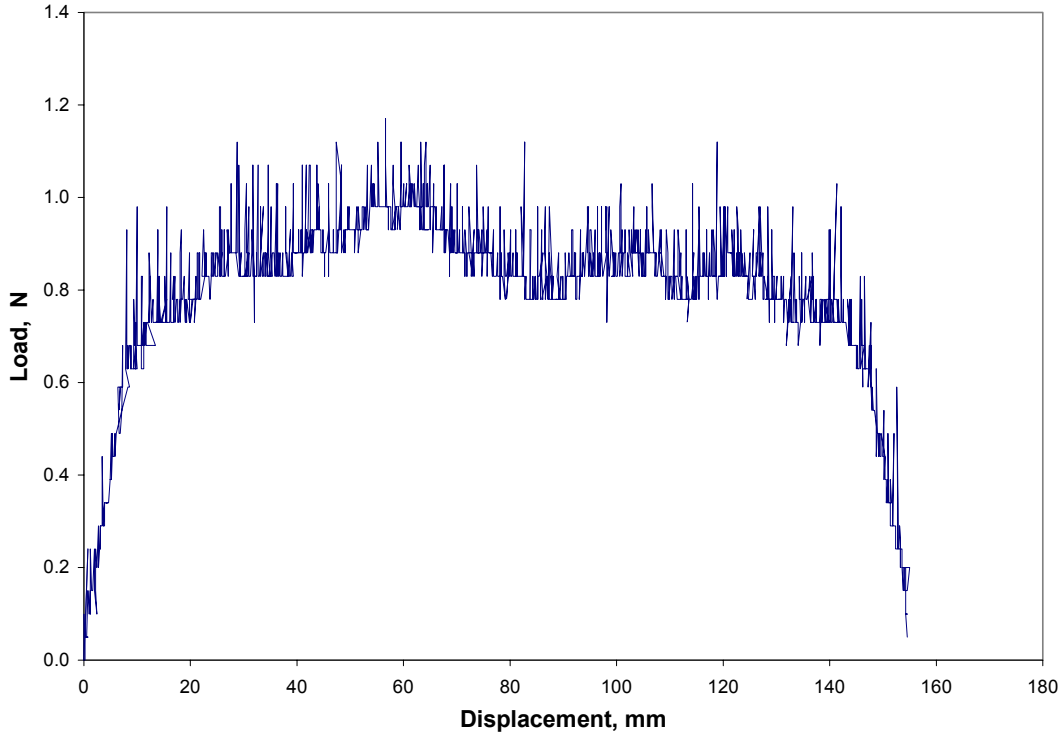

Figure B.125: Load Versus Displacement for Subject A, 180 degrees, 5 min, 500 mm/min, Test 2

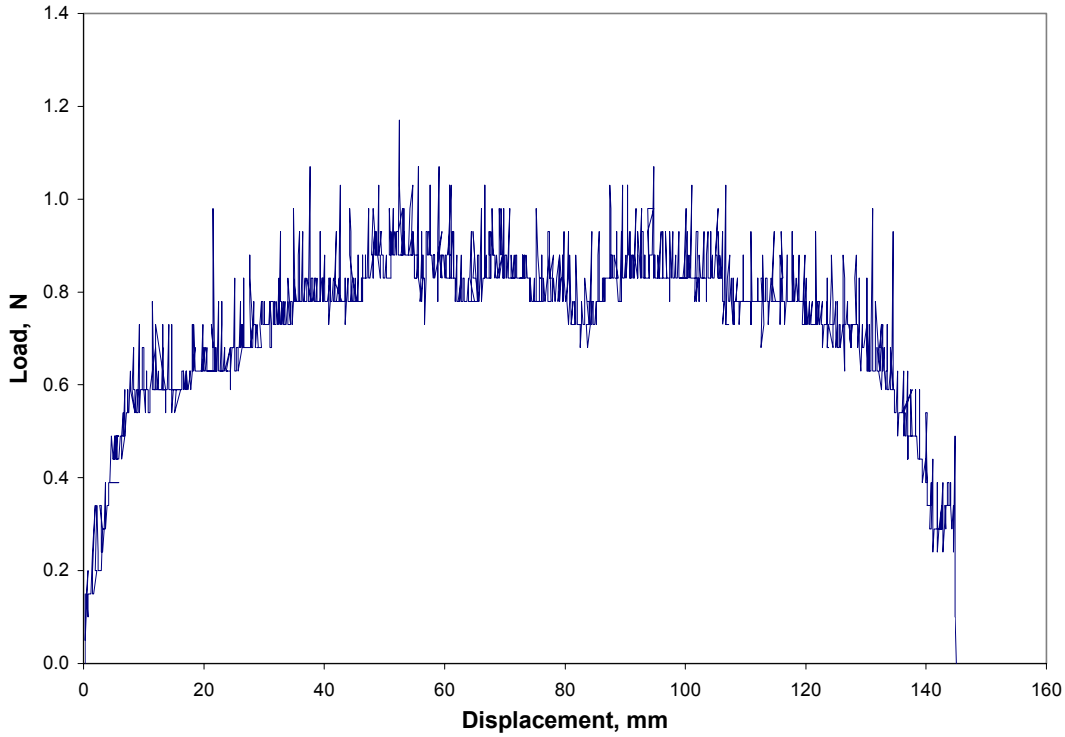

Figure B.126: Load Versus Displacement for Subject A, 180 degrees, 5 min, 500 mm/min, Test 3

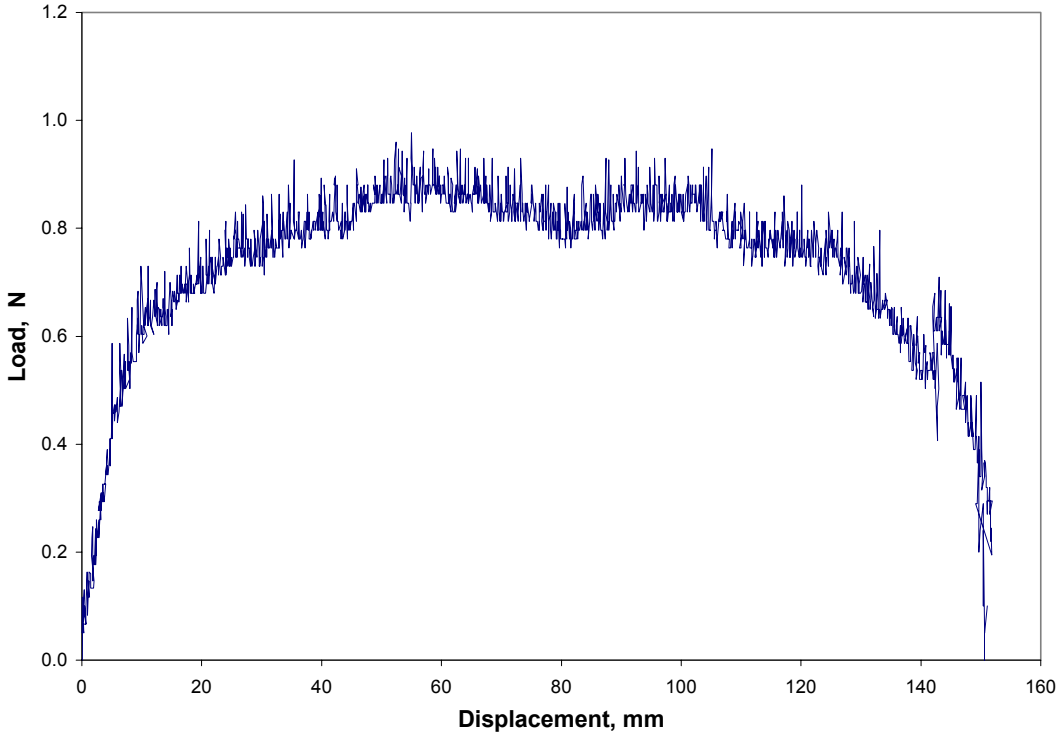

Figure B.127: Load Versus Displacement for Subject A, 180 degrees, 5 min, 500 mm/min, Average

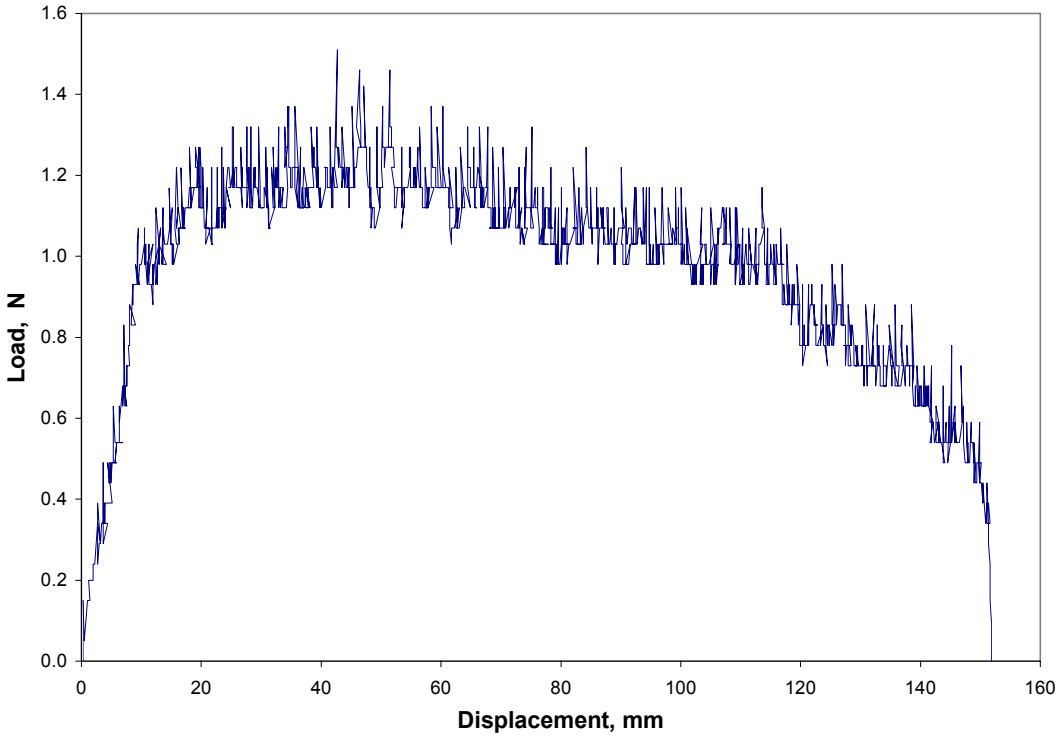

Figure B.128: Load Versus Displacement for Subject A, 180 degrees, 10 min, 500 mm/min, Test 1

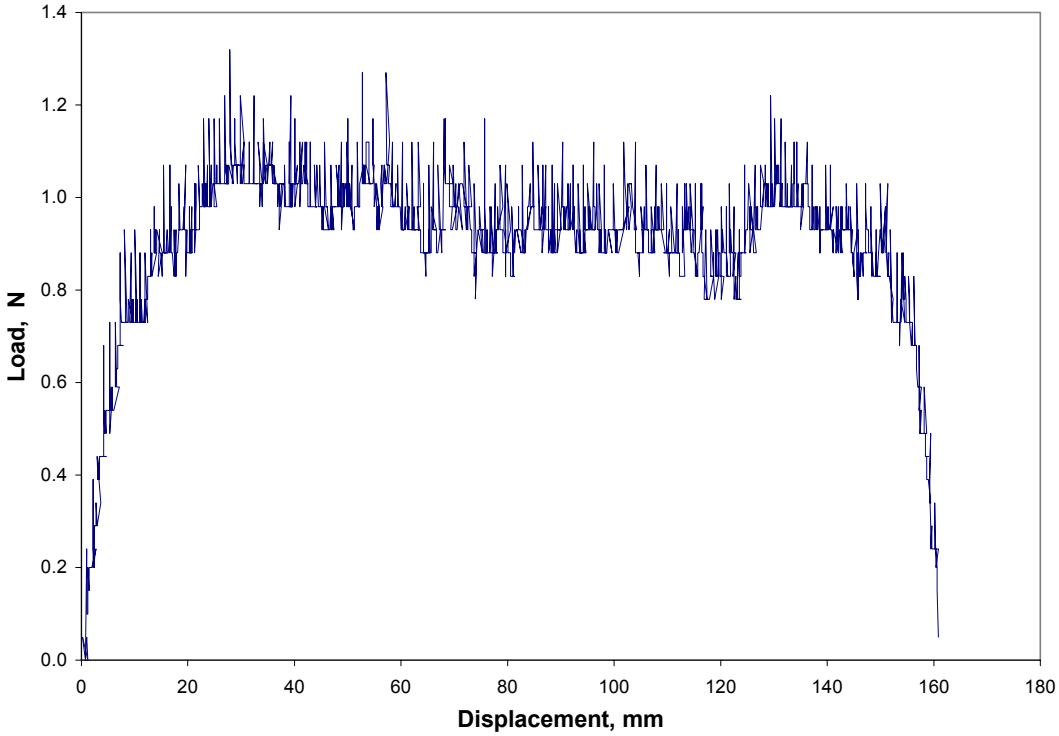

Figure B.129: Load Versus Displacement for Subject A, 180 degrees, 10 min, 500 mm/min, Test 2

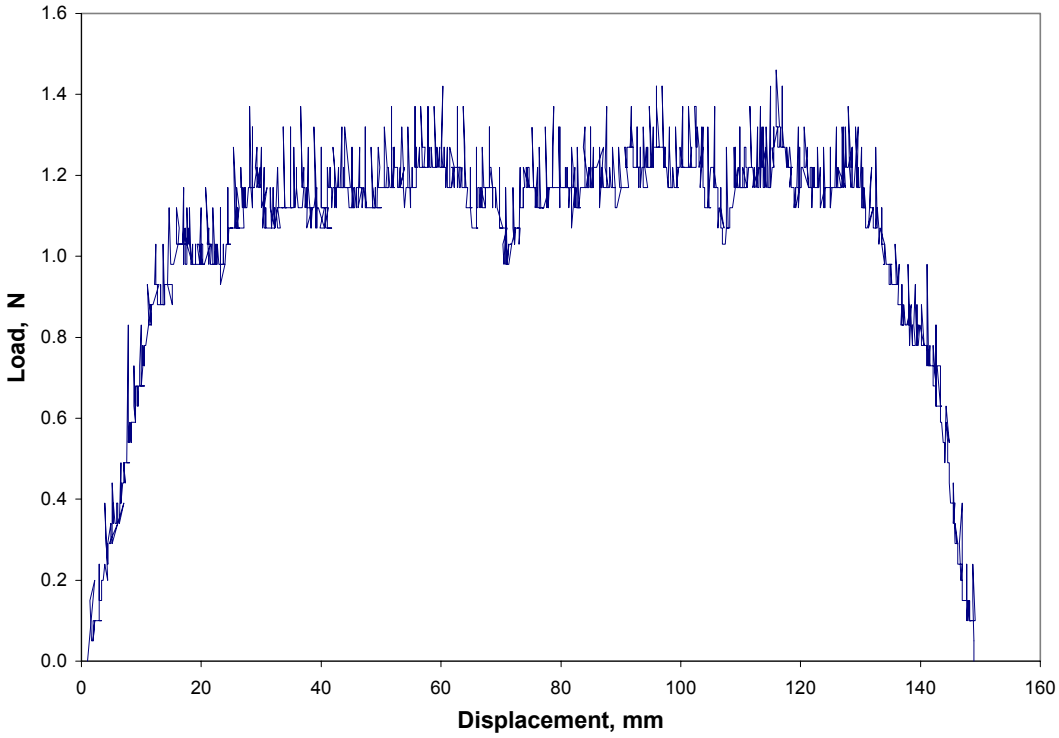

Figure B.130: Load Versus Displacement for Subject A, 180 degrees, 10 min, 500 mm/min, Test 3

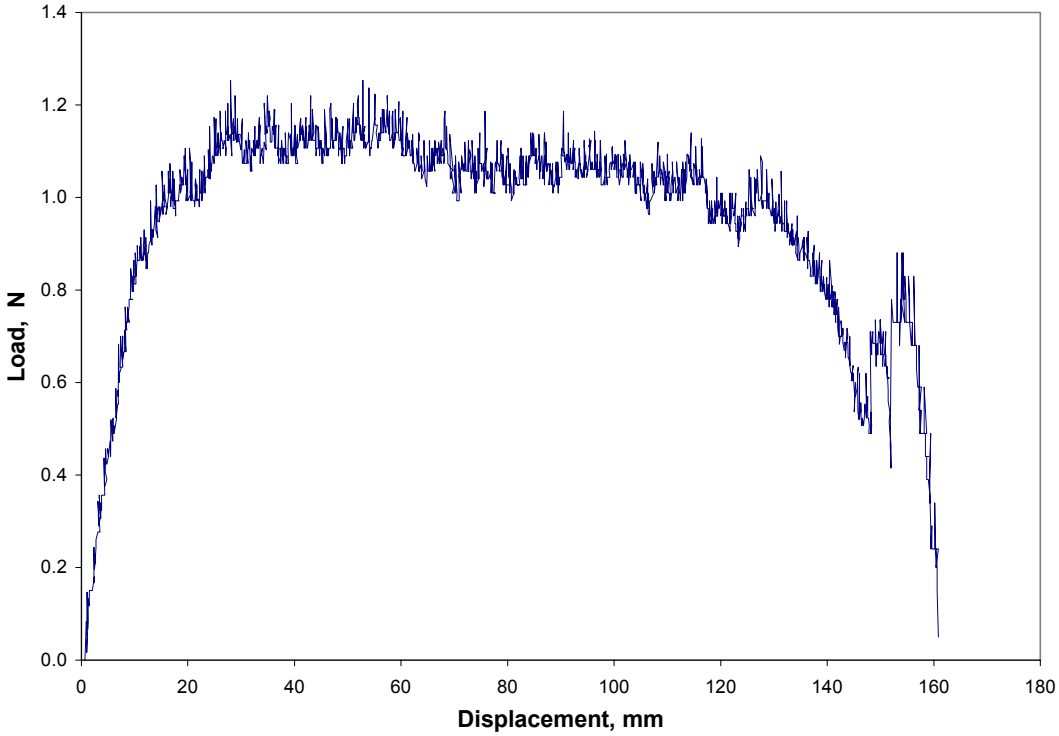

Figure B.131: Load Versus Displacement for Subject A, 180 degrees, 10 min, 500 mm/min, Average

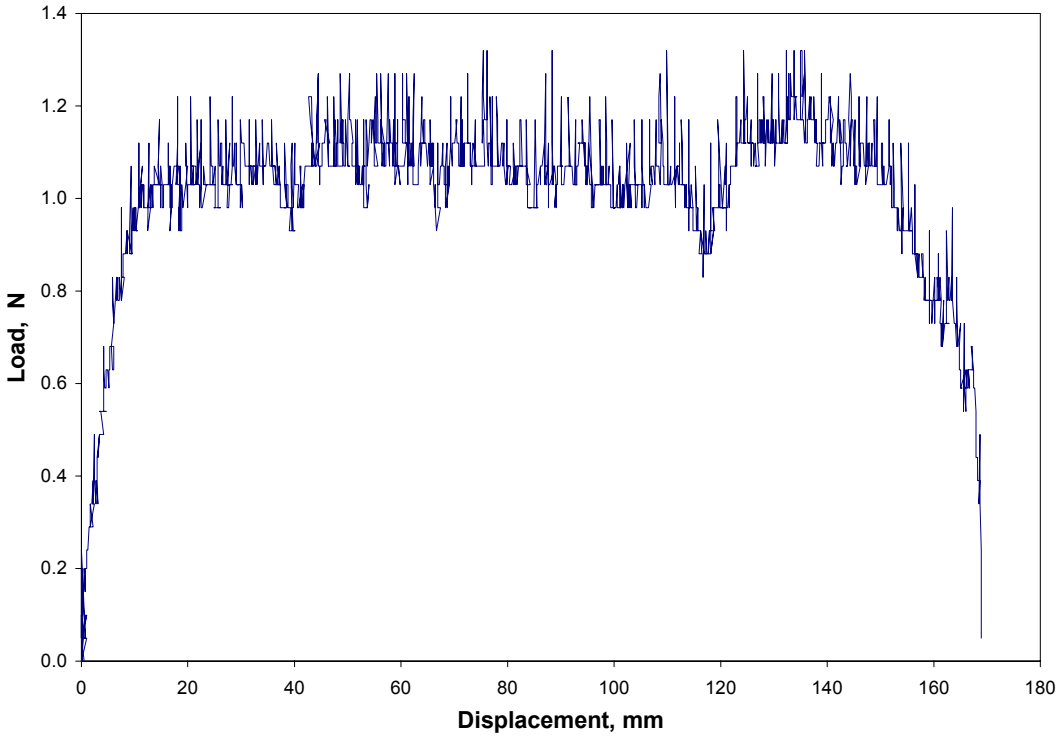

Figure B.132: Load Versus Displacement for Subject A, 180 degrees, 15 min, 500 mm/min, Test 1

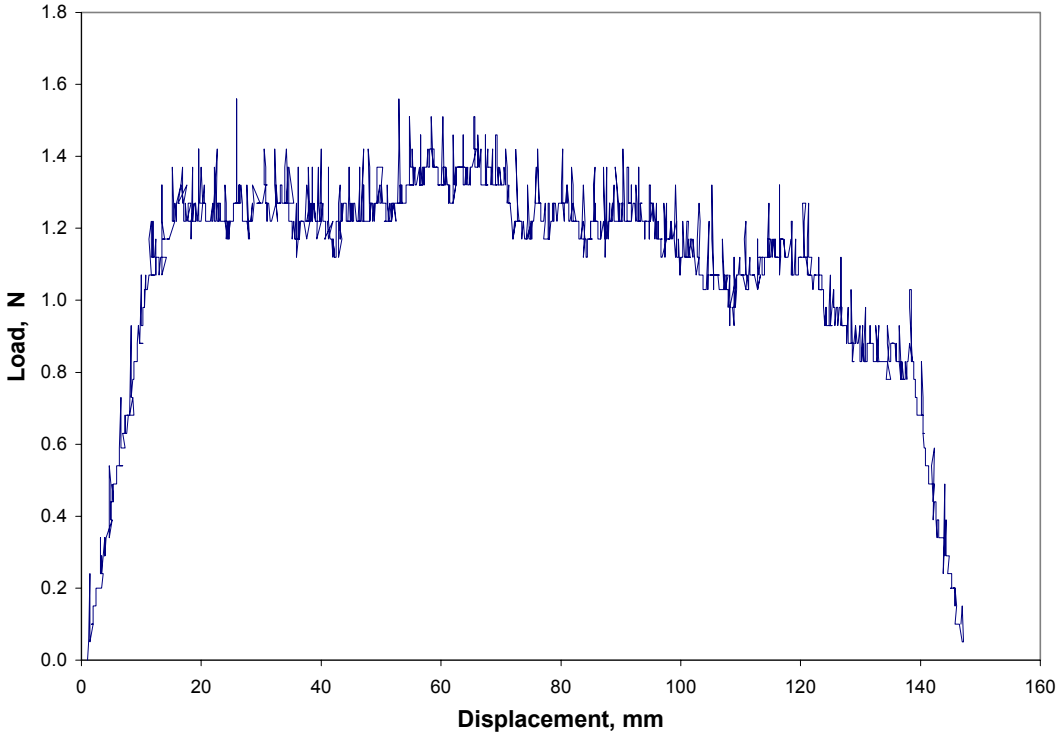

Figure B.133: Load Versus Displacement for Subject A, 180 degrees, 15 min, 500 mm/min, Test 2

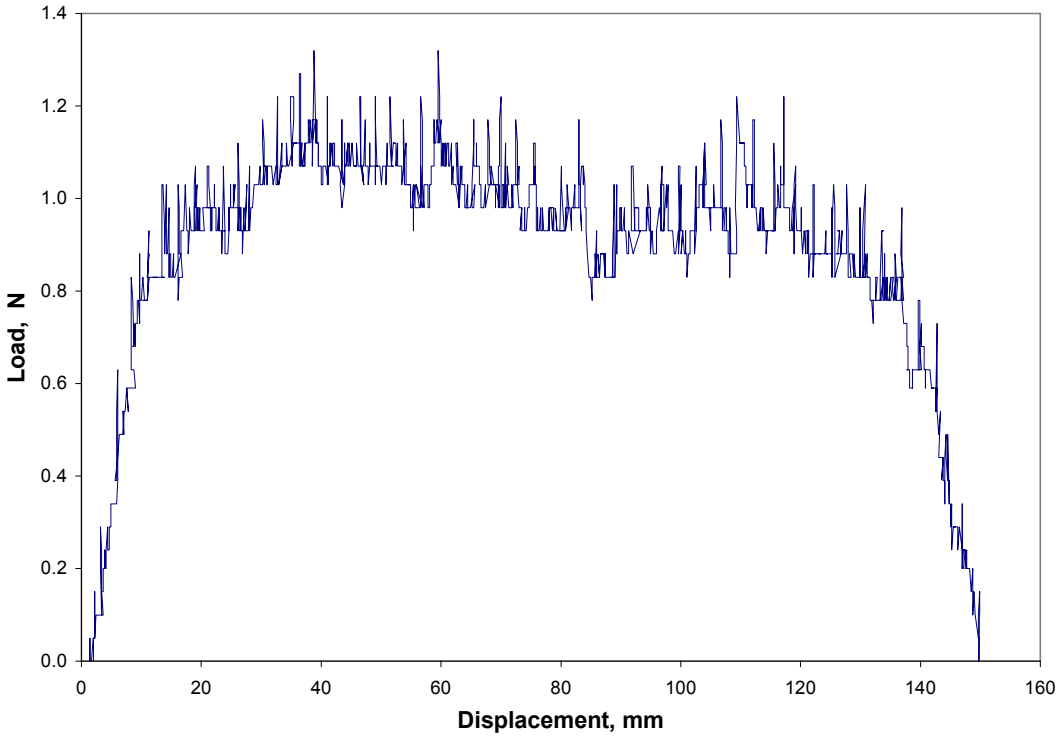

Figure B.134: Load Versus Displacement for Subject A, 180 degrees, 15 min, 500 mm/min, Test 3

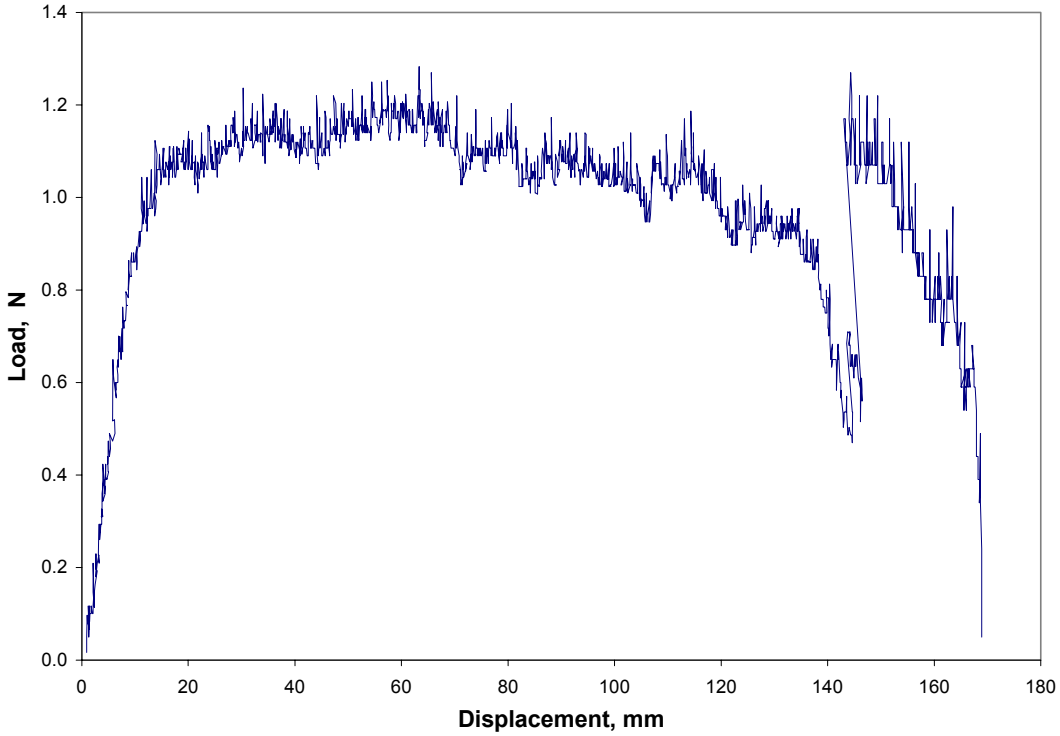

Figure B.135: Load Versus Displacement for Subject A, 180 degrees, 15 min, 500 mm/min, Average

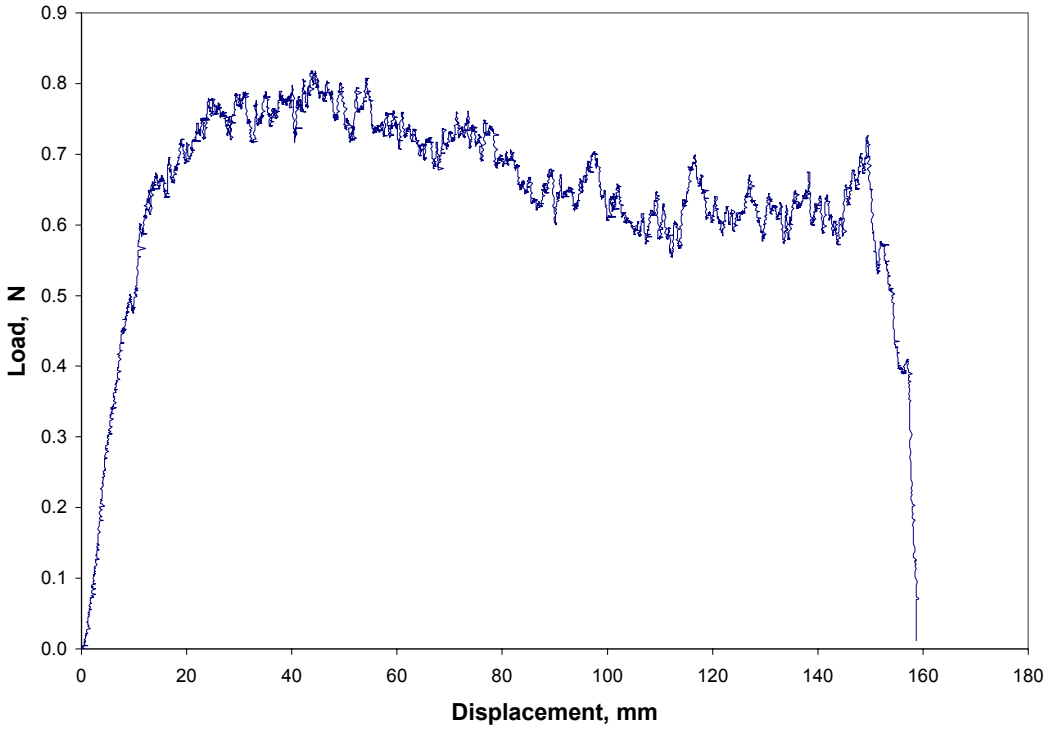

Figure B.136: Load Versus Displacement for Subject B, 180 degrees, 1 min, 100 mm/min, Test 1

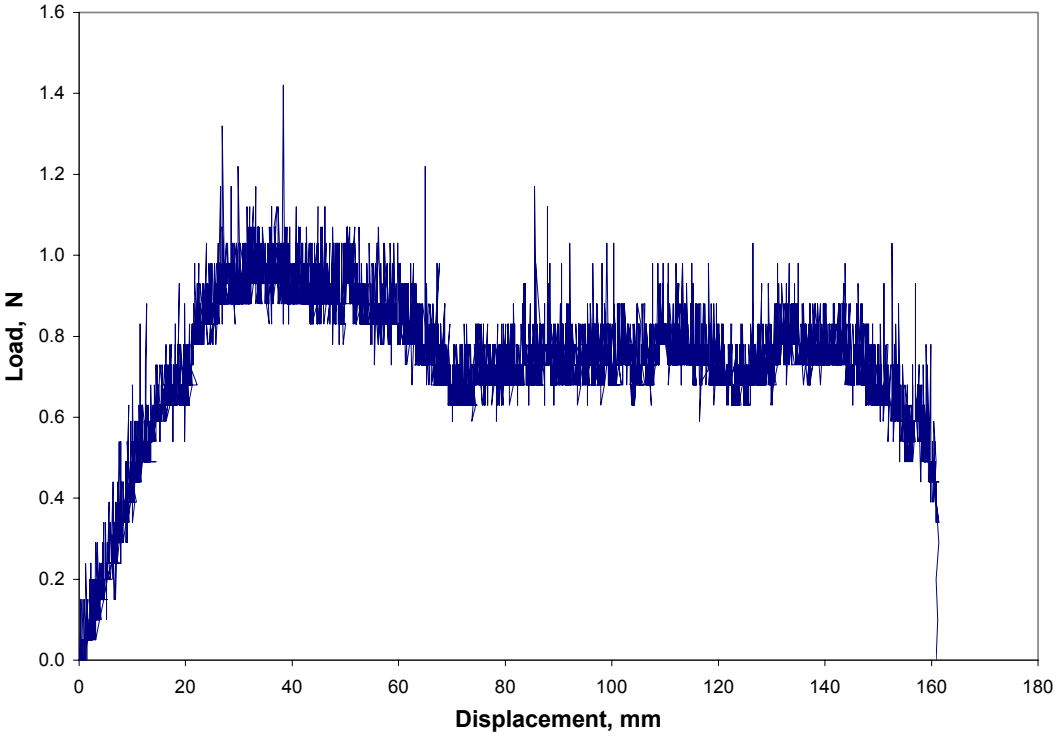

Figure B.137: Load Versus Displacement for Subject B, 180 degrees, 1 min, 100 mm/min, Test 2

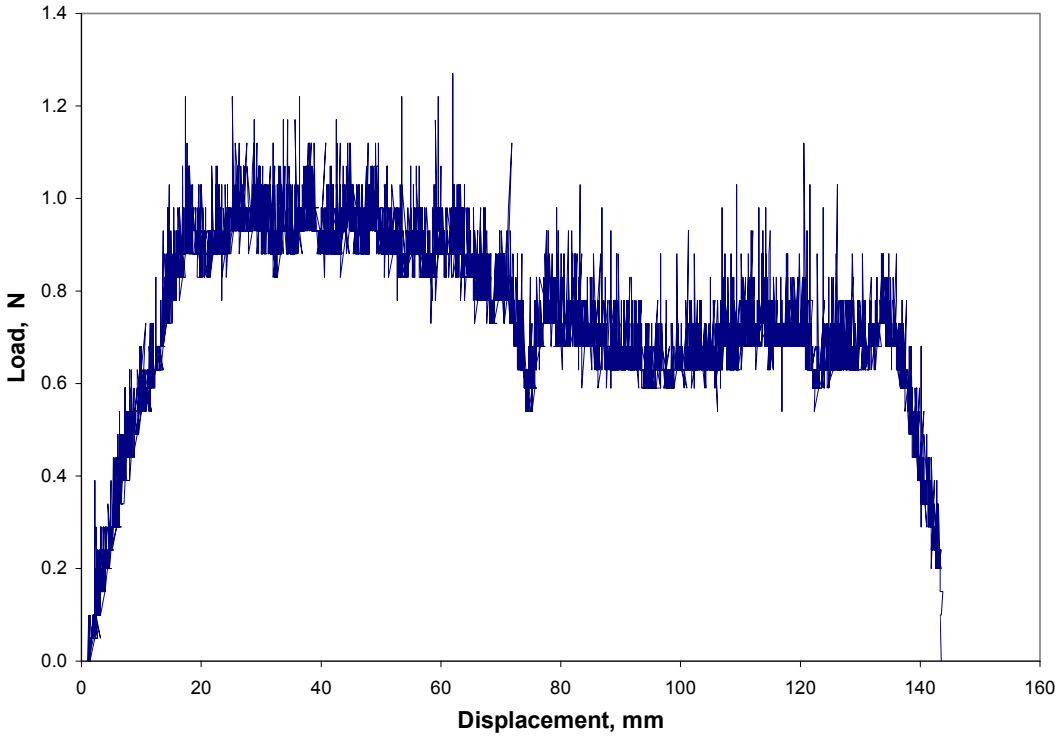

Figure B.138: Load Versus Displacement for Subject B, 180 degrees, 1 min, 100 mm/min, Test 3

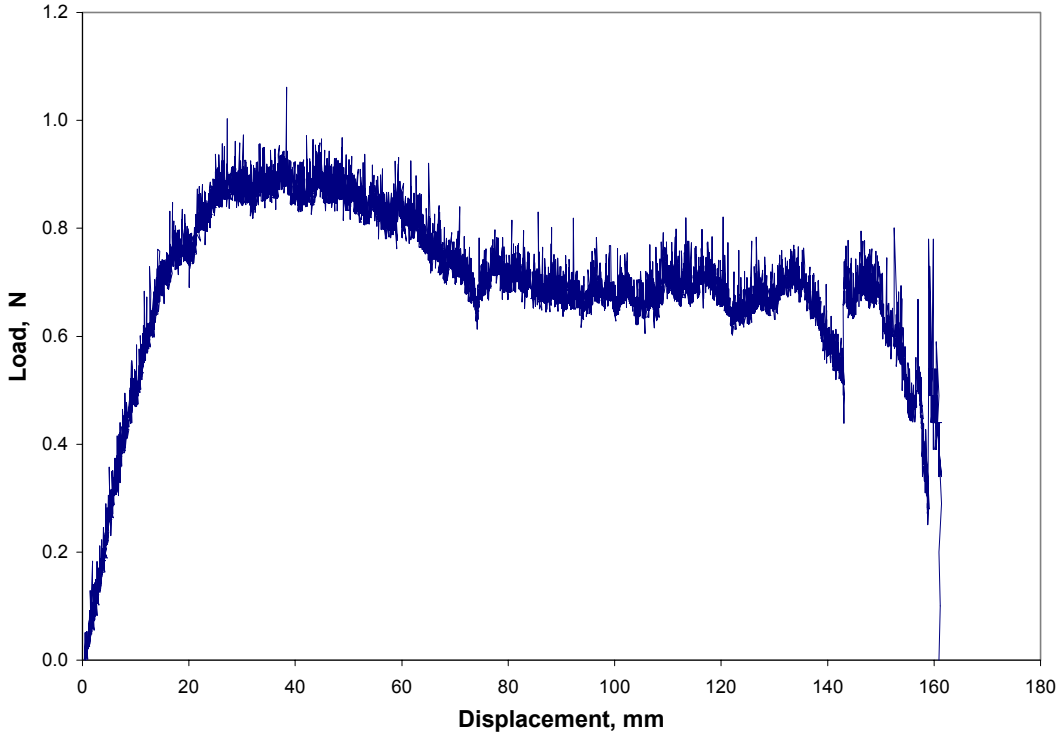

Figure B.139: Load Versus Displacement for Subject B, 180 degrees, 1 min, 100 mm/min, Average

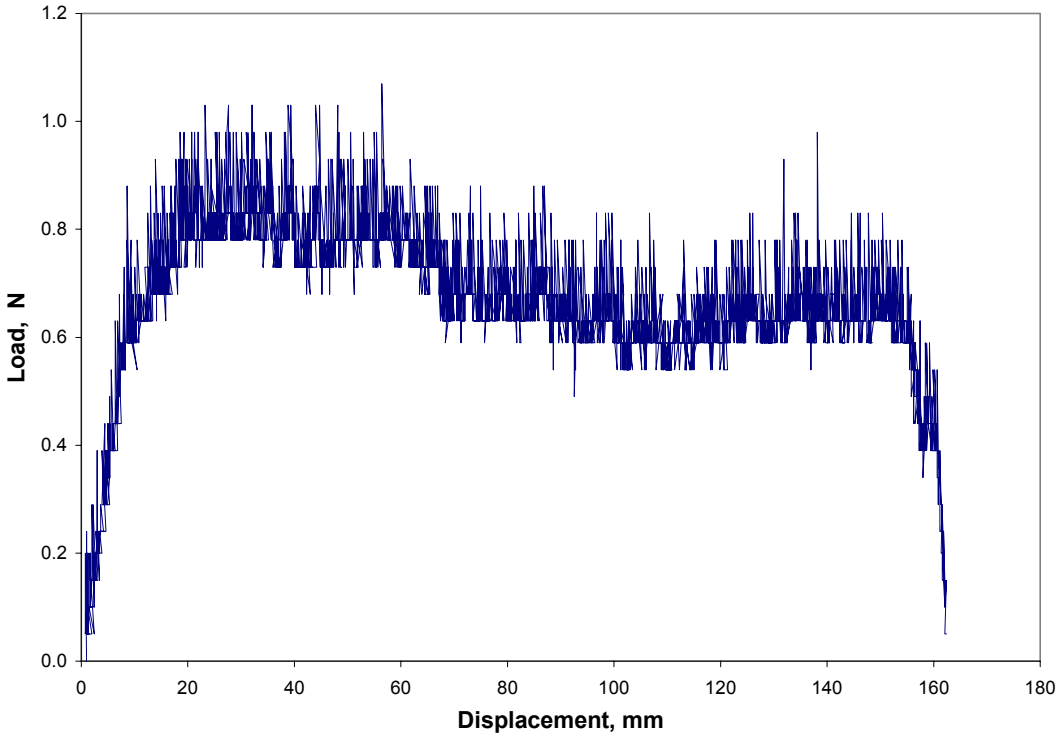

Figure B.140: Load Versus Displacement for Subject B, 180 degrees, 1 min, 200 mm/min, Test 1

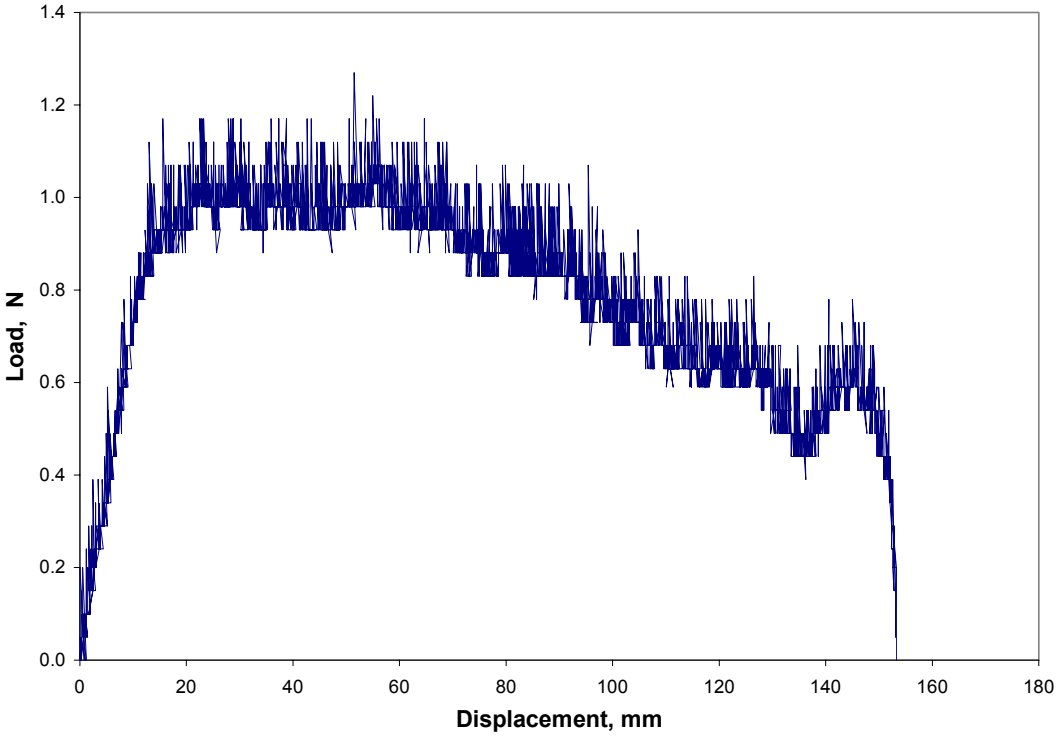

Figure B.141: Load Versus Displacement for Subject B, 180 degrees, 1 min, 200 mm/min, Test 2

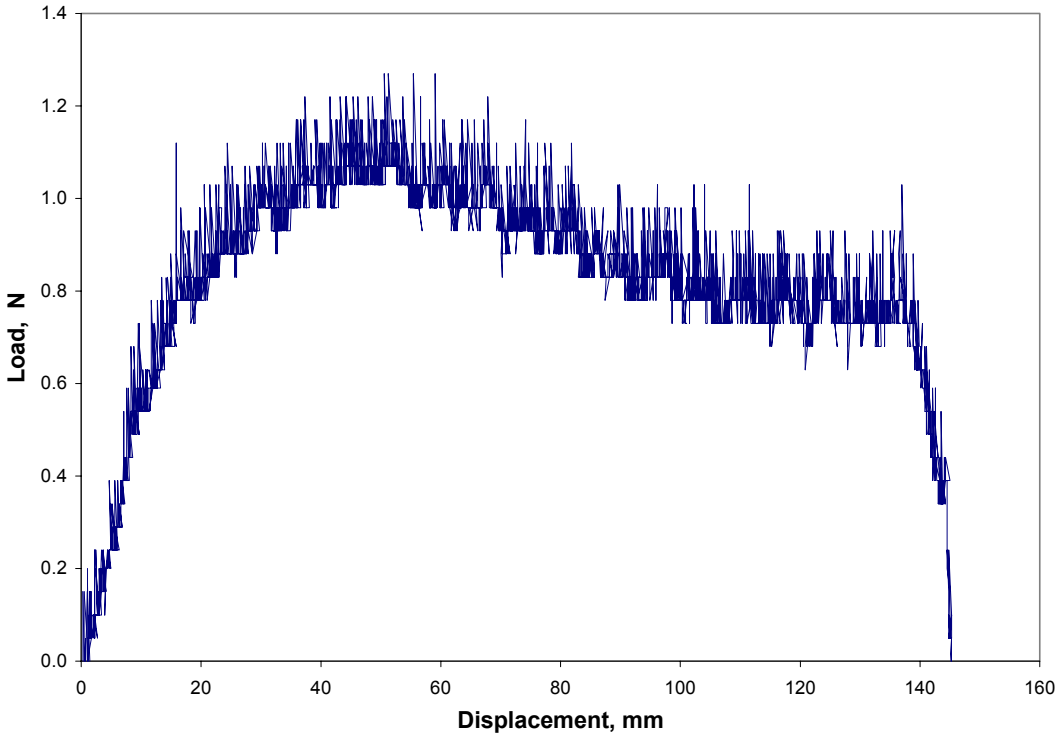

Figure B.142: Load Versus Displacement for Subject B, 180 degrees, 1 min, 200 mm/min, Test 3

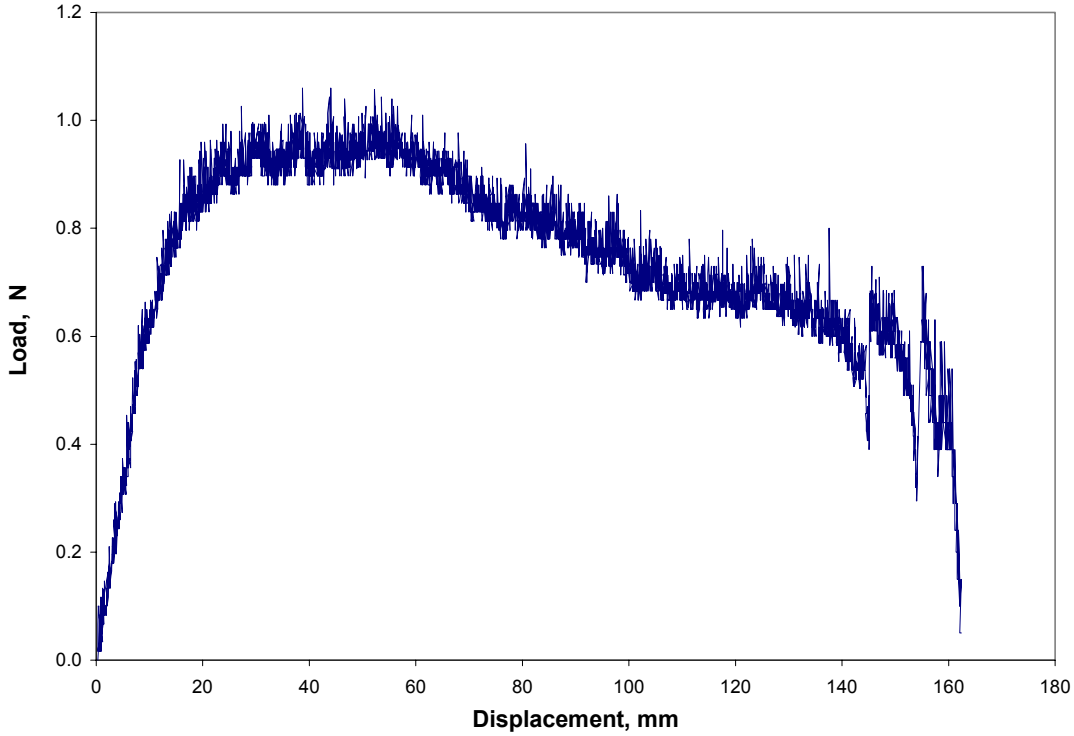

Figure B.143: Load Versus Displacement for Subject B, 180 degrees, 1 min, 200 mm/min, Average

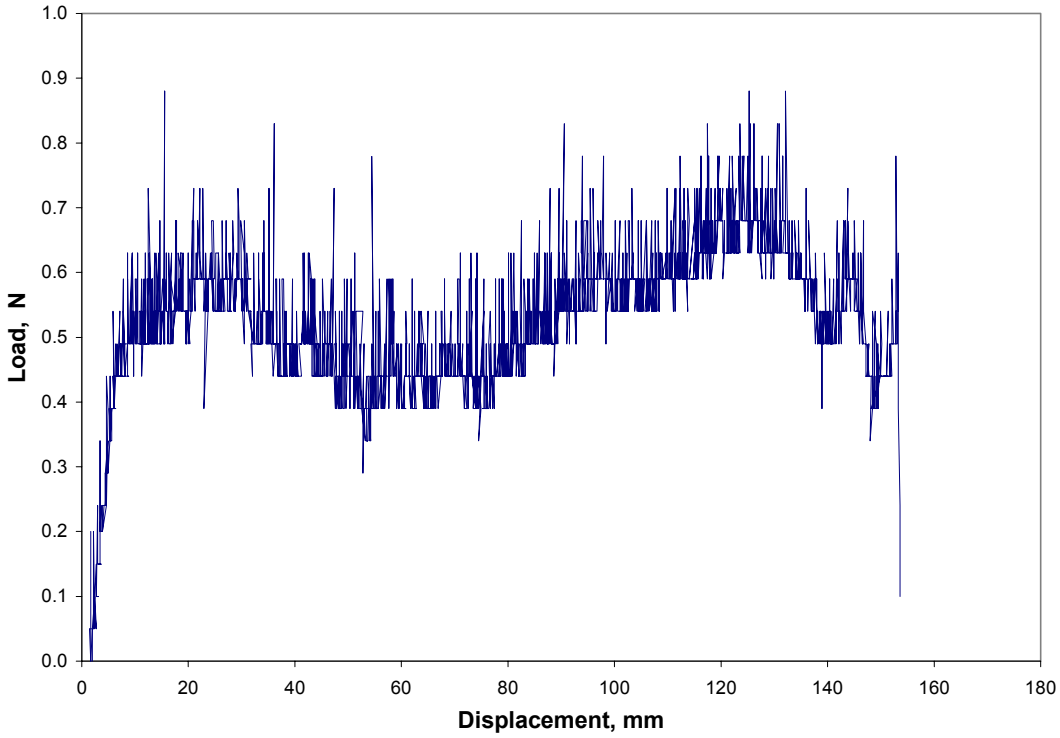

Figure B.144: Load Versus Displacement for Subject B, 180 degrees, 1 min, 300 mm/min, Test 1

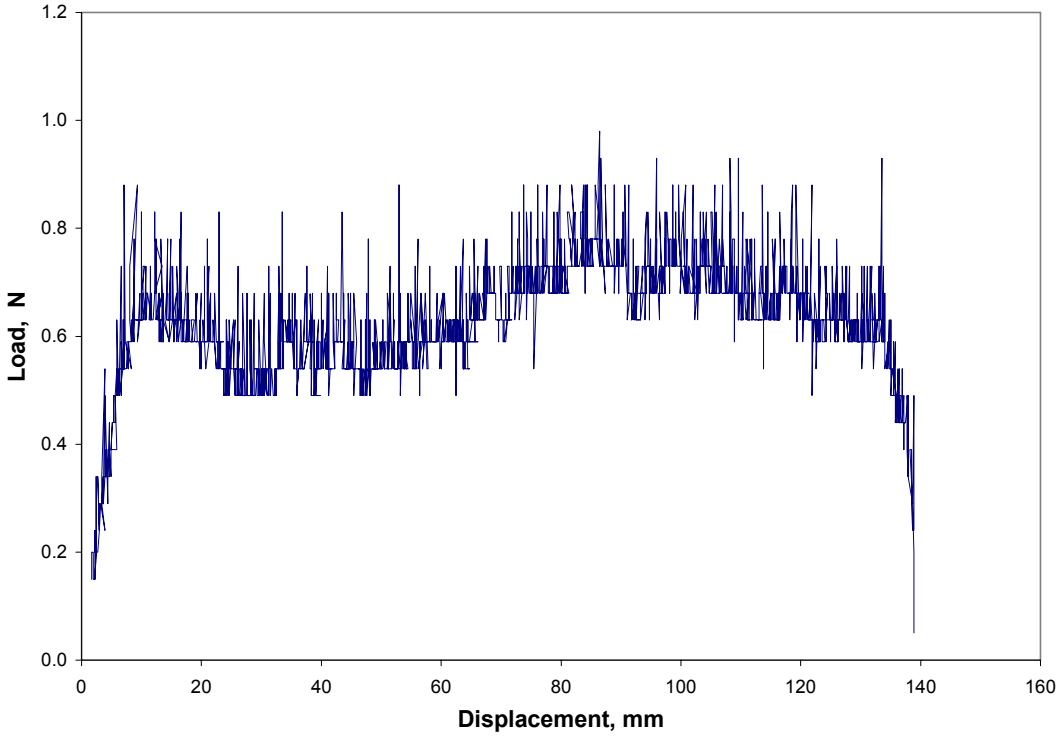

Figure B.145: Load Versus Displacement for Subject B, 180 degrees, 1 min, 300 mm/min, Test 2

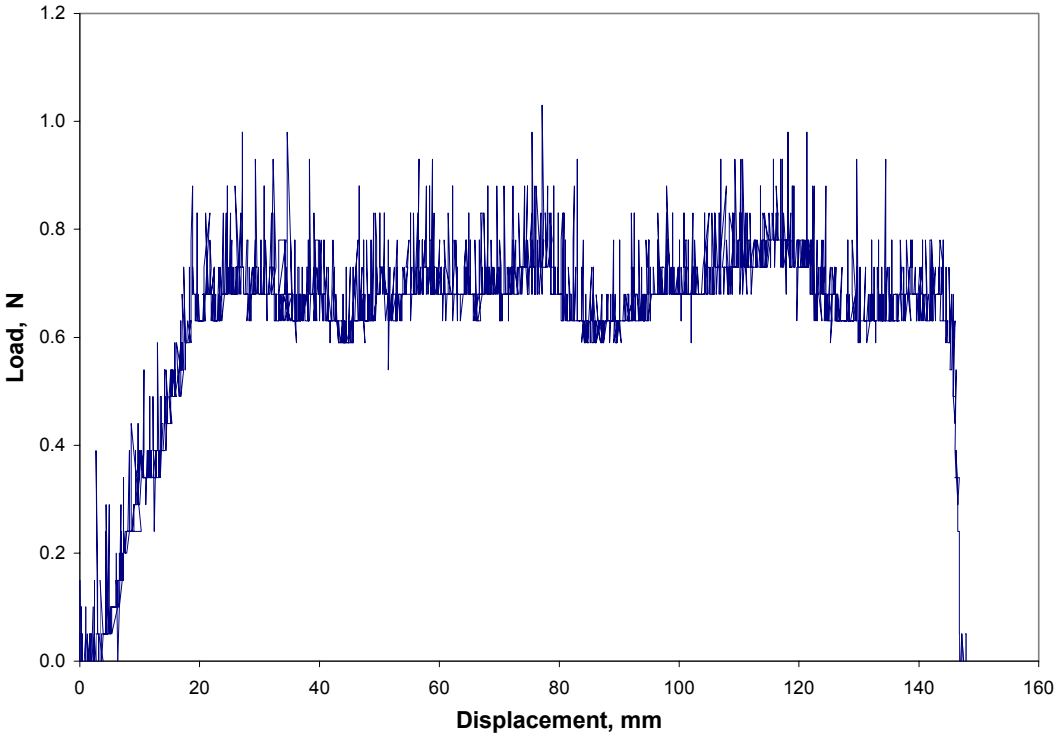

Figure B.146: Load Versus Displacement for Subject B, 180 degrees, 1 min, 300 mm/min, Test 3

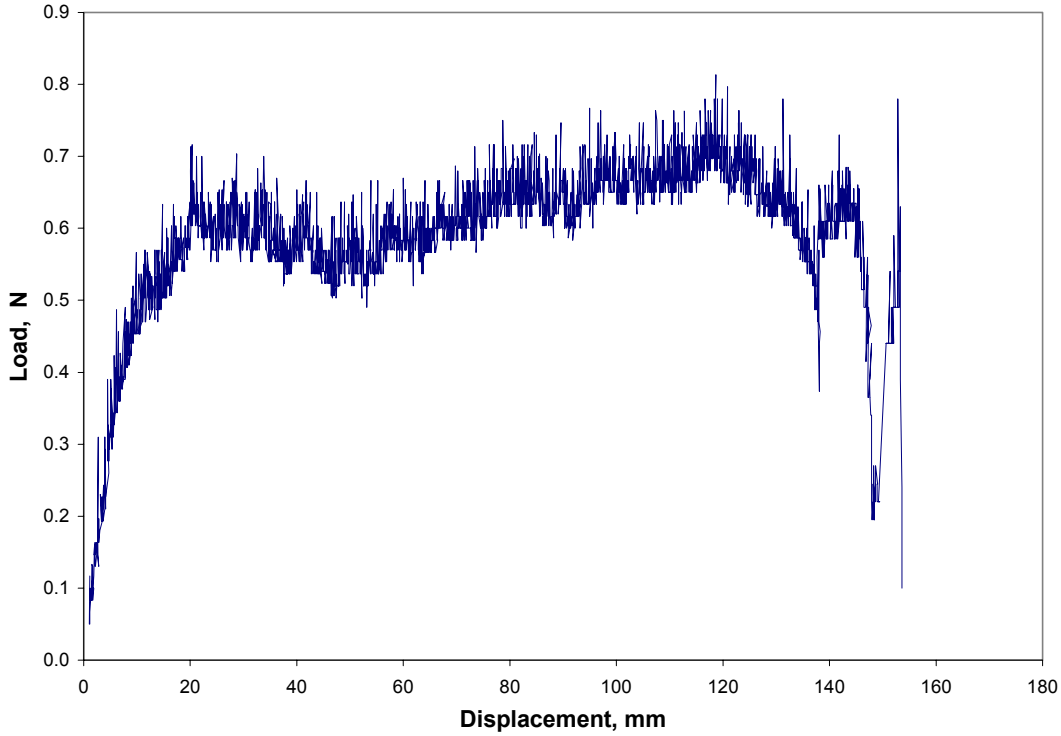

Figure B.147: Load Versus Displacement for Subject B, 180 degrees, 1 min, 300 mm/min, Average

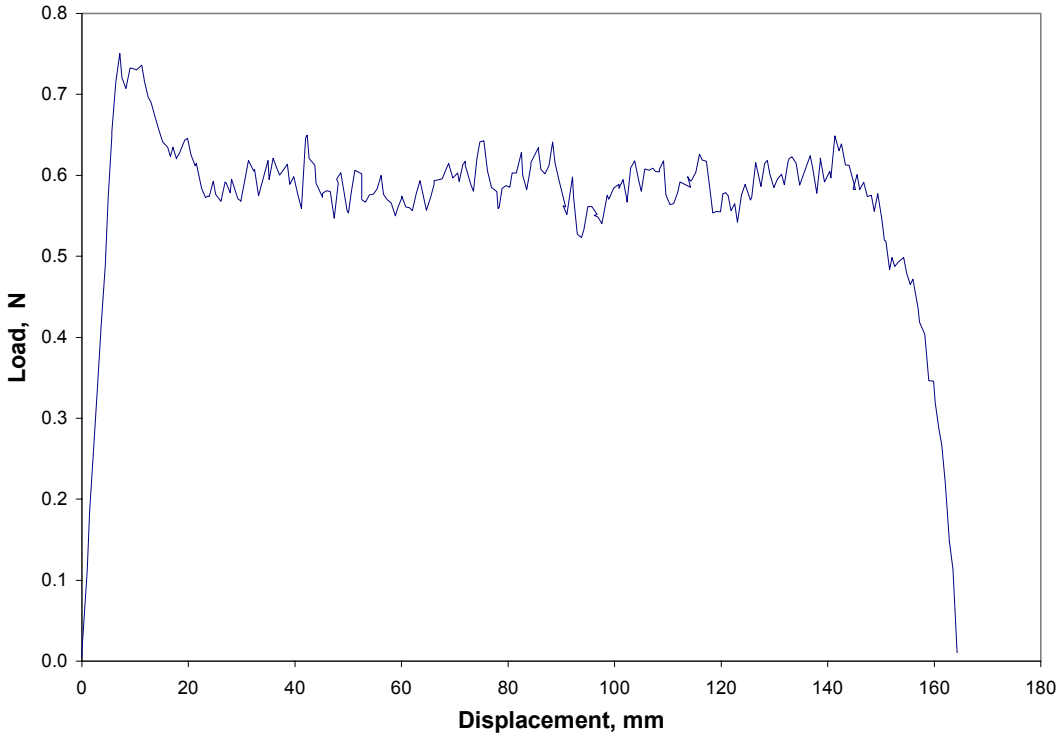

Figure B.148: Load Versus Displacement for Subject B, 180 degrees, 1 min, 400 mm/min, Test 1

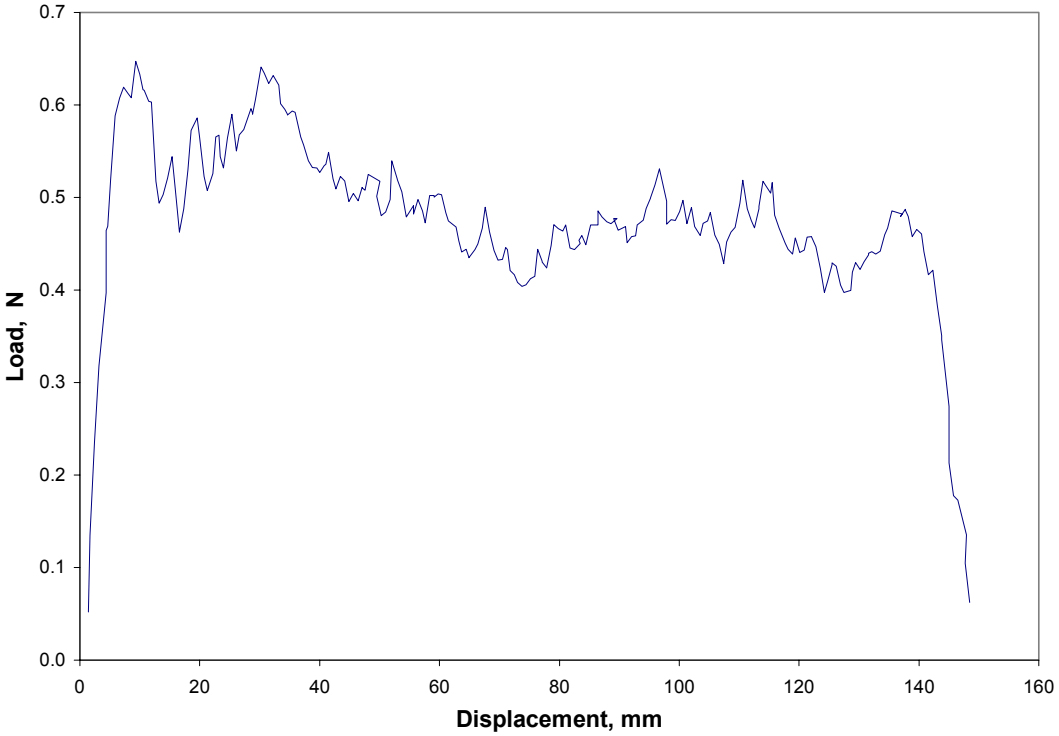

Figure B.149: Load Versus Displacement for Subject B, 180 degrees, 1 min, 400 mm/min, Test 2

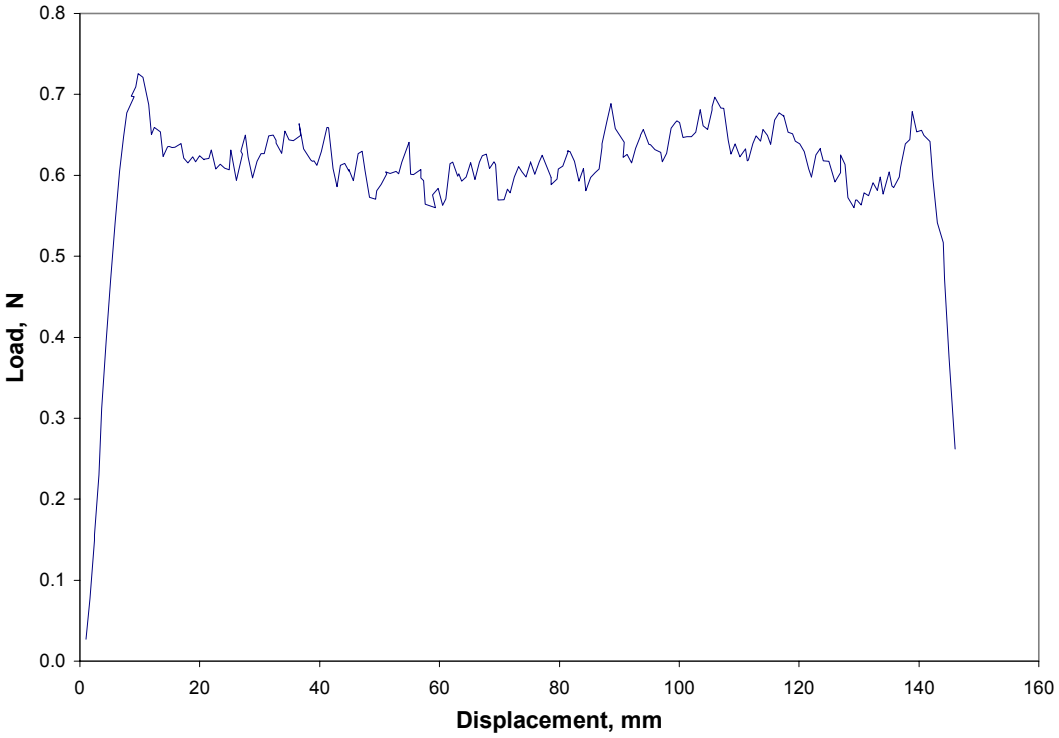

Figure B.150: Load Versus Displacement for Subject B, 180 degrees, 1 min, 400 mm/min, Test 3

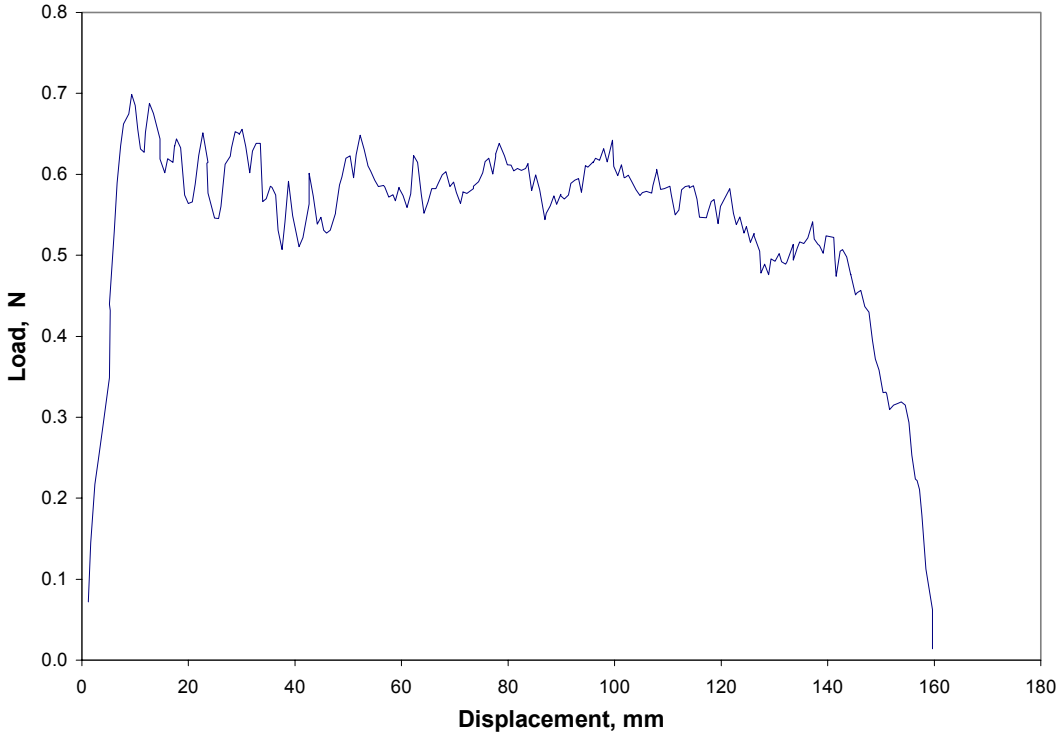

Figure B.151: Load Versus Displacement for Subject B, 180 degrees, 1 min, 400 mm/min, Test 4

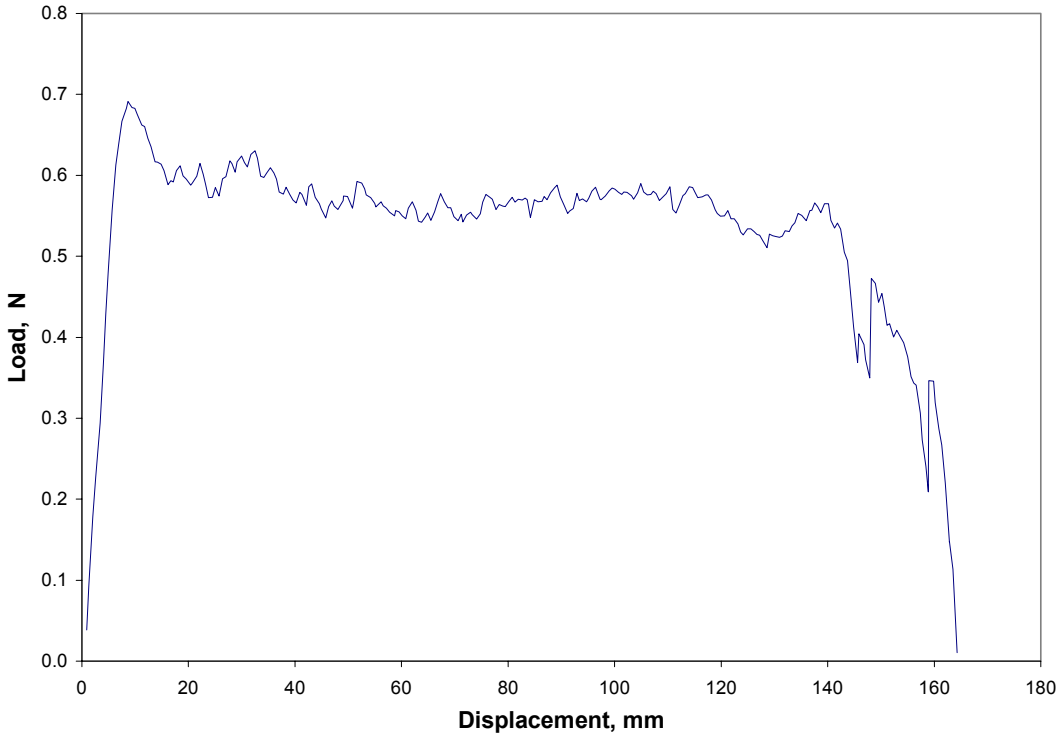

Figure B.152: Load Versus Displacement for Subject B, 180 degrees, 1 min, 400 mm/min, Average

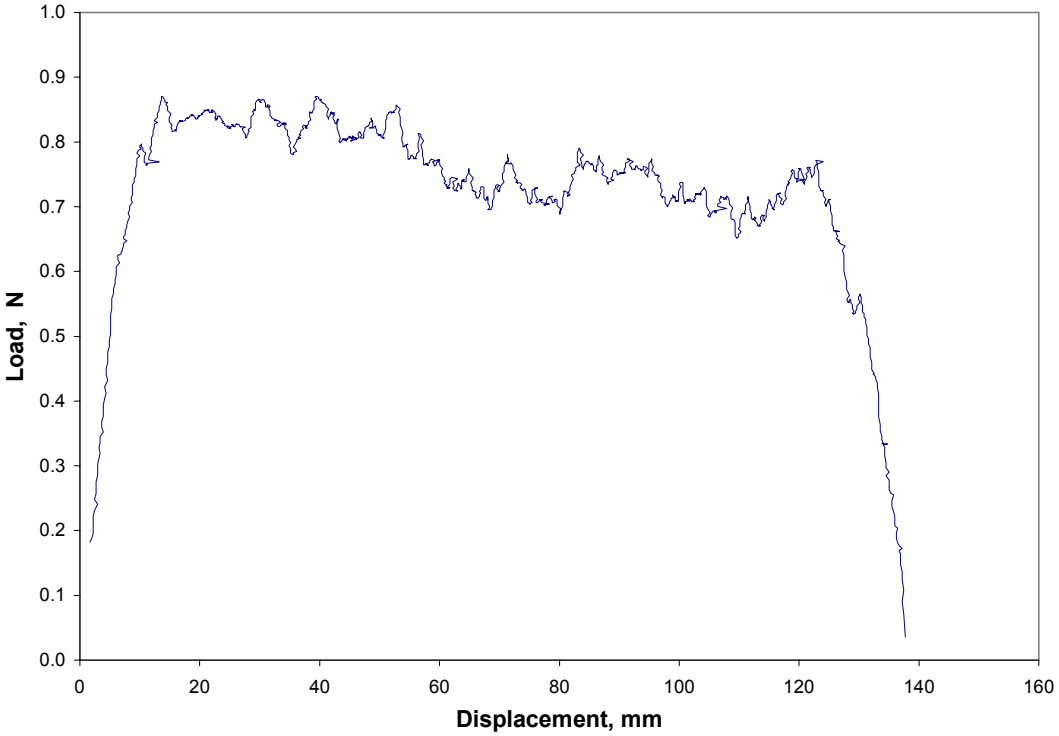

Figure B.153: Load Versus Displacement for Subject B, 180 degrees, 1 min, 500 mm/min, Test 1

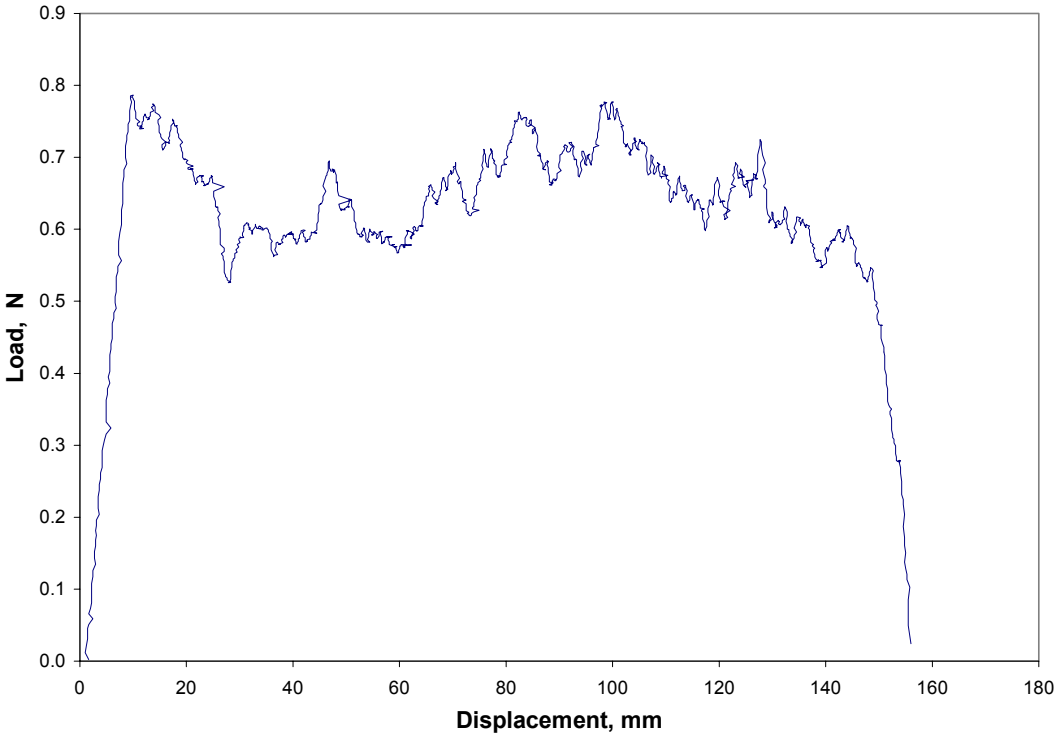

Figure B.154: Load Versus Displacement for Subject B, 180 degrees, 1 min, 500 mm/min, Test 2

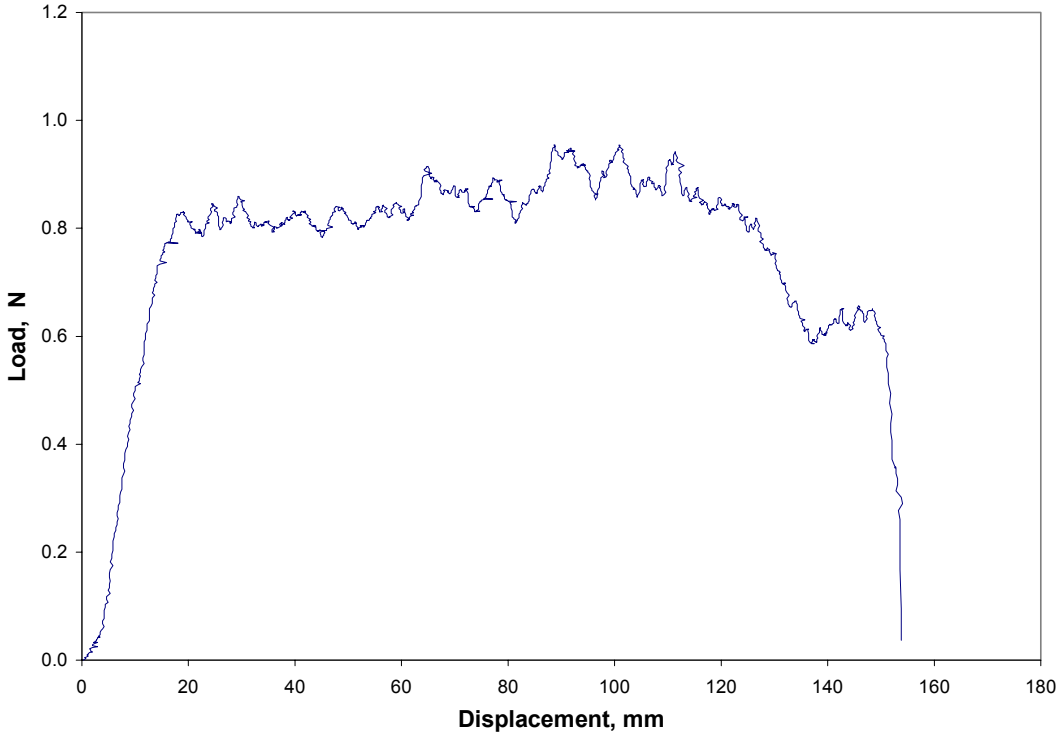

Figure B.155: Load Versus Displacement for Subject B, 180 degrees, 1 min, 500 mm/min, Test 3

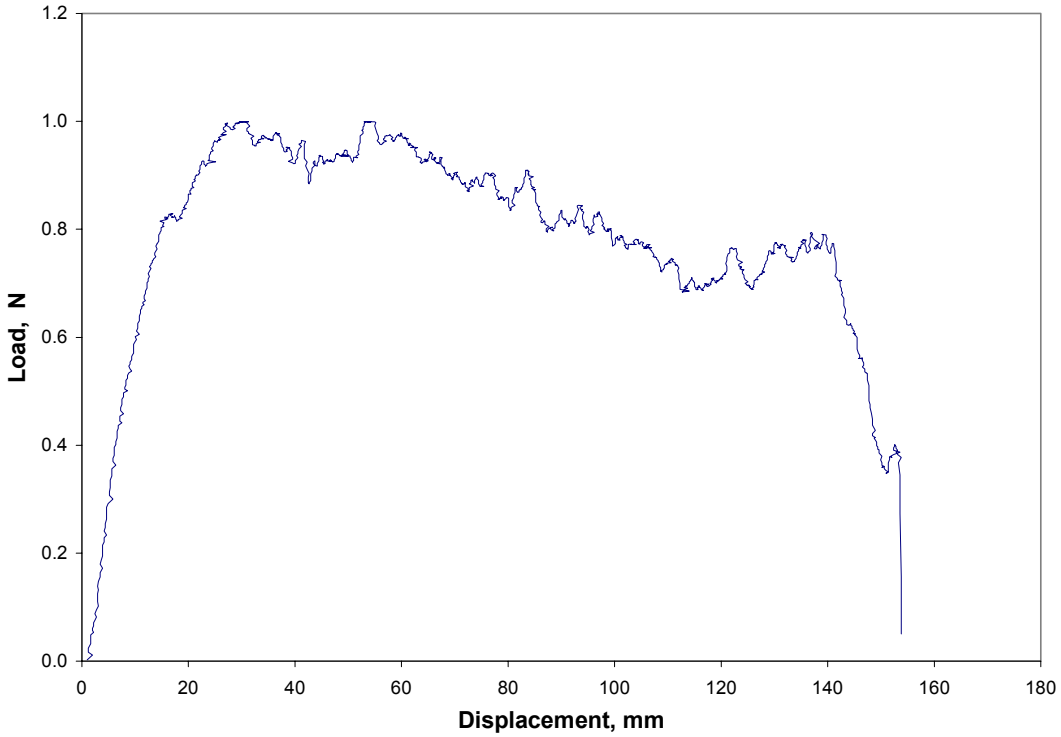

Figure B.156: Load Versus Displacement for Subject B, 180 degrees, 1 min, 500 mm/min, Test 4

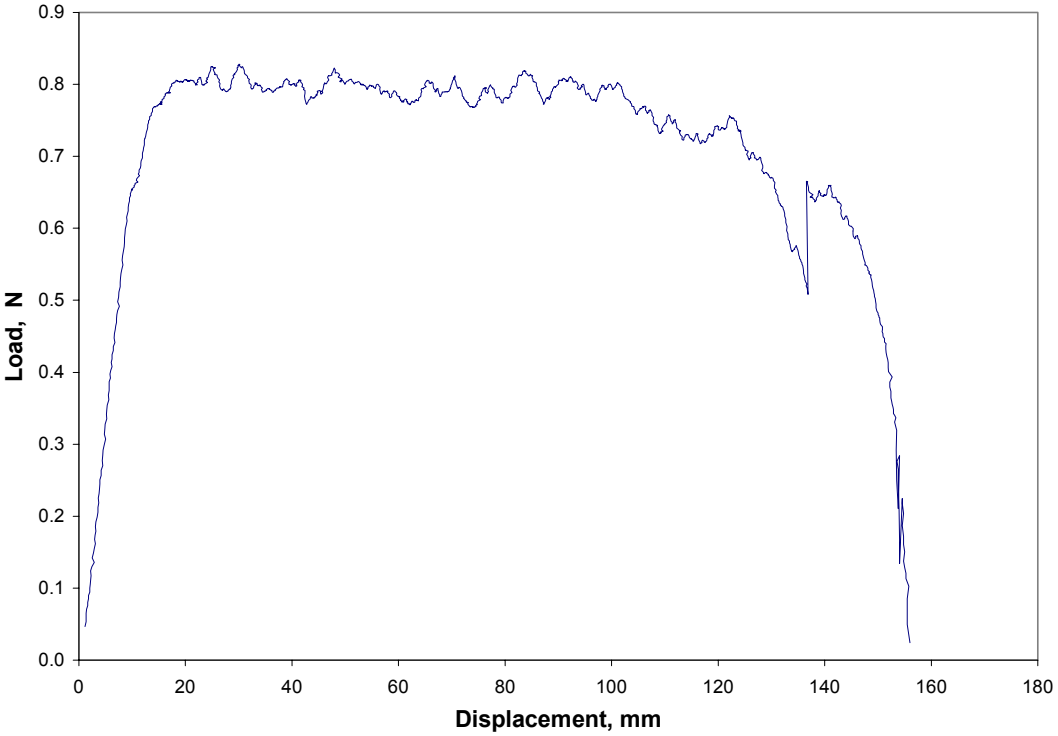

Figure B.157: Load Versus Displacement for Subject B, 180 degrees, 1 min, 500 mm/min, Average

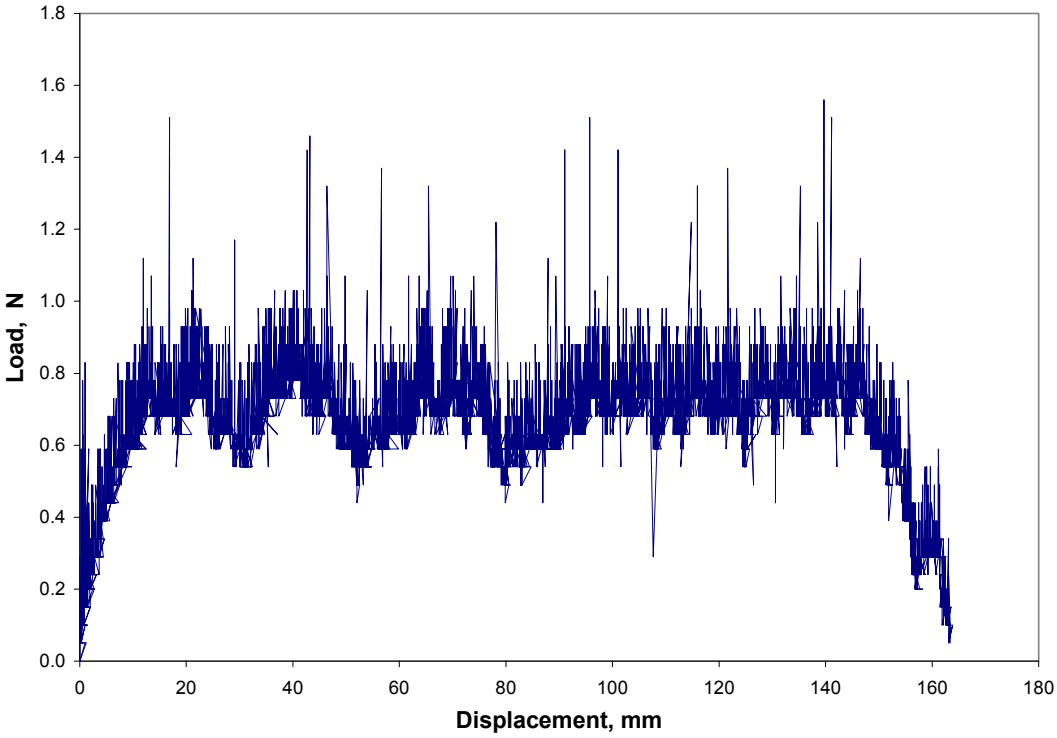

Figure B.158: Load Versus Displacement for Subject C, 180 degrees, 1 min, 100 mm/min, Test 1

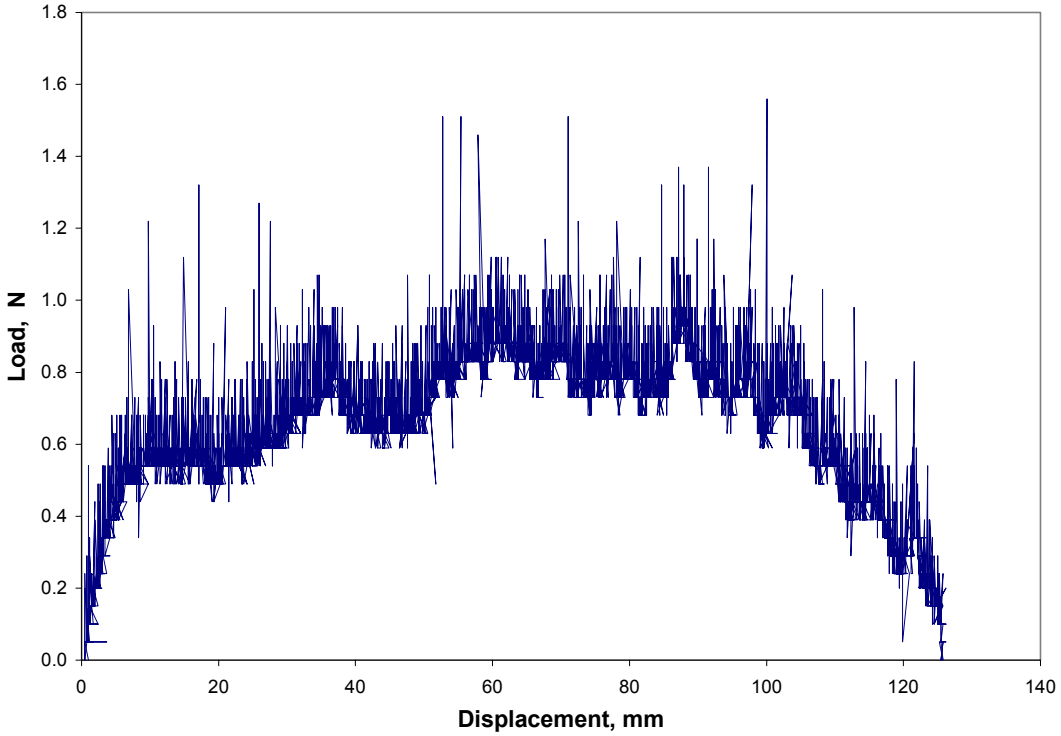

Figure B.159: Load Versus Displacement for Subject C, 180 degrees, 1 min, 100 mm/min, Test 2

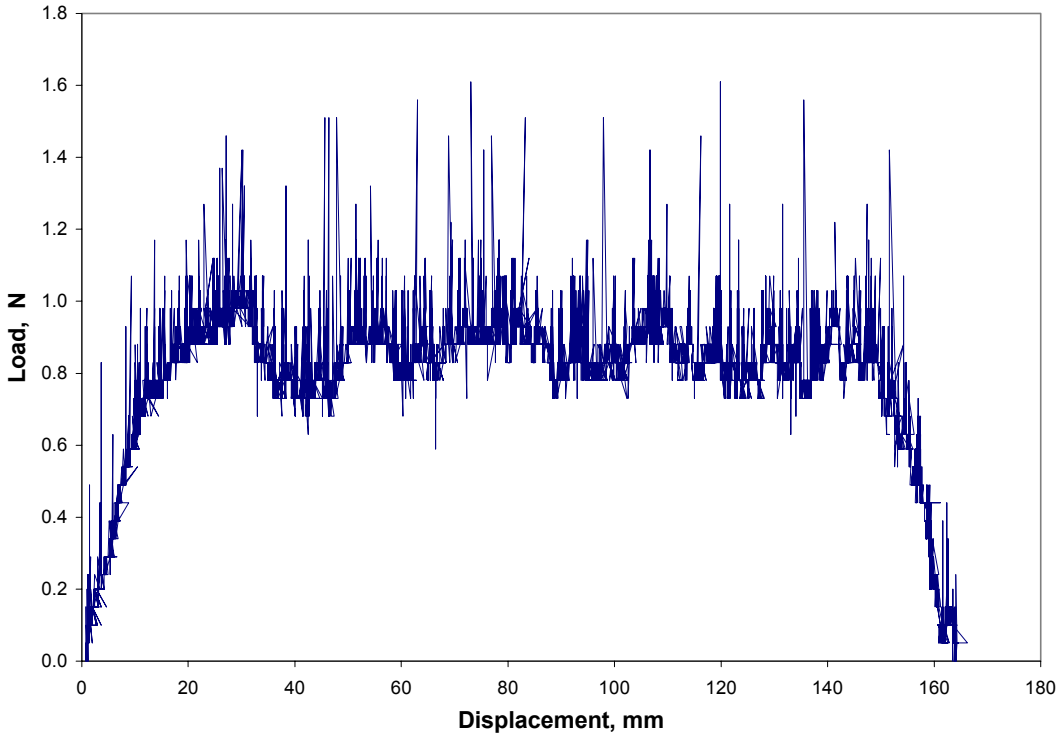

Figure B.160: Load Versus Displacement for Subject C, 180 degrees, 1 min, 100 mm/min, Test 3

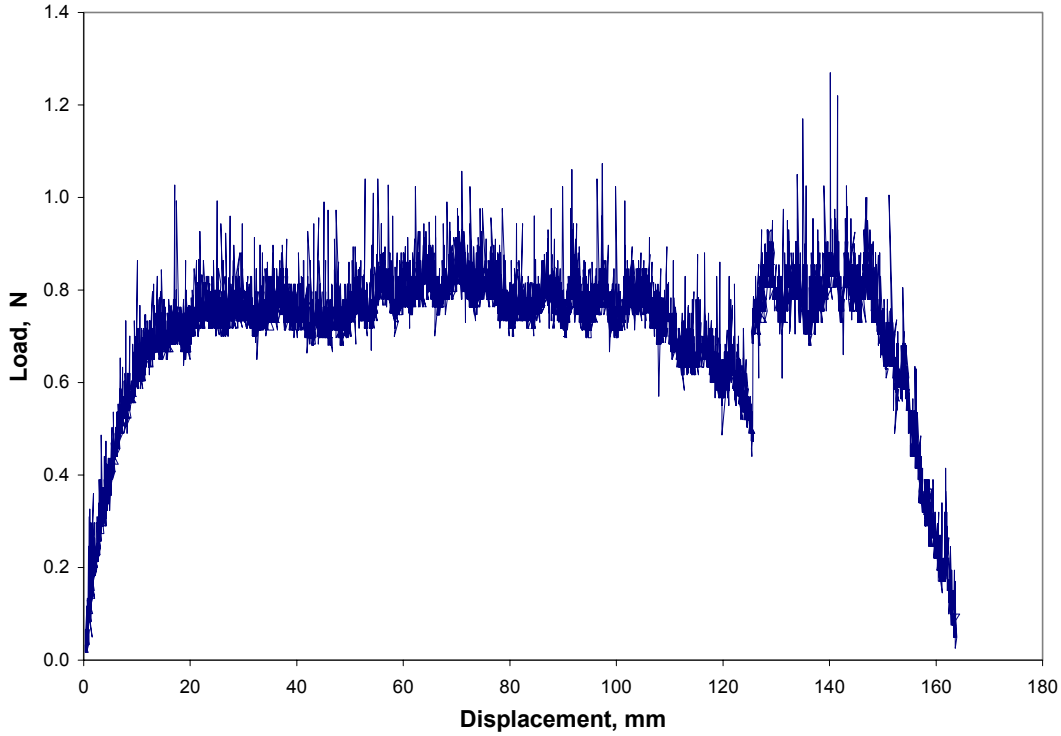

Figure B.161: Load Versus Displacement for Subject C, 180 degrees, 1 min, 100 mm/min, Average

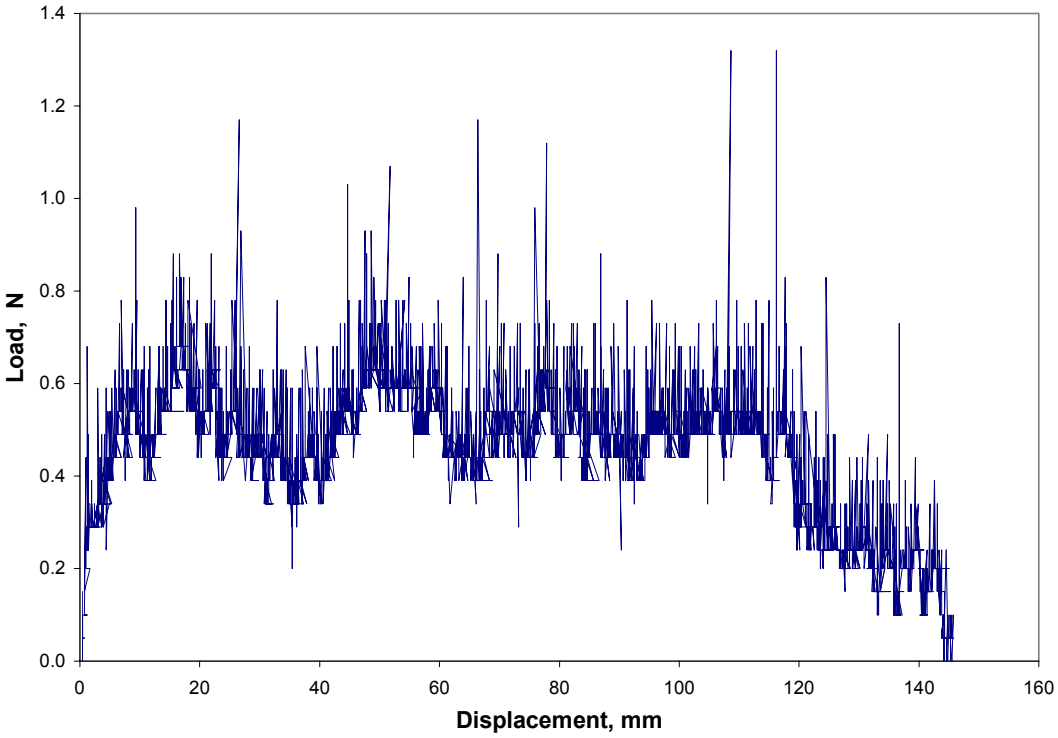

Figure B.162: Load Versus Displacement for Subject C, 180 degrees, 1 min, 200 mm/min, Test 1

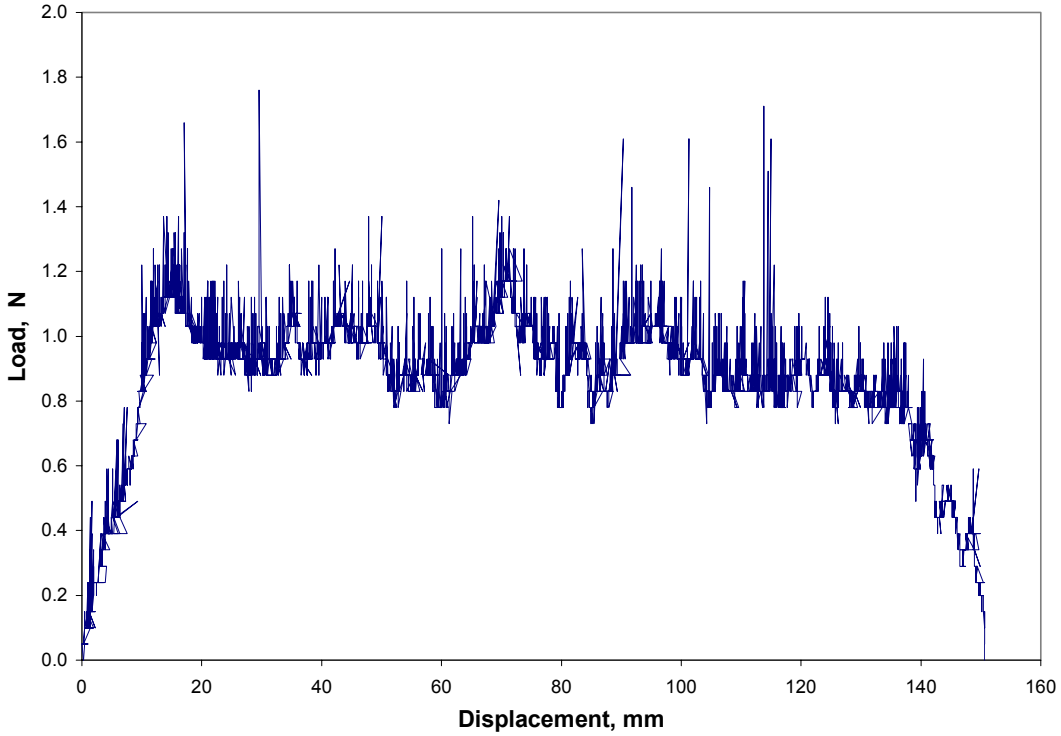

Figure B.163: Load Versus Displacement for Subject C, 180 degrees, 1 min, 200 mm/min, Test 2

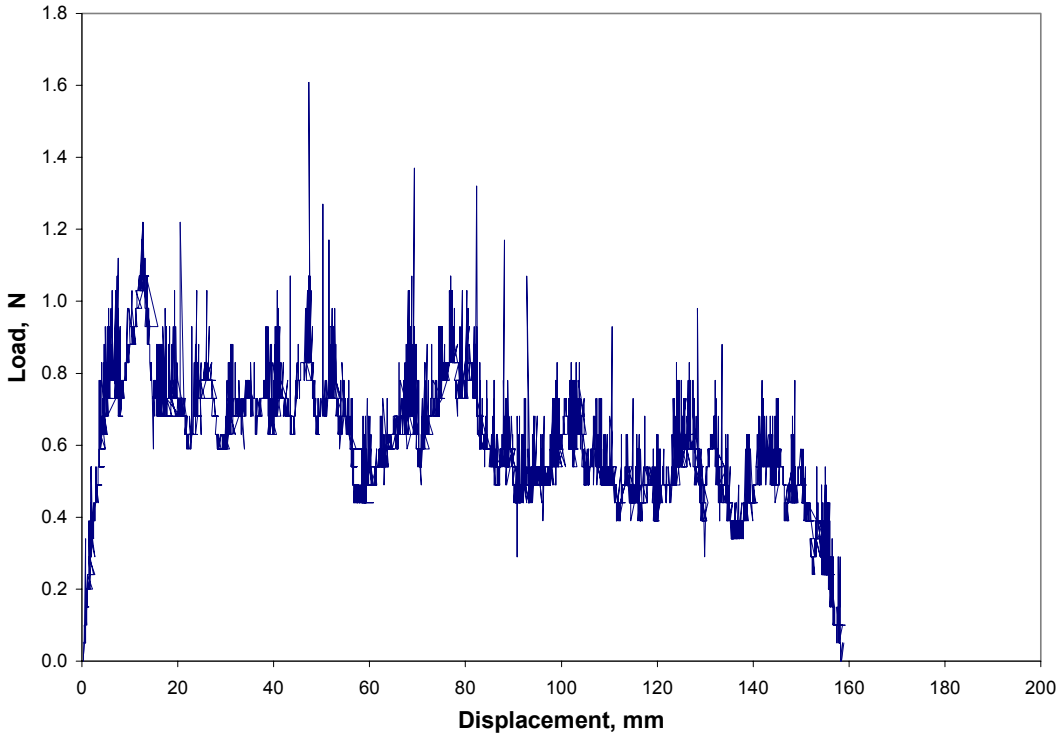

Figure B.164: Load Versus Displacement for Subject C, 180 degrees, 1 min, 200 mm/min, Test 3

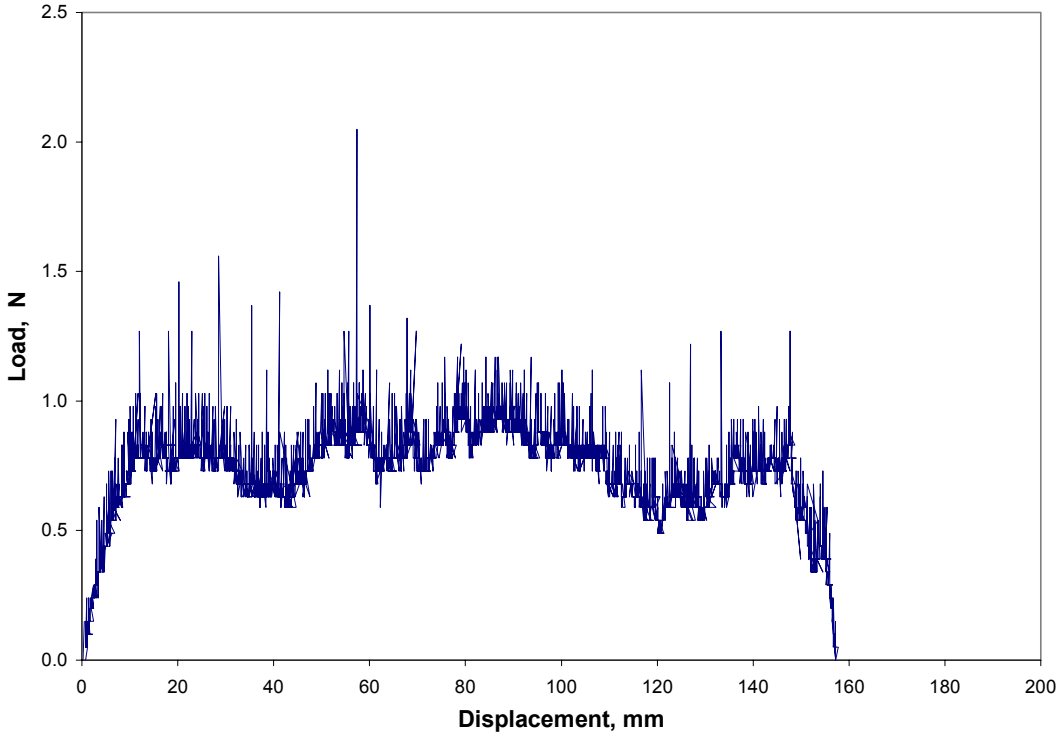

Figure B.165: Load Versus Displacement for Subject C, 180 degrees, 1 min, 200 mm/min, Test 4

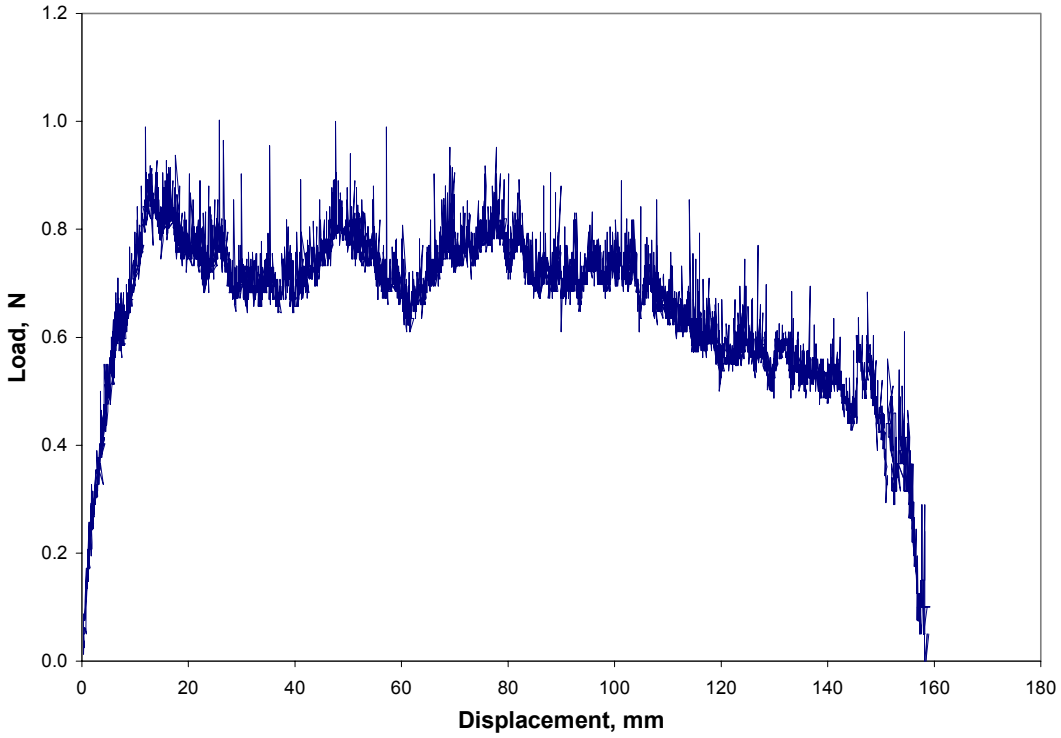

Figure B.166: Load Versus Displacement for Subject C, 180 degrees, 1 min, 200 mm/min, Average

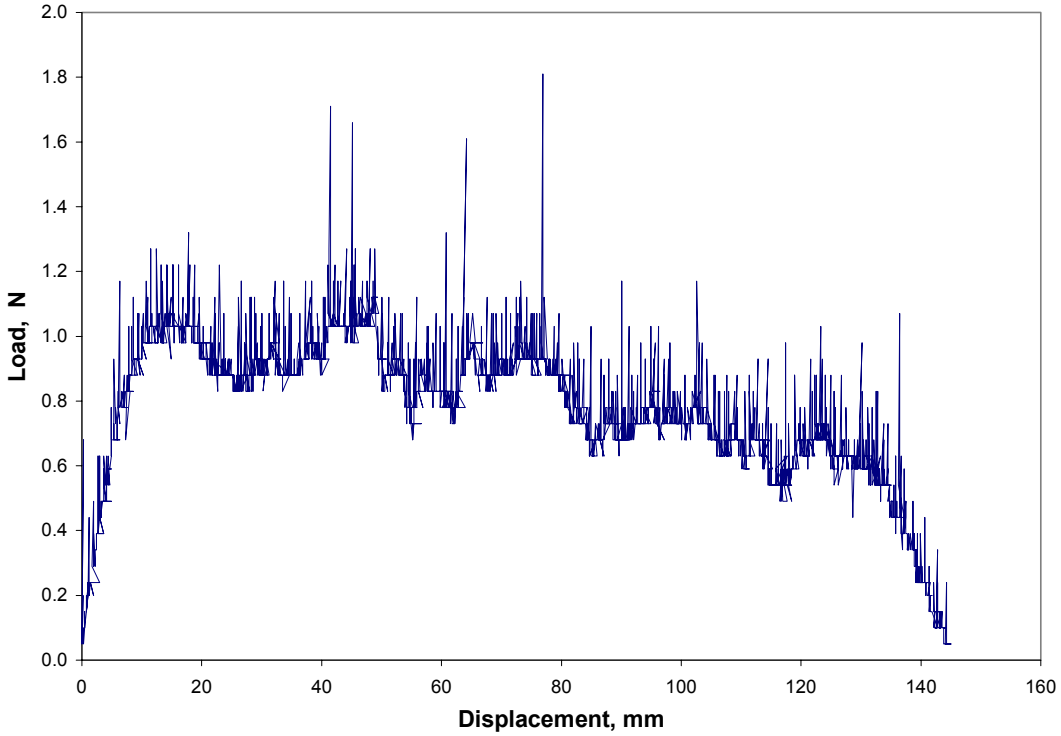

Figure B.167: Load Versus Displacement for Subject C, 180 degrees, 1 min, 300 mm/min, Test 1

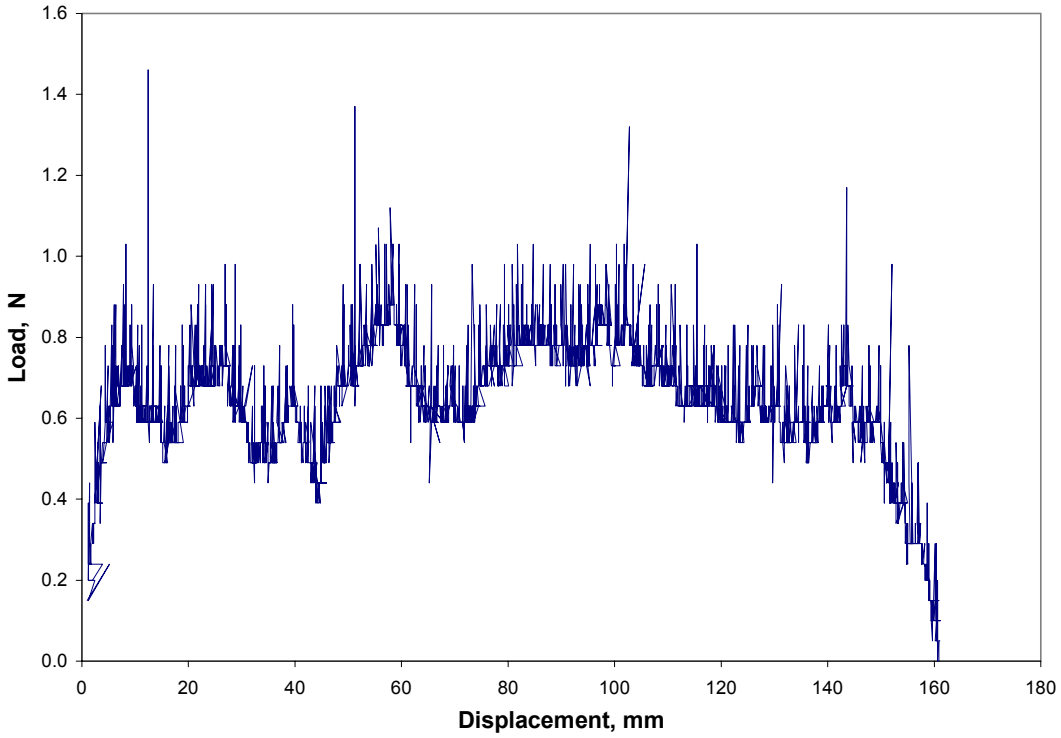

Figure B.168: Load Versus Displacement for Subject C, 180 degrees, 1 min, 300 mm/min, Test 2

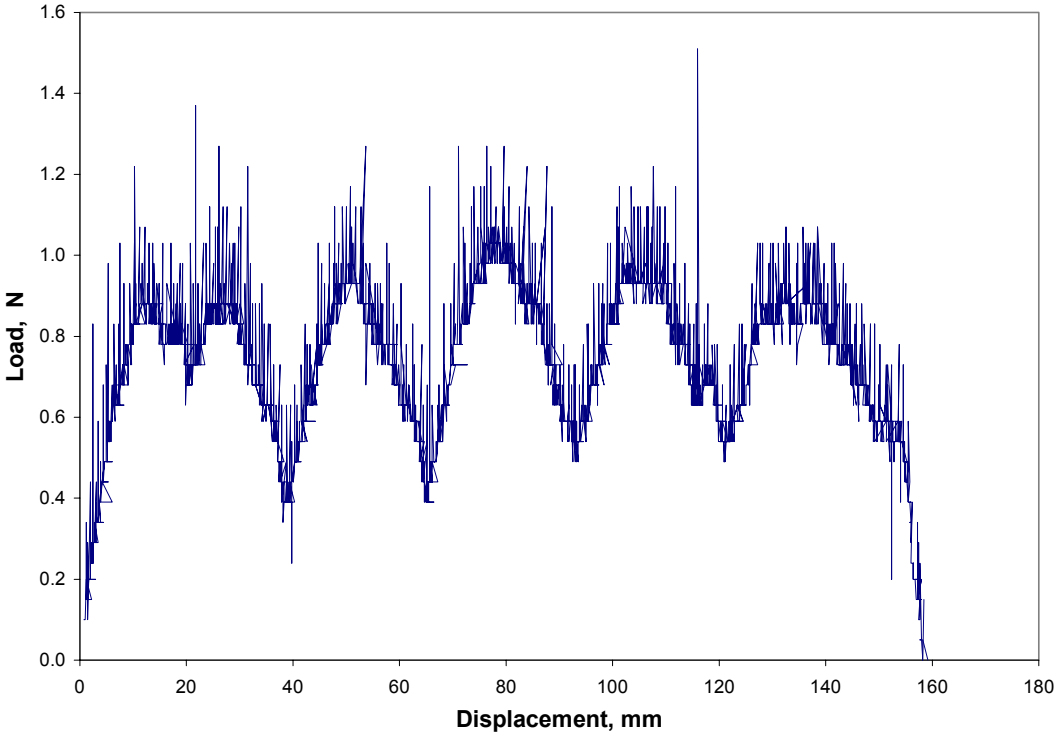

Figure B.169: Load Versus Displacement for Subject C, 180 degrees, 1 min, 300 mm/min, Test 3

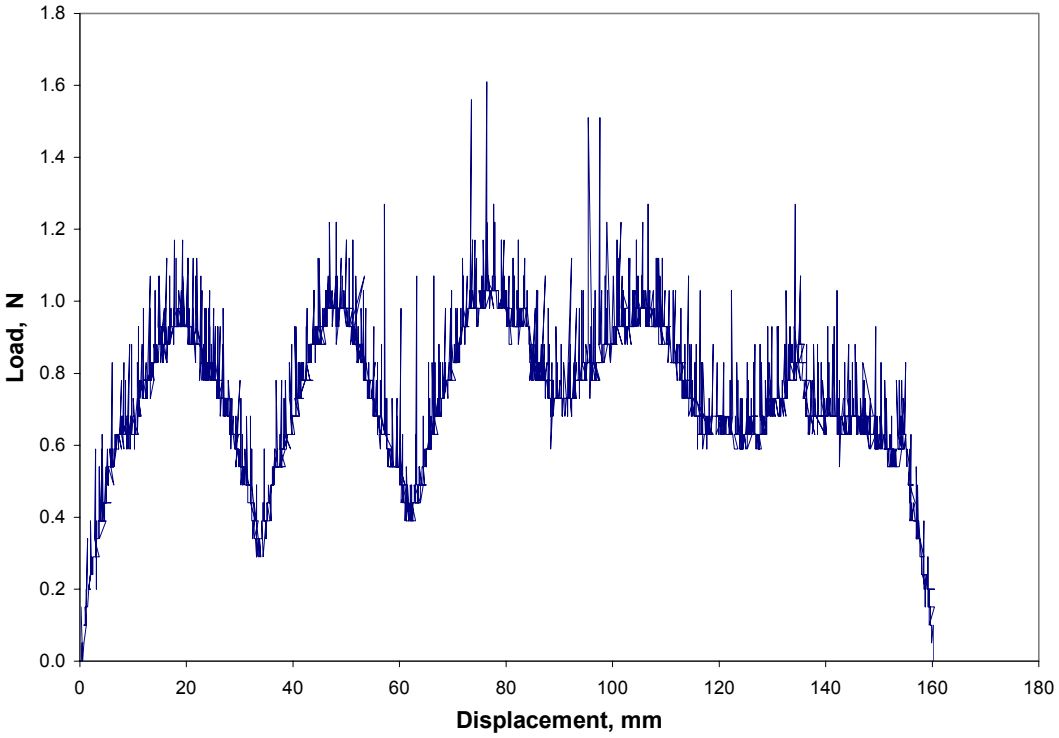

Figure B.170: Load Versus Displacement for Subject C, 180 degrees, 1 min, 300 mm/min, Test 4

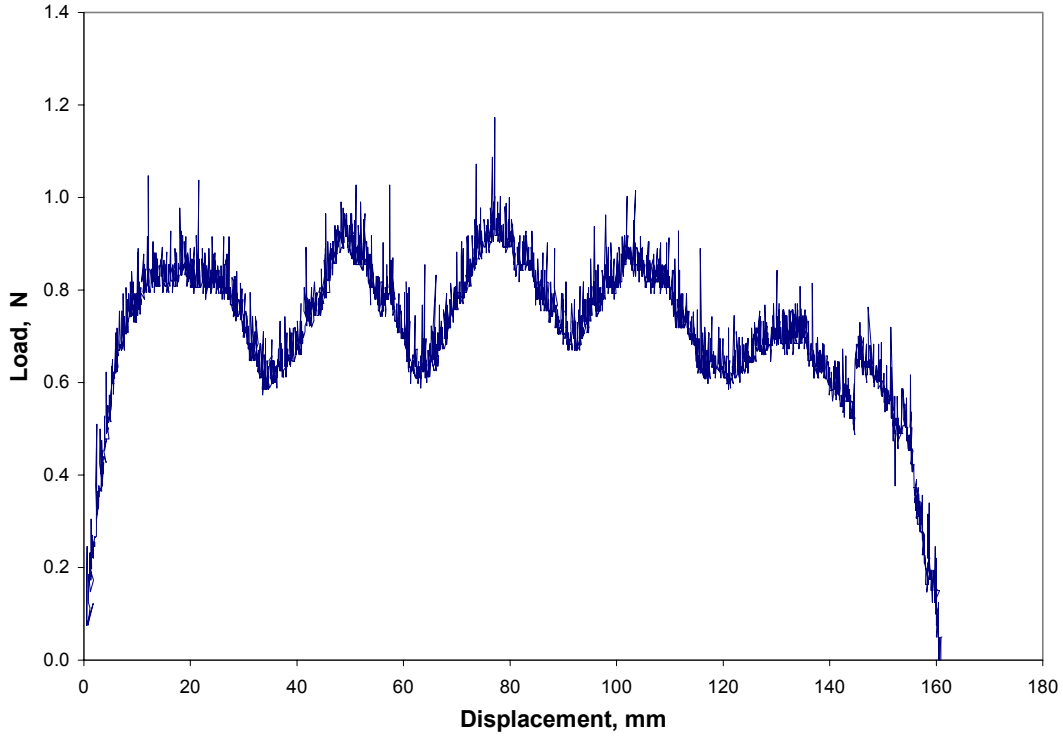

Figure B.171: Load Versus Displacement for Subject C, 180 degrees, 1 min, 300 mm/min, Average

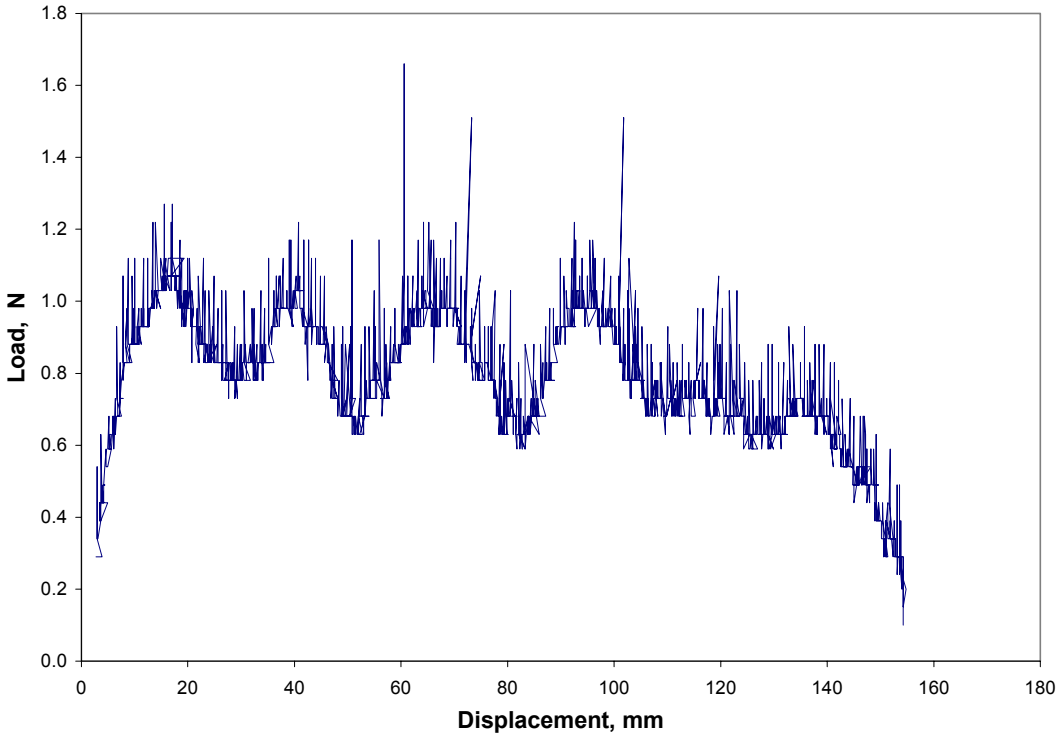

Figure B.172: Load Versus Displacement for Subject C, 180 degrees, 1 min, 400 mm/min, Test 1

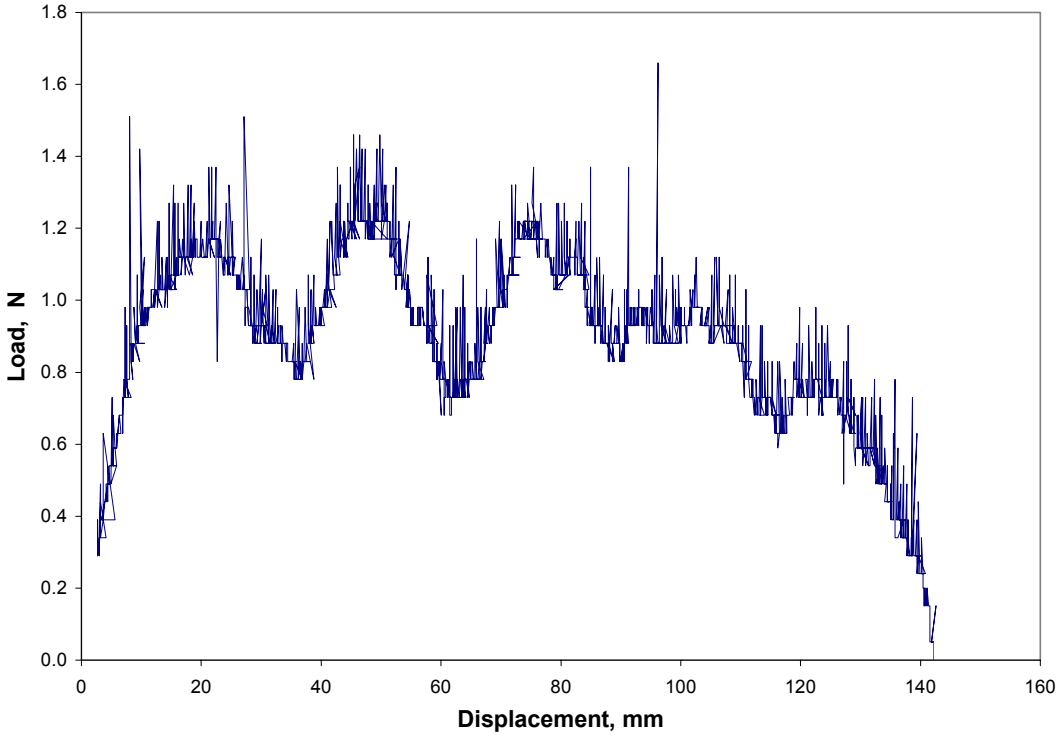

Figure B.173: Load Versus Displacement for Subject C, 180 degrees, 1 min, 400 mm/min, Test 2

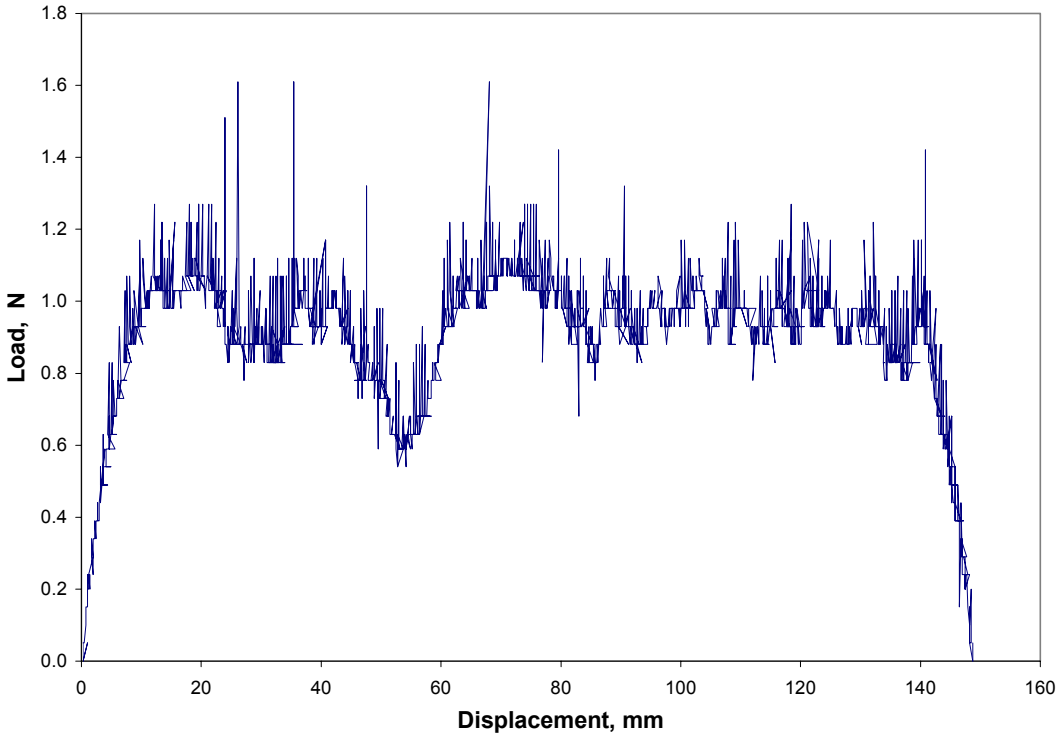

Figure B.174: Load Versus Displacement for Subject C, 180 degrees, 1 min, 400 mm/min, Test 3

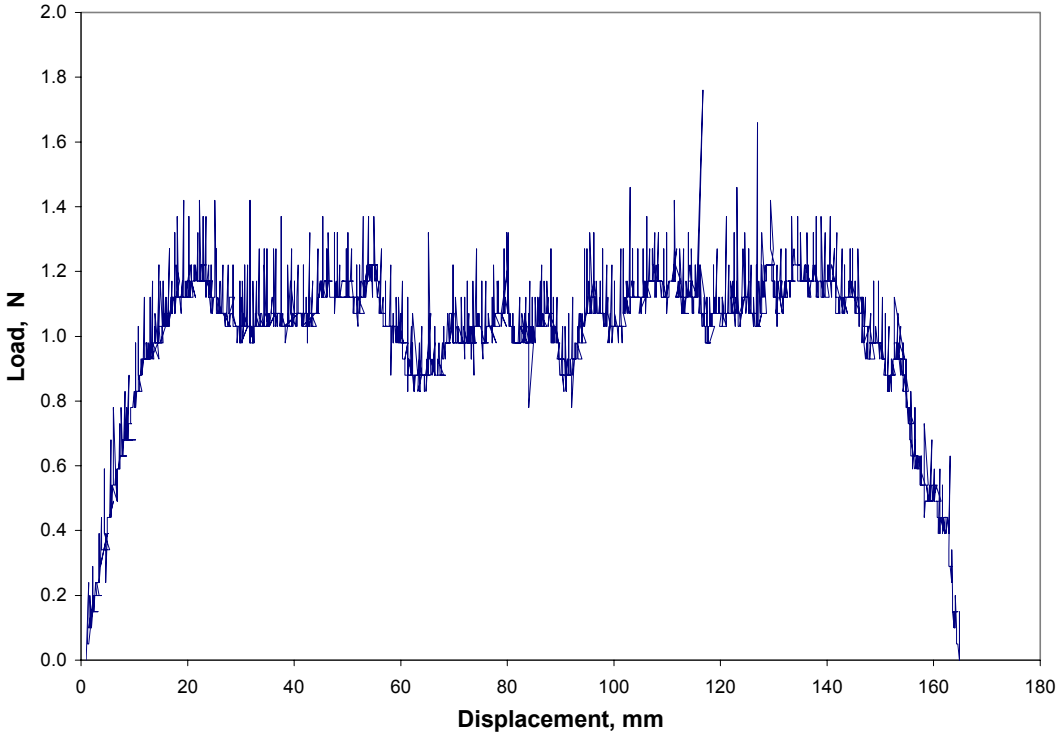

Figure B.175: Load Versus Displacement for Subject C, 180 degrees, 1 min, 400 mm/min, Test 4

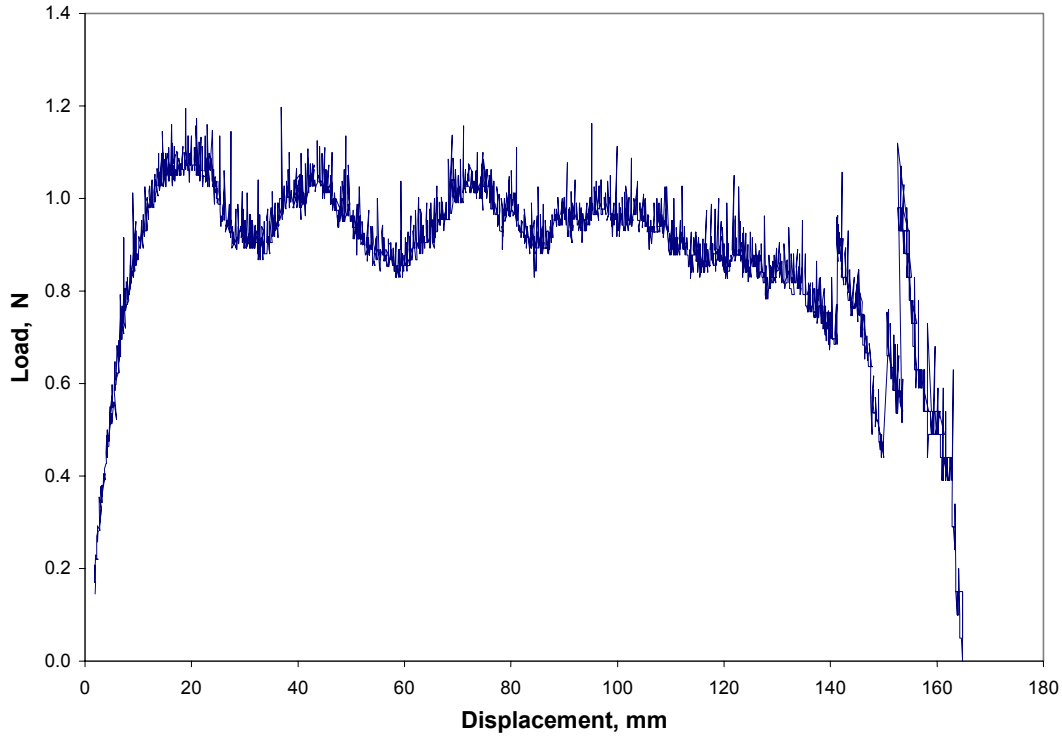

Figure B.176: Load Versus Displacement for Subject C, 180 degrees, 1 min, 400 mm/min, Average

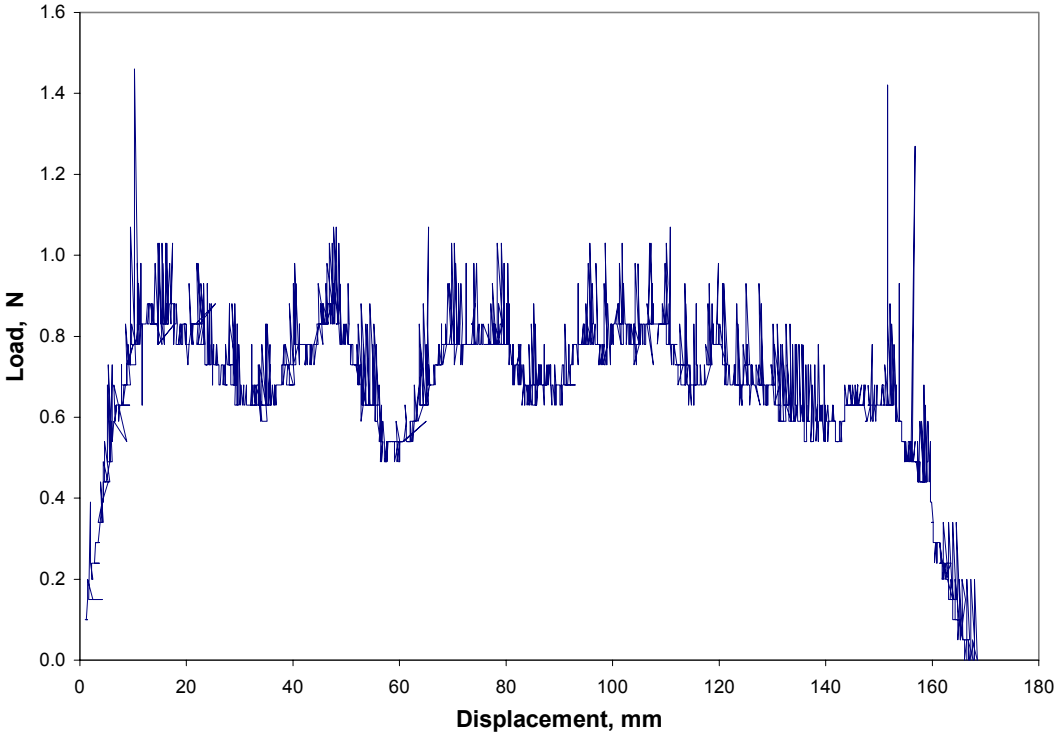

Figure B.177: Load Versus Displacement for Subject C, 180 degrees, 1 min, 500 mm/min, Test 1

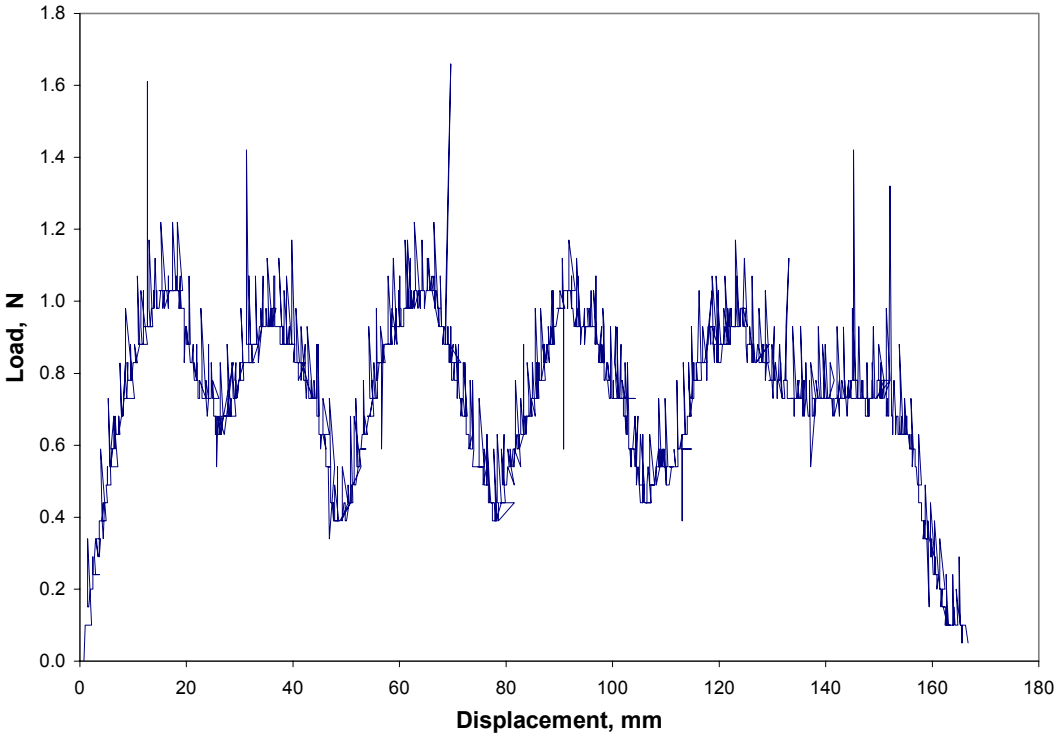

Figure B.178: Load Versus Displacement for Subject C, 180 degrees, 1 min, 500 mm/min, Test 2

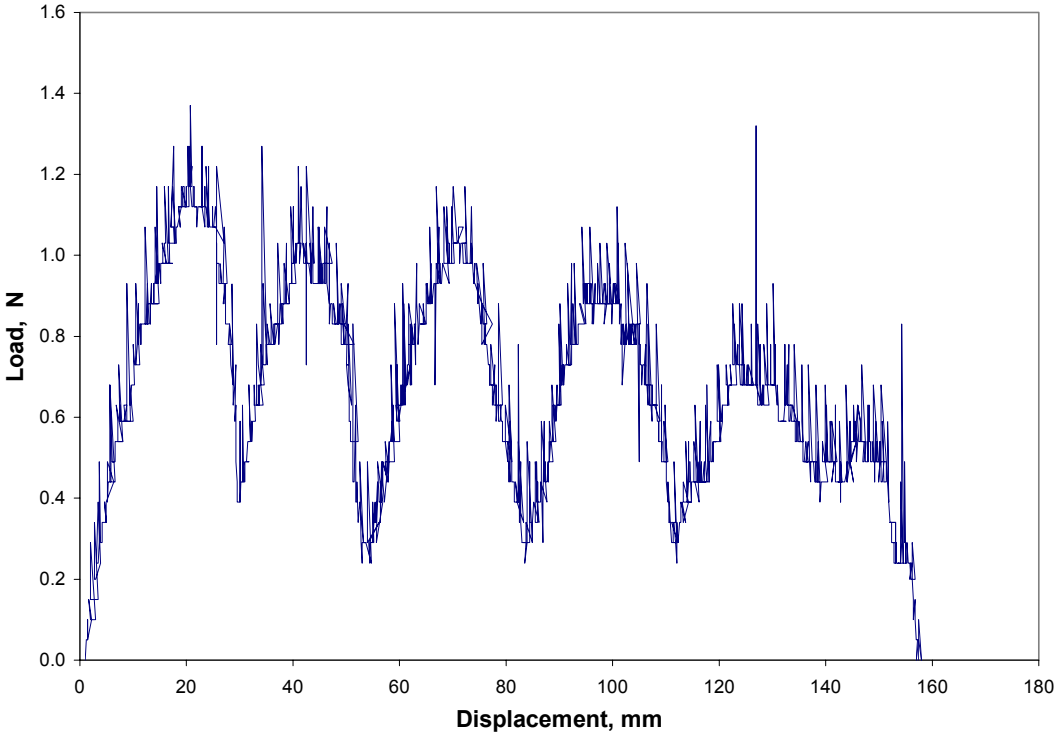

Figure B.179: Load Versus Displacement for Subject C, 180 degrees, 1 min, 500 mm/min, Test 3

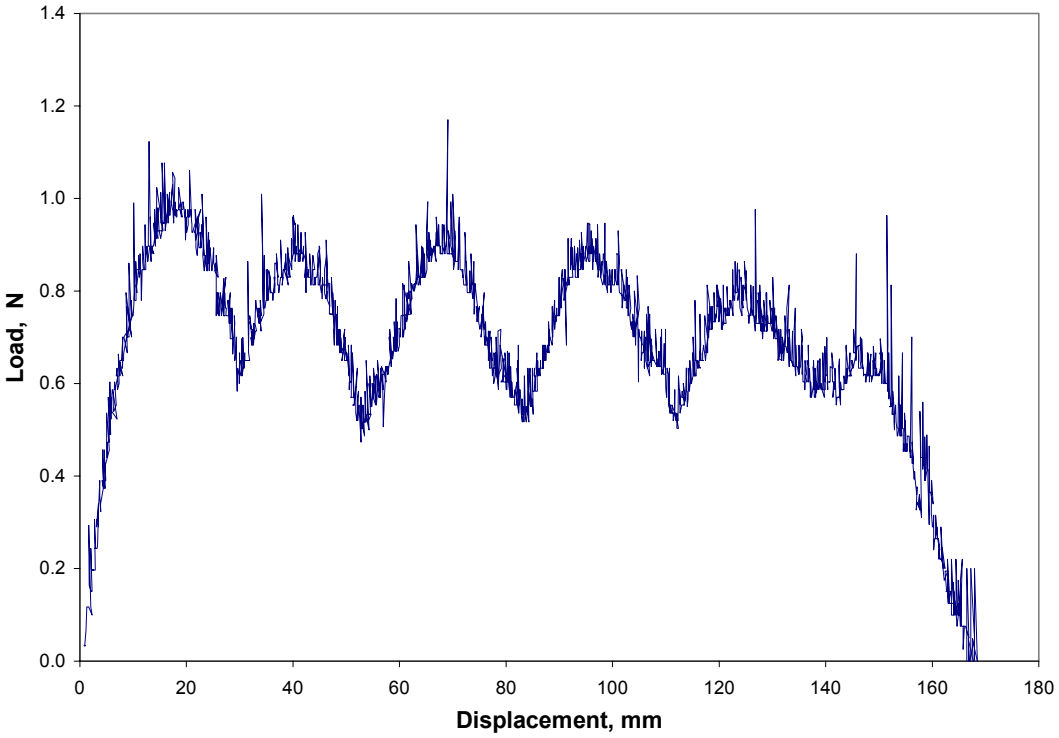

Figure B.180: Load Versus Displacement for Subject C, 180 degrees, 1 min, 500 mm/min, Average

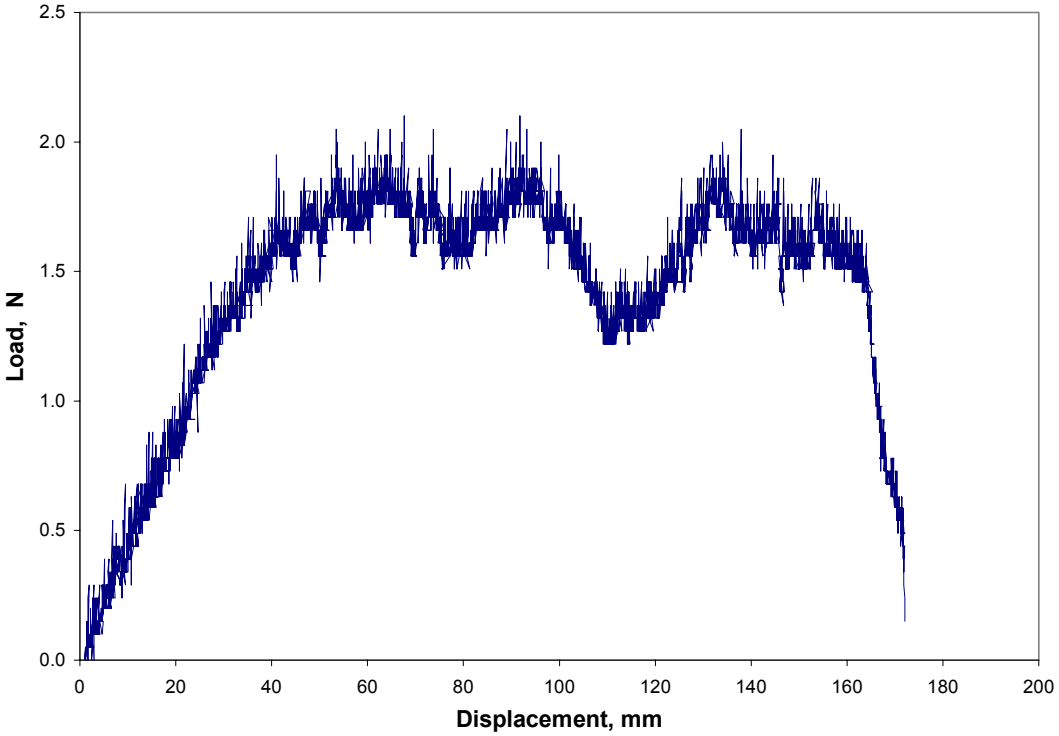

Figure B.181: Load Versus Displacement for Subject D, 180 degrees, 1 min, 100 mm/min, Test 1

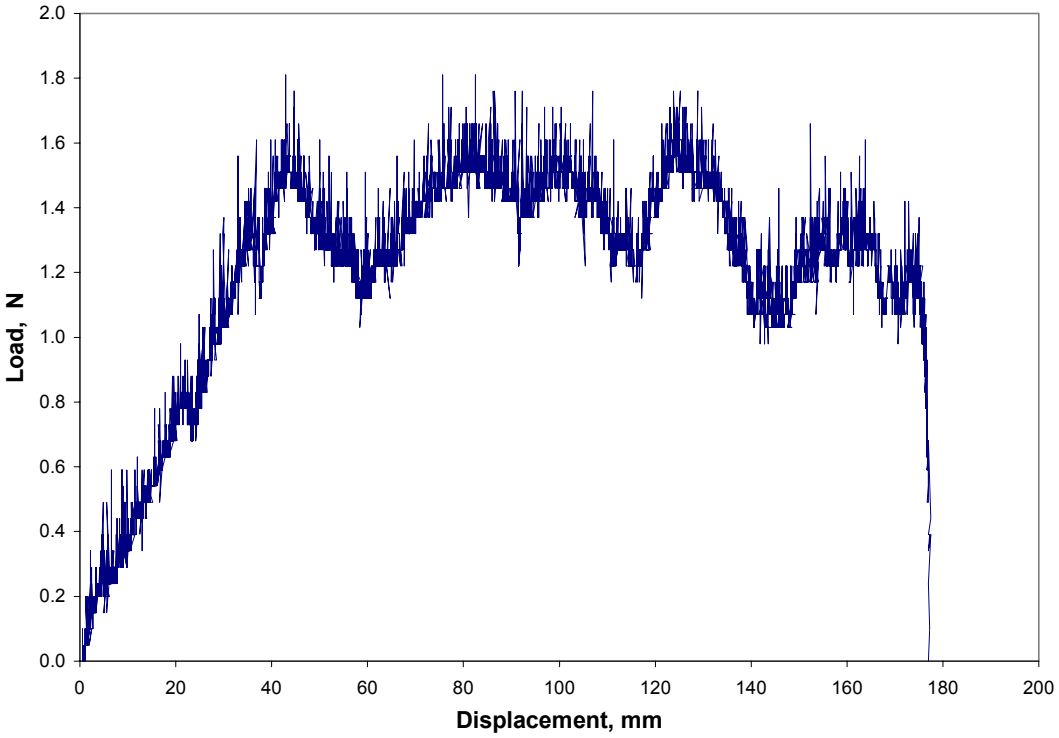

Figure B.182: Load Versus Displacement for Subject D, 180 degrees, 1 min, 100 mm/min, Test 2

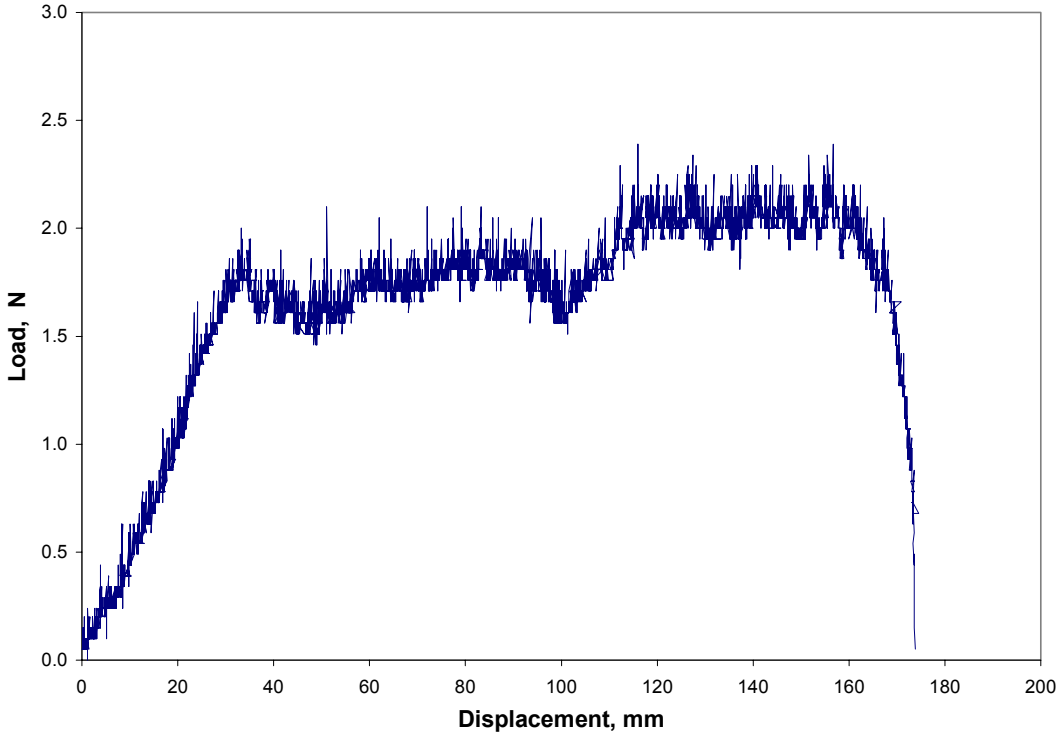

Figure B.183: Load Versus Displacement for Subject D, 180 degrees, 1 min, 100 mm/min, Test 3

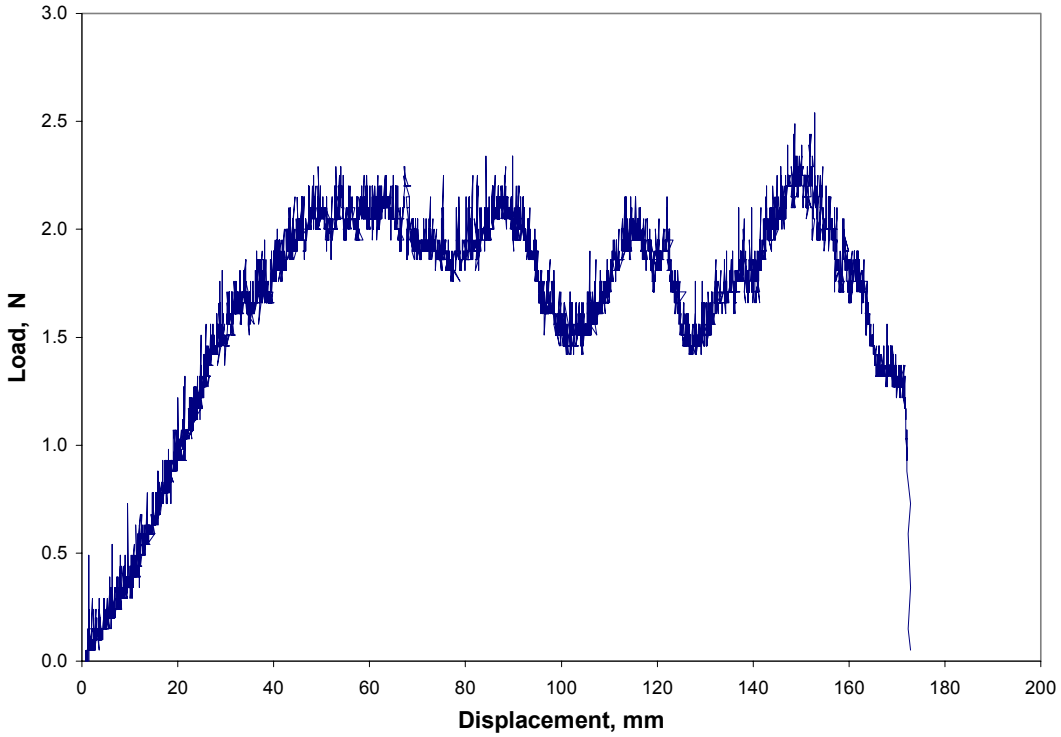

Figure B.184: Load Versus Displacement for Subject D, 180 degrees, 1 min, 100 mm/min, Test 4

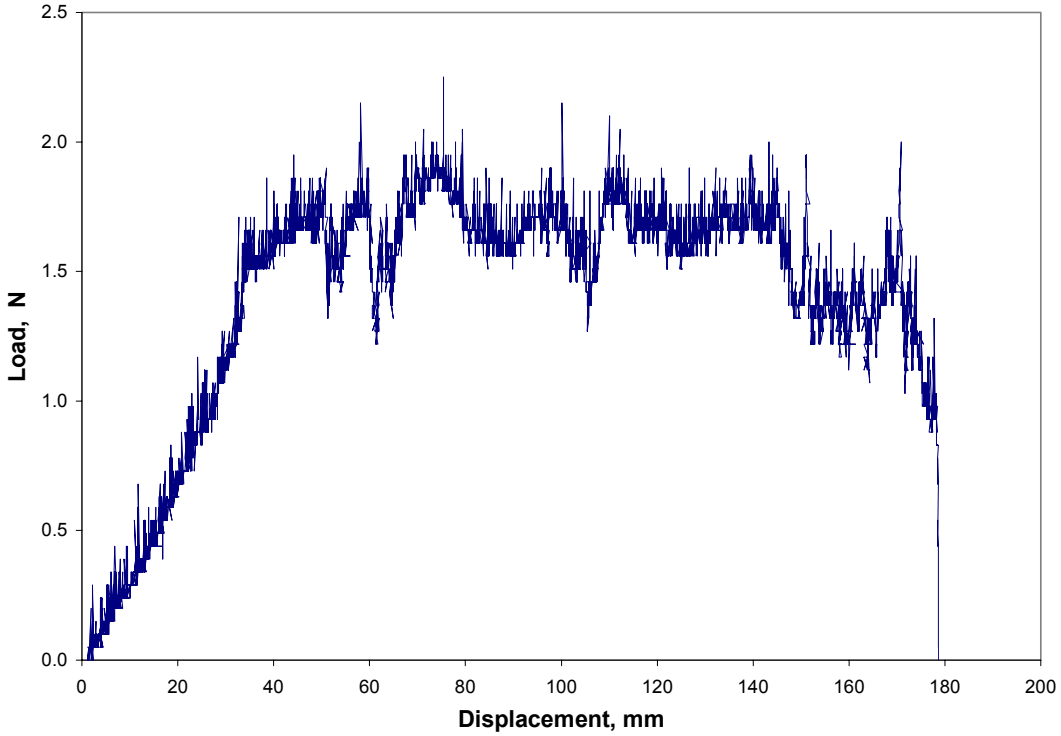

Figure B.185: Load Versus Displacement for Subject D, 180 degrees, 1 min, 100 mm/min, Test 5

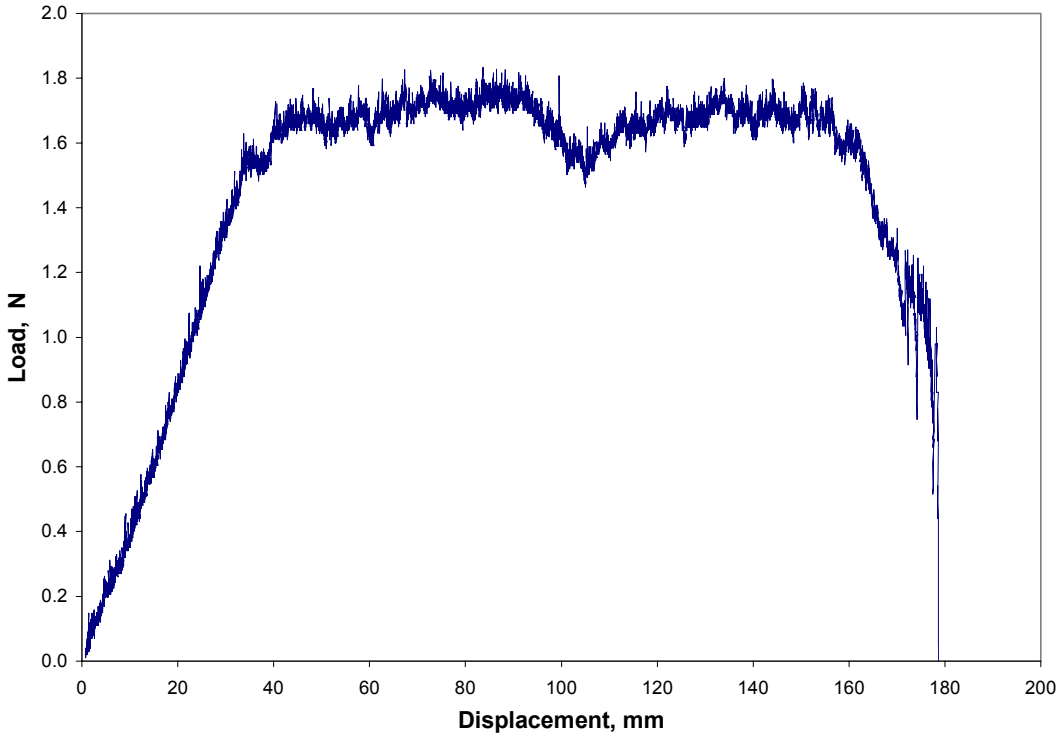

Figure B.186: Load Versus Displacement for Subject D, 180 degrees, 1 min, 100 mm/min, Average

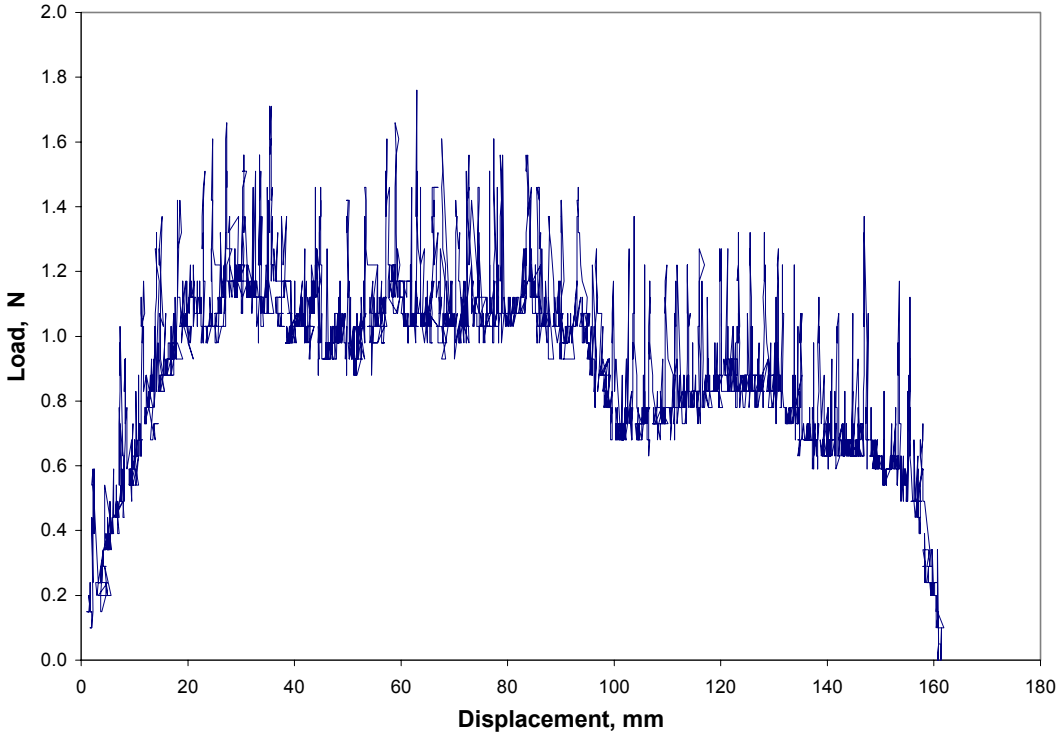

Figure B.187: Load Versus Displacement for Subject D, 180 degrees, 1 min, 200 mm/min, Test 1

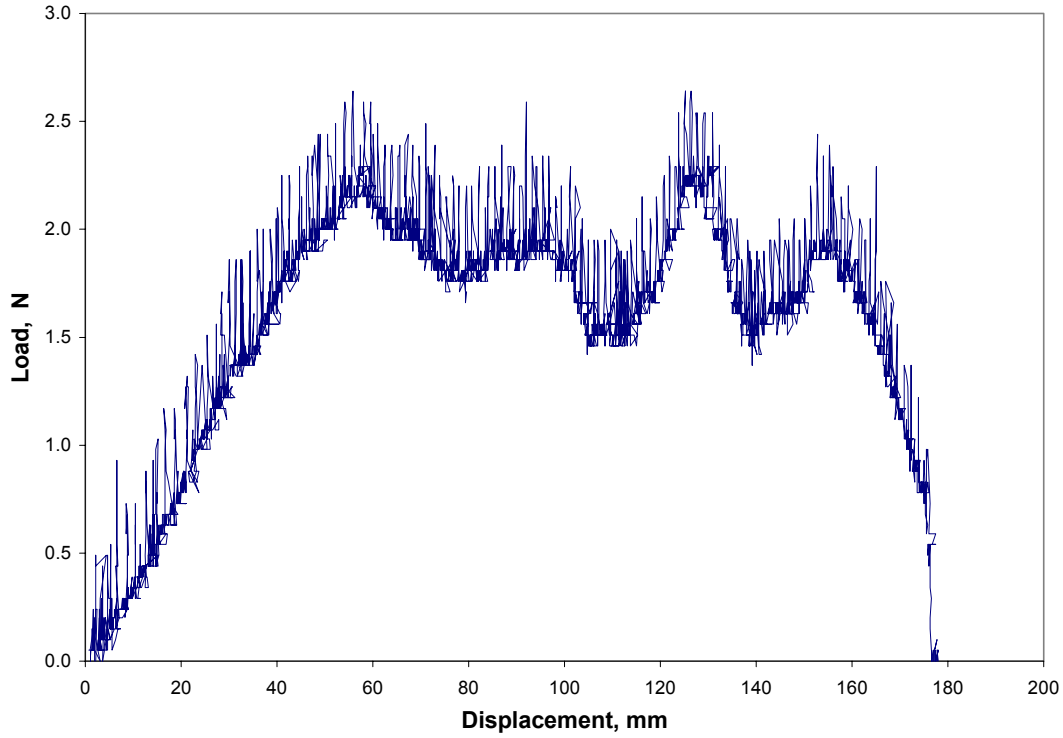

Figure B.188: Load Versus Displacement for Subject D, 180 degrees, 1 min, 200 mm/min, Test 2

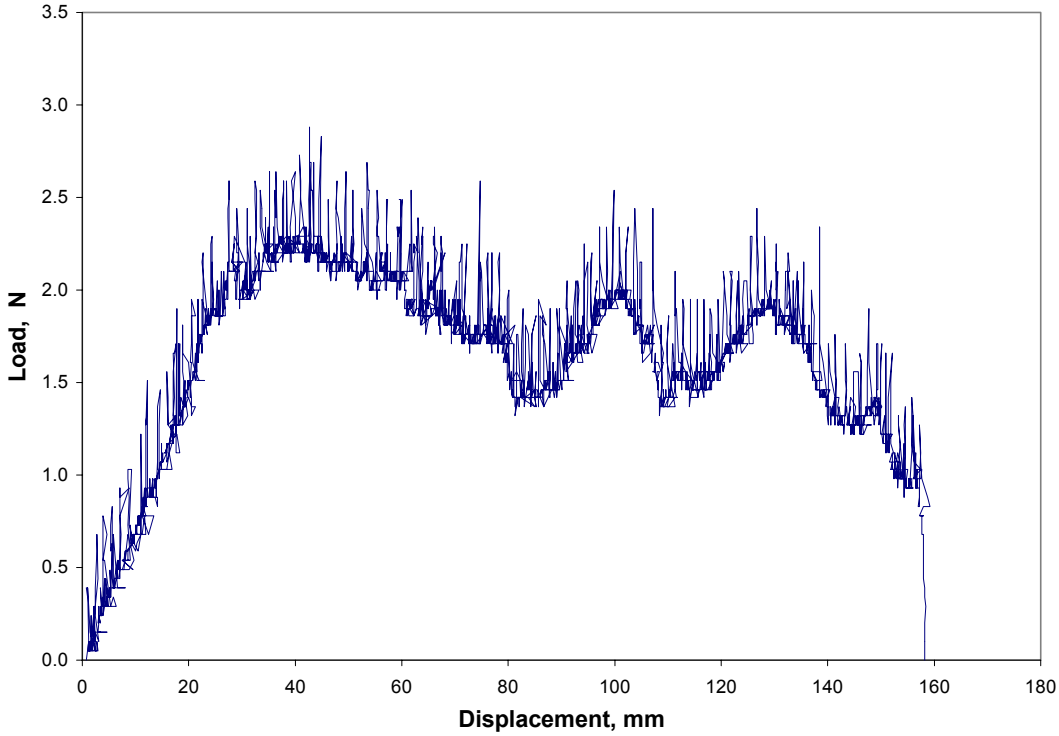

Figure B.189: Load Versus Displacement for Subject D, 180 degrees, 1 min, 200 mm/min, Test 3

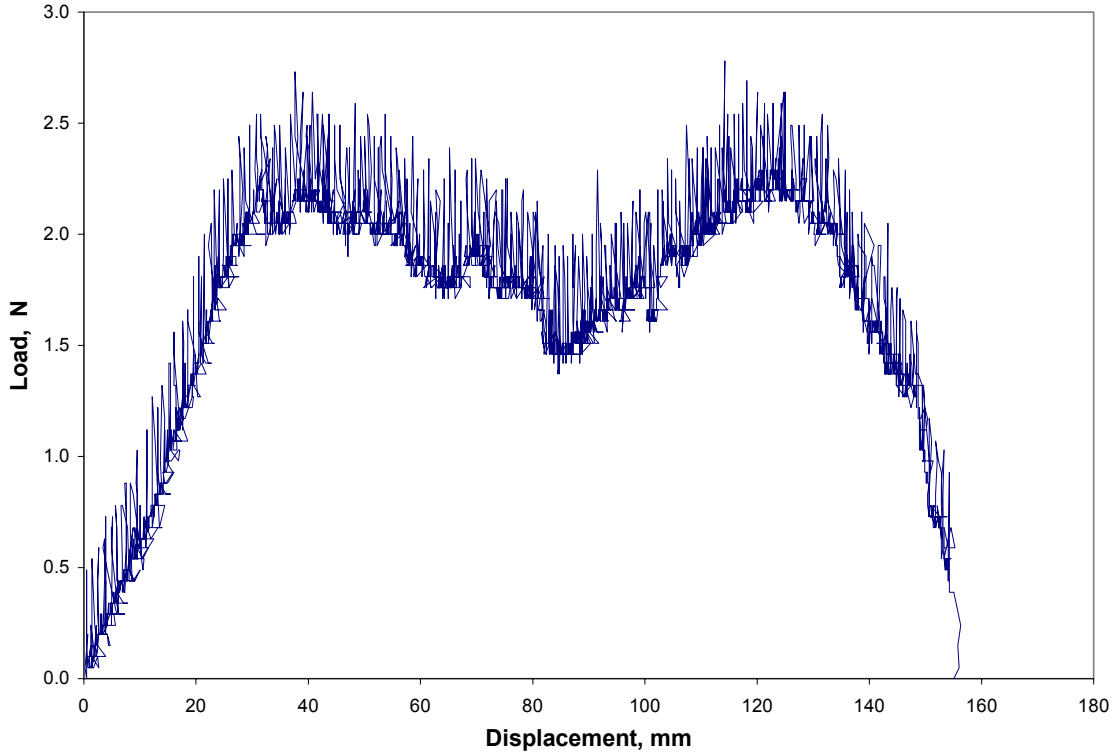

Figure B.190: Load Versus Displacement for Subject D, 180 degrees, 1 min, 200 mm/min, Test 4

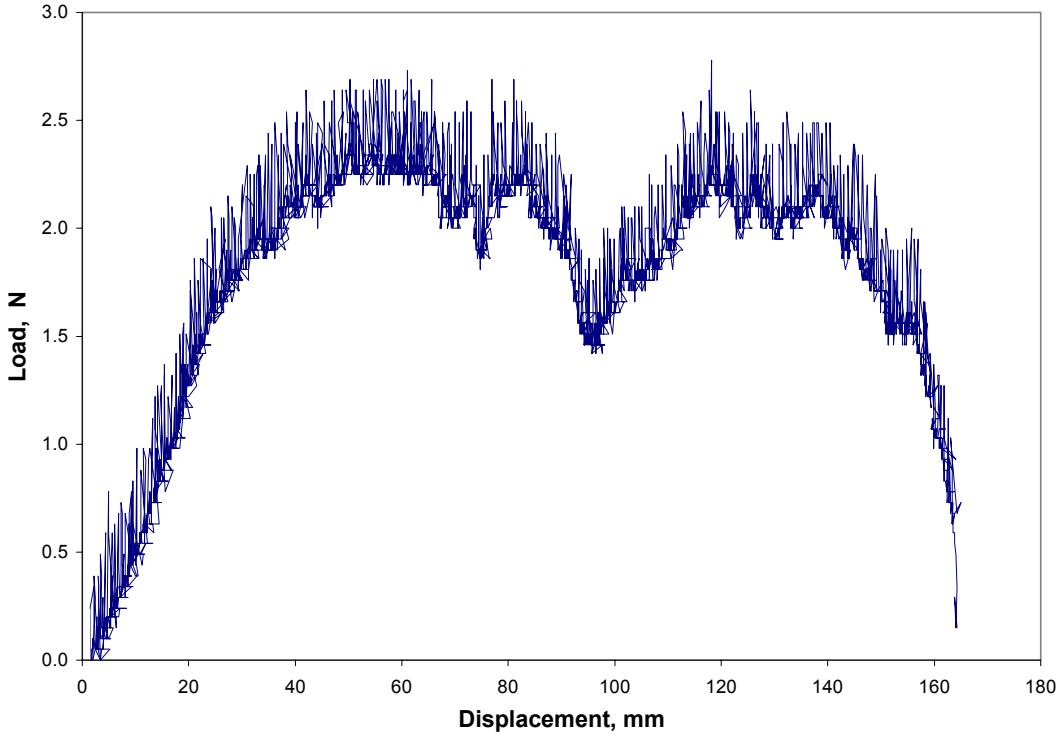

Figure B.191: Load Versus Displacement for Subject D, 180 degrees, 1 min, 200 mm/min, Test 5

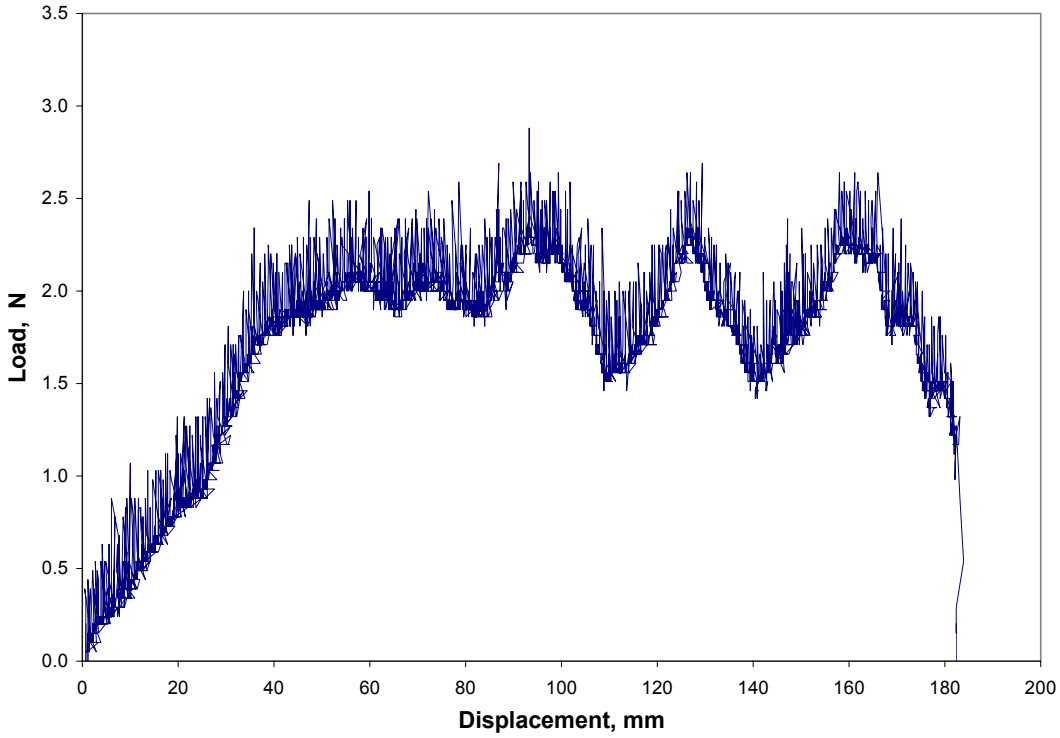

Figure B.192: Load Versus Displacement for Subject D, 180 degrees, 1 min, 200 mm/min, Test 6

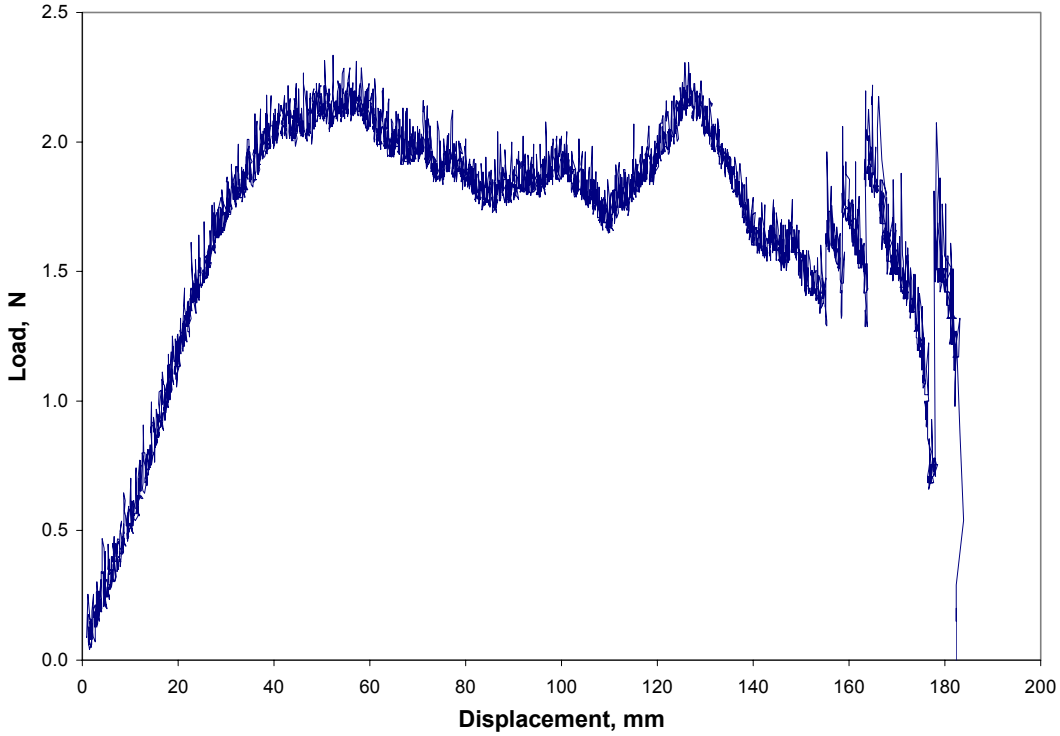

Figure B.193: Load Versus Displacement for Subject D, 180 degrees, 1 min, 200 mm/min, Average

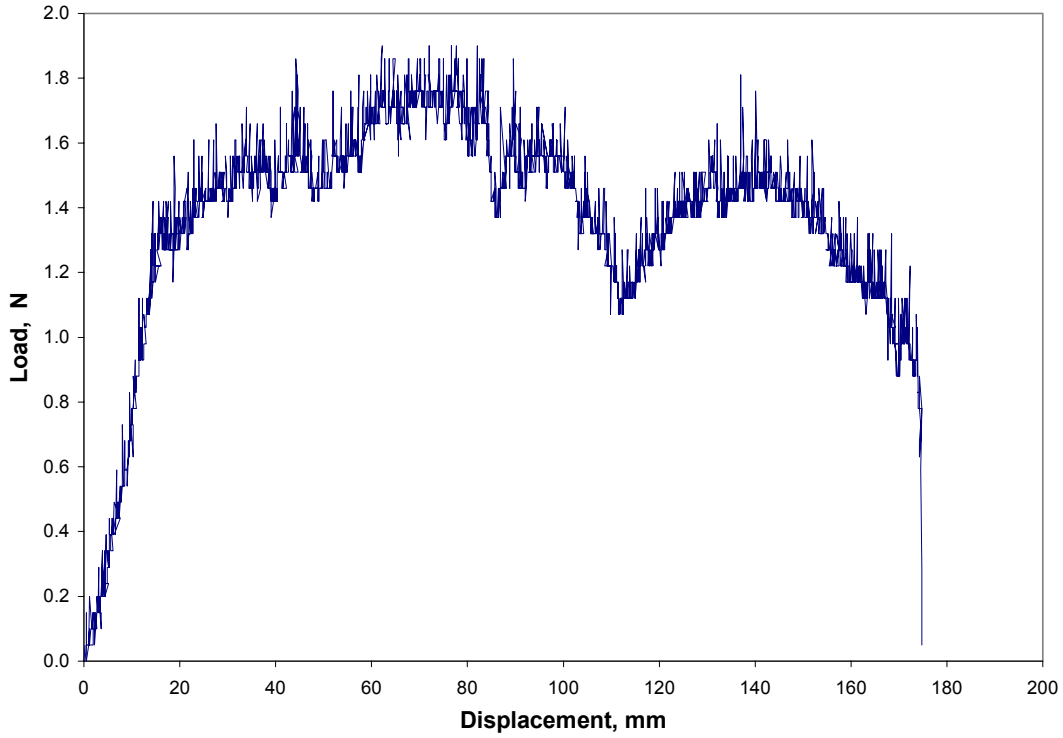

Figure B.194: Load Versus Displacement for Subject D, 180 degrees, 1 min, 300 mm/min, Test 1

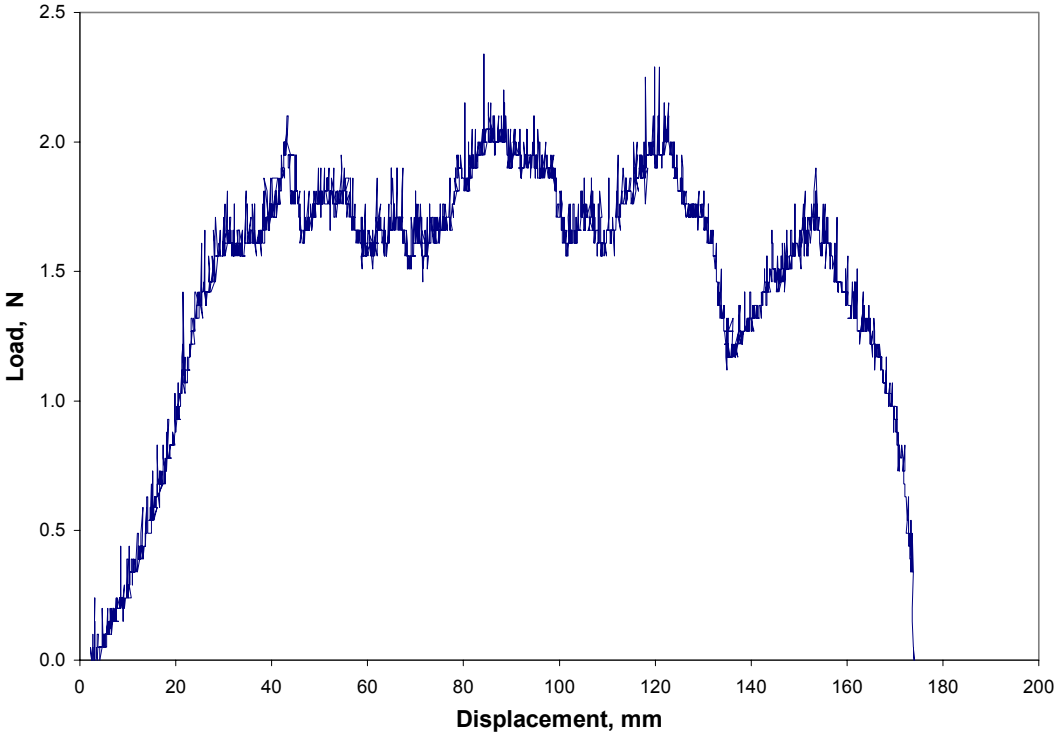

Figure B.195: Load Versus Displacement for Subject D, 180 degrees, 1 min, 300 mm/min, Test 2

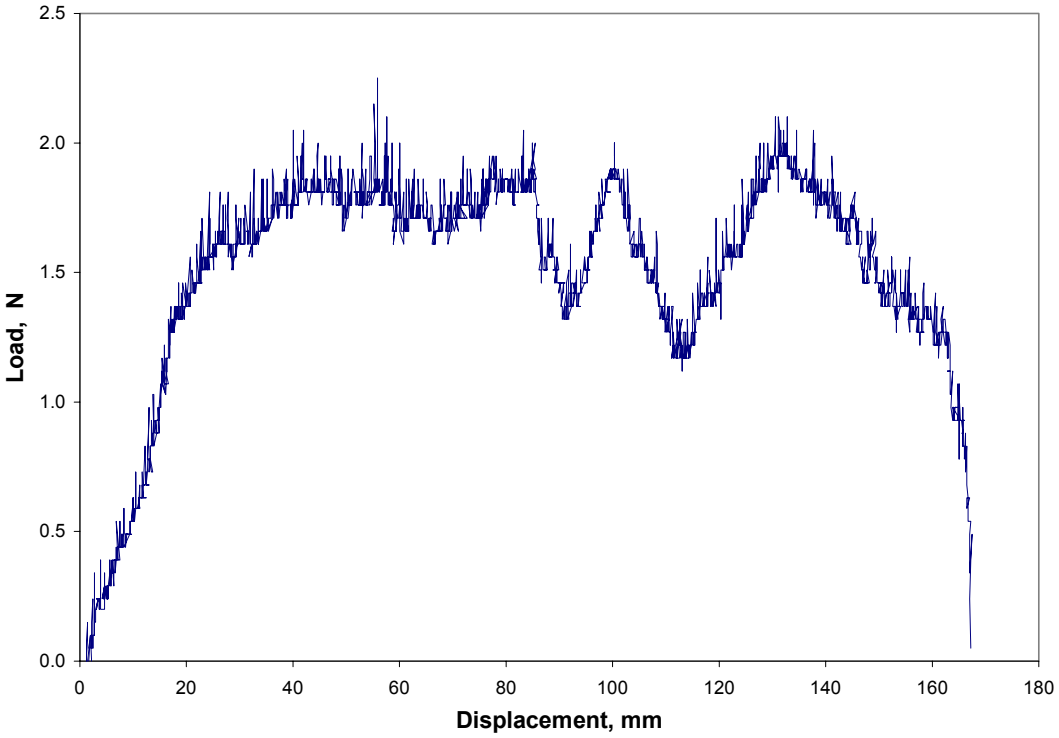

Figure B.196: Load Versus Displacement for Subject D, 180 degrees, 1 min, 300 mm/min, Test 3

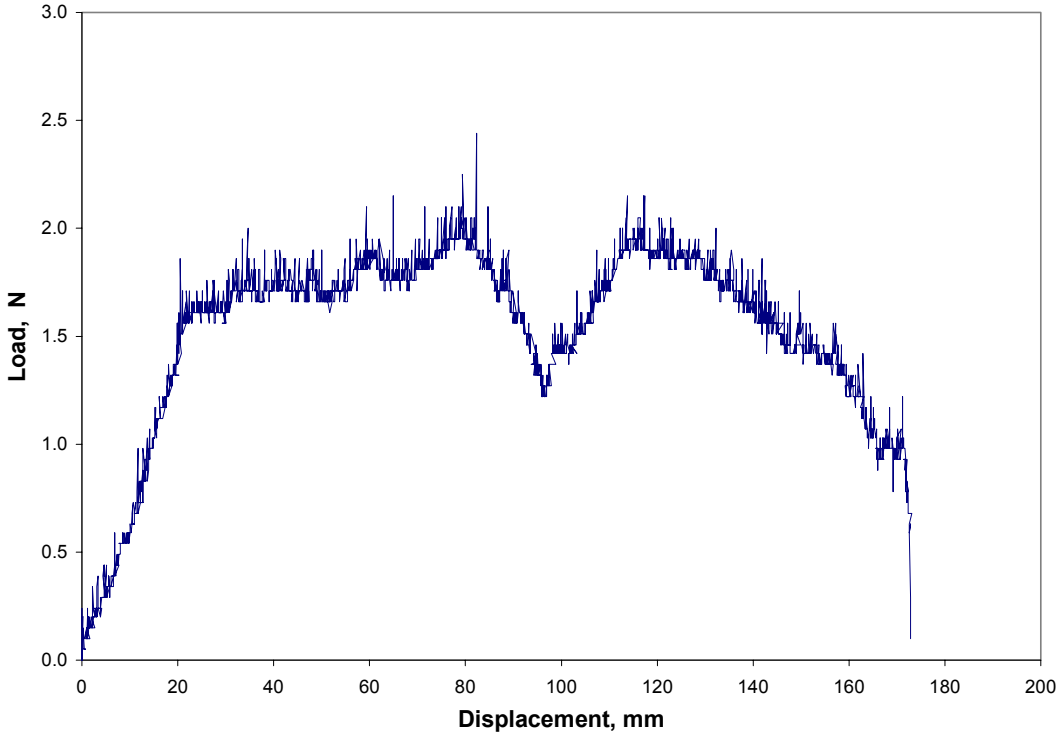

Figure B.197: Load Versus Displacement for Subject D, 180 degrees, 1 min, 300 mm/min, Test 4

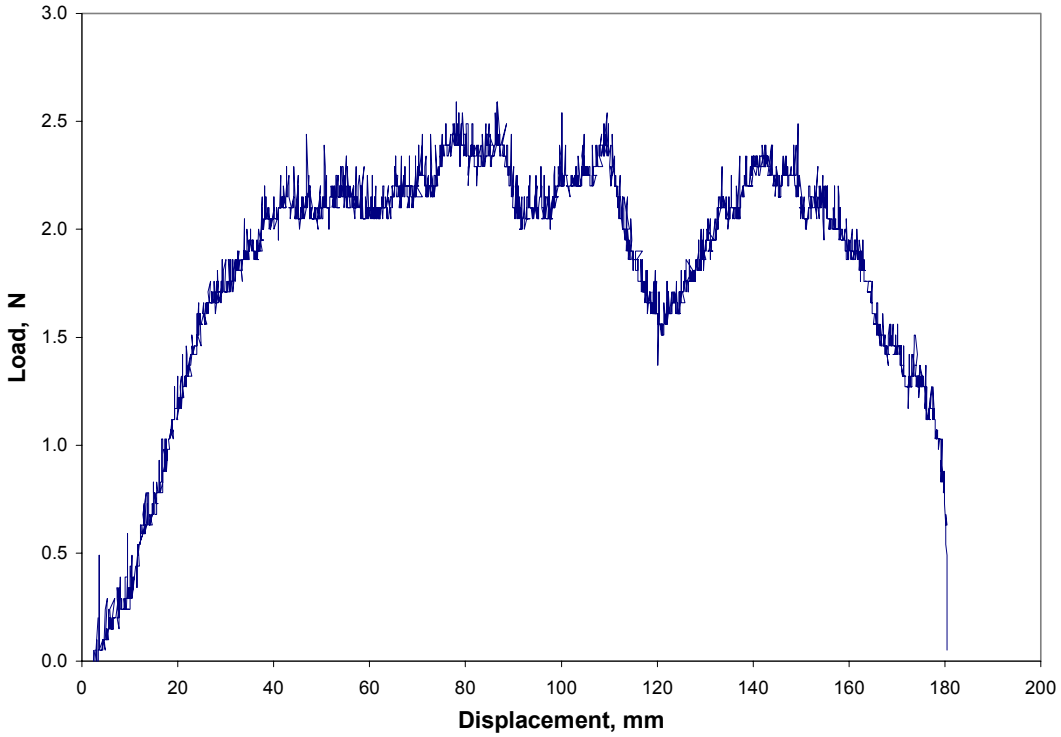

Figure B.198: Load Versus Displacement for Subject D, 180 degrees, 1 min, 300 mm/min, Test 5

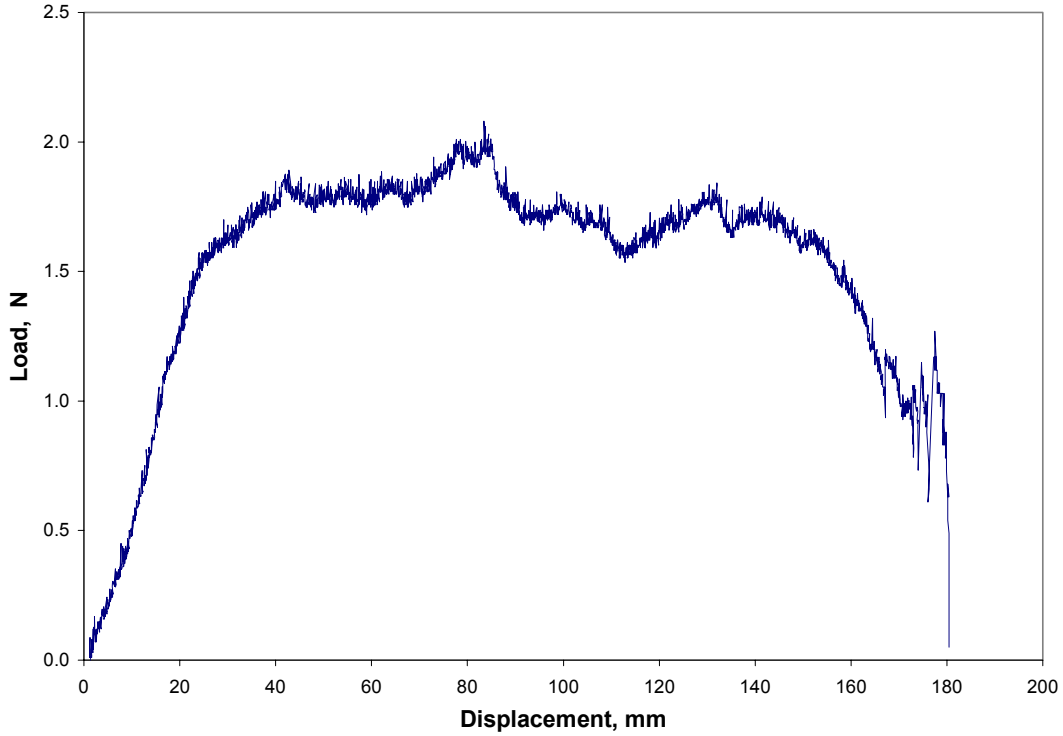

Figure B.199: Load Versus Displacement for Subject D, 180 degrees, 1 min, 300 mm/min, Average

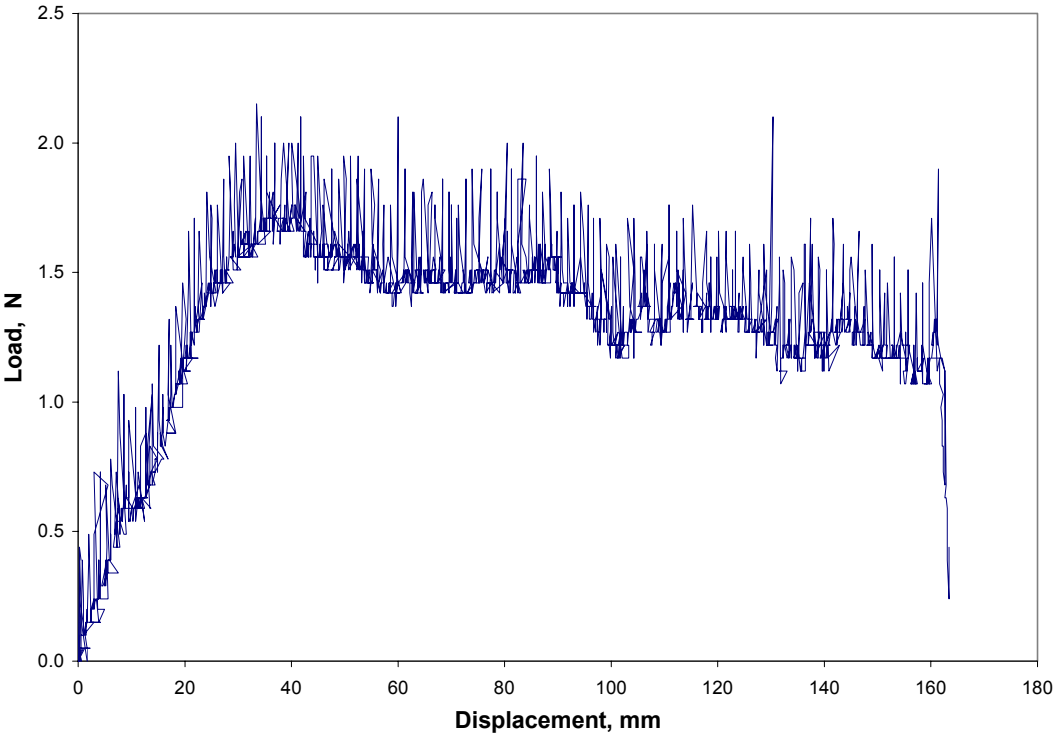

Figure B.200: Load Versus Displacement for Subject D, 180 degrees, 1 min, 400 mm/min, Test 1

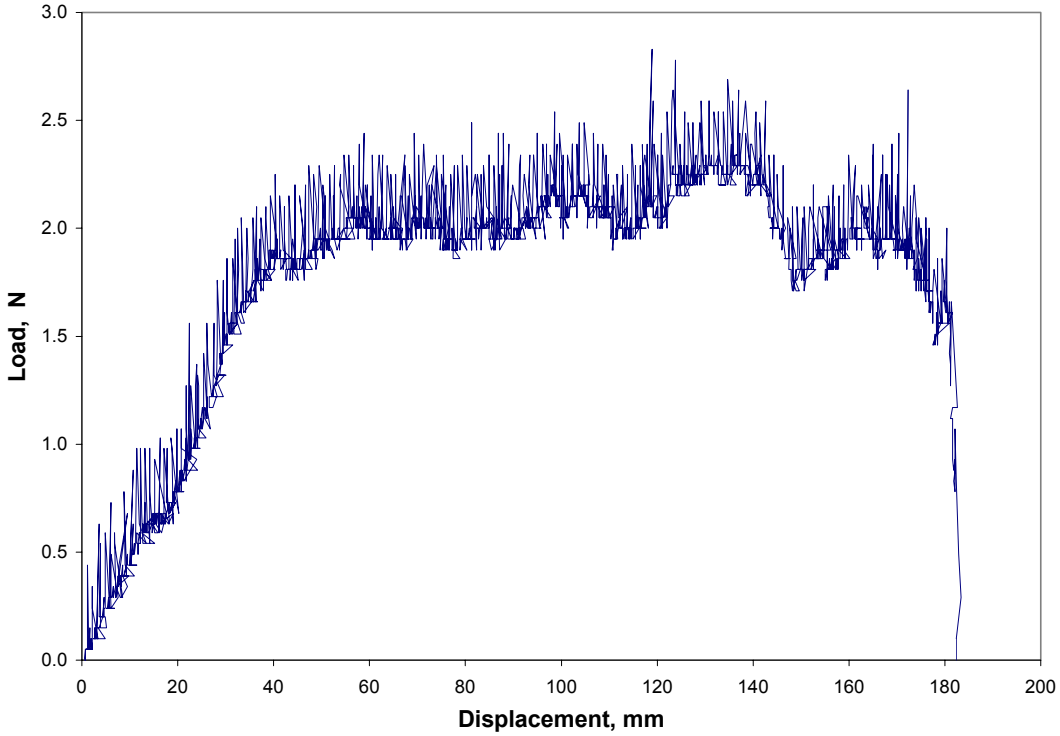

Figure B.201: Load Versus Displacement for Subject D, 180 degrees, 1 min, 400 mm/min, Test 2

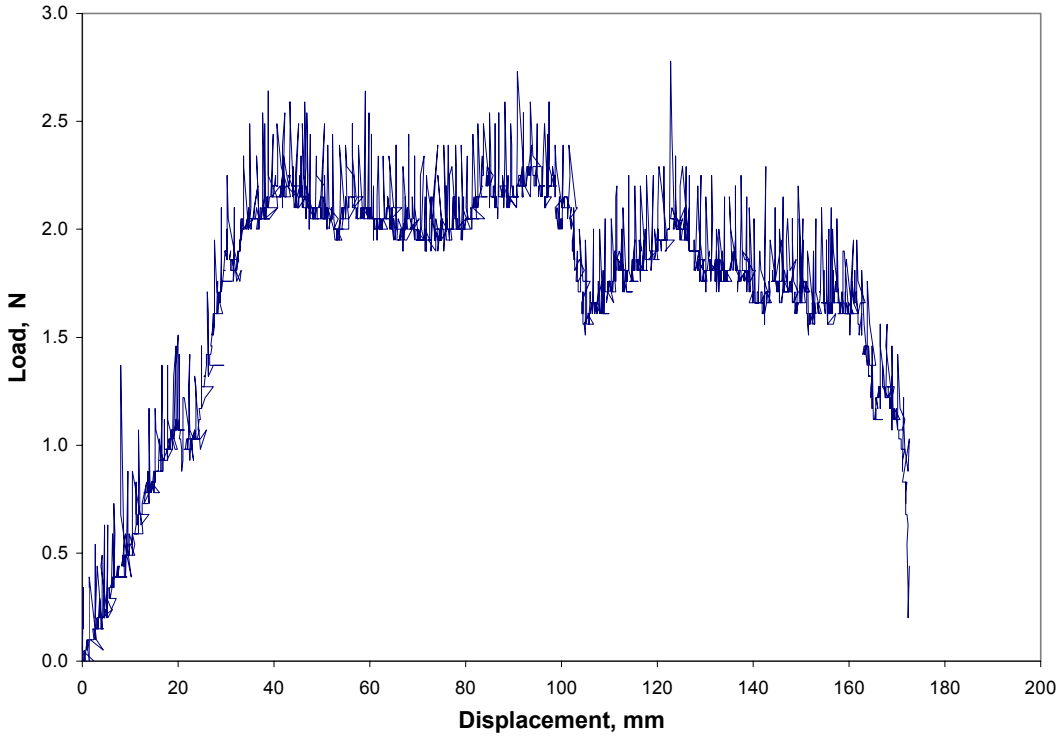

Figure B.202: Load Versus Displacement for Subject D, 180 degrees, 1 min, 400 mm/min, Test 3

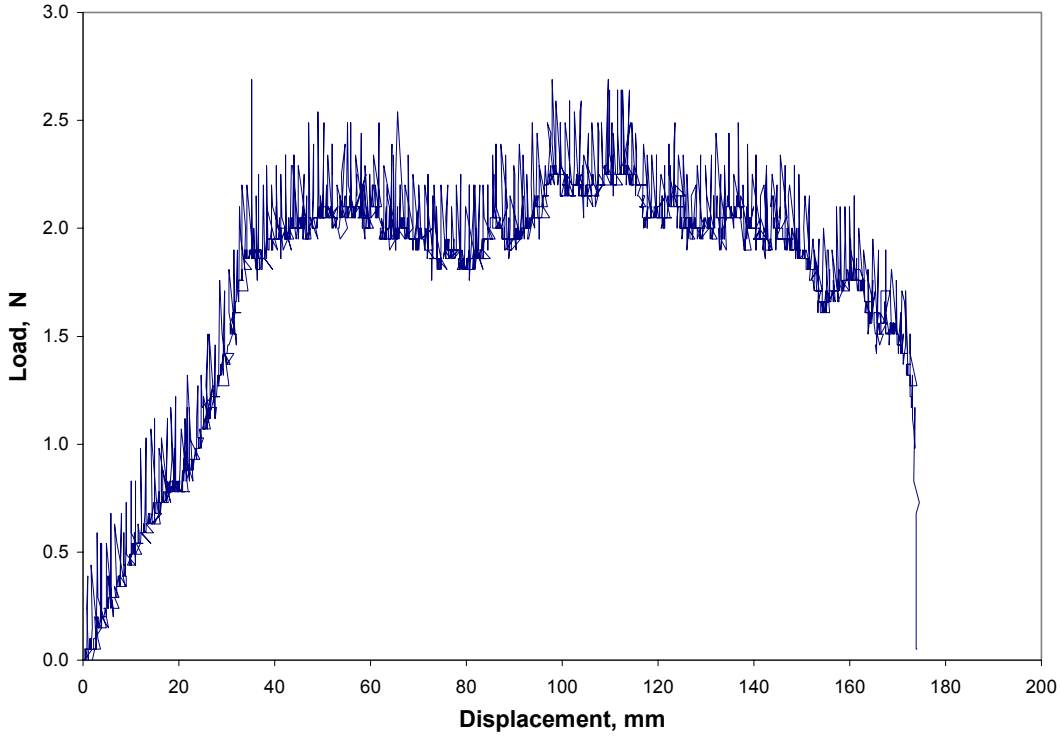

Figure B.203: Load Versus Displacement for Subject D, 180 degrees, 1 min, 400 mm/min, Test 4

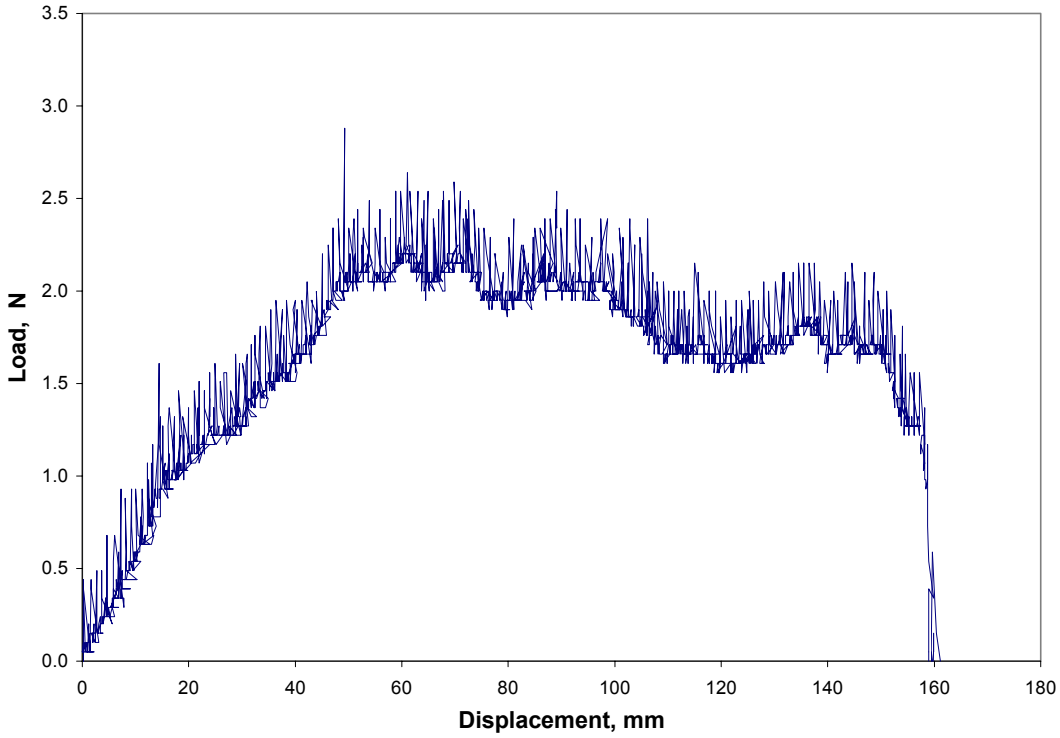

Figure B.204: Load Versus Displacement for Subject D, 180 degrees, 1 min, 400 mm/min, Test 5

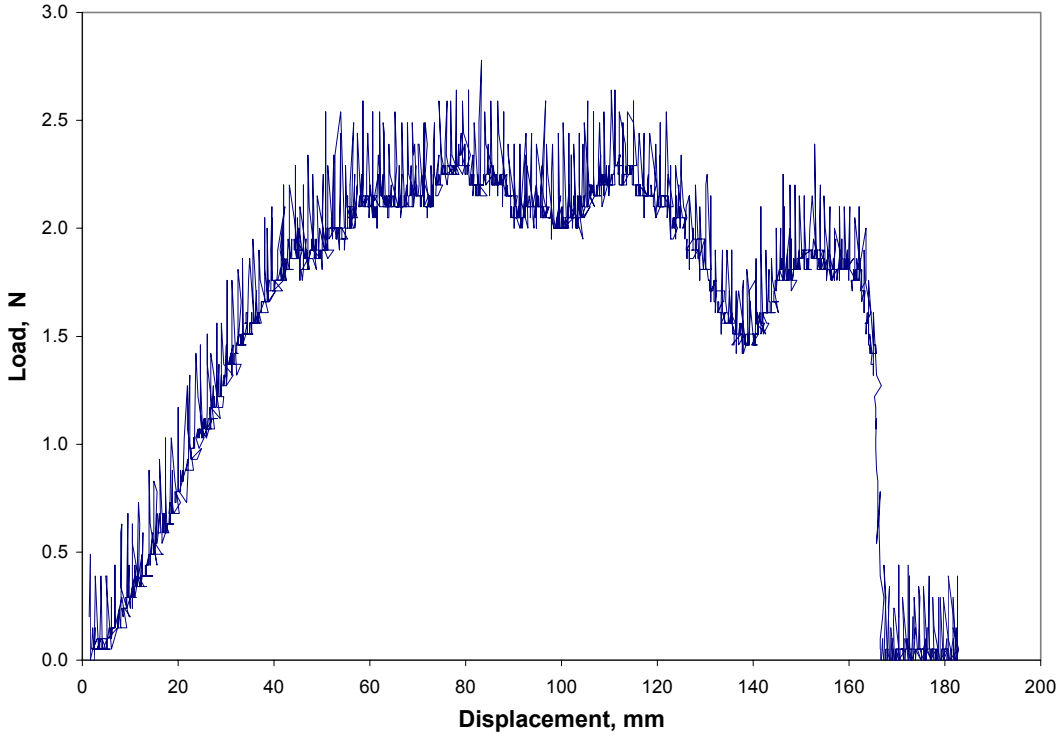

Figure B.205: Load Versus Displacement for Subject D, 180 degrees, 1 min, 400 mm/min, Test 6

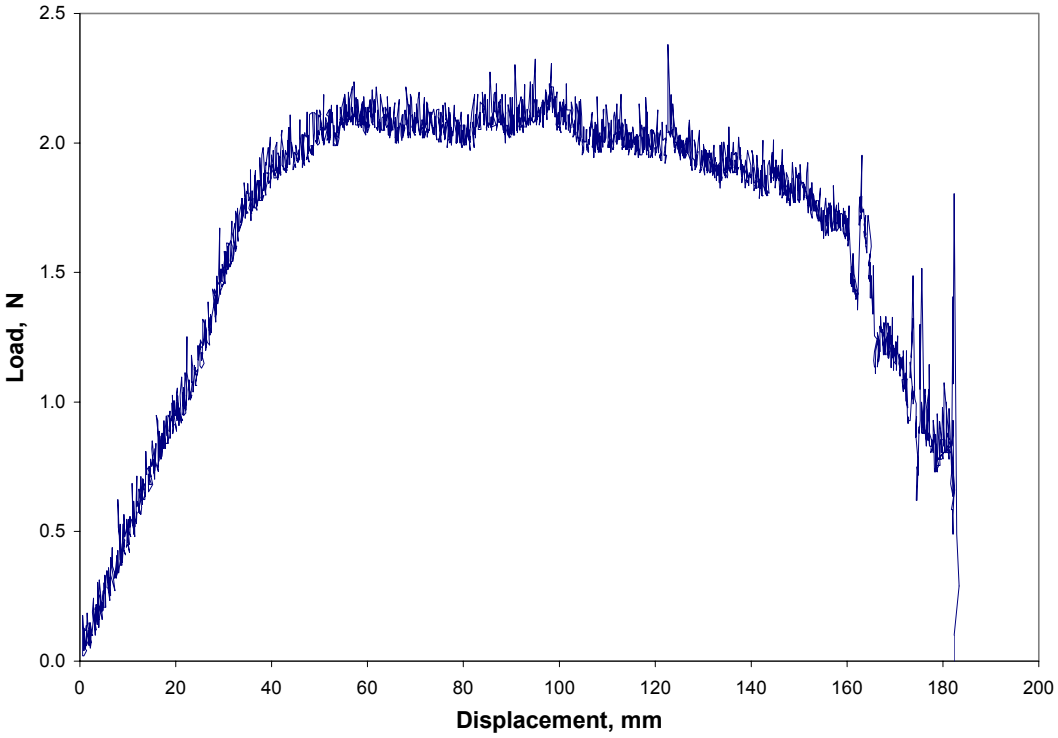

Figure B.206: Load Versus Displacement for Subject D, 180 degrees, 1 min, 400 mm/min, Average

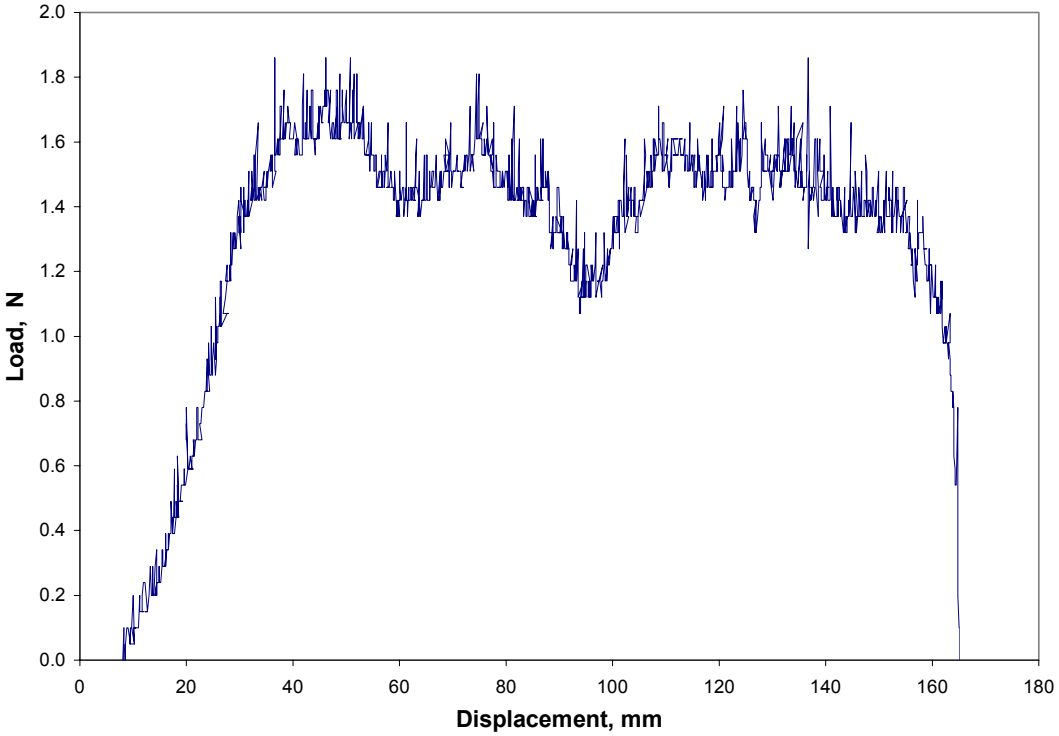

Figure B.207: Load Versus Displacement for Subject D, 180 degrees, 1 min, 500 mm/min, Test 1

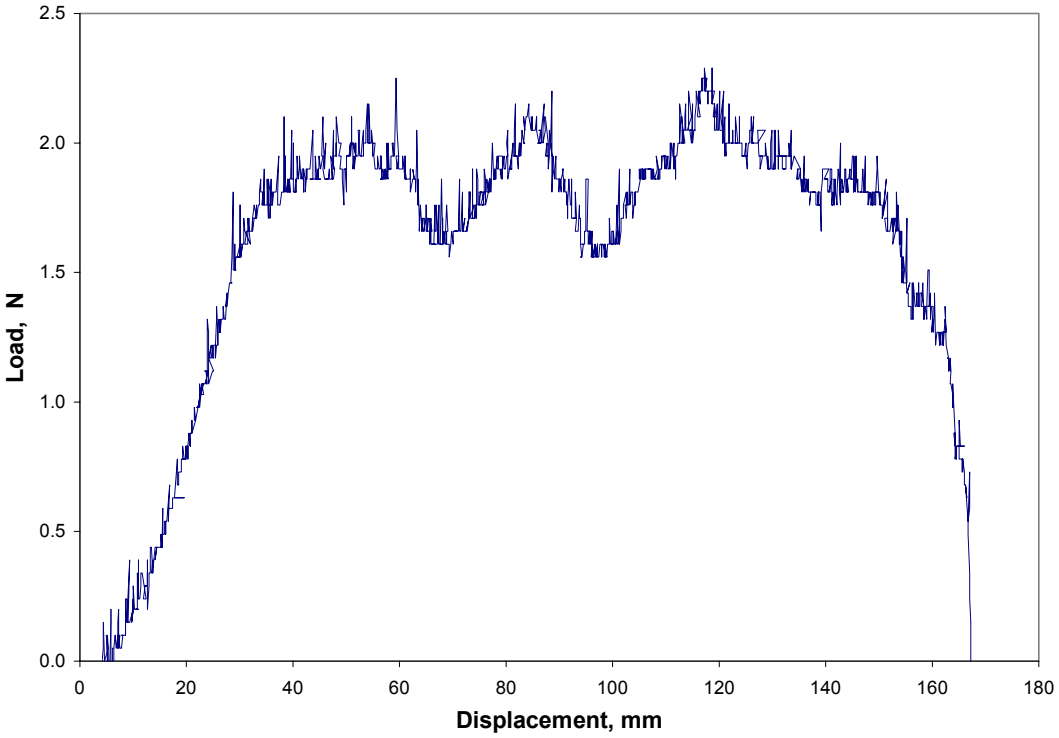

Figure B.208: Load Versus Displacement for Subject D, 180 degrees, 1 min, 500 mm/min, Test 2

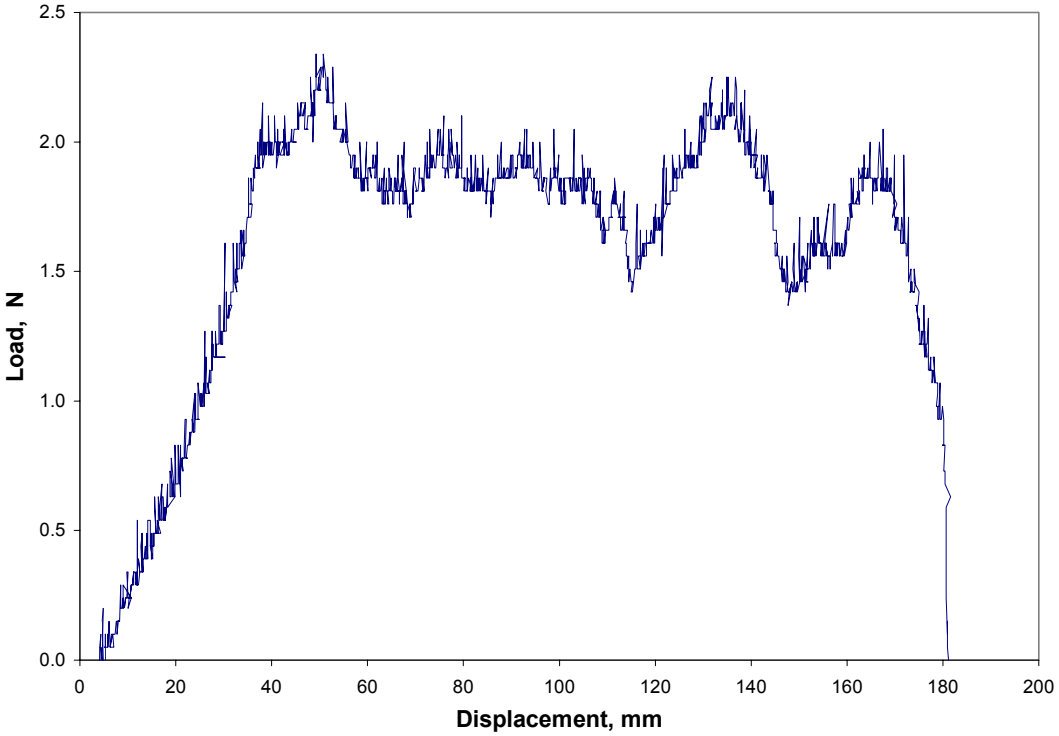

Figure B.209: Load Versus Displacement for Subject D, 180 degrees, 1 min, 500 mm/min, Test 3

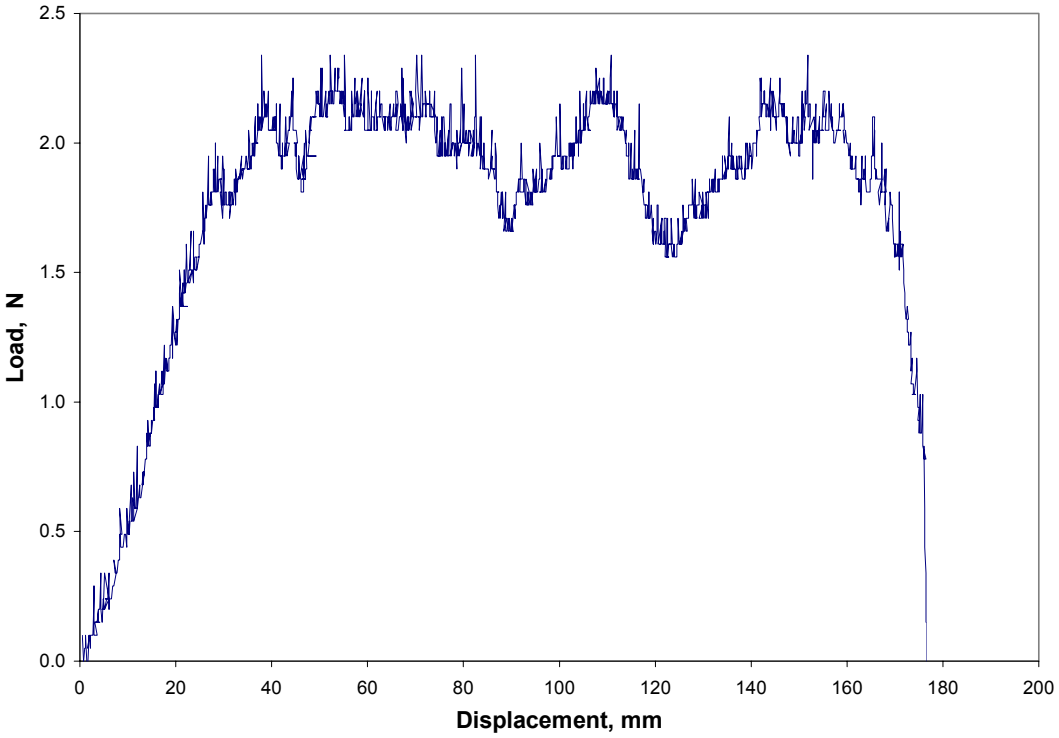

Figure B.210: Load Versus Displacement for Subject D, 180 degrees, 1 min, 500 mm/min, Test 4

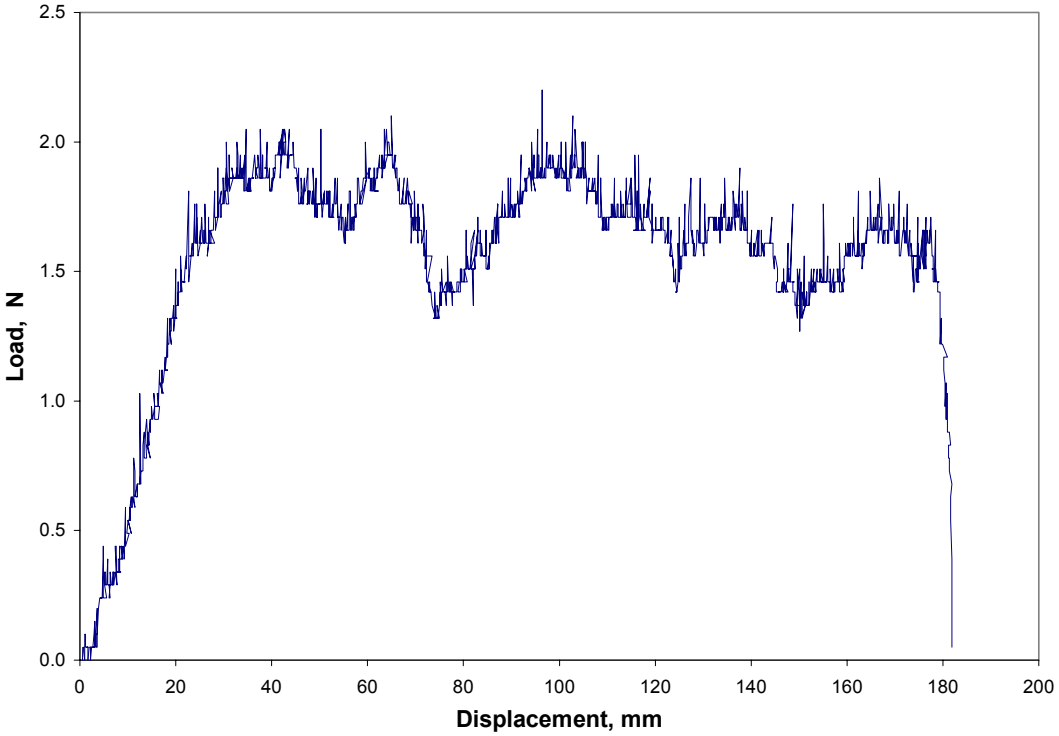

Figure B.211: Load Versus Displacement for Subject D, 180 degrees, 1 min, 500 mm/min, Test 5

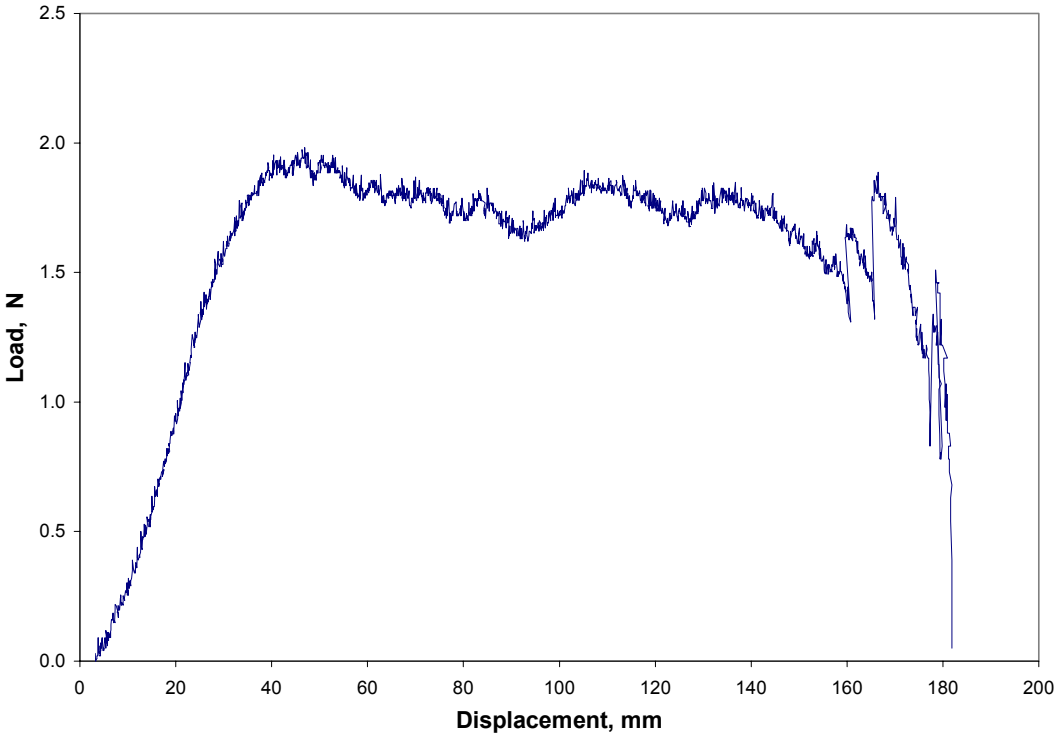

Figure B.212: Load Versus Displacement for Subject D, 180 degrees, 1 min, 500 mm/min, Average

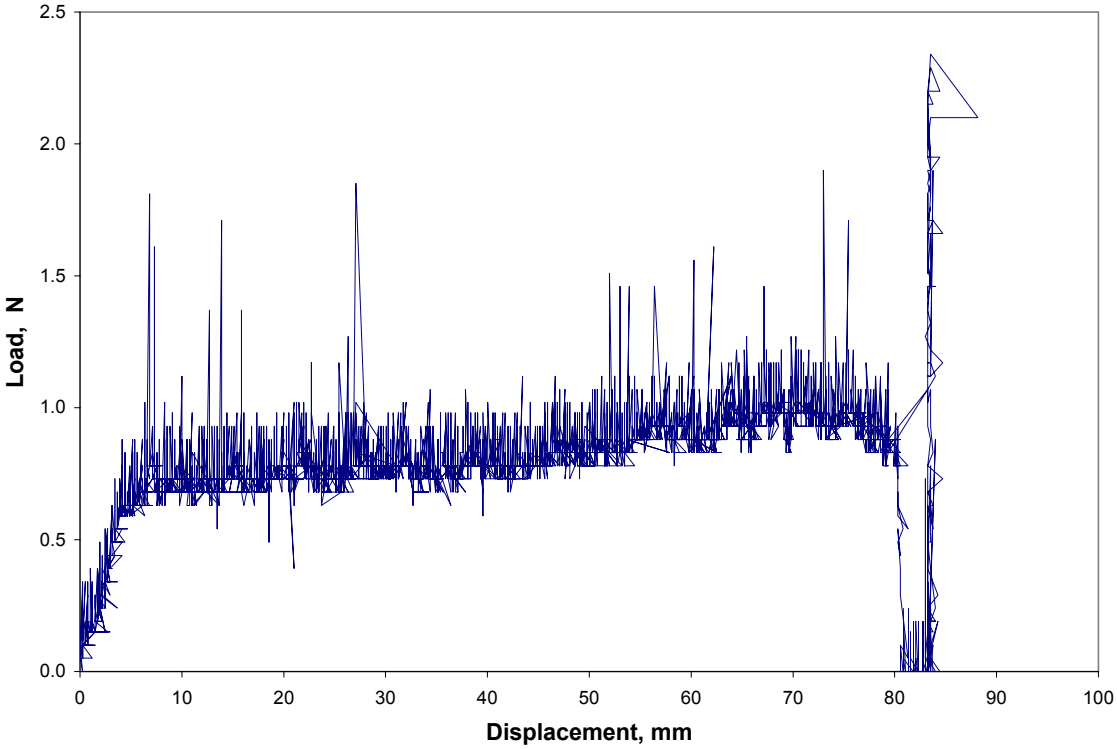

Figure B.213: Load Versus Displacement for Subject A, 120 degrees, 1 min, 100 mm/min, Test 1

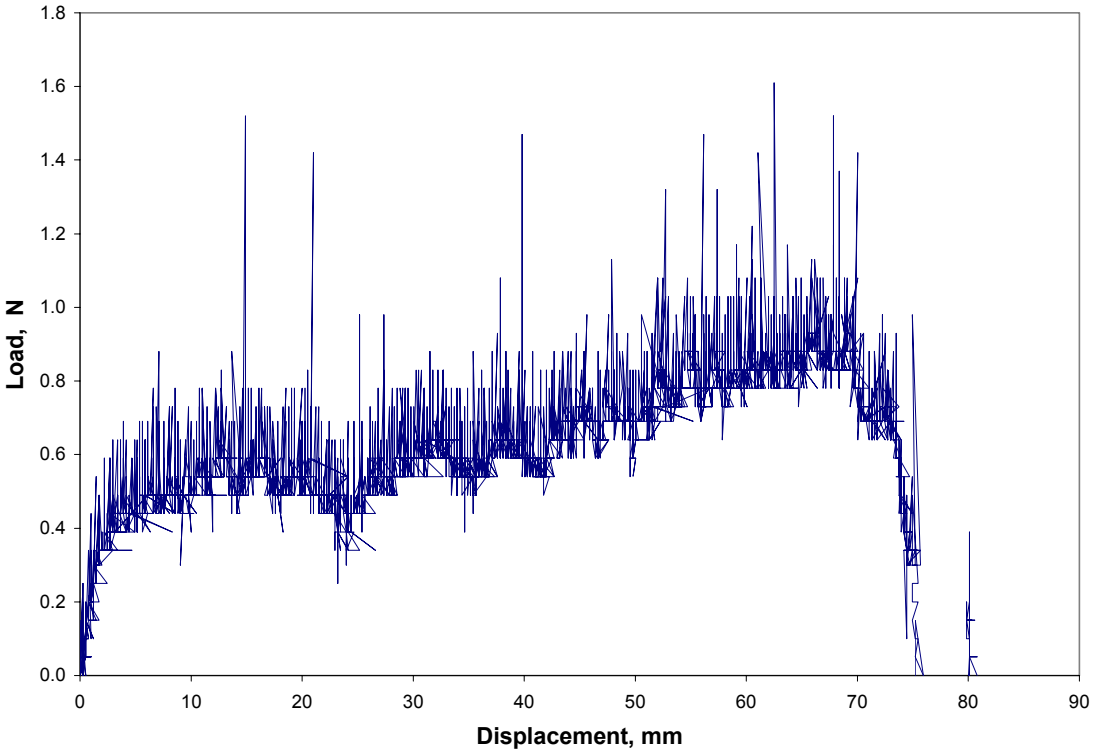

Figure B.214: Load Versus Displacement for Subject A, 120 degrees, 1 min, 100 mm/min, Test 2

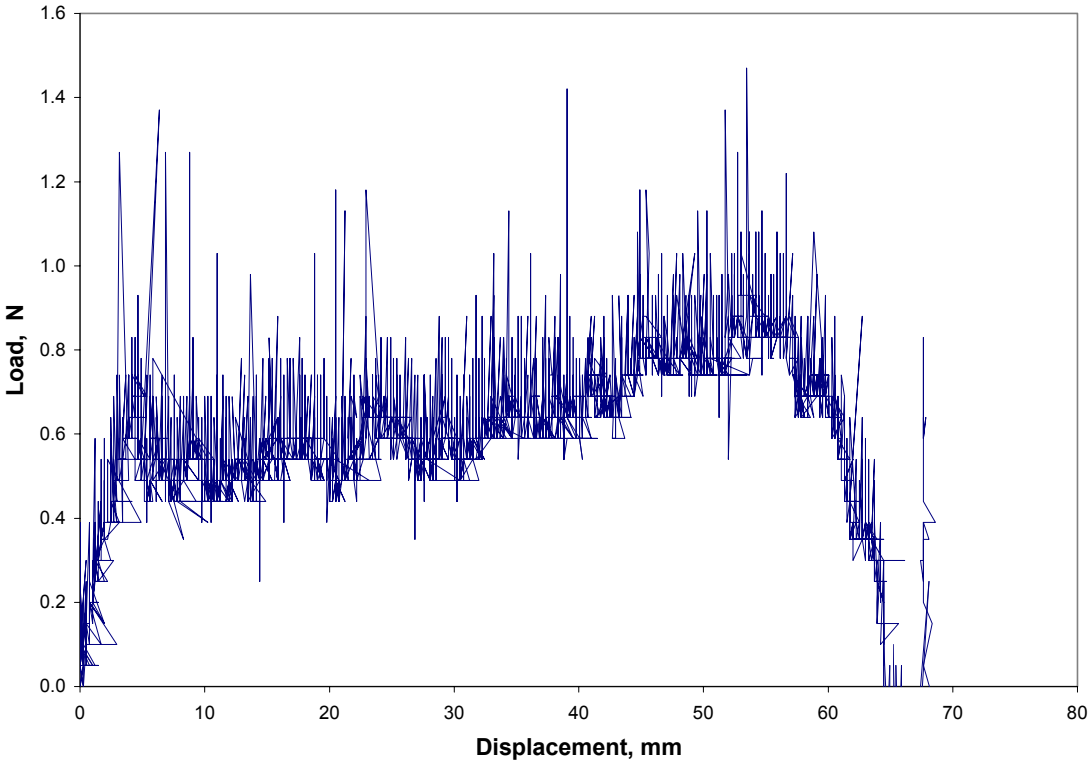

Figure B.215: Load Versus Displacement for Subject A, 120 degrees, 1 min, 100 mm/min, Test 3

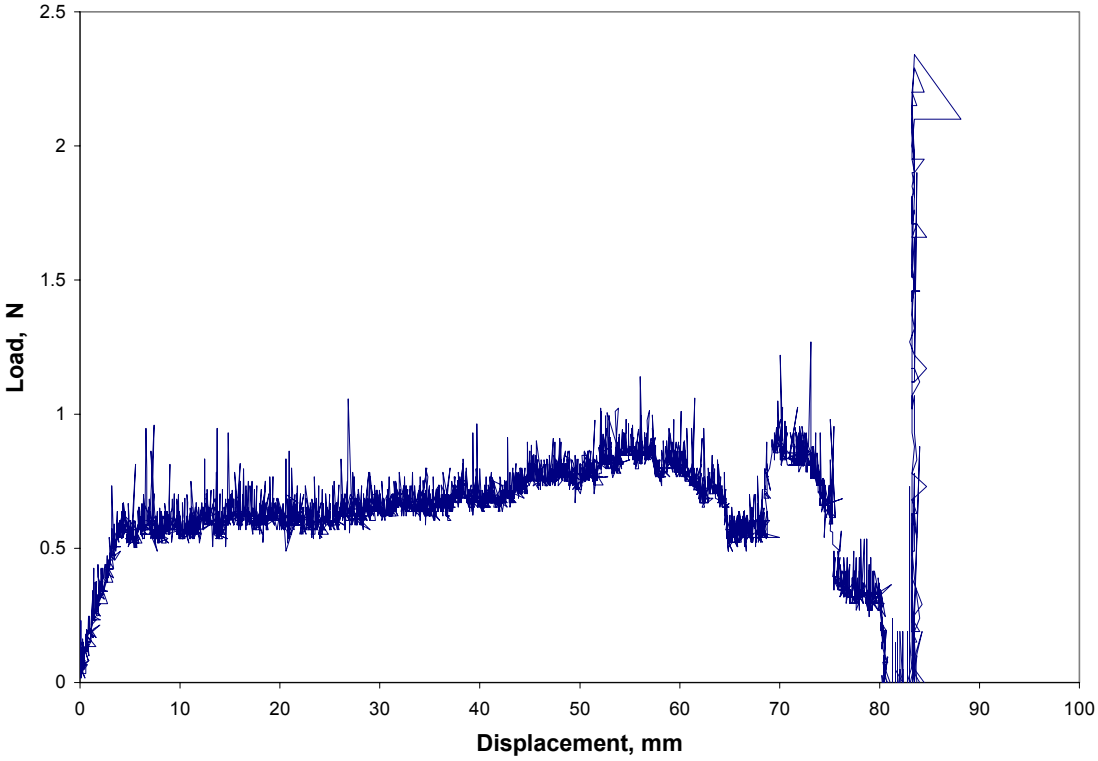

Figure B.216: Load Versus Displacement for Subject A, 120 degrees, 1 min, 100 mm/min, Average

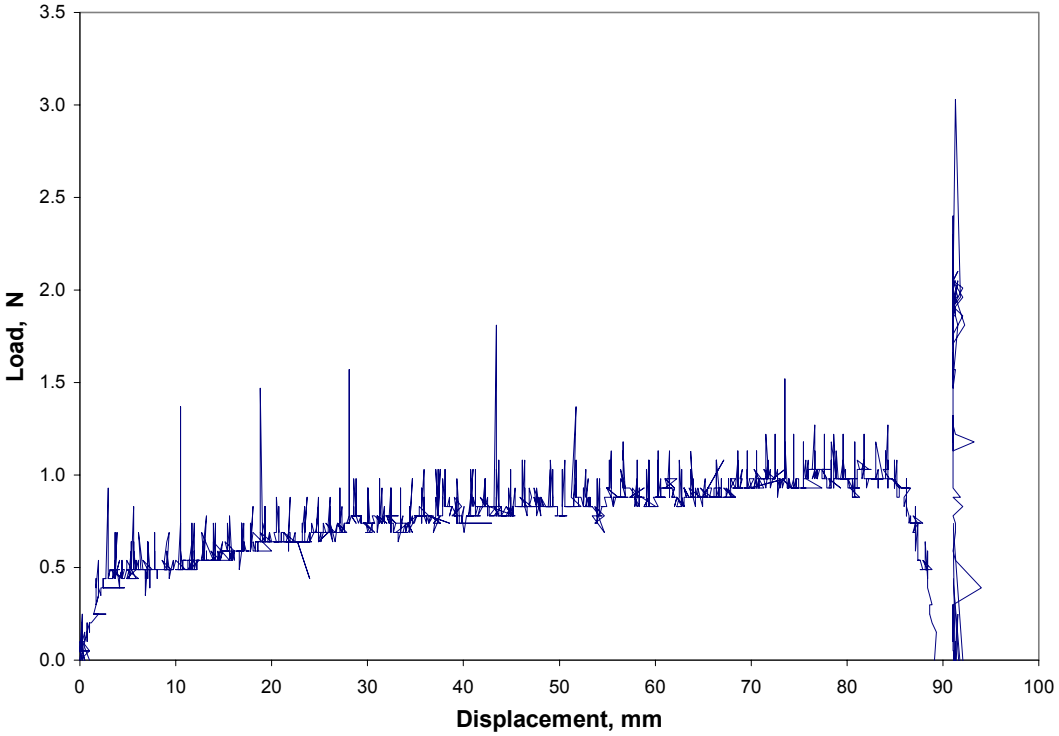

Figure B.217: Load Versus Displacement for Subject A, 120 degrees, 1 min, 300 mm/min, Test 1

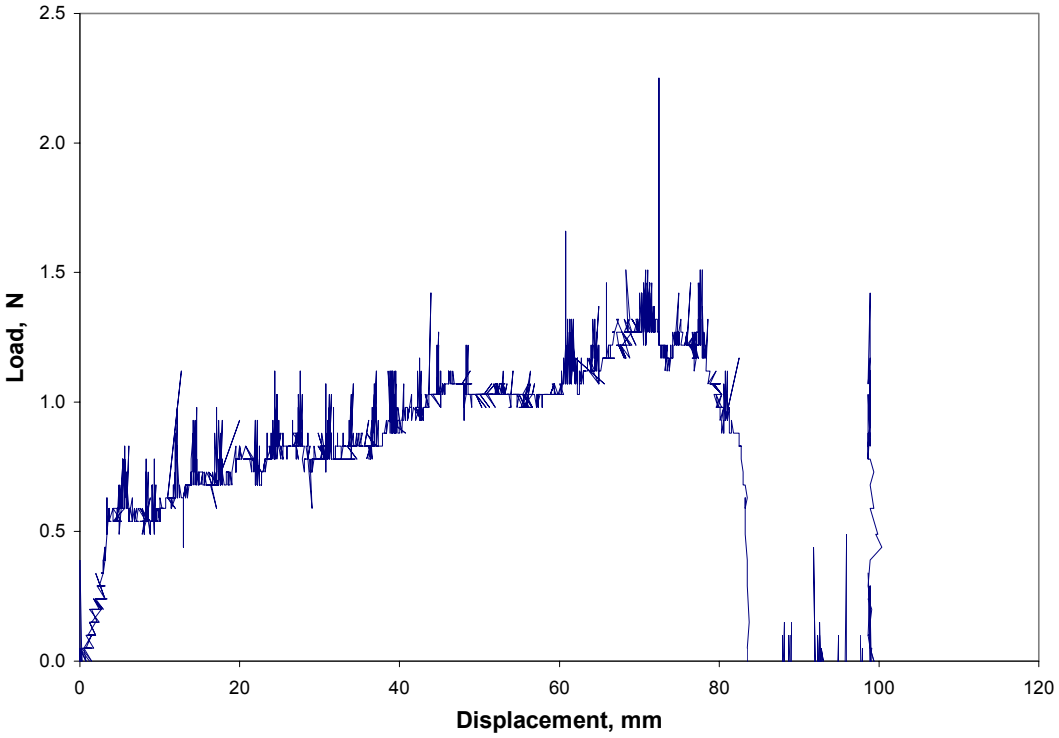

Figure B.218: Load Versus Displacement for Subject A, 120 degrees, 1 min, 300 mm/min, Test 2

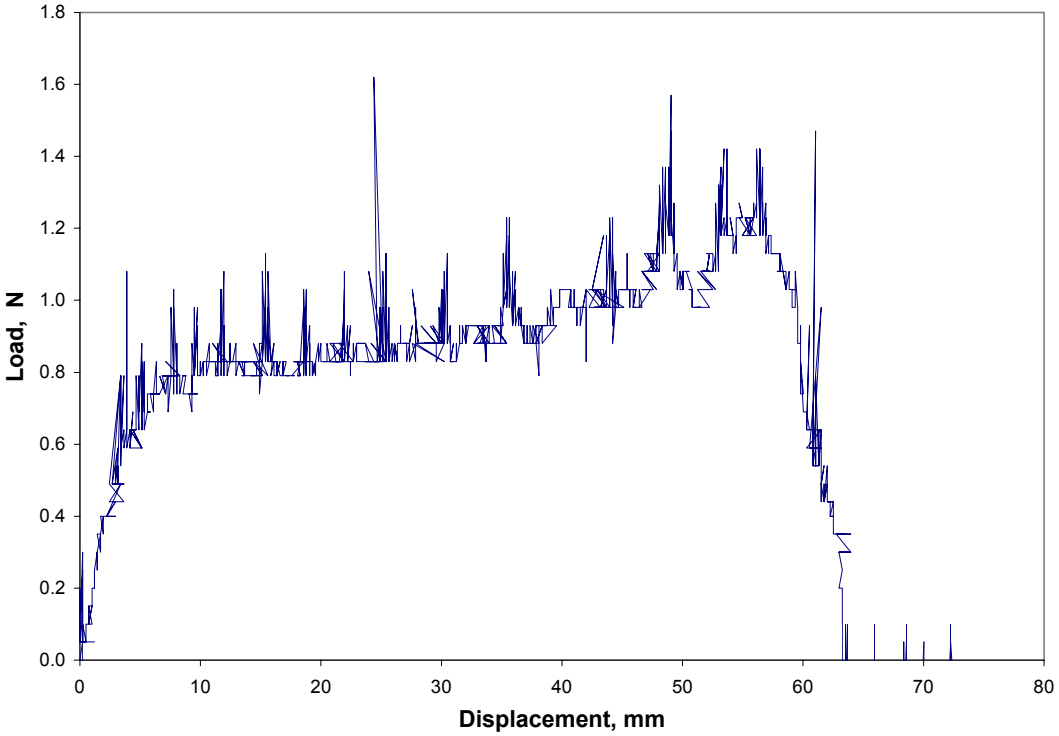

Figure B.219: Load Versus Displacement for Subject A, 120 degrees, 1 min, 300 mm/min, Test 3

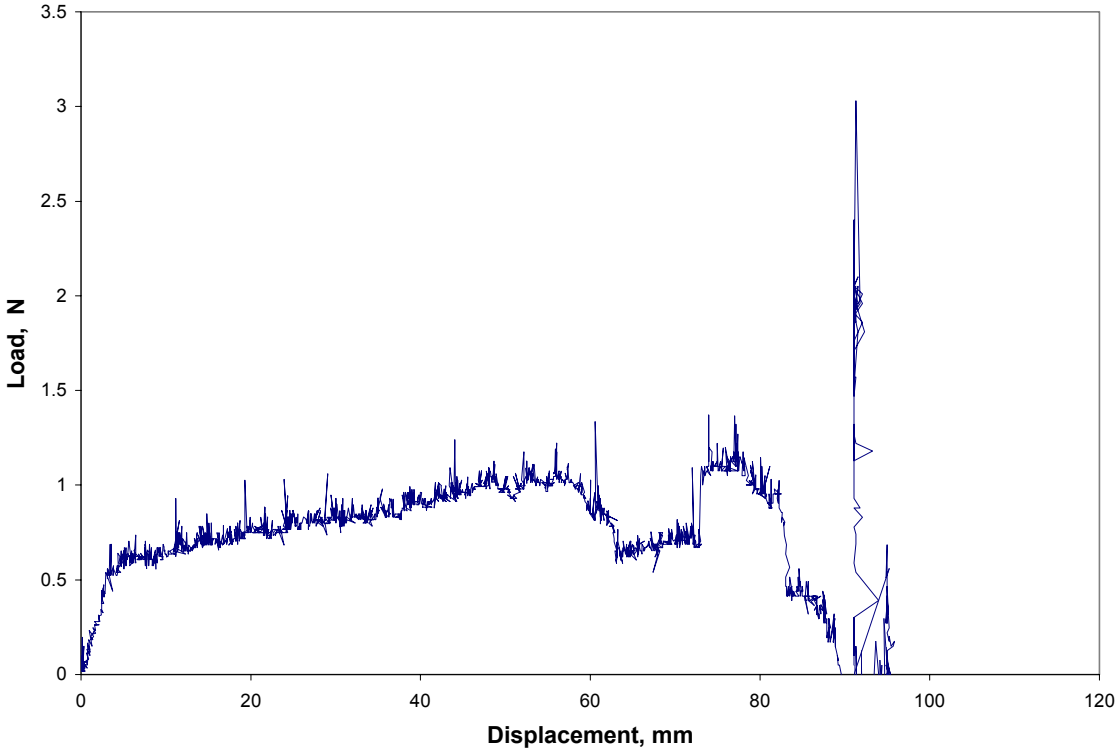

Figure B.220: Load Versus Displacement for Subject A, 120 degrees, 1 min, 300 mm/min, Average

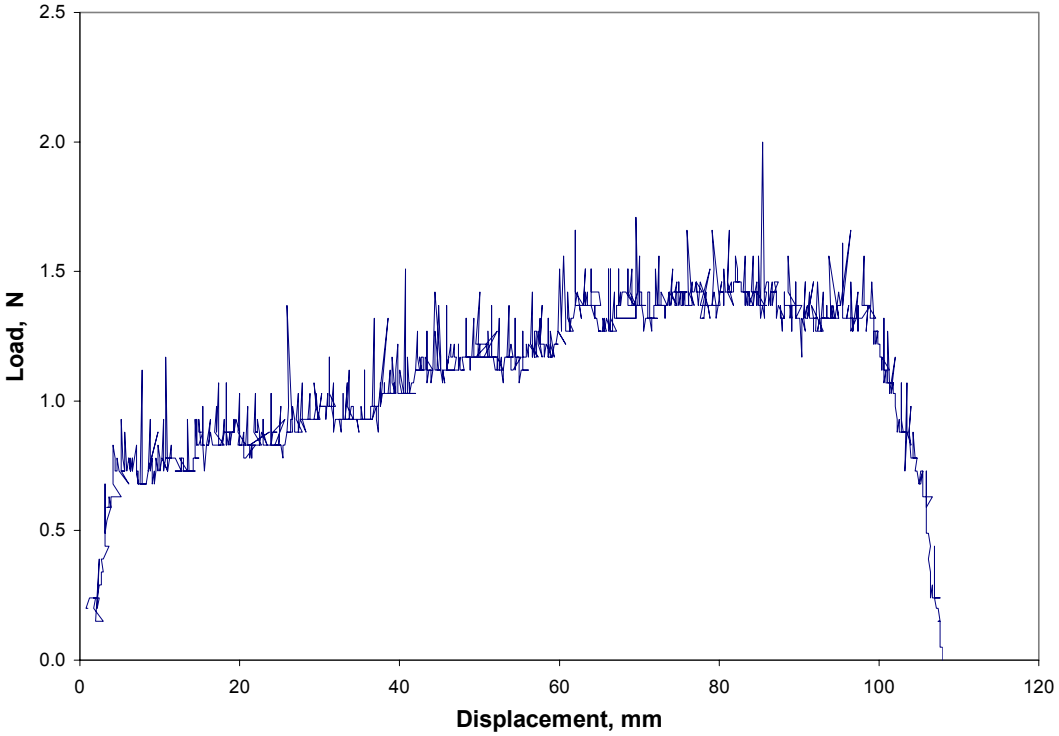

Figure B.221: Load Versus Displacement for Subject A, 120 degrees, 1 min, 500 mm/min, Test 1

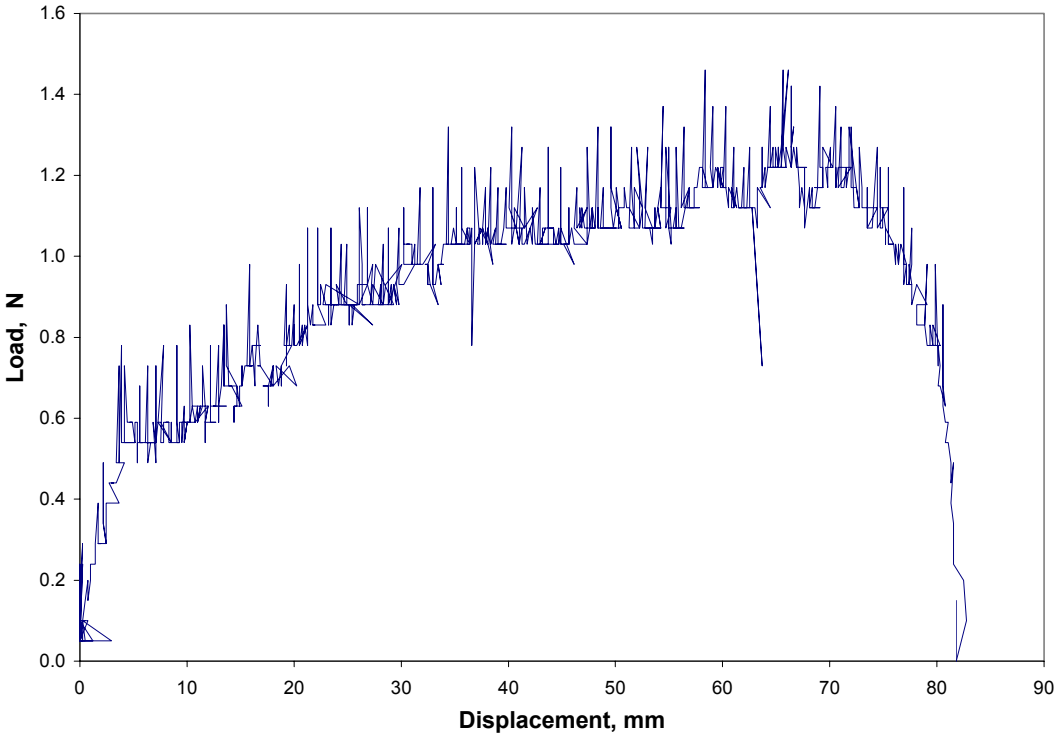

Figure B.222: Load Versus Displacement for Subject A, 120 degrees, 1 min, 500 mm/min, Test 2

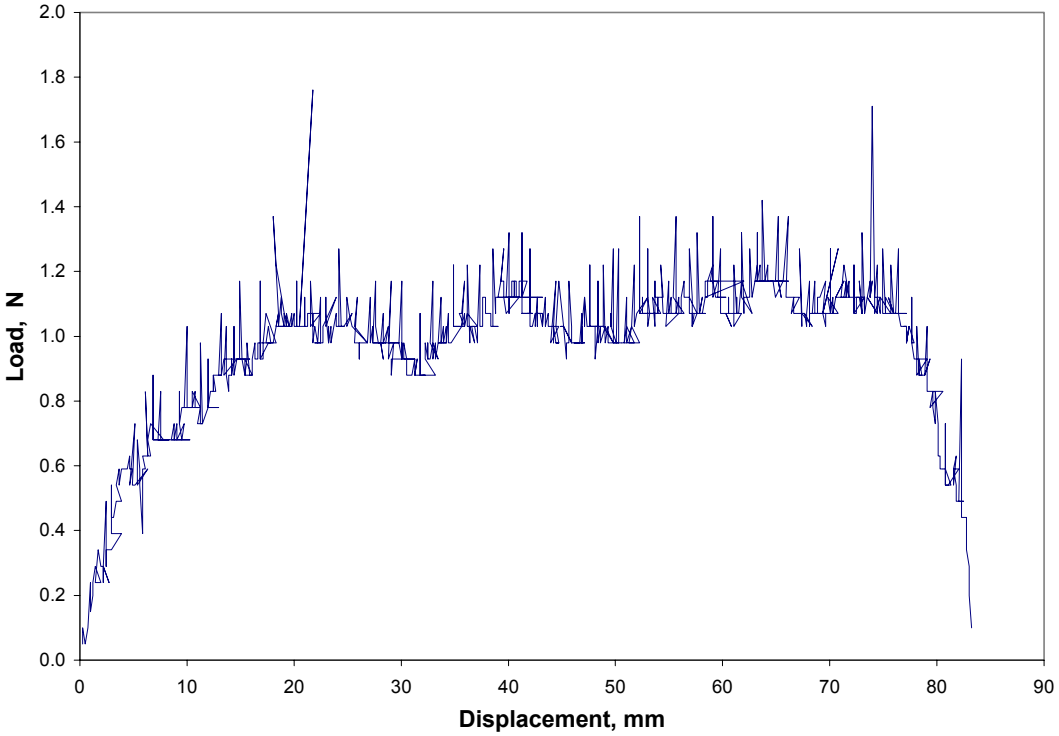

Figure B.223: Load Versus Displacement for Subject A, 120 degrees, 1 min, 500 mm/min, Test 3

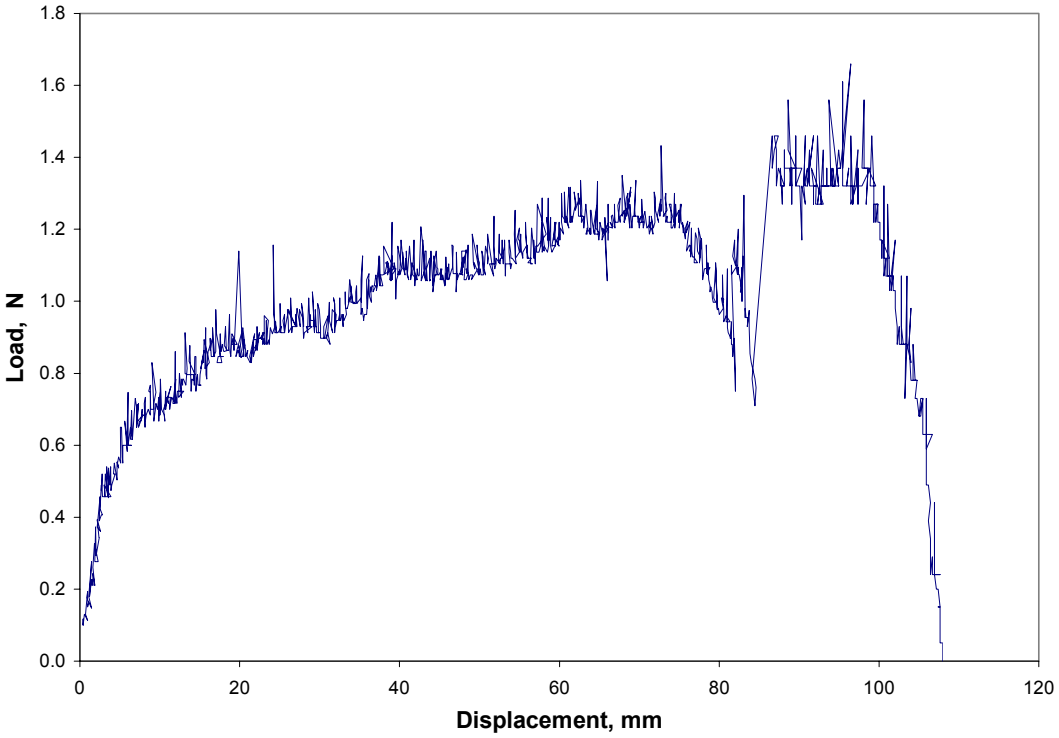

Figure B.224: Load Versus Displacement for Subject A, 120 degrees, 1 min, 500 mm/min, Average

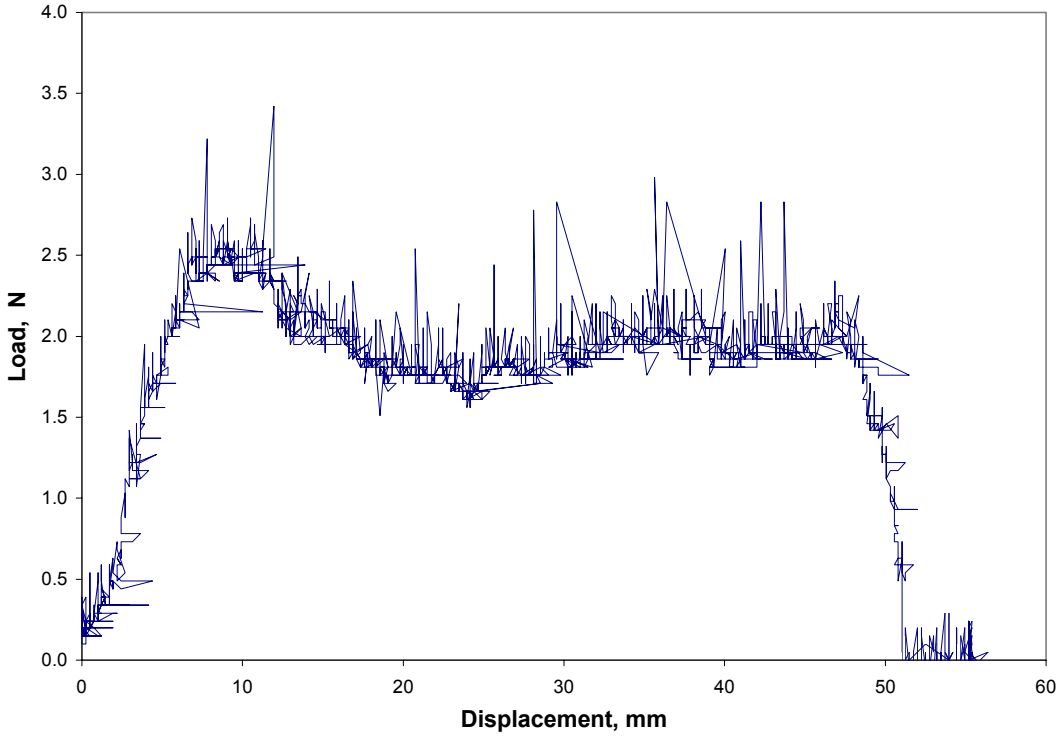

Figure B.225: Load Versus Displacement for Subject D, 120 degrees, 1 min, 100 mm/min, Test 1

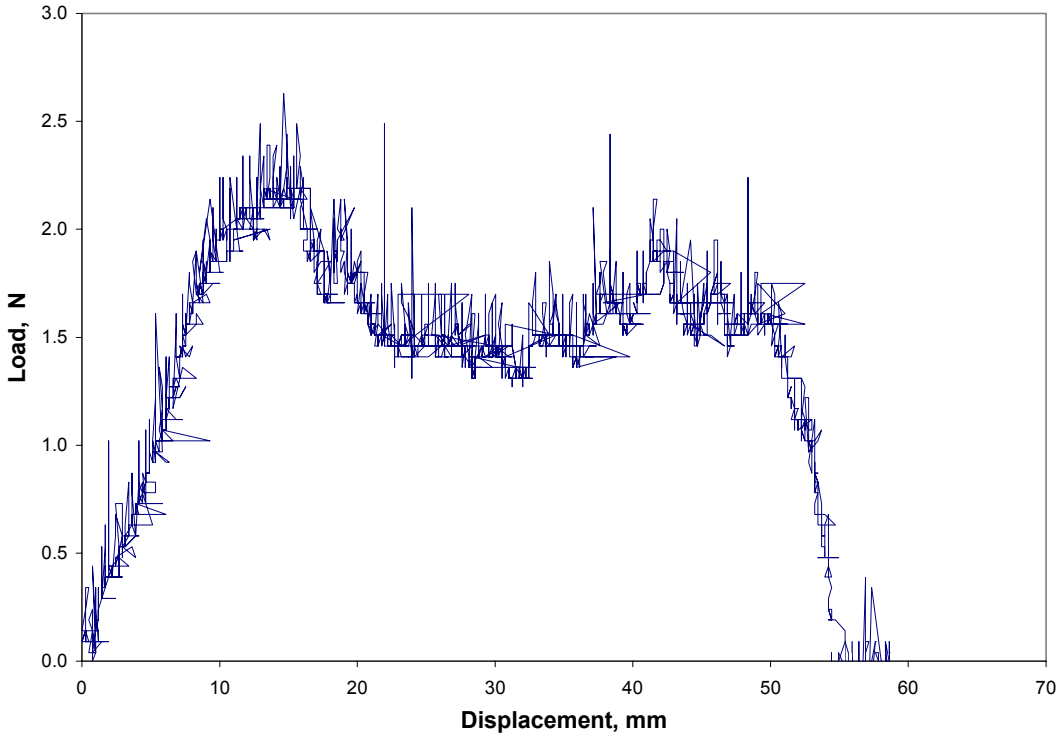

Figure B.226: Load Versus Displacement for Subject D, 120 degrees, 1 min, 100 mm/min, Test 2

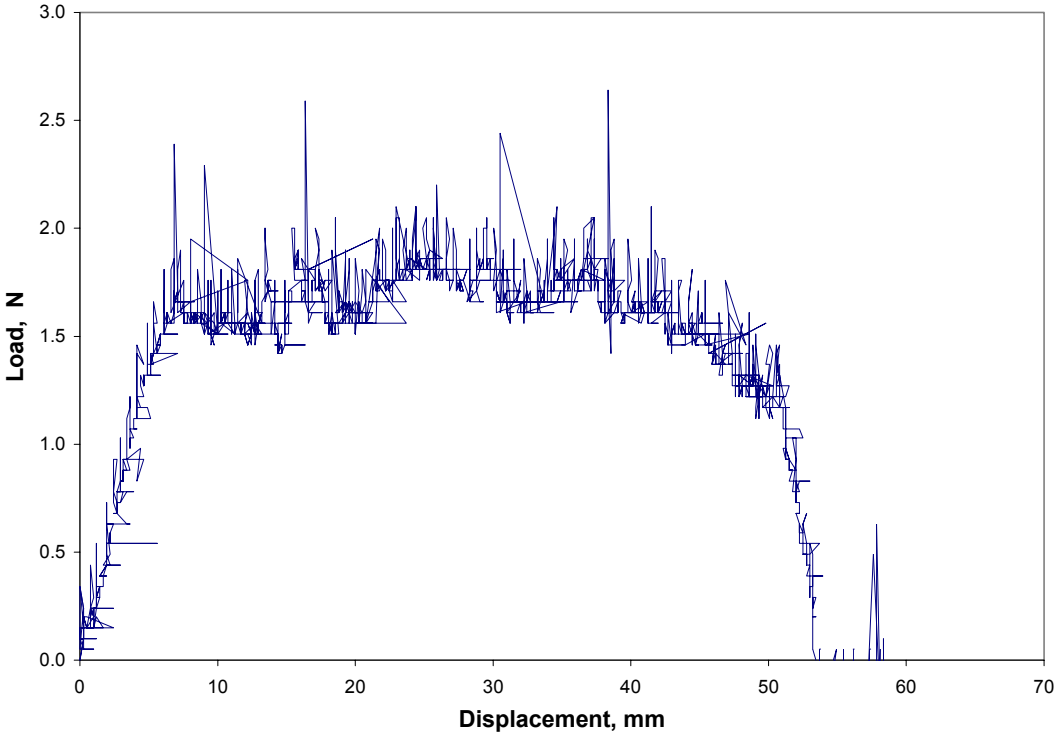

Figure B.227: Load Versus Displacement for Subject D, 120 degrees, 1 min, 100 mm/min, Test 3

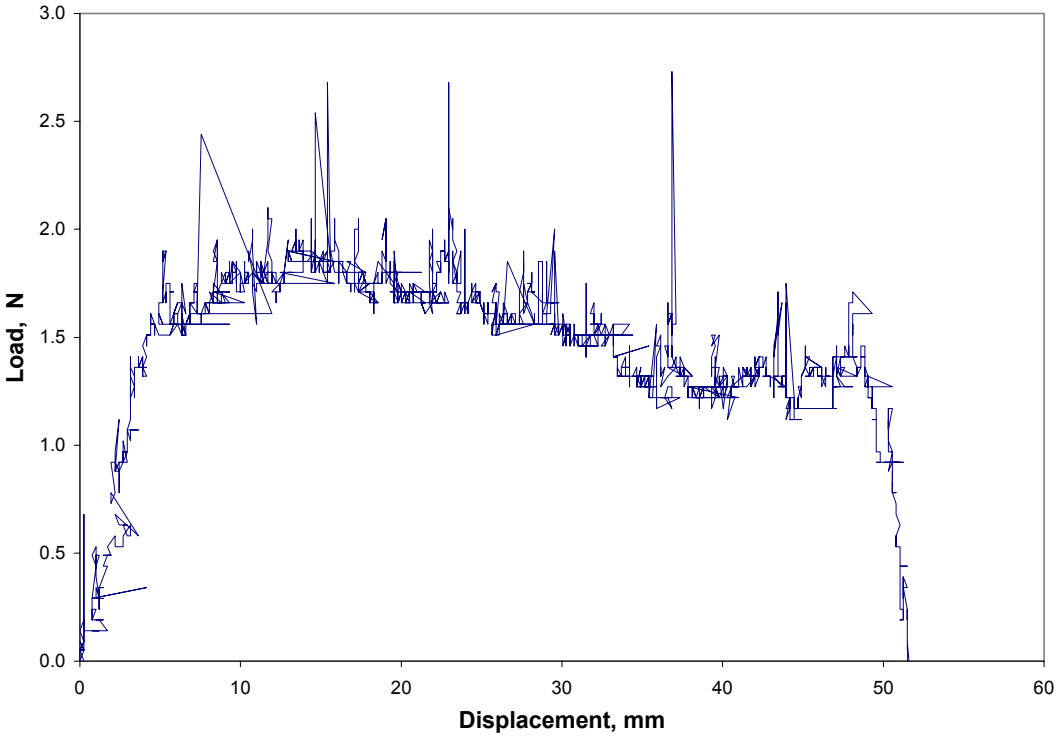

Figure B.228: Load Versus Displacement for Subject D, 120 degrees, 1 min, 100 mm/min, Test 4

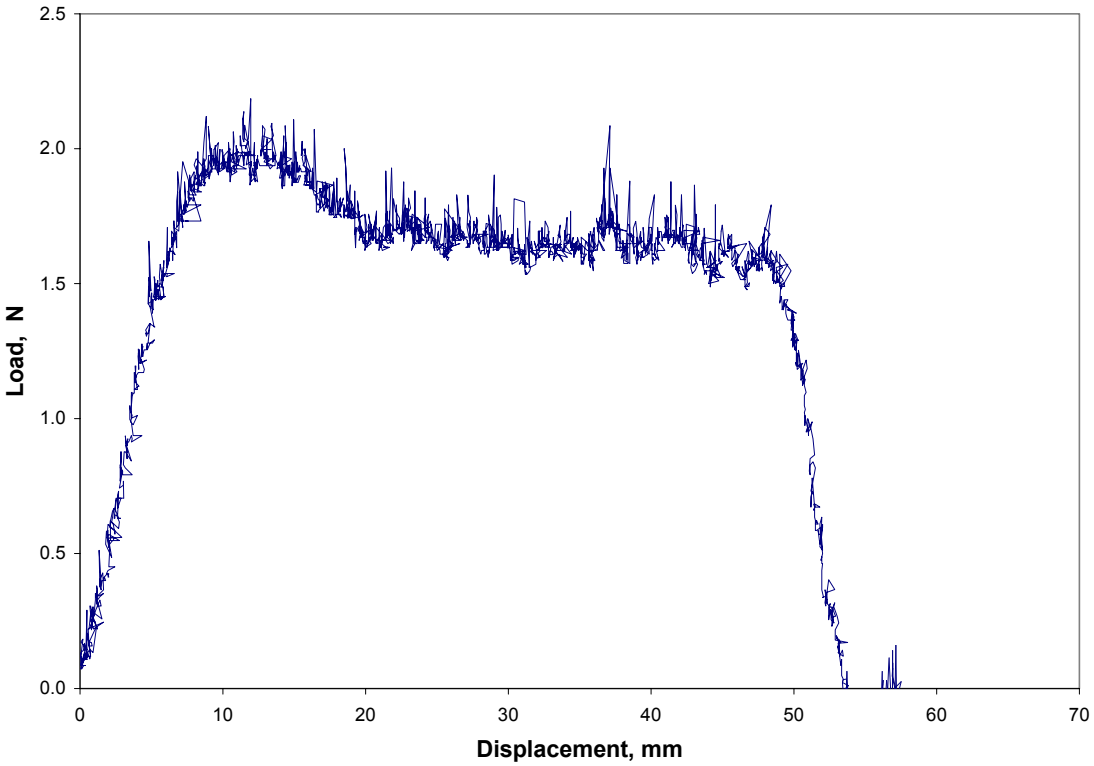

Figure B.229: Load Versus Displacement for Subject D, 120 degrees, 1 min, 100 mm/min, Average

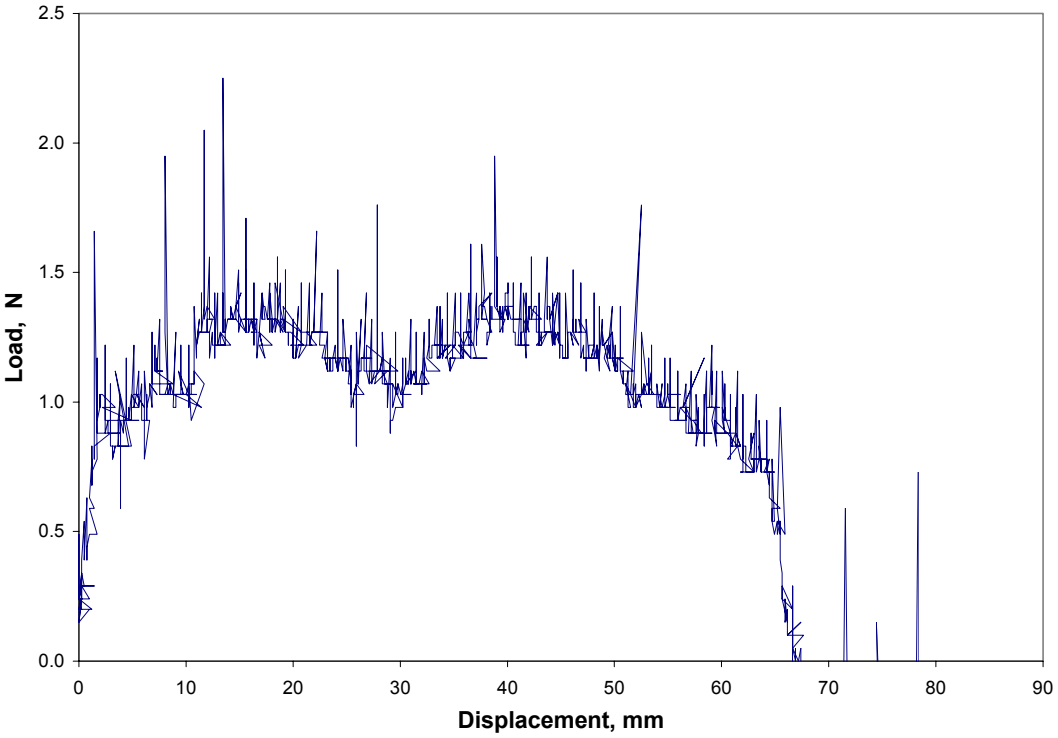

Figure B.230: Load Versus Displacement for Subject D, 120 degrees, 1 min, 300 mm/min, Test 1

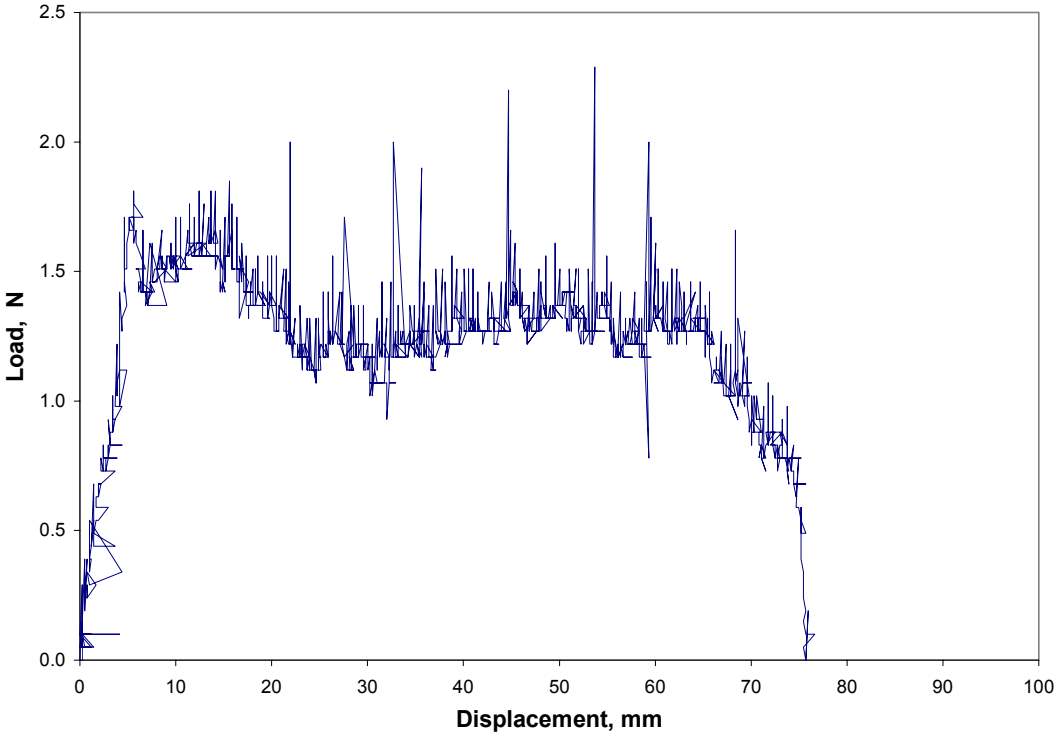

Figure B.231: Load Versus Displacement for Subject D, 120 degrees, 1 min, 300 mm/min, Test 2

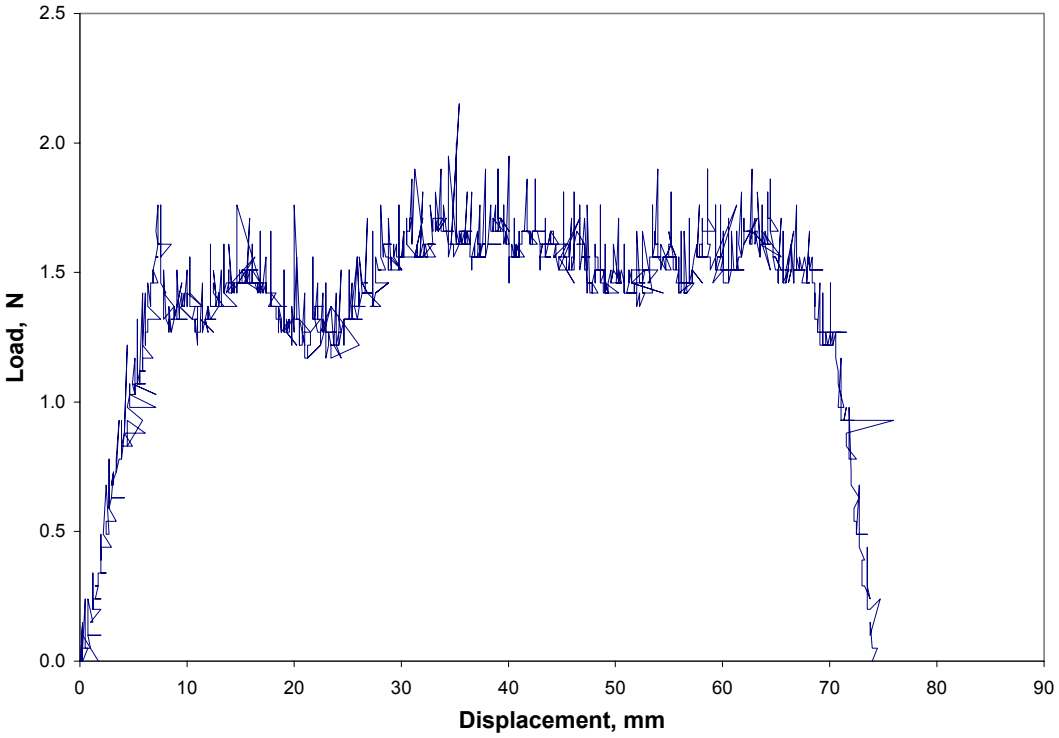

Figure B.232: Load Versus Displacement for Subject D, 120 degrees, 1 min, 300 mm/min, Test 3

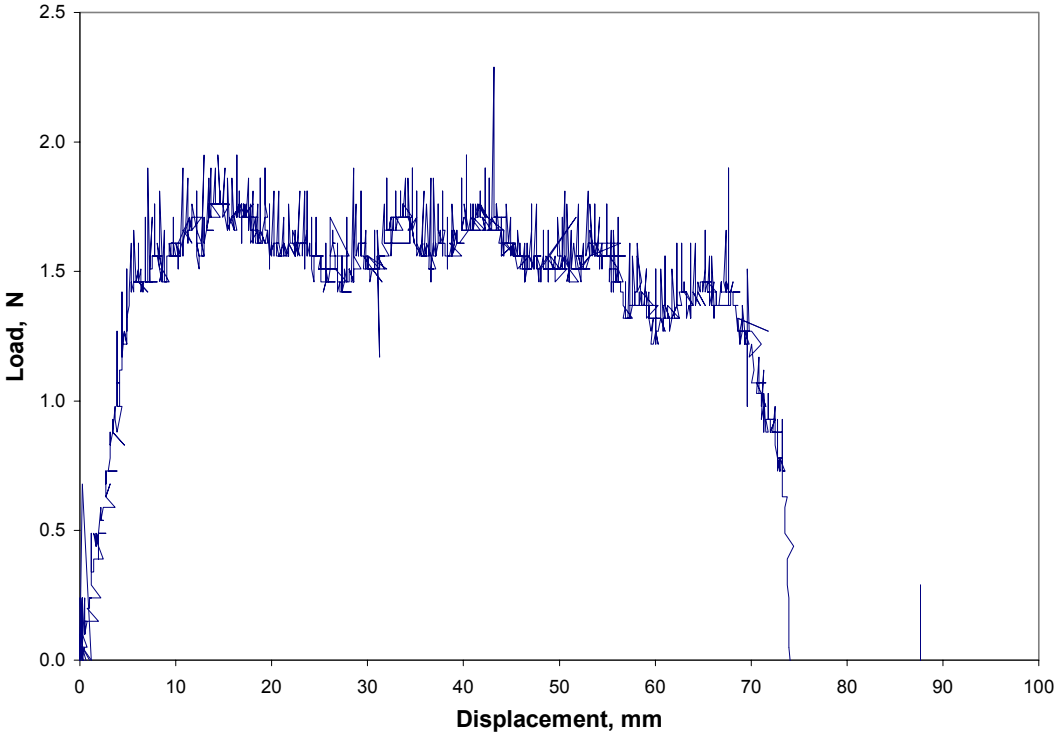

Figure B.233: Load Versus Displacement for Subject D, 120 degrees, 1 min, 300 mm/min, Test 4

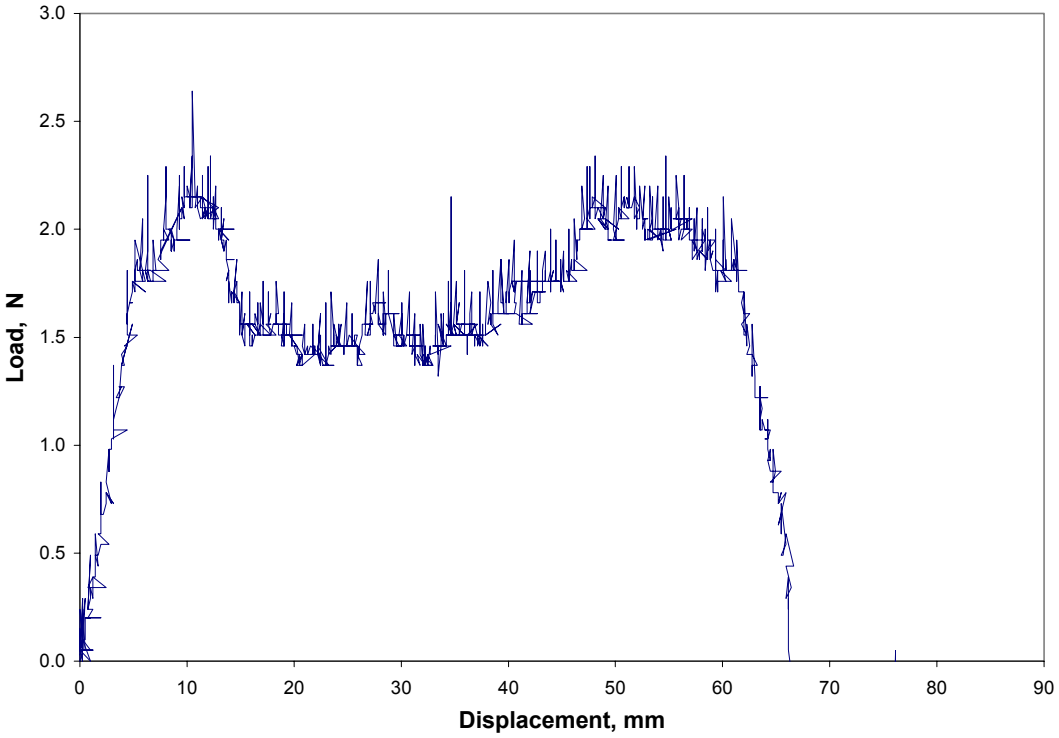

Figure B.234: Load Versus Displacement for Subject D, 120 degrees, 1 min, 300 mm/min, Test 5

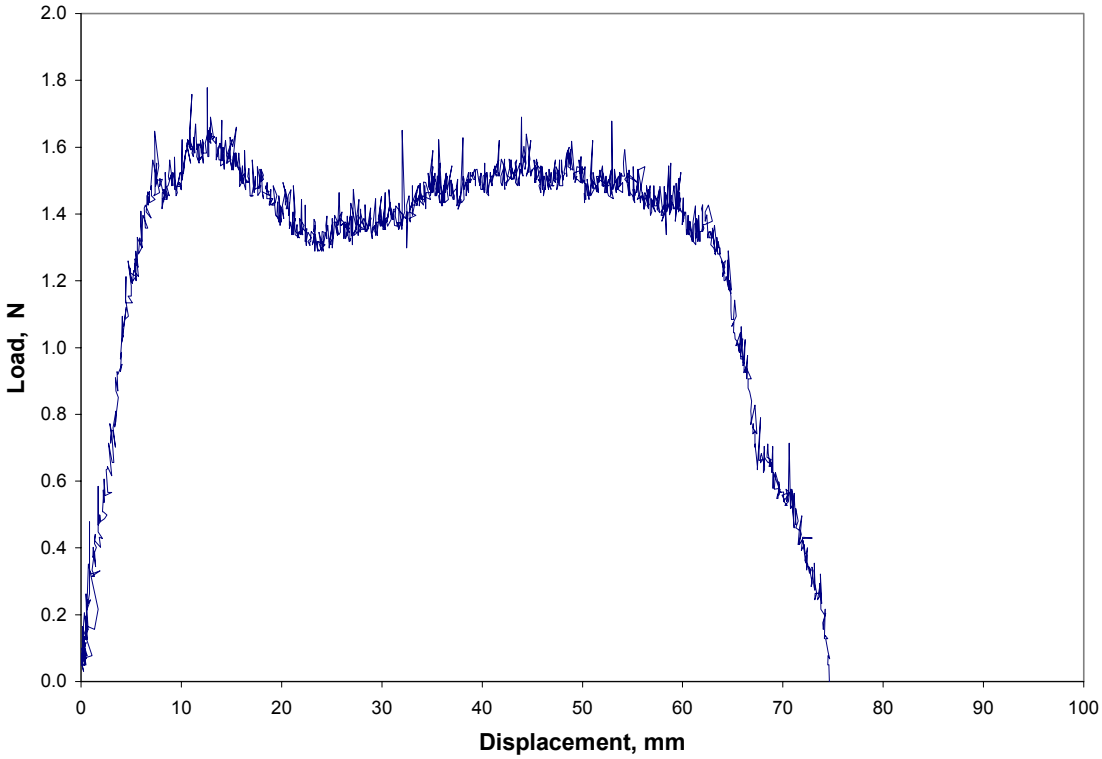

Figure B.235: Load Versus Displacement for Subject D, 120 degrees, 1 min, 300 mm/min, Average

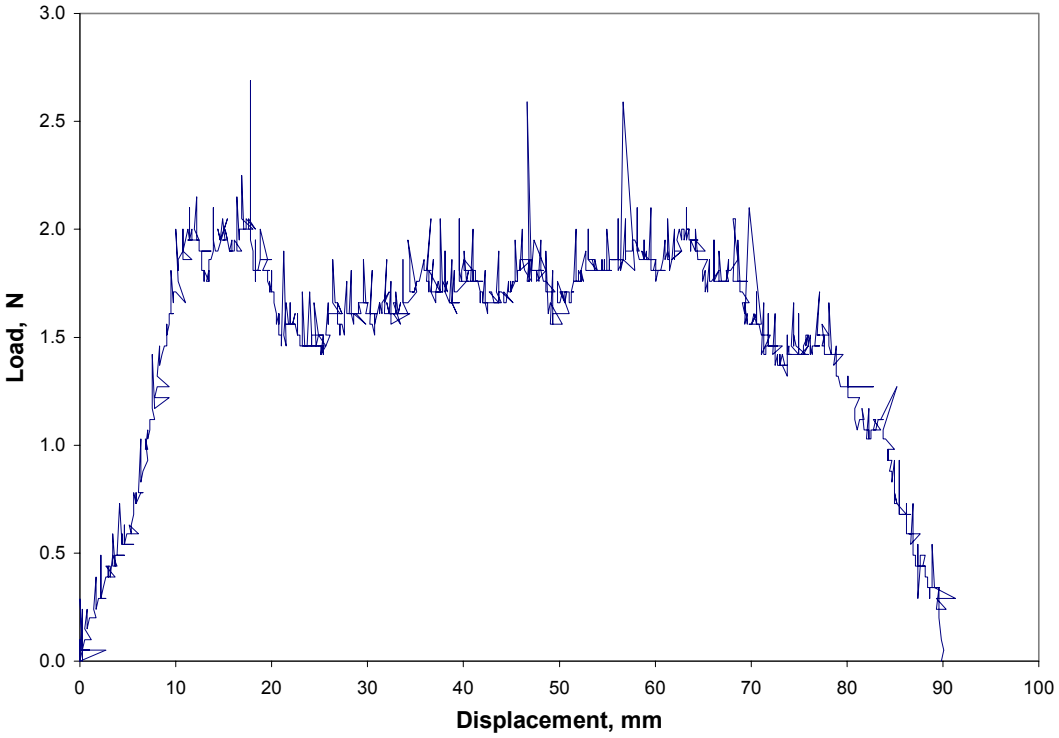

Figure B.236: Load Versus Displacement for Subject D, 120 degrees, 1 min, 500 mm/min, Test 1

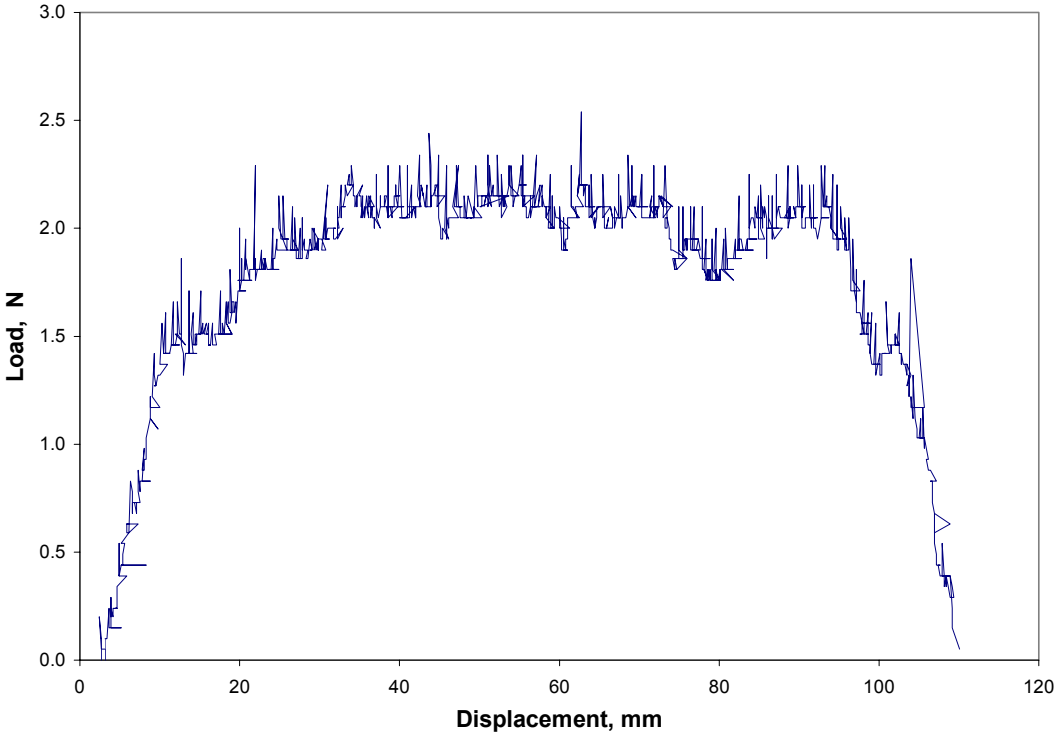

Figure B.237: Load Versus Displacement for Subject D, 120 degrees, 1 min, 500 mm/min, Test 2

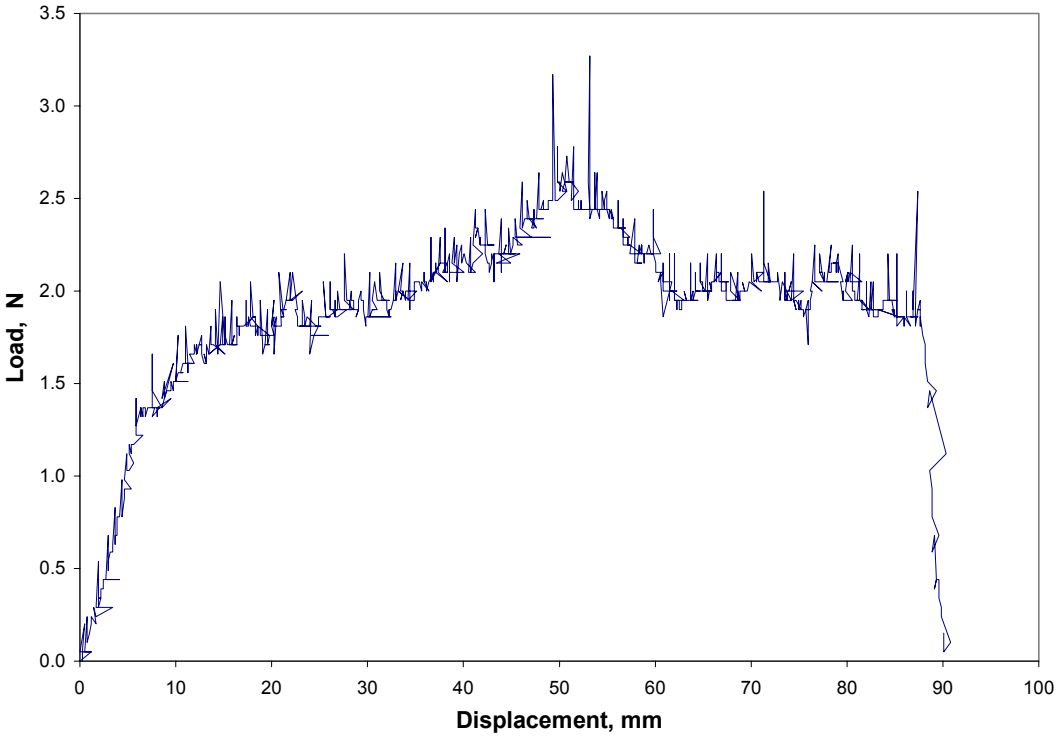

Figure B.238: Load Versus Displacement for Subject D, 120 degrees, 1 min, 500 mm/min, Test 3

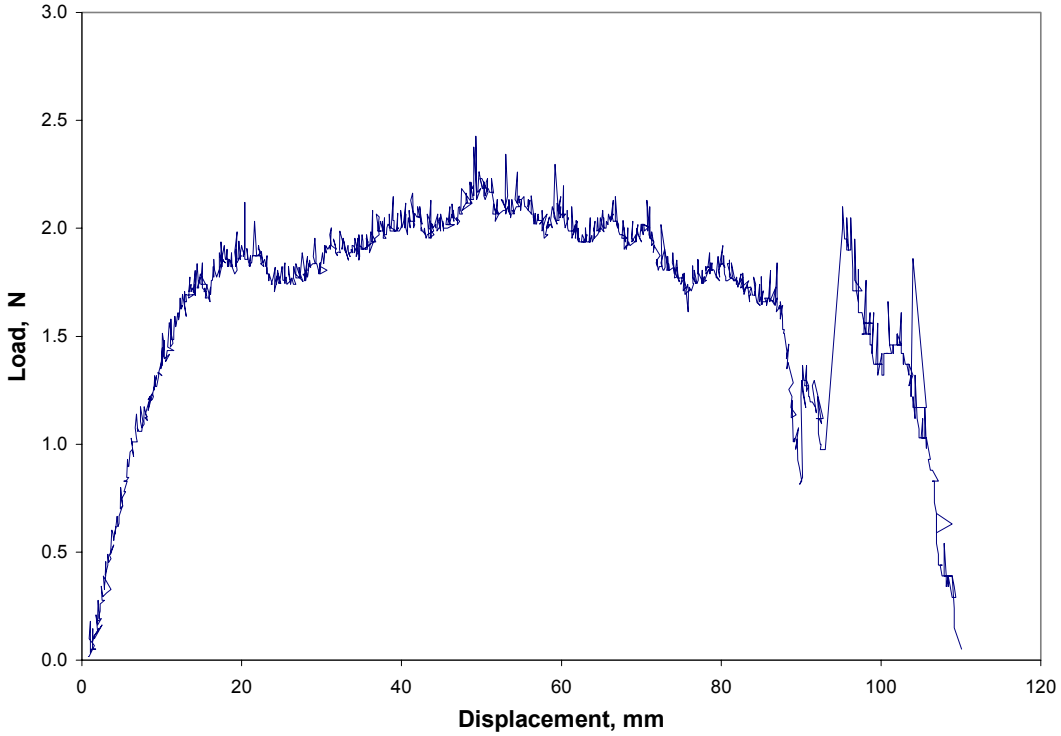

Figure B.239: Load Versus Displacement for Subject D, 120 degrees, 1 min, 500 mm/min, Average

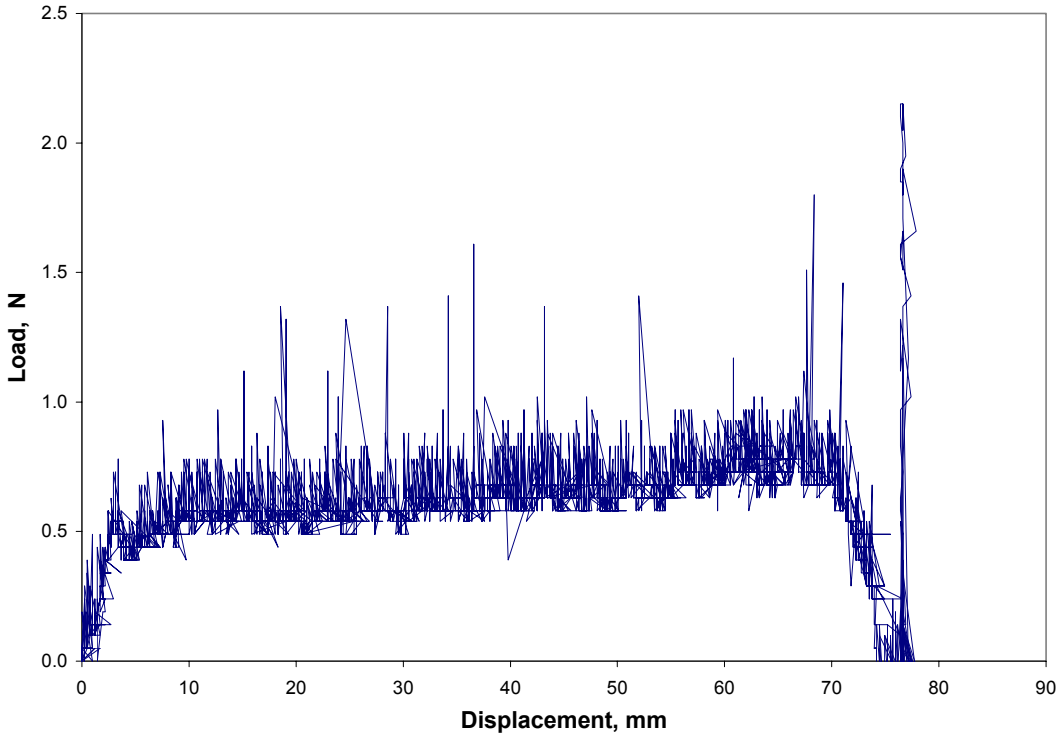

Figure B.240: Load Versus Displacement for Subject A, 150 degrees, 1 min, 100 mm/min, Test 1

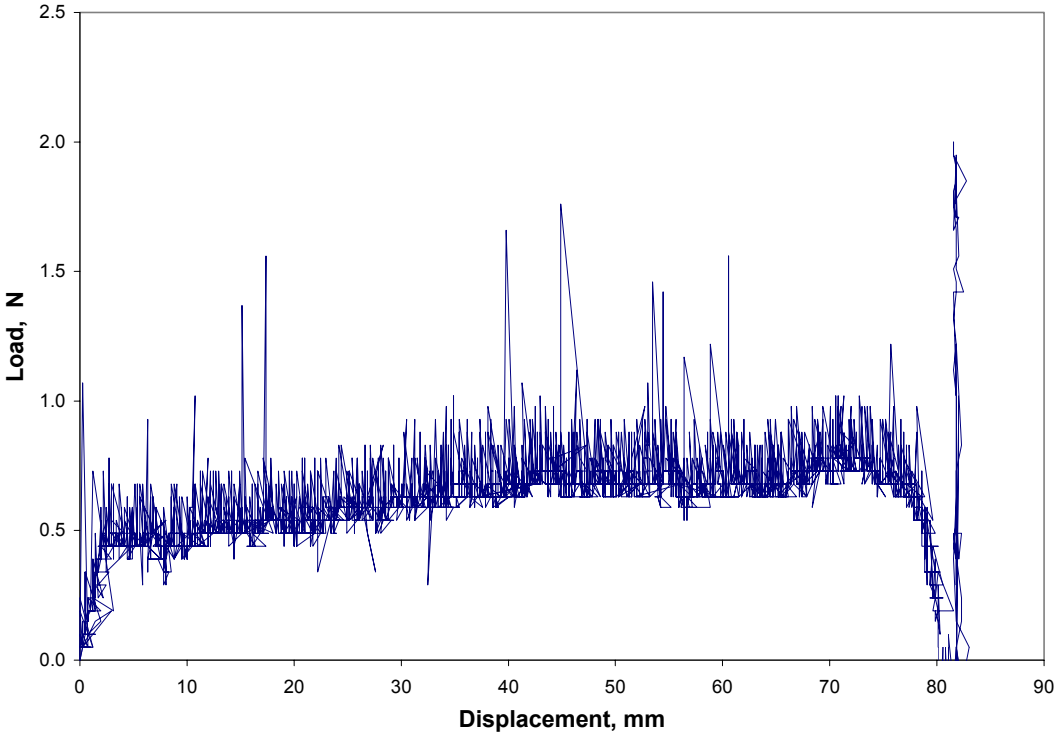

Figure B.241: Load Versus Displacement for Subject A, 150 degrees, 1 min, 100 mm/min, Test 2

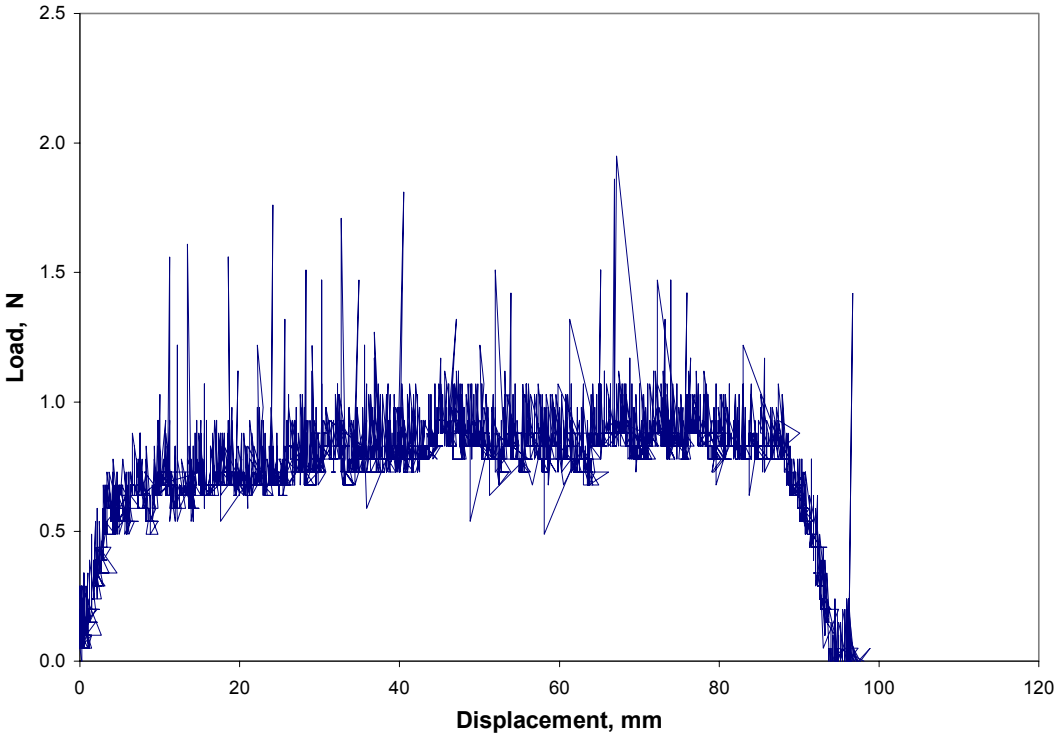

Figure B.242: Load Versus Displacement for Subject A, 150 degrees, 1 min, 100 mm/min, Test 3

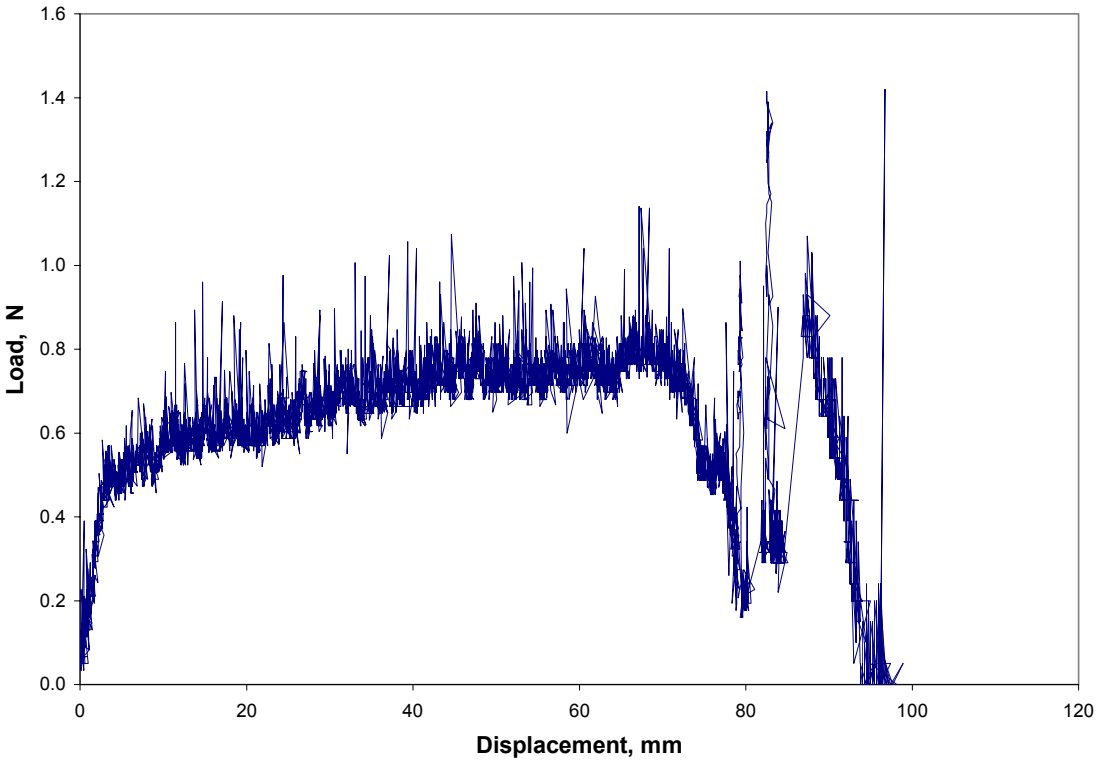

Figure B.243: Load Versus Displacement for Subject A, 150 degrees, 1 min, 100 mm/min, Average

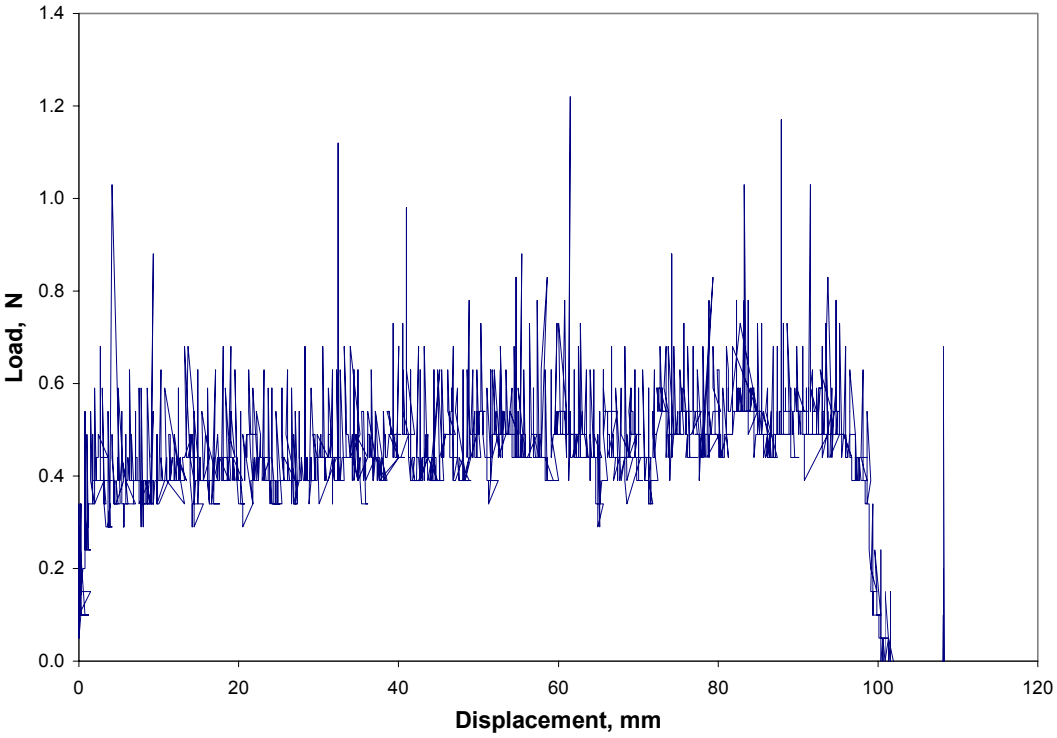

Figure B.244: Load Versus Displacement for Subject A, 150 degrees, 1 min, 300 mm/min, Test 1

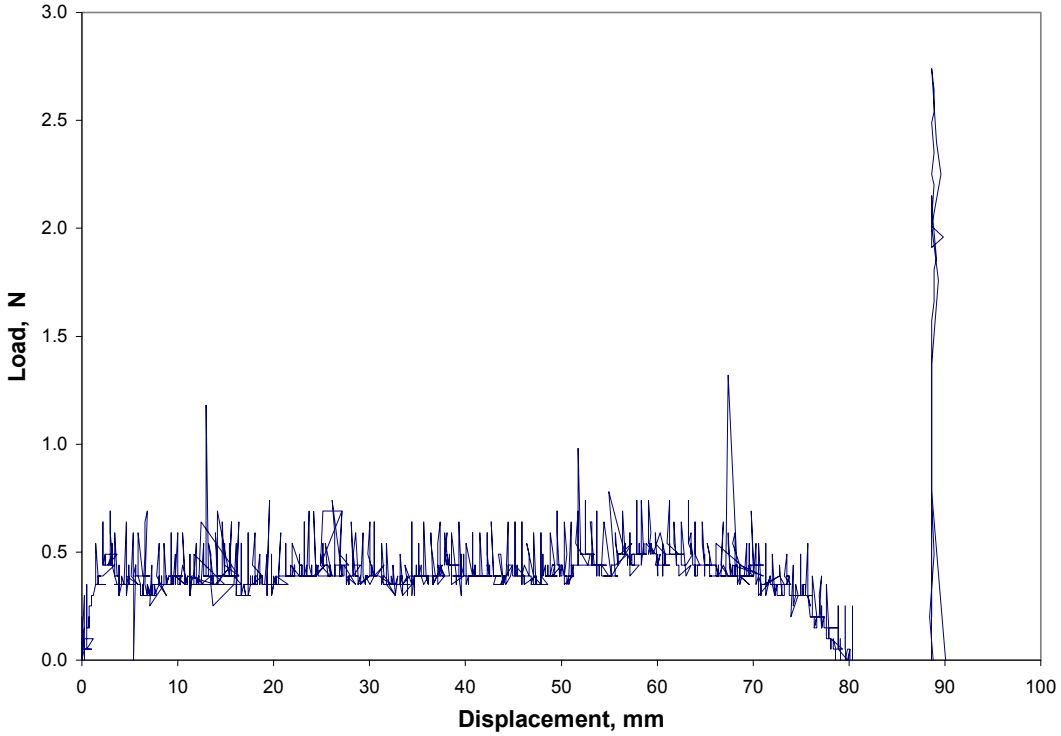

Figure B.245: Load Versus Displacement for Subject A, 150 degrees, 1 min, 300 mm/min, Test 2

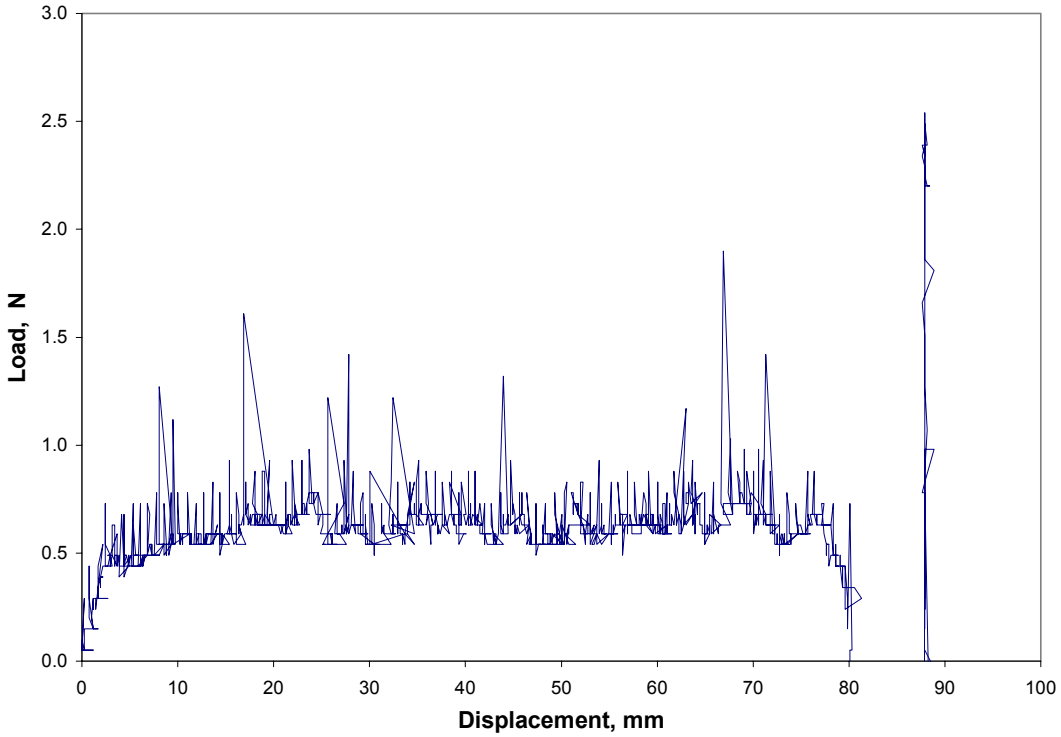

Figure B.246: Load Versus Displacement for Subject A, 150 degrees, 1 min, 300 mm/min, Test 3

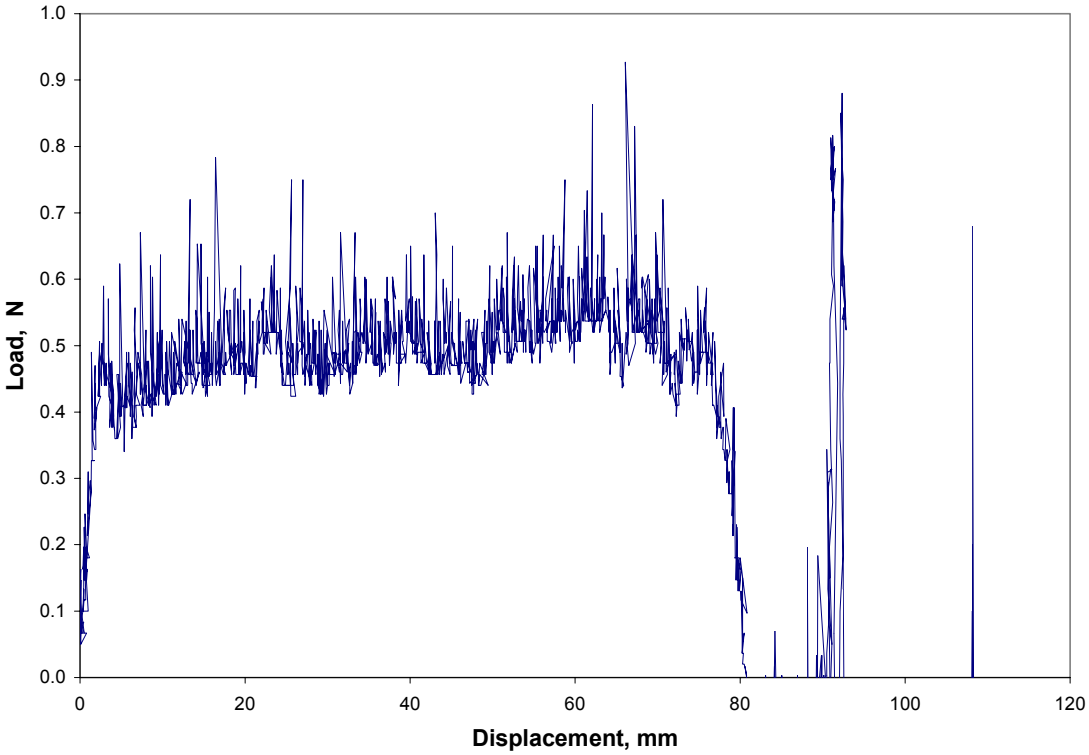

Figure B.247: Load Versus Displacement for Subject A, 150 degrees, 1 min, 300 mm/min, Average

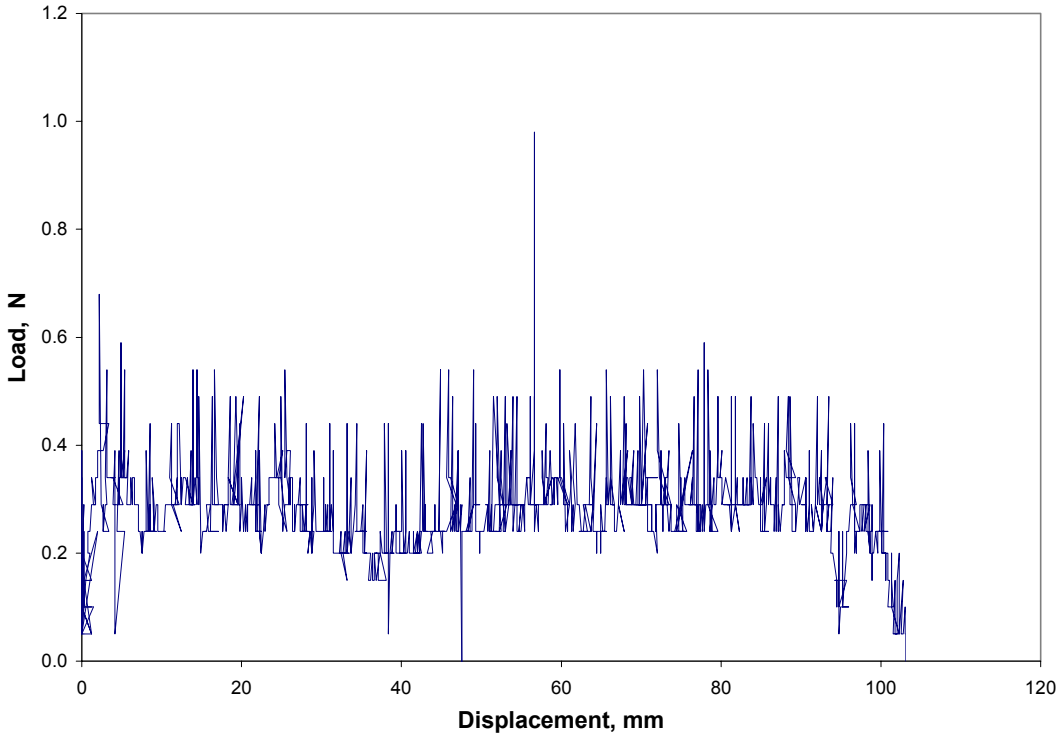

Figure B.248: Load Versus Displacement for Subject A, 150 degrees, 1 min, 500 mm/min, Test 1

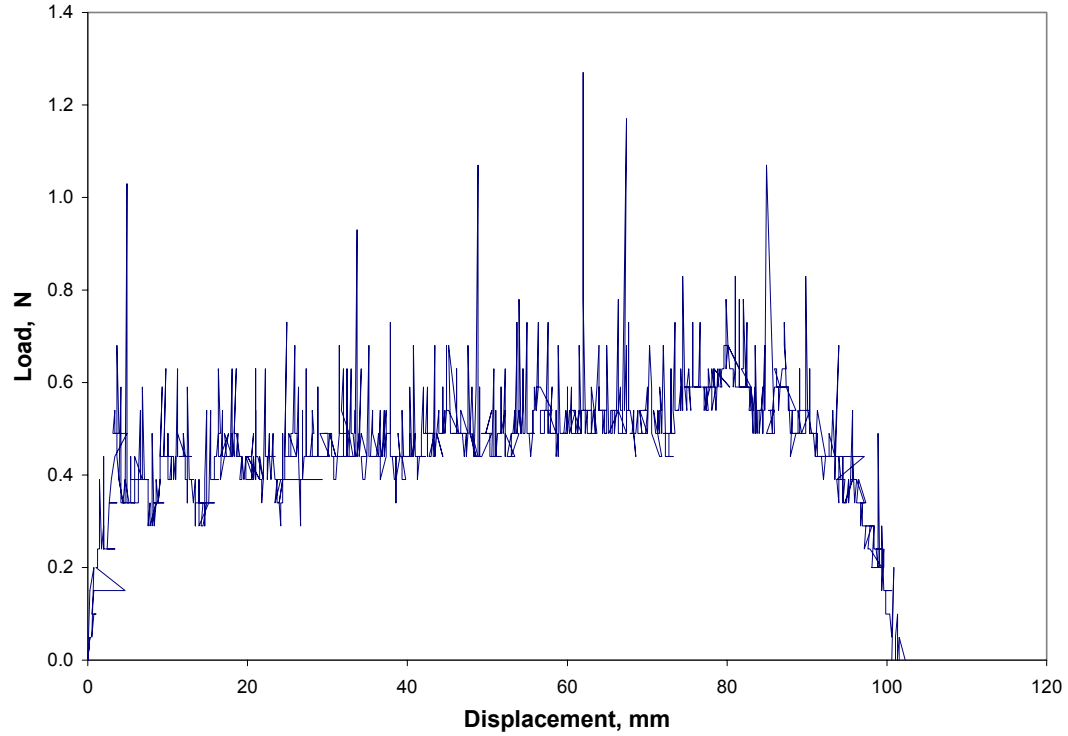

Figure B.249: Load Versus Displacement for Subject A, 150 degrees, 1 min, 500 mm/min, Test 2

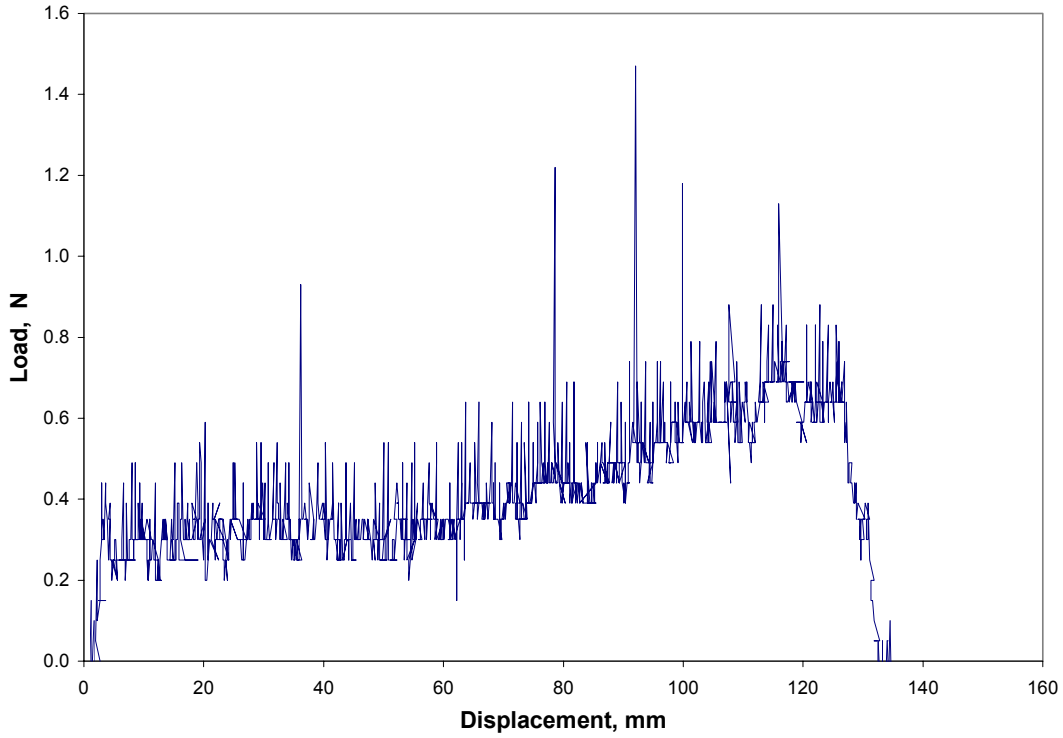

Figure B.250: Load Versus Displacement for Subject A, 150 degrees, 1 min, 500 mm/min, Test 3

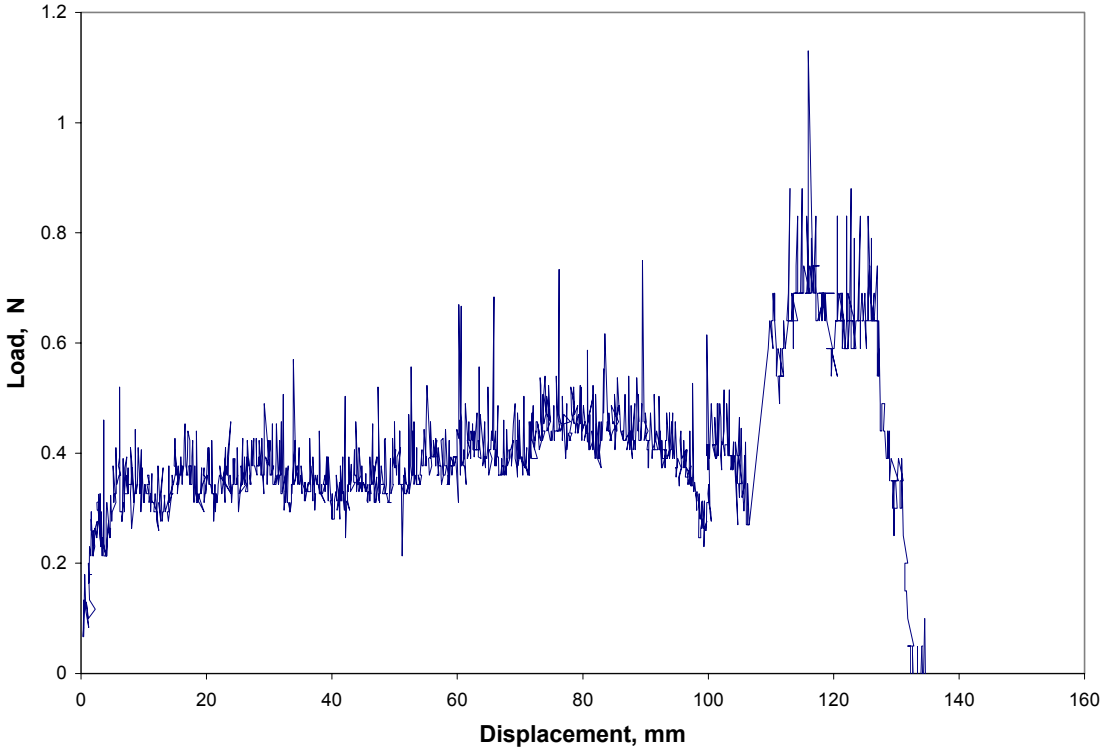

Figure B.251: Load Versus Displacement for Subject A, 150 degrees, 1 min, 500 mm/min, Average

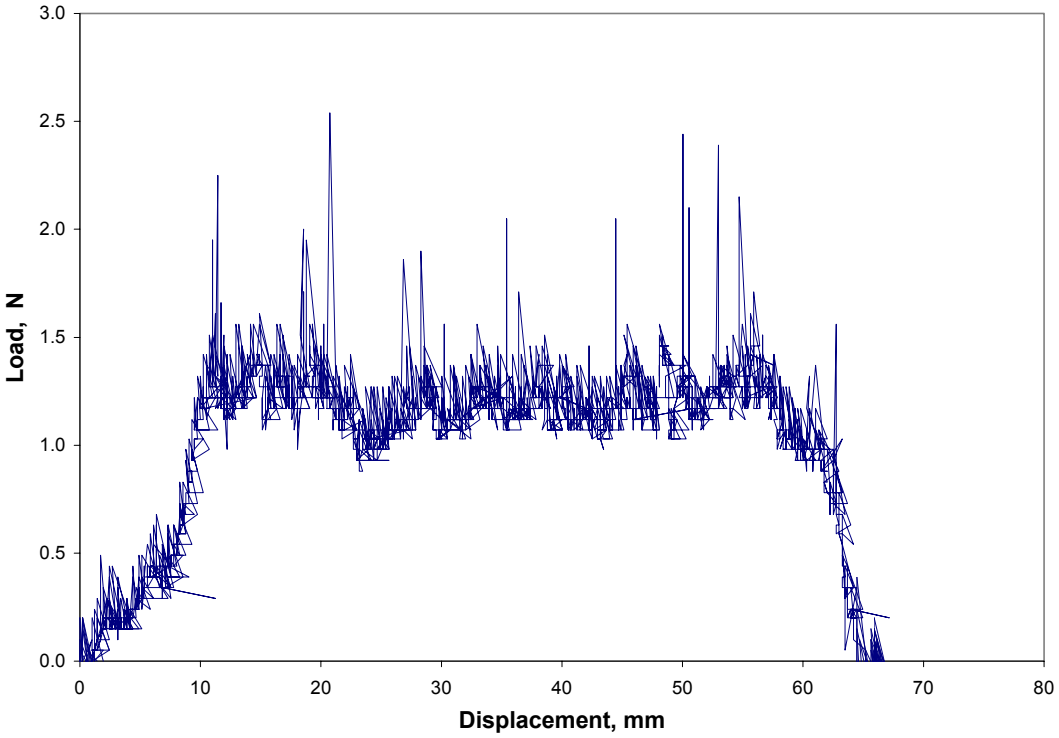

Figure B.252: Load Versus Displacement for Subject D, 150 degrees, 1 min, 100 mm/min, Test 1

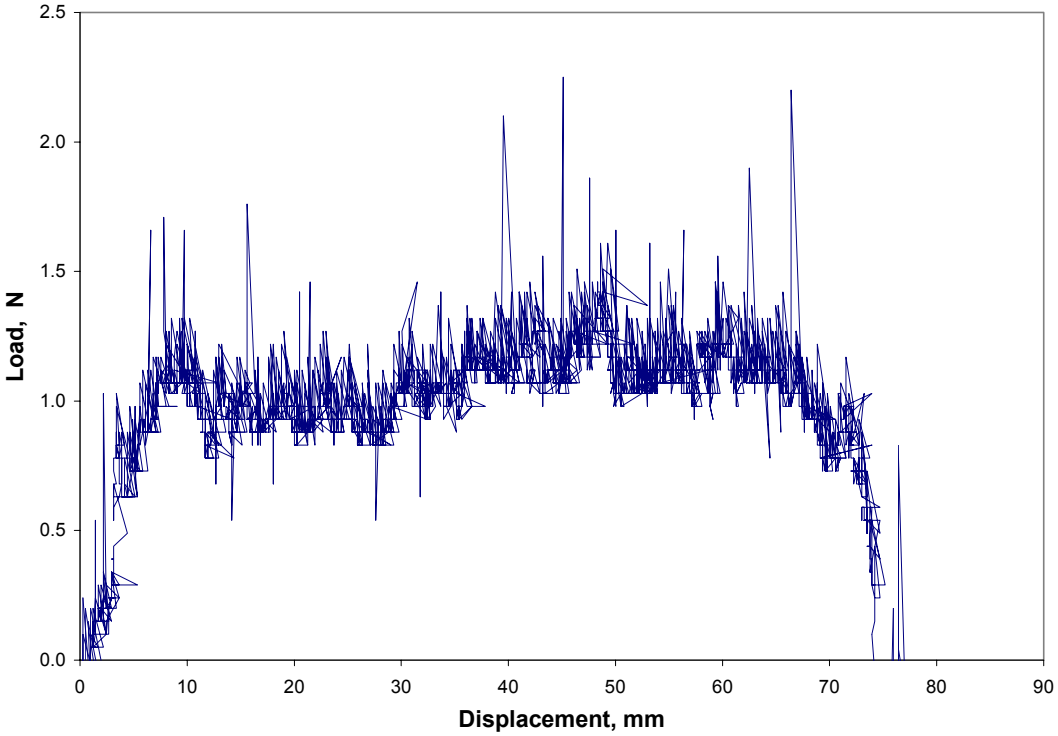

Figure B.253: Load Versus Displacement for Subject D, 150 degrees, 1 min, 100 mm/min, Test 2

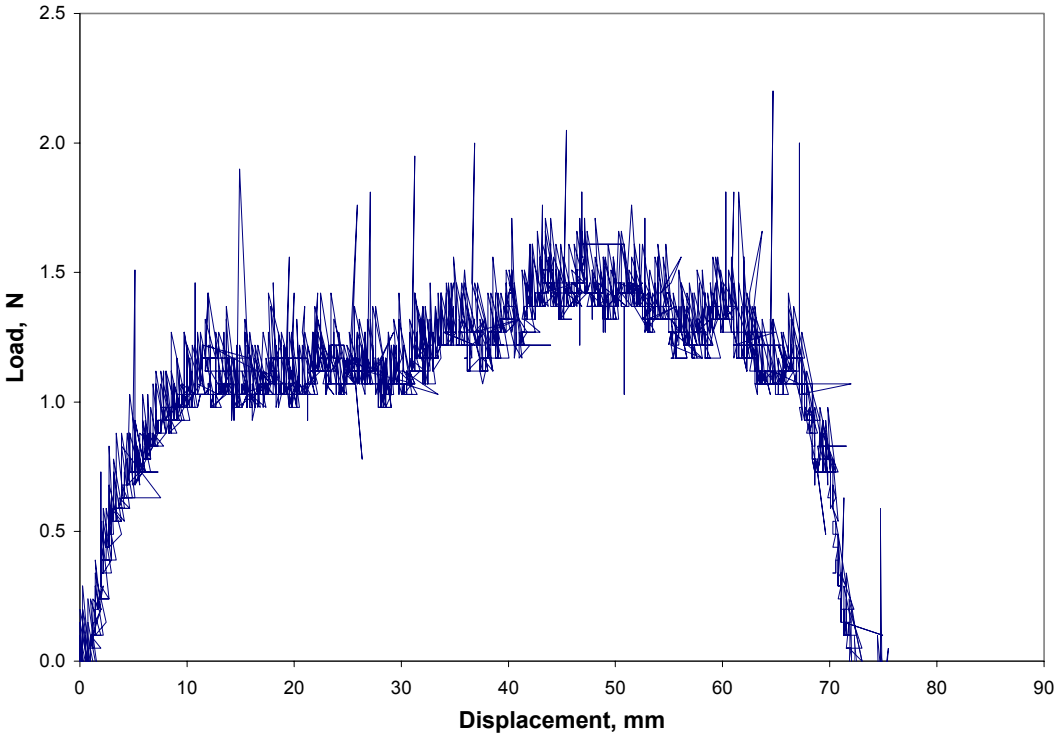

Figure B.254: Load Versus Displacement for Subject D, 150 degrees, 1 min, 100 mm/min, Test 3

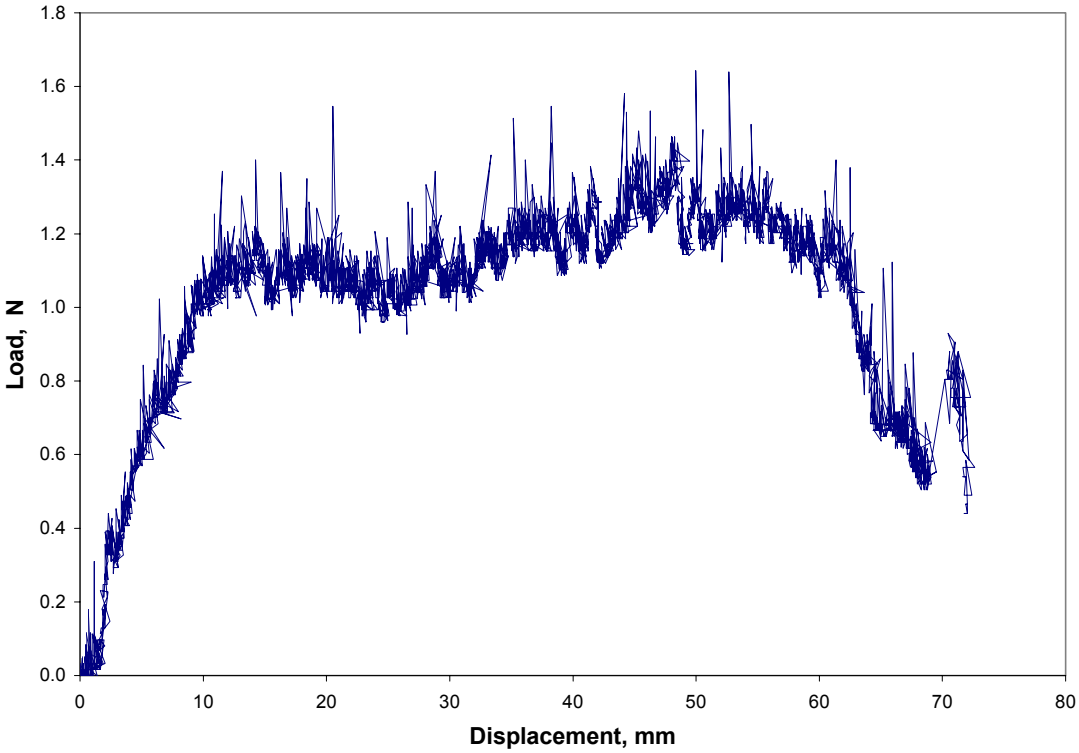

Figure B.255: Load Versus Displacement for Subject D, 150 degrees, 1 min, 100 mm/min, Average

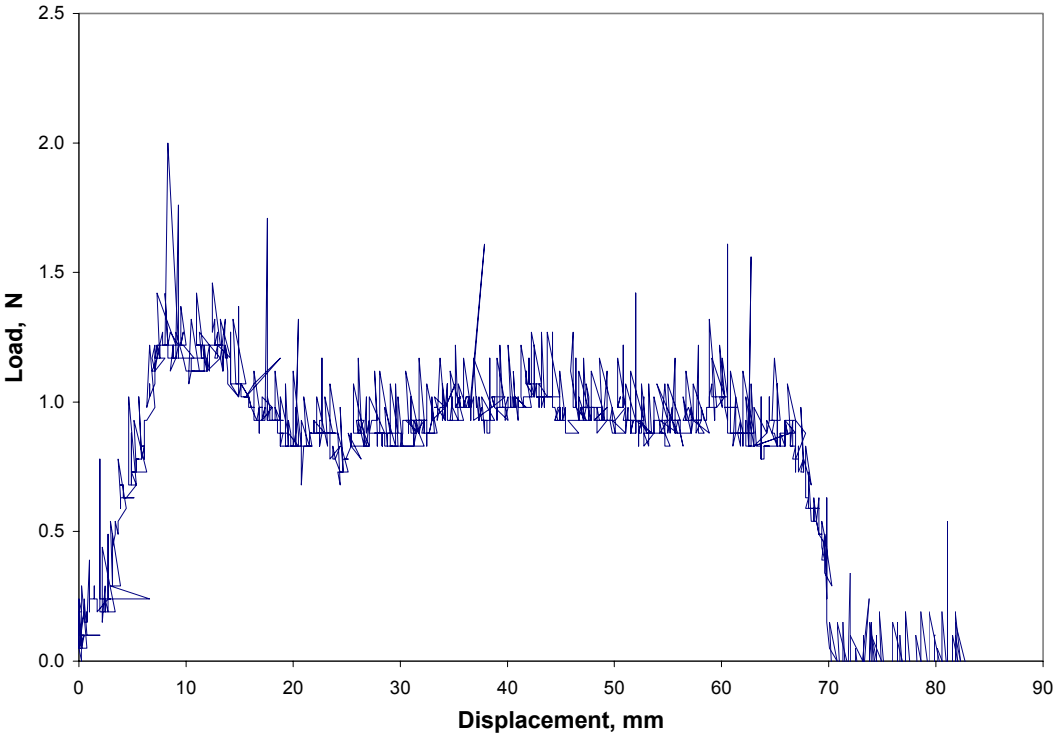

Figure B.256: Load Versus Displacement for Subject D, 150 degrees, 1 min, 300 mm/min, Test 1

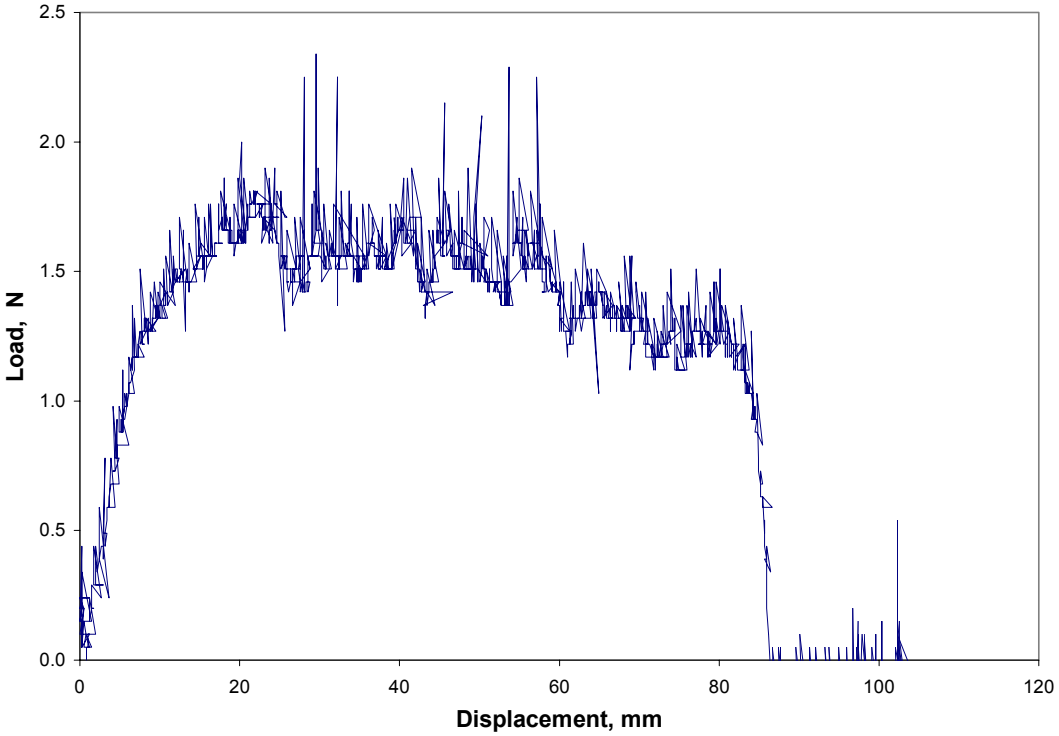

Figure B.257: Load Versus Displacement for Subject D, 150 degrees, 1 min, 300 mm/min, Test 2

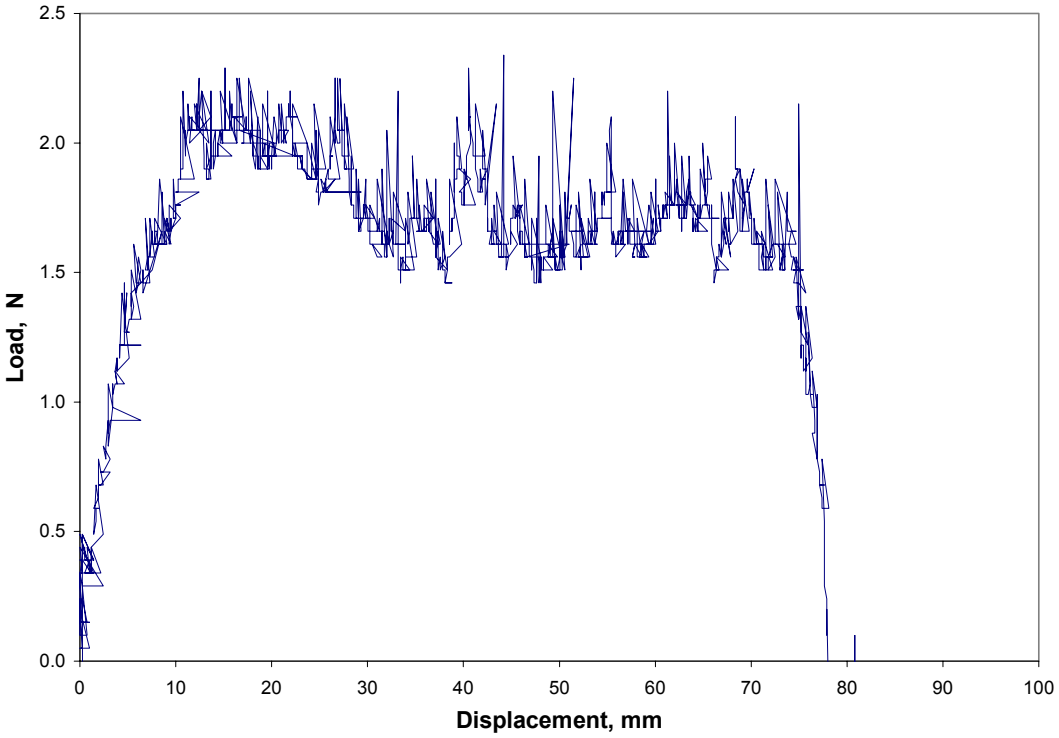

Figure B.258: Load Versus Displacement for Subject D, 150 degrees, 1 min, 300 mm/min, Test 3

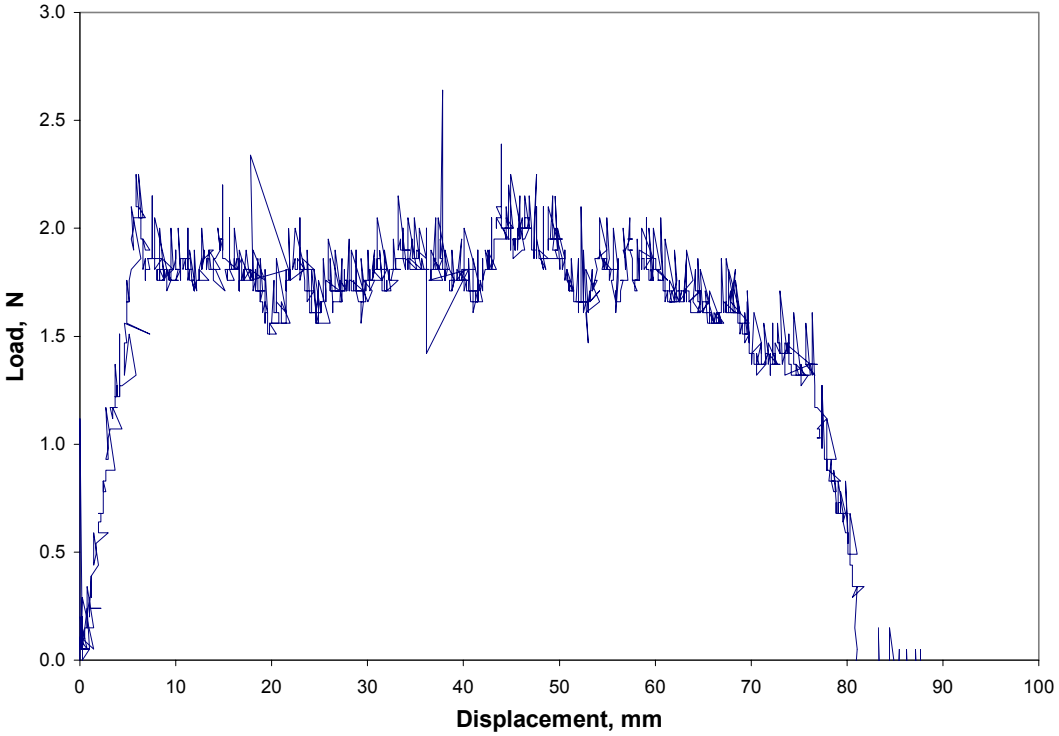

Figure B.259: Load Versus Displacement for Subject D, 150 degrees, 1 min, 300 mm/min, Test 4

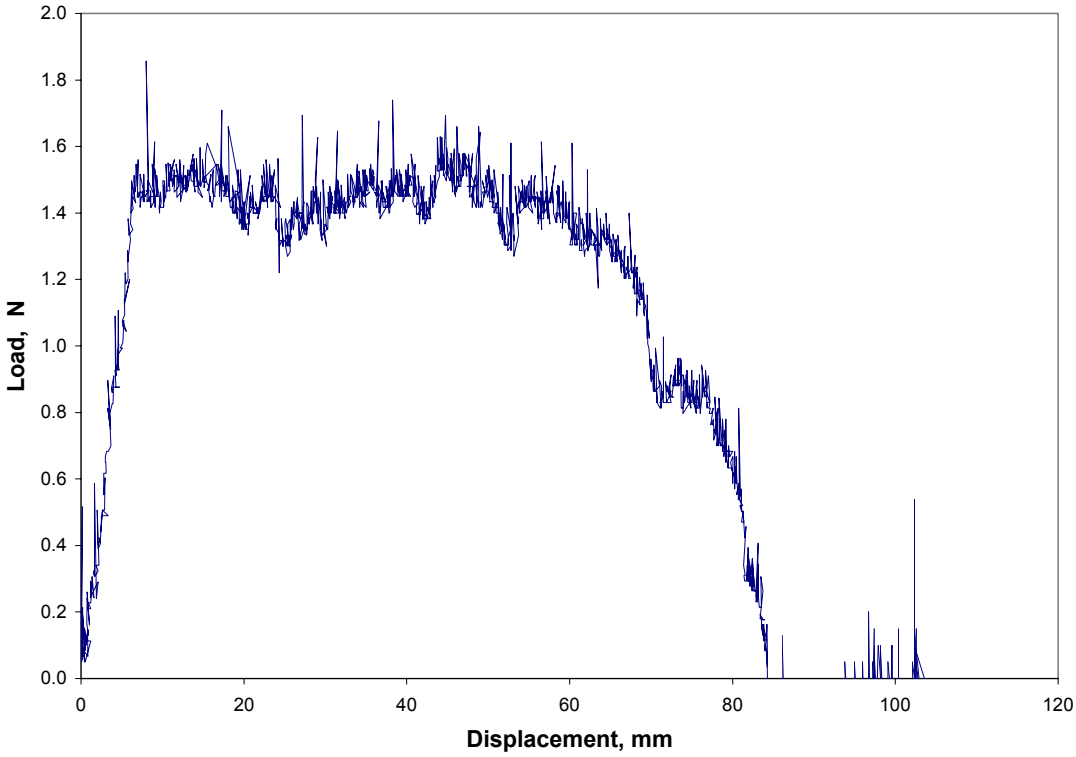

Figure B.260: Load Versus Displacement for Subject D, 150 degrees, 1 min, 300 mm/min, Average

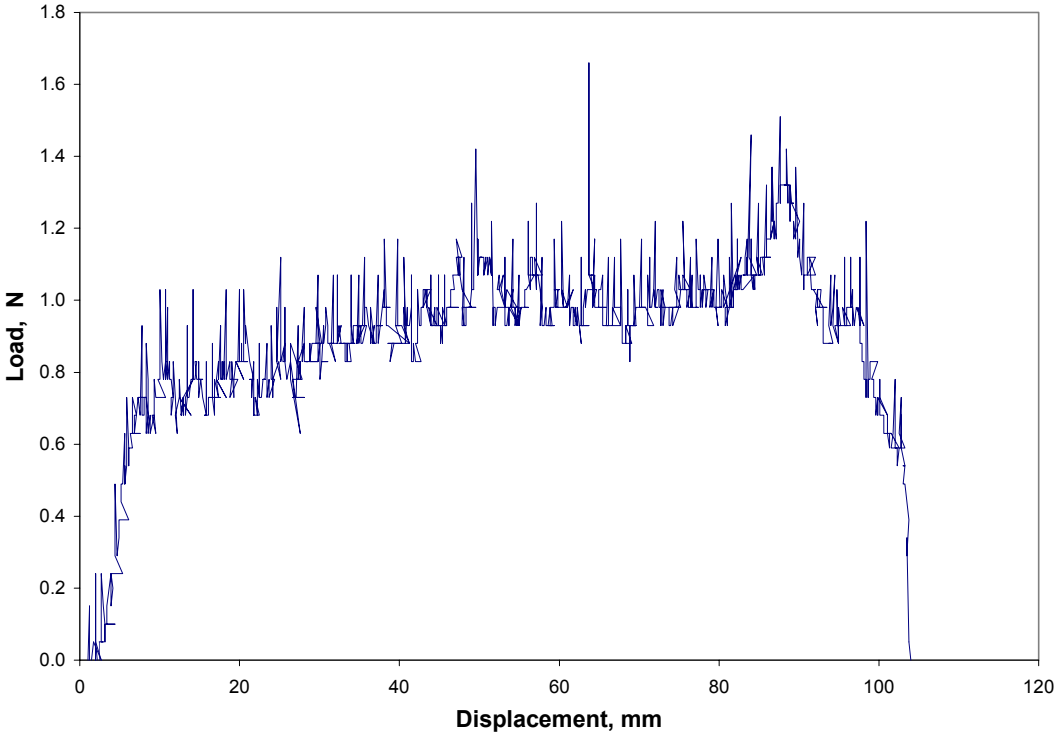

Figure B.261: Load Versus Displacement for Subject D, 150 degrees, 1 min, 500 mm/min, Test 1

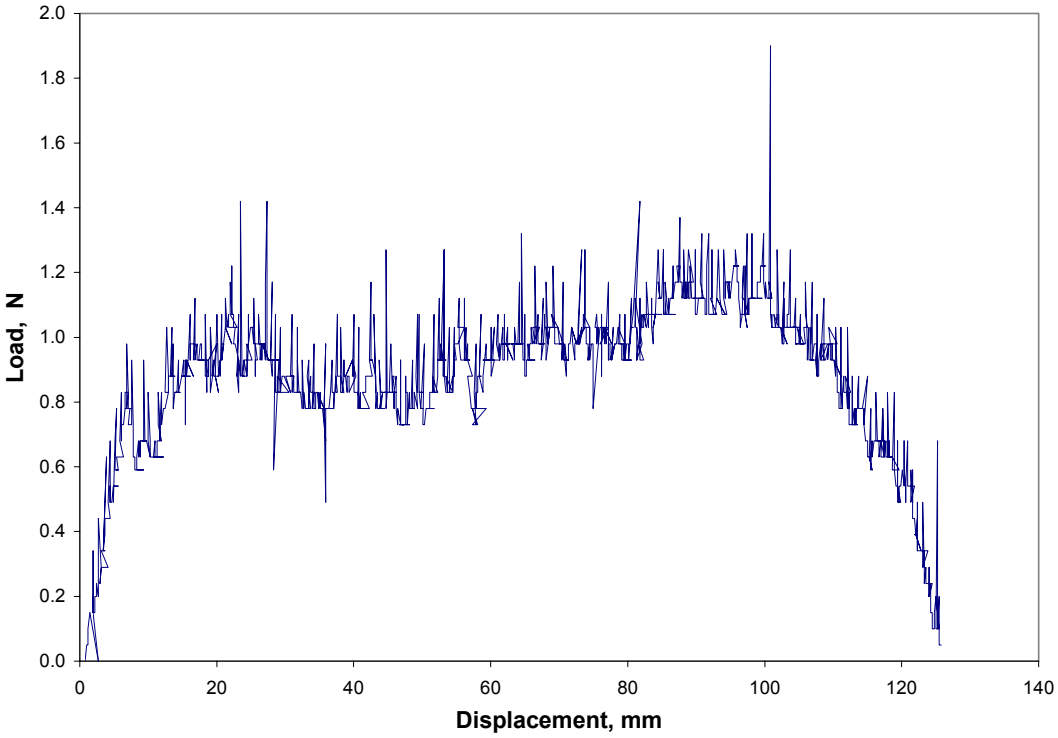

Figure B.262: Load Versus Displacement for Subject D, 150 degrees, 1 min, 500 mm/min, Test 2

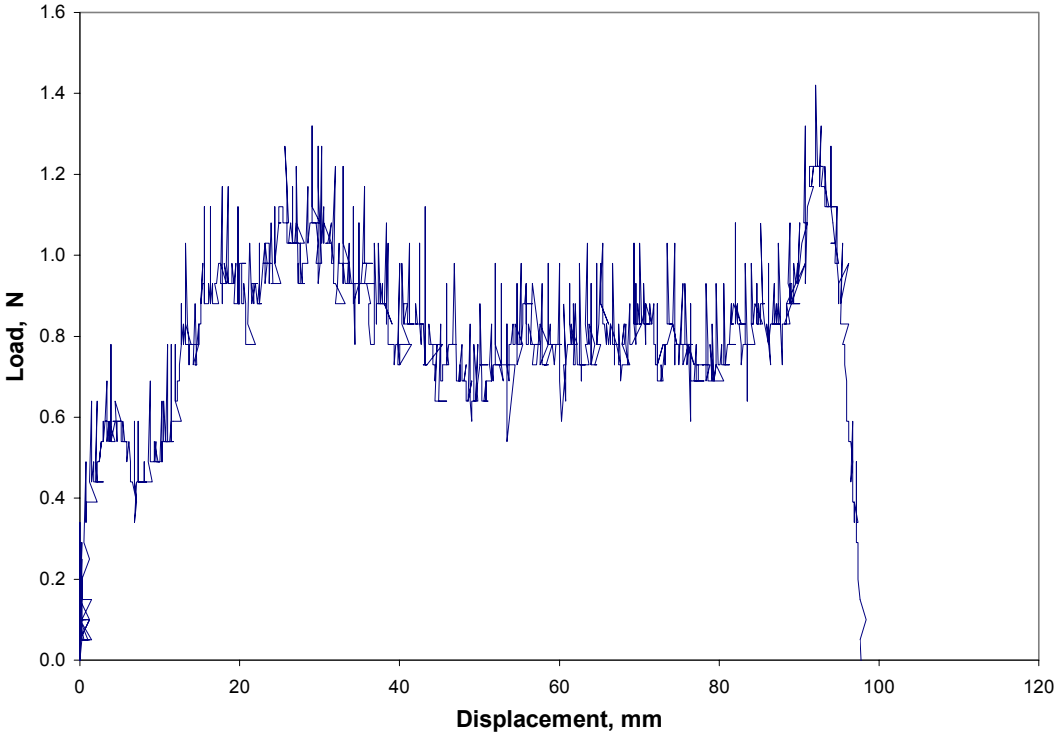

Figure B.263: Load Versus Displacement for Subject D, 150 degrees, 1 min, 500 mm/min, Test 3

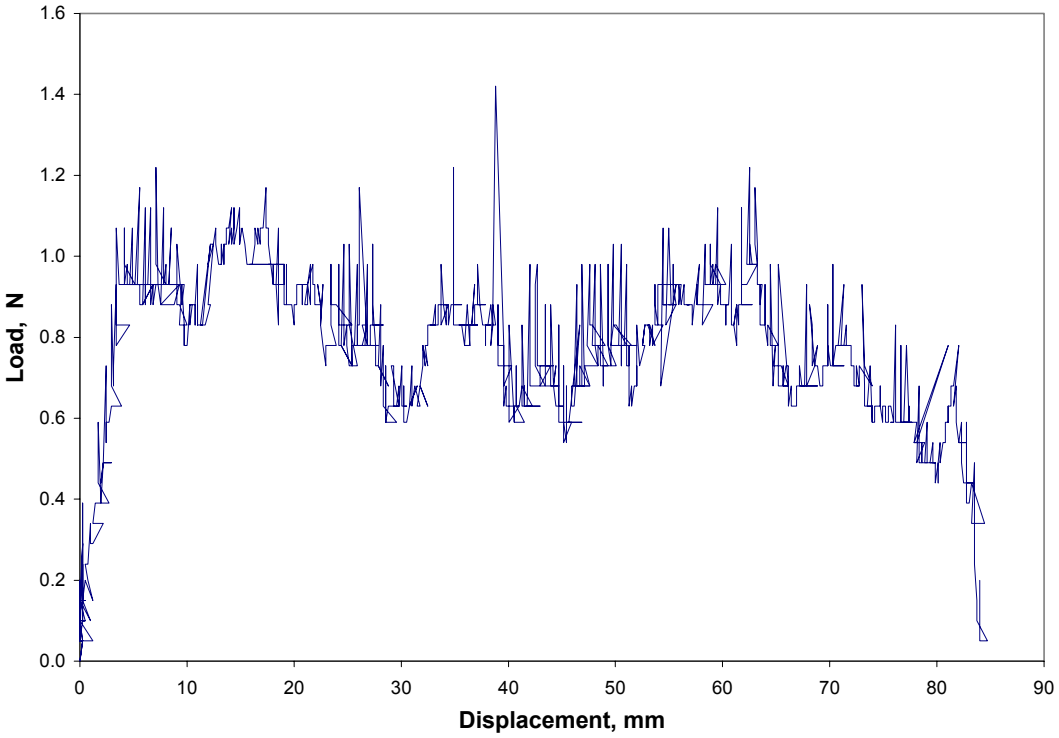

Figure B.264: Load Versus Displacement for Subject D, 150 degrees, 1 min, 500 mm/min, Test 4

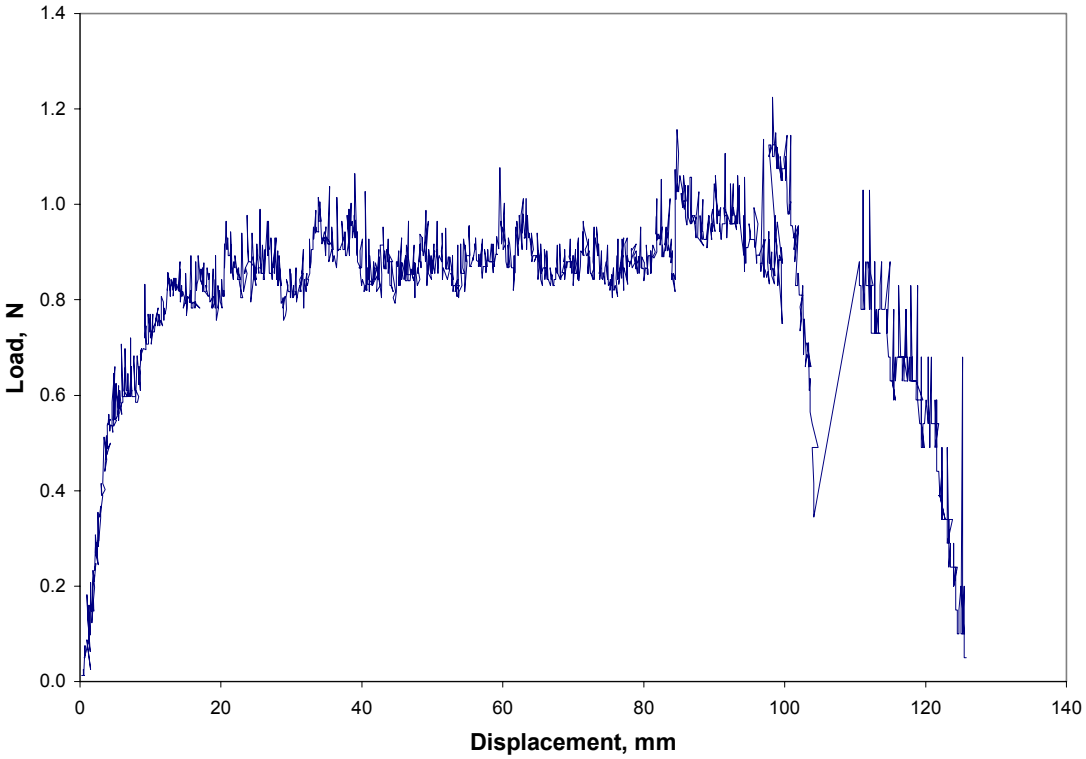

Figure B.265: Load Versus Displacement for Subject D, 150 degrees, 1 min, 500 mm/min, Average

Appendix C

Experimentation Series Two Results

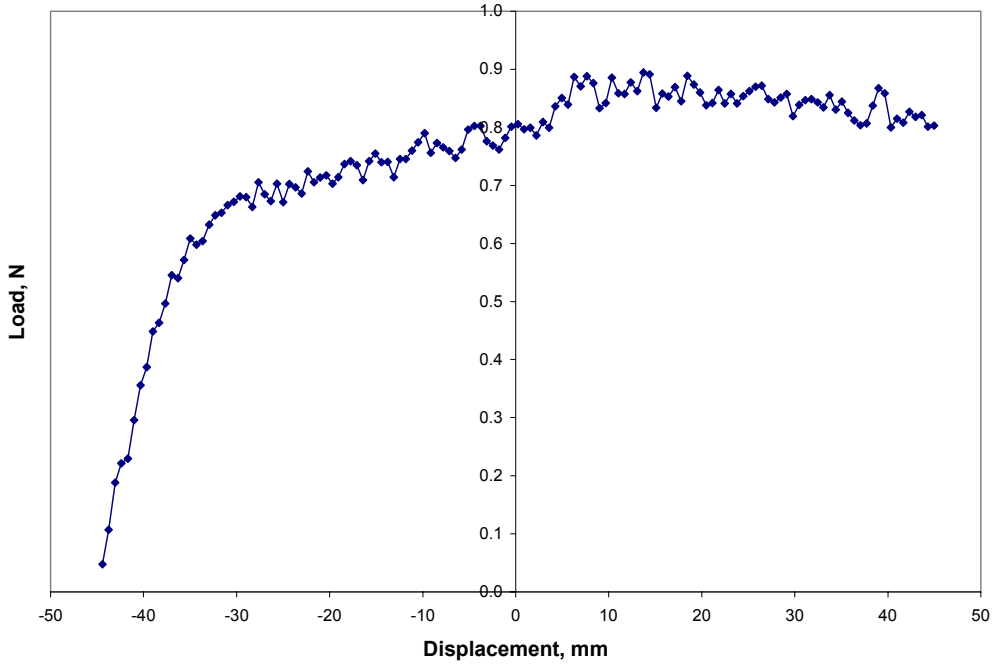

Figure C.1: Load Versus Displacement for Subject A, 180 degrees, 200 mm/min, Test 1

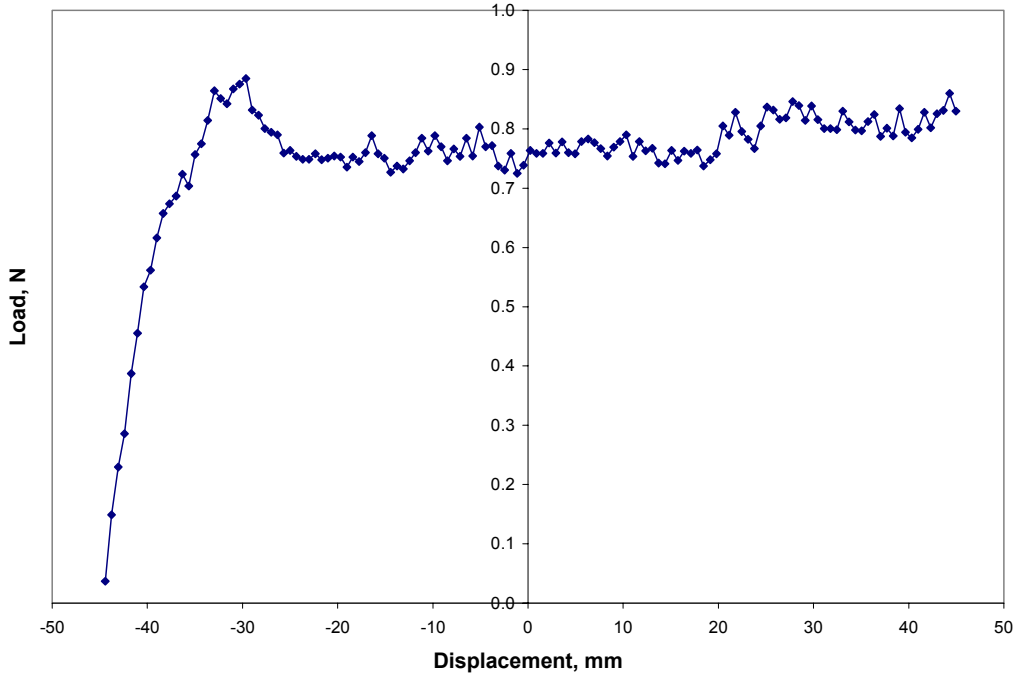

Figure C.2: Load Versus Displacement for Subject A, 180 degrees, 200 mm/min, Test 2

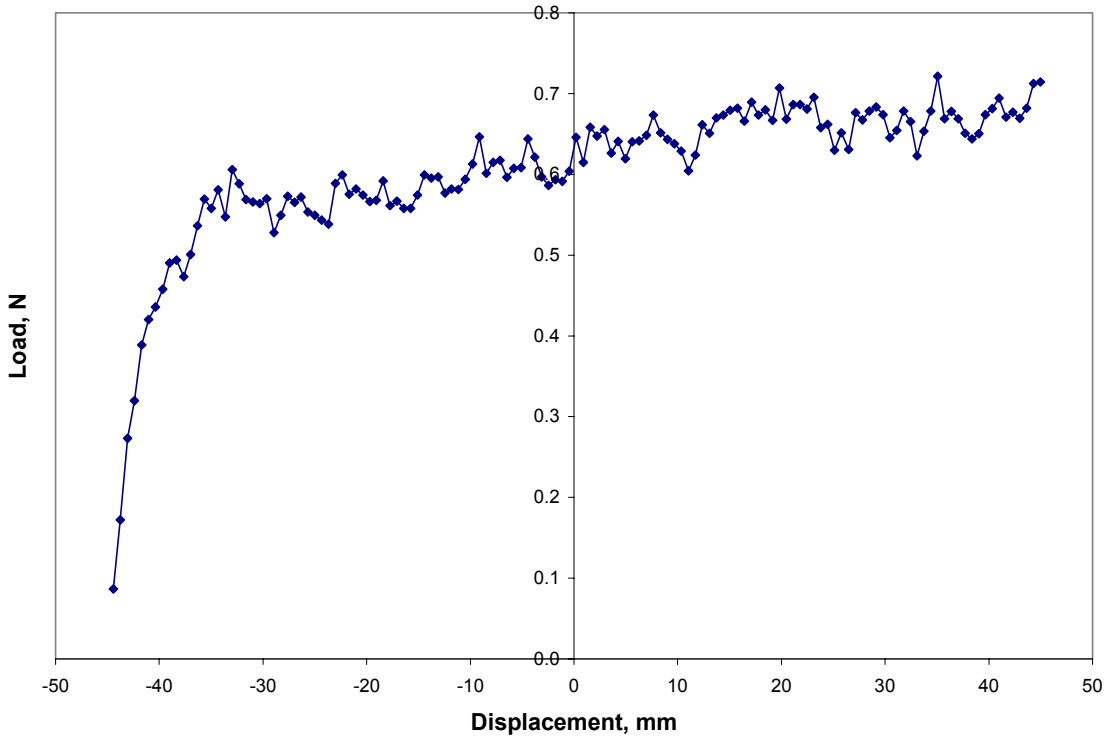

Figure C.3: Load Versus Displacement for Subject A, 180 degrees, 200 mm/min, Test 3

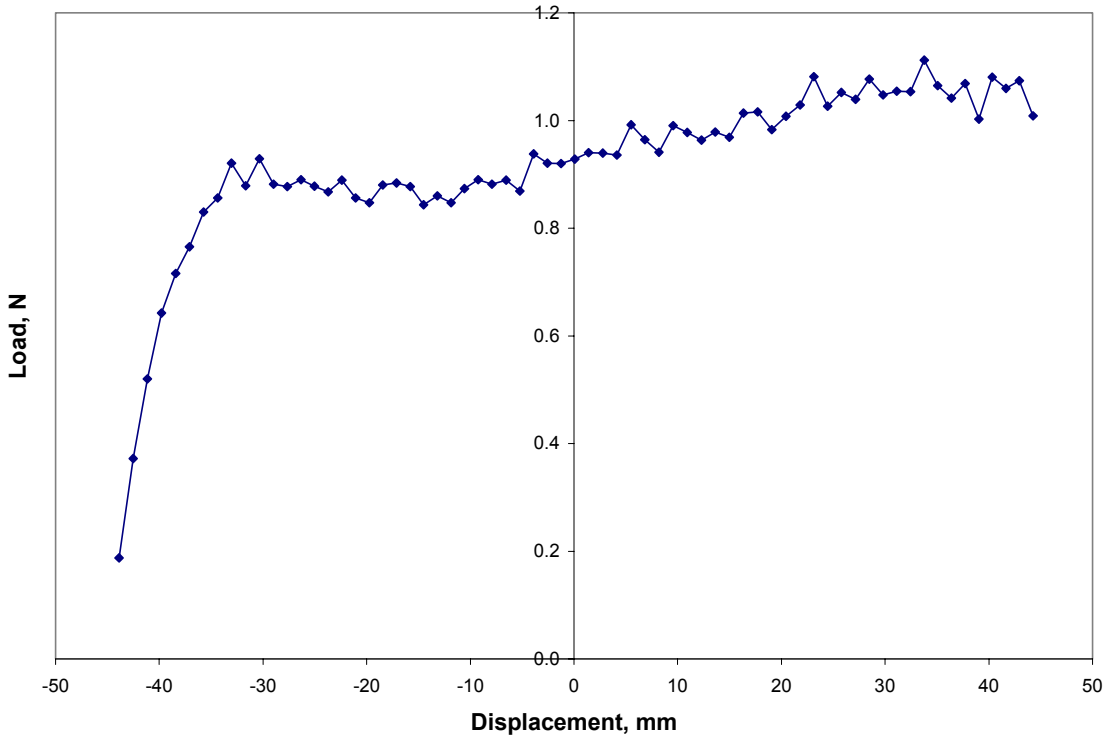

Figure C.4: Load Versus Displacement for Subject A, 180 degrees, 400 mm/min, Test 1

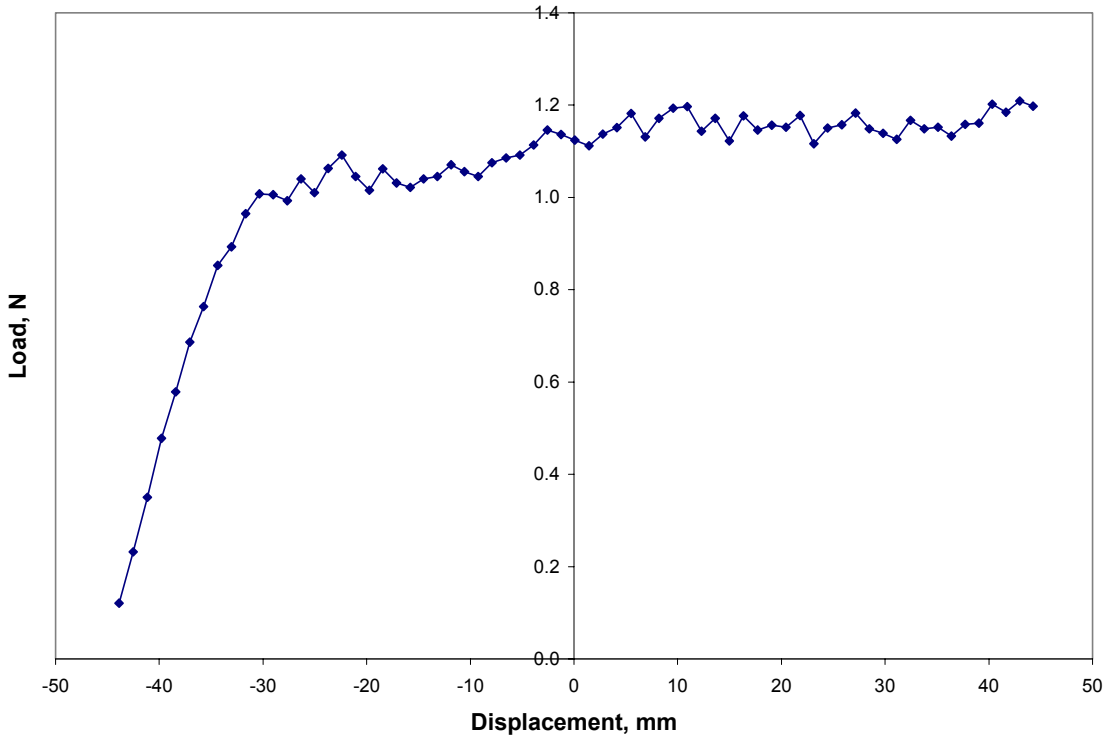

Figure C.5: Load Versus Displacement for Subject A, 180 degrees, 400 mm/min, Test 2

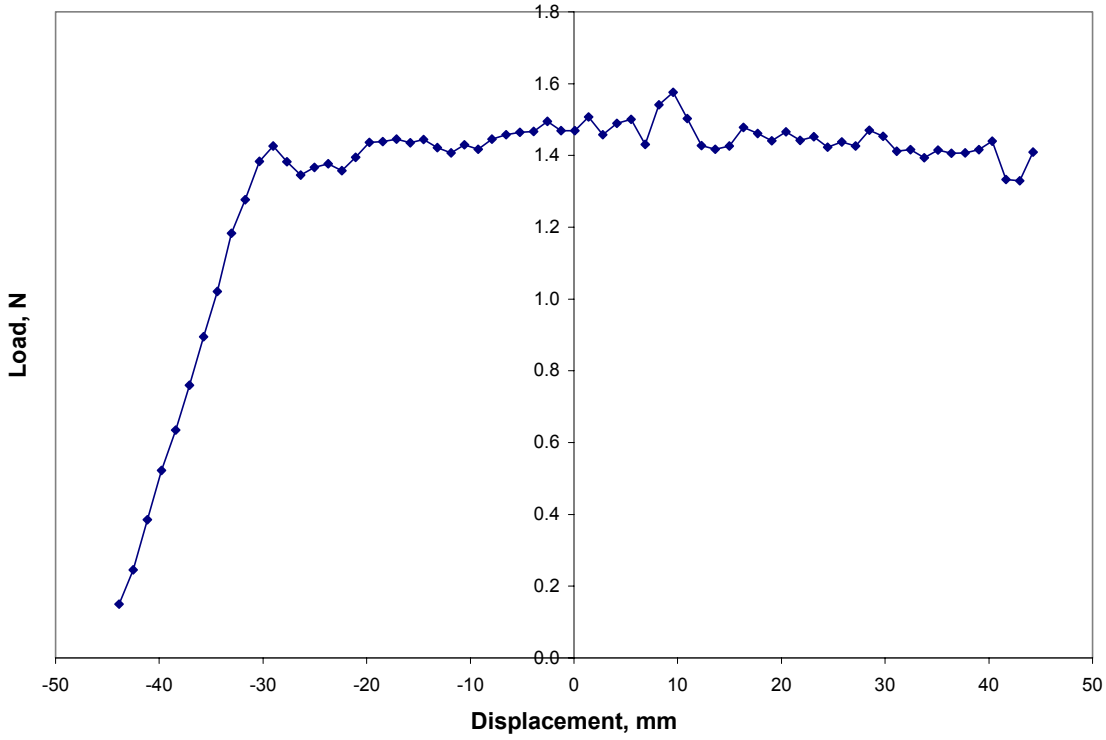

Figure C.6: Load Versus Displacement for Subject A, 180 degrees, 400 mm/min, Test 3

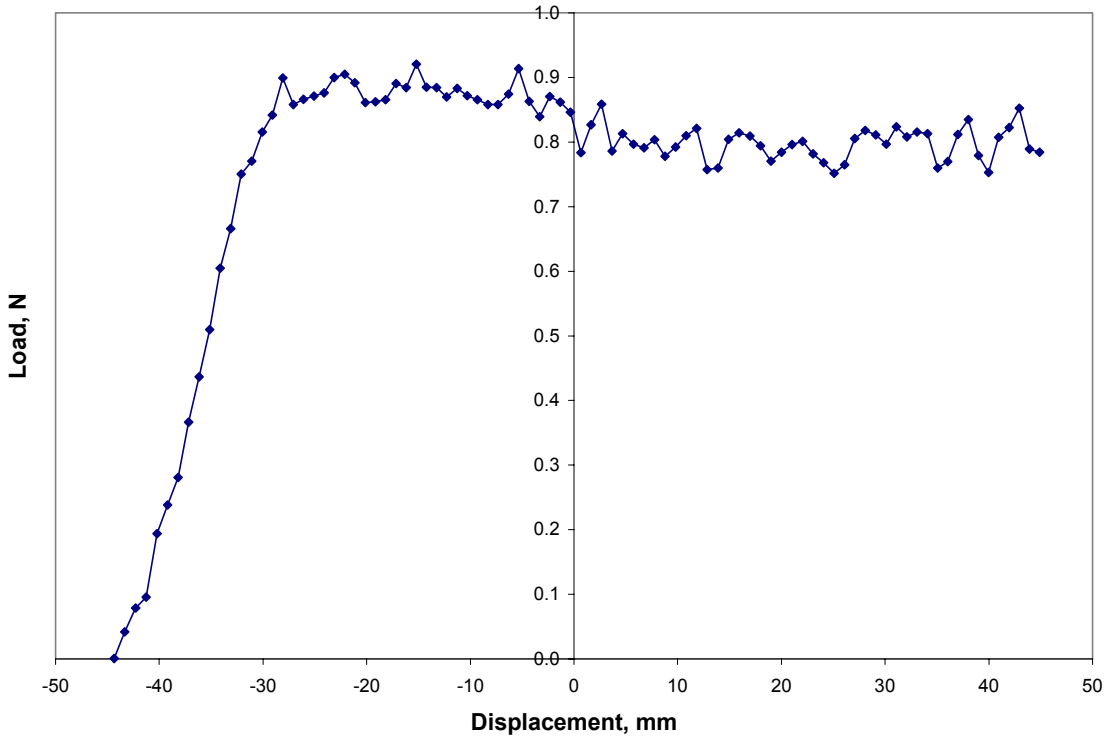

Figure C.7: Load Versus Displacement for Subject A, 180 degrees, 600 mm/min, Test 1

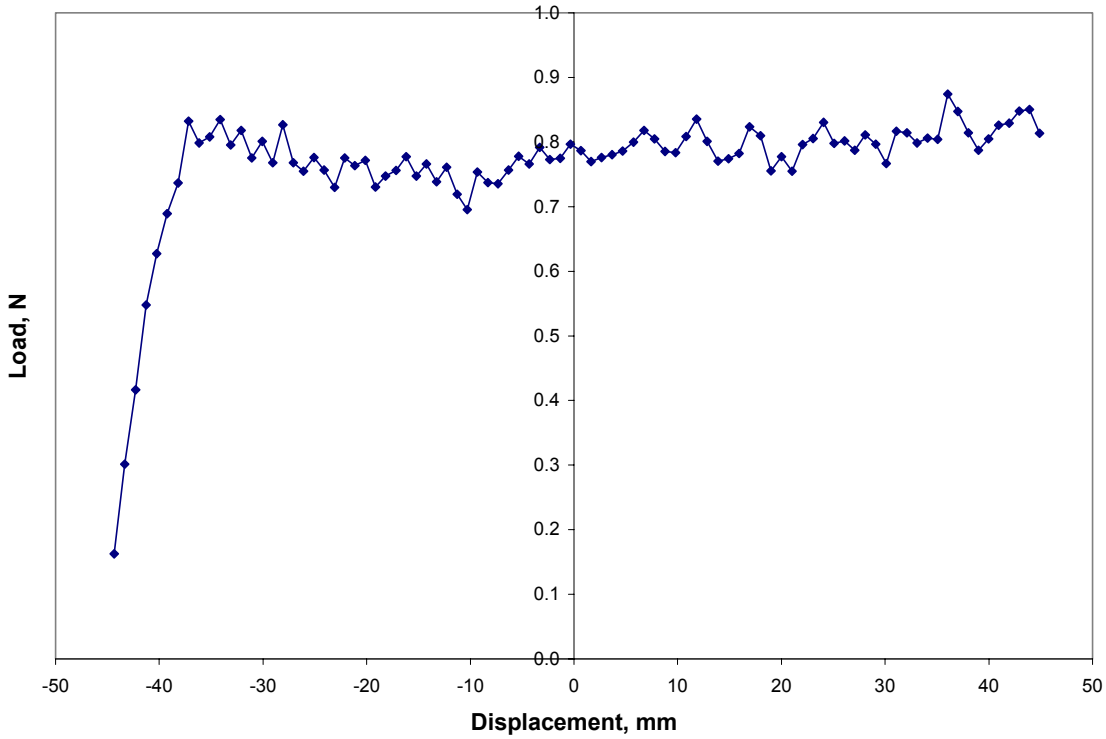

Figure C.8: Load Versus Displacement for Subject A, 180 degrees, 600 mm/min, Test 2

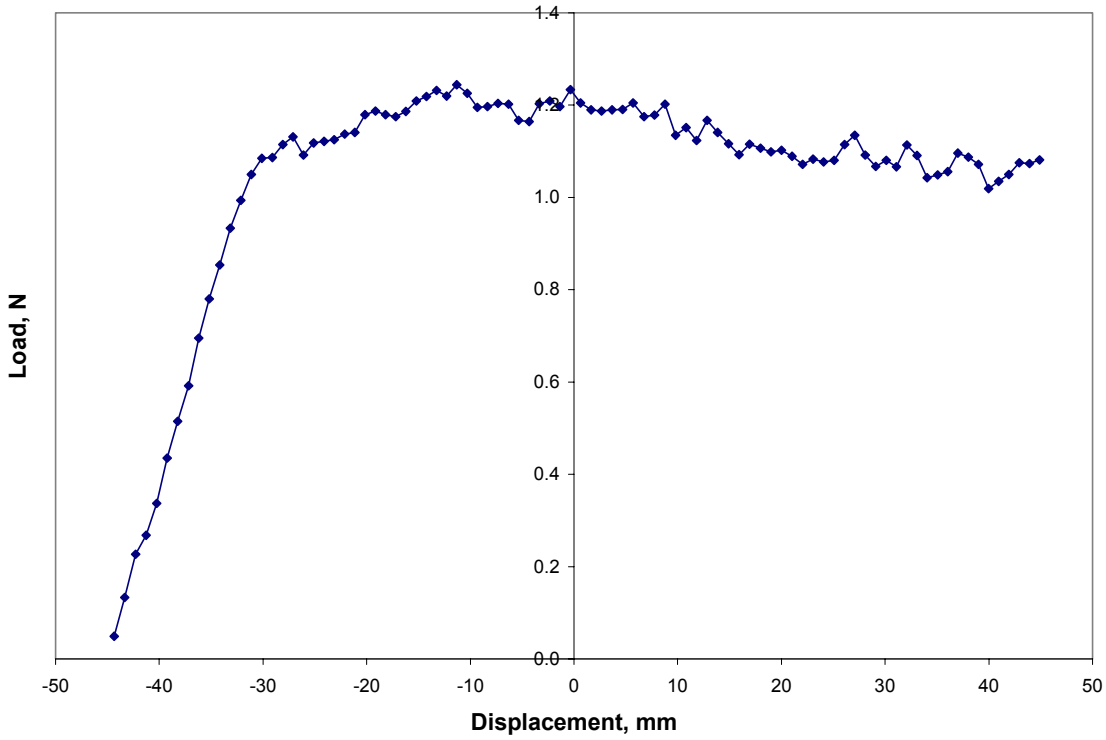

Figure C.9: Load Versus Displacement for Subject A, 180 degrees, 600 mm/min, Test 3

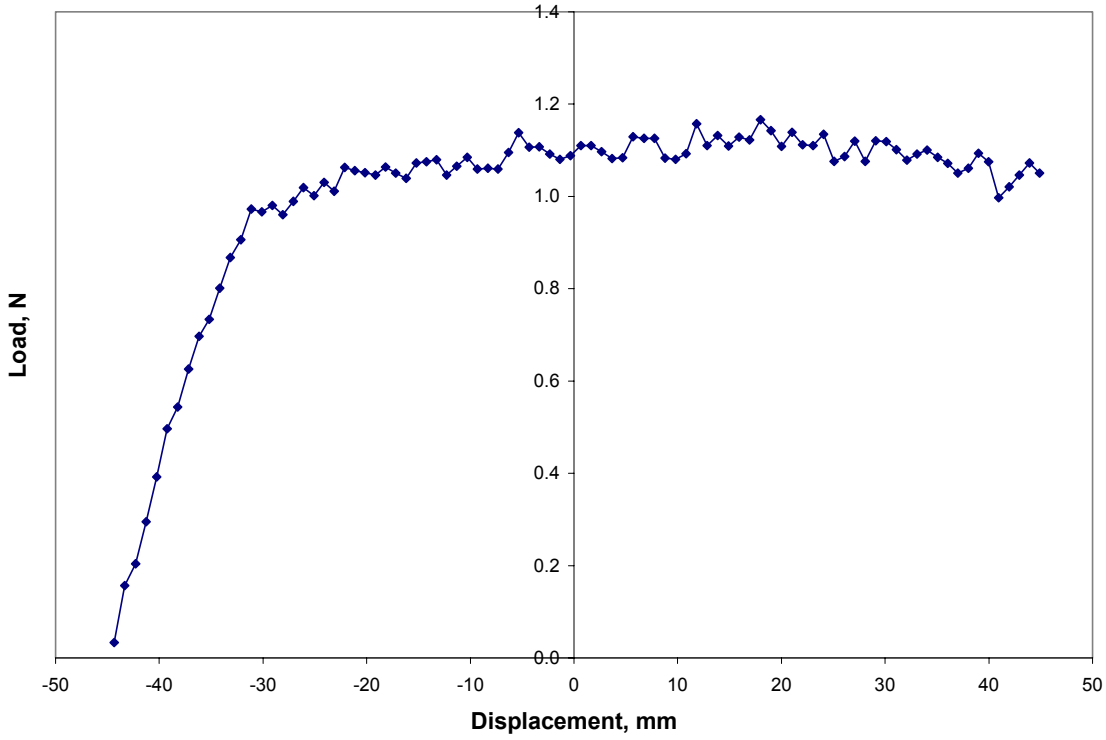

Figure C.10: Load Versus Displacement for Subject A, 180 degrees, 600 mm/min, Test 4

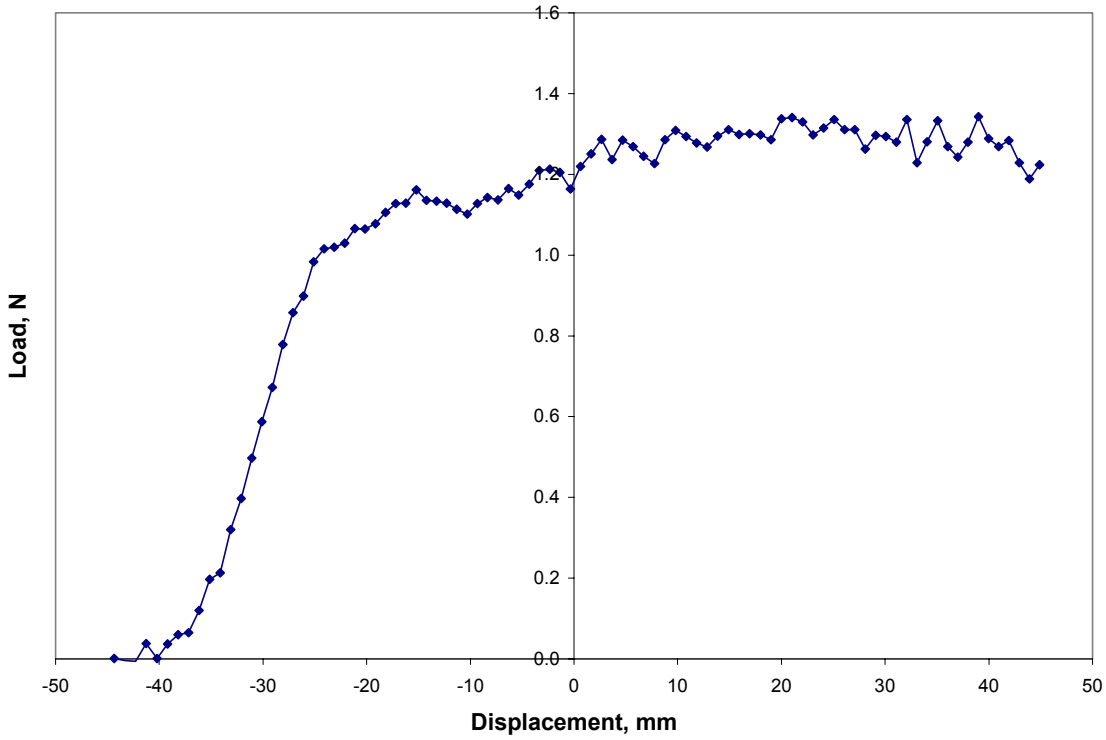

Figure C.11: Load Versus Displacement for Subject A, 180 degrees, 600 mm/min, Test 5

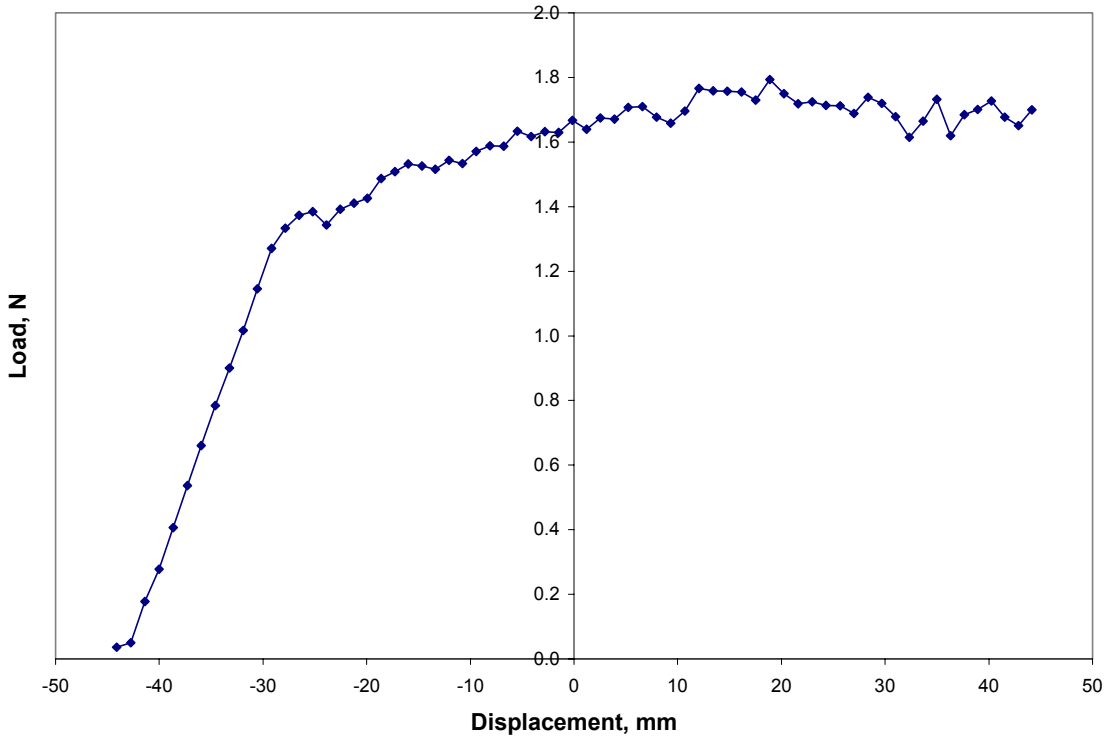

Figure C.12: Load Versus Displacement for Subject A, 180 degrees, 800 mm/min, Test 1

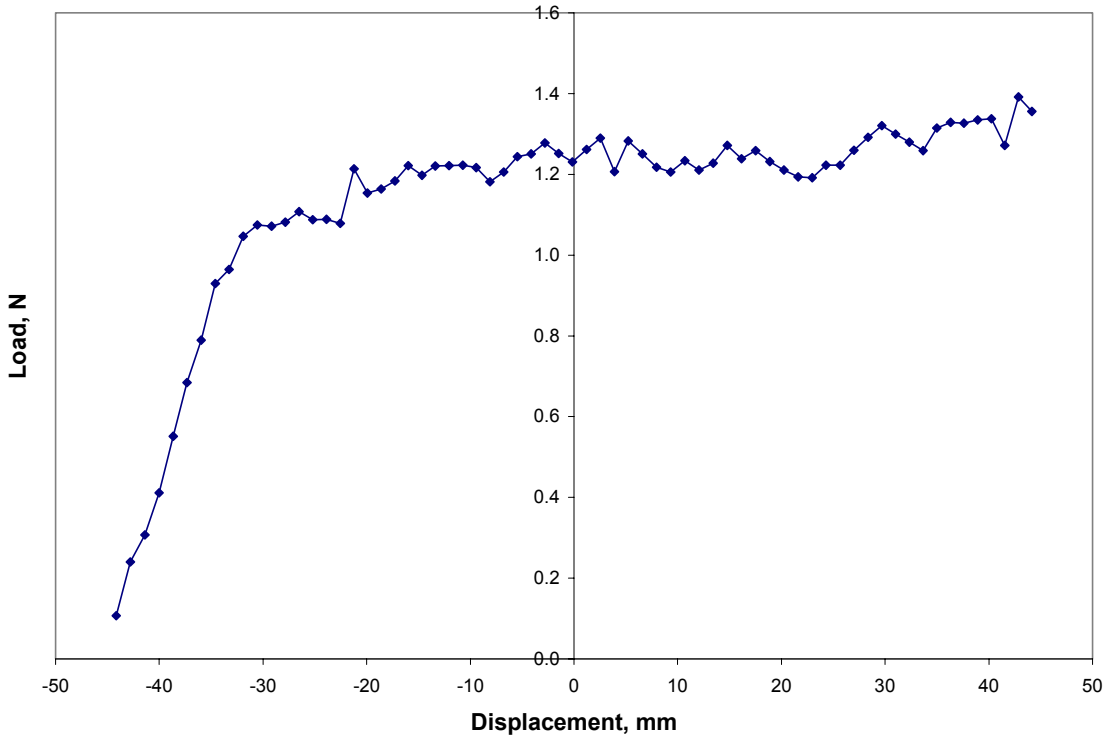

Figure C.13: Load Versus Displacement for Subject A, 180 degrees, 800 mm/min, Test 2

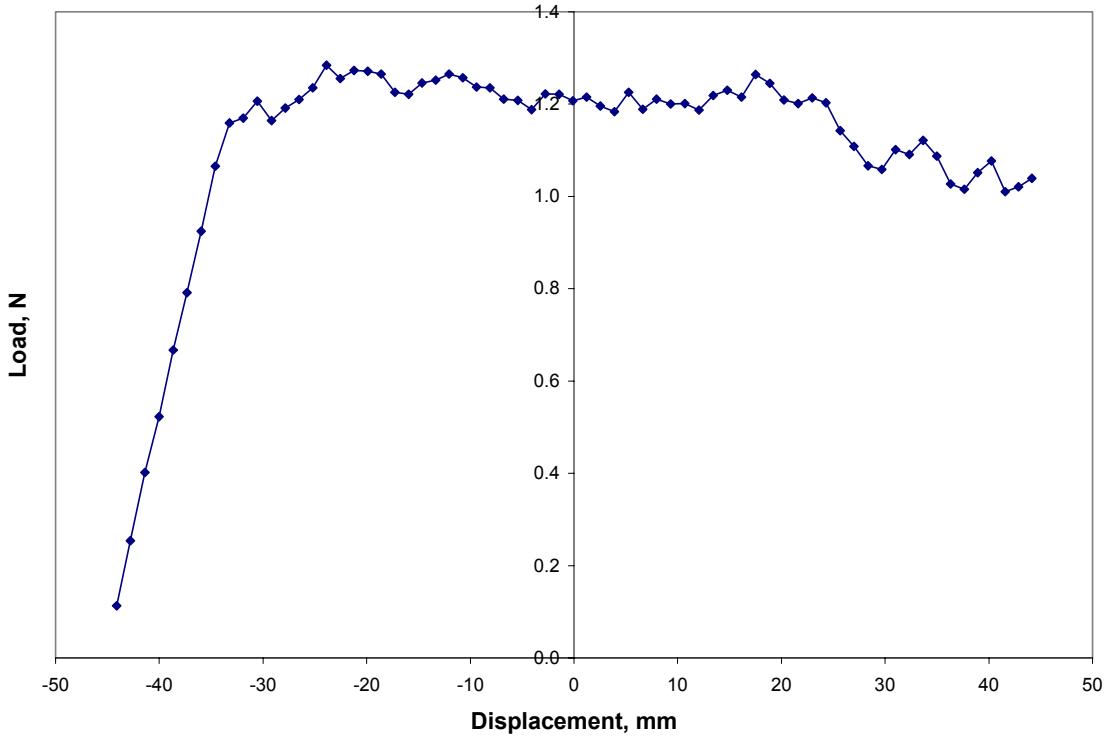

Figure C.14: Load Versus Displacement for Subject A, 180 degrees, 800 mm/min, Test 3

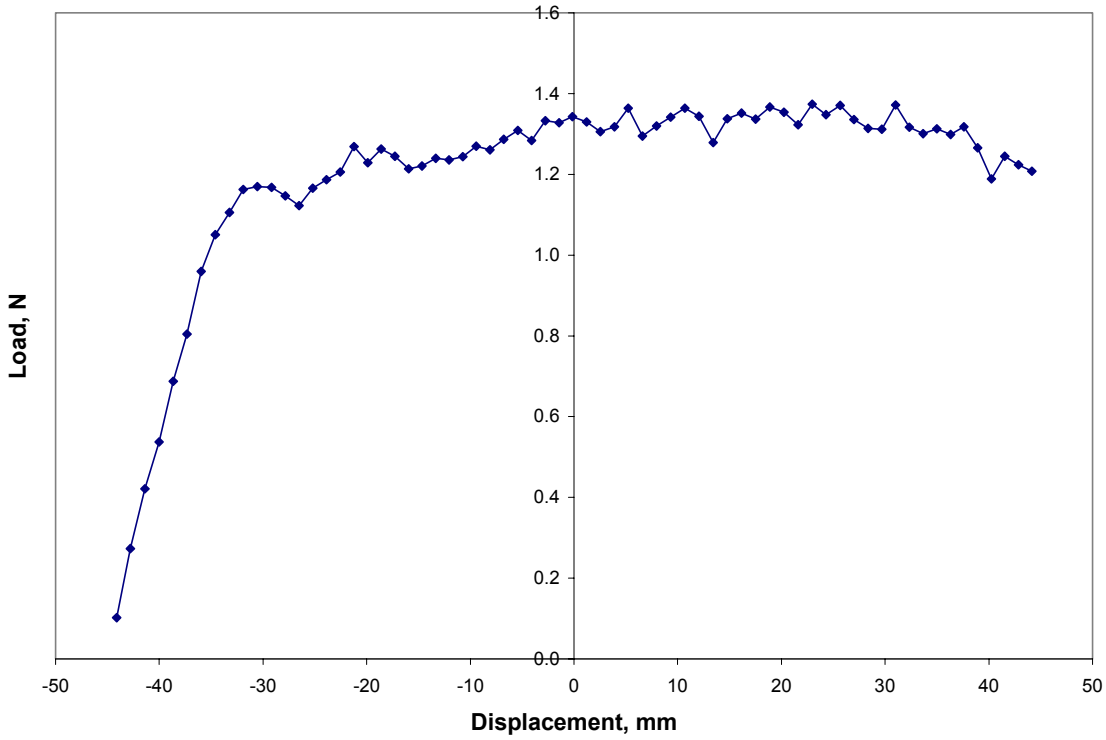

Figure C.15: Load Versus Displacement for Subject A, 180 degrees, 800 mm/min, Test 4

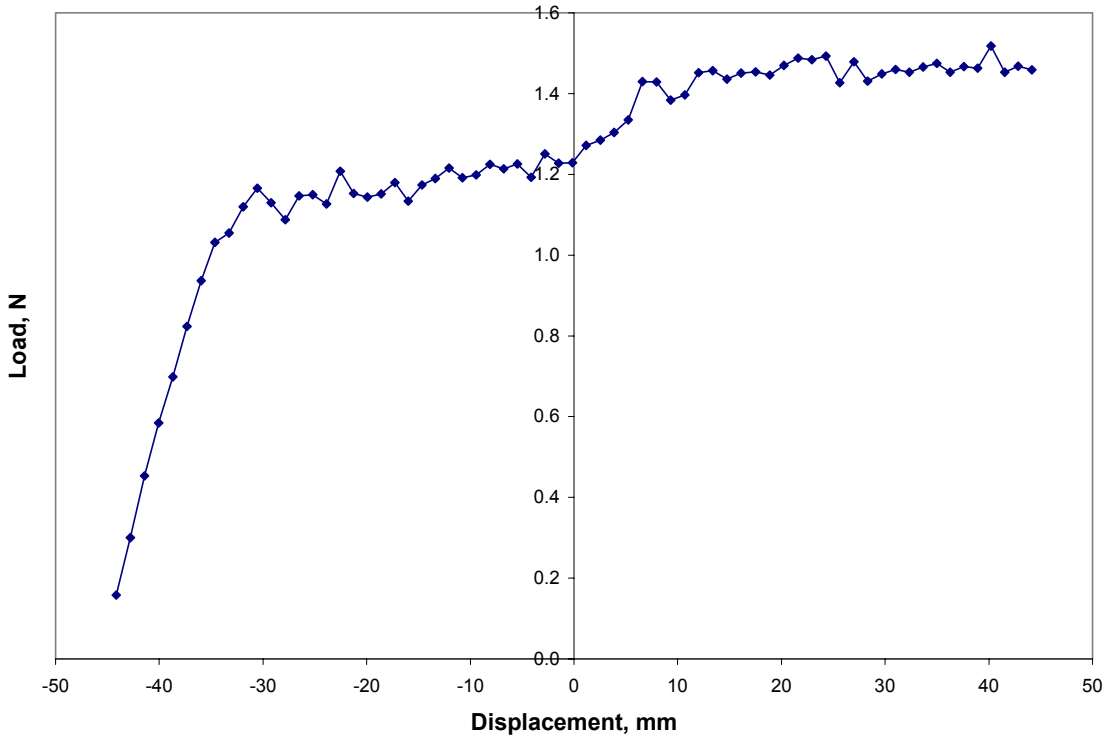

Figure C.16: Load Versus Displacement for Subject A, 180 degrees, 800 mm/min, Test 5

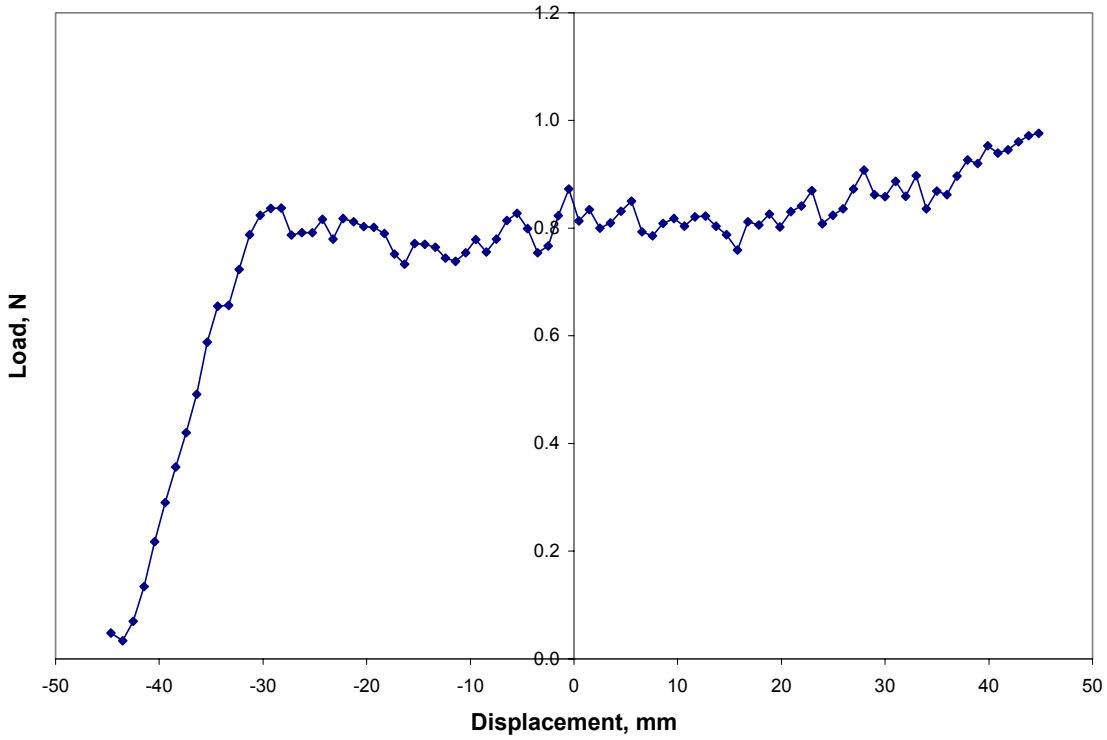

Figure C.17: Load Versus Displacement for Subject A, 180 degrees, 1000 mm/min, Test 1

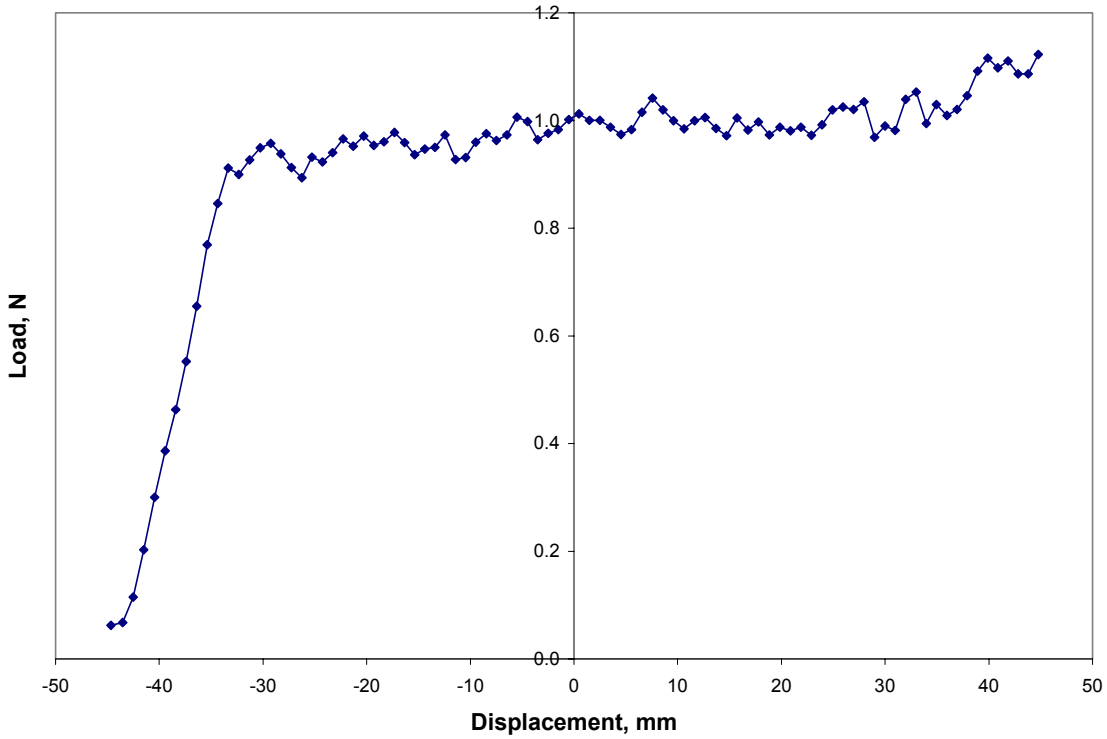

Figure C.18: Load Versus Displacement for Subject A, 180 degrees, 1000 mm/min, Test 2

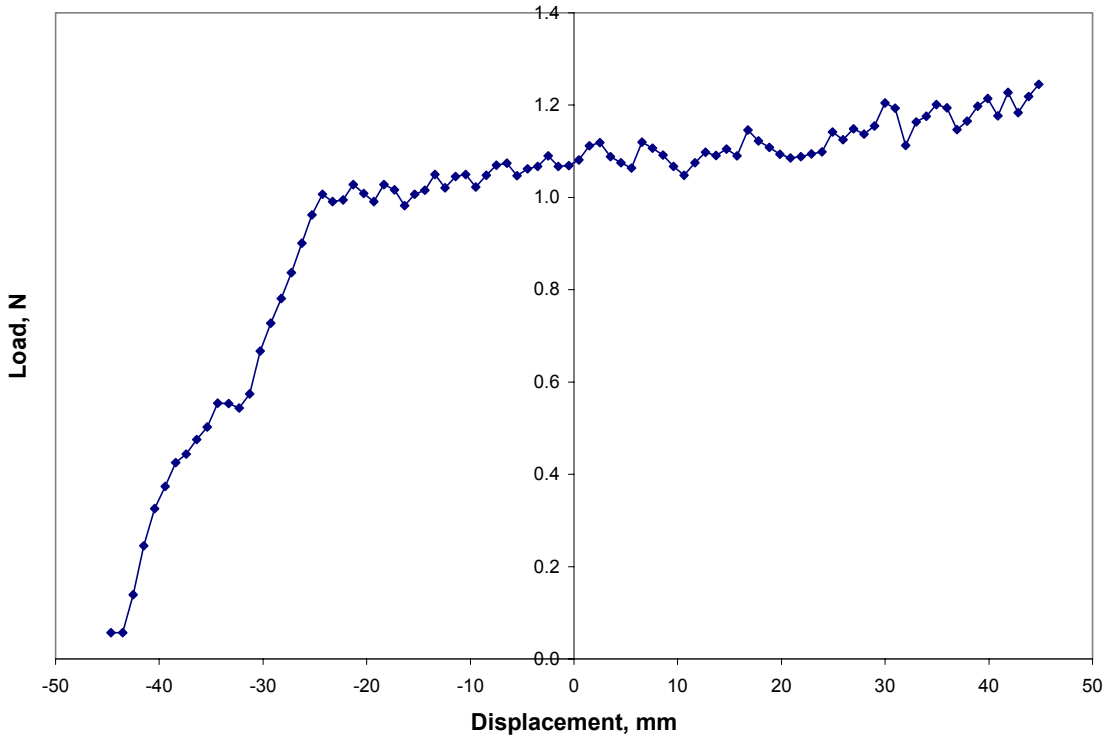

Figure C.19: Load Versus Displacement for Subject A, 180 degrees, 1000 mm/min, Test 3

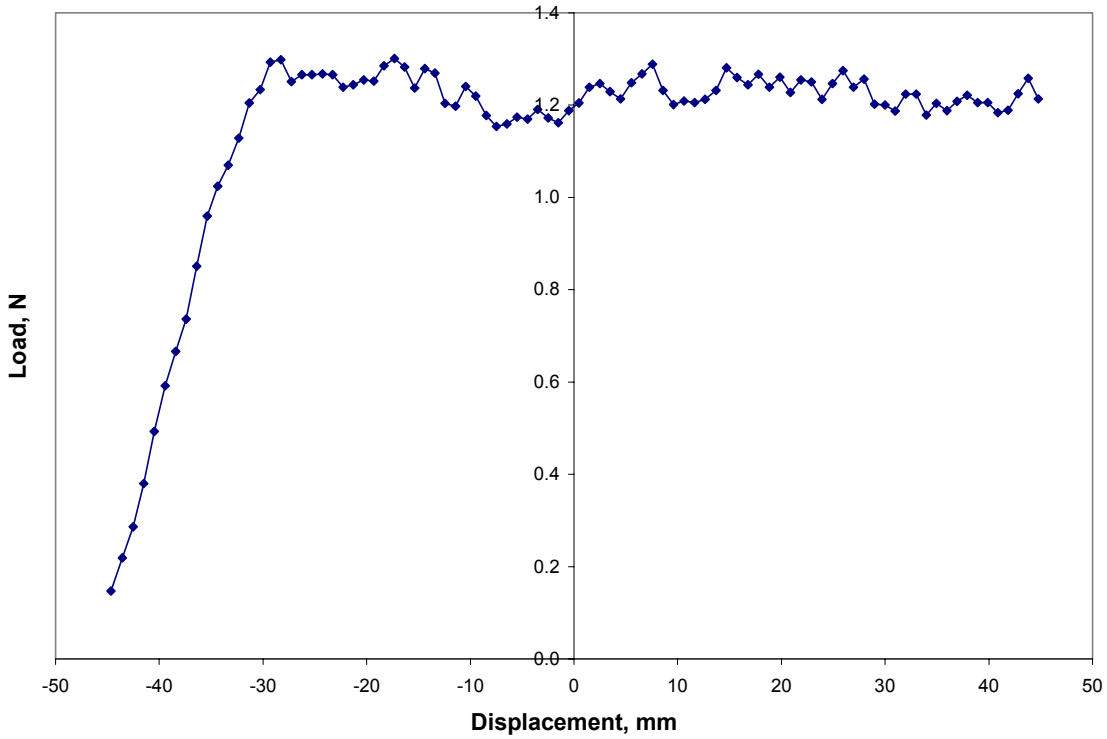

Figure C.20: Load Versus Displacement for Subject A, 180 degrees, 1000 mm/min, Test 4

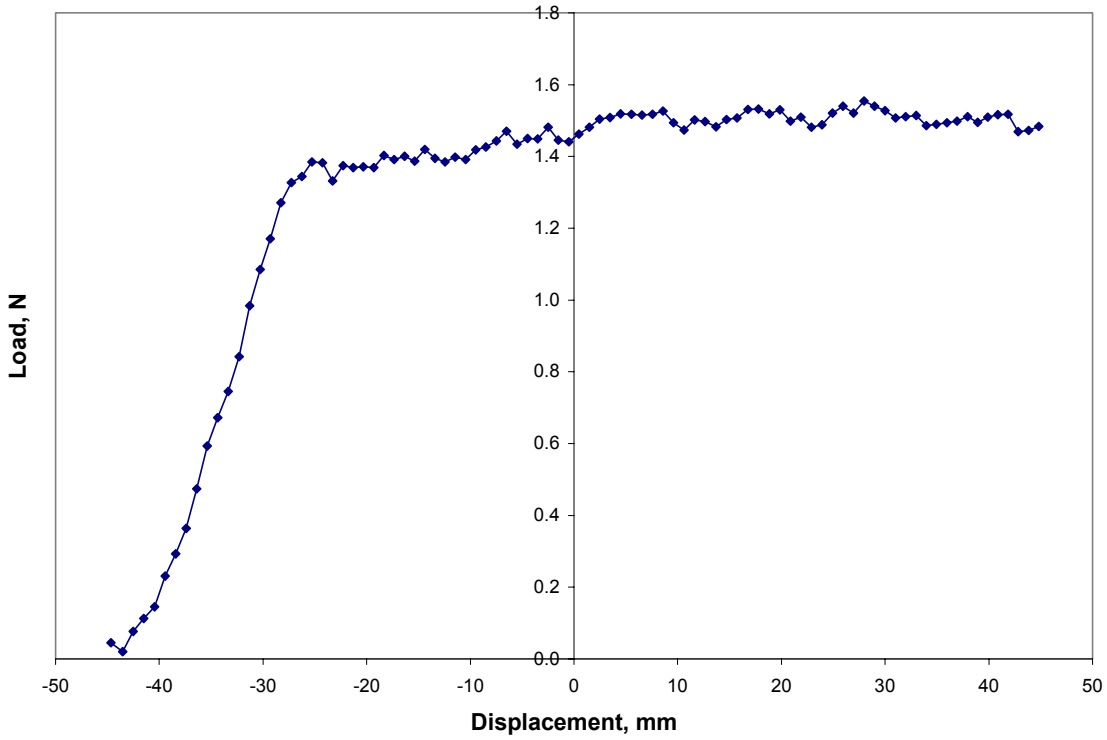

Figure C.21: Load Versus Displacement for Subject A, 180 degrees, 1000 mm/min, Test 5

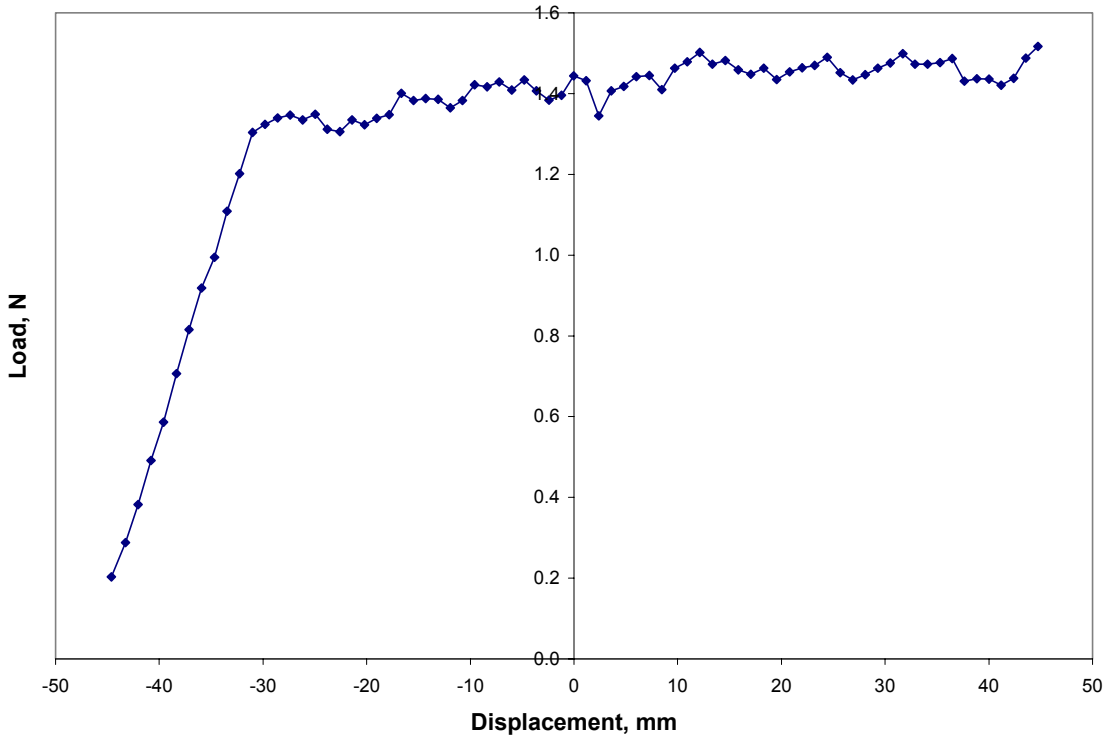

Figure C.22: Load Versus Displacement for Subject A, 180 degrees, 1200 mm/min, Test 1

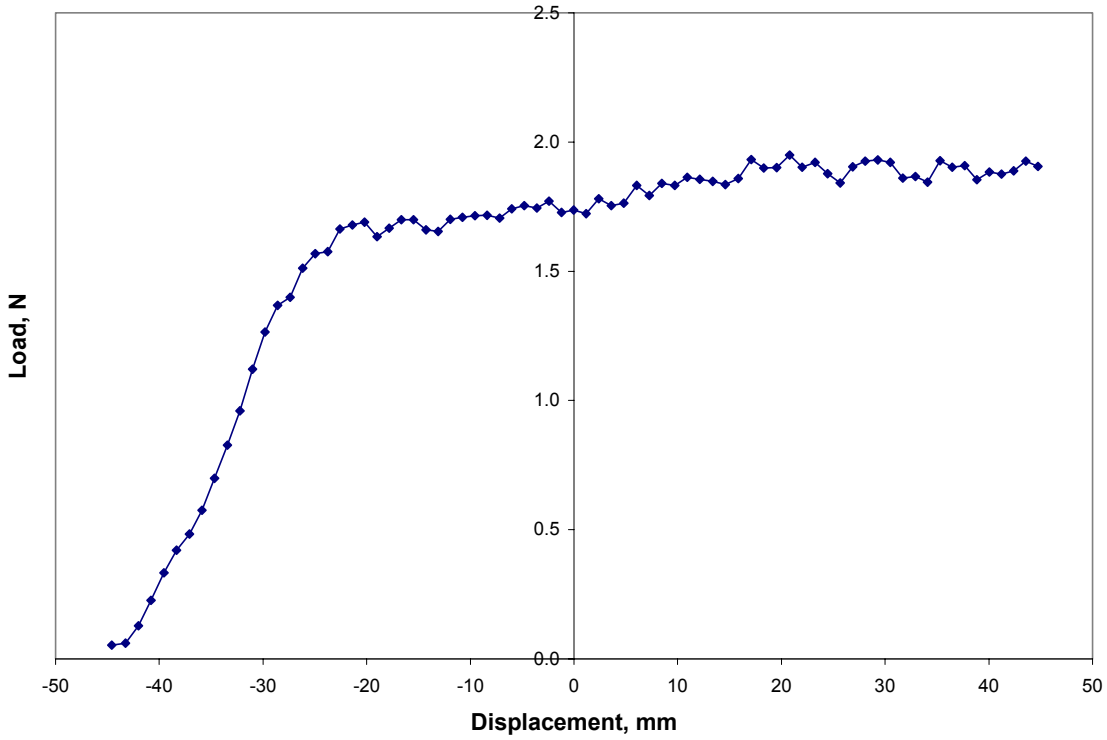

Figure C.23: Load Versus Displacement for Subject A, 180 degrees, 1200 mm/min, Test 2

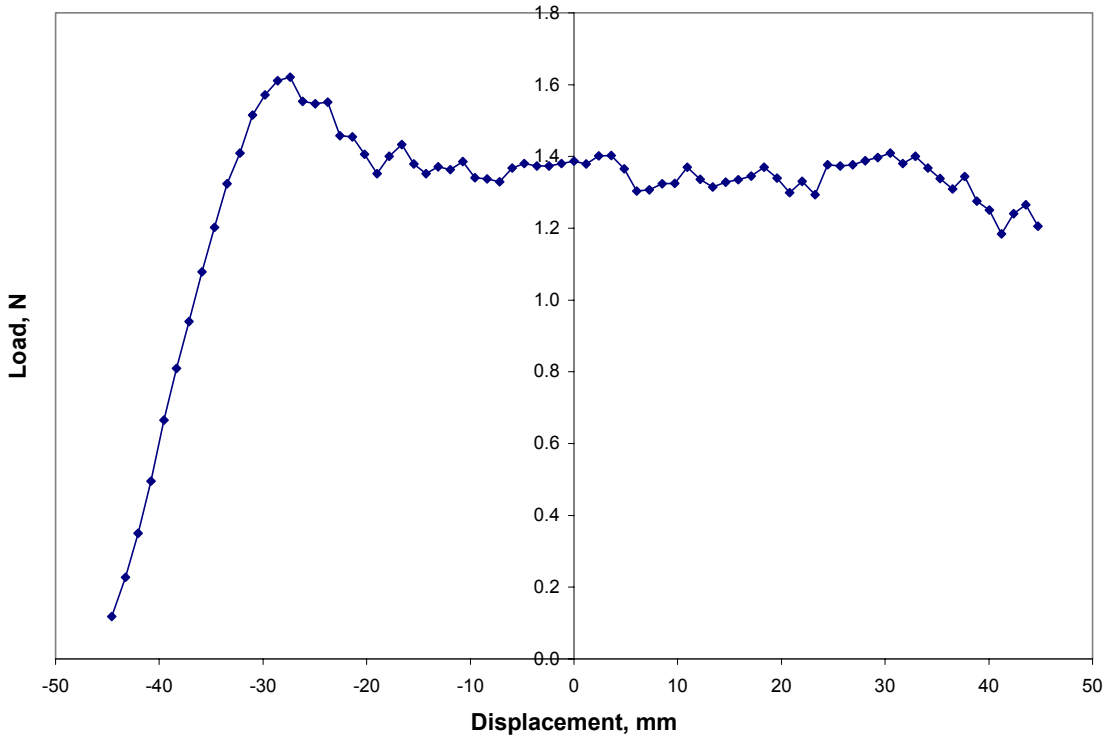

Figure C.24: Load Versus Displacement for Subject A, 180 degrees, 1200 mm/min, Test 3

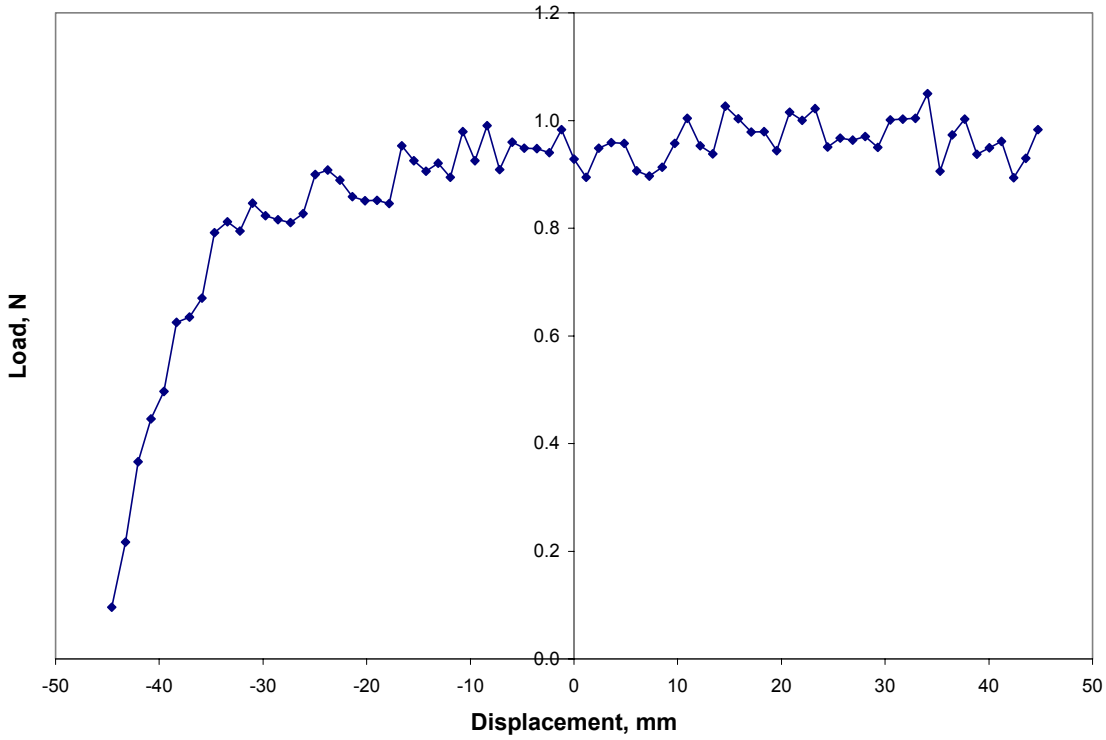

Figure C.25: Load Versus Displacement for Subject A, 180 degrees, 1200 mm/min, Test 4

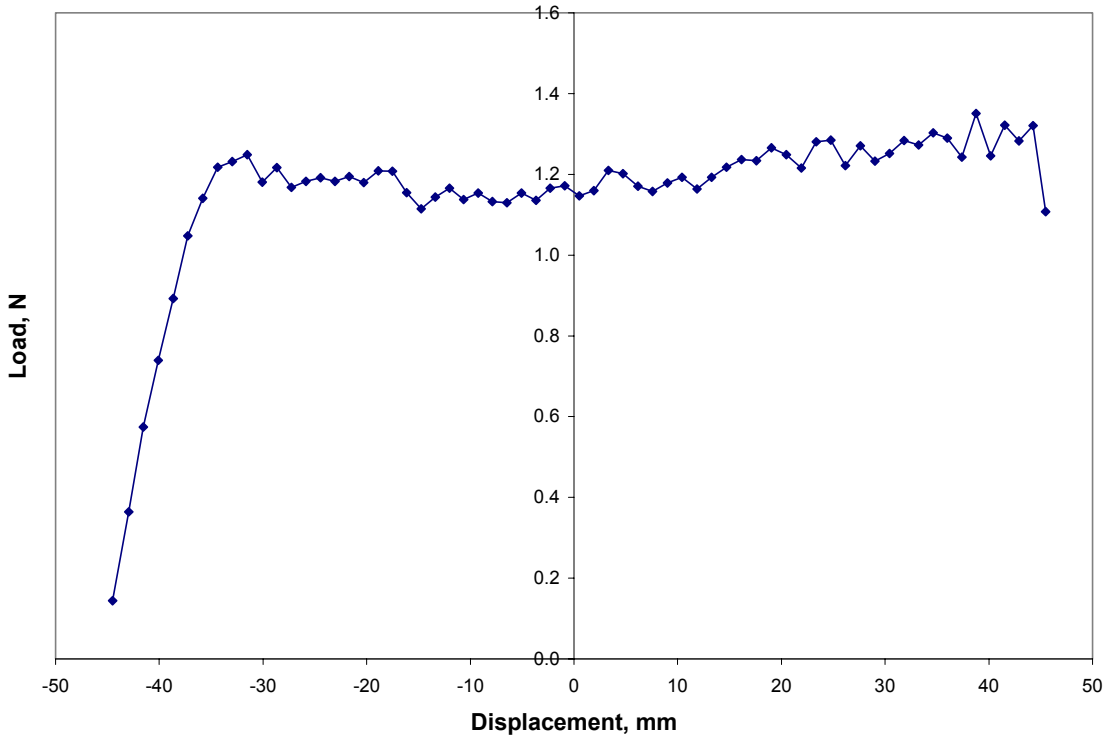

Figure C.26: Load Versus Displacement for Subject A, 180 degrees, 1400 mm/min, Test 1

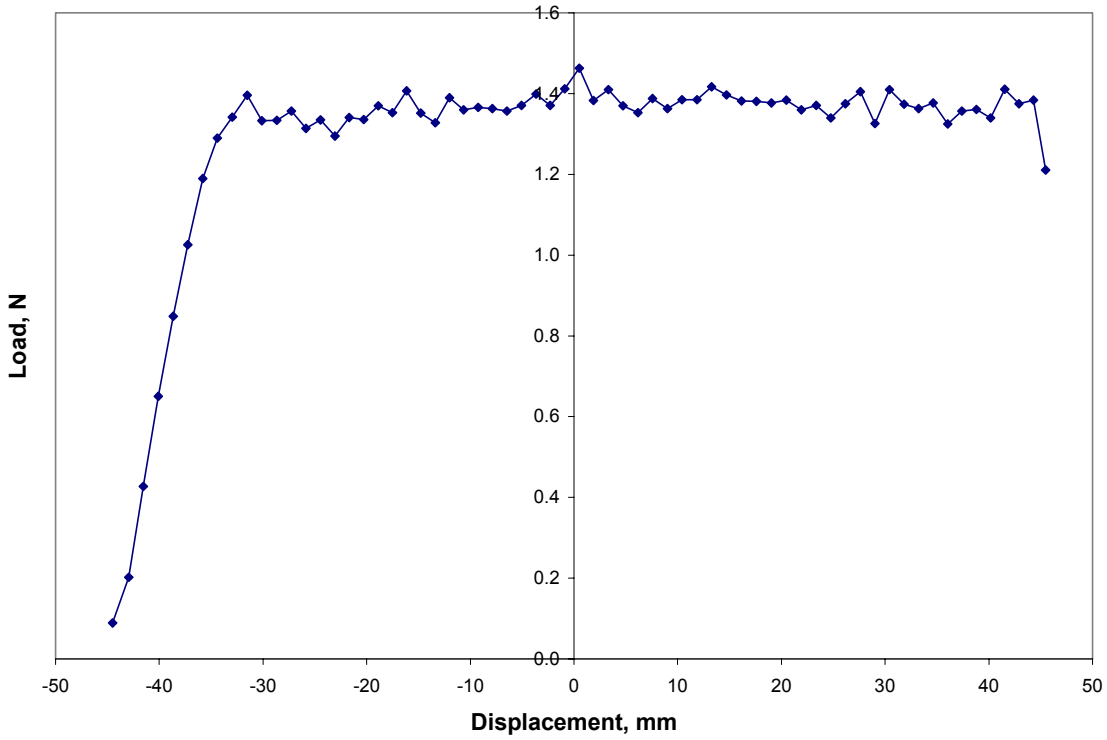

Figure C.27: Load Versus Displacement for Subject A, 180 degrees, 1400 mm/min, Test 2

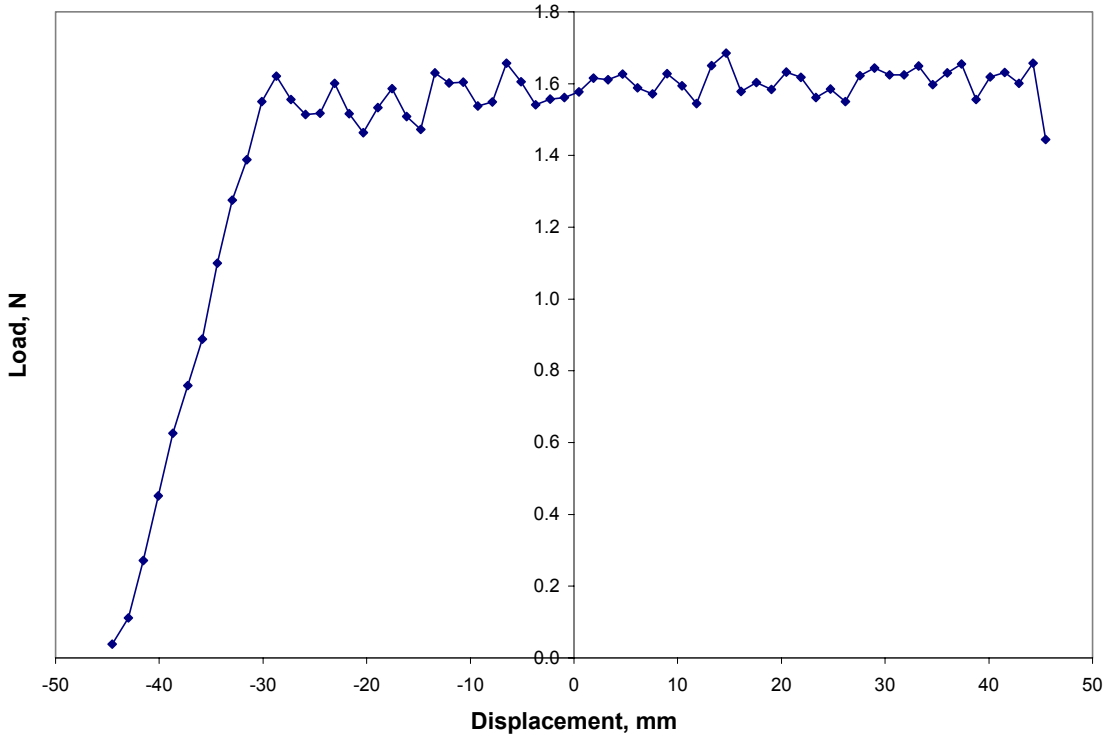

Figure C.28: Load Versus Displacement for Subject A, 180 degrees, 1400 mm/min, Test 3

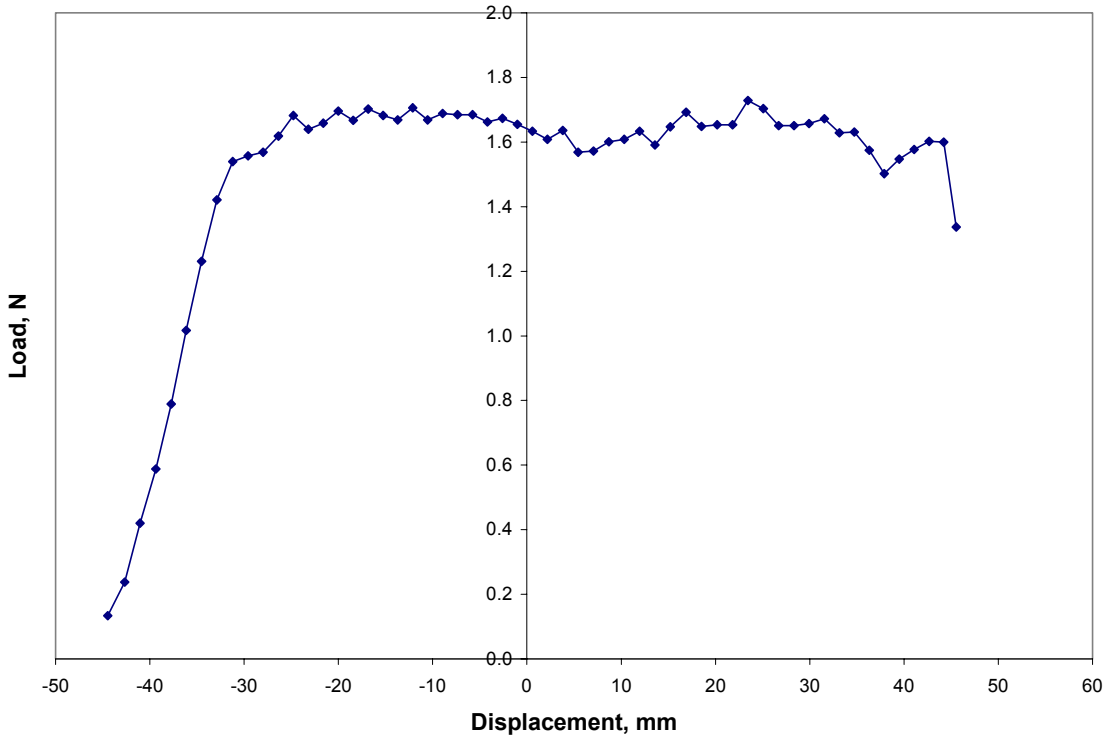

Figure C.29: Load Versus Displacement for Subject A, 180 degrees, 1600 mm/min, Test 1

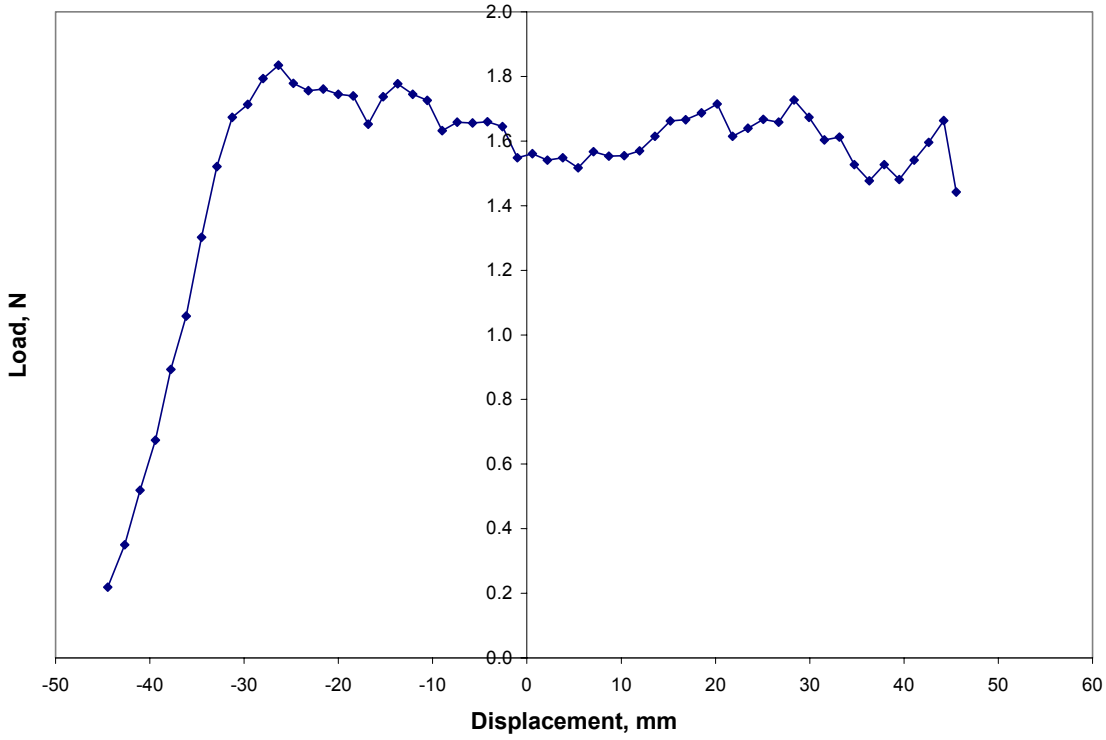

Figure C.30: Load Versus Displacement for Subject A, 180 degrees, 1600 mm/min, Test 2

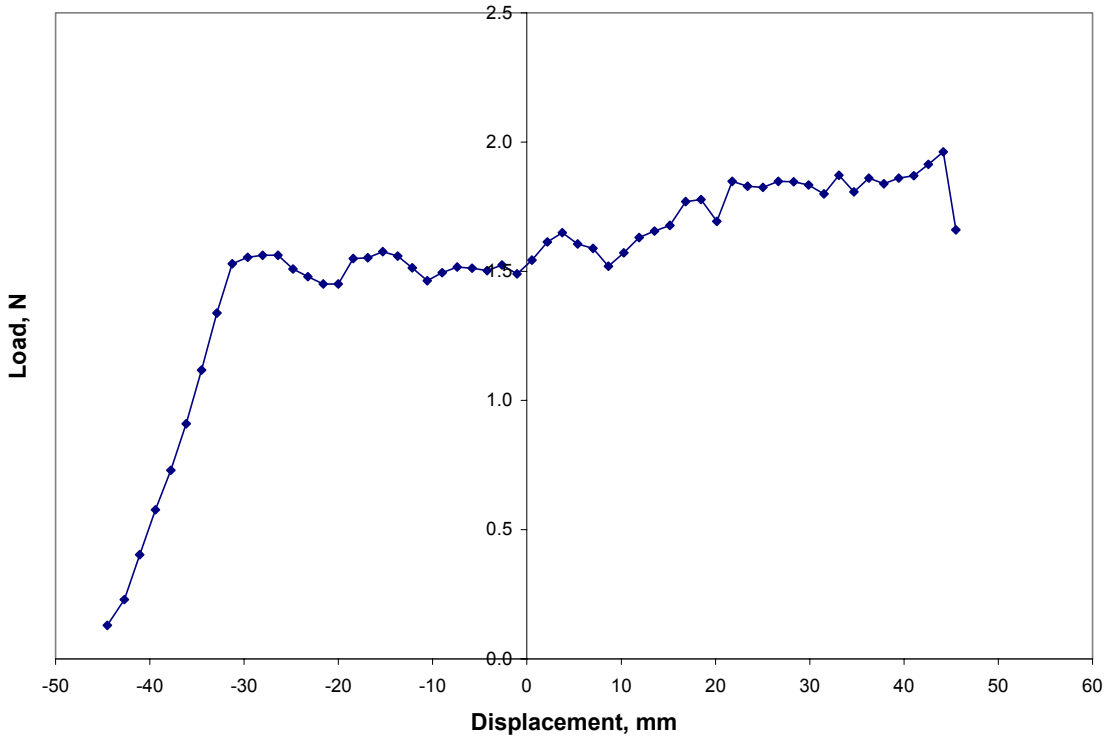

Figure C.31: Load Versus Displacement for Subject A, 180 degrees, 1600 mm/min, Test 3

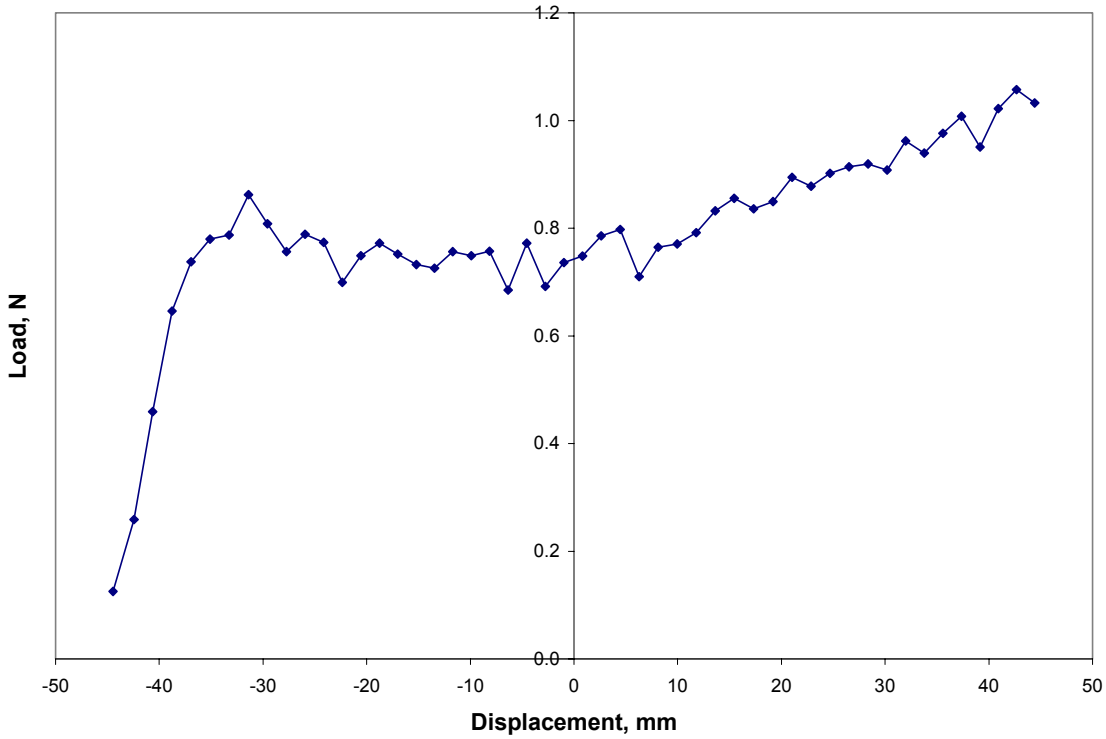

Figure C.32: Load Versus Displacement for Subject A, 180 degrees, 1800 mm/min, Test 1

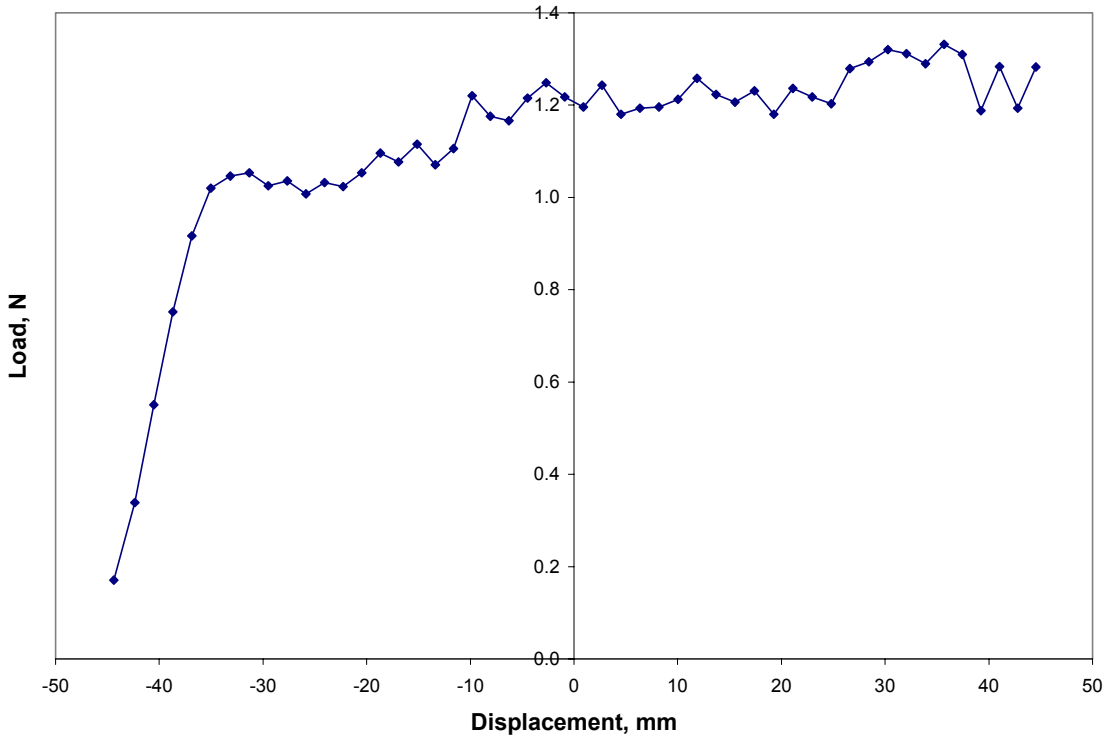

Figure C.33: Load Versus Displacement for Subject A, 180 degrees, 1800 mm/min, Test 2

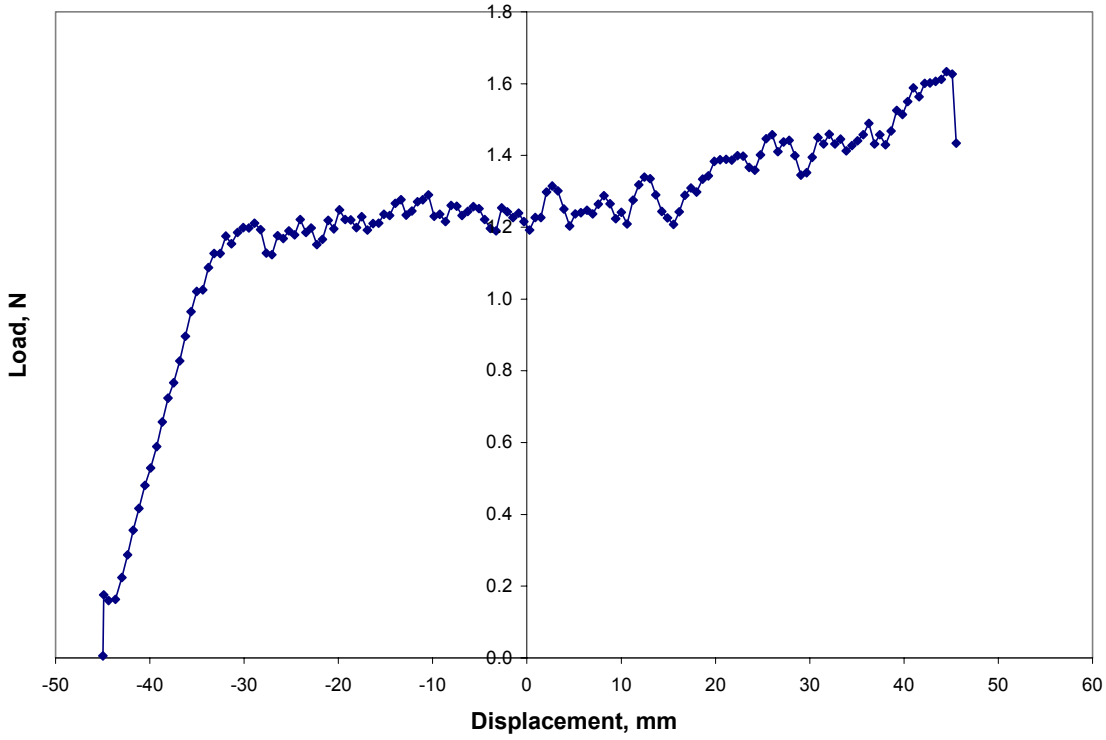

Figure C.34: Load Versus Displacement for Subject A, 180 degrees, 1800 mm/min, Test 3

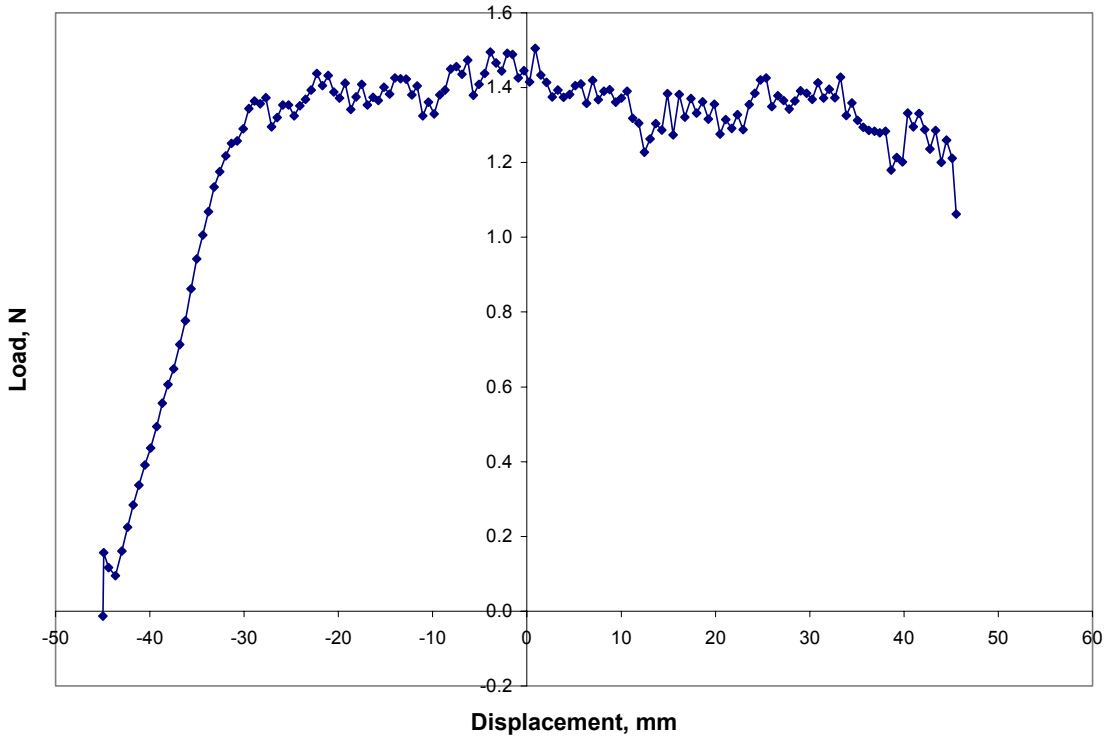

Figure C.35: Load Versus Displacement for Subject A, 180 degrees, 1800 mm/min, Test 4

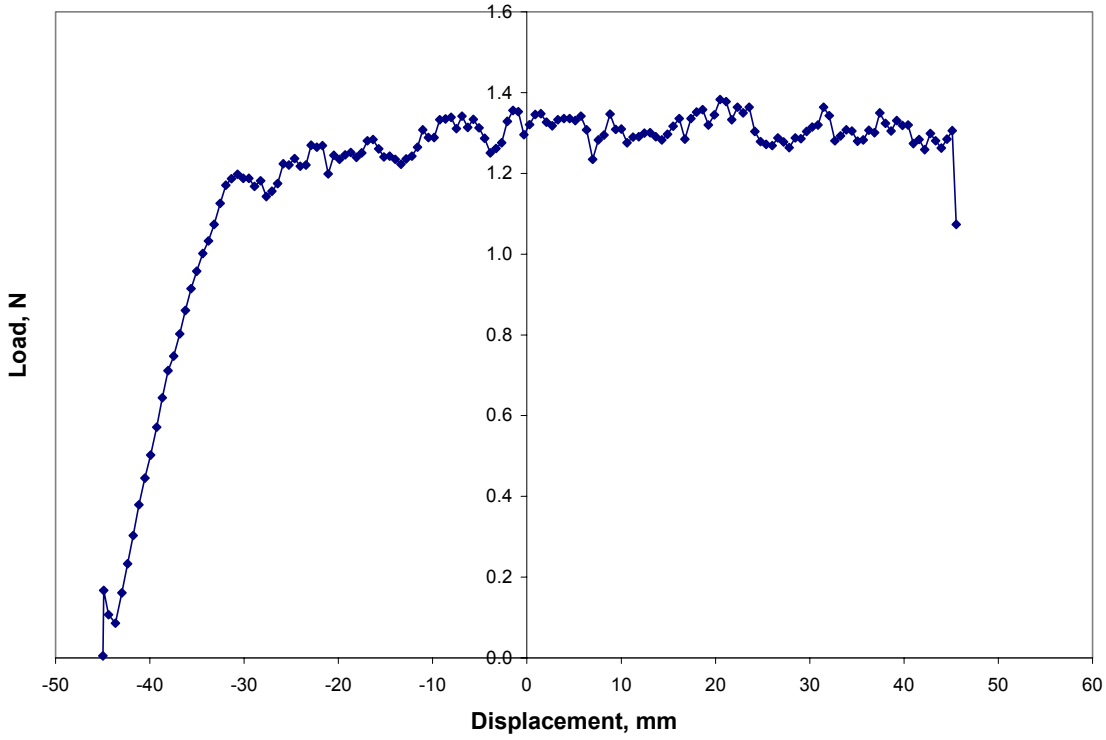

Figure C.36: Load Versus Displacement for Subject A, 180 degrees, 1800 mm/min, Test 5

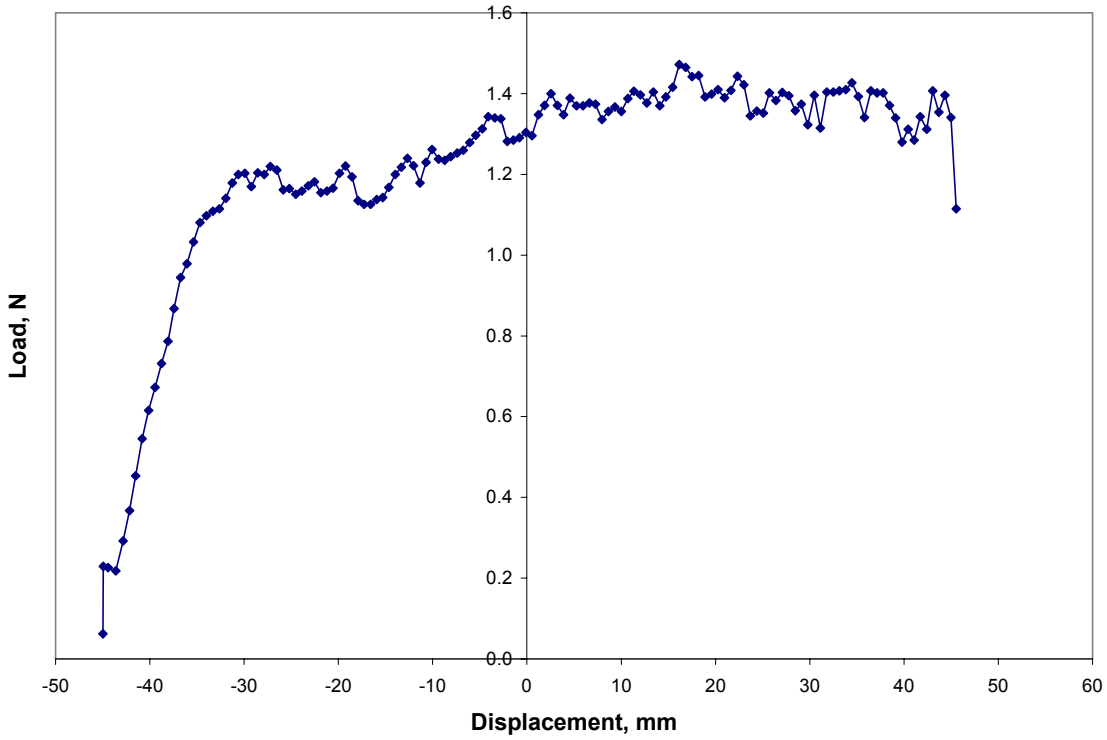

Figure C.37: Load Versus Displacement for Subject A, 180 degrees, 2000 mm/min, Test 1

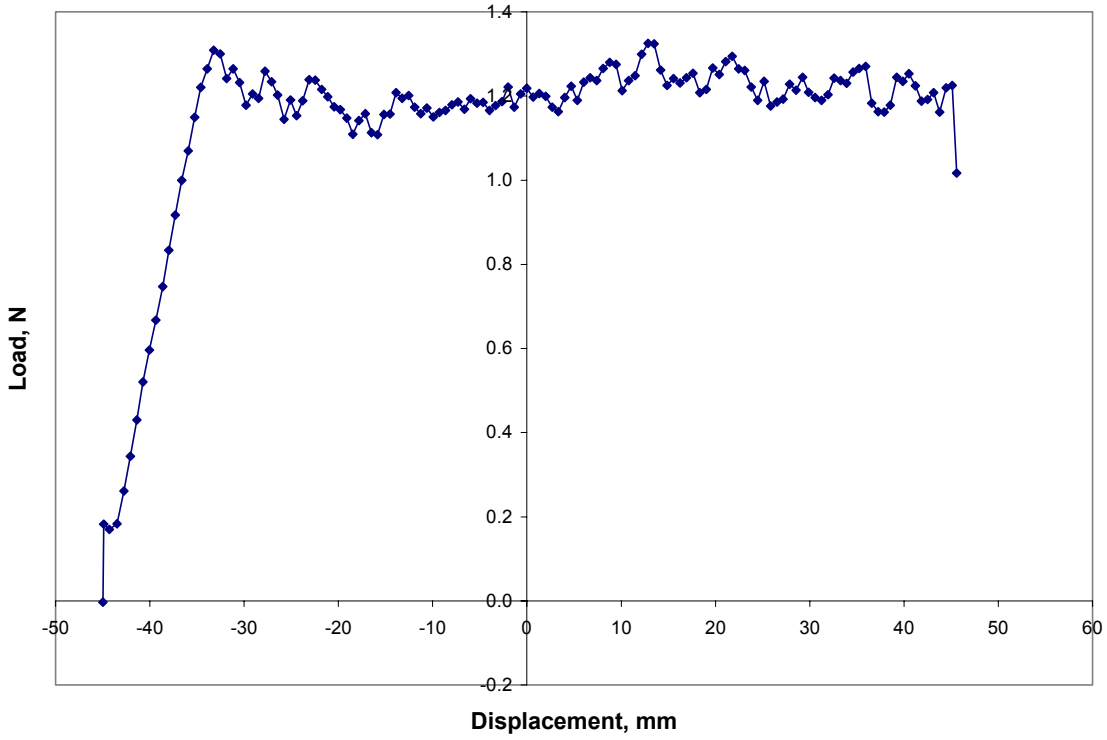

Figure C.38: Load Versus Displacement for Subject A, 180 degrees, 2000 mm/min, Test 2

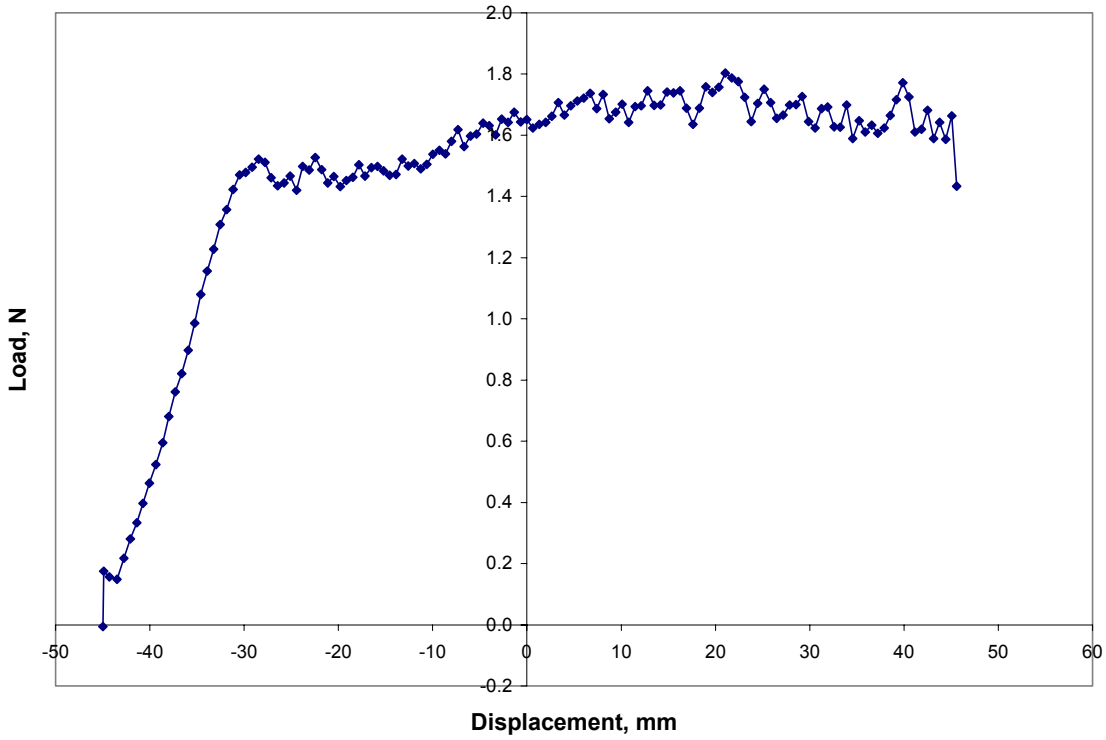

Figure C.39: Load Versus Displacement for Subject A, 180 degrees, 2000 mm/min, Test 3

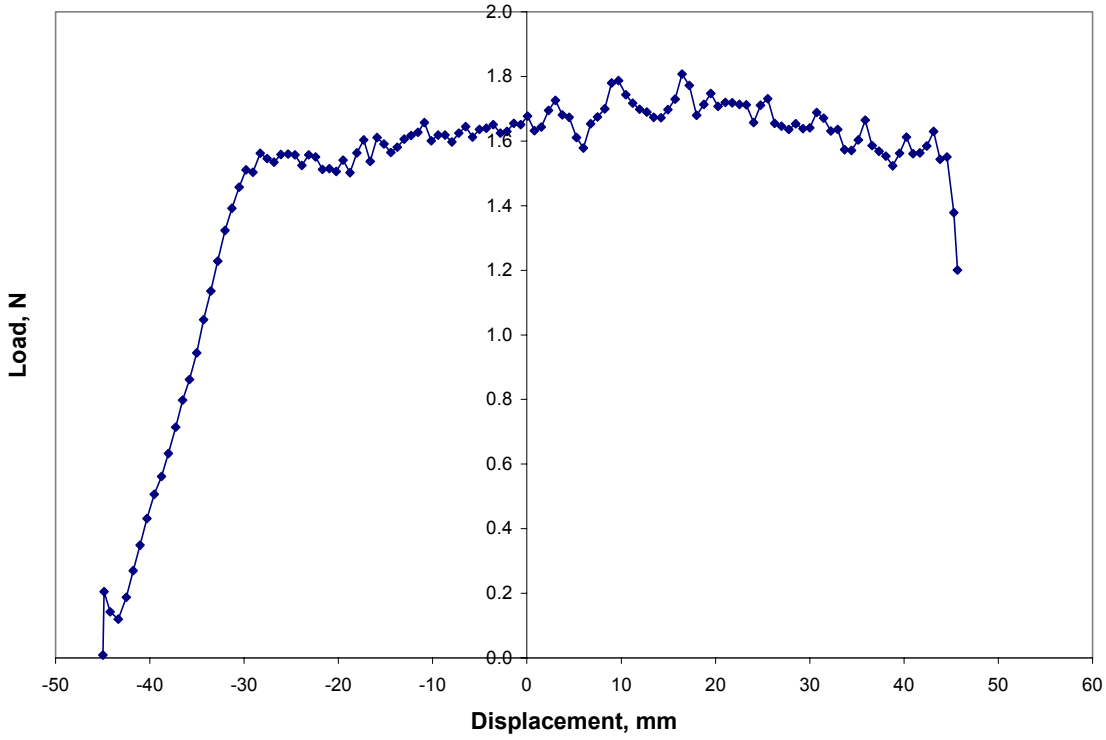

Figure C.40: Load Versus Displacement for Subject A, 180 degrees, 2200 mm/min, Test 1

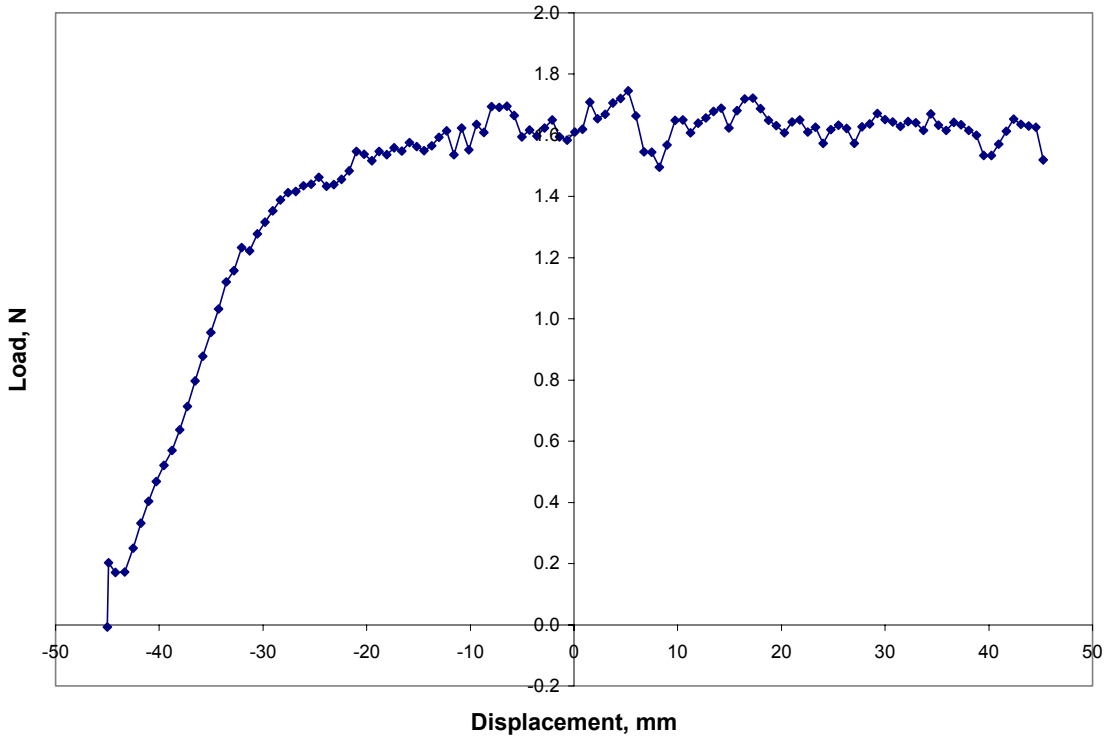

Figure C.41: Load Versus Displacement for Subject A, 180 degrees, 2200 mm/min, Test 2

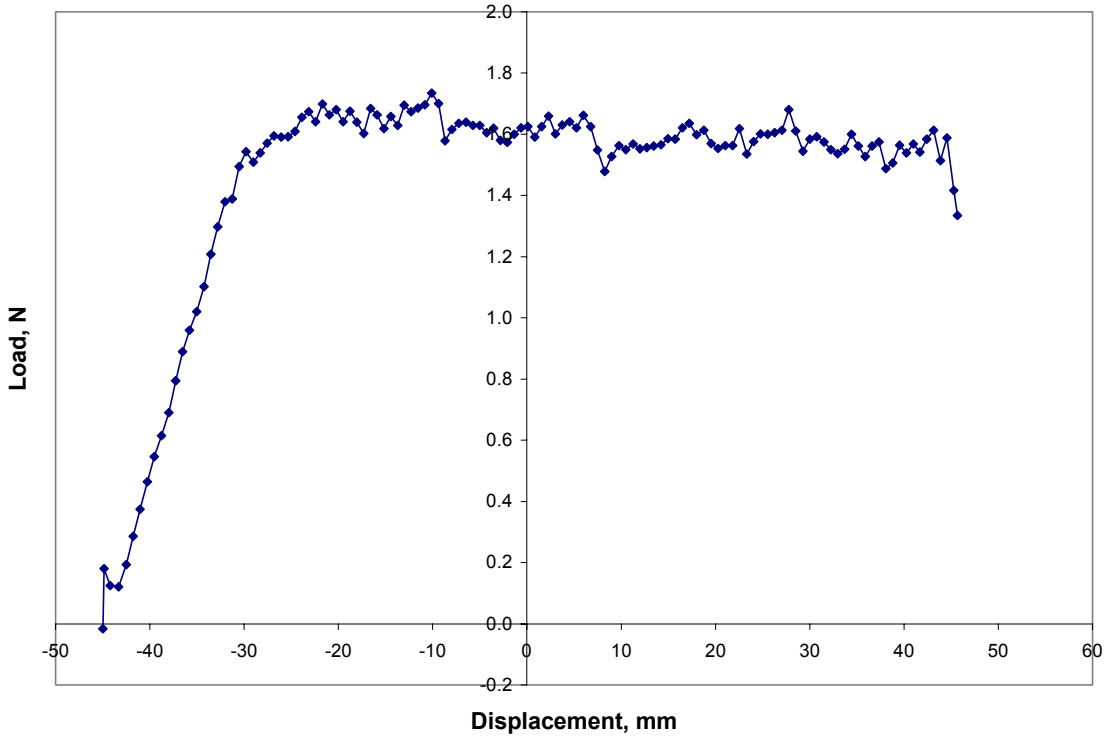

Figure C.42: Load Versus Displacement for Subject A, 180 degrees, 2200 mm/min, Test 3

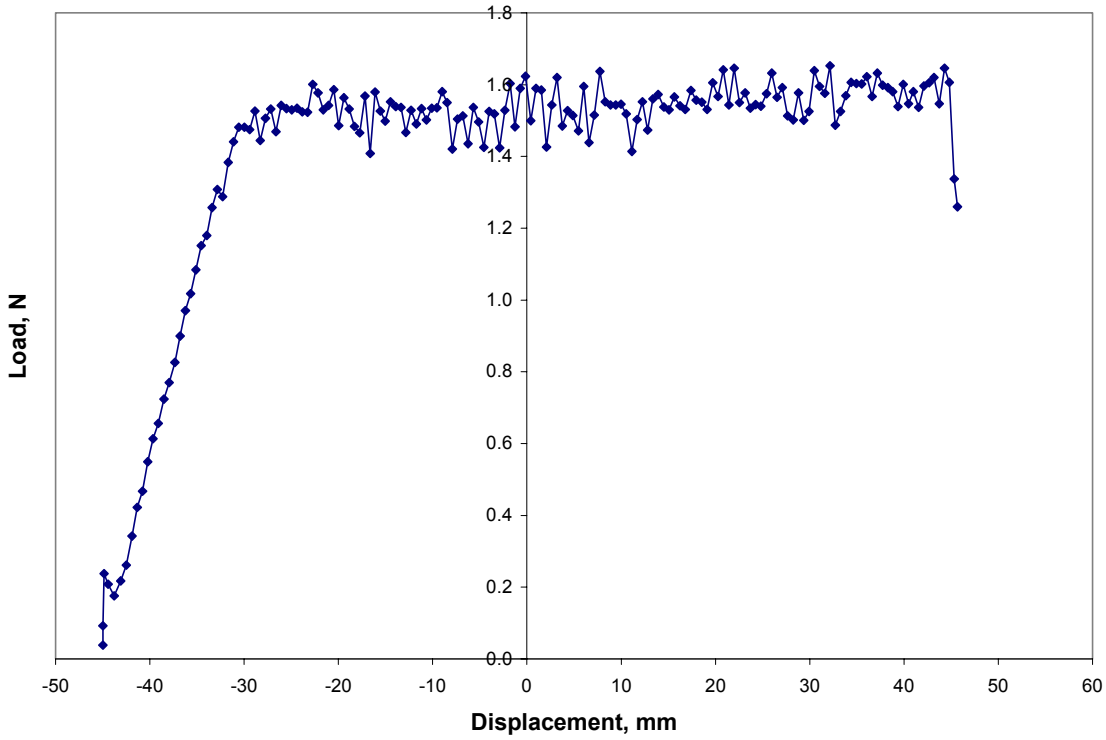

Figure C.43: Load Versus Displacement for Subject A, 180 degrees, 2400 mm/min, Test 1

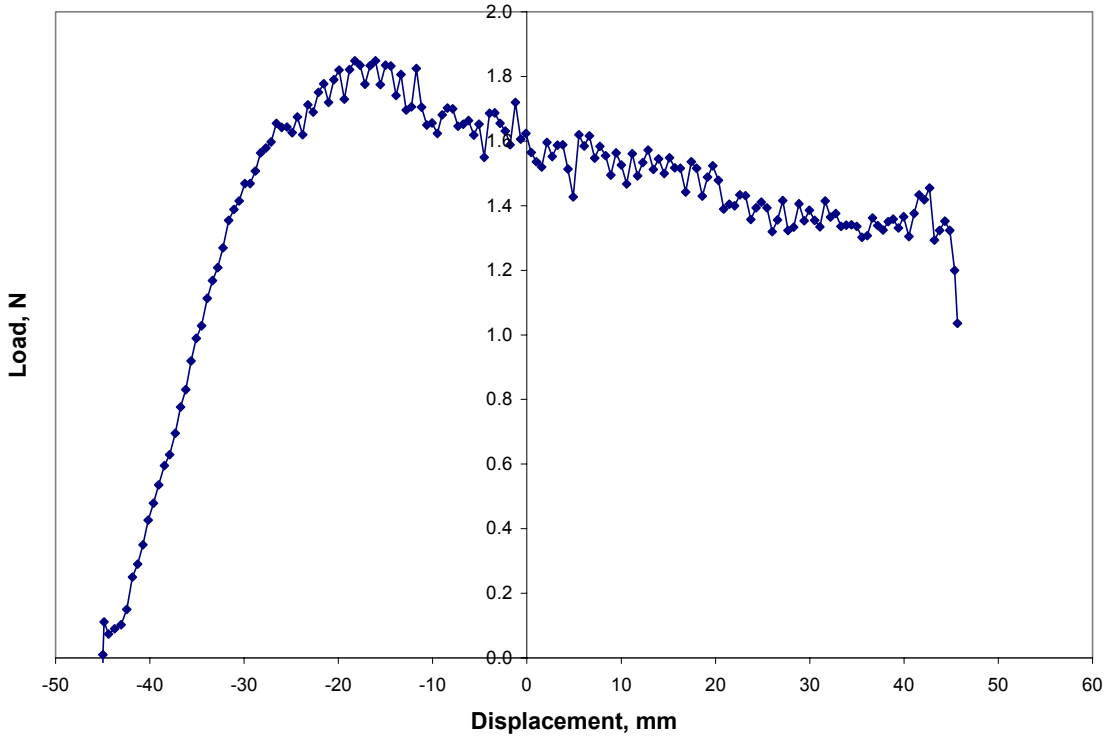

Figure C.44: Load Versus Displacement for Subject A, 180 degrees, 2400 mm/min, Test 2

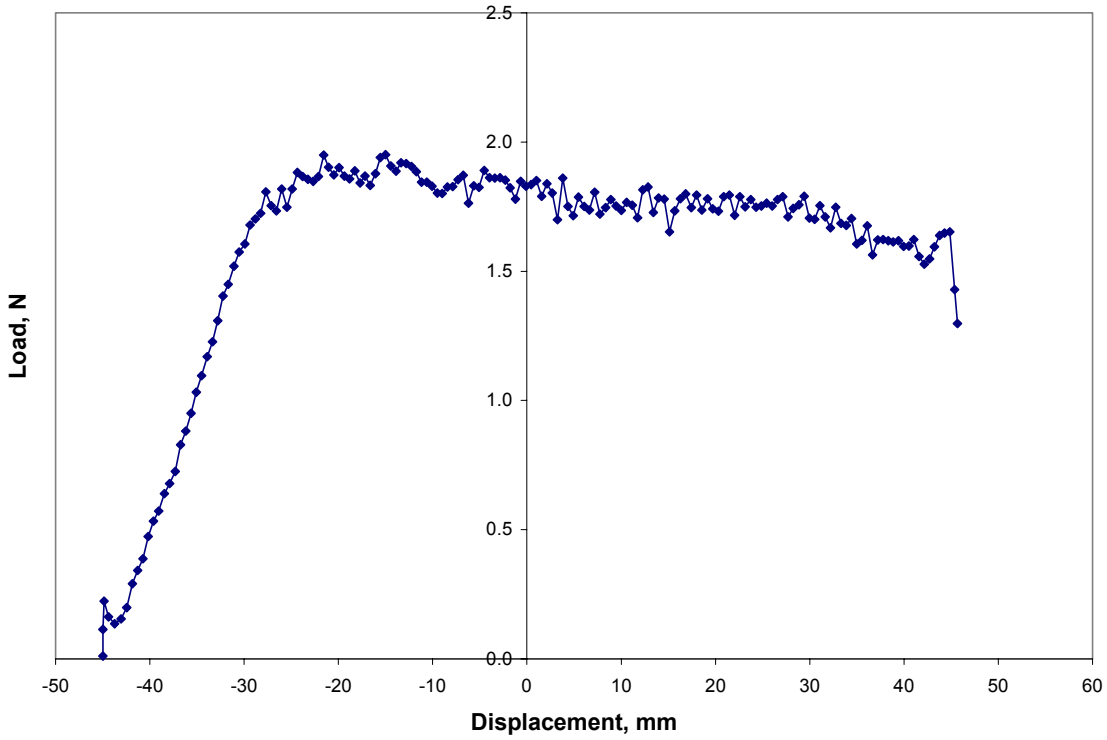

Figure C.45: Load Versus Displacement for Subject A, 180 degrees, 2400 mm/min, Test 3

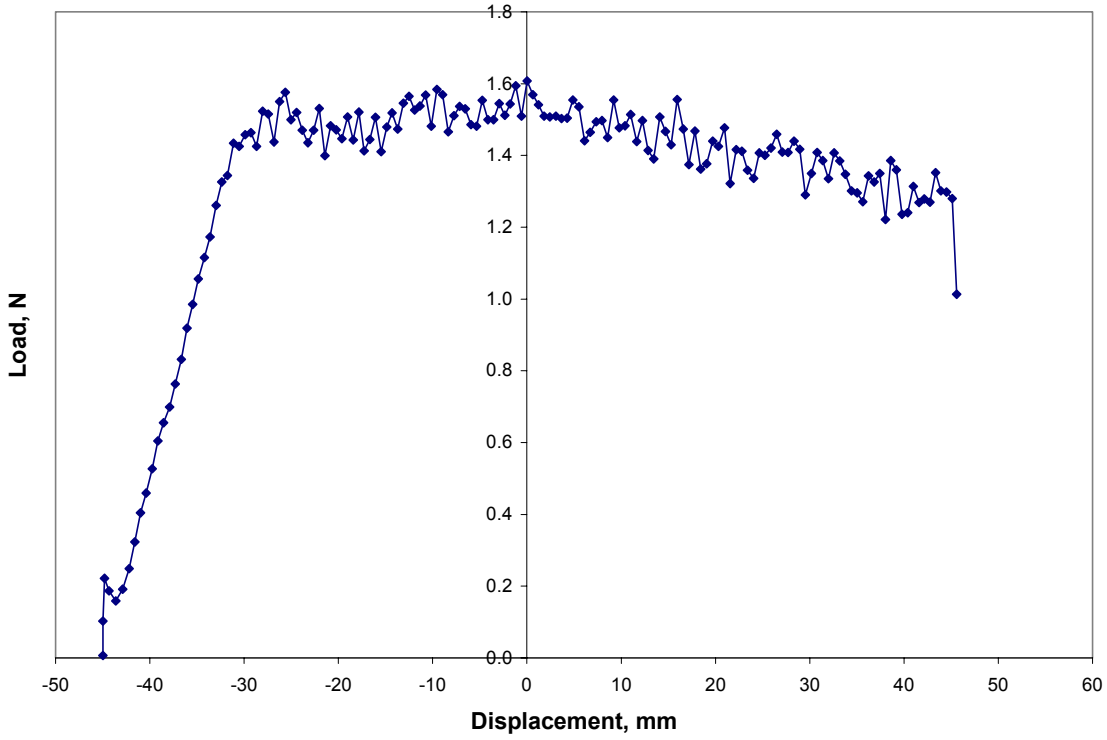

Figure C.46: Load Versus Displacement for Subject A, 180 degrees, 2600 mm/min, Test 1

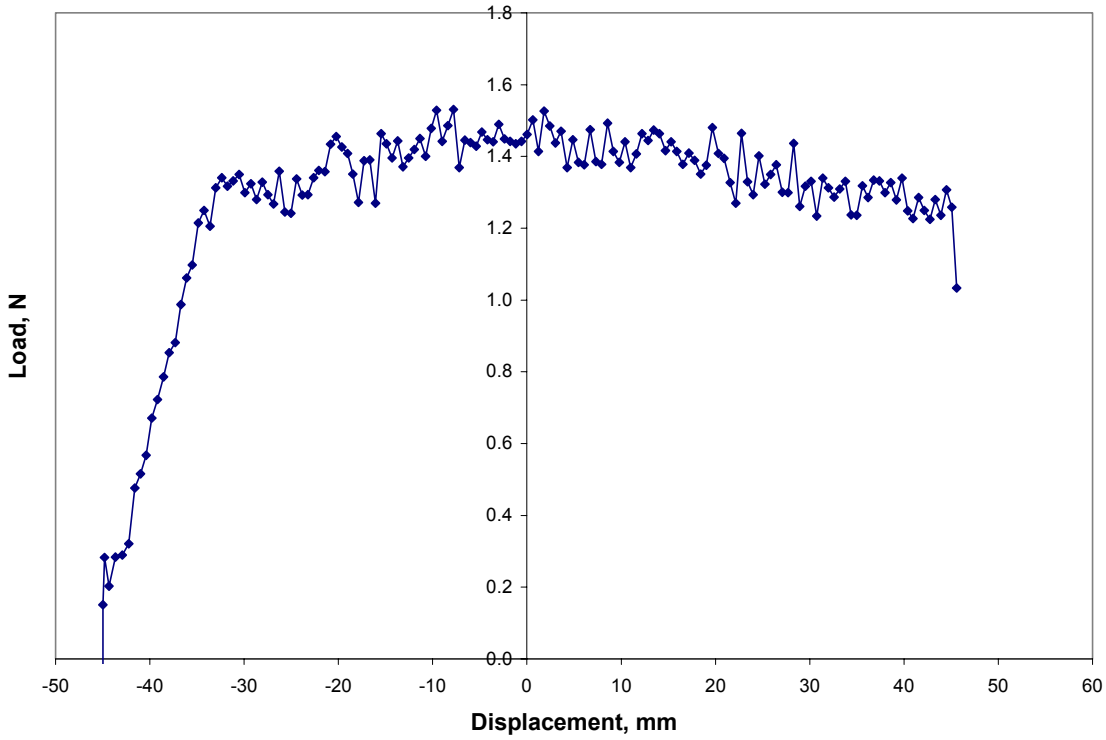

Figure C.47: Load Versus Displacement for Subject A, 180 degrees, 2600 mm/min, Test 2

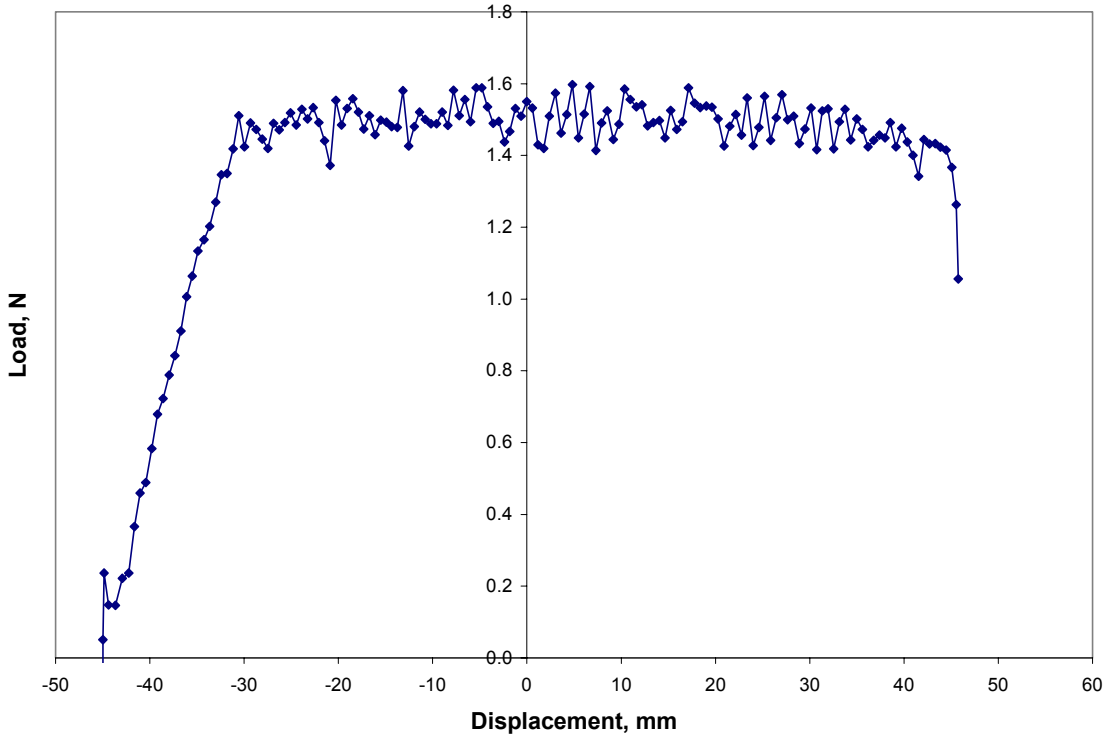

Figure C.48: Load Versus Displacement for Subject A, 180 degrees, 2600 mm/min, Test 3

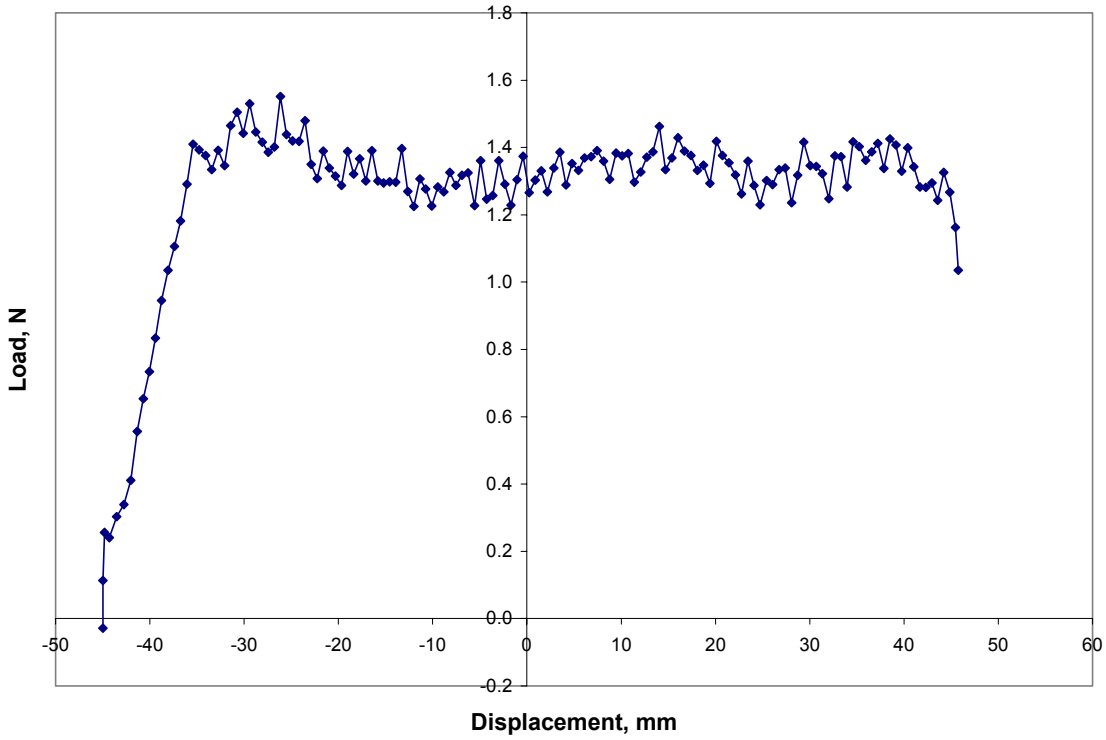

Figure C.49: Load Versus Displacement for Subject A, 180 degrees, 2800 mm/min, Test 1

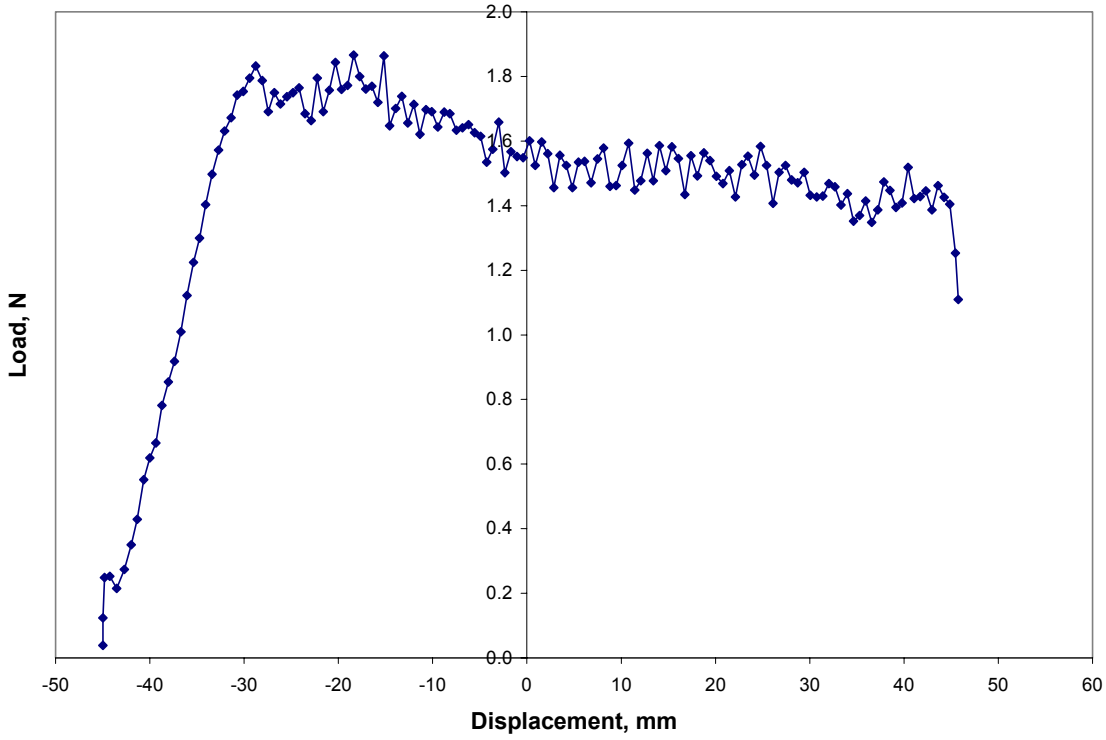

Figure C.50: Load Versus Displacement for Subject A, 180 degrees, 2800 mm/min, Test 2

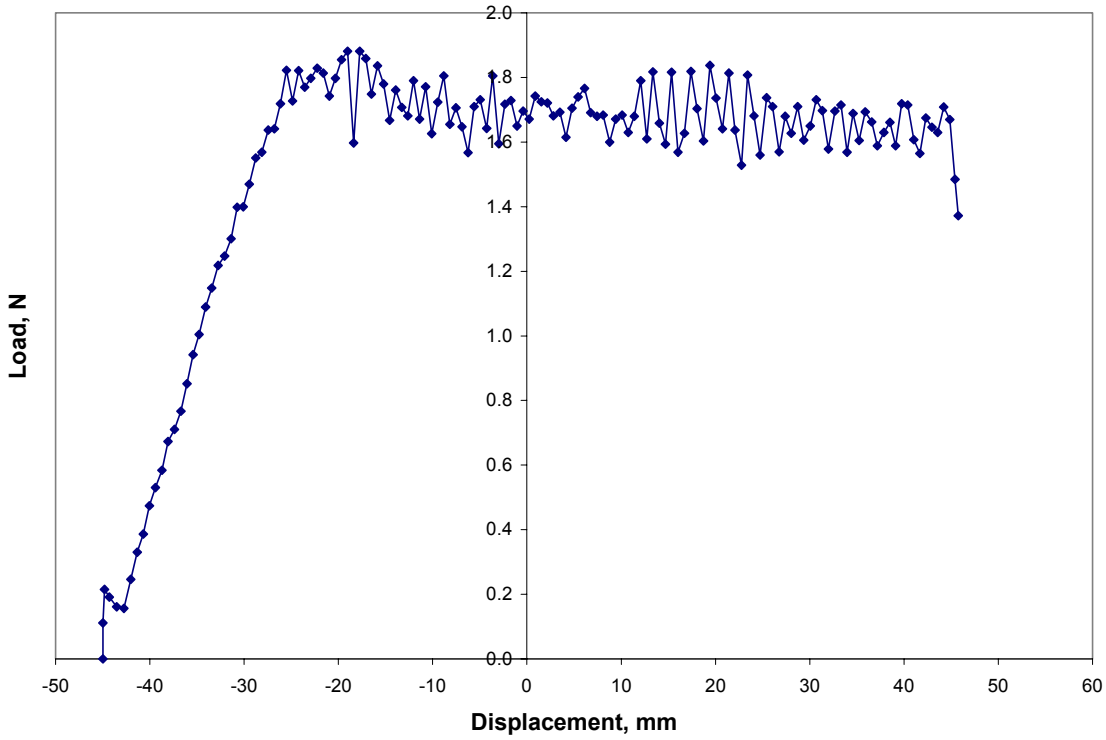

Figure C.51: Load Versus Displacement for Subject A, 180 degrees, 2800 mm/min, Test 3

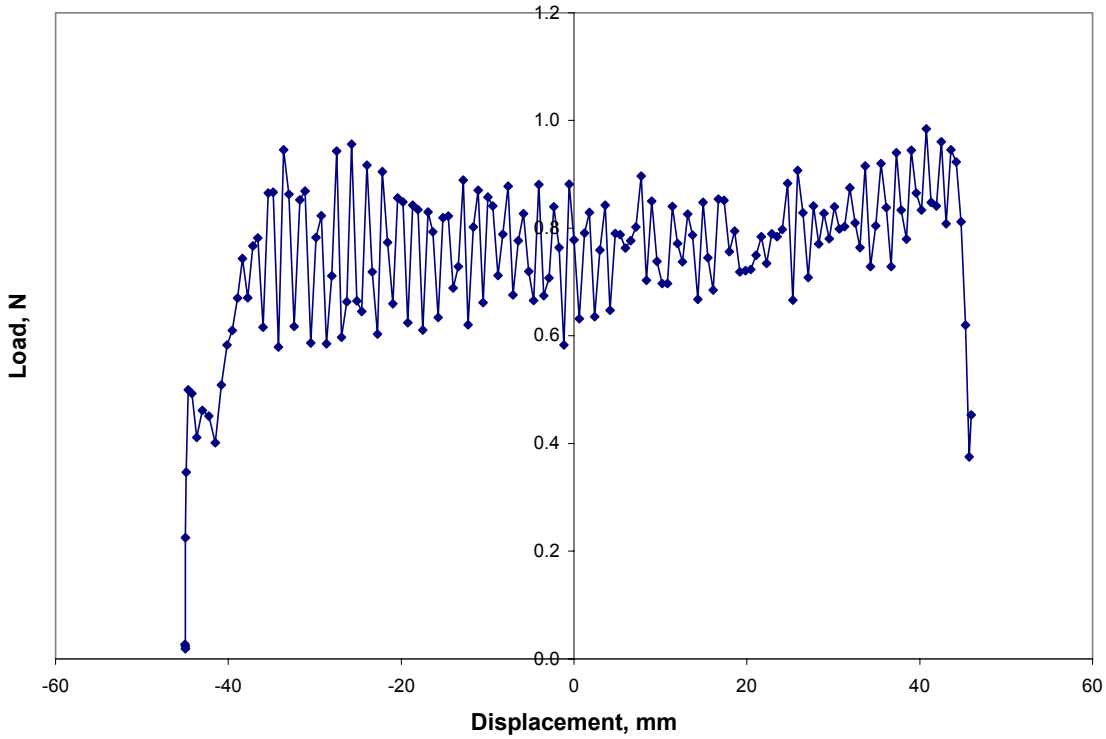

Figure C.52: Load Versus Displacement for Subject A, 180 degrees, 5000 mm/min, Test 1

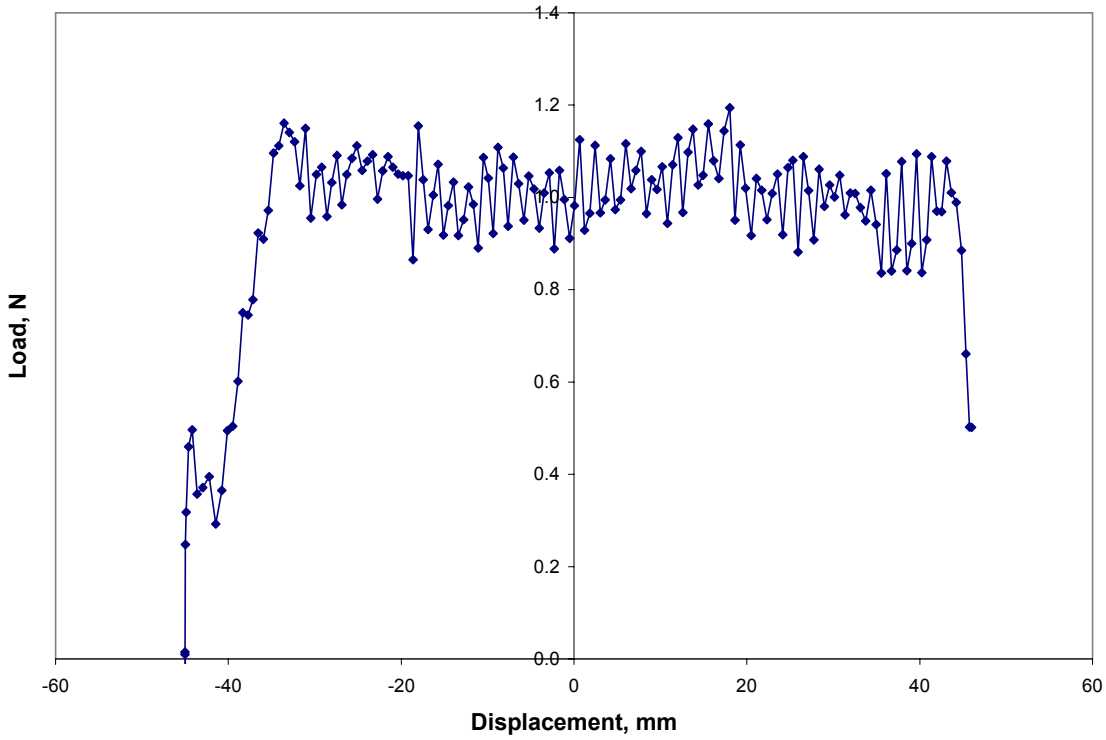

Figure C.53: Load Versus Displacement for Subject A, 180 degrees, 5000 mm/min, Test 2

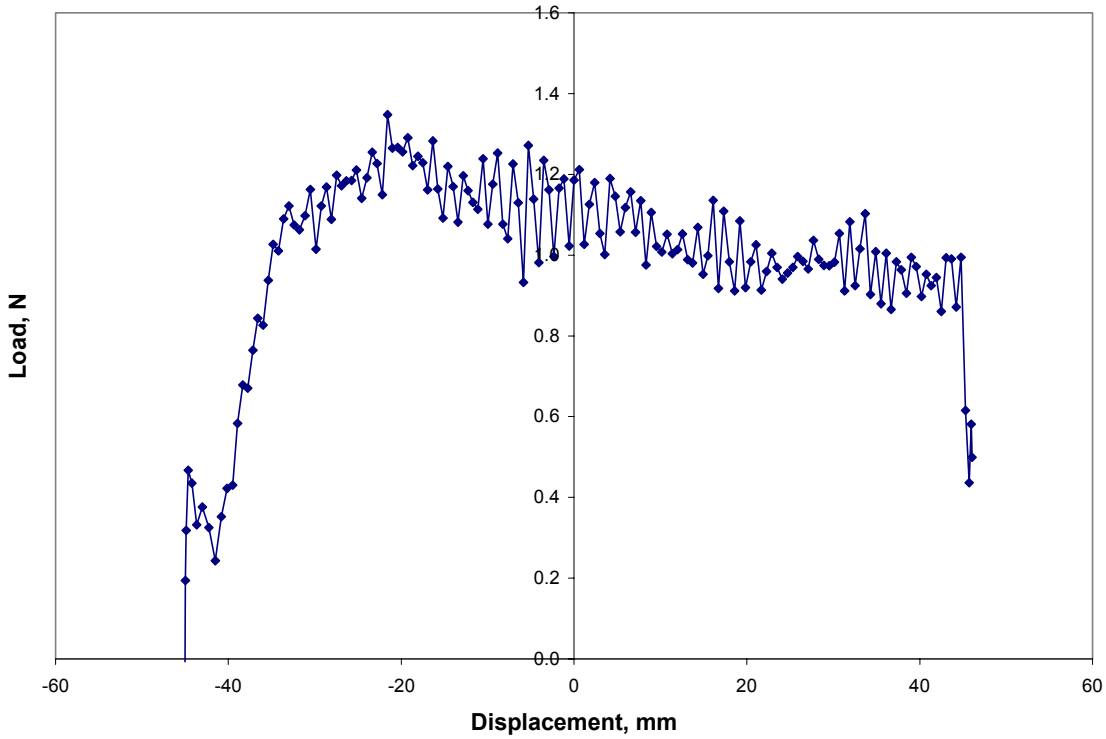

Figure C.54: Load Versus Displacement for Subject A, 180 degrees, 5000 mm/min, Test 3

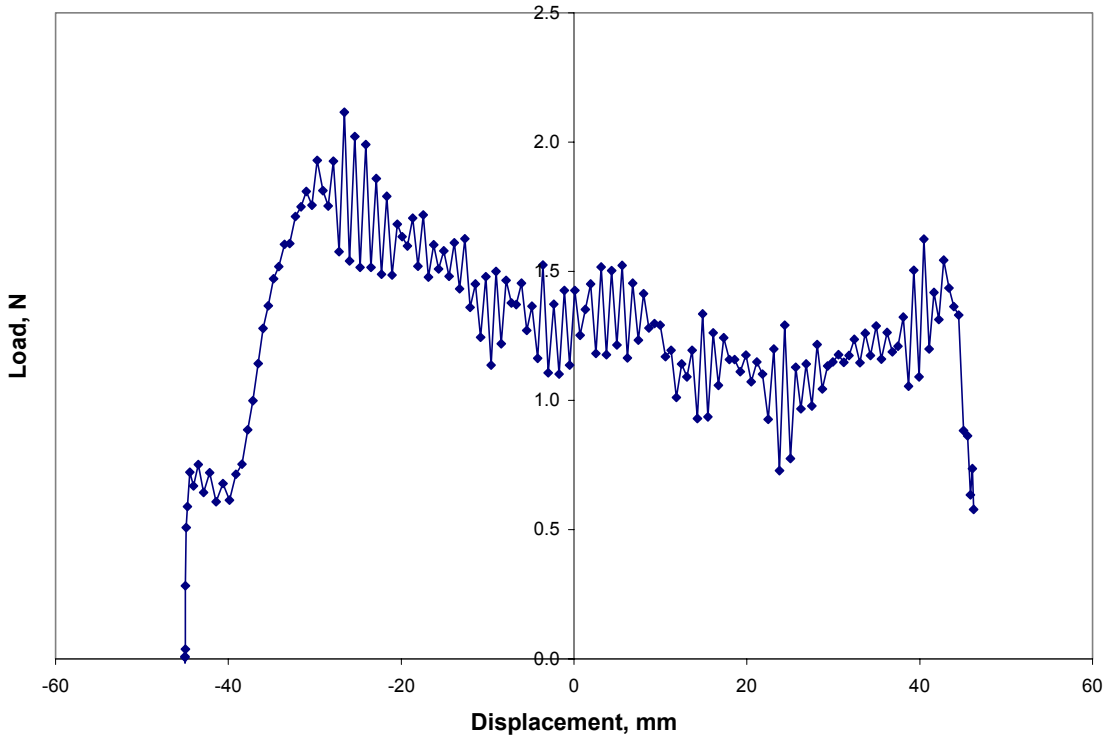

Figure C.55: Load Versus Displacement for Subject A, 180 degrees, 7500 mm/min, Test 1

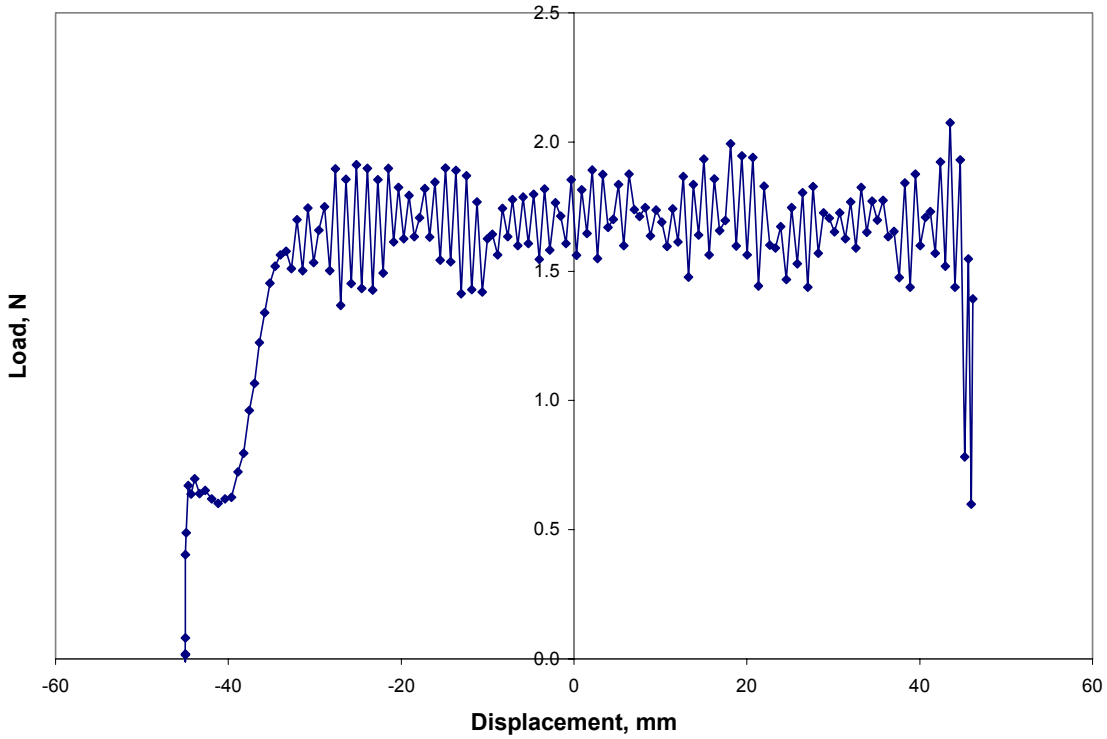

Figure C.56: Load Versus Displacement for Subject A, 180 degrees, 7500 mm/min, Test 2

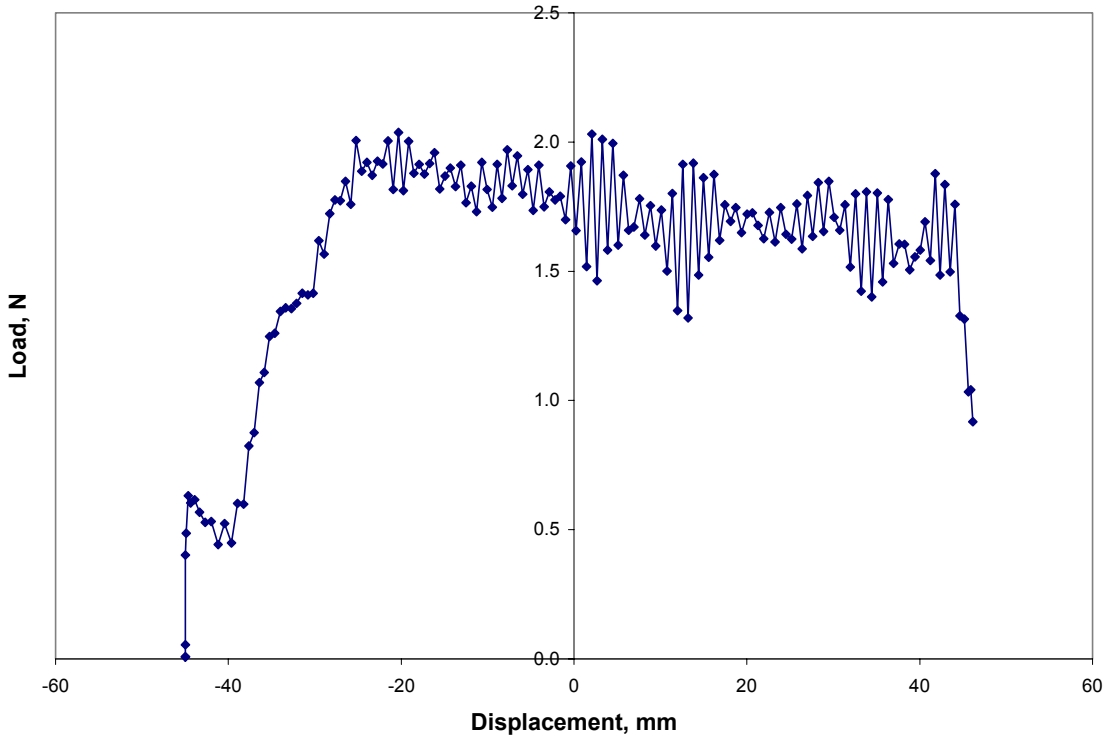

Figure C.57: Load Versus Displacement for Subject A, 180 degrees, 7500 mm/min, Test 3

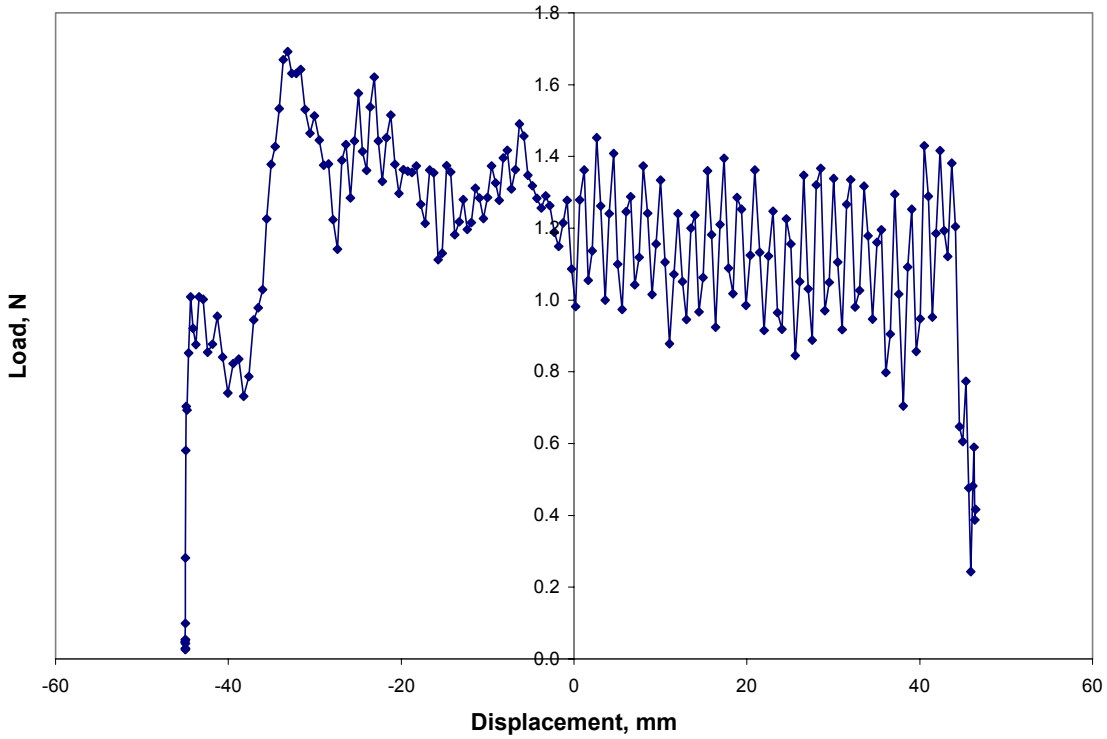

Figure C.58: Load Versus Displacement for Subject A, 180 degrees, 10,000 mm/min, Test 1

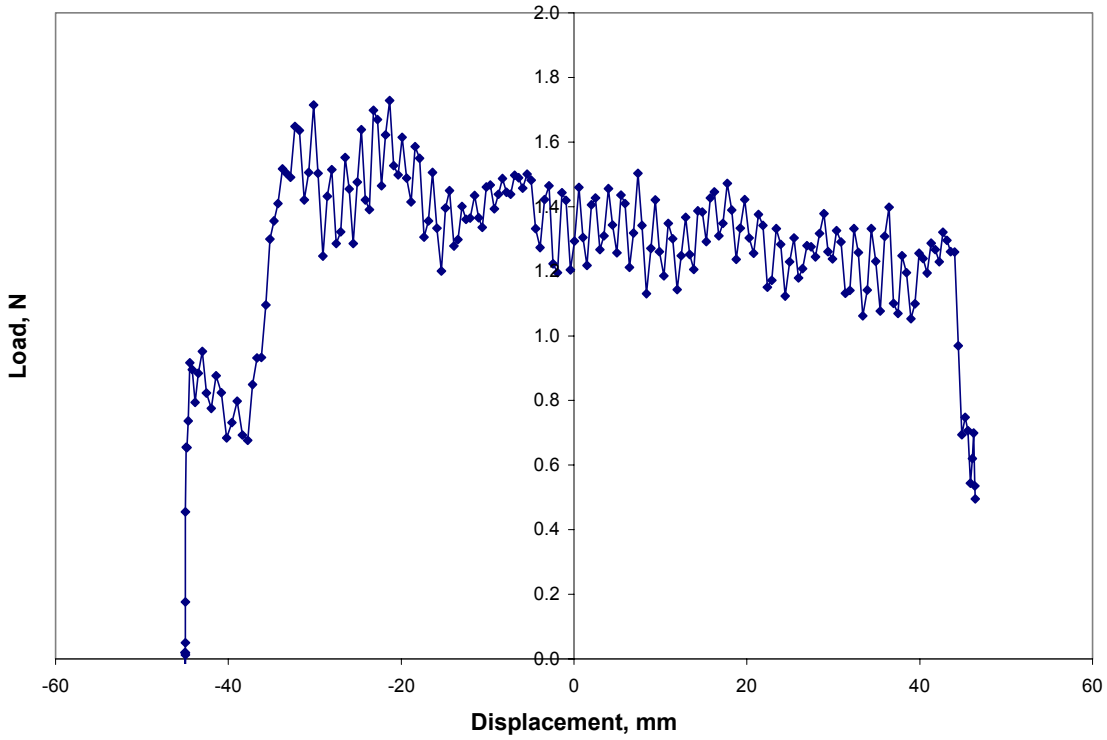

Figure C.59: Load Versus Displacement for Subject A, 180 degrees, 10,000 mm/min, Test 2

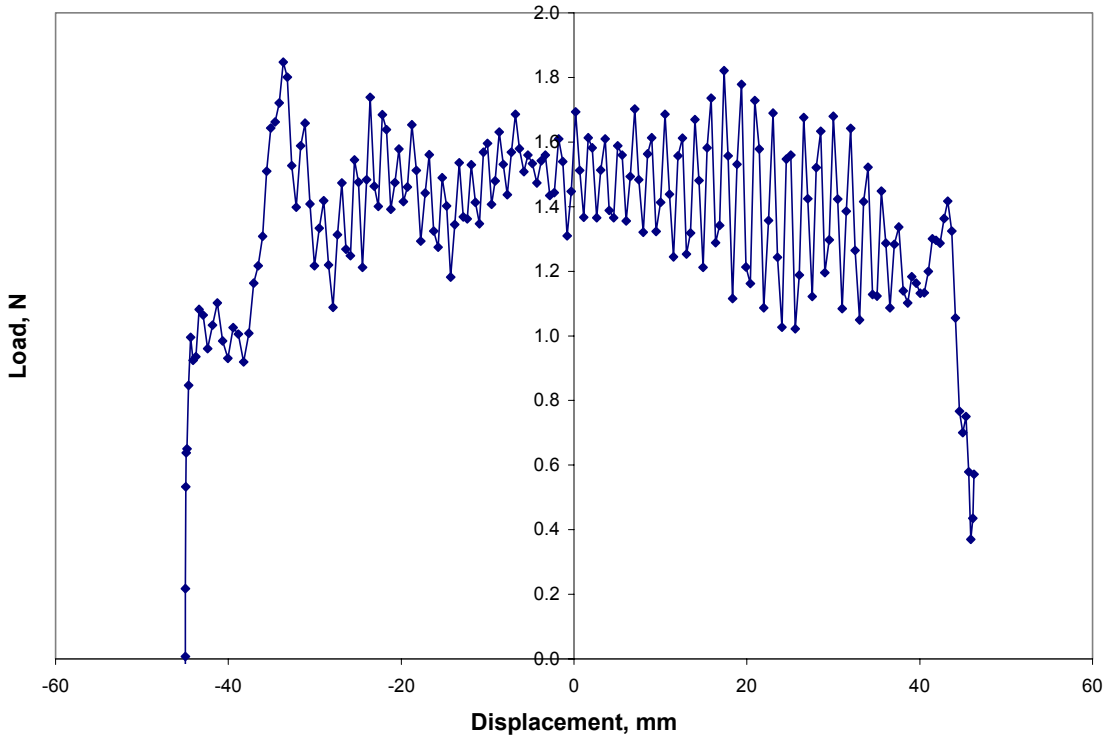

Figure C.60: Load Versus Displacement for Subject A, 180 degrees, 10,000 mm/min, Test 3

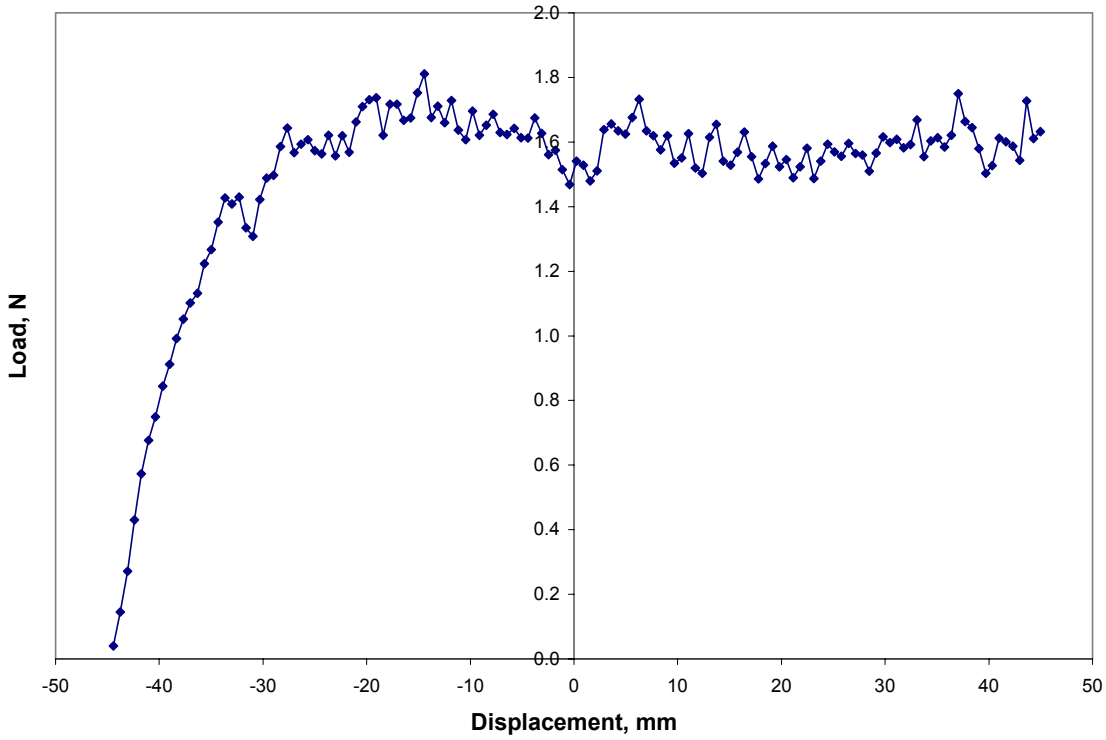

Figure C.61: Load Versus Displacement for Subject D, 180 degrees, 200 mm/min, Test 1

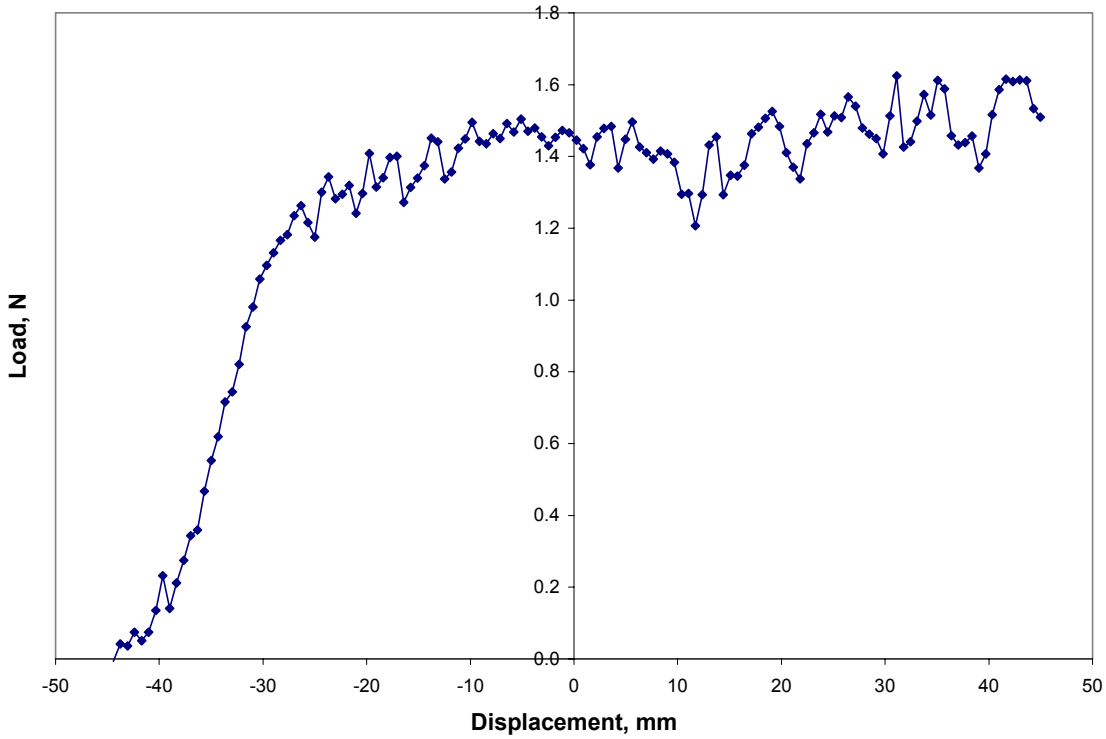

Figure C.62: Load Versus Displacement for Subject D, 180 degrees, 200 mm/min, Test 2

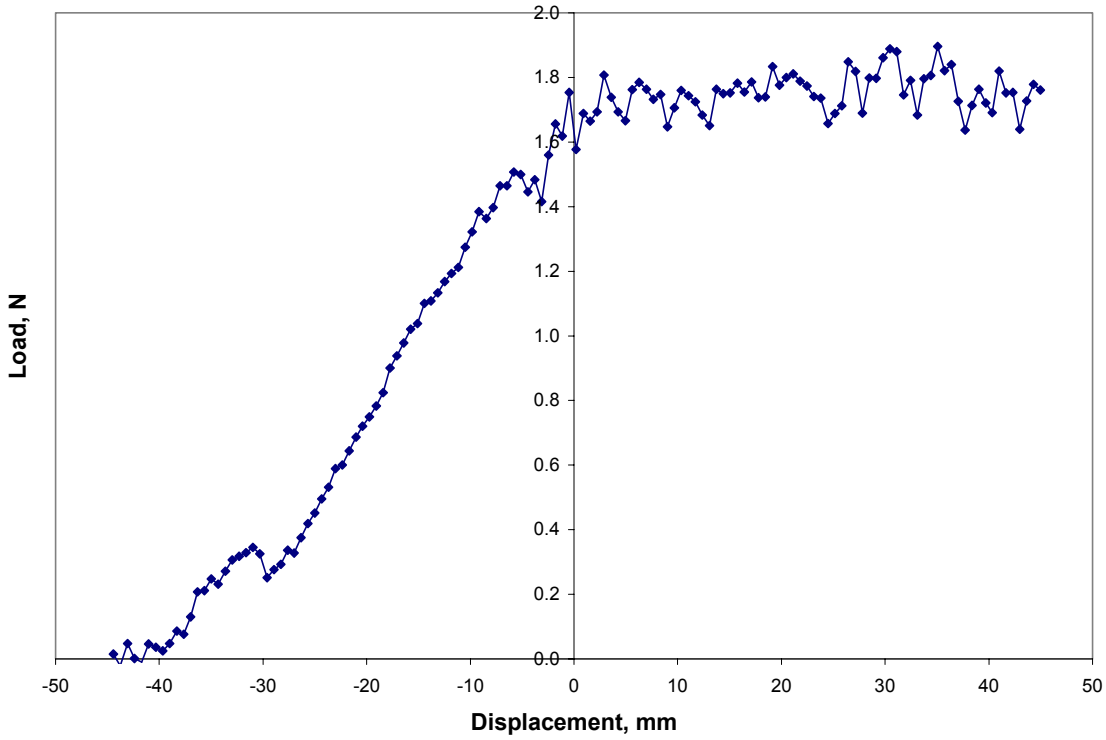

Figure C.63: Load Versus Displacement for Subject D, 180 degrees, 200 mm/min, Test 3

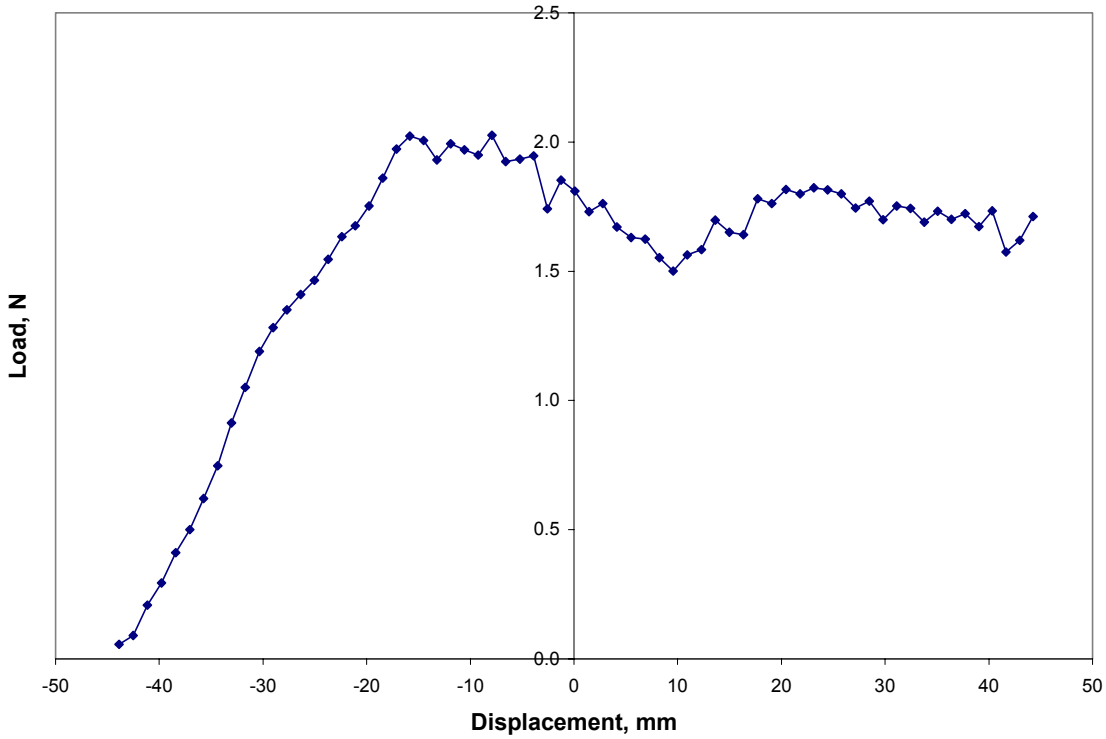

Figure C.64: Load Versus Displacement for Subject D, 180 degrees, 400 mm/min, Test 1

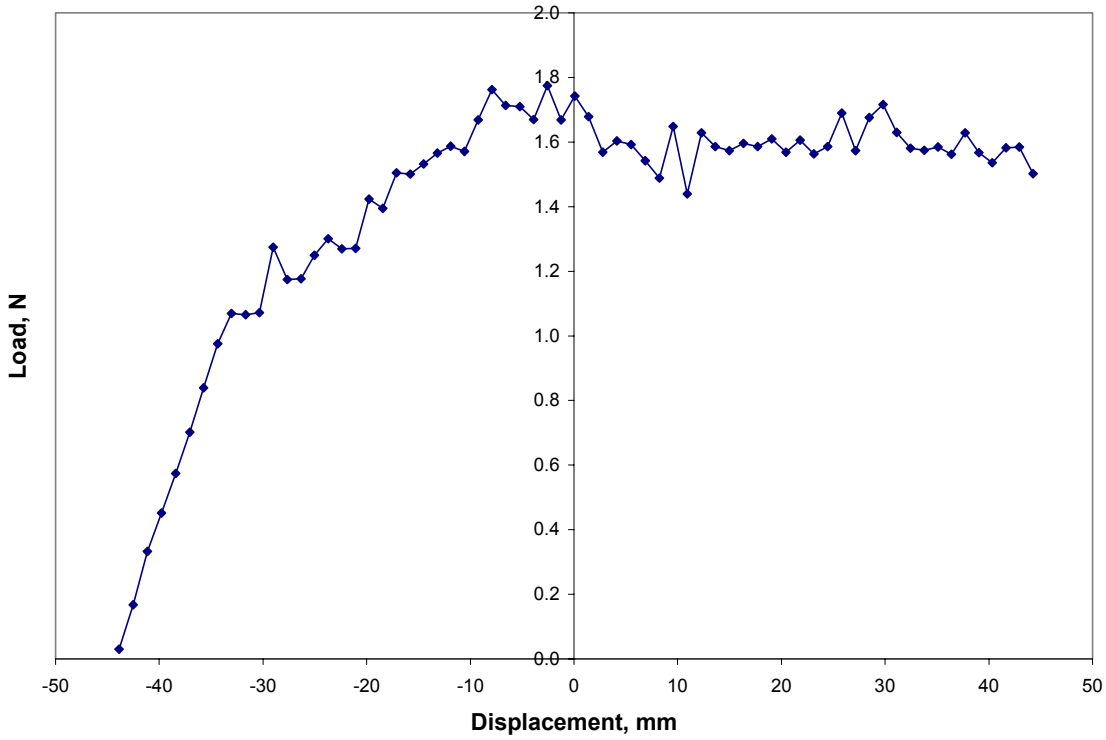

Figure C.65: Load Versus Displacement for Subject D, 180 degrees, 400 mm/min, Test 2

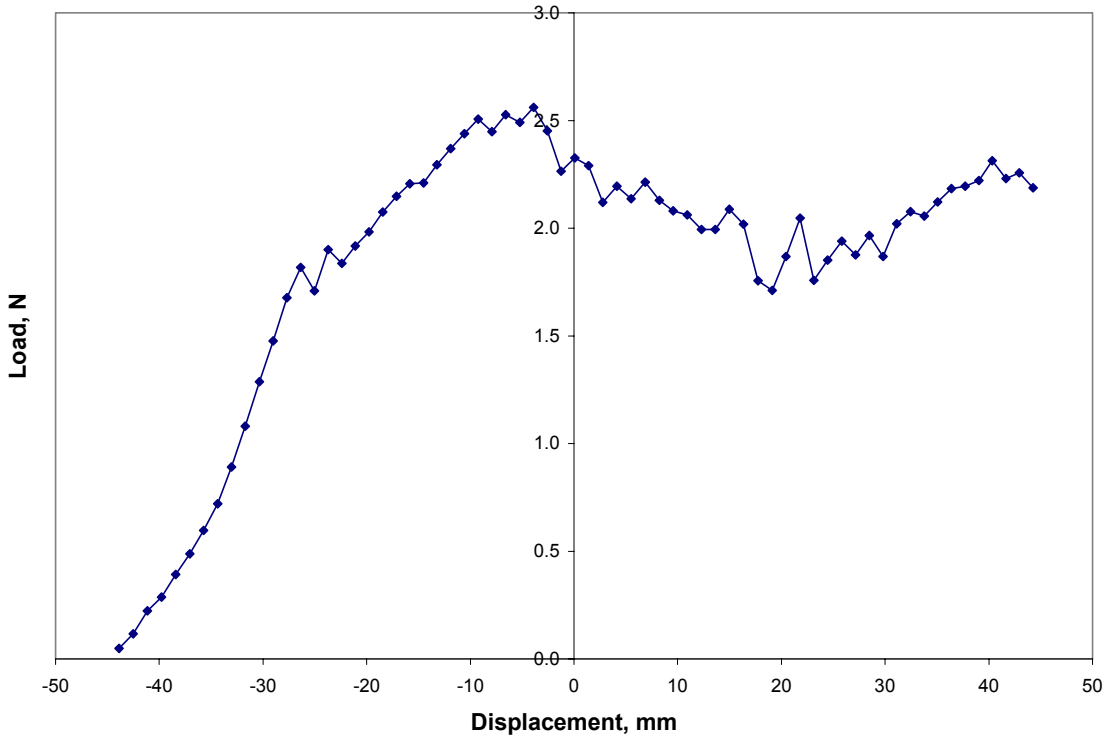

Figure C.66: Load Versus Displacement for Subject D, 180 degrees, 400 mm/min, Test 3

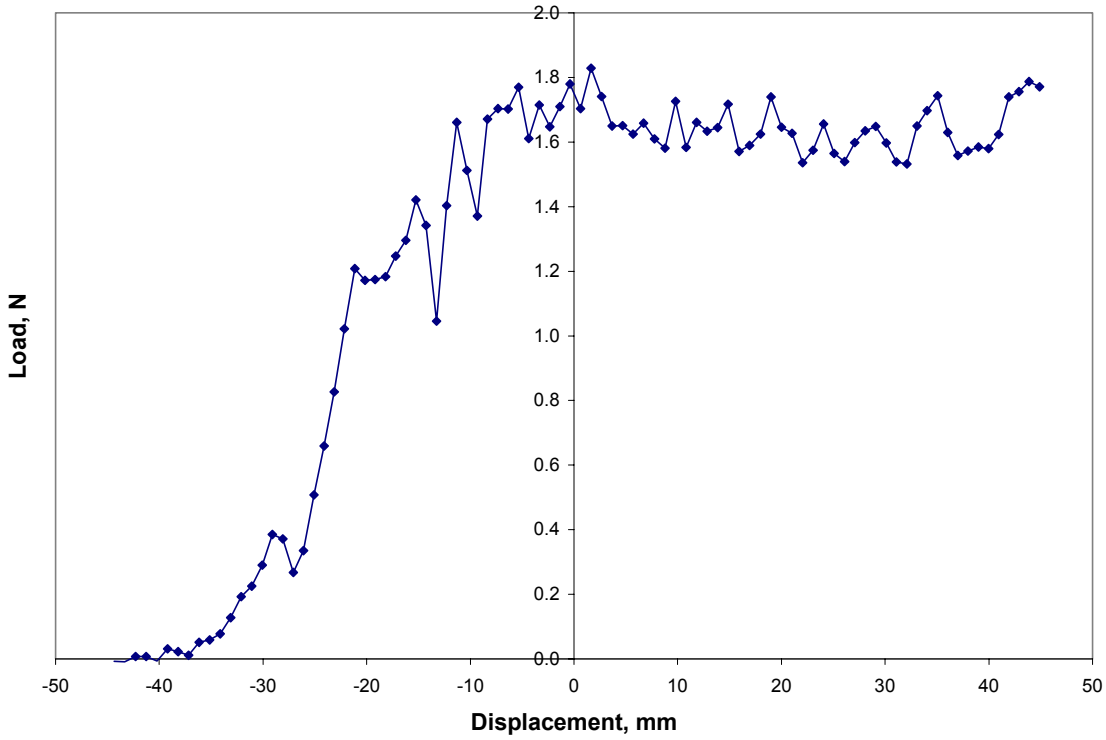

Figure C.67: Load Versus Displacement for Subject D, 180 degrees, 600 mm/min, Test 1

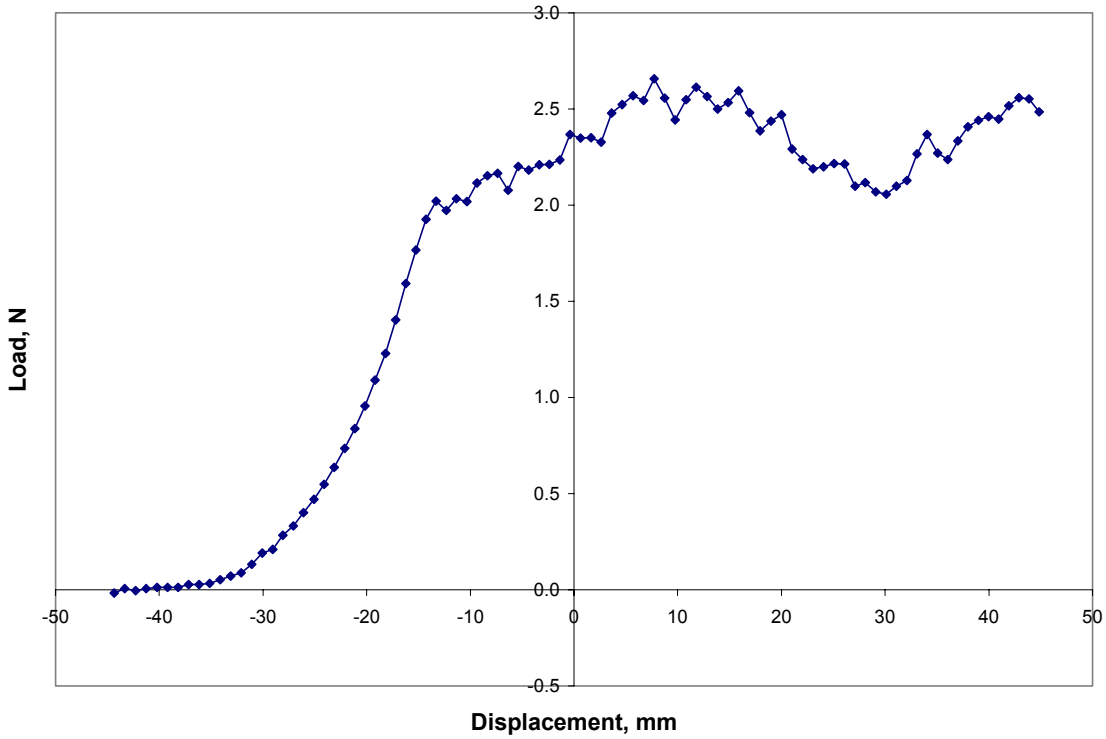

Figure C.68: Load Versus Displacement for Subject D, 180 degrees, 600 mm/min, Test 2

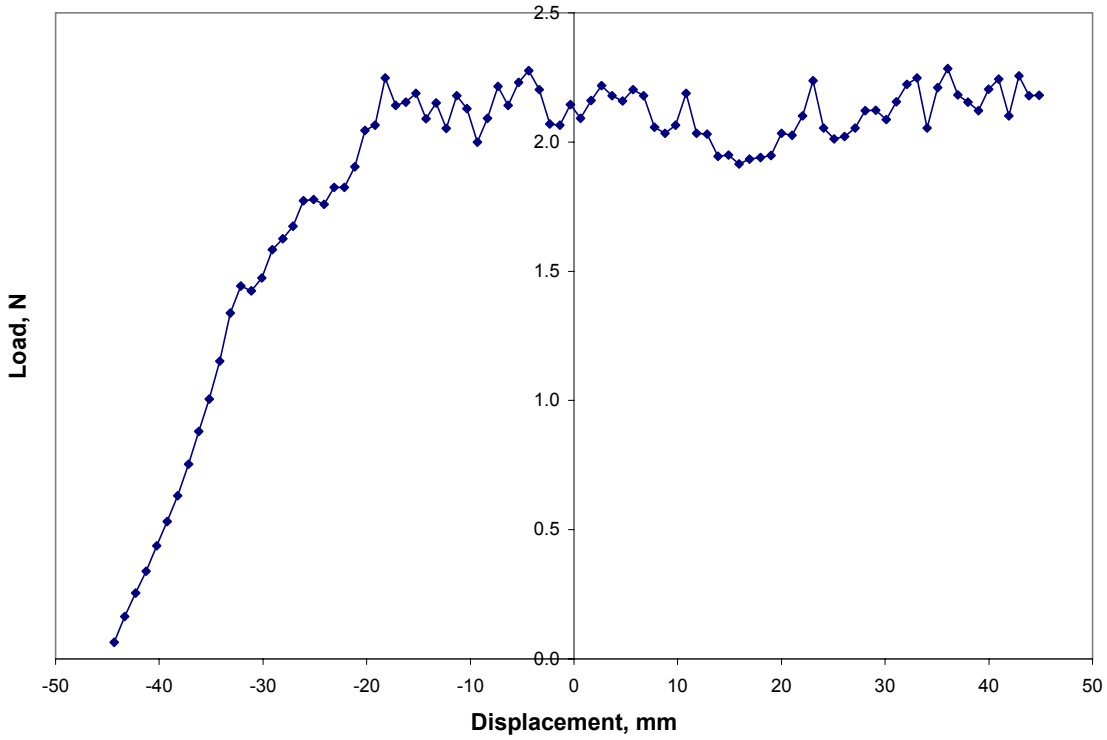

Figure C.69: Load Versus Displacement for Subject D, 180 degrees, 600 mm/min, Test 3

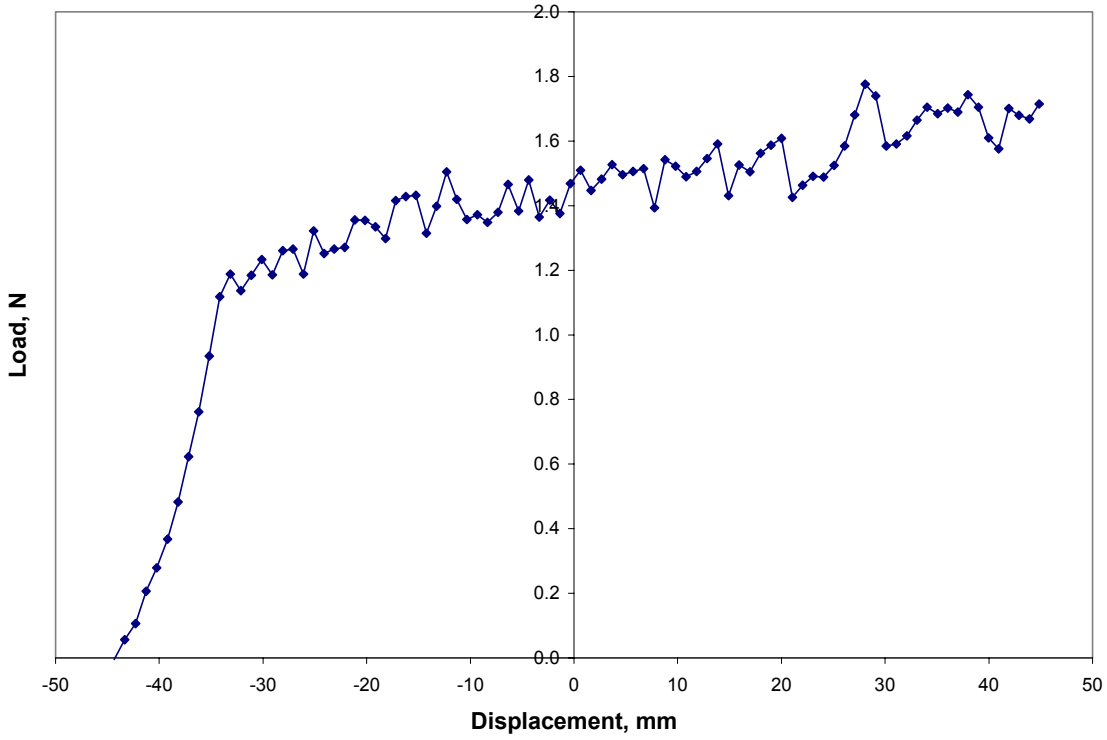

Figure C.70: Load Versus Displacement for Subject D, 180 degrees, 600 mm/min, Test 4

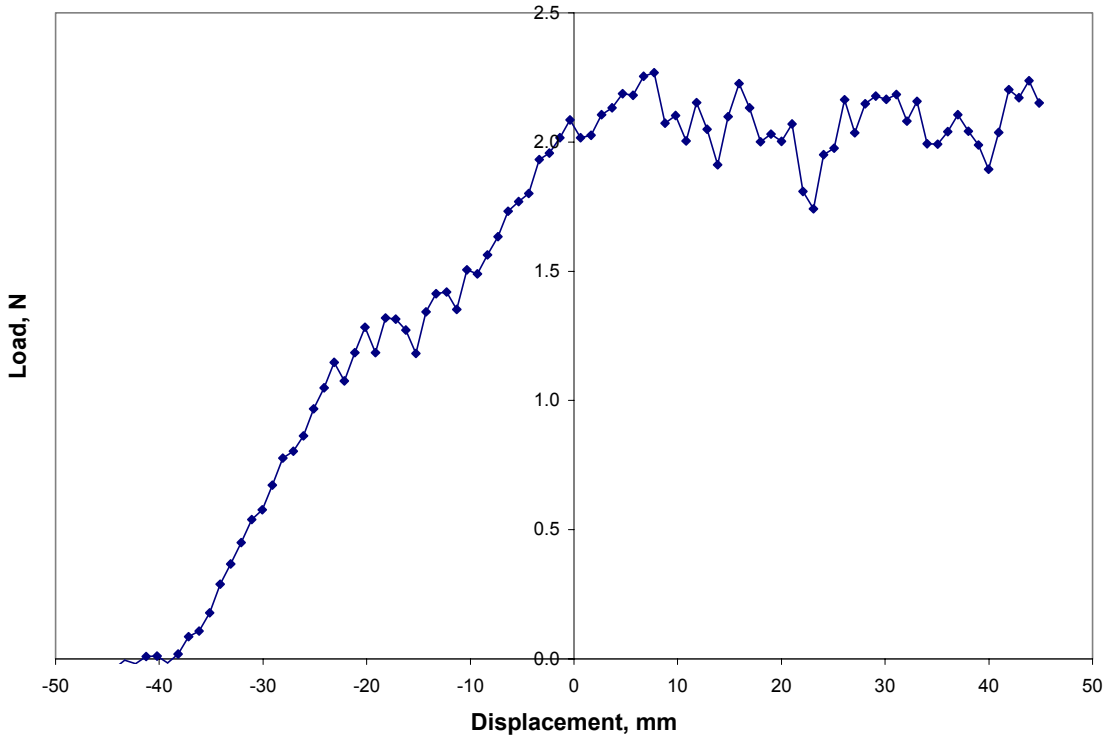

Figure C.71: Load Versus Displacement for Subject D, 180 degrees, 600 mm/min, Test 5

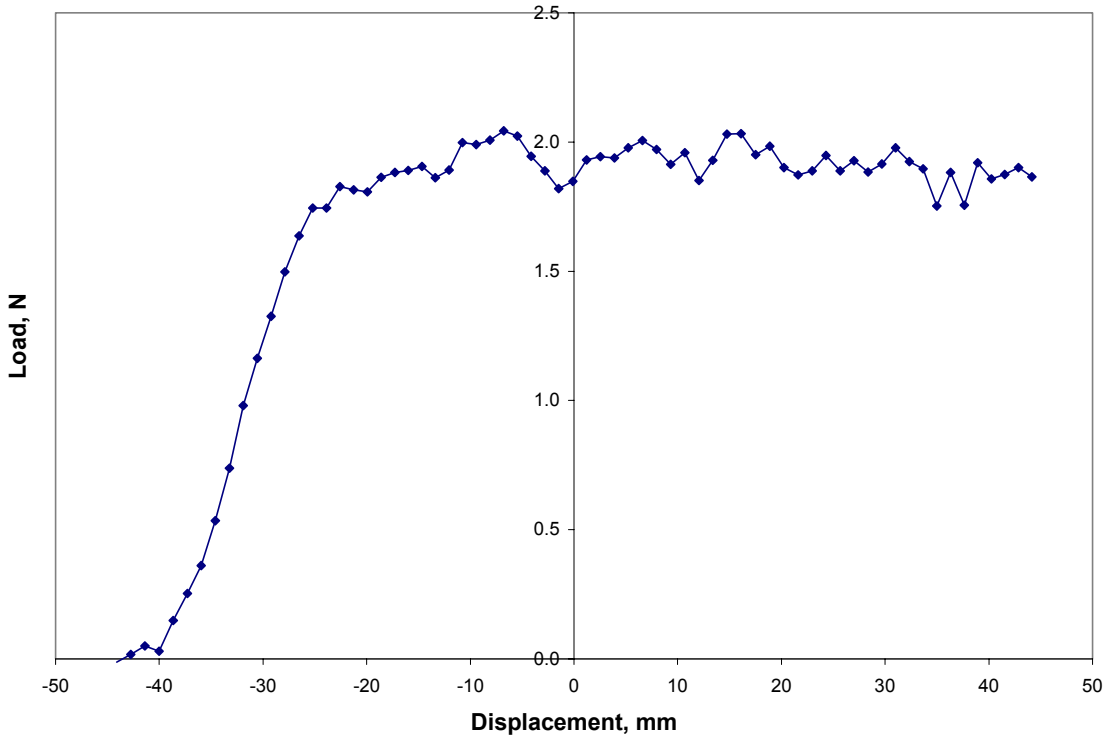

Figure C.72: Load Versus Displacement for Subject D, 180 degrees, 800 mm/min, Test 1

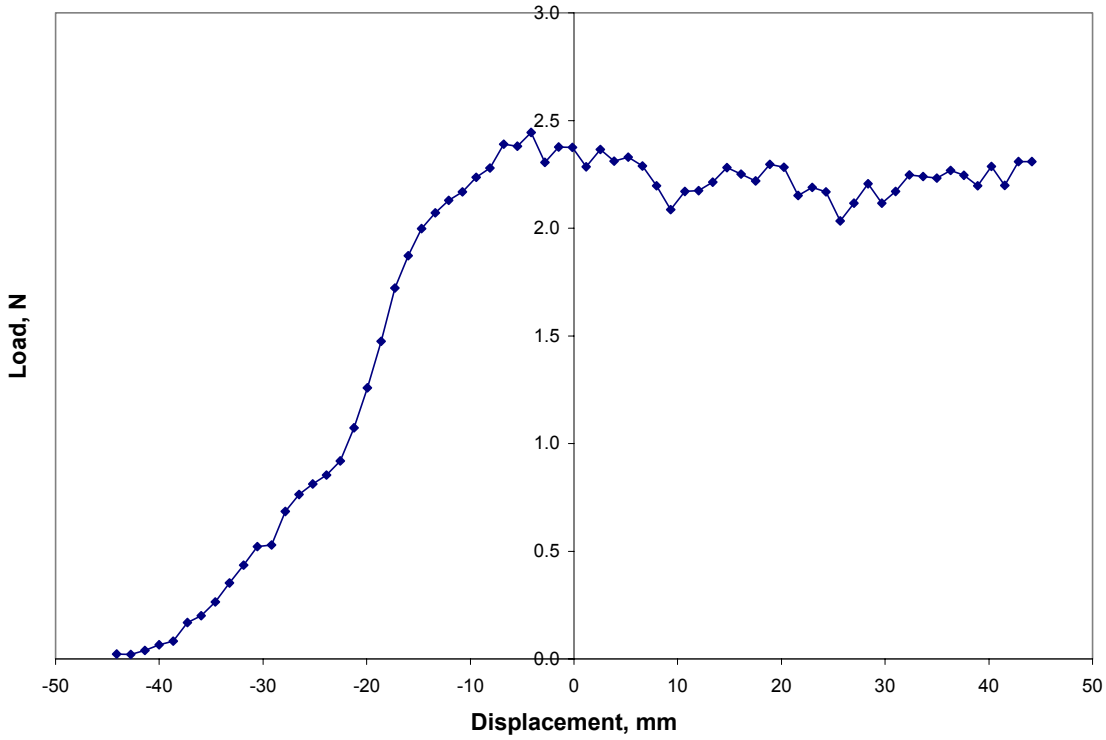

Figure C.73: Load Versus Displacement for Subject D, 180 degrees, 800 mm/min, Test 2

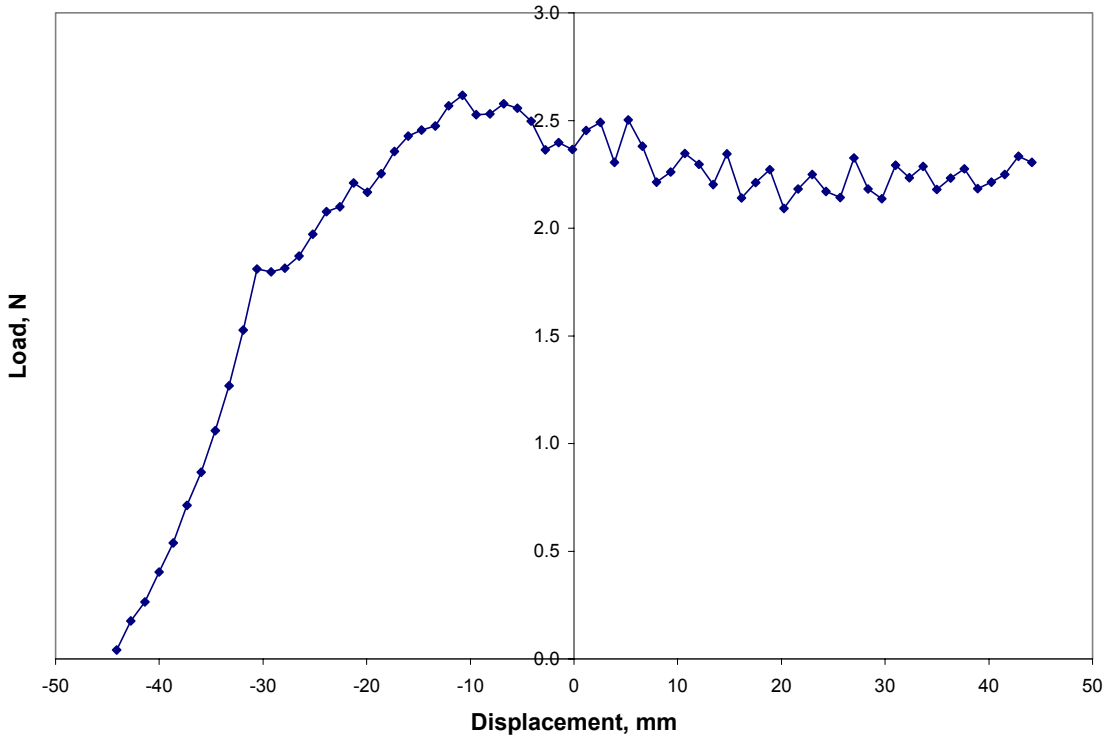

Figure C.74: Load Versus Displacement for Subject D, 180 degrees, 800 mm/min, Test 3

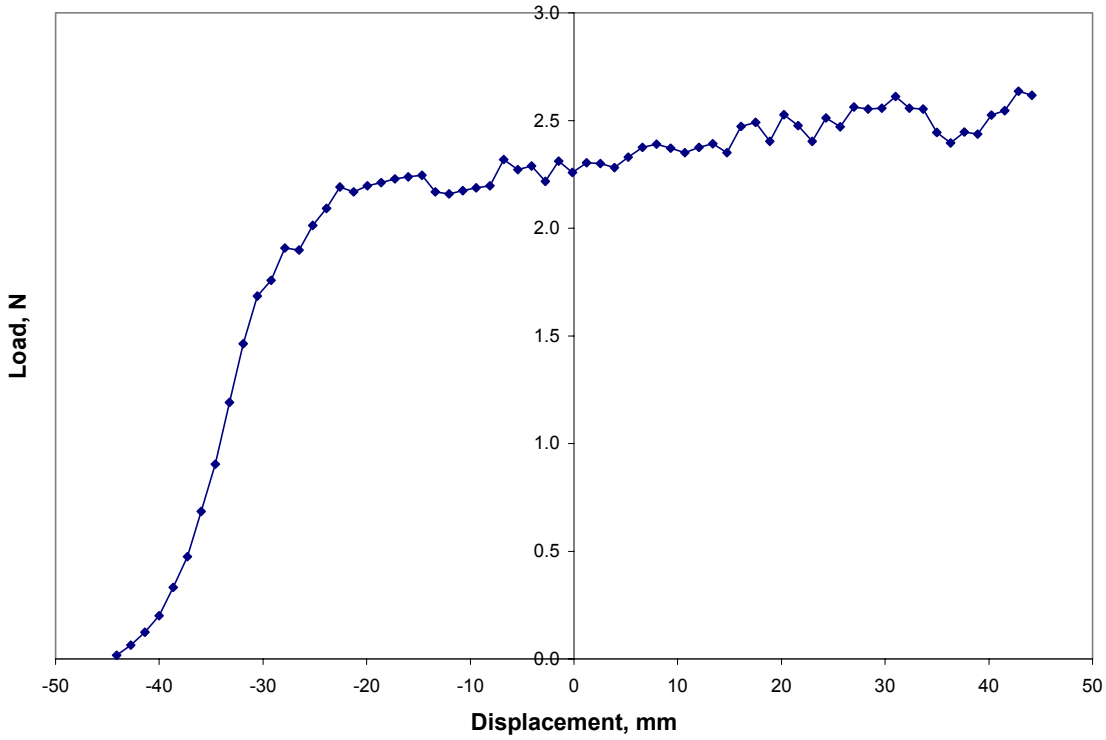

Figure C.75: Load Versus Displacement for Subject D, 180 degrees, 800 mm/min, Test 4

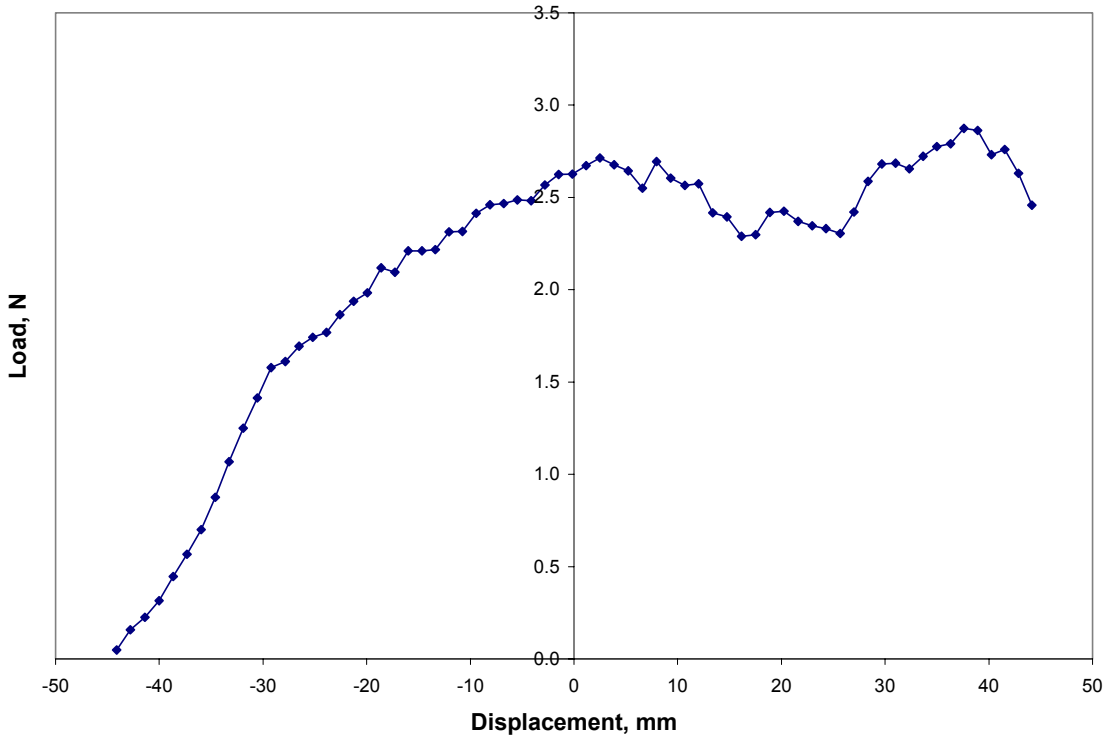

Figure C.76: Load Versus Displacement for Subject D, 180 degrees, 800 mm/min, Test 5

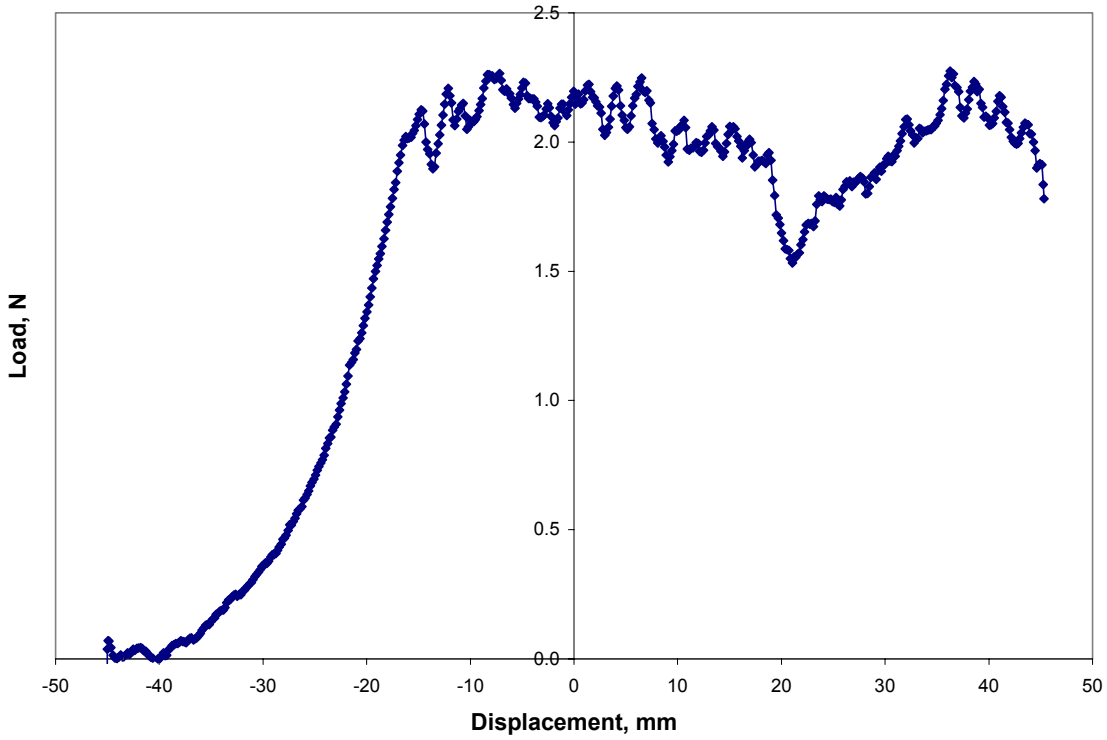

Figure C.77: Load Versus Displacement for Subject D, 180 degrees, 1000 mm/min, Test 1

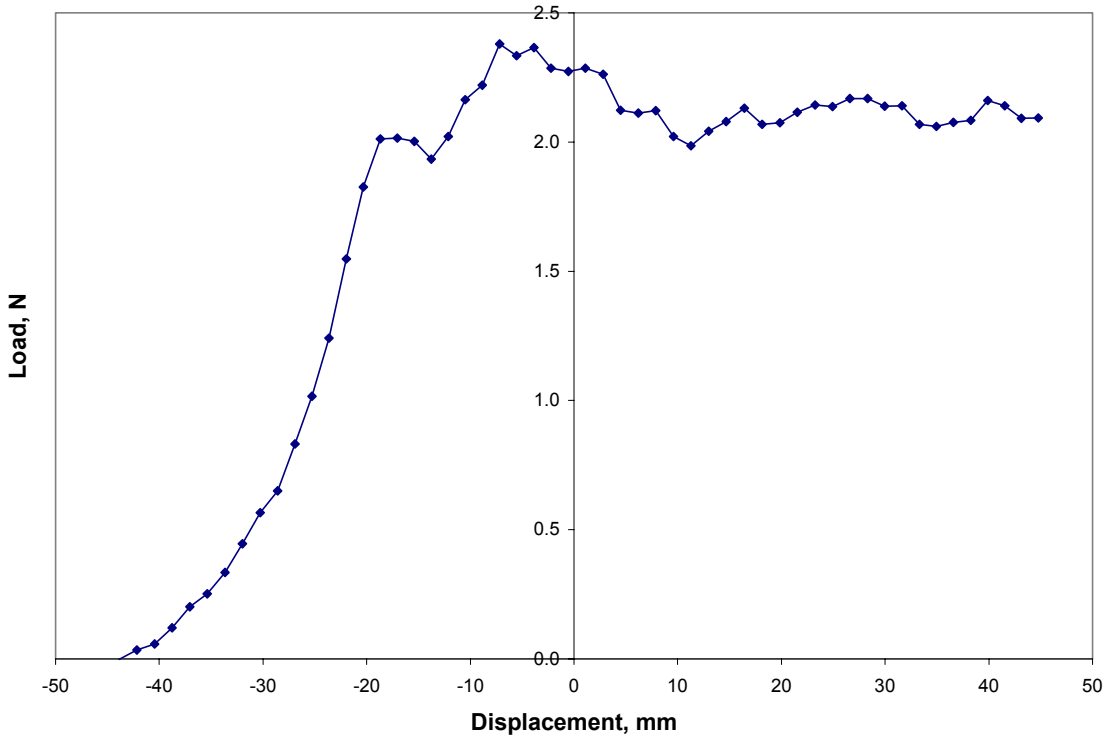

Figure C.78: Load Versus Displacement for Subject D, 180 degrees, 1000 mm/min, Test 2

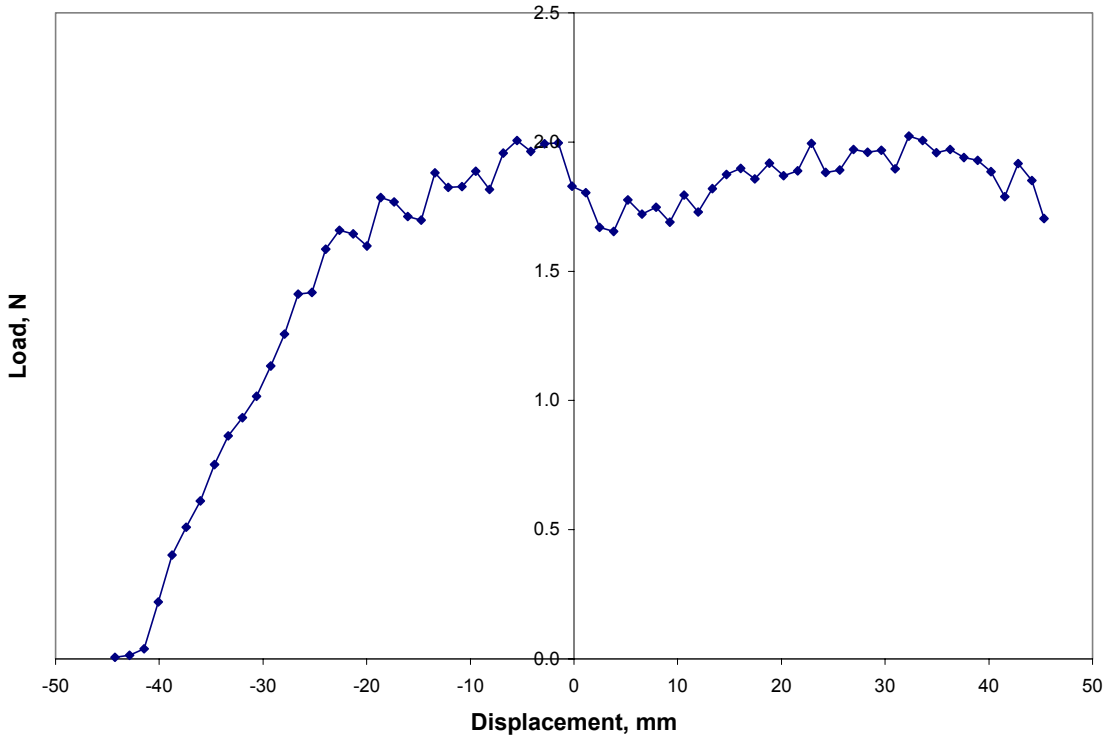

Figure C.79: Load Versus Displacement for Subject D, 180 degrees, 1000 mm/min, Test 3

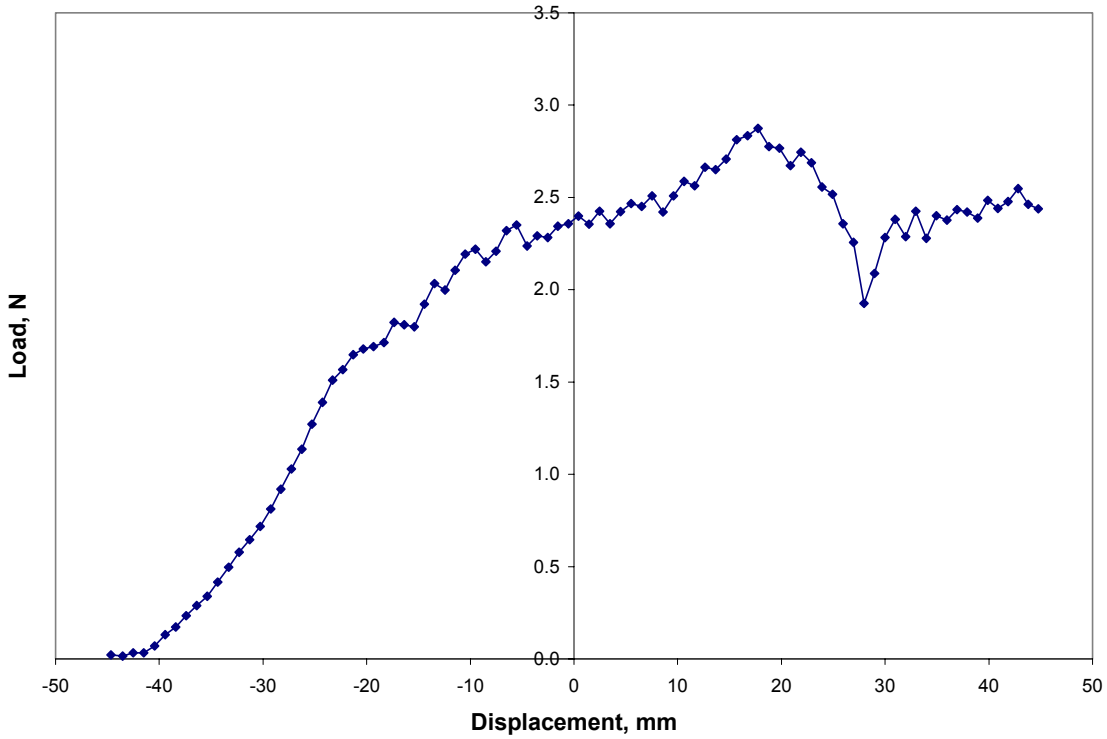

Figure C.80: Load Versus Displacement for Subject D, 180 degrees, 1000 mm/min, Test 4

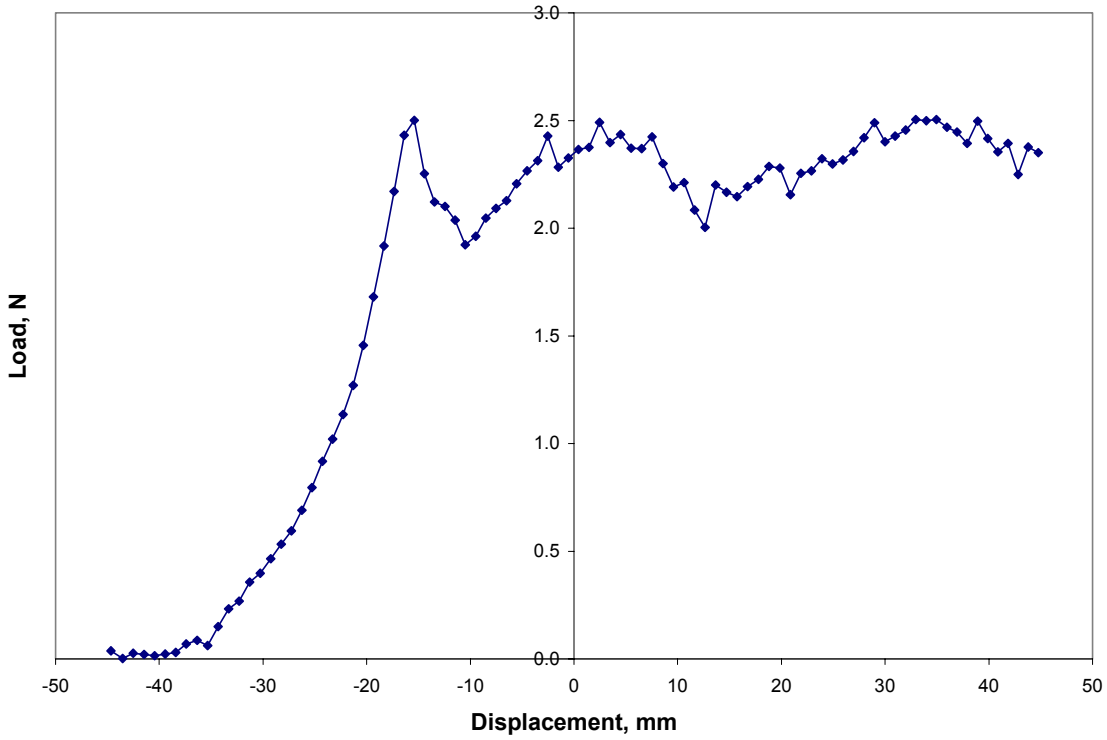

Figure C.81: Load Versus Displacement for Subject D, 180 degrees, 1000 mm/min, Test 5

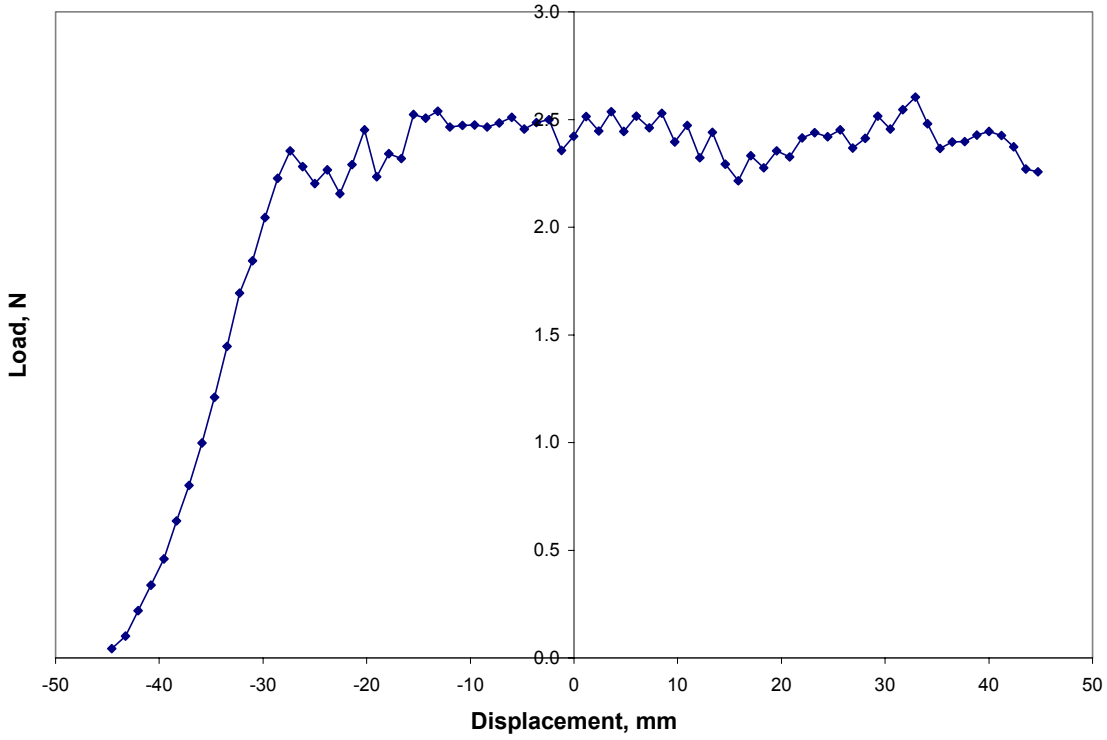

Figure C.82: Load Versus Displacement for Subject D, 180 degrees, 1200 mm/min, Test 1

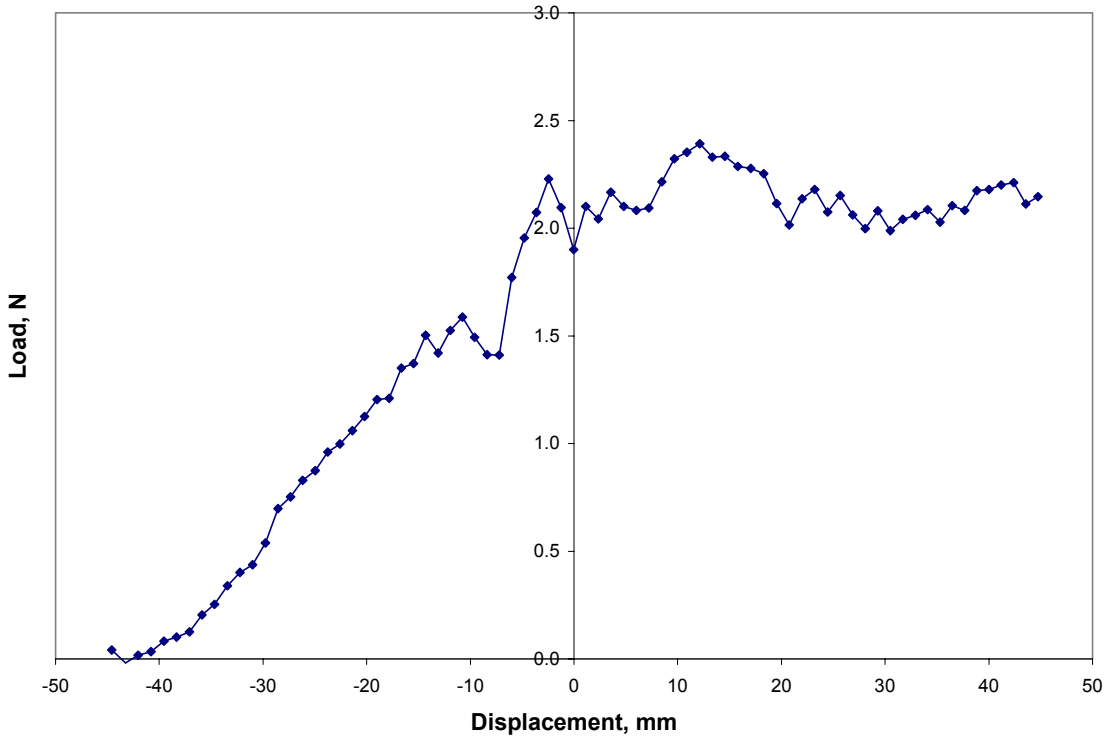

Figure C.83: Load Versus Displacement for Subject D, 180 degrees, 1200 mm/min, Test 2

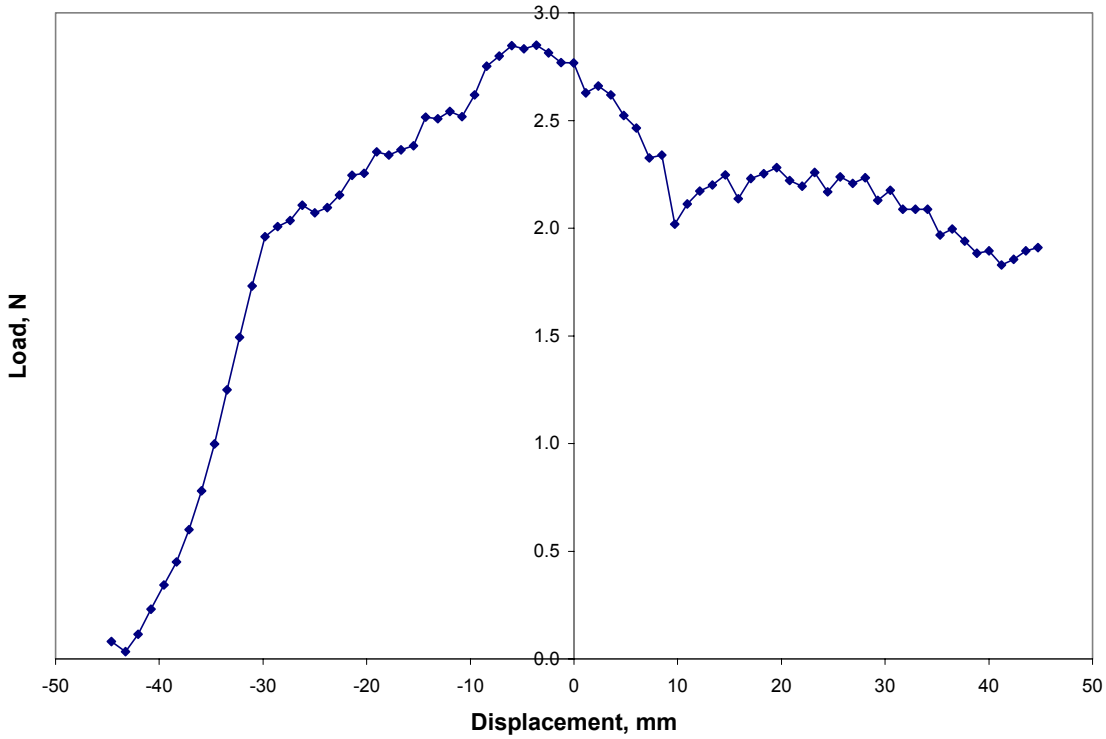

Figure C.84: Load Versus Displacement for Subject D, 180 degrees, 1200 mm/min, Test 3

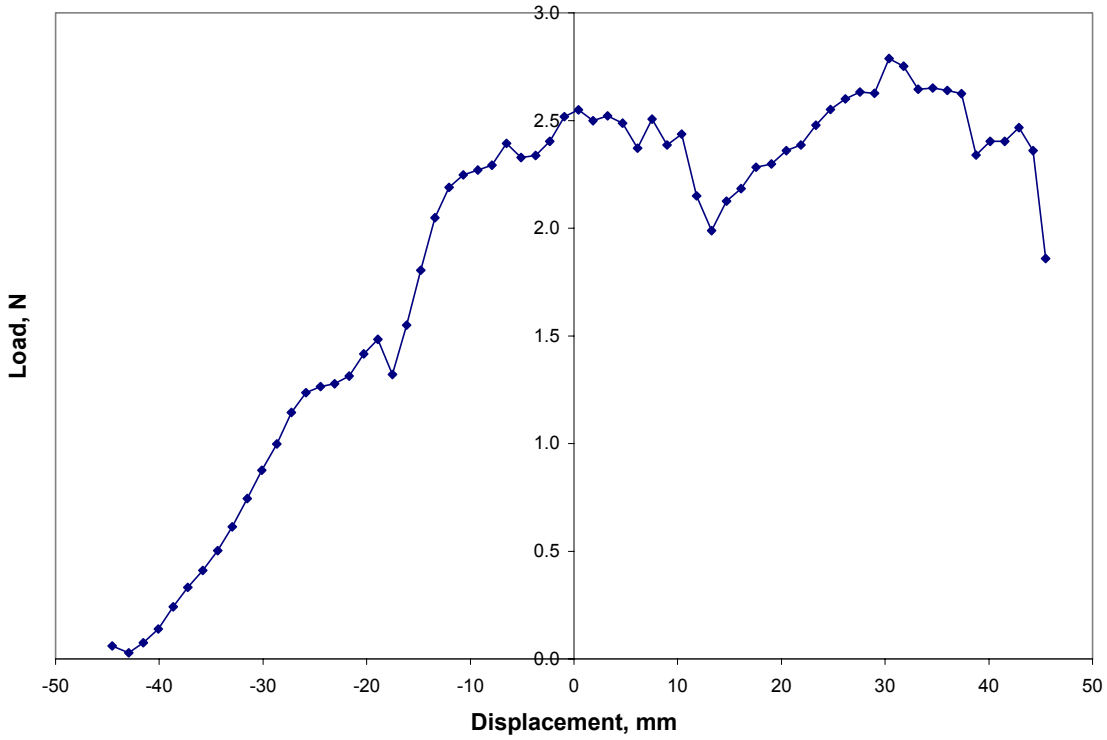

Figure C.85: Load Versus Displacement for Subject D, 180 degrees, 1400 mm/min, Test 1

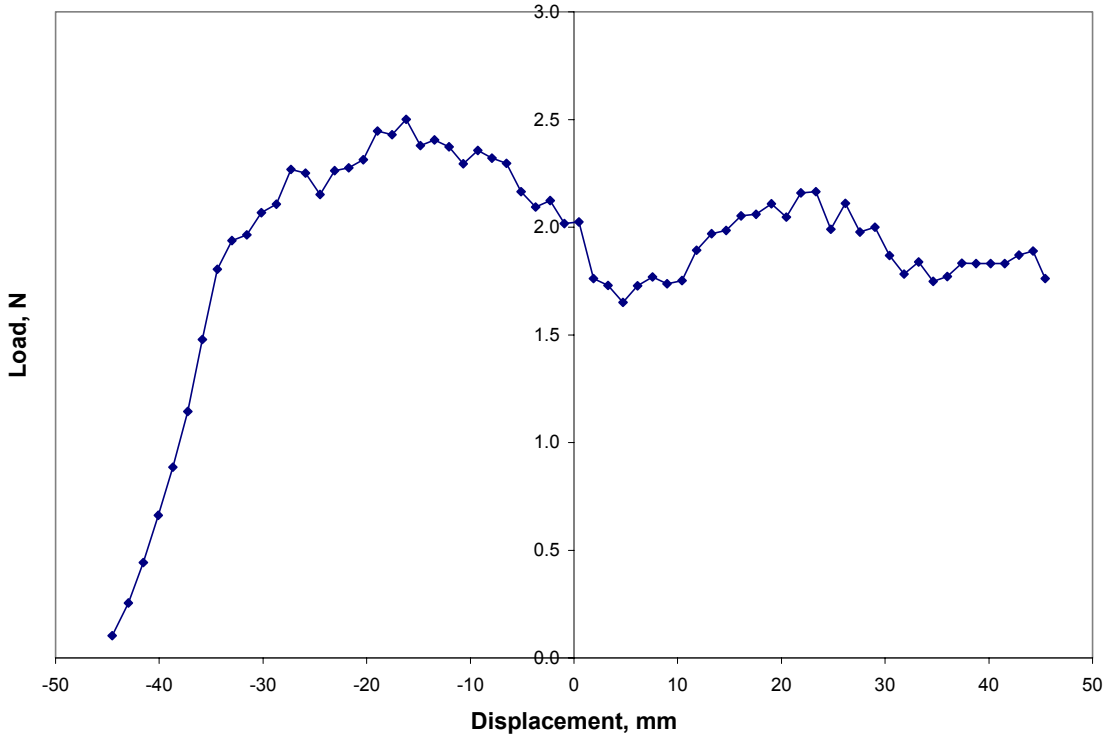

Figure C.86: Load Versus Displacement for Subject D, 180 degrees, 1400 mm/min, Test 2

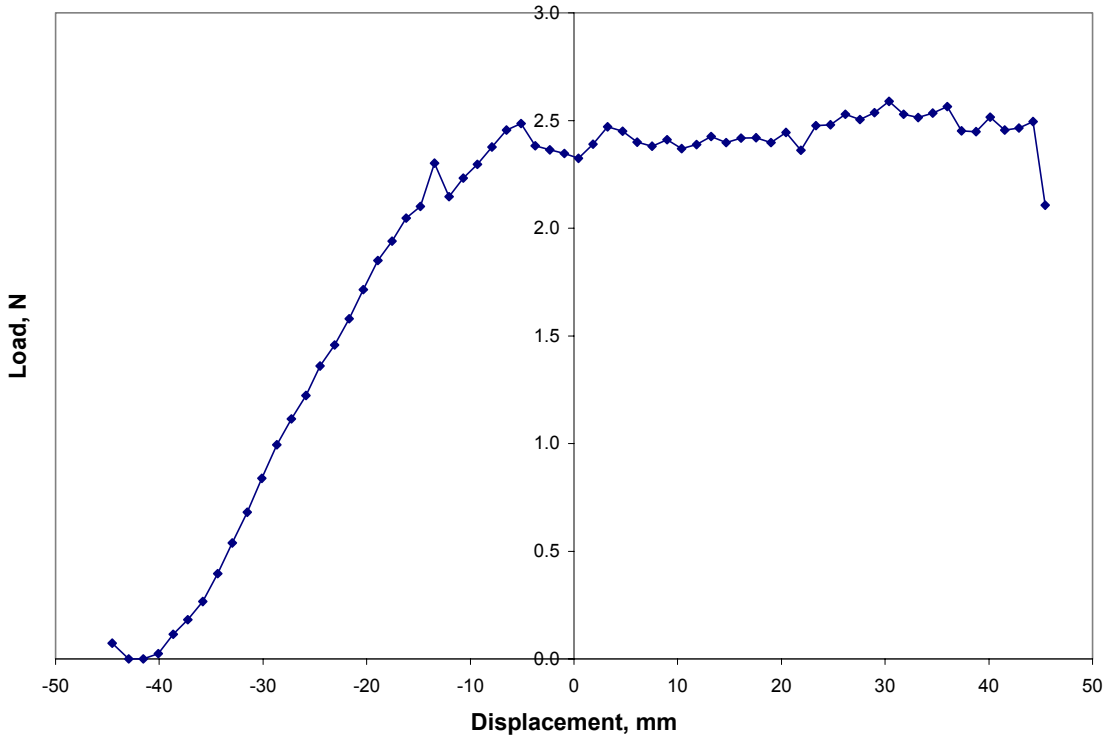

Figure C.87: Load Versus Displacement for Subject D, 180 degrees, 1400 mm/min, Test 3

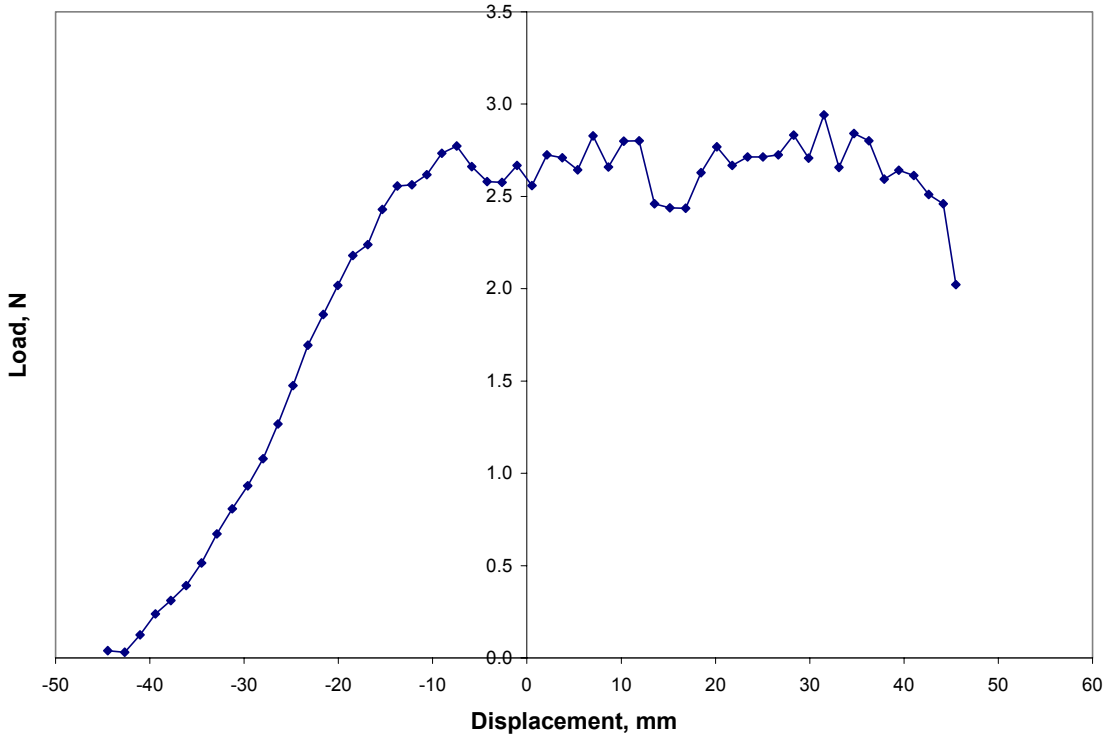

Figure C.88: Load Versus Displacement for Subject D, 180 degrees, 1600 mm/min, Test 1

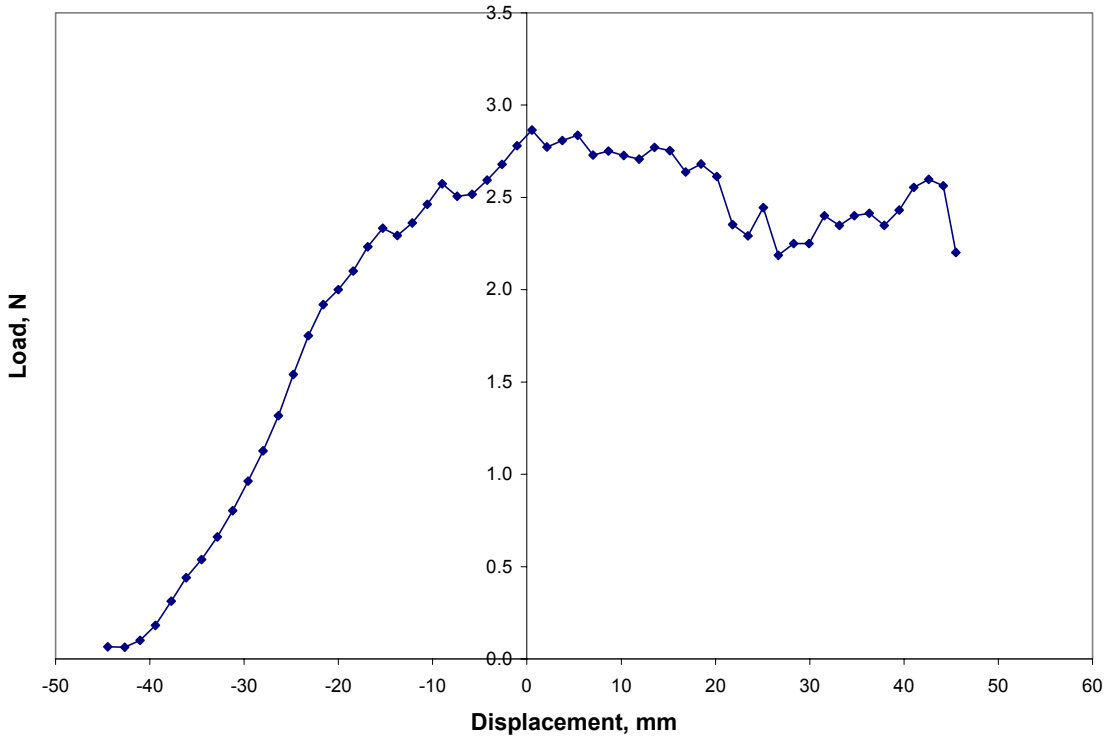

Figure C.89: Load Versus Displacement for Subject D, 180 degrees, 1600 mm/min, Test 2

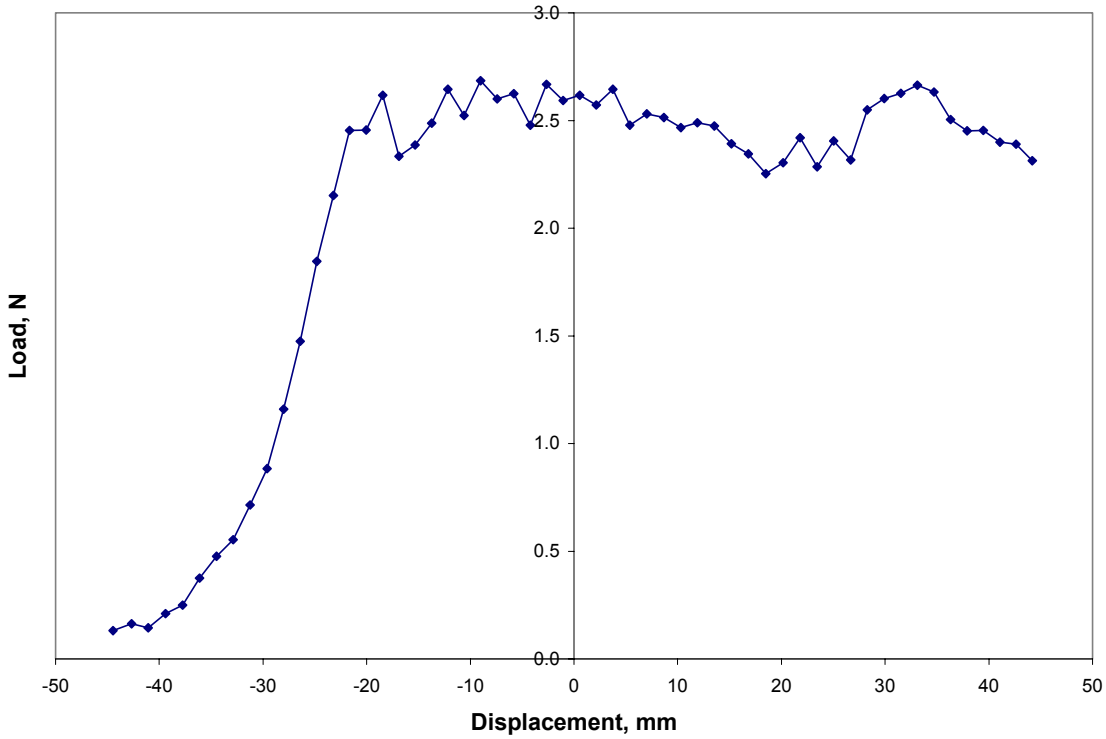

Figure C.90: Load Versus Displacement for Subject D, 180 degrees, 1600 mm/min, Test 3

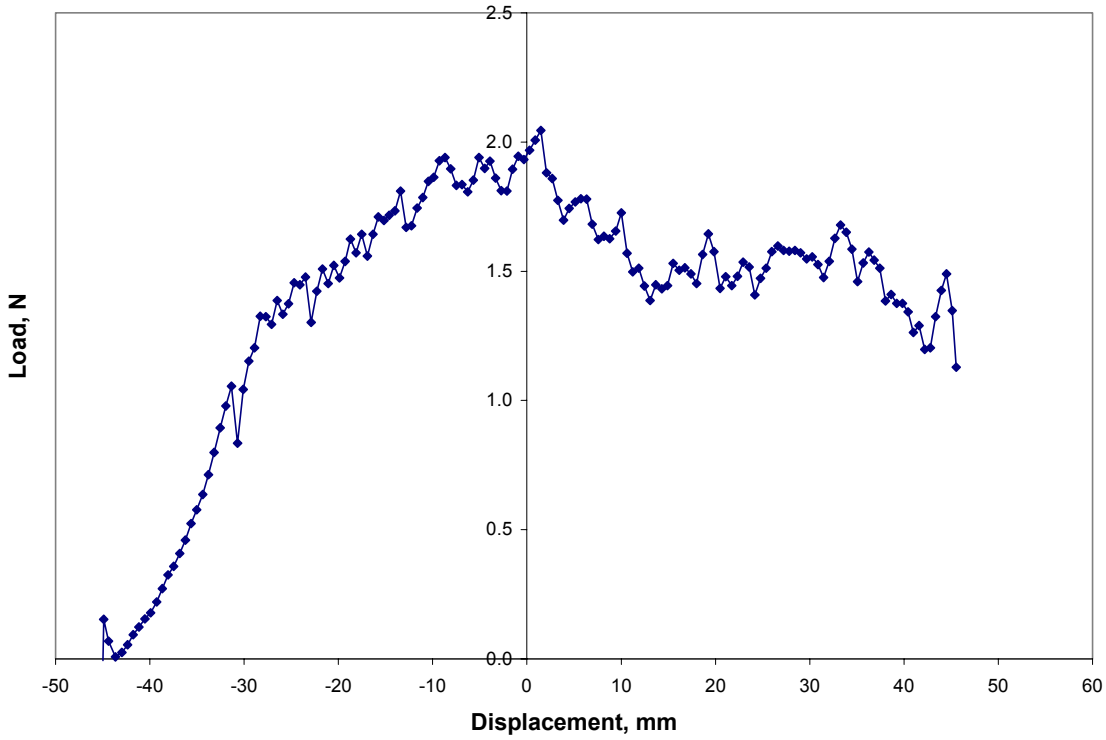

Figure C.91: Load Versus Displacement for Subject D, 180 degrees, 1800 mm/min, Test 1

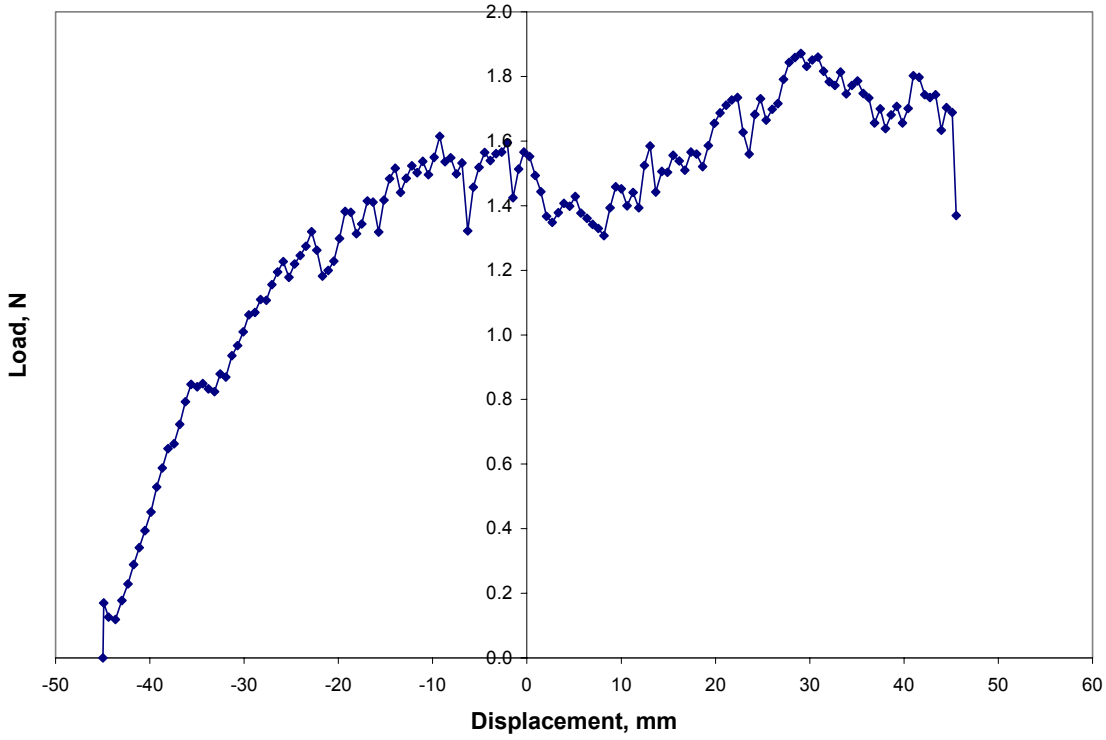

Figure C.92: Load Versus Displacement for Subject D, 180 degrees, 1800 mm/min, Test 2

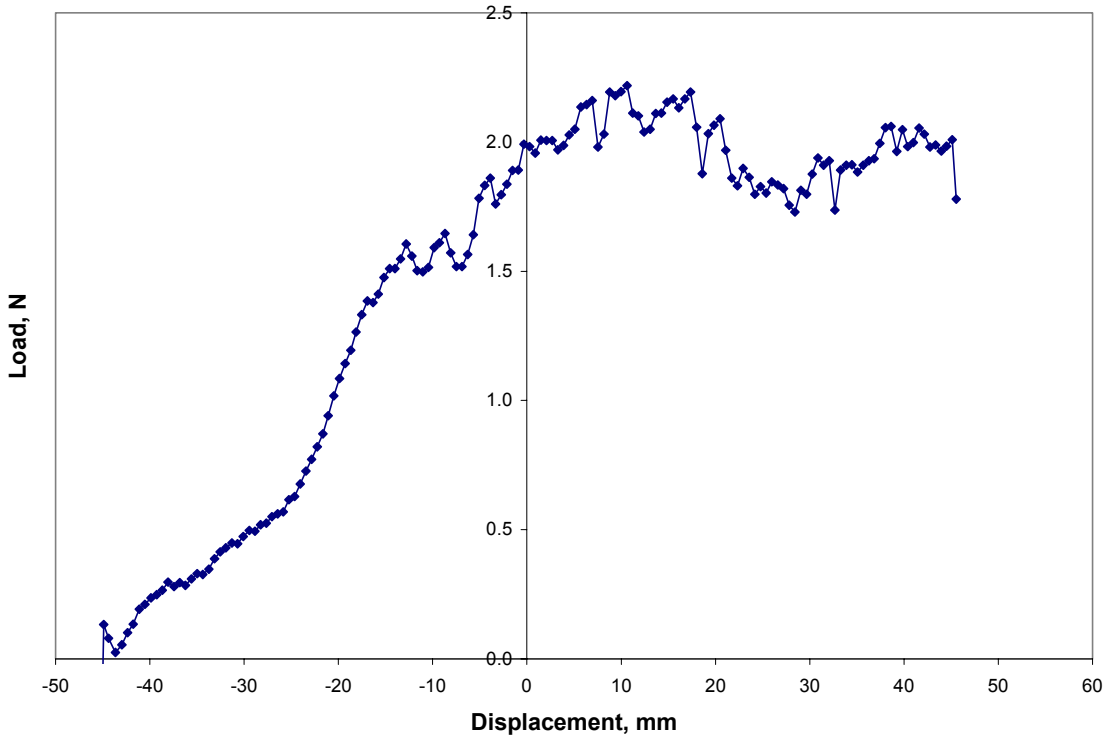

Figure C.93: Load Versus Displacement for Subject D, 180 degrees, 1800 mm/min, Test 3

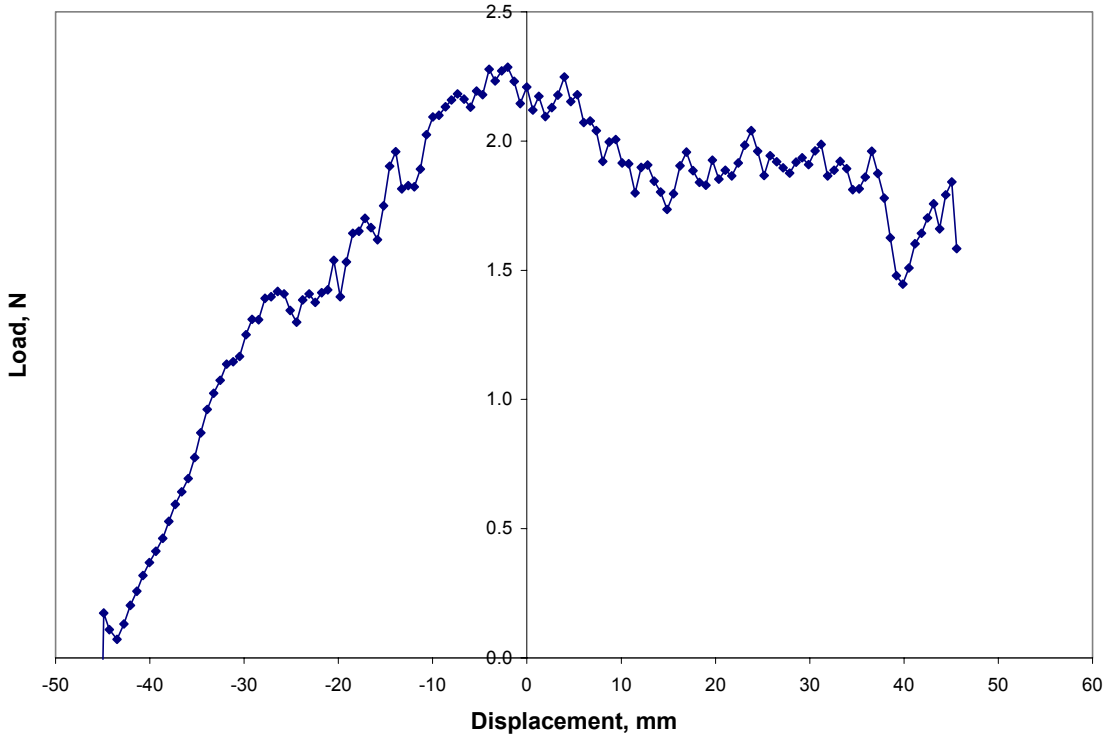

Figure C.94: Load Versus Displacement for Subject D, 180 degrees, 2000 mm/min, Test 1

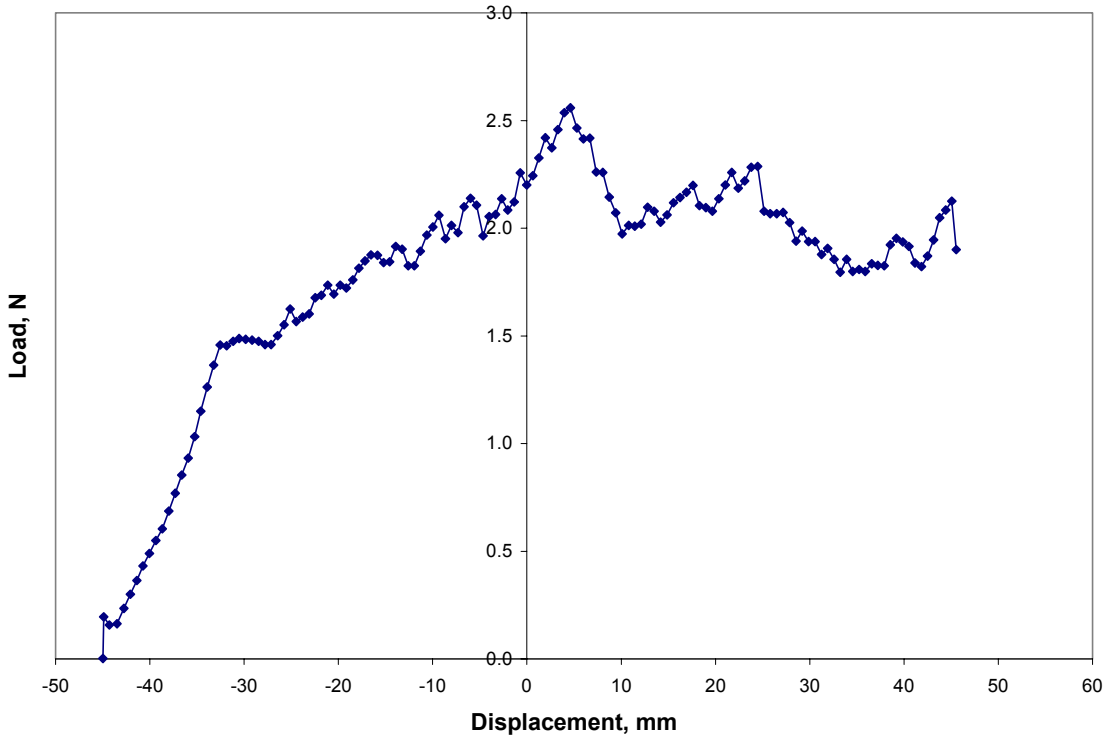

Figure C.95: Load Versus Displacement for Subject D, 180 degrees, 2000 mm/min, Test 2

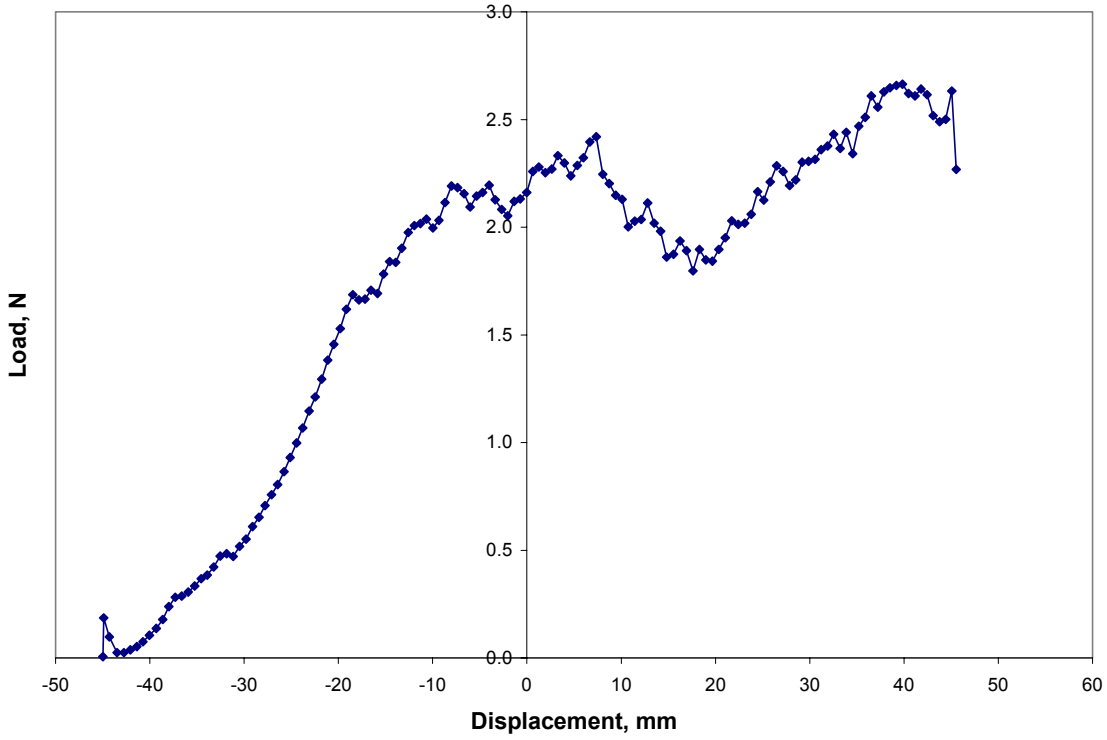

Figure C.96: Load Versus Displacement for Subject D, 180 degrees, 2000 mm/min, Test 3

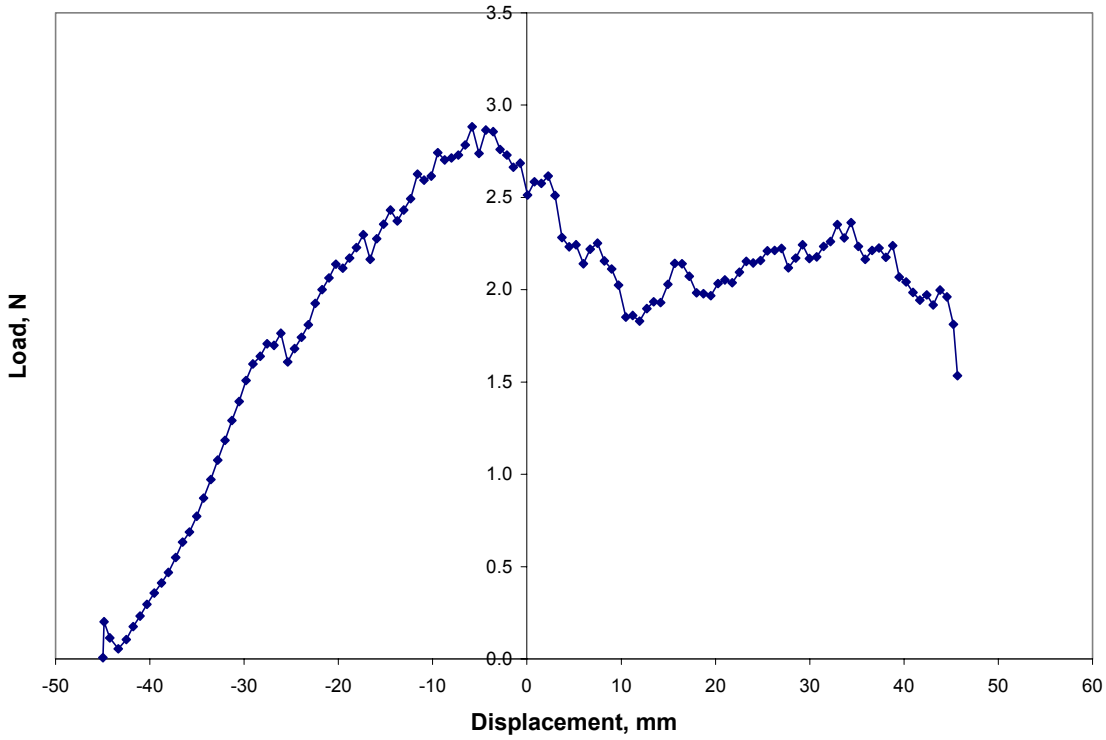

Figure C.97: Load Versus Displacement for Subject D, 180 degrees, 2200 mm/min, Test 1

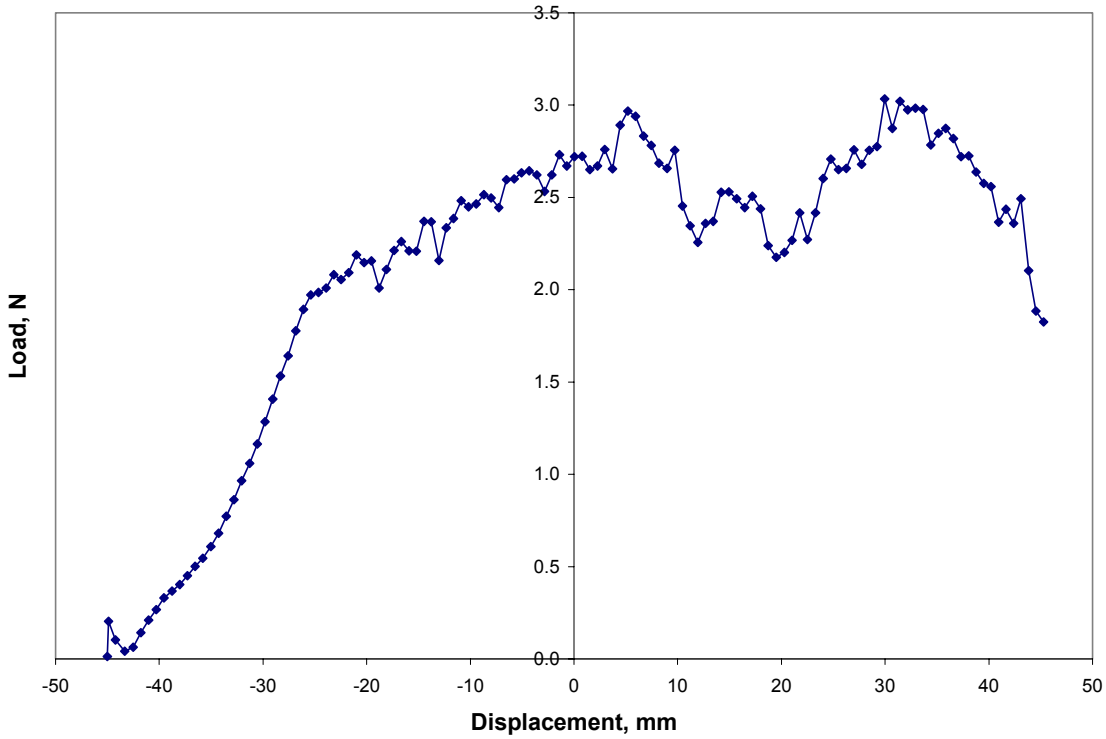

Figure C.98: Load Versus Displacement for Subject D, 180 degrees, 2200 mm/min, Test 2

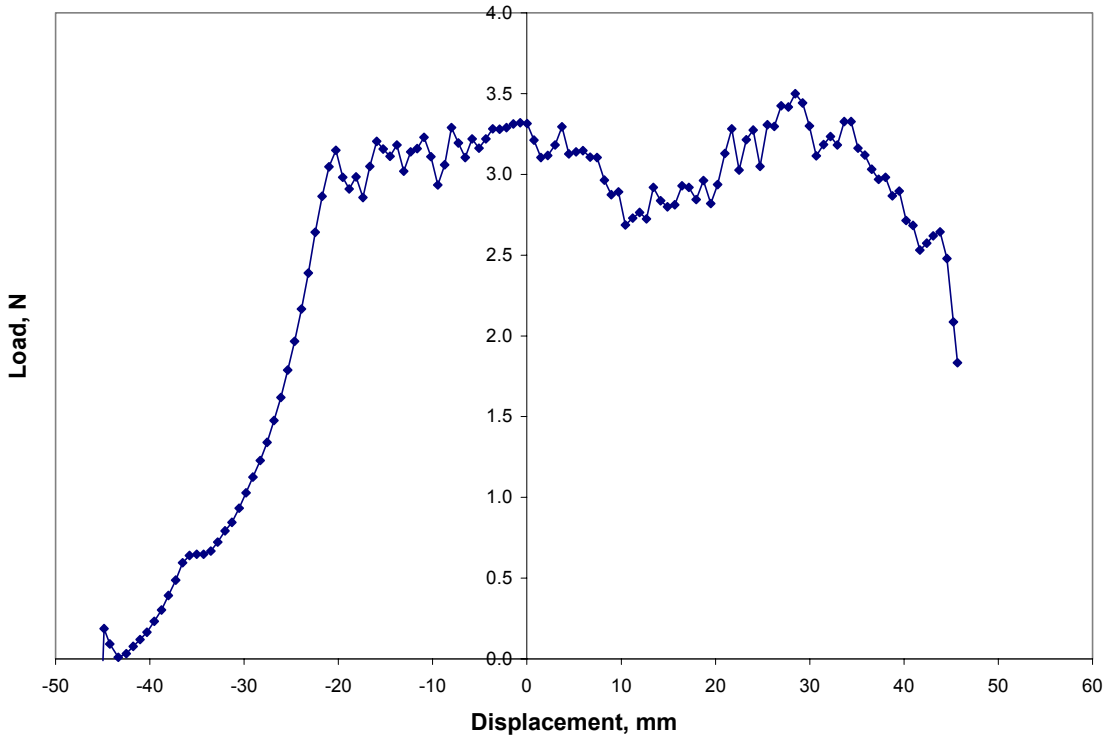

Figure C.99: Load Versus Displacement for Subject D, 180 degrees, 2200 mm/min, Test 3

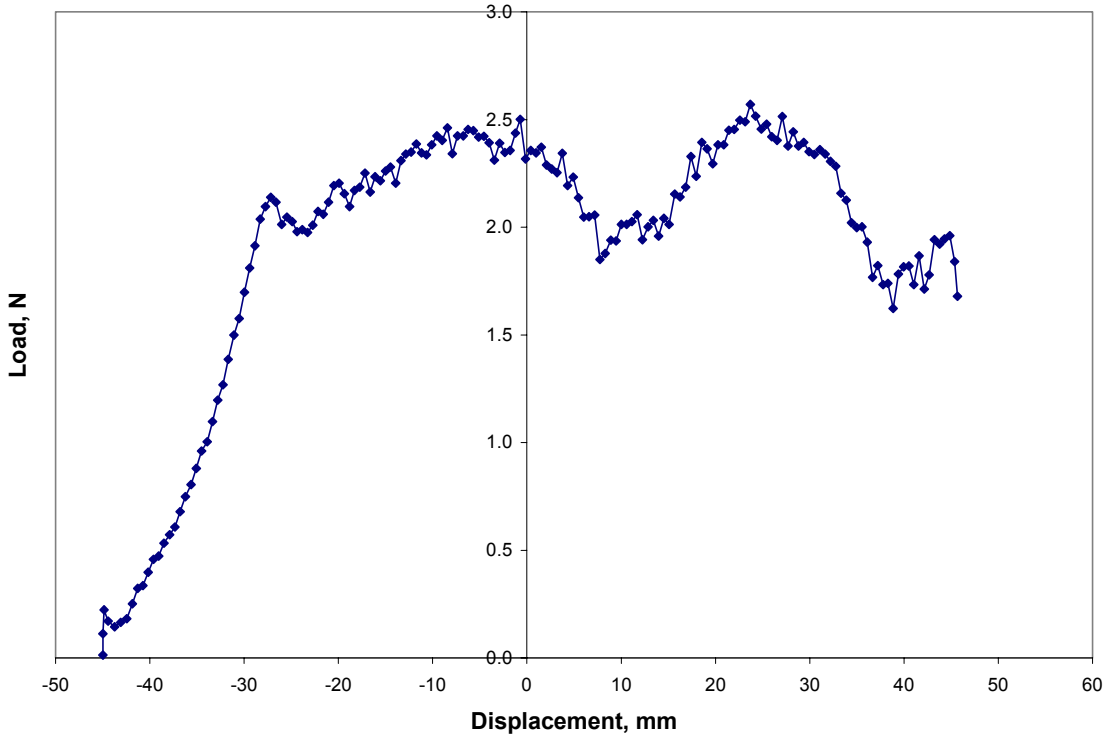

Figure C.100: Load Versus Displacement for Subject D, 180 degrees, 2400 mm/min, Test 1

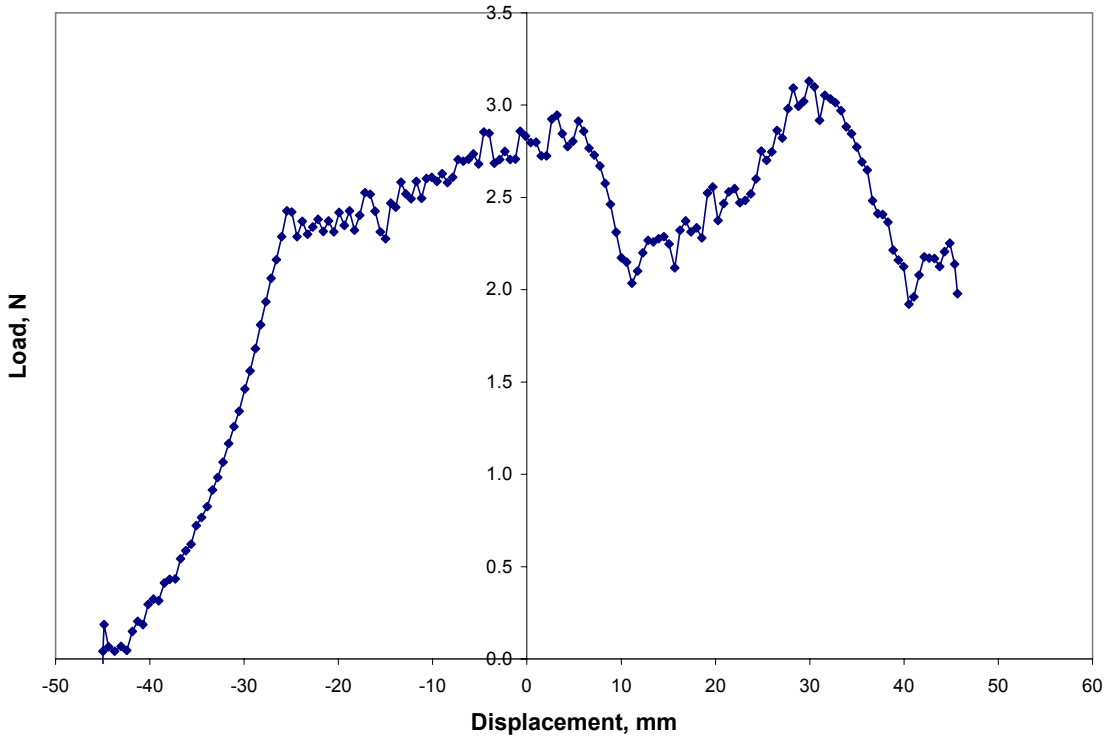

Figure C.101: Load Versus Displacement for Subject D, 180 degrees, 2400 mm/min, Test 2

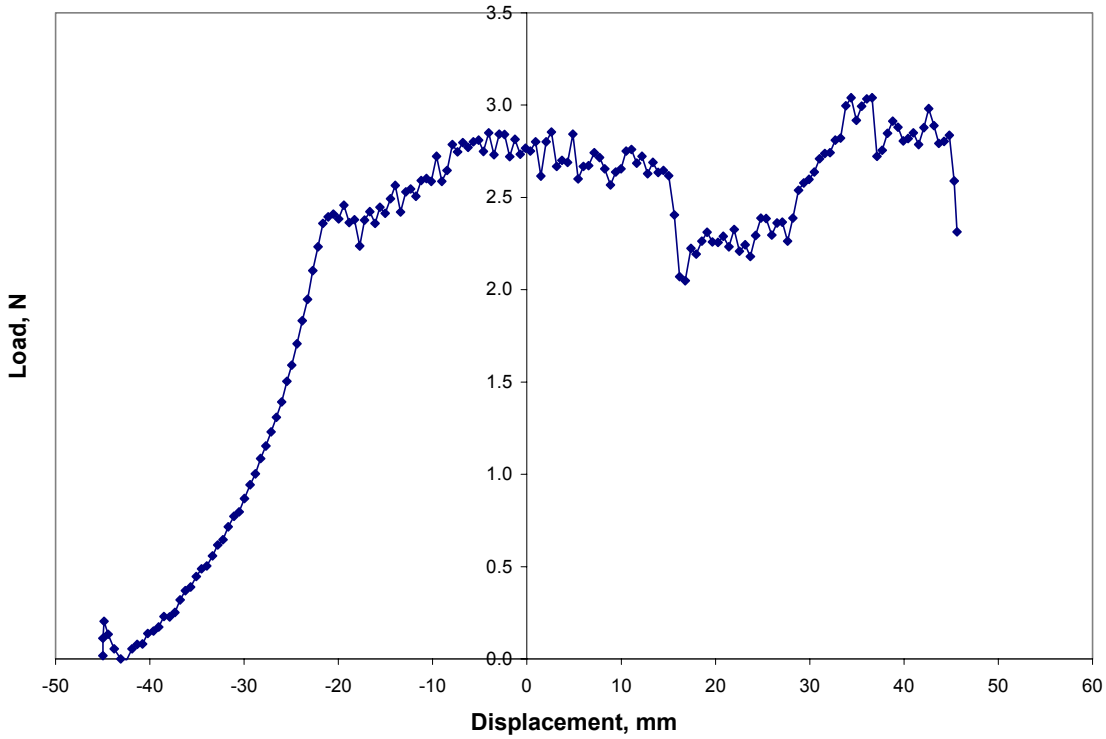

Figure C.102: Load Versus Displacement for Subject D, 180 degrees, 2400 mm/min, Test 3

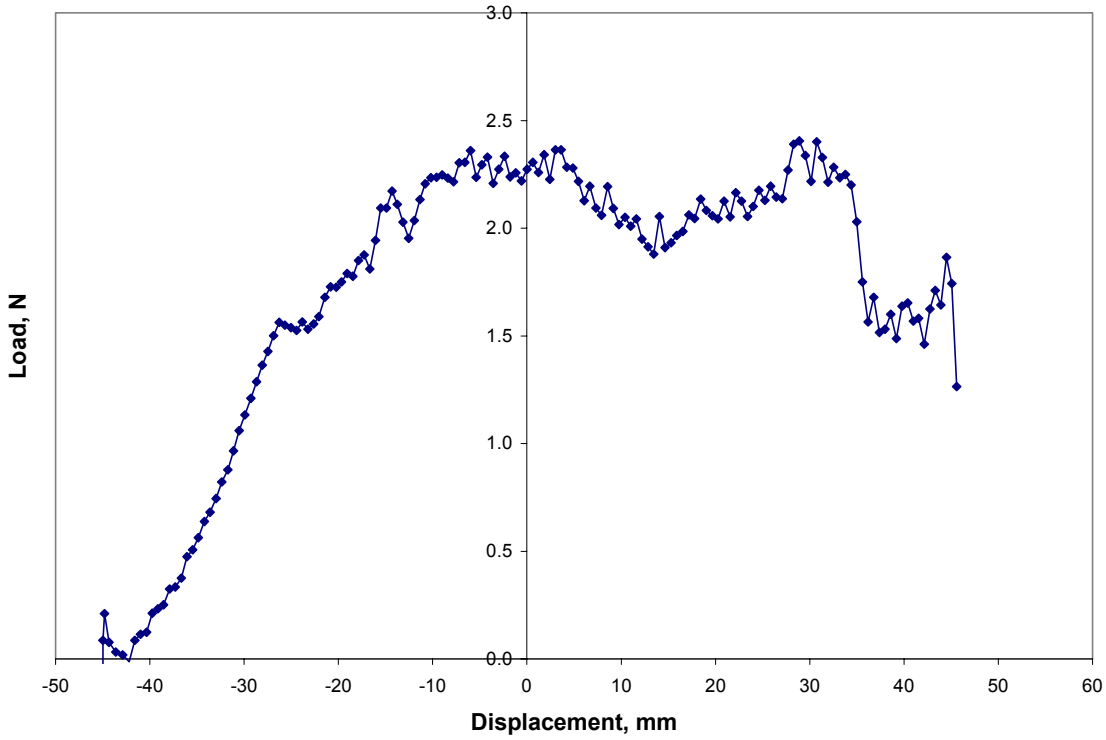

Figure C.103: Load Versus Displacement for Subject D, 180 degrees, 2600 mm/min, Test 1

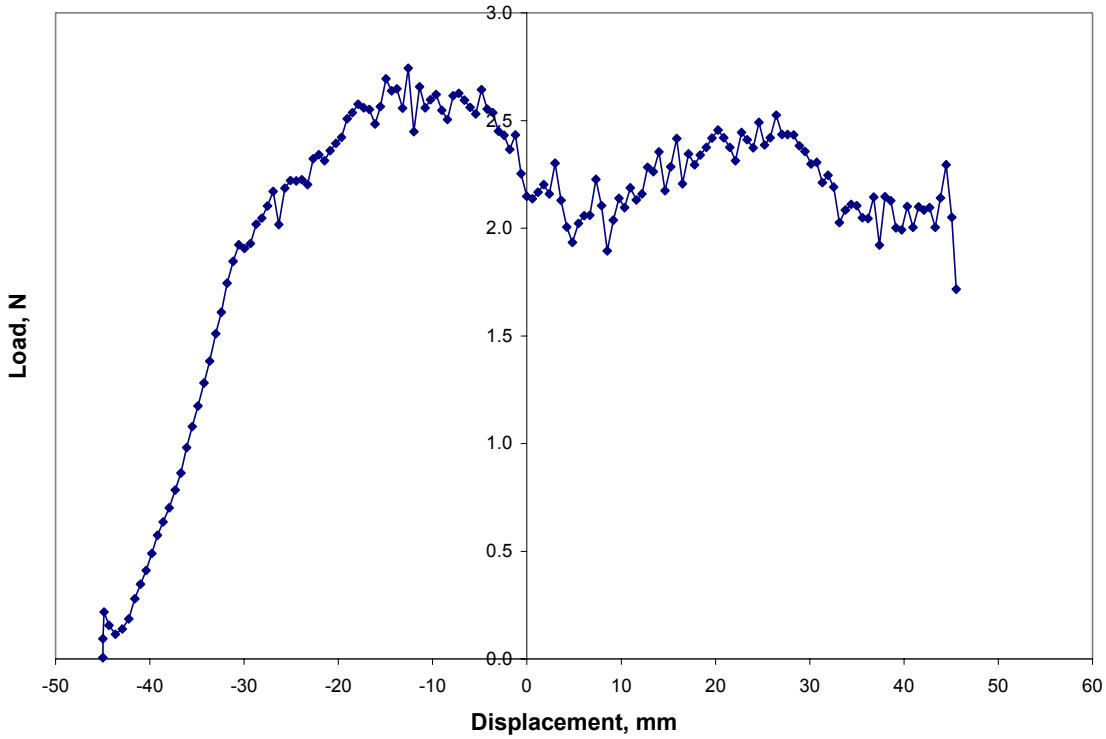

Figure C.104: Load Versus Displacement for Subject D, 180 degrees, 2600 mm/min, Test 2

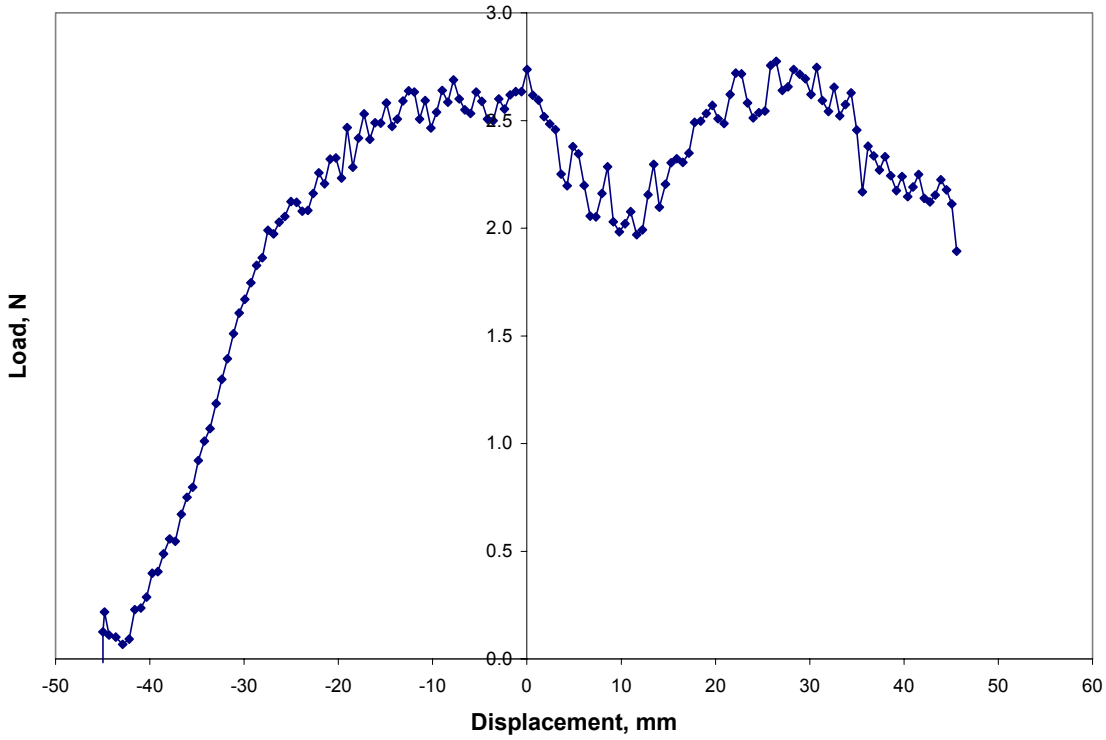

Figure C.105: Load Versus Displacement for Subject D, 180 degrees, 2600 mm/min, Test 3

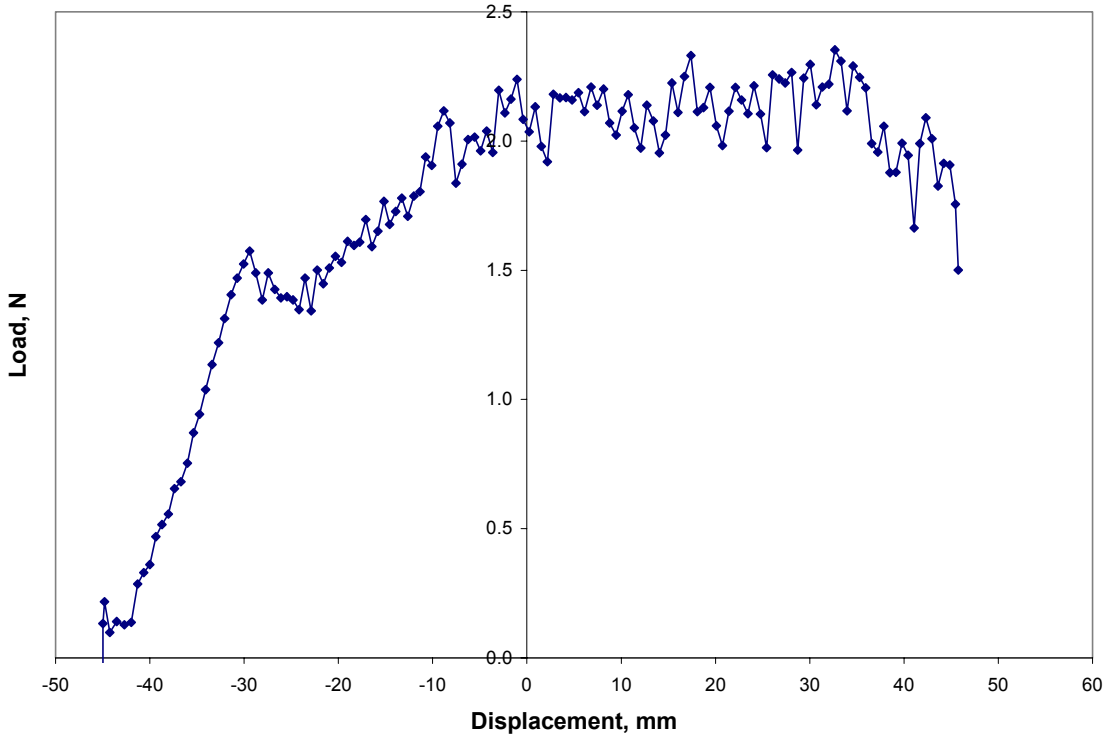

Figure C.106: Load Versus Displacement for Subject D, 180 degrees, 2800 mm/min, Test 1

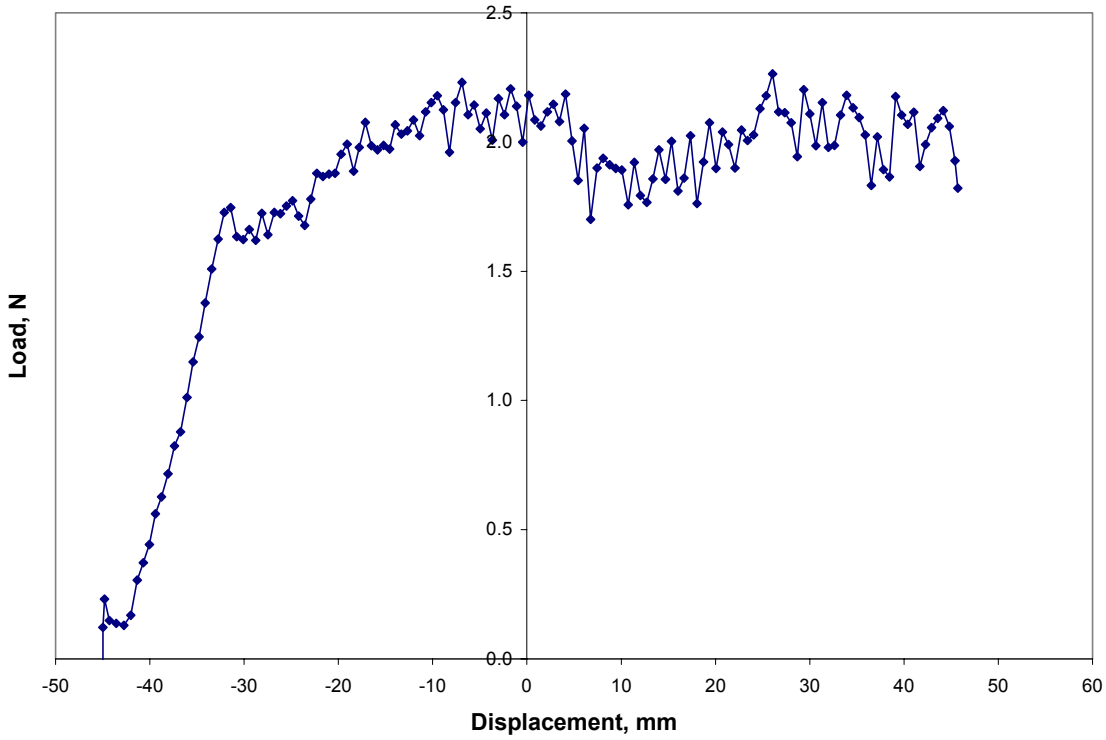

Figure C.107: Load Versus Displacement for Subject D, 180 degrees, 2800 mm/min, Test 2

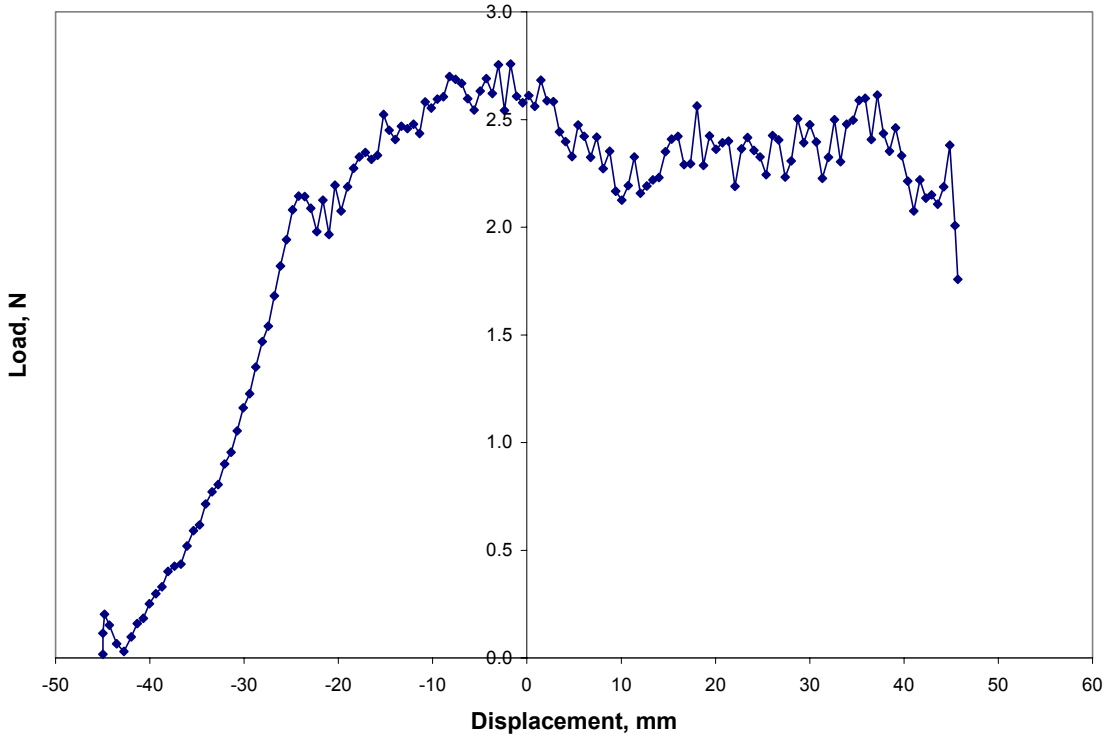

Figure C.108: Load Versus Displacement for Subject D, 180 degrees, 2800 mm/min, Test 3

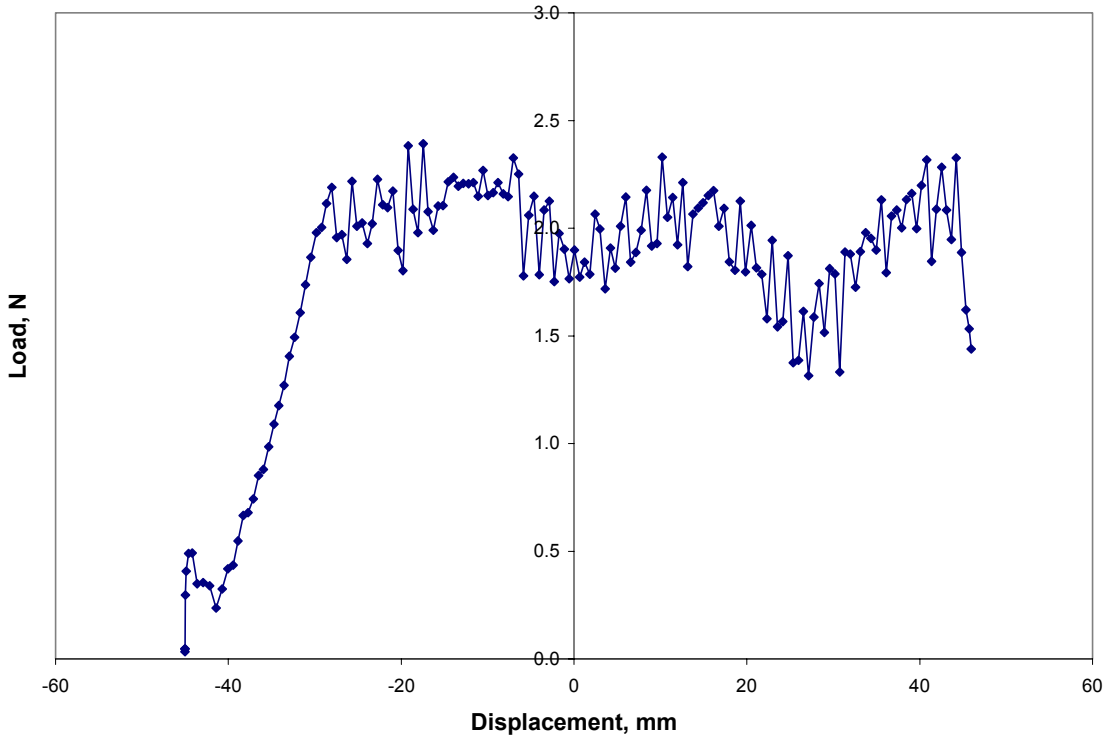

Figure C.109: Load Versus Displacement for Subject D, 180 degrees, 5000 mm/min, Test 1

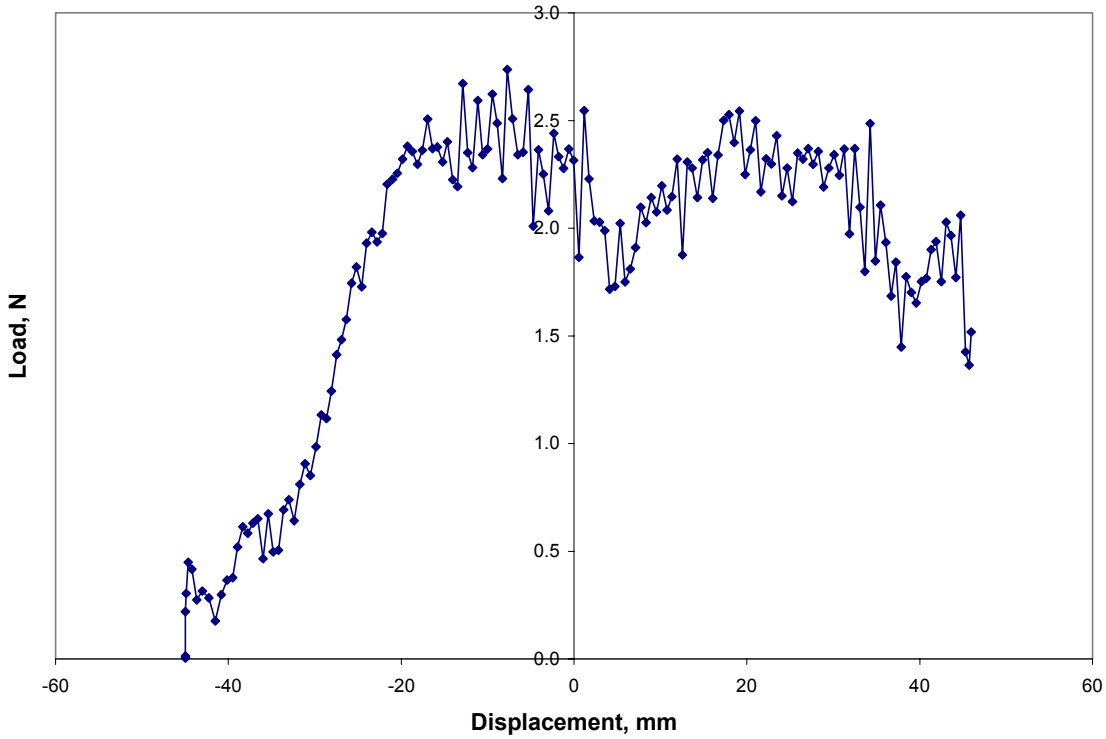

Figure C.110: Load Versus Displacement for Subject D, 180 degrees, 5000 mm/min, Test 2

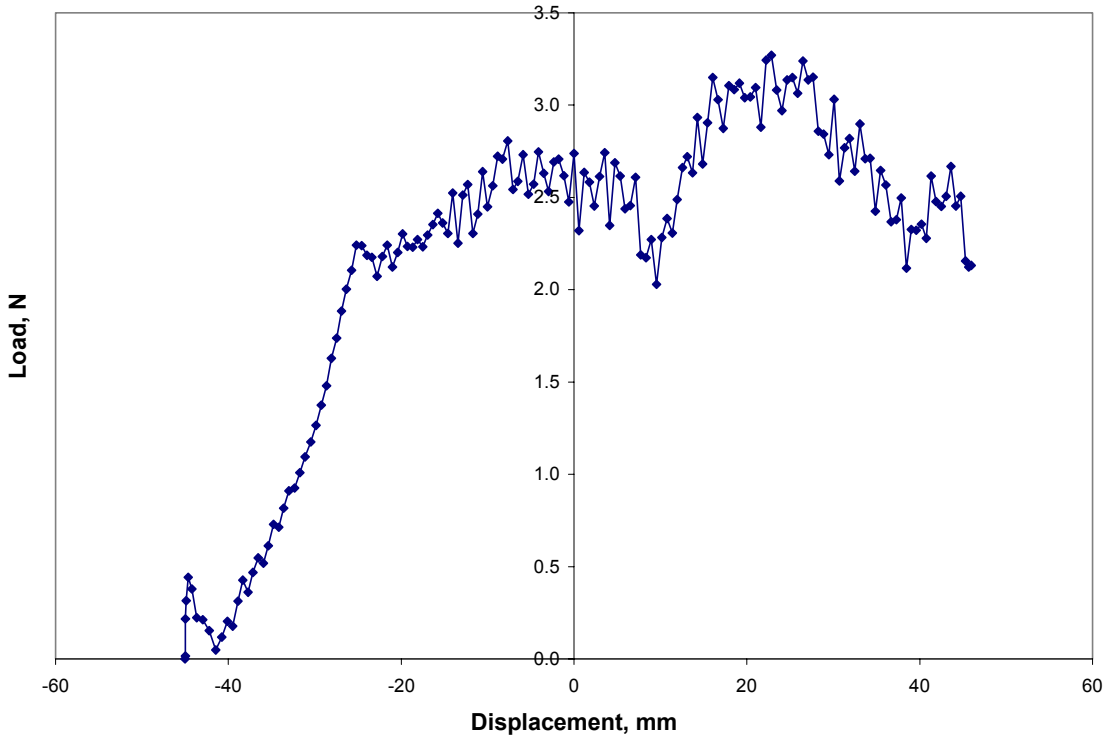

Figure C.111: Load Versus Displacement for Subject D, 180 degrees, 5000 mm/min, Test 3

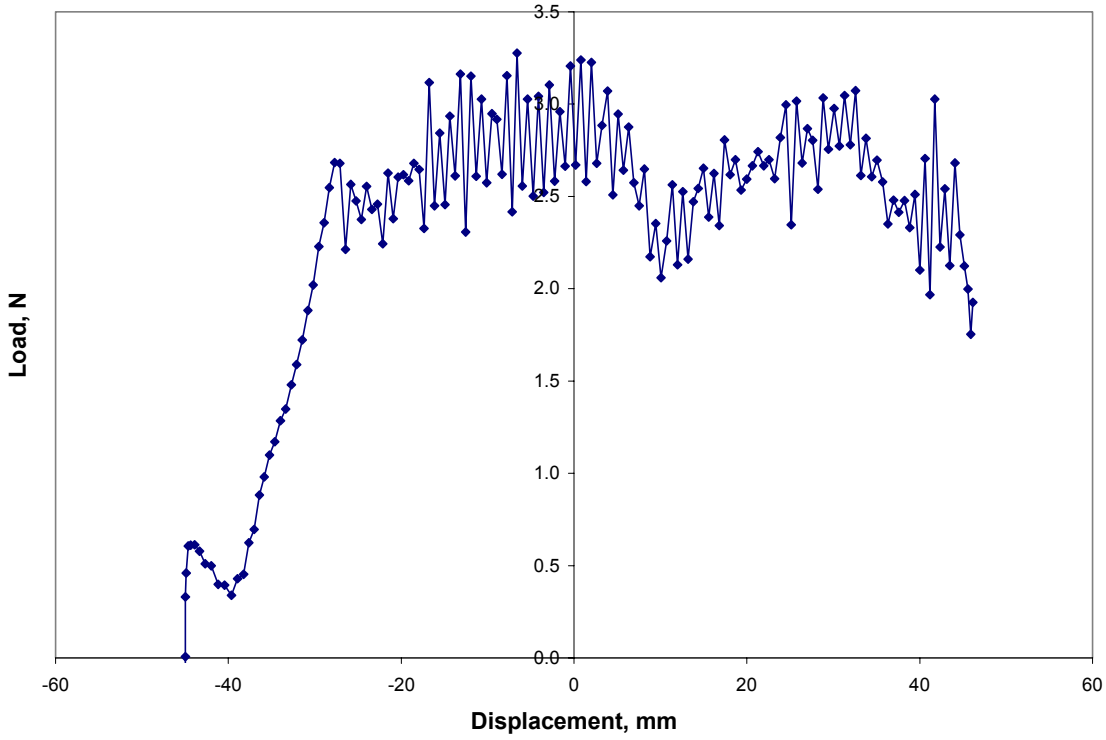

Figure C.112: Load Versus Displacement for Subject D, 180 degrees, 7500 mm/min, Test 1

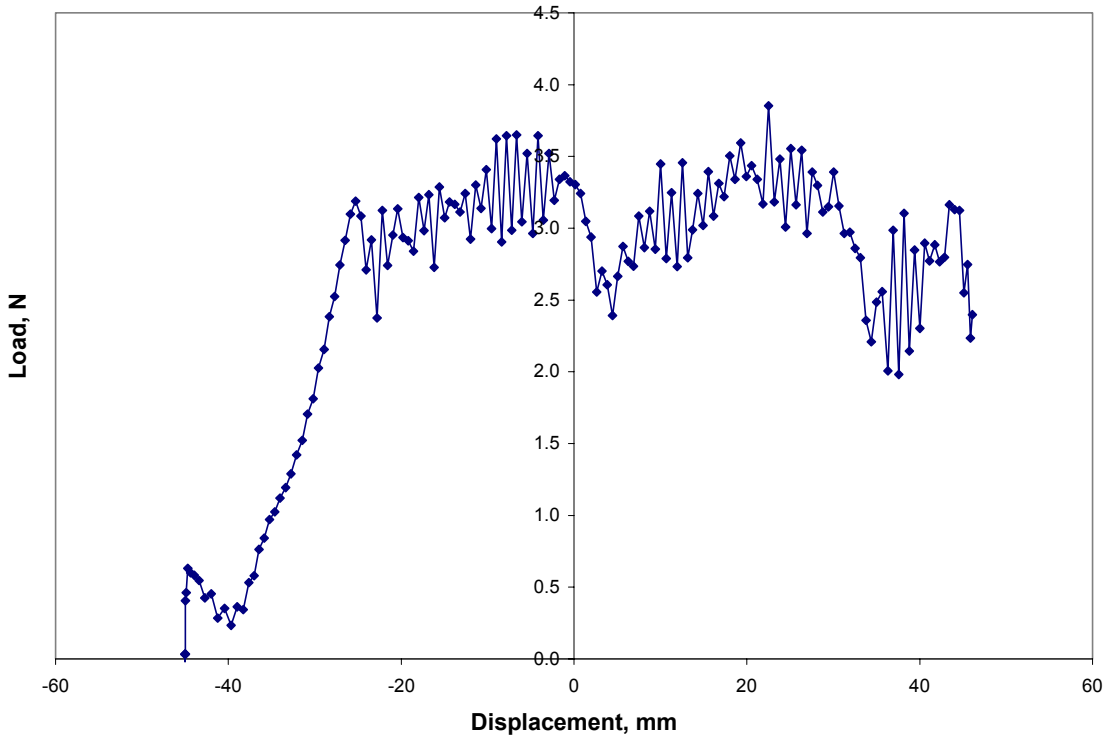

Figure C.113: Load Versus Displacement for Subject D, 180 degrees, 7500 mm/min, Test 2

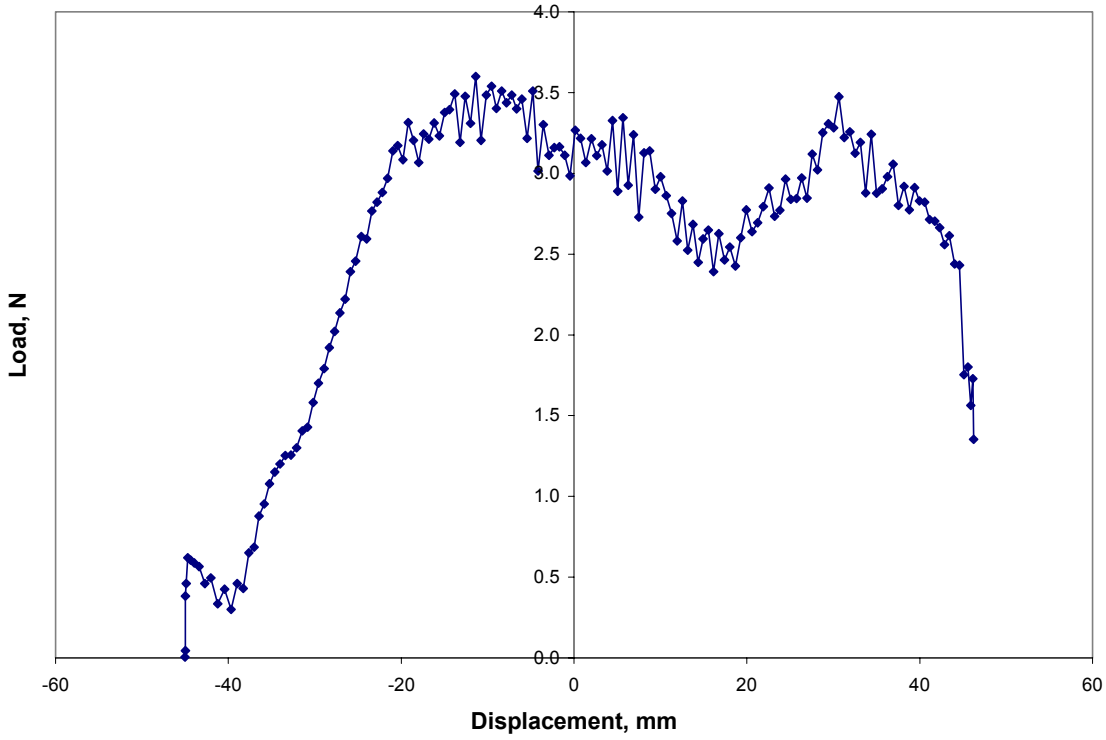

Figure C.114: Load Versus Displacement for Subject D, 180 degrees, 7500 mm/min, Test 3

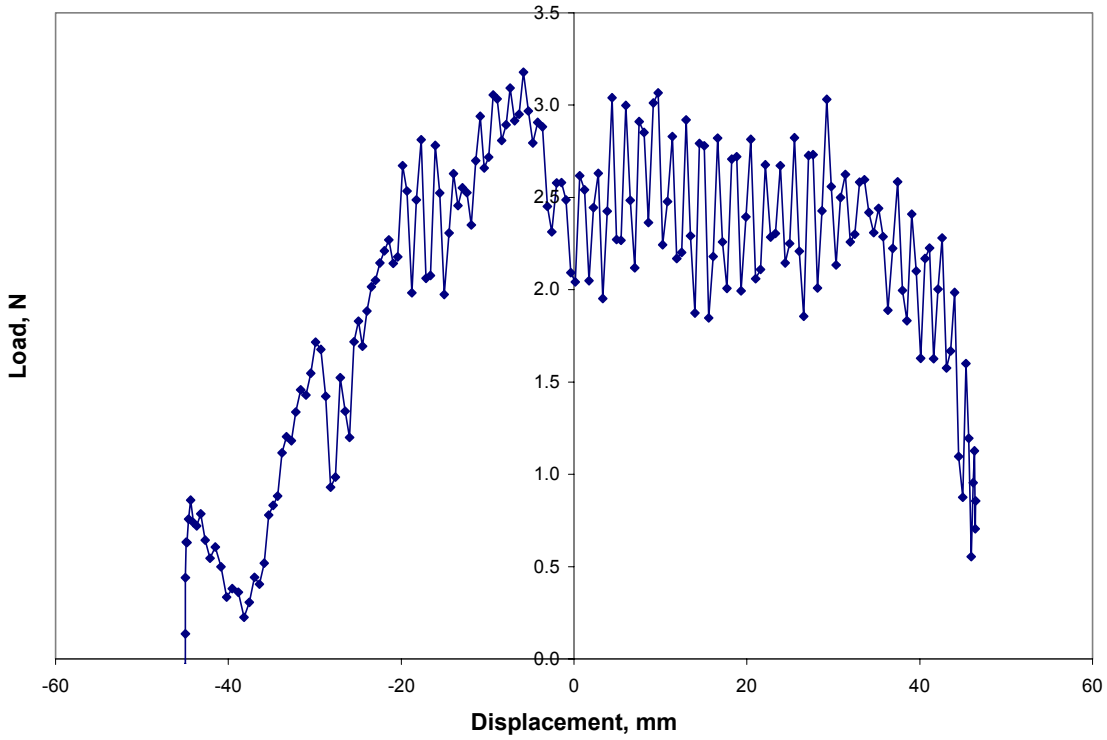

Figure C.115: Load Versus Displacement for Subject D, 180 degrees, 10,000 mm/min, Test 1

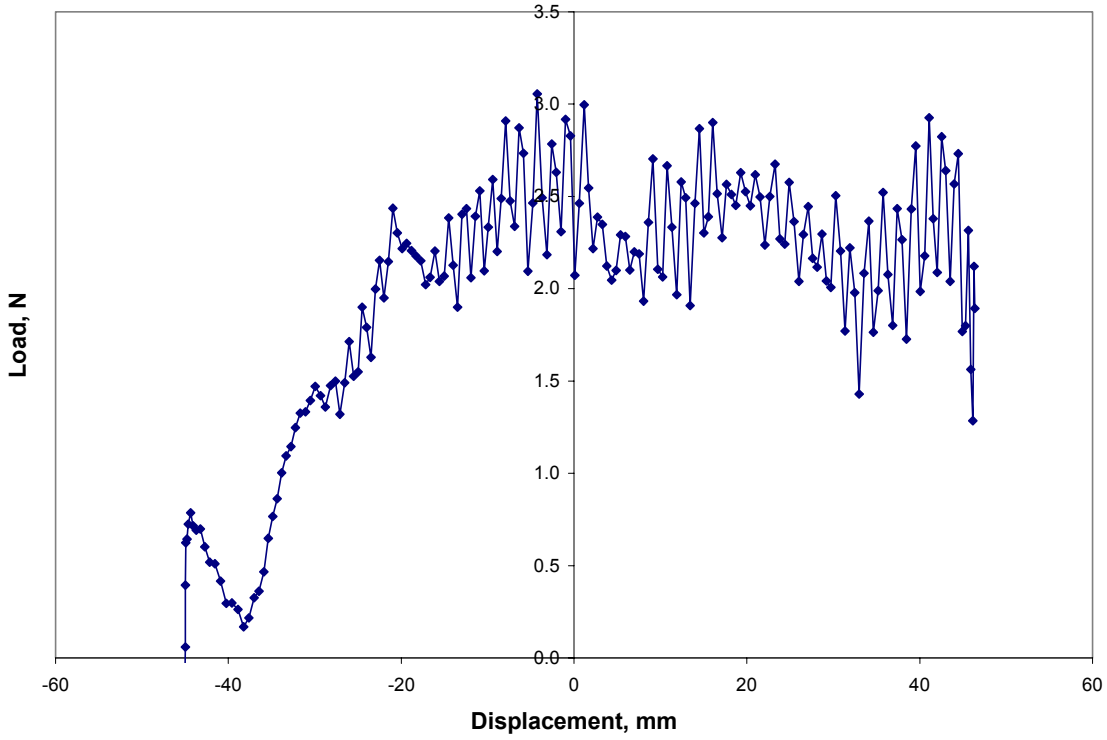

Figure C.116: Load Versus Displacement for Subject D, 180 degrees, 10,000 mm/min, Test 2

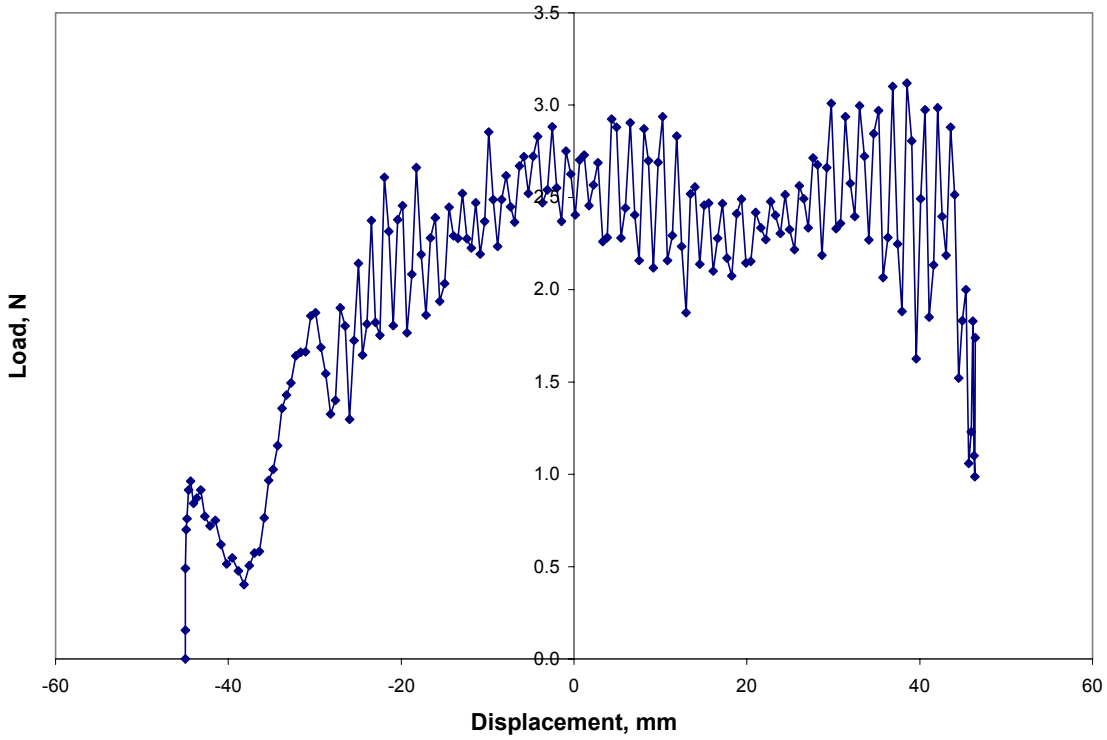

Figure C.117: Load Versus Displacement for Subject D, 180 degrees, 10,000 mm/min, Test 3

Appendix D

Rigid Substrate Testing Results

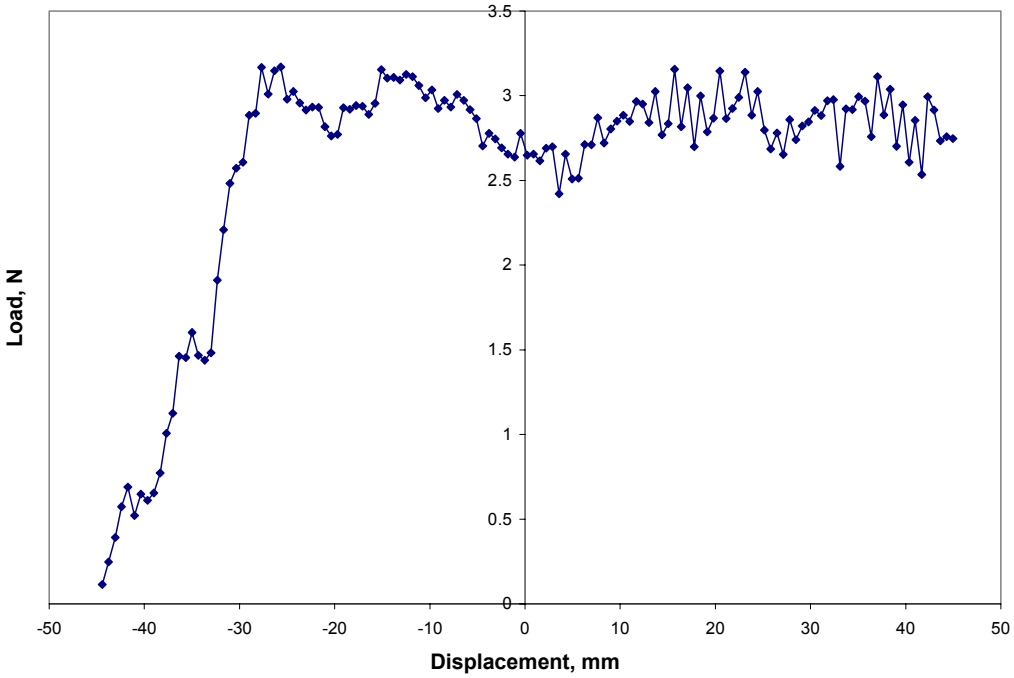

Figure D.1: Load Versus Displacement for Aluminum, 180 degrees, 200 mm/min, Test 1

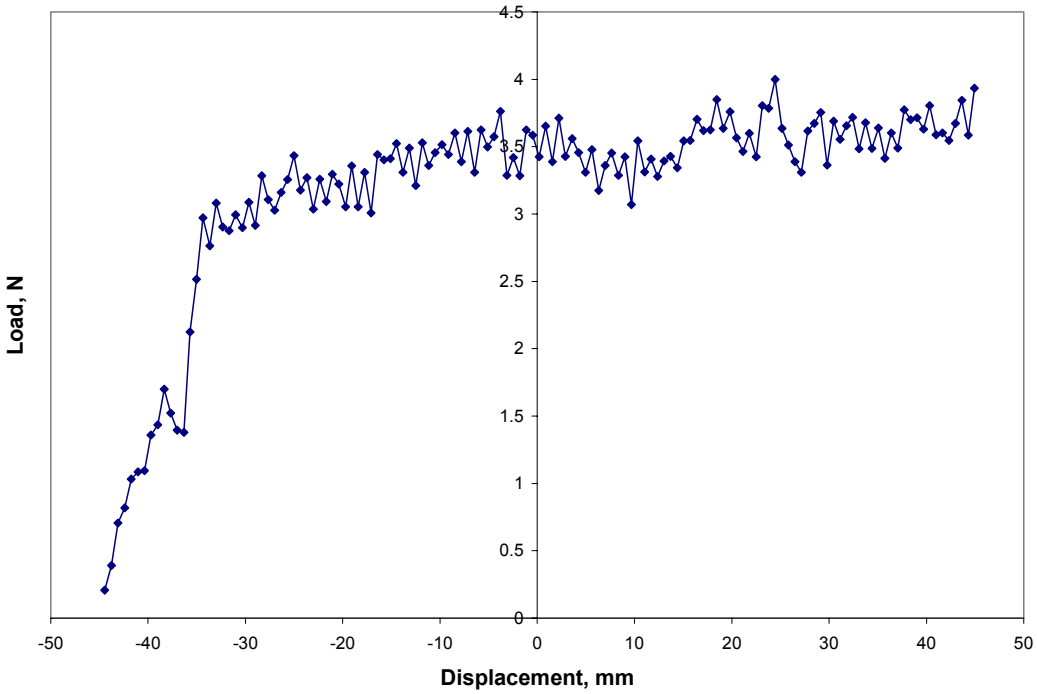

Figure D.2: Load Versus Displacement for Aluminum, 180 degrees, 200 mm/min, Test 2

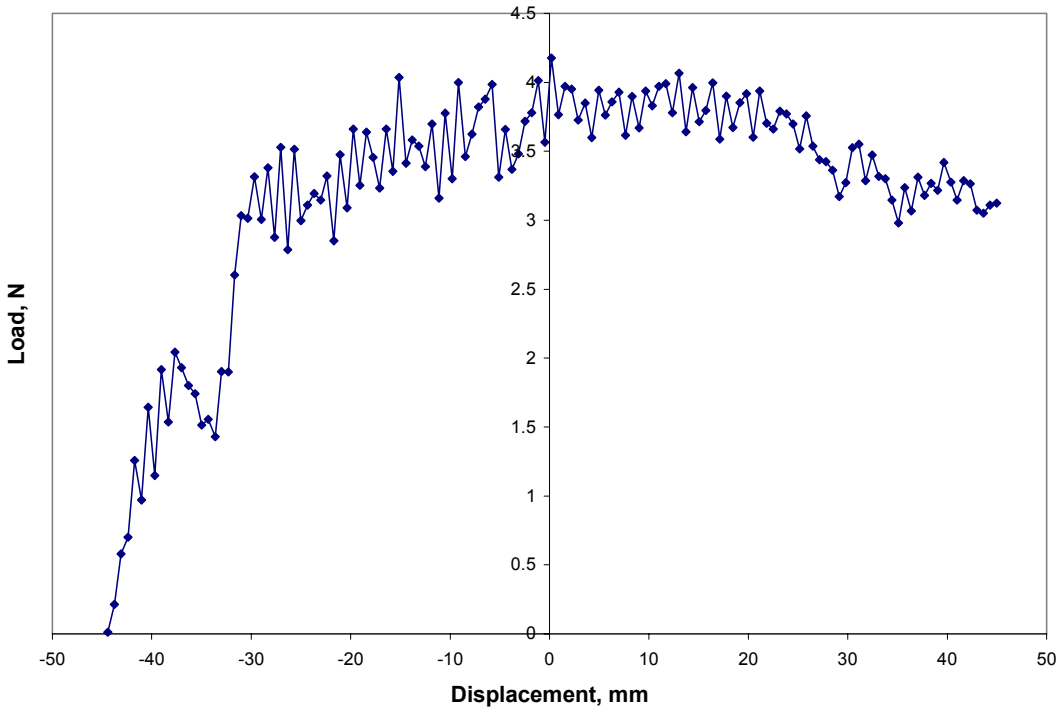

Figure D.3: Load Versus Displacement for Aluminum, 180 degrees, 200 mm/min, Test 3

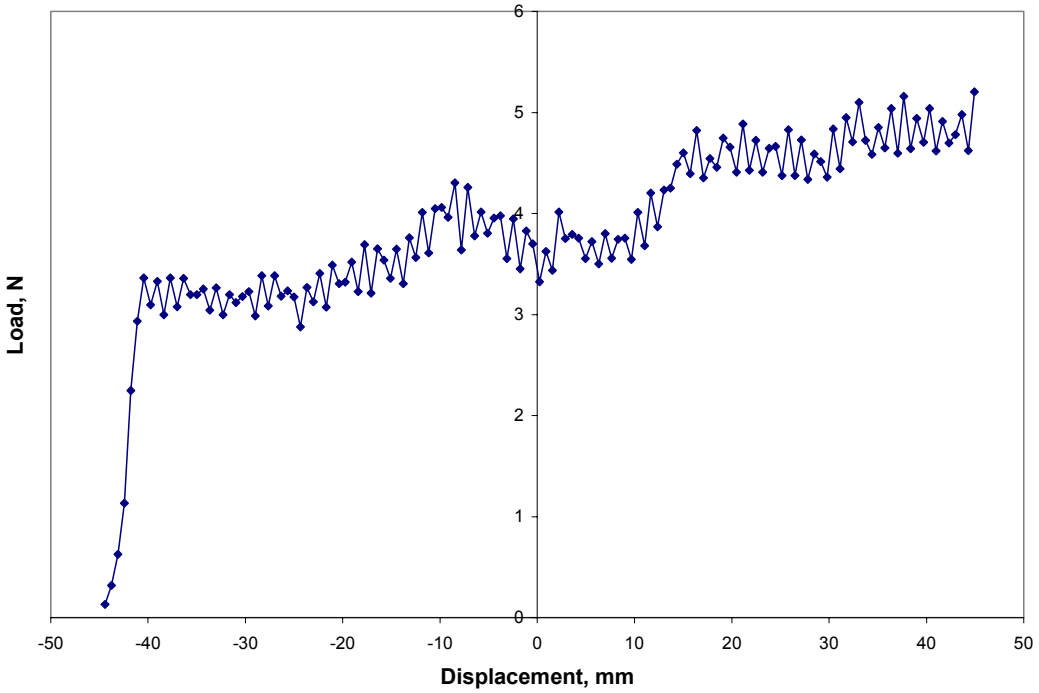

Figure D.4: Load Versus Displacement for Polycarbonate, 180 degrees, 200 mm/min, Test 1

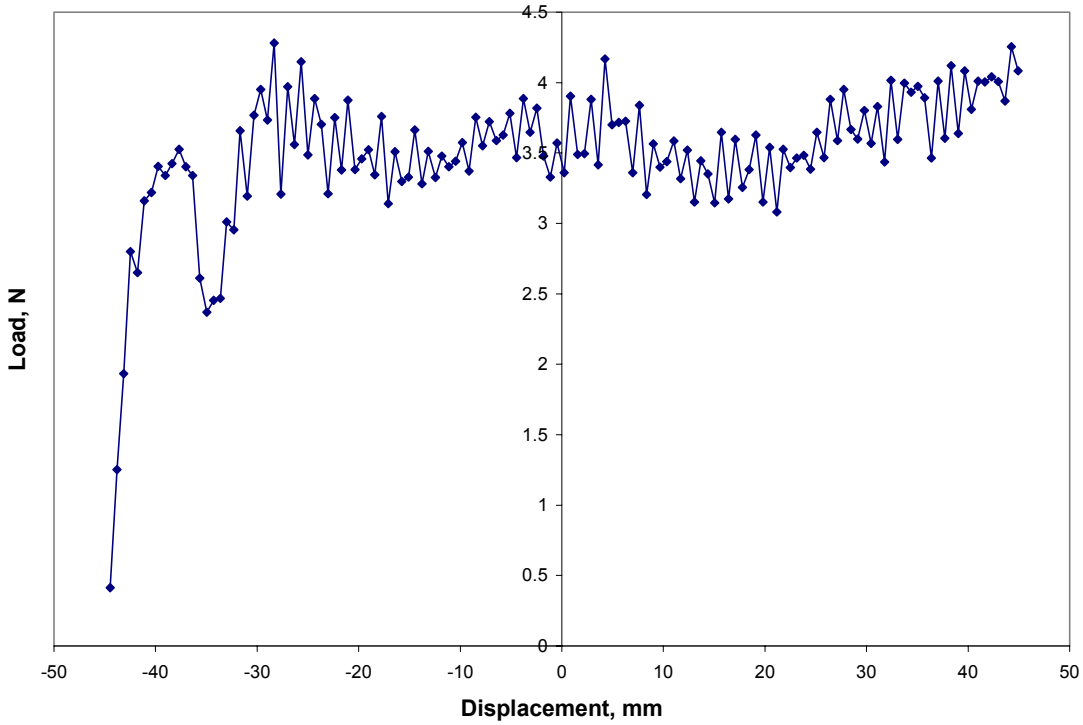

Figure D.5: Load Versus Displacement for Polycarbonate, 180 degrees, 200 mm/min, Test 2

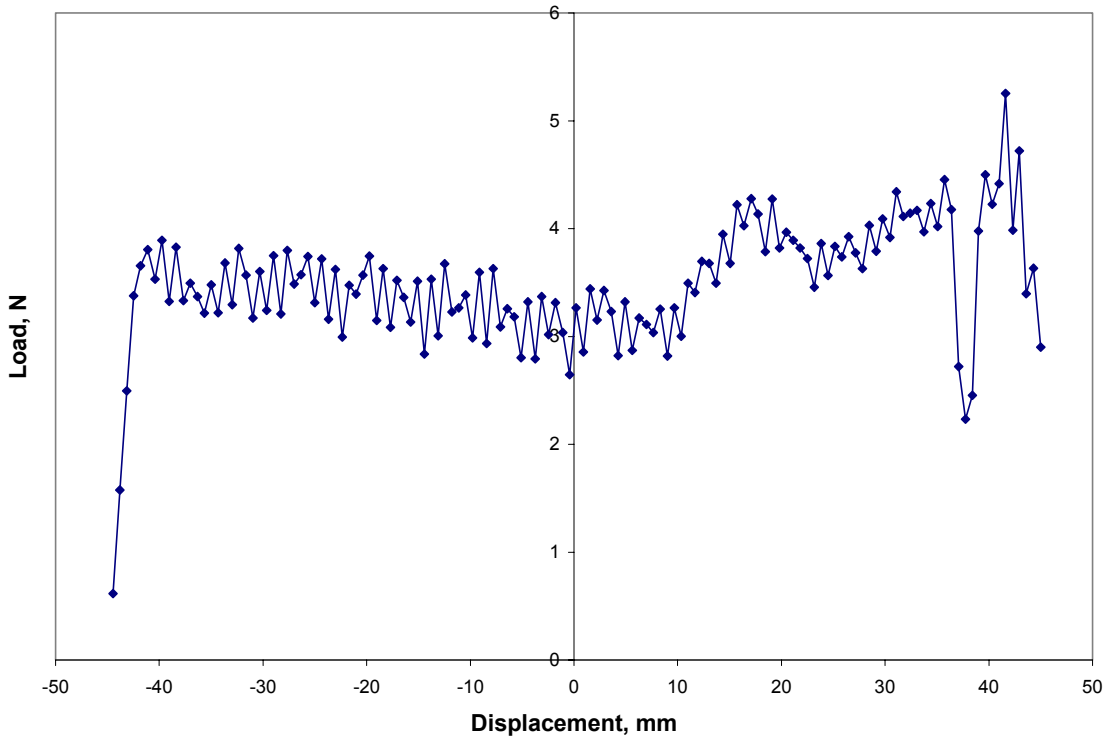

Figure D.6: Load Versus Displacement for Polycarbonate, 180 degrees, 200 mm/min, Test 3

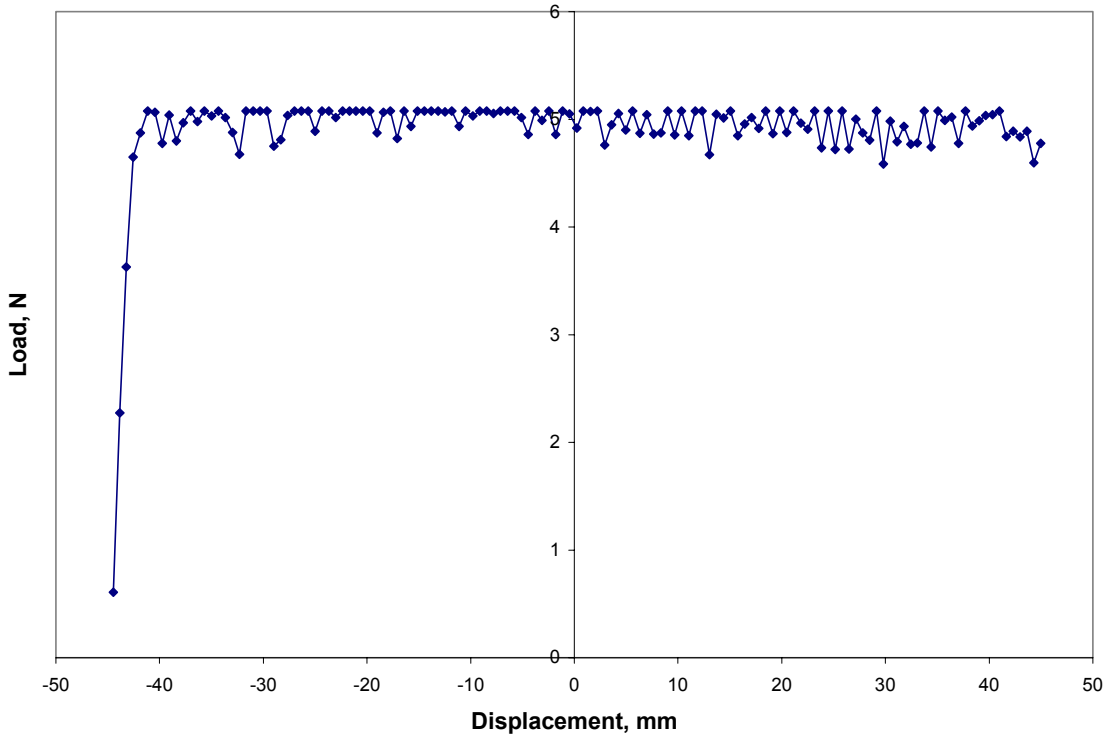

Figure D.7: Load Versus Displacement for Steel, 180 degrees, 200 mm/min, Test 1

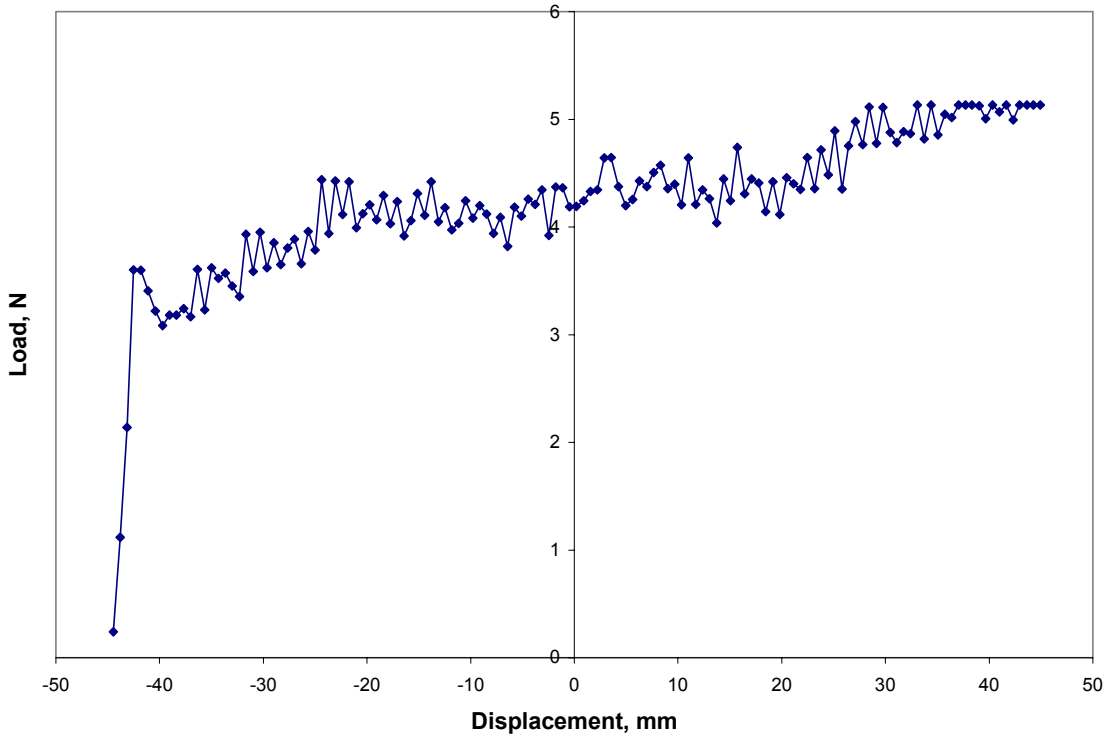

Figure D.8: Load Versus Displacement for Steel, 180 degrees, 200 mm/min, Test 2

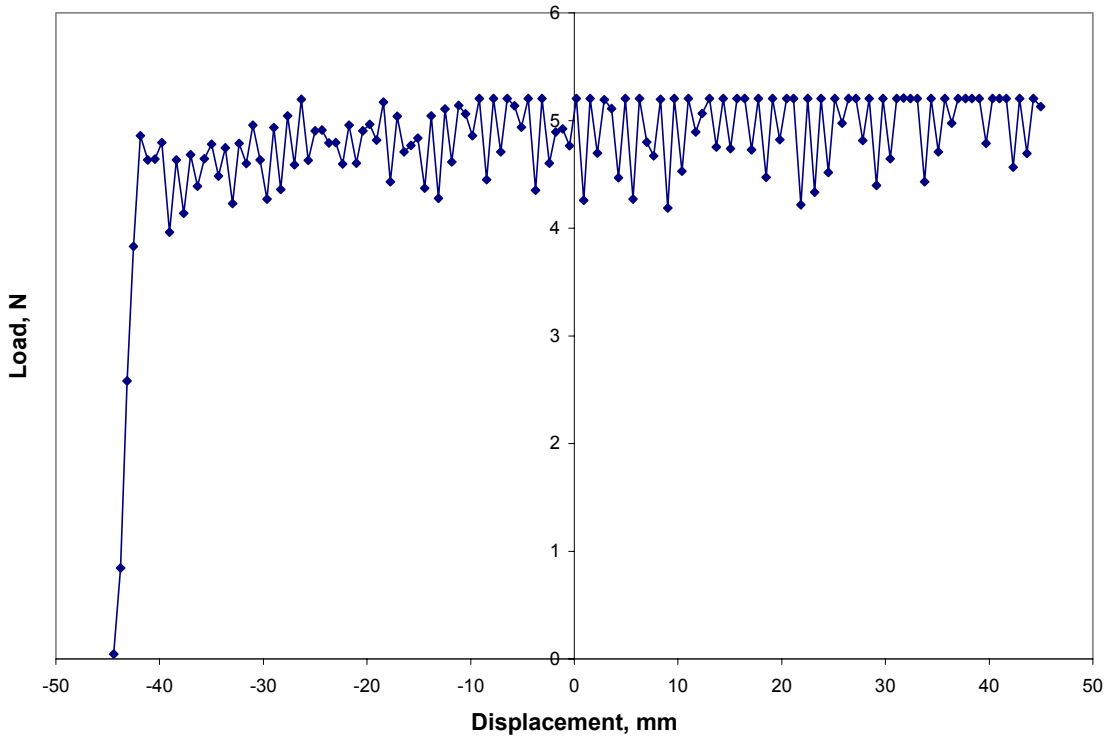

Figure D.9: Load Versus Displacement for Steel, 180 degrees, 200 mm/min, Test 3

Appendix E

Mathematica Printouts

Model 1

In this program, y1 represents x, y2 represents y, y3 represents θ, y4 represents m, y5 represents q, y6 represents p, and t represents s.

```
Clear[eta, ha, hb, θo, mB, gxA, gyA, gθA]
pi = Pi;
eta = 1;
ha = 0.0005;
hb = 0.005;
θo = 27*pi/36;
mB = 0;
gxA = -0.0002;
gyA = 0.003;
gθA = -0.0001;
```

**The above three variables are initial guesses.

```
de[y1_, y2_, y3_, y4_, y5_, y6_, xA_, yA_] :=
 {y1'[t] == Cos[y3[t]], y2'[t] == Sin[y3[t]], y3'[t] == y4[t],
  y4'[t] == If[(yA + y2[t] - 0.5*hb*Cos[y3[t]]) > ha,
    y5[t]*Cos[y3[t]] + y6[t]*Sin[y3[t]] -
     (hb/2)*eta*
      (1/(√((-t + xA + 0.5*hb*Sin[y3[t]] + y1[t])^2 + (yA - 0.5*hb*Cos[y3[t]] + y2[t])^2)) -
       1/ha)*((y2[t] + yA - 0.5*hb*Cos[y3[t]])*Sin[y3[t]] +
       (y1[t] + xA + 0.5*hb*Sin[y3[t]] - t)*Cos[y3[t]]),
    y5[t]*Cos[y3[t]] + (hb/(2*ha))*eta*(y2[t] + yA - 0.5*hb*Cos[y3[t]] - ha)*Sin[y3[t]]],
  y5'[t] == If[(yA + y2[t] - 0.5*hb*Cos[y3[t]]) > ha,
    eta*
     (1/(√((-t + xA + 0.5*hb*Sin[y3[t]] + y1[t])^2 + (yA - 0.5*hb*Cos[y3[t]] + y2[t])^2)) -
       1/ha)*(y2[t] + yA - 0.5*hb*Cos[y3[t]]),
    (-eta/ha)*(y2[t] + yA - 0.5*hb*Cos[y3[t]] - ha)],
  y6'[t] == If[(yA + y2[t] - 0.5*hb*Cos[y3[t]]) > ha,
    eta*
     (1/(√((-t + xA + 0.5*hb*Sin[y3[t]] + y1[t])^2 + (yA - 0.5*hb*Cos[y3[t]] + y2[t])^2)) -
       1/ha)*(-1)*(-t + y1[t] + xA + 0.5*hb*Sin[y3[t]]),
    0.35*eta*((y1[t] + xA + 0.5*hb*Sin[y3[t]] - t)/ha)]}
```

```
leftBC[θA_] := {y1[0] == 0, y2[0] == 0, y3[0] == θA, y4[0] == 0, y5[0] == 0, y6[0] == 0}
soln := NDSolve[Flatten[Append[de[y1, y2, y3, y4, y5, y6, xA, yA], leftBC[θA]]],
  {y1, y2, y3, y4, y5, y6}, {t, 0, 1}, MaxSteps → 1000]
endpt[xA_, yA_, θA_] :=
  {y1[t], y2[t], y3[t], y4[t], y5[t], y6[t]} /.
    First[NDSolve[Flatten[Append[de[y1, y2, y3, y4, y5, y6, xA, yA], leftBC[θA]]],
      {y1[t], y2[t], y3[t], y4[t], y5[t], y6[t]}, {t, 0, 1}, MaxSteps → 1000]] /. t → 1;
endpt[gxA, gyA, gθA]
{1., 0.000444767, -0.00105738, -0.030687, -0.241086, -0.132909}
Clear[xA, yA, θA]
rts :=
 FindRoot[{endpt[xA, yA, θA][[4]] == mB,
   endpt[xA, yA, θA][[5]] / endpt[xA, yA, θA][[6]] == -Tan[θo],
   (√(((yA - 0.5 * hb * Cos[endpt[xA, yA, θA][[3]]]) + endpt[xA, yA, θA][[2]])^2 +
         (endpt[xA, yA, θA][[1]] + (xA + 0.5 * hb * Sin[endpt[xA, yA, θA][[3]]]) - 1)^2) - ha) /
     ha == 2}, {xA, {gxA, 0.9 * gxA}}, {yA, {gyA, 0.9 * gyA}}, {θA, {gθA, 0.9 * gθA}},
  AccuracyGoal → 3, MaxIterations → 200]
rts
{xA → -0.000290269, yA → 0.00300269, θA → -0.0000934928}
xA = xA /. rts
-0.000290269
yA = yA /. rts
0.00300269
θA = θA /. rts
-0.0000934928
endpt[xA, yA, θA]
{0.999998, 0.000970936, 0.00472985, -0.0000249968, -0.209644, -0.209534}
{yy1[t_], yy2[t_], yy3[t_], yy4[t_], yy5[t_], yy6[t_]} =
  {y1[t], y2[t], y3[t], y4[t], y5[t], y6[t]} /. First[soln];
fo = √(yy5[1]^2 + yy6[1]^2)
0.296404
TableForm[Table[Evaluate[{yy1[t], yy2[t], yy4[t], yy5[t], yy6[t]}], {t, 0, 1, (1/100)}],
  TableHeadings → {None, {"x", "y", "m", "q", "p"}}];
```

Plot of y versus x

```
ParametricPlot[Evaluate[{yy1[t], yy2[t]}], {t, 0, 1}, PlotRange → All,
  PlotPoints → 1000, AxesLabel → {"x", "y"}];
```

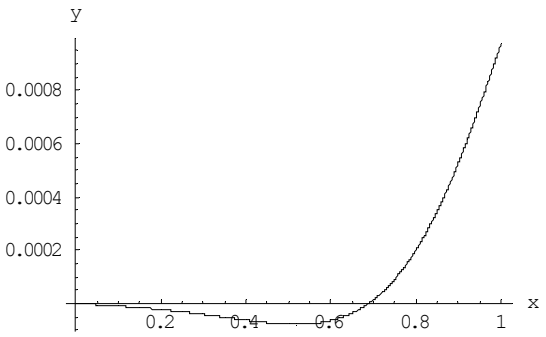

Output y versus x Graph Data to Text File

```
0 >> A2graphdata1.txt
Do[{N[yy1[t]], N[yy2[t]]} >>> A2graphdata1.txt, {t, 0, 1, (1 / 100)}]
```

Plot of (y + yA - 0.5*hb*Cosθ) versus x

```
Clear[g, t]
g[t_] := yy2[t] + yA - 0.5 * hb * Cos[yy3[t]];
ParametricPlot[Evaluate[{yy1[t], g[t]}], {t, 0, 1}, PlotRange → All,
  PlotPoints → 1000, AxesOrigin → {0, 0}, AxesLabel → {"x", "y + yA - 0.5*hb*Cosθ"}];
```

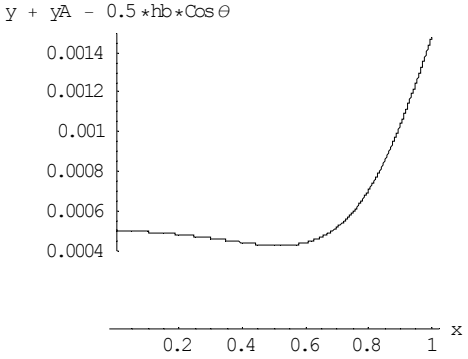

Output (y + yA) versus x Graph Data to Text File

```
0 >> A2graphdata2.txt
Do[{N[yy1[t]], N[yy2[t]]} >>> A2graphdata2.txt, {t, 0, 1, (1 / 100)}]
```

Performing Check to Assure Spring Does Not Wrap Around Backing

```
Clear[f1, f2, f3, f4]
f1[t_] := Cos[yy3[t]]
f2[t_] := (yy1[t] + xA + 0.5 * hb * Sin[yy3[t]] - t) /
  (√((-t + xA + 0.5 * hb * Sin[yy3[t]] + yy1[t])^2 + (yA - 0.5 * hb * Cos[yy3[t]] + yy2[t])^2))
f3[t_] := f1[t] - f2[t]
f4[t_] := If[f3[t] > 0, "okay", "no good"]
```

```
TableForm[Table[Evaluate[{f1[t], f2[t], f3[t], f4[t]}], {t, 0, 1, (1/100)}],
 TableHeadings→
  {None,
   {"Cos[y3[t]]",
    "(yy1[t] + xA + 0.5*hb*Sin[yy3[t]] - t) /
       (√((-t+ xA + 0.5*hb*Sin[yy3[t]] + yy1[t])^2 +
           (yA - 0.5*hb*Cos[yy3[t]] + yy2[t])^2))", "difference", "conclusion"}}];
```

Extensional Strain in the Adhesive

```
ε[t_] :=
 (√(((yA - 0.5*hb*Cos[yy3[t]]) + yy2[t])^2 + (yy1[t] + (xA + 0.5*hb* Sin[yy3[t]]) - t)^2) -
    ha) / ha
```

Maximum Strain

```
ε[1]
```

```
2.00011
```

```
ParametricPlot[
  Evaluate[
   {yy1[t],
    (√(((yA - 0.5*hb*Cos[yy3[t]]) + yy2[t])^2 + (yy1[t] + (xA + 0.5*hb* Sin[yy3[t]]) - t)^2) -
       ha) / ha}], {t, 0, 1}, PlotRange→ All, PlotPoints→ 1000, AxesOrigin→ {0, 0},
  AxesLabel→ {"x", "ε"}];
```

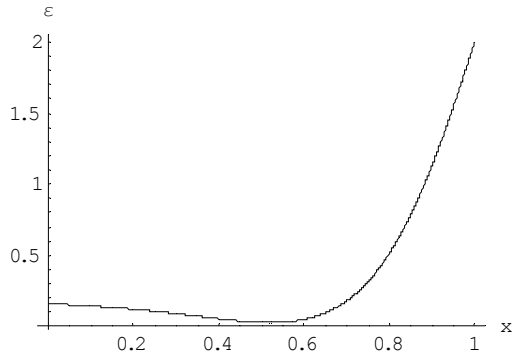

Model 2

In this program, y1 represents x, y2 represents y, y3 represents θ, y4 represents m, y5 represents q, y6 represents p, and t represents s.

```
Clear[eta, ha, hb, θo, mB, gxA, gyA, gθA]
pi = Pi;
eta = 1;
ha = 0.0005;
hb = 0.005;
θo = 27 * pi / 36;
mB = 0;
gxA = -0.0002;
gyA = 0.003;
gθA = -0.0001;
```

**The above three variables are initial guesses.

```
de[y1_, y2_, y3_, y4_, y5_, y6_, xA_, yA_] :=
 {y1'[t] == Cos[y3[t]], y2'[t] == Sin[y3[t]], y3'[t] == y4[t],
  y4'[t] == If[(yA + y2[t] - 0.5 * hb * Cos[y3[t]]) > ha,
    y5[t] * Cos[y3[t]] + y6[t] * Sin[y3[t]] -
     (hb/2) * eta *
      (1 / (√((-t + xA + 0.5 * hb * Sin[y3[t]] + y1[t])^2 + (yA - 0.5 * hb * Cos[y3[t]] + y2[t])^2)) -
       1/ha) * ((y2[t] + yA - 0.5 * hb * Cos[y3[t]]) * Sin[y3[t]] +
       (y1[t] + xA + 0.5 * hb * Sin[y3[t]] - t) * Cos[y3[t]]),
    y5[t] * Cos[y3[t]] + (hb/(2 * ha)) * eta * (y2[t] + yA - 0.5 * hb * Cos[y3[t]] - ha) * Sin[y3[t]]],
  y5'[t] == If[(yA + y2[t] - 0.5 * hb * Cos[y3[t]]) > ha,
    eta *
     (1 / (√((-t + xA + 0.5 * hb * Sin[y3[t]] + y1[t])^2 + (yA - 0.5 * hb * Cos[y3[t]] + y2[t])^2)) -
      1/ha) * (y2[t] + yA - 0.5 * hb * Cos[y3[t]]),
    -eta/ha * (y2[t] + yA - 0.5 * hb * Cos[y3[t]] - ha)],
  y6'[t] == If[(yA + y2[t] - 0.5 * hb * Cos[y3[t]]) > ha,
    eta *
     (1 / (√((-t + xA + 0.5 * hb * Sin[y3[t]] + y1[t])^2 + (yA - 0.5 * hb * Cos[y3[t]] + y2[t])^2)) -
      1/ha) * (-1) * (-t + y1[t] + xA + 0.5 * hb * Sin[y3[t]]),
    0.35 * eta * ((y1[t] + xA + 0.5 * hb * Sin[y3[t]] - t) / ha)]}
leftBC[θA_] := {y1[0] == 0, y2[0] == 0, y3[0] == θA, y4[0] == 0, y5[0] == 0, y6[0] == 0}
soln := NDSolve[Flatten[Append[de[y1, y2, y3, y4, y5, y6, xA, yA], leftBC[θA]]],
  {y1, y2, y3, y4, y5, y6}, {t, 0, 1}, MaxSteps → 1000]
```

```
endpt[xA_, yA_, θA_] :=
  {y1[t], y2[t], y3[t], y4[t], y5[t], y6[t]} /.
    First[NDSolve[Flatten[Append[de[y1, y2, y3, y4, y5, y6, xA, yA], leftBC[θA]]],
      {y1[t], y2[t], y3[t], y4[t], y5[t], y6[t]}, {t, 0, 1}, MaxSteps → 1000]] /. t → 1;
endpt[gxA, gyA, gθA]
{1., 0.000444767, -0.00105738, -0.030687, -0.241086, -0.132909}
Clear[xA, yA, θA]
rts :=
 FindRoot[{endpt[xA, yA, θA][[4]] == mB,
   endpt[xA, yA, θA][[5]] / endpt[xA, yA, θA][[6]] == -Tan[θo],
   (√(((yA - 0.5 * hb * Cos[endpt[xA, yA, θA][[3]]]) + endpt[xA, yA, θA][[2]])^2 +
          (endpt[xA, yA, θA][[1]] + (xA + 0.5 * hb * Sin[endpt[xA, yA, θA][[3]]]) - 1)^2) - ha) /
     ha == 2}, {xA, {gxA, 0.9 * gxA}}, {yA, {gyA, 0.9 * gyA}}, {θA, {gθA, 0.9 * gθA}},
  AccuracyGoal → 3, MaxIterations → 200]
rts
{xA → -0.000290269, yA → 0.00300269, θA → -0.0000934928}
xA = xA /. rts
-0.000290269
yA = yA /. rts
0.00300269
θA = θA /. rts
-0.0000934928
endpt[xA, yA, θA]
{0.999998, 0.000970936, 0.00472985, -0.0000249968, -0.209644, -0.209534}
{yy1[t_], yy2[t_], yy3[t_], yy4[t_], yy5[t_], yy6[t_]} =
  {y1[t], y2[t], y3[t], y4[t], y5[t], y6[t]} /. First[soln];
fo = √(yy5[1]^2 + yy6[1]^2)
0.296404
TableForm[Table[Evaluate[{yy1[t], yy2[t], yy4[t], yy5[t], yy6[t]}], {t, 0, 1, (1/100)}],
  TableHeadings → {None, {"x", "y", "m", "q", "p"}}];
```

Plot of y versus x

```
ParametricPlot[Evaluate[{yy1[t], yy2[t]}], {t, 0, 1}, PlotRange → All,
  PlotPoints → 1000, AxesLabel → {"x", "y"}];
```

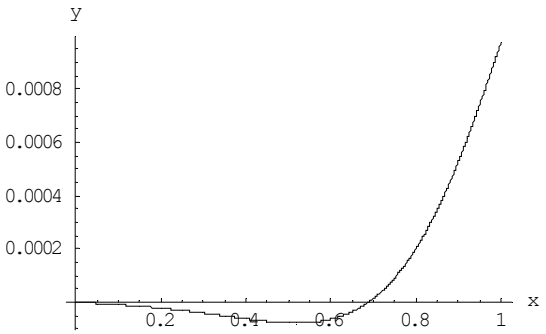

Output y versus x Graph Data to Text File

```
0>> A2graphdata1.txt
Do[{N[yy1[t]], N[yy2[t]]} >>> A2graphdata1.txt, {t, 0, 1, (1 / 100)}]
```

Plot of (y + yA - 0.5*hb*Cosθ) versus x

```
Clear[g, t]
g[t_] := yy2[t] + yA - 0.5 * hb * Cos[yy3[t]];
ParametricPlot[Evaluate[{yy1[t], g[t]}], {t, 0, 1}, PlotRange → All,
  PlotPoints → 1000, AxesOrigin → {0, 0}, AxesLabel → {"x", "y + yA - 0.5*hb*Cosθ"}];
```

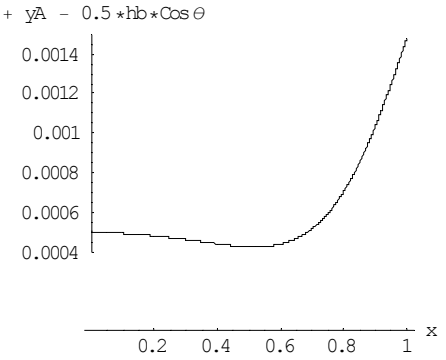

Output (y + yA) versus x Graph Data to Text File

```
0>> A2graphdata2.txt
Do[{N[yy1[t]], N[yy2[t]]} >>> A2graphdata2.txt, {t, 0, 1, (1 / 100)}]
```

Performing Check to Assure Spring Does Not Wrap Around Backing

```
Clear[f1, f2, f3, f4]
f1[t_] := Cos[yy3[t]]
f2[t_] := (yy1[t] + xA + 0.5 * hb * Sin[yy3[t]] - t) /
  (√((-t + xA + 0.5 * hb * Sin[yy3[t]] + yy1[t])^2 + (yA - 0.5 * hb * Cos[yy3[t]] + yy2[t])^2))
f3[t_] := f1[t] - f2[t]
f4[t_] := If[f3[t] > 0, "okay", "no good"]
TableForm[Table[Evaluate[{f1[t], f2[t], f3[t], f4[t]}], {t, 0, 1, (1 / 100)}],
 TableHeadings →
  {None,
   {"Cos[y3[t]]",
    "(yy1[t] + xA + 0.5 * hb * Sin[yy3[t]] - t) /
       (√((-t + xA + 0.5 * hb * Sin[yy3[t]] + yy1[t])^2 +
           (yA - 0.5 * hb * Cos[yy3[t]] + yy2[t])^2))", "difference", "conclusion"}}];
```

Extensional Strain in the Adhesive

```
ε[t_] :=
 (√(((yA - 0.5 * hb * Cos[yy3[t]]) + yy2[t])^2 + (yy1[t] + (xA + 0.5 * hb * Sin[yy3[t]]) - t)^2) -
    ha) / ha
```

Maximum Strain

```
ε[1]
```

```
2.00011
```

```
ParametricPlot[
  Evaluate[
   {yy1[t],
    (√(((yA - 0.5*hb*Cos[yy3[t]]) + yy2[t])^2 + (yy1[t] + (xA + 0.5*hb* Sin[yy3[t]]) - t)^2) -
       ha) / ha}], {t, 0, 1}, PlotRange → All, PlotPoints → 1000, AxesOrigin → {0, 0},
  AxesLabel → {"x", "ε"}];
```

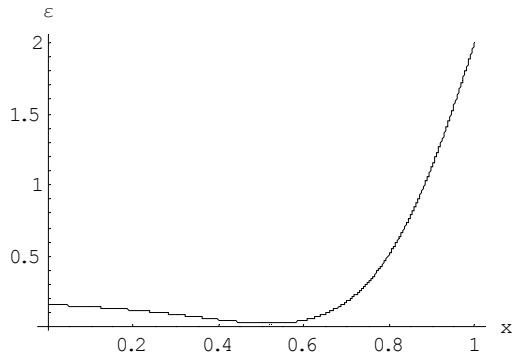

Model 5

In this program, y1 represents x1, y2 represents y1, y3 represents θ1, y4 represents m1, y5 represents q1, y6 represents x2, y7 represents y2, y8 represents θ2, y9 represents m2, and y10 represents q2. For y1 through y6, t represents s and for y7 through y10, t represents z.

```
Clear[F, a, c, theta, k, K1, eta, gy40, gy50, gy90, gy100, gT1];
pi = N[Pi];
F = 2000;
a = 0.4;
c = 1;
theta = pi/2;
k = 1;
K1 = 100;
eta = 100;
n = 3;
gy40 = 365; gy50 = -927; gy90 = 11; gy100 = -73; gT1 = 1.1;
```

**The above five variables are initial guesses.

```
de[y2_, y3_, y4_, y5_, y7_, y8_, y9_, y10_, T1_] :=
 {y1'[t] == a*Cos[y3[t]], y2'[t] == a*Sin[y3[t]], y3'[t] == a*y4[t]/eta,
  y4'[t] == a*(y5[t]*Cos[y3[t]] + T1*Sin[y3[t]]), y5'[t] == -a*k*(y2[t]^n),
  y6'[t] == (1 - a)*Cos[y8[t]], y7'[t] == (1 - a)*Sin[y8[t]], y8'[t] == (1 - a)*y9[t],
  y9'[t] == (1 - a)*y10[t]*Cos[y8[t]] + (1 - a)*(T1 - F*Cos[theta])*Sin[y8[t]],
  y10'[t] == -(1 - a)*k*(y7[t]^n)}
leftBC[y40_, y50_, y90_, y100_, T1_] :=
 {y1[0] == (T1/K1)^(1/n), y2[0] == 0, y3[0] == 0, y4[0] == y40, y5[0] == y50,
  y6[0] == 0, y7[0] == 0, y8[0] == 0, y9[0] == y90, y10[0] == y100}
soln :=
 NDSolve[Flatten[Append[de[y2, y3, y4, y5, y7, y8, y9, y10, T1],
    leftBC[y40, y50, y90, y100, T1]]], {y1, y2, y3, y4, y5, y6, y7, y8, y9, y10},
  {t, 0, 1}, MaxSteps -> 2000]
endpt[y40_, y50_, y90_, y100_, T1_] :=
 {y1[t], y2[t], y3[t], y4[t], y5[t], y6[t], y7[t], y8[t], y9[t], y10[t]} /.
   First[
    NDSolve[Flatten[Append[de[y2, y3, y4, y5, y7, y8, y9, y10, T1],
       leftBC[y40, y50, y90, y100, T1]]],
     {y1[t], y2[t], y3[t], y4[t], y5[t], y6[t], y7[t], y8[t], y9[t], y10[t]},
     {t, 0, 1}, MaxSteps -> 2000]] /. t -> 1
endpt[gy40, gy50, gy90, gy100, gT1]
{0.564522, 0.186426, 0.7845, 48.0565, -927.,
 0.333378, 0.122251, -2.79914, -13.2023, -73.0034}
Clear[y40, y50, y90, y100, T1]
```

```
rts := FindRoot[{endpt[y40, y50, y90, y100, T1][[2]] == endpt[y40, y50, y90, y100, T1][[7]],
   endpt[y40, y50, y90, y100, T1][[1]] + endpt[y40, y50, y90, y100, T1][[6]] == c,
   endpt[y40, y50, y90, y100, T1][[5]] + endpt[y40, y50, y90, y100, T1][[10]] +
     F*Sin[theta] == 0,
   endpt[y40, y50, y90, y100, T1][[8]] + endpt[y40, y50, y90, y100, T1][[3]] == 0,
   endpt[y40, y50, y90, y100, T1][[9]] == endpt[y40, y50, y90, y100, T1][[4]]},
  {y40, {gy40, 0.99*gy40}}, {y50, {gy50, 0.99*gy50}}, {y90, {gy90, 0.99*gy90}},
  {y100, {gy100, 0.99*gy100}}, {T1, {gT1, 0.99*gT1}}, AccuracyGoal -> 6,
  MaxIterations -> 500]
rts
{y40 → 570.215, y50 → -1957.87, y90 → 8.10724, y100 → -42.1252, T1 → 1.15422}
y40 = Re[y40 /. rts]
570.215
y50 = Re[y50 /. rts]
-1957.87
y90 = Re[y90 /. rts]
8.10724
y100 = Re[y100 /. rts]
-42.1252
T1 = Re[T1 /. rts]
1.15422
endpt[y40, y50, y90, y100, T1]
{0.523351, 0.242592, 0.979588, -11.6923,
 -1957.87, 0.476649, 0.242592, -0.979588, -11.6923, -42.1306}
{yy1[t_], yy2[t_], yy3[t_], yy4[t_], yy5[t_], yy6[t_], yy7[t_], yy8[t_], yy9[t_],
   yy10[t_]} = {y1[t], y2[t], y3[t], y4[t], y5[t], y6[t], y7[t], y8[t], y9[t], y10[t]} /.
   First[soln];
TableForm[Table[Evaluate[{yy1[t], yy2[t], c - yy6[t], yy7[t]}], {t, 0, 1, 0.1}],
 TableHeadings → {None, {"x1", "y1", "x2", "y2"}}]
```

x1	y1	x2	y2
0.225993	1.85793×10^{-24}	1.	2.22305×10^{-24}
0.265682	0.00433675	0.941838	0.012903
0.303772	0.0163681	0.891176	0.0446929
0.33934	0.0345832	0.848424	0.0866994
0.372039	0.057575	0.810525	0.133202
0.40192	0.0841411	0.773415	0.180346
0.429282	0.113304	0.732922	0.22457
0.454569	0.14429	0.685438	0.261031
0.478301	0.176485	0.629635	0.282187
0.501038	0.209394	0.570412	0.278112
0.523351	0.242592	0.523351	0.242592

```
plot1 = ParametricPlot[Evaluate[{yy1[t], yy2[t]}], {t, 0, 1}, PlotRange → All,
   PlotPoints → 1000, AxesLabel → {"x", "y"}];
```

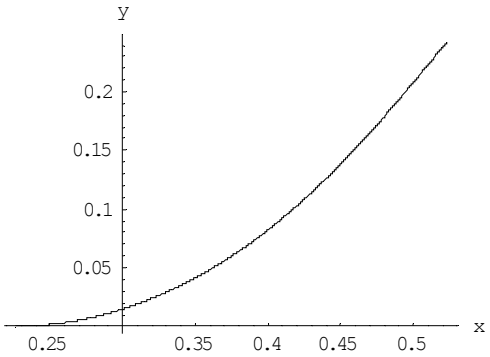


```
plot2 = ParametricPlot[Evaluate[{c - yy6[t], yy7[t]}], {t, 0, 1}, PlotRange → All,
    PlotPoints → 1000, AxesLabel → {"x", "y"},
    PlotStyle → {Thickness[.01], RGBColor[0, 0, 1]}];
```

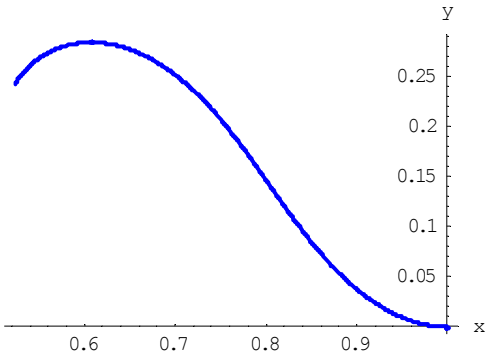


```
Show[plot1, plot2];
```

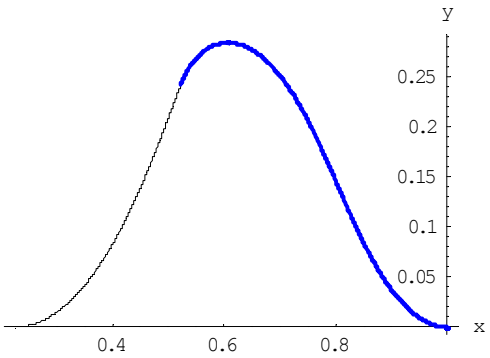


```
0 >> Fshape1.txt
Do[{N[yy1[t]], N[yy2[t]]} >>> Fshape1.txt, {t, 0, 1, (1 / 100)}]
0 >> Fshape2.txt
Do[{N[c - yy6[t]], N[yy7[t]]} >>> Fshape2.txt, {t, 0, 1, (1 / 100)}]
```

Model 7

In this program, y1 represents x1, y2 represents y1, y3 represents θ1, y4 represents m1, y5 represents q1, y6 represents x2, y7 represents y2, y8 represents θ2, y9 represents m2, and y10 represents q2. For y1 through y6, t represents s and for y7 through y10, t represents z.

```
Clear[a, c, theta, k, K1, eta, F, gy40, gy50, gy90, gy100, gT1];
F = 50; pi = N[Pi]; a = 0.4; c = 1; theta = pi/2; k = 1; K1 = 1; eta = 100;
n = 3;
gy40 = 19.1148198039341 86`-1.8656625709775084`*^-6 i;
gy50 = -48.83496025510005`+2.6825938613370645`*^-6 i;
gy90 = 0.28706391674456916`+8.130431789660515`*^-7 i;
gy100 = -1.16503974574999 37`-2.6825482181723483`*^-6 i;
gT1 = -8.355631049099125`*^-11+2.2776176668237474`*^-12 i;
```

**The above five variables are initial guesses.

```
de[y2_, y3_, y4_, y5_, y7_, y8_, y9_, y10_, T1_] :=
 {y1'[t] == a*Cos[y3[t]], y2'[t] == a*Sin[y3[t]], y3'[t] == a*y4[t]/eta,
  y4'[t] == a*(y5[t]*Cos[y3[t]]+T1*Sin[y3[t]]), y5'[t] == -a*k*(y2[t]^n),
  y6'[t] == (1-a)*Cos[y8[t]], y7'[t] == (1-a)*Sin[y8[t]], y8'[t] == (1-a)*y9[t],
  y9'[t] == (1-a)*y10[t]*Cos[y8[t]]+(1-a)*(T1-F*Cos[theta])*Sin[y8[t]],
  y10'[t] == -(1-a)*k*(y7[t]^n)}
leftBC[y40_, y50_, y90_, y100_, T1_] :=
 {y1[0] == (T1/K1)^(1/n), y2[0] == 0, y3[0] == 0, y4[0] == y40, y5[0] == y50,
  y6[0] == 0, y7[0] == ((T1-F*Cos[theta])/K1)^(1/n), y8[0] == 0, y9[0] == y90,
  y10[0] == y100}
soln :=
 NDSolve[Flatten[Append[de[y2, y3, y4, y5, y7, y8, y9, y10, T1],
    leftBC[y40, y50, y90, y100, T1]]], {y1, y2, y3, y4, y5, y6, y7, y8, y9, y10},
  {t, 0, 1}, MaxSteps -> 2000]
endpt[y40_, y50_, y90_, y100_, T1_] :=
 {y1[t], y2[t], y3[t], y4[t], y5[t], y6[t], y7[t], y8[t], y9[t], y10[t]} /.
   First[
    NDSolve[Flatten[Append[de[y2, y3, y4, y5, y7, y8, y9, y10, T1],
       leftBC[y40, y50, y90, y100, T1]]],
     {y1[t], y2[t], y3[t], y4[t], y5[t], y6[t], y7[t], y8[t], y9[t], y10[t]},
     {t, 0, 1}, MaxSteps -> 2000]] /. t -> 1
endpt[gy40, gy50, gy90, gy100, gT1];
Clear[y40, y50, y90, y100, T1]
```

```
rts := FindRoot[{endpt[y40, y50, y90, y100, T1][[2]] == endpt[y40, y50, y90, y100, T1][[7]],
    endpt[y40, y50, y90, y100, T1][[1]] + endpt[y40, y50, y90, y100, T1][[6]] == c,
    endpt[y40, y50, y90, y100, T1][[5]] + endpt[y40, y50, y90, y100, T1][[10]] +
      F*Sin[theta] == 0,
    endpt[y40, y50, y90, y100, T1][[8]] + endpt[y40, y50, y90, y100, T1][[3]] == 0,
    endpt[y40, y50, y90, y100, T1][[9]] == endpt[y40, y50, y90, y100, T1][[4]]},
  {y40, {gy40, 0.99*gy40}}, {y50, {gy50, 0.99*gy50}}, {y90, {gy90, 0.99*gy90}},
  {y100, {gy100, 0.99*gy100}}, {T1, {gT1, 0.99*gT1}}, AccuracyGoal -> 6,
  MaxIterations -> 500]
rts
{y40 → 19.1148 - 3.68784×10^-10 i,
 y50 → -48.8349 + 5.3155×10^-10 i, y90 → 0.287077 + 1.60694×10^-10 i,
 y100 → -1.16508 - 5.31005×10^-10 i, T1 → 3.9207×10^-11 + 4.22685×10^-14 i}
y40 = Re[y40 /. rts];
y50 = Re[y50 /. rts];
y90 = Re[y90 /. rts];
y100 = Re[y100 /. rts];
T1 = Re[T1 /. rts];
endpt[y40, y50, y90, y100, T1];
{yy1[t_], yy2[t_], yy3[t_], yy4[t_], yy5[t_], yy6[t_], yy7[t_], yy8[t_], yy9[t_],
   yy10[t_]} = {y1[t], y2[t], y3[t], y4[t], y5[t], y6[t], y7[t], y8[t], y9[t], y10[t]} /.
   First[soln];
yyy2aa = yy2[1]
0.010082
yy1[0]
0.00033972
(T1 / K1) ^ (1 / n)
0.00033972
N[100^(1 / 3)]
4.64159
```

Model 7—symmetrical

In this program, y1 represents x1, y2 represents y1, y3 represents θ1, y4 represents m1, y5 represents q1, y6 represents x2, y7 represents y2, y8 represents θ2, y9 represents m2, and y10 represents q2. For y1 through y6, t represents s and for y7 through y10, t represents z.

```
Clear[a, c, theta, k, K1, eta, F, gy40, gy50, gT1];
F = 50; pi = N[Pi]; a = 0.5; c = 1; theta = pi/2; k = 1; K1 = 1; eta = 1;
n = 1;
gy40 = 5.53; gy50 = -25; gT1 = 6.176954386942746`*^-7;
```

**The above three variables are initial guesses.

```
de[y2_, y3_, y4_, y5_, T1_] :=
 {y1'[t] == a*Cos[y3[t]], y2'[t] == a*Sin[y3[t]], y3'[t] == a*y4[t]/eta,
  y4'[t] == a*(y5[t]*Cos[y3[t]] + T1*Sin[y3[t]]), y5'[t] == -a*k*(y2[t]^n)}
leftBC[y40_, y50_, T1_] := {y1[0] == (T1/K1)^(1/n), y2[0] == 0, y3[0] == 0,
  y4[0] == y40, y5[0] == y50}
soln := NDSolve[Flatten[Append[de[y2, y3, y4, y5, T1], leftBC[y40, y50, T1]]],
  {y1, y2, y3, y4, y5}, {t, 0, 1}, MaxSteps -> 2000]
endpt[y40_, y50_, T1_] :=
 {y1[t], y2[t], y3[t], y4[t], y5[t]} /.
   First[NDSolve[Flatten[Append[de[y2, y3, y4, y5, T1], leftBC[y40, y50, T1]]],
     {y1[t], y2[t], y3[t], y4[t], y5[t]}, {t, 0, 1}, MaxSteps -> 2000]] /. t -> 1
endpt[gy40, gy50, gT1];
Clear[y40, y50, T1]
rts := FindRoot[{endpt[y40, y50, T1][[5]] == -F/2, endpt[y40, y50, T1][[3]] == 0,
   endpt[y40, y50, T1][[1]] == c/2}, {y40, {gy40, 0.99*gy40}}, {y50, {gy50, 0.99*gy50}},
  {T1, {gT1, 0.99*gT1}}, AccuracyGoal -> 6, MaxIterations -> 500]
rts
{y40 → 5.52068, y50 → -24.9473, T1 → 0.057058}
y40 = Re[y40 /. rts];
y50 = Re[y50 /. rts];
T1 = Re[T1 /. rts];
endpt[y40, y50, T1];
{yy1[t_], yy2[t_], yy3[t_], yy4[t_], yy5[t_]} =
  {y1[t], y2[t], y3[t], y4[t], y5[t]} /. First[soln];
yyy2aa = yy2[1]
0.210901
```

Plot of shape

```
plot1 = ParametricPlot[Evaluate[{yy1[t], yy2[t]}], {t, 0, 1}, PlotRange → All,
   PlotPoints → 1000, AxesLabel → {"x", "y"}];
```

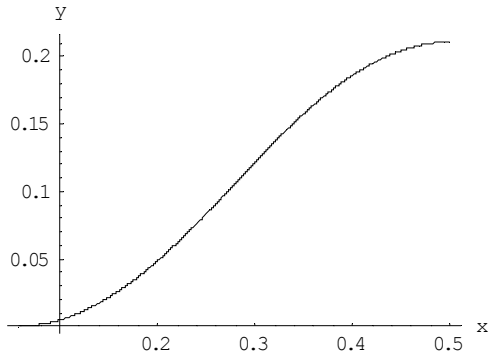


```
0 >> Hchangen1.txt
Do[{N[yy1[t]], N[yy2[t]]} >>> Hchangen1.txt, {t, 0, 1, (1 / 100)}]
```

Model 9

In this program, y1 = x1, y2 = z1, y3 = θ1, y4 = m1, y5 = p1, y6 = q1, y7 = x2, y8 = z2, y9 = θ2, y10 = m2, y11 = p2, y12 = q2, and t = s.

```
Clear[ao, bo, k1, k2, ks, n, eta, fo, θo, d]
ao = 0.1;
bo = 0.5;
d = 1;
k1 = 200;
k2 = 200;
ks = 1;
fo = 120;
mo = 0;
θo = Pi / 2;
n = 1;
eta = 10;
gm10 = 24.63;
gp10 = 33.79;
gq10 = -59.90;
gx20 = 1.017;
gz20 = 0.499;
gth20 = 0.540;
gm20 = -9.329;
gp20 = 33.84;
gq20 = 39.84;
```

**The above nine variables are initial guesses.

```
de[y1_, y2_, y3_, y4_, y5_, y6_, y7_, y8_, y9_, y10_, y11_, y12_] :=
 {y1'[t] == Cos[y3[t]],
  y2'[t] == Sin[y3[t]],
  y3'[t] == y4[t] / eta,
  y4'[t] == y5[t] * Sin[y3[t]] + y6[t] * Cos[y3[t]],
  y5'[t] == -2 * (t - y1[t]) * ks / Sqrt[(ao + y2[t])^2 + bo^2 + (t - y1[t])^2] *
    (Sqrt[(ao + y2[t])^2 + bo^2 + (t - y1[t])^2] / Sqrt[ao^2 + bo^2] - 1)^n,
  y6'[t] == -2 * (ao + y2[t]) * ks / Sqrt[(ao + y2[t])^2 + bo^2 + (t - y1[t])^2] *
    (Sqrt[(ao + y2[t])^2 + bo^2 + (t - y1[t])^2] / Sqrt[ao^2 + bo^2] - 1)^n,
  y7'[t] == d * Cos[y9[t]],
  y8'[t] == d * Sin[y9[t]],
  y9'[t] == d * y10[t],
  y10'[t] == d * (y11[t] * Sin[y9[t]] + y12[t] * Cos[y9[t]]),
  y11'[t] == -2 * d * (1 + d * t - y7[t]) * ks /
    Sqrt[(ao + y8[t])^2 + bo^2 + (1 + t - y7[t])^2] *
    (Sqrt[(ao + y8[t])^2 + bo^2 + (1 + t - y7[t])^2] / Sqrt[ao^2 + bo^2] - 1)^n,
  y12'[t] == -2 * d * (ao + y8[t]) * ks /
    Sqrt[(ao + y8[t])^2 + bo^2 + (1 + t - y7[t])^2] *
    (Sqrt[(ao + y8[t])^2 + bo^2 + (1 + t - y7[t])^2] / Sqrt[ao^2 + bo^2] - 1)^n}
leftBC[m10_, p10_, q10_, x20_, z20_, th20_, m20_, p20_, q20_] :=
 {y1[0] == Abs[(p10 / k1)^(1/n)], y2[0] == 0, y3[0] == 0, y4[0] == m10, y5[0] == p10, y6[0] == q10,
  y7[0] == x20, y8[0] == z20, y9[0] == th20, y10[0] == m20, y11[0] == p20, y12[0] == q20}
soln :=
 NDSolve[Flatten[Append[de[y1, y2, y3, y4, y5, y6, y7, y8, y9, y10, y11, y12],
    leftBC[m10, p10, q10, x20, z20, th20, m20, p20, q20]]],
  {y1, y2, y3, y4, y5, y6, y7, y8, y9, y10, y11, y12}, {t, 0, 1}, MaxSteps → 9000]
endpt[m10_, p10_, q10_, x20_, z20_, th20_, m20_, p20_, q20_] :=
  {y1[t], y2[t], y3[t], y4[t], y5[t], y6[t], y7[t], y8[t], y9[t], y10[t], y11[t], y12[t]} /.
    First[
     NDSolve[Flatten[Append[de[y1, y2, y3, y4, y5, y6, y7, y8, y9, y10, y11, y12],
        leftBC[m10, p10, q10, x20, z20, th20, m20, p20, q20]]],
      {y1[t], y2[t], y3[t], y4[t], y5[t], y6[t], y7[t], y8[t], y9[t], y10[t],
       y11[t], y12[t]}, {t, 0, 1}, MaxSteps → 8500]] /. t → 1;
endpt[gm10, gp10, gq10, gx20, gz20, gth20, gm20, gp20, gq20]
{1.0167, 0.498868, 0.540206, -9.32999, 33.8411,
 -60.1585, 1.82401, -0.0146368, -0.117527, 5.23069, 33.813, 39.467}
Clear[m10, p10, q10, x20, z20, th20, m20, p20, q20]
```

```
rts :=
 FindRoot[{1 + d - endpt[m10, p10, q10, x20, z20, th20, m20, p20, q20][[7]] == Abs[(p20/k2)^(1/n)],
   endpt[m10, p10, q10, x20, z20, th20, m20, p20, q20][[8]] == 0,
   endpt[m10, p10, q10, x20, z20, th20, m20, p20, q20][[9]] == 0,
   endpt[m10, p10, q10, x20, z20, th20, m20, p20, q20][[3]] == th20,
   endpt[m10, p10, q10, x20, z20, th20, m20, p20, q20][[4]] == m20 + mo,
   endpt[m10, p10, q10, x20, z20, th20, m20, p20, q20][[5]] == p20 + fo*Cos[θo],
   endpt[m10, p10, q10, x20, z20, th20, m20, p20, q20][[6]] == q20 - fo*Sin[θo],
   endpt[m10, p10, q10, x20, z20, th20, m20, p20, q20][[1]] == x20,
   endpt[m10, p10, q10, x20, z20, th20, m20, p20, q20][[2]] == z20},
  {m10, {gm10, 0.97*gm10}}, {p10, {gp10, 0.97*gp10}}, {q10, {gq10, 0.97*gq10}},
  {x20, {gx20, 0.97*gx20}}, {z20, {gz20, 0.97*gz20}}, {th20, {gth20, 0.97*gth20}},
  {m20, {gm20, 0.97*gm20}}, {p20, {gp20, 0.97*gp20}}, {q20, {gq20, 0.97*gq20}},
  AccuracyGoal → 3, MaxIterations → 3000]
rts
{m10 → 27.5082, p10 → 38.7508, q10 → -71.1915, x20 → 1.01783,
 z20 → 0.533289, th20 → 0.5705, m20 → -10.5312, p20 → 38.8162, q20 → 48.5115}
m10 = m10 /. rts
27.5082
p10 = p10 /. rts
38.7508
q10 = q10 /. rts
-71.1915
x20 = x20 /. rts
1.01783
z20 = z20 /. rts
0.533289
th20 = th20 /. rts
0.5705
m20 = m20 /. rts
-10.5312
p20 = p20 /. rts
38.8162
q20 = q20 /. rts
48.5115
endpt[m10, p10, q10, x20, z20, th20, m20, p20, q20]
{1.01783, 0.533289, 0.5705, -10.5312, 38.8162, -71.4885,
 1.80592, -3.33649×10^-7, 7.25902×10^-6, 6.77299, 38.7796, 48.0941}
{yy1[t_], yy2[t_], yy3[t_], yy4[t_], yy5[t_], yy6[t_], yy7[t_], yy8[t_], yy9[t_],
   yy10[t_], yy11[t_], yy12[t_]} =
  {y1[t], y2[t], y3[t], y4[t], y5[t], y6[t], y7[t], y8[t], y9[t], y10[t], y11[t], y12[t]} /.
   First[soln];
```

```
F = ParametricPlot[Evaluate[{yy1[t], yy2[t]}], {t, 0, 1}, PlotRange → All,
    PlotPoints → 1000, AxesLabel → {"x1", "z1"}];
G = ParametricPlot[Evaluate[{yy7[t], yy8[t]}], {t, 0, 1}, PlotRange → All,
    PlotPoints → 1000, AxesOrigin → {0, 0}, AxesLabel → {"x2", "z2"}];
H = Show[F, G]
```

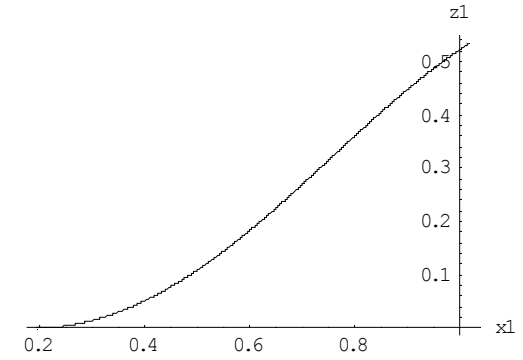

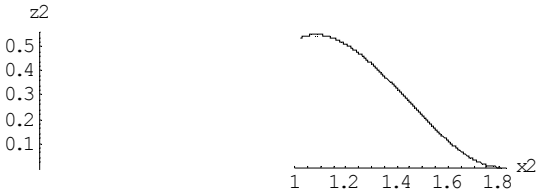

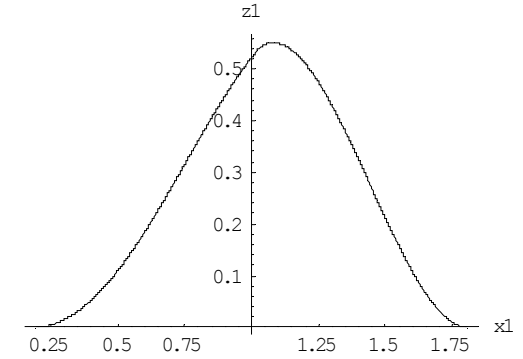

- Graphics -

```
0 >> Jgraphdata1.txt
Do[{N[yy1[t]], N[yy2[t]]} >>> Jgraphdata1.txt, {t, 0, 1, (1 / 100)}]
0 >> Jgraphdata2.txt
Do[{N[yy7[t]], N[yy8[t]]} >>> Jgraphdata2.txt, {t, 0, 1, (1 / 100)}]
Do[{N[yy7[t]], N[yy8[t]]} >>> Jgraphdata2.txt, {t, 0, 1, (1 / 100)}]
```

Model 10

In this program, y1 = x, y2 = z, y3 = θ, y4 = m, y5 = p, y6 = q, and t = s.

```
Clear[ao, bo, k1, k2, ks, n, eta, fA, θo, d]
ao = 0.1;
bo = 0.5;
d = 1;
k1 = 200;
k2 = 200;
ks = 1;
fA = 410;
n = 1;
eta = 10;
beta = 50;

gm10 = 2;
gp10 = 0.4;
gq10 = -3;
```

**The above three variables are initial guesses.

$$\text{de}[y1\_, y2\_, y3\_, y4\_, y5\_, y6\_] :=$$

$$\{y1'[t] == \text{Cos}[y3[t]],$$

$$y2'[t] == \text{Sin}[y3[t]],$$

$$y3'[t] == \text{If}[t <= 1, y4[t]/\text{eta}, y4[t]], y4'[t] == y5[t]*\text{Sin}[y3[t]] + y6[t]*\text{Cos}[y3[t]],$$

$$y5'[t] ==$$

$$\text{If}\left[t <= 1, \frac{-2*(t-y1[t])*ks}{\sqrt{(ao+y2[t])^2+bo^2+(t-y1[t])^2}}*\left(\frac{\sqrt{(ao+y2[t])^2+bo^2+(t-y1[t])^2}}{\sqrt{ao^2+bo^2}}-1\right)^n + fA*\text{Exp}[\text{beta}*(t-1)]*\text{Cos}[\text{beta}*(t-1)]*\text{Sin}[y3[t]], \frac{-2*(t-y1[t])*ks}{\sqrt{(ao+y2[t])^2+bo^2+(t-y1[t])^2}}*\left(\frac{\sqrt{(ao+y2[t])^2+bo^2+(t-y1[t])^2}}{\sqrt{ao^2+bo^2}}-1\right)^n\right],$$

$$y6'[t] ==$$

$$\text{If}\left[t <= 1, \frac{-2*(ao+y2[t])*ks}{\sqrt{(ao+y2[t])^2+bo^2+(t-y1[t])^2}}*\left(\frac{\sqrt{(ao+y2[t])^2+bo^2+(t-y1[t])^2}}{\sqrt{ao^2+bo^2}}-1\right)^n + fA*\text{Exp}[\text{beta}*(t-1)]*\text{Cos}[\text{beta}*(t-1)]*\text{Cos}[y3[t]], \frac{-2*(ao+y2[t])*ks}{\sqrt{(ao+y2[t])^2+bo^2+(t-y1[t])^2}}*\left(\frac{\sqrt{(ao+y2[t])^2+bo^2+(t-y1[t])^2}}{\sqrt{ao^2+bo^2}}-1\right)^n\right]\}$$

$$\text{leftBC}[m10\_, p10\_, q10\_] := \left\{y1[0] == \left(\frac{p10}{k1}\right)^{\frac{1}{n}}, y2[0] == 0, y3[0] == 0, y4[0] == m10,\right.$$

$$\left.y5[0] == p10, y6[0] == q10\right\}$$

$$\text{soln} := \text{NDSolve}[\text{Flatten}[\text{Append}[\text{de}[y1, y2, y3, y4, y5, y6], \text{leftBC}[m10, p10, q10]]],$$

$$\{y1, y2, y3, y4, y5, y6\}, \{t, 0, 1+d\}, \text{MaxSteps} \to 9000]$$

```
endpt[m10_, p10_, q10_] :=
  {y1[t], y2[t], y3[t], y4[t], y5[t], y6[t]} /.
    First[NDSolve[Flatten[Append[de[y1, y2, y3, y4, y5, y6], leftBC[m10, p10, q10]]],
      {y1[t], y2[t], y3[t], y4[t], y5[t], y6[t]}, {t, 0, 1 + d}, MaxSteps → 8500]] /.
   t → 1 + d;
endpt[gm10, gp10, gq10]
{1.95283, -0.21748, -0.454558, -0.104924, 0.609289, 1.0864}
Clear[m10, p10, q10]
rts := FindRoot[{1 + d - endpt[m10, p10, q10][[1]] == (endpt[m10, p10, q10][[5]] / k2)^(1/n),
   endpt[m10, p10, q10][[2]] == 0, endpt[m10, p10, q10][[3]] == 0},
  {m10, {gm10, 0.97*gm10}}, {p10, {gp10, 0.97*gp10}}, {q10, {gq10, 0.97*gq10}},
  AccuracyGoal → 3, MaxIterations → 300]
rts
{m10 → 2.15265, p10 → 0.357353, q10 → -2.84924}
m10 = m10 /. rts
2.15265
p10 = p10 /. rts
0.357353
q10 = q10 /. rts
-2.84924
endpt[m10, p10, q10]
{1.99669, -0.000143234, -0.000189746, 0.512522, 0.659691, 1.22365}
{yy1[t_], yy2[t_], yy3[t_], yy4[t_], yy5[t_], yy6[t_]} =
  {y1[t], y2[t], y3[t], y4[t], y5[t], y6[t]} /. First[soln];

F = ParametricPlot[Evaluate[{yy1[t], yy2[t]}], {t, 0, 1 + d}, PlotRange → All,
   PlotPoints → 1000, AxesLabel → {"x", "z"}];
```

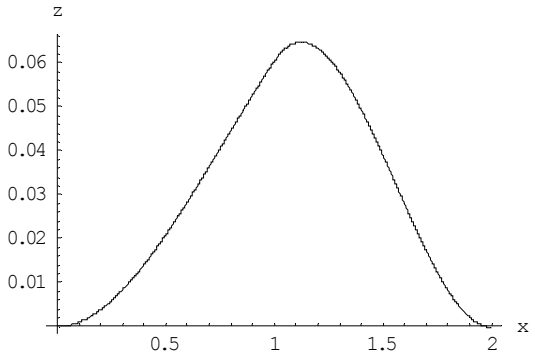


```
0 >> Kgraphdata.txt
Do[{N[yy1[t]], N[yy2[t]]} >>> Kgraphdata.txt, {t, 0, 1 + d, (1/100)}]
```

Model 11

In this program, y1 represents x1, y2 represents y1, y3 represents θ1, y4 represents m1, y5 represents x2, y6 represents y2, y7 represents θ2, y8 represents m2, y9 represents x3, y10 represents y3, y11 rperesents θ3, y12 represents m3, and t represents s.

```
Clear[fo, θo, r, d, η2, η3, k2, k3, gm1, gm2, gm3, gq1, gq2, gp2]
pi = Pi;
fo = 5;
θo = pi / 2;
r = 1;
d = 1;
η2 = 0.05;
η3 = 0.005;
k2 = 0.01;
k3 = 0;
gq1 = -3.5;
gp2 = 0.002;
gq2 = -0.5;
gm1 = 1.6;
gm2 = 0.2;
gm3 = 6.3*10^-15;
```

**The above six variables are initial guesses.

```
de[y3_, y4_, y7_, y8_, y11_, y12_, q1_, p2_, q2_] :=
 {y1'[t] == Cos[y3[t]], y2'[t] == Sin[y3[t]], y3'[t] == y4[t],
  y4'[t] == q1*Cos[y3[t]] + (p2 + fo*Cos[y3[t]])*Sin[y3[t]], y5'[t] == r*Cos[y7[t]],
  y6'[t] == r*Sin[y7[t]], y7'[t] == r*y8[t]/η2, y8'[t] == r*(q2*Cos[y7[t]] + p2*Sin[y7[t]]),
  y9'[t] == d*Cos[y11[t]], y10'[t] == d*Sin[y11[t]], y11'[t] == d*y12[t]/η3,
  y12'[t] == d*(-fo*Sin[θo]*Cos[y11[t]] - fo*Cos[θo]*Sin[y11[t]])}
leftBC[m1_, m2_, m3_] := {y1[0] == 0, y2[0] == 0, y3[0] == 0, y4[0] == m1, y5[0] == 0,
  y6[0] == 0, y7[0] == 0, y8[0] == m2, y9[0] == 0, y10[0] == 0, y11[0] == pi - θo, y12[0] == m3}
soln :=
 NDSolve[Flatten[Append[de[y3, y4, y7, y8, y11, y12, q1, p2, q2], leftBC[m1, m2, m3]]],
  {y1, y2, y3, y4, y5, y6, y7, y8, y9, y10, y11, y12}, {t, 0, 1}, MaxSteps → 2000]
endpt[q1_, p2_, q2_, m1_, m2_, m3_] :=
  {y1[t], y2[t], y3[t], y4[t], y5[t], y6[t], y7[t], y8[t], y9[t], y10[t], y11[t], y12[t]} /.
    First[
     NDSolve[Flatten[Append[de[y3, y4, y7, y8, y11, y12, q1, p2, q2],
        leftBC[m1, m2, m3]]], {y1[t], y2[t], y3[t], y4[t], y5[t], y6[t], y7[t],
       y8[t], y9[t], y10[t], y11[t], y12[t]}, {t, 0, 1}, MaxSteps → 1000]] /. t → 1;
endpt[gq1, gp2, gq2, gm1, gm2, gm3]
{0.881129, 0.430486, 0.717353, 0.3465, 0.765037, 0.593134,
 0.142897, -0.181332, -0.0267655, 0.994056, 2.44476, 0.133827}
```

```
Clear[q1, p2, q2, m1, m2, m3]
rts := FindRoot[{endpt[q1, p2, q2, m1, m2, m3][[2]] == endpt[q1, p2, q2, m1, m2, m3][[6]],
   endpt[q1, p2, q2, m1, m2, m3][[3]] + endpt[q1, p2, q2, m1, m2, m3][[11]] == pi,
   endpt[q1, p2, q2, m1, m2, m3][[7]] == -endpt[q1, p2, q2, m1, m2, m3][[3]],
   k3 * endpt[q1, p2, q2, m1, m2, m3][[2]] == q2 + q1 + (fo * Sin[θo]),
   endpt[q1, p2, q2, m1, m2, m3][[12]] + endpt[q1, p2, q2, m1, m2, m3][[8]] ==
    endpt[q1, p2, q2, m1, m2, m3][[4]],
   k2 * (1 + r - endpt[q1, p2, q2, m1, m2, m3][[1]] - endpt[q1, p2, q2, m1, m2, m3][[5]]) ==
    p2}, {q1, {gq1, 0.9 * gq1}}, {p2, {gp2, 0.9 * gp2}}, {q2, {gq2, 0.9 * gq2}},
  {m1, {gm1, 0.9 * gm1}}, {m2, {gm2, 0.9 * gm2}}, {m3, {gm3, 0.9 * gm3}},
  AccuracyGoal → 4, MaxIterations → 500]
rts
{q1 → -4.38832, p2 → 0.0029685, q2 → -0.611681,
 m1 → 1.84895, m2 → 0.215321, m3 → 6.39566 × 10^-15}
q1 = q1 /. rts
-4.38832
p2 = p2 /. rts
0.0029685
q2 = q2 /. rts
-0.611681
m1 = m1 /. rts
1.84895
m2 = m2 /. rts
0.215321
m3 = m3 /. rts
6.39566 × 10^-15
endpt[q1, p2, q2, m1, m2, m3]
{0.881658, 0.437856, 0.61526, -0.140471, 0.821492, 0.437856,
 -0.61526, -0.28587, -0.0290814, 0.992916, 2.52639, 0.145407}
{yy1[t_], yy2[t_], yy3[t_], yy4[t_], yy5[t_], yy6[t_], yy7[t_], yy8[t_], yy9[t_],
   yy10[t_], yy11[t_], yy12[t_]} =
  {y1[t], y2[t], y3[t], y4[t], y5[t], y6[t], y7[t], y8[t], y9[t], y10[t], y11[t], y12[t]} /.
   First[soln];
plot1 = ParametricPlot[Evaluate[{yy1[t], yy2[t]}], {t, 0, 1}, PlotRange → All,
   PlotPoints → 1000, AxesLabel → {"x", "y"}];
```

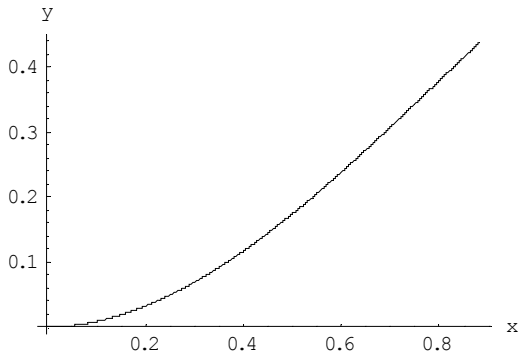


```
0 >> Mgraphdata1.txt
```

```
Do[{N[yy1[t]], N[yy2[t]]} >>> Mgraphdata1.txt, {t, 0, 1, (1/100)}]
plot2 = ParametricPlot[Evaluate[{((yy5[1] + yy1[1]) - yy5[t]), yy6[t]}],
   {t, 0, 1}, PlotRange → All, PlotPoints → 1000, AxesLabel → {"x", "y"}];
```

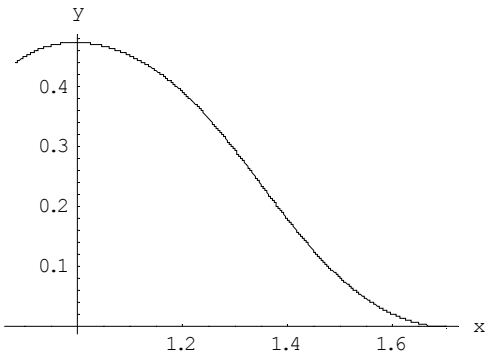


```
0 >> Mgraphdata2.txt
Do[{N[yy5[1] + yy1[1] - yy5[t]], N[yy6[t]]} >>> Mgraphdata2.txt, {t, 0, 1, (1/100)}]
Show[plot1, plot2];
```

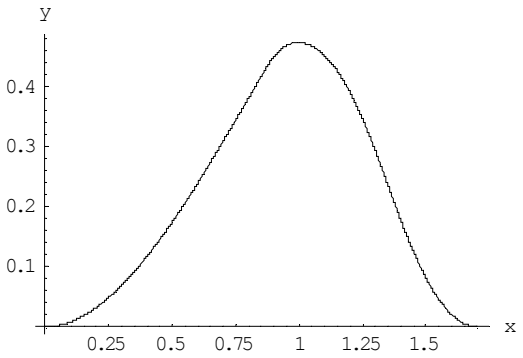

Adding Free Piece to Graph

```
ParametricPlot[Evaluate[{(yy9[t]), yy10[t]}], {t, 0, 1}, PlotRange → All,
  PlotPoints → 1000, AxesLabel → {"x", "y"}];
```

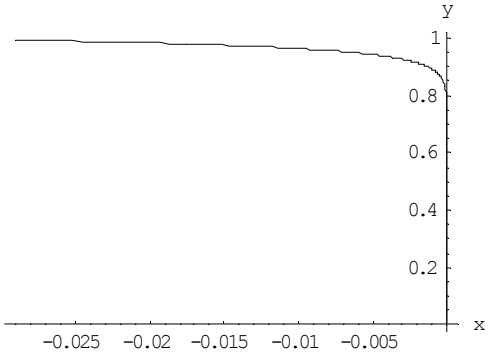


```
plot3 =
  ParametricPlot[Evaluate[{(yy1[1] - yy9[1] + yy9[t]), (yy2[1] + yy10[1] - yy10[t])}],
   {t, 0, 1}, PlotRange → All, PlotPoints → 1000, AxesLabel → {"x", "y"}];
```

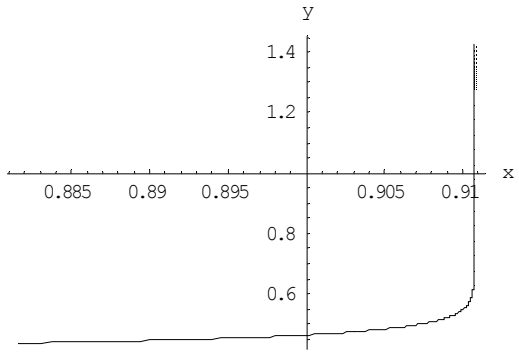


```
0 >> Mgraphdata3.txt
Do[{N[yy1[1] - yy9[1] + yy9[t]], N[yy2[1] + yy10[1] - yy10[t]]} >>> Mgraphdata3.txt,
 {t, 0, 1, (1/100)}]
Show[plot1, plot2, plot3];
```

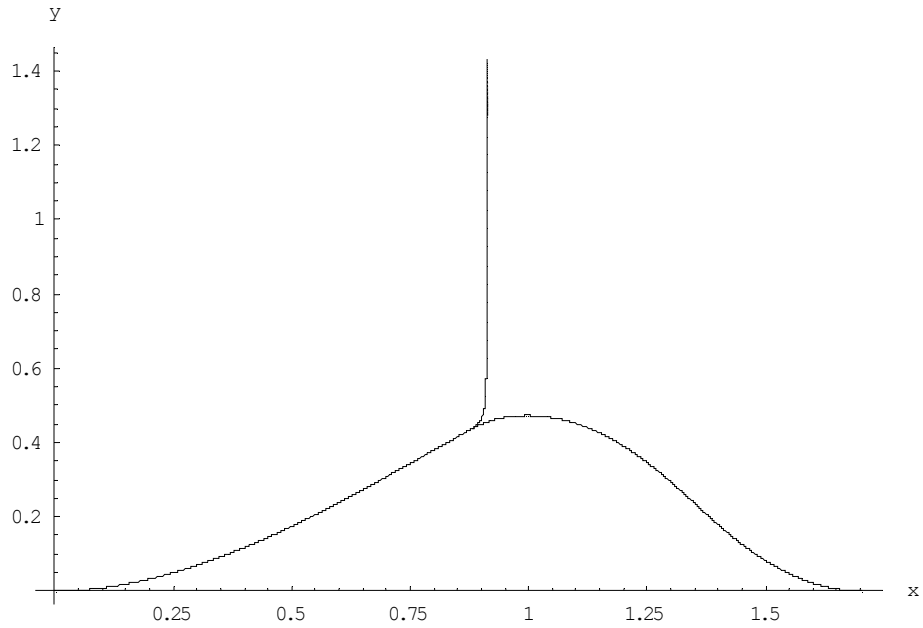


```
z = (yy2[1] + yy10[1]) / Sin[θo]
```

1.43077

```
md = yy12[1] - yy8[1]
```

0.431278

```
fn = fo * Sin[θo - yy3[1]] + p2 * Sin[yy3[1]] - q2 * Cos[yy3[1]]
```

4.58434

```
ft = -p2 * Cos[yy3[1]] - q2 * Sin[yy3[1]] + fo * Cos[θo - yy3[1]]
```

3.23647

Model 11—plastic hinges

In this program, y1 represents x1, y2 represents y1, y3 represents θ1, y4 represents m1, y5 represents x2, y6 represents y2, y7 represents θ2, y8 represents m2, y9 represents x3, y10 represents y3, y11 rperesents θ3, y12 represents m3, and t represents s.

```
Clear[fo, θo, r, d, η2, η3, k2, k3, gm1, gm2, gm3, gq1, gq2, gp2]
pi = Pi;
fo = 32;
θo = 0.8 * pi;
r = 1;
d = 0.4;
η2 = 0.1;
η3 = 0.5;
k2 = 0.01;
k3 = 0;
mt = 0.1;
ms = 0.1;
gq1 = -18.6;
gp2 = 0.0028;
gq2 = -0.19;
gm1 = 3.29;
gm2 = 0.16;
gm3 = 0.008;
```

**The above six variables are initial guesses.

```
de[y3_, y4_, y7_, y8_, y11_, y12_, q1_, p2_, q2_] :=
 {y1'[t] == Cos[y3[t]], y2'[t] == Sin[y3[t]], y3'[t] == y4[t],
  y4'[t] == q1 * Cos[y3[t]] + (p2 + fo * Cos[y3[t]]) * Sin[y3[t]], y5'[t] == r * Cos[y7[t]],
  y6'[t] == r * Sin[y7[t]], y7'[t] == r * y8[t] / η2, y8'[t] == r * (q2 * Cos[y7[t]] + p2 * Sin[y7[t]]),
  y9'[t] == d * Cos[y11[t]], y10'[t] == d * Sin[y11[t]], y11'[t] == d * y12[t] / η3,
  y12'[t] == d * (-fo * Sin[θo] * Cos[y11[t]] - fo * Cos[θo] * Sin[y11[t]])}
leftBC[m1_, m2_, m3_] := {y1[0] == 0, y2[0] == 0, y3[0] == 0, y4[0] == m1, y5[0] == 0,
  y6[0] == 0, y7[0] == 0, y8[0] == m2, y9[0] == 0, y10[0] == 0, y11[0] == pi - θo, y12[0] == m3}
soln :=
 NDSolve[Flatten[Append[de[y3, y4, y7, y8, y11, y12, q1, p2, q2], leftBC[m1, m2, m3]]],
  {y1, y2, y3, y4, y5, y6, y7, y8, y9, y10, y11, y12}, {t, 0, 1}, MaxSteps → 1000]
endpt[q1_, p2_, q2_, m1_, m2_, m3_] :=
  {y1[t], y2[t], y3[t], y4[t], y5[t], y6[t], y7[t], y8[t], y9[t], y10[t], y11[t], y12[t]} /.
    First[
     NDSolve[Flatten[Append[de[y3, y4, y7, y8, y11, y12, q1, p2, q2], leftBC[m1, m2, m3]]],
      {y1[t], y2[t], y3[t], y4[t], y5[t], y6[t], y7[t], y8[t], y9[t], y10[t],
       y11[t], y12[t]}, {t, 0, 1}, MaxSteps → 1000]] /. t → 1;
endpt[gq1, gp2, gq2, gm1, gm2, gm3]
```

```
{0.865046, 0.477731, 0.645589, 0.16516, 0.853356, 0.47373,
 0.744447, -0.000811278, 0.321933, 0.237386, 0.65281, 0.0982897}
Clear[q1, p2, q2, m1, m2, m3]
rts := FindRoot[{endpt[q1, p2, q2, m1, m2, m3][[2]] == endpt[q1, p2, q2, m1, m2, m3][[6]],
   endpt[q1, p2, q2, m1, m2, m3][[8]] == -ms, endpt[q1, p2, q2, m1, m2, m3][[12]] == mt,
   k3 * endpt[q1, p2, q2, m1, m2, m3][[2]] == q2 + q1 + (fo * Sin[θo]),
   endpt[q1, p2, q2, m1, m2, m3][[12]] + endpt[q1, p2, q2, m1, m2, m3][[8]] ==
    endpt[q1, p2, q2, m1, m2, m3][[4]],
   k2 * (1 + r - endpt[q1, p2, q2, m1, m2, m3][[1]] - endpt[q1, p2, q2, m1, m2, m3][[5]]) ==
    p2}, {q1, {gq1, 0.9*gq1}}, {p2, {gp2, 0.9*gp2}}, {q2, {gq2, 0.9*gq2}},
  {m1, {gm1, 0.9*gm1}}, {m2, {gm2, 0.9*gm2}}, {m3, {gm3, 0.9*gm3}},
  AccuracyGoal → 3, MaxIterations → 200]
rts
{q1 → -18.4521, p2 → 0.00262219,
 q2 → -0.357018, m1 → 3.26141, m2 → 0.208058, m3 → 0.00813922}
q1 = q1 /. rts
-18.4521
p2 = p2 /. rts
0.00262219
q2 = q2 /. rts
-0.357018
m1 = m1 /. rts
3.26141
m2 = m2 /. rts
0.208058
m3 = m3 /. rts
0.00813922
endpt[q1, p2, q2, m1, m2, m3]
{0.871484, 0.467962, 0.604258, -0.000499258, 0.866283,
 0.467976, 0.485966, -0.0999941, 0.321904, 0.237425, 0.653236, 0.1}
{yy1[t_], yy2[t_], yy3[t_], yy4[t_], yy5[t_], yy6[t_], yy7[t_], yy8[t_], yy9[t_],
   yy10[t_], yy11[t_], yy12[t_]} =
  {y1[t], y2[t], y3[t], y4[t], y5[t], y6[t], y7[t], y8[t], y9[t], y10[t], y11[t], y12[t]} /.
   First[soln];
plot1 = ParametricPlot[Evaluate[{yy1[t], yy2[t]}], {t, 0, 1}, PlotRange → All,
   PlotPoints → 1000, AxesLabel → {"x", "y"}];
```

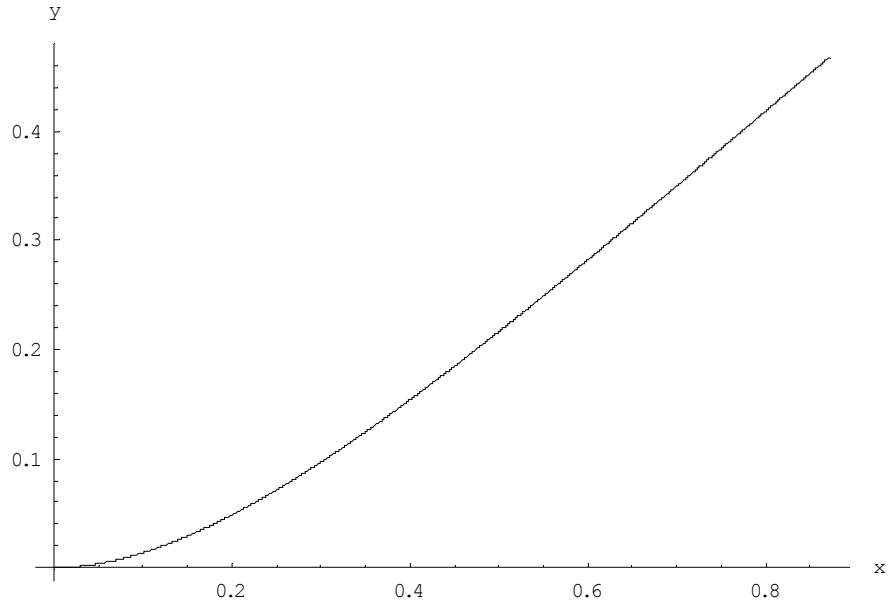


```
0 >> Ographdata1.txt
Do[{N[yy1[t]], N[yy2[t]]} >>> Ographdata1.txt, {t, 0, 1, (1 / 100)}]
plot2 = ParametricPlot[Evaluate[{((yy5[1] + yy1[1]) - yy5[t]), yy6[t]}], {t, 0, 1},
   PlotRange → All, PlotPoints → 1000, AxesLabel → {"x", "y"}];
```

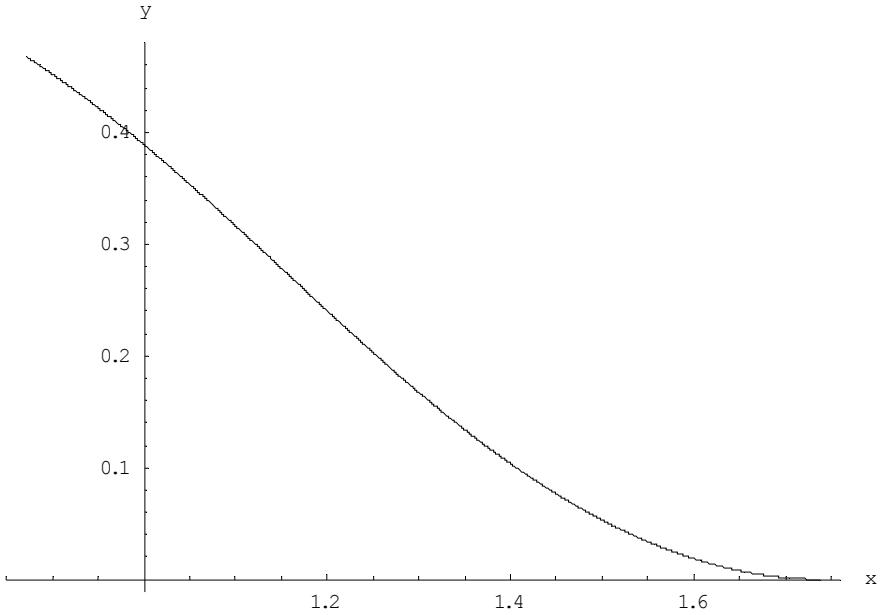


```
0 >> Ographdata2.txt
Do[{N[((yy5[1] + yy1[1]) - yy5[t])], N[yy6[t]]} >>> Ographdata2.txt, {t, 0, 1, (1 / 100)}]
Show[plot1, plot2];
```

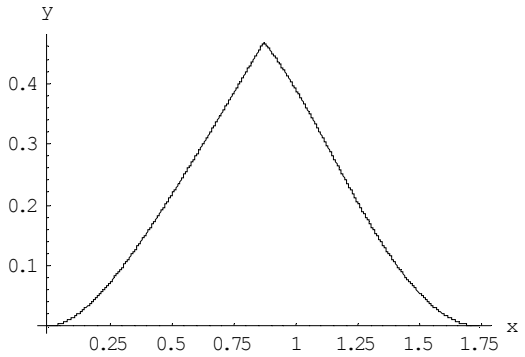

Adding Free Piece to Graph

```
ParametricPlot[Evaluate[{(yy9[t]), yy10[t]}], {t, 0, 1}, PlotRange → All,
  PlotPoints → 1000, AxesLabel → {"x", "y"}];
```

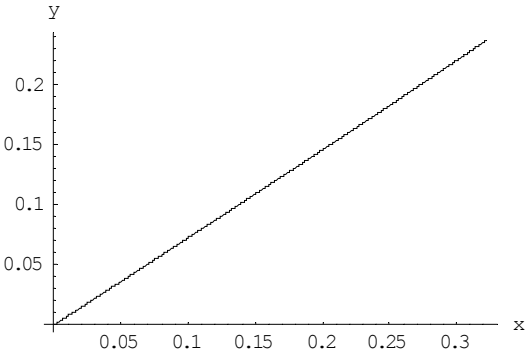


```
plot3 =
  ParametricPlot[Evaluate[{(yy1[1] - yy9[1] + yy9[t]), (yy2[1] + yy10[1] - yy10[t])}],
   {t, 0, 1}, PlotRange → All, PlotPoints → 1000, AxesLabel → {"x", "y"}];
```

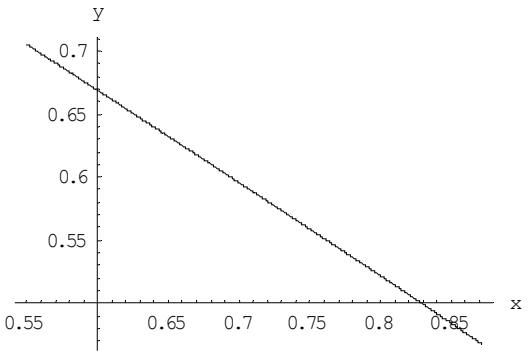


```
0 >> Ographdata3.txt
Do[{N[(yy1[1] - yy9[1] + yy9[t])], N[(yy2[1] + yy10[1] - yy10[t])]} >>> Ographdata3.txt,
 {t, 0, 1, (1 / 100)}]
Show[plot1, plot2, plot3];
```

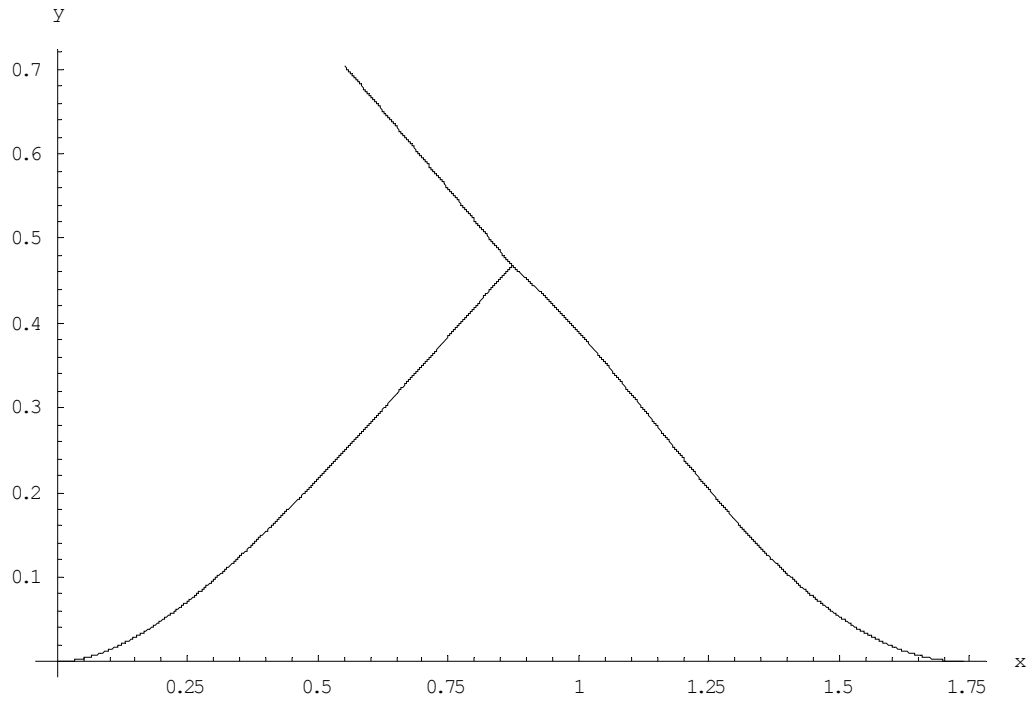
y
0.7
0.6
0.5
0.4
0.3
0.2
0.1
0.25
0.5
0.75
1
1.25
1.5
1.75
x

Vita

Alicia Corrine Karwoski was born on October 25, 1979 in Smithsburg, Maryland. She graduated from Virginia Tech with her Bachelor of Science degree in Civil Engineering in May 2002 and went on to complete her Master of Science degree in Civil Engineering in May 2003. After completing her graduate degree, she will work for Pulte Homes Sciences in Manassas, Virginia, designing houses.